JAERI-M
88-065

NEANDC(J) 127/U
INDC(JPN) 113/L

PROCEEDINGS OF THE 1987 SEMINAR ON NUCLEAR DATA

March 1988

(Ed.) Tsuneo NAKAGAWA and Atsushi ZUKERAN*

日本原子力研究所
Japan Atomic Energy Research Institute

JAERI-Mレポートは，日本原子力研究所が不定期に公刊している研究報告書です。
入手の問合わせは，日本原子力研究所技術情報部情報資料課（〒319-11茨城県那珂郡東海村）あて，お申しこしください。なお，このほかに財団法人原子力弘済会資料センター（〒319-11 茨城県那珂郡東海村日本原子力研究所内）で複写による実費頒布をおこなっております。

JAERI-M reports are issued irregularly.
Inquiries about availability of the reports should be addressed to Information Division Department of Technical Information, Japan Atomic Energy Research Institute, Tokai-mura, Naka-gun, Ibaraki-ken 319-11, Japan.

©Japan Atomic Energy Research Institute, 1988

編集兼発行　日本原子力研究所
印　　刷　いばらき印刷㈱

JAERI-M 88-065

Proceedings of the 1987 Seminar on Nuclear Data

(Ed.) Tsuneo NAKAGAWA and Atsushi ZUKERAN*

Japanese Nuclear Data Committee
Tokai Research Establishment
Japan Atomic Energy Research Institute
Tokai-mura, Naka-gun, Ibaraki-ken

(Received February 9, 1988)

The 1987 Seminar on Nuclear Data was held by the Japanese Nuclear Data committee and the Nuclear Data Center, at the Tokai Research Establishment of the Japan Atomic Energy Research Institute, on November 12 and 13, 1987. Main topics of the seminar were 1) evaluation of nuclear data for JENDL-3 and 2) benchmark test of JENDL-3T. Some topical review presentations were also made on interesting fields for post-JENDL-3 activity. This report containes the 36 papers given at the seminar.

Keywords: Proceedings, Seminar, Nuclear Data, JENDL, Evaluation, Benchmark Test

* Hitachi, Ltd.

Program Committee

A. Zukeran(Chairman)	(Hitachi, Ltd.)
T. Fukahori	(Japan Atomic Energy Research Institute)
K. Hide	(Nippon Atomic Industry Group Co., Ltd.)
M. Igashira	(Tokyo Institute of Technology)
J. Katakura	(Japan Atomic Energy Research Institute)
K. Kitao	(National Institute of Radiological Sciences)
H. Maekawa	(Japan Atomic Energy Research Institute)
H. Matsunobu	(Sumitomo Atomic Energy Industries, Ltd.)
M. Mizumoto	(Japan Atomic Energy Research Institute)
T. Nakagawa	(Japan Atomic Energy Research Institute)
H. Nakamura	(Fuji Electric Co., Ltd.)
M. Nakazawa	(University of Tokyo)
M. Sasaki	(Mitsubishi Atomic Power Industries, Ltd.)
K. Shibata	(Japan Atomic Energy Research Institute)
H. Takano	(Japan Atomic Energy Research Institute)

JAERI－M 88－065

1987年核データ研究会報文集

日本原子力研究所東海研究所シグマ研究委員会
（編）中川　庸雄・瑞慶覧　篤*

（1988年2月9日受理）

シグマ研究委員会と核データセンターにより，1987年核データ研究会が，1987年11月12日と13日の両日，日本原子力研究所東海研究所において開催された。今回の研究会の主なテーマは，1）ＪＥＮＤＬ－３のための核データ評価と，2）ＪＥＮＤＬ－３Ｔ のベンチマークテストであった。さらに，ＪＥＮＤＬ－３以降の核データ活動に関して興味深いテーマの講演も行われた。本報告は，研究会で報告された36件の論文をまとめたものである。

プログラム委員会

瑞慶覧　篤（委員長）	((株）日立製作所エネルギー研究所）
深堀　智生	（日本原子力研究所）
肥田　和毅	（日本原子力事業（株））
井頭　政之	（東京工業大学）
片倉　純一	（日本原子力研究所）
喜多尾憲助	（放射線医学総合研究所）
前川　　洋	（日本原子力研究所）
松延　廣幸	（住友原子力工業（株））
水本　元治	（日本原子力研究所）
中川　庸雄	（日本原子力研究所）
中村　　久	（富士電機（株））
中沢　正治	（東京大学）
佐々木　誠	（三菱原子力工業（株））
柴田　恵一	（日本原子力研究所）
高野　秀機	（日本原子力研究所）

東海研究所：〒319－11 茨城県那珂郡東海村白根2－4
* （株）日立製作所

Contents

目　　次

1. Program of Seminar

The 1987 Seminar on Nuclear Data was held at the Tokai Research Establishment of the Japan Atomic Energy Research Institute on November 12-13, 1987, according to the following program.

November 12 (Thursday)		Speaker
11:00-11:02	1. Opening address	N. Shikazono (JAERI)
11:02-11:10	2. Report from secretariat	A. Zukeran (Hitachi)
	3. Compilation of JENDL-3	
	Chairman:	H. Matsunobu (SAEI)
11:10-11:30	3.1 An Outline of JENDL-3T	T. Asami (JAERI)
11:30-12:00	3.2 Evaluation of Nuclear Data for Heavy Nuclides	T. Nakagawa (JAERI)
Lunch		
13:00-13:25	3.3 Nuclear Data Evaluation for Medium and Heavy Nuclei	M. Mizumoto (JAERI)
13:25-13:50	3.4 Evaluation of Neutron Cross Sections of Fission Products for JENDL-3	M. Kawai (NAIG)
	4. Benchmark Tests of JENDL-3T	
	Chairman:	S. Iijima (NAIG)
13:50-14:20	4.1 Thermal Reactor and High Conversion Light Water Reactor	H. Takano (JAERI)
14:20-15:00	4.2 Fast Breeder Reactor	T. Takeda (Osaka Univ.)
Coffee Break		
15:10-15:35	4.3 Fission Product Cross Section Integral Tests and Adjustment Based on Integral Data	T. Watanabe (KHI)
15:35-16:00	4.4 Shielding Benchmark Test	A. Hasegawa (JAERI)
16:00-16:25	4.5 Dosimetry Benchmark Test	M. Nakazawa (Univ. of Tokyo)

5. Free Discussion on JENDL-3

Chairman: A. Zukeran (Hitachi)

16:25-17:45 (Free discussion)

18:30-20:30 Reception (at Tokai Kaikan)

November 13 (Friday)		Speaker
	6. Poster Session	
9:00-10:20	(18 papers were presented)	
	7. Topics	Chairman: K. Harada (Nippon Energy)
10:20-11:05	7.1 Energy Spectra of Particles Emitted from (p,α), (n,α), (p,n) and (n,p) Reactions on Nuclei around Magic Number	I. Kumabe (Kyushu Univ.)
11:05-11:35	7.2 Activity on Atomic and Molecular Data for Fusion	T. Shirai (JAERI)
11:35-12:05	7.3 Free-Electron Laser	Y. Kawarasaki (JAERI)
Lunch		
		Chairman: Y. Nakahara (JAERI)
13:00-13:30	7.4 A Basic Study on the Transmutation of Radioactive Wastes by Photonuclear Reactions	T. Nakamura (Tohoku Univ.)
13:30-14:00	7.5 Analysis of Transmutation of Transuranic Wastes by Nuclear Spallation Reactions	T. Nishida (JAERI)
14:00-14:15	Discussion	
		Chairman: T. Nakamura (JAERI)
14:15-14:40	7.6 The Measurement of Leakage Neutron Spectra from Various Sphere Piles with 14 MeV Neutrons	C. Ichihara (Kyoto Univ.)

14:40-15:05	7.7 Angle-integrated Neutron Emission Spectra at 14 MeV for Be, F, Mg, Al, Si, V, Fe, Cr, Cu, Pb and Bi	A. Takahashi (Osaka Univ.)

Coffee Break

8. Nuclear Data for Fusion Reactor in JENDL-3T

Chairman: Y. Kanda (Kyushu Univ.)

15:15-15:40	8.1 Evaluation of the Fusion-Related Neutron Data	S. Chiba (JAERI)
15:40-16:05	8.2 Fusion Neutronics Integral Test for JENDL-3T	H. Maekawa (JAERI)
16:05-16:25	Discussion	
16:25-16:30	9. Closing Address	S. Igarasi (JAERI)

2. Orally Presented Papers

2.1 Compilation of JENDL-3

2.1.1 An Outline of JENDL-3T

Tetuso Asami
Nuclear Data Center
Japan Atomic Energy Research Institute

The compilation of the Japanese Evaluated Nuclear Data Library, Version 3 (JENDL-3) is now in progress aiming at the completion in 1988. The data evaluation has been almost finished, and the data assembling, the error checks, the consistency checks and so on have been continued. On the other hand, various benchmark tests started at the beginning of 1987 for these data of some important nuclides. JENDL-3T is a temporary file which was particularly prepared for these benchmark tests. The data in JENDL-3T could be revised partly in the basis of the results of the benchmarks. An outline of JENDL-3T is given together with various problems encountered in the compilation work for JENDL-3.

1. What is JENDL-3T?

The project of Japanese Evaluated Nuclear Data Library, Version 3 (JENDL-3) was planned in Japanese Nuclear Data Committee(JNDC) about five years ago, and the data evaluation has been made ever since. The data evaluation has been performed by thirty-odd evaluators in the Subcommittee on Nuclear Data in JNDC, and the compilation of the evaluated data have been carried out in JENDL Compilation Group of JAERI Nuclear Data Center. On the other hand, various benchmark tests for the data of main nuclides started at the beginning of 1987 in the working groups in the Subcommittee on Reactor Constants in JNDC. The evaluated data used in the benchmark tests were compiled in a temporary file named as JENDL-3T. JENDL-3T is not final one and their data could be revised partly at least before the completion of JENDL-3. Therefore, we should be recognized JENDL-3T to be indeed different from JENDL-3. As the outline of JENDL-3 plan have been described elsewhe $\varepsilon^{1)}$, we will discuss only on JENDL-3T here.

Table 1 is a list of the nuclides whose evaluated data are to be stored in JENDL-3. At the present (December in 1987) the evaluated data for 73 nuclides have been stored in JENDL-3T. In Table 1, the nuclides in JENDL-3T are shown with underlines. Table 2 shows the numbers of the nuclides stored in JENDL-3T, compared with those of JENDL-1, -2 and -3. Table 2 also shows the number of nuclides with photon production data which were adopted newly in JENDL-3. The

evaluated data were compiled in the ENDF/B-V format.

2. Work in the JENDL Compilation Group

The compilation of the JENDL-3T data have been made in the JENDL Compilation Group. This Group consists of six persons in JAERI Nuclear Data Center and three in other laboratories in JAERI and was organized in JAERI Nuclear DAta Center in September of 1986. The main tasks for this group were (1) to do the work of file-making, (2) to examine the problems on the file-making and the evaluated data, (3) to establish the processes for the file-making and (4) to keep in close contact with data evaluators and data users.

In order to discuss the above tasks and to solve troublesome problems in the compilation, the group meetings were held about thirty times so far. Through the discussions at the meetings a sheet for data checking was prepared as a part of establishing a system for error check. Main checks for erroneous data and format errors were made with the use of several computer codes (for example, CHECKER, FIZCON, PSYCHE etc.), and by examining plotted data. In the data evaluation and the file making many computer codes and systems have been used effectively. In particular RESENDD[2], NDES[3] and GAMFIL[4] were much useful in the file making. In the checks of the compiled data the data of neutron-emission double-differential cross sections(DDX) and of photon spectra were examined in detail in comparing with their experimental data. In plotting the DDX data DDXPLOT[5] was much useful.

The JENDL News were prepared to serve close contacts with the data evaluators, the data users and the compilation group, and have been issued once a month roughly.

In the course of the JENDL-3 compilation we faced several problems on the file-making. The main problems were on the data format used and their format rules, and on the relation with user's processing codes, except for laborious work in the file making. Although all the evaluated data in JENDL-3 were compiled in the ENDF/B-V format as described above, several problems happened on the format and the format rule.

Here we will give some examples for the problems on the file making. The first is on the File 6. For the data evaluations for the secondary neutrons of ^{6}Li and ^{7}Li, the use of File 6 was essential. In fact, the use of the File 6 representation has been recommended[6] for presenting the actual physical process more precisely. The use of File 6, however, is not permitted in the ENDF/B-V format, being available in the ENDF/B-VI format. Considering the relation of user's processing codes, therefore, the data for File 6 were to be converted to File 4 and File 5. However, taking account of that the ENDF/B-VI format will be adopted in the major library in the world in near future, we will have an another

auxiliary file used File 6 .

The second is on the formalism of resonance parameters. The resolved resonance parameters of ^{239}Pu were evaluated with the formalism of Reich-Moore which is not permitted in the ENDF/B-V format[7]. However, since the use of the Reich-Moore formalism was unavoidable in this case, we decided to use this formalism in JENDL-3 in spite of the violation for the format rule.

In some cases the JENDL-3T data were not accepted in the user's processing codes. One of the cause resulted from the subsections in the File 5 and File 15. We suppose that the use of the subsections in File 5 would be allowed in the ENDF/B-V format although the use of the subsections in File 15 may be the violation of the format rules. Generally we consider that troublesome problems occurred in the data processing should be solved by data users except for the violation of the format rule. In JENDL-3, however, the subsections in File 5 and File 15 will be removed in taking account of user's processing codes.

Although in the file making we have followed the rule of the ENDF/B-V format, we had to permit minor violations. According to the format rule, for example, the upper limit of resolved resonance region must coincide between stable isotopes included. However, we have permitted this violation of the format rule since the upper limits of resonance region depend directly on their level spacings which in general are fairly different among isotopes, in order to utilize detailed information on the resonance parameters as much as possible.

Aside from the format rule we had another problem such as the following. The JENDL-3T data for the resolved resonance parameter of ^{238}U and ^{239}Pu have included a large number of levels, and much times for computing were required in reproducing the pointwise cross sections from these parameters. This is a serious problem in the general uses of the data library.

3. Remaining Work in the process from JENDL-3T to JENDL-3

The results of the benchmark tests for JENDL-3T which have been pointed out in this seminar, will be effectively used in revising the JENDL-3T data by each data evaluator. The another test for the revised data would be necessary. As the expected revisions of the JENDL-3T data and the data to be revised based on the benchmark tests will be described by several authors later, we don't touch these problems in this paper further.

Before the completion of JENDL-3 a large amount of work remains in the revision of the JENDL-3T data and the compilation of the JENDL-3 data. In particular the compilation for the evaluated data for FP nuclides is a little late.

In JENDL-3 the data on fission-product yields and decays in File 8 will be taken from a new version of the JNDC Decay Data File. The scattering law data for thermal neutrons used in File 7 will be taken from the evaluation due to the

Subworking group on thermal neutron scattering law in JNDC.

The completion of the file-making for JENDL-3 is expected in April of 1988. Before the completion, however, there are some problems to be solved: for example, problems on final checks of all the evaluated data to be stored in JENDL-3 and the choice of their MAT number. The former is concerns with steps for the final check of the evaluated data and how to make the data checking efficiently and rapidly. The latter is not so difficult but the MAT number had to be decided in relating to the special file which will be added to the general file of JENDL-3.

References

1) T. Asami, Proceedings of the 1986 Seminar on Nuclear Data, JAERI-M 87-025 (1987) p. 1.
2) T. Nakagawa, "Program RESENDD (Version 84-07) : A Program for Reconstruction of Resonance Cross Sections from Evaluated Nuclear Data in the ENDF/B format (Modified Version of RESEND)", JAERI-M 84-192 (1984).
3) T. Nakagawa, "Neutron Data Evaluation System" (in Japanese), J. At. Energy society of Japan 22, 559 (1980).
4) K. Hida: "GAMFIL: A Computer Program for Generating Photon Produc tion Nuclear Data File" (in Japanese), JAERI-M 86-150 (1986).
5) T. Iguchi and N. Yamano, "DDXPLOT : A Program to plot the Energy Angle Double-Differential Cross Sections" (in Japanese), JAERI-M 84-033 (1984).
6) the report of Subgroup, Proceedings of Specialist' Meeting on Nuclear Data for Fusion Neutronics, JAERI-M 86-029 (1986) p.196.
7) R. Kinsey (revised), "ENDF-102 Data Formats and Procedures for the Evaluated Nuclear Data", BNL-NCS-50496(ENDF 102) 2nd Edition (ENDF/B-V) (1979).

Table I List of Nuclides in JENDL-3 and JENDL-3T.
The underlines denote the nuclides stored in JENDL-3T(as of December 1987).
The asteriskes show the nuclides with the evaluated data for photon production.
The nuclides with the parenthisis are only with the specific data.

Z	Nuclide
1	*^{1}H, ^{2}H
2	^{3}He, ^{4}He
3	*^{6}Li, *^{7}Li
4	*^{9}Be
5	^{10}B, ^{11}B
6	*^{12}C
7	*^{14}N
8	*^{16}O
9	*^{19}F
11	*^{23}Na
12	*Mg, ^{24}Mg, ^{25}Mg, ^{26}Mg
13	*^{27}Al
14	*Si, ^{28}Si, ^{29}Si, ^{30}Si
15	^{31}P
16	S, ^{32}S, ^{33}S, ^{34}S, ^{36}S
17	Cl, ^{35}Cl, ^{37}Cl
18	^{40}Ar
19	K, ^{39}K, ^{40}K, ^{41}K
20	*Ca, ^{40}Ca, ^{42}Ca, ^{43}Ca, ^{44}Ca ^{46}Ca, ^{48}Ca
21	^{45}Sc
22	*Ti, ^{40}Ti, ^{47}Ti, ^{48}Ti, ^{49}Ti, ^{50}Ti
23	^{51}V
24	*Cr, ^{50}Cr, ^{52}Cr, ^{53}Cr, ^{54}Cr
25	*^{55}Mn
26	*Fe, *^{54}Fe, *^{56}Fe, *^{57}Fe, *^{58}Fe
27	^{59}Co
28	*Ni, *^{58}Ni, (^{59}Ni), *^{60}Ni, ^{61}Ni, ^{62}Ni, ^{64}Ni
29	*Cu, *^{63}Cu, *^{65}Cu
40	*Zr, ^{90}Zr, ^{91}Zr, ^{92}Zr, ^{94}Zr, ^{96}Zr
41	*^{93}Nb, (^{94}Nb)
42	*Mo, ^{92}Mo, ^{94}Mo, ^{95}Mo, ^{96}Mo, ^{97}Mo, ^{98}Mo, ^{100}Mo
47	Ag, ^{107}Ag, ^{109}Ag
48	Cd
51	Sb, ^{121}Sb, ^{123}Sb
63	*Eu, ^{151}Eu, ^{153}Eu
72	*Hf, ^{174}Hf, ^{176}Hf, ^{177}Hf, ^{178}Hf, ^{179}Hf, ^{180}Hf
73	*^{181}Ta
74	*W, ^{180}W, ^{182}W, ^{183}W, ^{184}W, ^{186}W
82	*Pb, *^{204}Pb, *^{206}Pb, *^{207}Pb, *^{208}Pb
83	*^{209}Bi
90	^{228}Th, ^{230}Th, ^{232}Th, ^{233}Th, ^{234}Th
91	^{231}Pa, ^{233}Pa
92	^{232}U, ^{233}U, ^{234}U, *^{235}U, ^{236}U, *^{238}U
93	^{237}Np, ^{239}Np
94	^{236}Pu, ^{238}Pu, *^{239}Pu, ^{240}Pu, ^{241}Pu, ^{242}Pu
95	^{241}Am, ^{242g}Am, ^{242m}Am, ^{243}Am
96	^{242}Cm, ^{243}Cm, ^{244}Cm, ^{245}Cm, ^{246}Cm, ^{247}Cm, ^{248}Cm, ^{249}Cm
97	^{249}Bk
98	^{249}Cf, ^{250}Cf, ^{251}Cf

JAERI - M 88 - 065

Table 2 The Comparison of the Numbers of Nuclides in JENDL-3T with Those in JENDL-1, -2 and -3. The figures in the parenthesis stand for the number of nuclides with photon-production data.

	JENDL-1 (1977)	JENDL-2 (1982)	JENDL-3T (1987)	(JENDL-3) (1988?)
light nuclides (z= 1 ~ 19)	7	11	28(10)	37(12)
structural materials nuclides (z= 20 ~ 30)	20	30	20(13)	37(15)
FP nuclides (z= 31 ~ 69)	34	101	1(1)	178(3)
medium weight nuclides (z= 70 ~ 89)	1	12	5(5)	20(9)
heavy nuclides (z= 90 ~ 94)	9	19	15(3)	21(3)
transplutonium (z= 95 ~ 98)	1	8	4(0)	18(0)
TOTAL	72(0)	181(0)	73(32)	311(42)

JAERI-M 88-065

2 1.2 Evaluation of Nuclear Data for Heavy Nuclides

Tsuneo NAKAGAWA

Japan Atomic Energy Research Institute
Tokai-mura, Naka-gun, Ibaraki-ken 319-11, Japan

Abstract

For JENDL-3, nuclear data of nuclides from Th to Pu were evaluated by members of JNDC Subworking Group on Heavy Nuclides Data. In this presentation, status of the evaluated heavy nuclide data stored in JENDL-3T is given.

1. Introduction

In JENDL-3, nuclear data of 40 heavy nuclides will be stored. Among them, evaluation for nuclides from Am to Cf was performed by the Nuclear Data Center, JAERI, and that for Th, Pa, U and Pu isotopes was carried out by the member of JNDC Subworking Group on Heavy Nuclide Nuclear Data*) as shown in Table 1. Those evaluated data were compiled as JENDL-3T**),1) for benchmark test. In this presentation, the present status of the evaluated data stored in JENDL-3T is briefly described.

---

*) Current member of the subworking group:
K. Hida, Y. Kanda, M. Kawai, K. Kawakita, H. Matsunobu, T. Murata, T. Nakagawa, T. Ohsawa, T. Yoshida and A. Zukeran.
T. Asami, T. Houjuyama, Y. Kikuchi, Y. Nakajima, M. Sasaki and T. Watanabe were also member of the subworking group.

**) JENDL-3T is a temporary file for testing the evaluated data for JENDL-3. The data in JENDL-3T will be partly revised in JENDL-3.

2. Simultaneous Evaluation

The fission cross sections of ^{235}U, ^{238}U, ^{239}Pu, ^{240}Pu and ^{241}Pu, and the capture cross section of ^{238}U were evaluated with a simultaneous evaluation method in the energy range from 50 keV to 20 MeV. A computer program developed by Uenohara and Kanda[2] was used. In this program, best fit values are obtained by means of the generalized least-squares fitting by appling B-spline functions.

Experimental data reported mainly after 1970 were taken into consideration together with their covariance matrices constructed from reported information on experimental errors.

Figure 1 shows a result of ^{235}U fission cross section. The present result (solid line) reproduces experimental data very well, except in a high energy region where the result is lower than the experimental data because of ratio data to the other reactions. In the energy range below 1 MeV, the present result is lower by about 3% in average than JENDL-2 shown with a dashed line.

Figure 2 compares ratio data of ^{239}Pu and ^{235}U fission cross sections. The present result is also lower than JENDL-2 below 1 MeV. These experimental ratio data are transformed to the ^{239}Pu fission cross section by multipling the ^{235}U fission cross section and shown in Fig. 3 as well as absolute measurements. The evaluated cross section below 1 MeV is obviously lower than JENDL-2, but in good agreement with recent measurements. The data of JENDL-2 were evaluated by selecting large values in this energy range in order to meet requirement from reactor physics for getting reasonable k_{eff} values of integral experiments. However, the present evaluation was purely based on experimental data.

The capture cross section of ^{238}U is given in Fig. 4. The result of the simultaneous evaluation is larger than JENDL-2 and has structure at high energies. In JENDL-3T, this result was adopted from 100 keV to 3 MeV。 However, that will be replaced to final JENDL-3 with a more smooth curve in the high energy region.

3. Inelastic Scattering Cross Section

A direct process is very important for the inelastic scattering cross sections in a high energy region. However, it was not taken into account for JENDL-2. For JENDL-3, improvement of the inelastic scattering cross section was made for several important nuclides by adopting coupled-channel and/or DWBA calculations.

In the case of the ^{238}U inelastic scattering cross section, the contributions from the direct process to the first and second excited levels were calculated with a coupled-channel calculation code ECIS[3] and those for other levels with a DWBA code DWUCK-4[4]. The compound process was estimated with CASTHY.[5] Thus obtained total inelastic scattering cross section is largely different from JENDL-2 and ENDF/B-IV above 1 MeV. No experimental data are available to be compared with the calculated total inelastic scattering cross section. The cross section to the first excited state is compared in Fig. 5-a. It is seemed that the evaluation for JENDL-3 is in better agreement with experimental data than JENDL-2. Figure 5-b shows the data of 732-keV level. The JENDL-3 evaluation agrees very well with experimental data.

The direct process was also considered for ^{232}Th, ^{233}U, ^{234}U, ^{235}U, ^{239}Pu, ^{240}Pu and ^{242}Pu inelastic scattering cross sections.

4. Other Cross Sections in High Energy Region

Figure 6 is the ^{239}Pu (n,2n) reaction cross section. The solid curve was calculated with GNASH[6] for JENDL-3, and in agreement with a recent measurement by Frehaut[7]. However, below about 8 MeV the cross section will be modified a little to reproduce better the experimental data. The data obtained by Mather[8] are larger than Frehant's new data.

For the other nuclides, the evaluation was made on the basis of new experimental data if available.

The ^{235}U total cross section is shown in Fig. 7. JENDL-3T was based on the data measured by Poenitz[9]. In the cases of other nuclides, a lot of experimental data is also available to determine accurate total cross sections.

In many cases, the elastic scattering cross section was obtained as (total cross section - sum of partial cross sections). Experimental data are not so many, but as shown in Fig. 8, the evaluated elastic scattering cross section is in agreement with existing experimental data. In this figure, the inelastic scattering cross section to the first excited level of ^{235}U is included in the evaluated data.

5. Resonance Parameters

After JENDL-2 evaluation, several experiments and analyses were made for resonance parameters of important heavy nuclides. Those of ^{238}U were newly obtained in the energy region up to 10 keV by Olsen[10]

by means of the shape analysis to transmission data measured at ORNL. The present evaluation was mainly based on Olsen's data and JENDL-2. The parameters for 356 s-wave resonances and 485 p-wave ones were given in the multi-level Breit-Wigner formula. The upper limit of the resolved resonance region was extended up to 9.5 keV. As a result, it takes a very long CPU time to reconstruct resonance cross sections from the parameters and the number of energy points generated is very large.

Another extensive analysis of ^{238}U resonance parameters is in progress at Harwell. Unfortunately, Harwell's result could not be taken into consideration.

The parameters of the Reich-Moore multi-level formula obtained by Derrien et al.[11] were tentatively adopted for ^{239}Pu. The upper boundary of resolved resonance regin was set to be 1 keV. Since the Reich-Moore formula cannot be stored in the ENDF/B-V format adopted for JENDL-3, the ENDF/B-IV format was used only for MF=2 of the ^{239}Pu data.

The resonance parameters of ^{232}Th and ^{240}Pu were also modified from JENDL-2. The same values of total spin J as a target spin were adopted in JENDL-2 for the resonances of odd mass nuclides whose J values had not been determined experimentally. They were modified to physically reasonable values in the case where the multi-level Breit-Wiguer formula was adopted.

Unresolved resonance parameters were determined with ASREP[12] so as to reproduce cross sections evaluated in the unresolved resonance region. An example in Fig. 9 shows the fission cross sections of ^{235}U. Experimental data in the figure are those measured in 1980's. The solid curve is the present result and the dashed one JENDL-2. The solid curve is lower than the dashed curve. The unresolved resonance parameters of ^{235}U will be investigated more, because such low fission cross section of ^{235}U is not preferable from the viewpoint of reactor physics.

6. Thermal Cross Sections and Resonance Integrals

Table 2 lists the 2200-m/s cross sections and resonance integrals of important six nuclides. Those recommended by Mughabghab[13] are also given for comparison.

7. Fission Spectra

The fission spectra were mainly taken from recommendation of Madland and Nix[14]. Figure 10 shows the prompt neutron spectrum from

200-keV neutron-induced fission of ^{239}Pu. The upper half of the figure is comparison of normalized spectra with JENDL-2 and experimental data. And the lower half shows the ratio to JENDL-2. From this figure it is seen that the Madland-Nix type spectra are harder than evaporation spectra adopted in JENDL-2.

The spectra of delayed neutrons were adopted from the evaluation work done by Saphier et al.[15].

8. Number of Neutrons per Fission

In JENDL-3T, the numbers of prompt neutrons per fission of ^{235}U and ^{239}Pu were largely changed from JENDL-2. This evaluation was based on the relatively large experimental data and the new evaluated data by Frehant[16]. However, the large value and structure of $\bar{\nu}_p$ in JENDL-3T, especially that of ^{235}U, resulted in undesirable conclusions of benchmark calculation[17]. They will be modified to the final JENDL-3.

9. Concluding Remarks

Status of important data of heavy nuclides was summarized. The evaluated data in JENDL-3T have been benchmark-tested and their problems are reported in this Nuclear Data Seminar. On the other hand, data checking with graphes which compare JENDL-3T with experimental data and other evaluated data such as JENDL-2, ENDF/B-IV, and comparison with deduced values such as 2200m/s values and resonance integrals were performed at JNDC Subworking Group on Heavy Nuclide Data. Each evaluator is now reevaluating partly the data whose problems were pointed out.

References

1) JENDL Compilation Group (Nuclear Data Center, JAERI): JENDL-3T, private communication (1987).
2) Uenohara, Y. and Kanda, Y.: "Simultaneous Evaluation of Neutron Cross Section and Their Covariances for Some Reaction of Heavy Nuclei", Proc. International Conf. on Nuclear Data for Science and Technology, 1982 Antwerp, 639 (1983).
3) Raynal, J.: "Optical Model and Coupled-Channel Calculations in Nuclear Physics", IEAE SMR-9/8 (1970).
4) Kunz, P.D.: DWUCK4, unpublished.

5) Igarasi, S.: J. Nucl. Sci. Technol., 12, 67 (1975).
6) Young, P.G. and Arthur E.D.: "GNASH: A Preequilibrium, Statistical Nuclear-Model Code for Calculation of Cross Sections and Emission Spectra", LA-6947 (1977).
7) Frehaut, J., et al.: "(n,2n) Cross Sections of ^{2}H and ^{239}Pu", Proc. International Conference on Nuclear Data for Basic and Applied Science, 1985 Santa Fe, vol.2, 1561 (1986).
8) Mather, D.S., et al.: "Measurement of (n,2n) Cross Sections for Incident Energies between 6 and 14 MeV", AWRE O 72/72 (1972).
9) Poenitz, W.P. and Whalen, J.F.: "Neutron Total Cross Section Measurements in the Energy Region from 47 keV to 20 MeV", ANL/NDM-80 (1983).
10) Olsen, D.K.: Nucl. Sci. Eng., 94, 102 (1986).
11) Derrien, H., et al.: "R-Matrix Analysis of the ^{239}Pu Cross Sections up to 1 keV", ORNL/TM-10098 (1986).
12) Kikuchi, Y.: private communication.
13) Mughabghab, S.F.: "Neutron Cross Sections, Vol.1, Neutron Resonance Parameters and Thermal Cross Sections, Part B: Z=61-100", Academic Press (1984).
14) Madland, D.G. and Nix, J.R.: Nucl. Sci. Eng., 81, 213 (1982), Madland, D.G.: Computer program FISPEK, private communication (1987).
15) Saphier, D.: Nucl. Sci. Eng., 62, 660 (1977).
16) Frehaut, J.: "Coherent Evaluation of $\bar{\nu}_p$ for ^{235}U, ^{238}U and ^{239}Pu", NEANDC(E) 238/L (1986).
17) Takano, H.: presented in this seminar.
Komuro, Y.: private communication (1987).

Table 1 Evaluators of Nuclear Data for Heavy Nuclides.

Nuclides	Evaluators
Th-228, 230, 232, 233, 234	T. Ohsawa
Pa-231, 233, U-232	T. Ohsawa, T. Nakagawa
U-233	H. Matsunobu
U-234	T. Asami, T. Watanabe
U-235	H. Matsunobu, Y. Nakajima, K. Hida
U-236	T. Yoshida
U-238	Y. Kanda, Y. Uenohara, T. Nakagawa, K. Hida
Np-237	Y. Uenohara, Y. Kanda
Pu-236	T. Hojuyama
Pu-238	K. Kawakita
Pu-239	M. Kawai, T. Yoshida, K. Hida
Pu-240	T. Murata, A. Zukeran
Pu-241	Y. Kikuchi, T. Nakagawa
Pu-242	M. Kawai, T. Murata

Table 2 2200-m/s cross sections and resonance integrals

(barns)

	2200m/s values		Resonance Integral	
	Capture	fission	Capture	fission
^{232}Th	7.37±0.06 7.40	<0.0025mb 0.0	85±3 84.4	 0.64
^{235}U	98.3±0.8 96	582.6±1.1 584	144±6 152	275±5 276
^{238}U	2.680±0.019 2.68	0.004mb 0.011mb	277±3 279	1.54±0.15mb 2.02
^{239}Pu	269.3±2.9 268.6	748.1±2.0 744.5	200±20 186	301±10 297
^{240}Pu	289.5±1.4 289.4	0.056±0.030 0.0588	8100±200 8110	8.8 8.94
^{241}Pu	358.2±5.1 363	1011.1±6.2 1015	162±8 187	570±15 590

upper: Mughabghab[13], lower: JENDL-3T

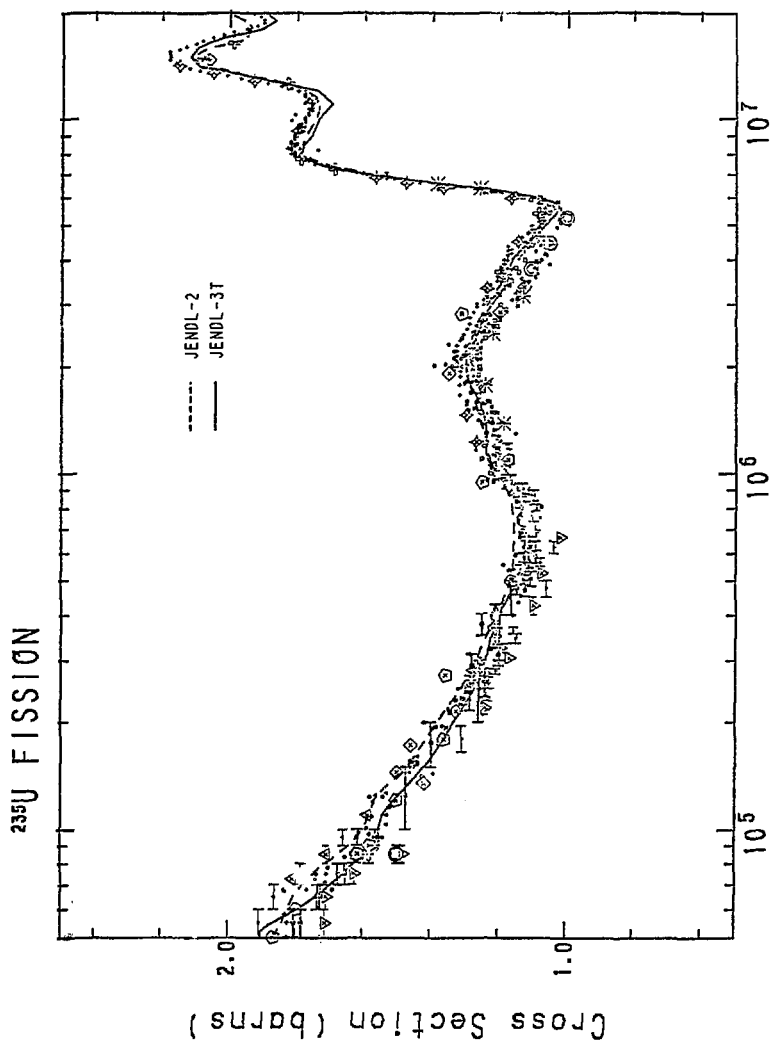

Fig. 1 ^{235}U fission cross section

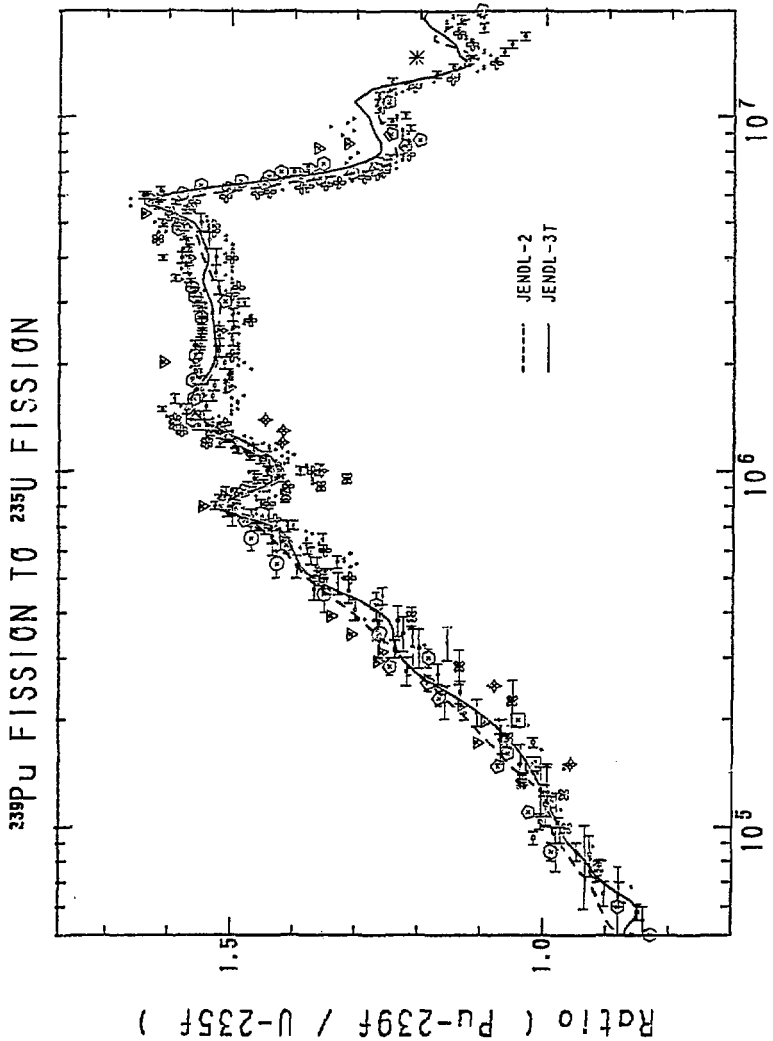

Fig. 2 Ratio data of ^{239}Pu to ^{235}U fission cross sections

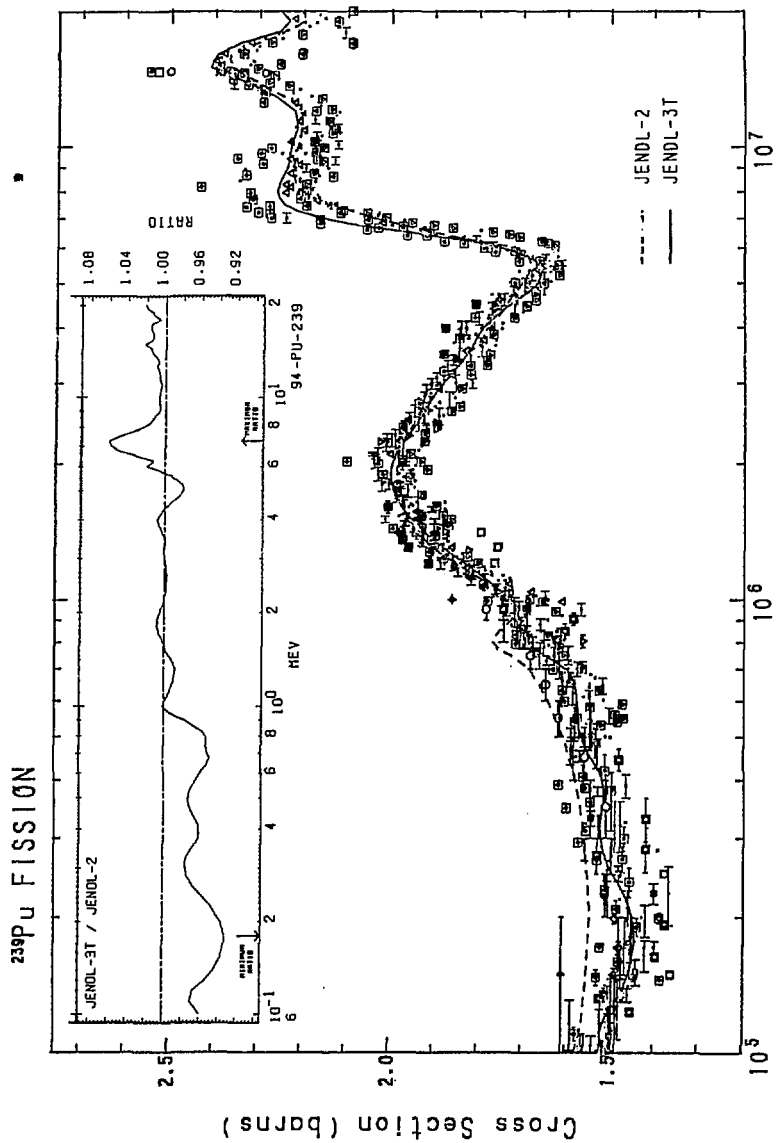

Fig. 3 ^{239}Pu fission cross section

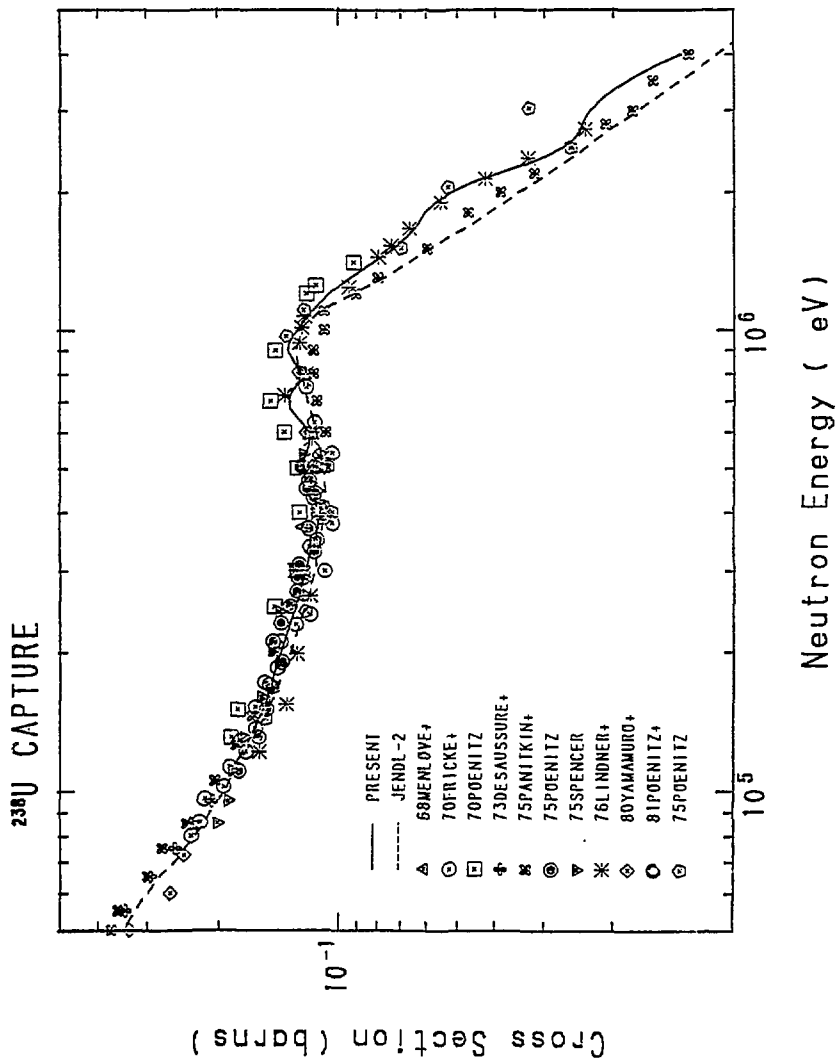

Fig. 4 ^{238}U capture cross section

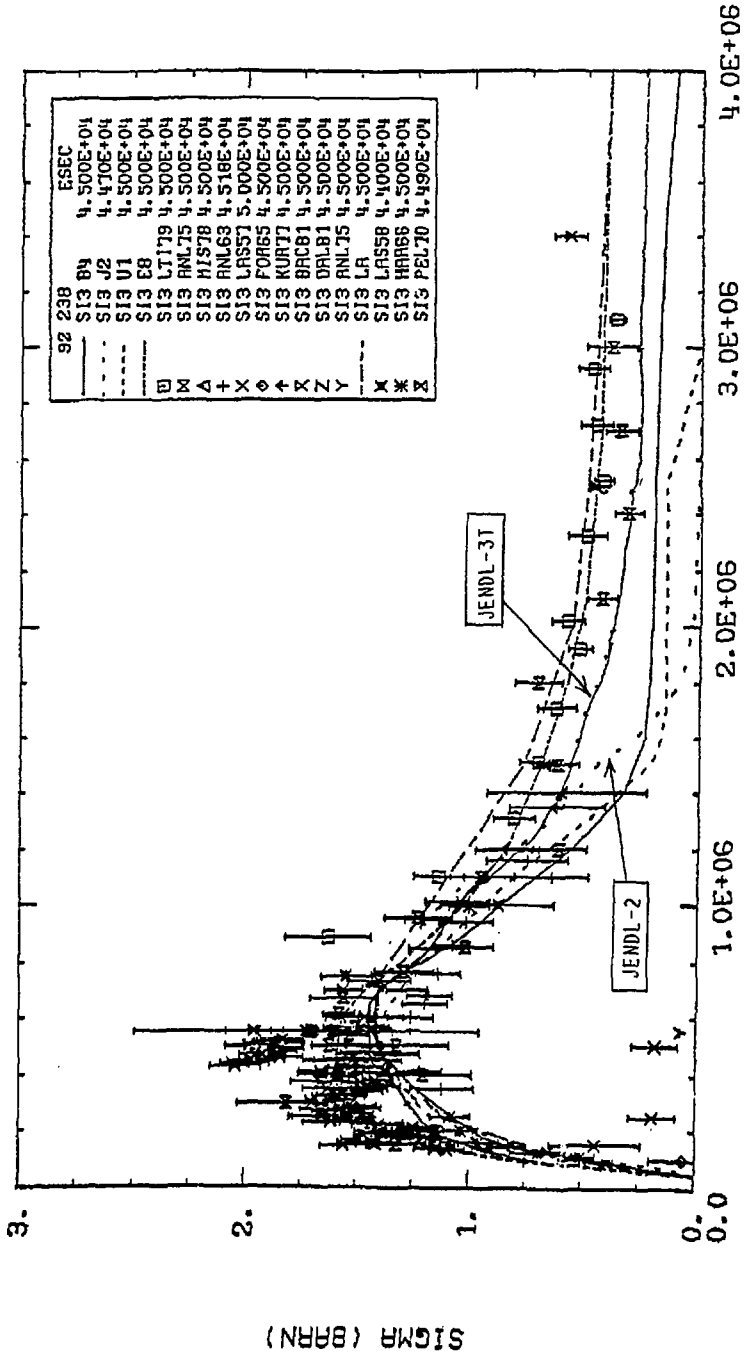

Fig. 5-a Inelastic scattering cross section to the first level of ^{238}U

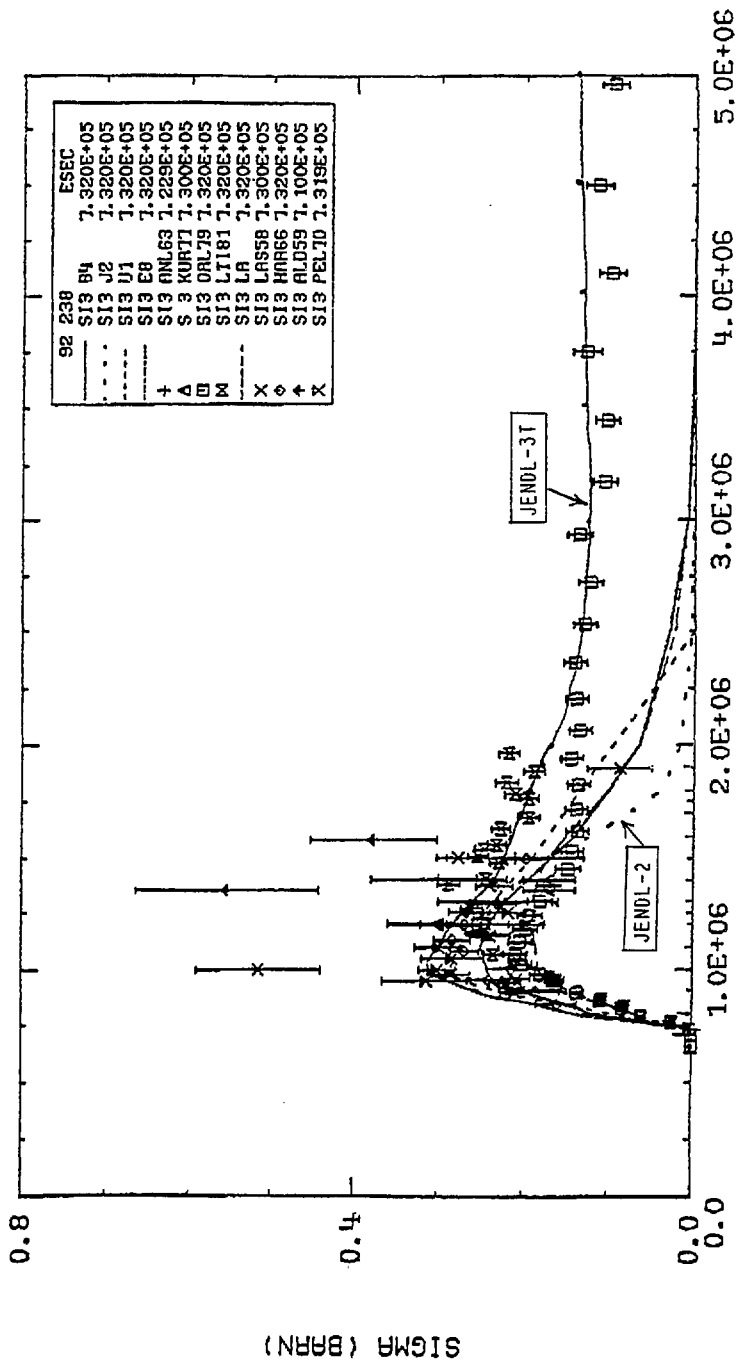

Fig. 5-b Inelastic scattering cross section to 732-keV level of ^{238}U

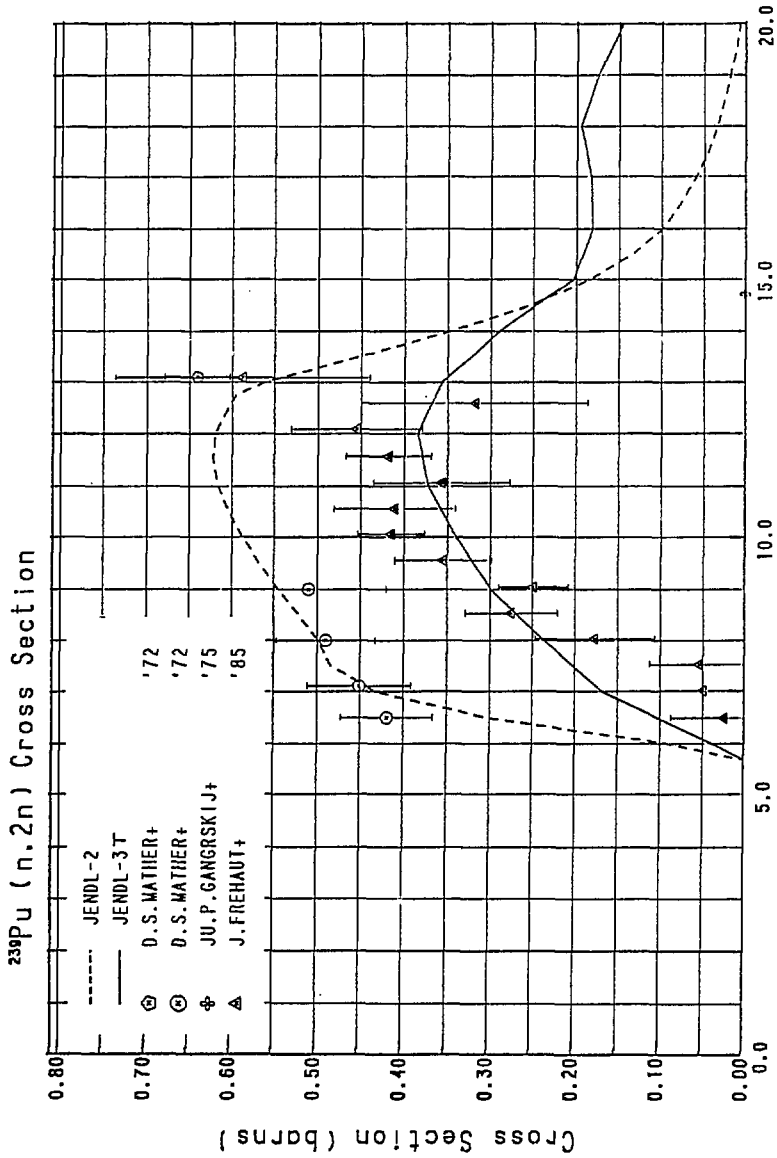

Fig. 6 ^{239}Pu (n,2n) reaction cross section

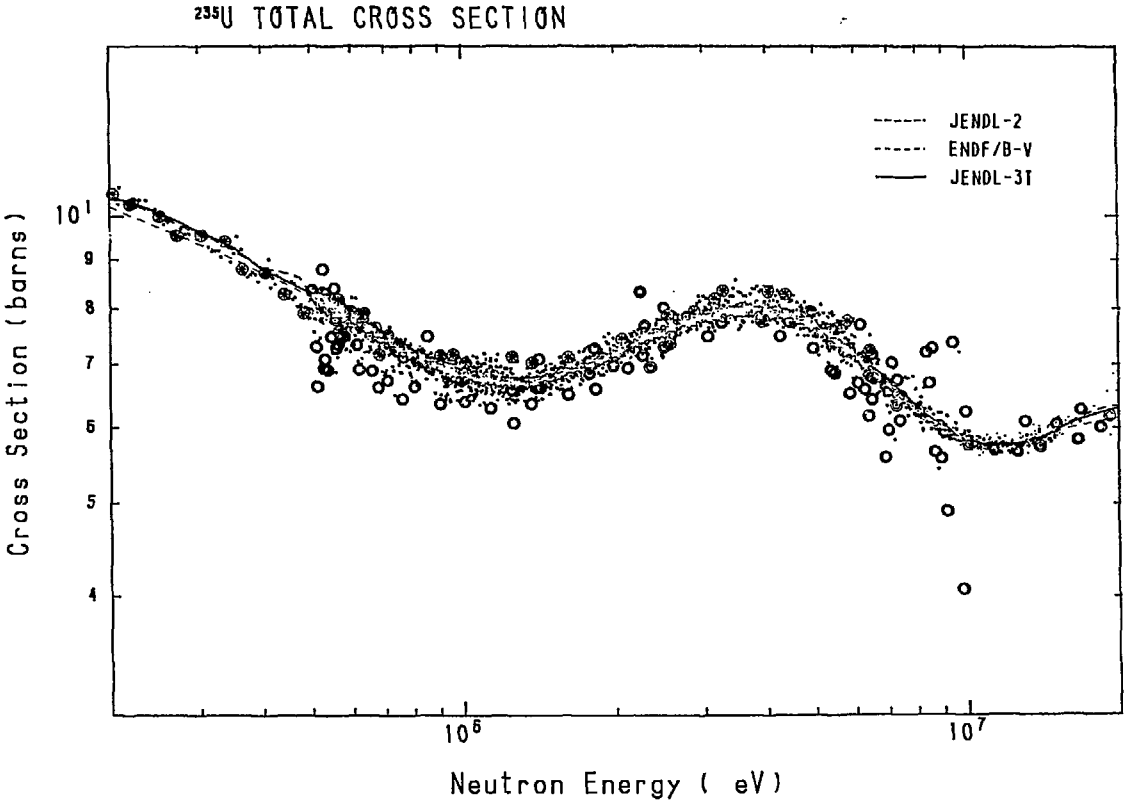

Fig. 7 ^{235}U total cross section

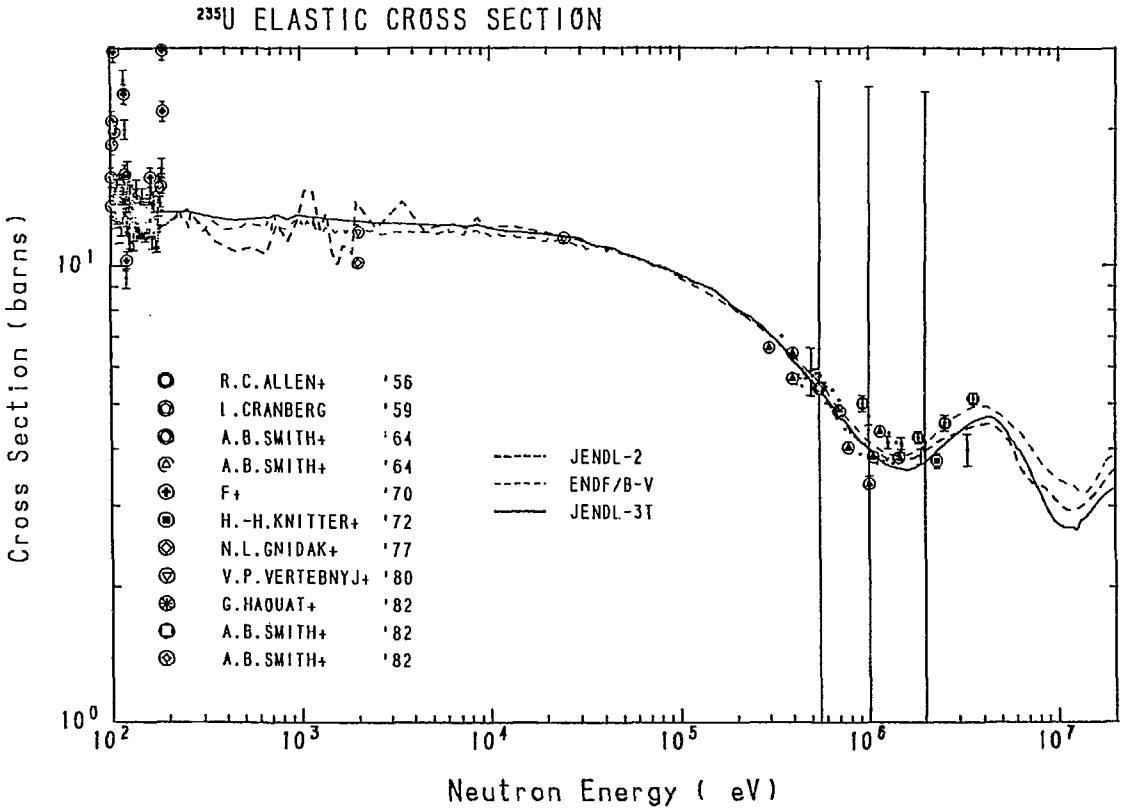

Fig. 8 ^{235}U Elastic scattering cross section

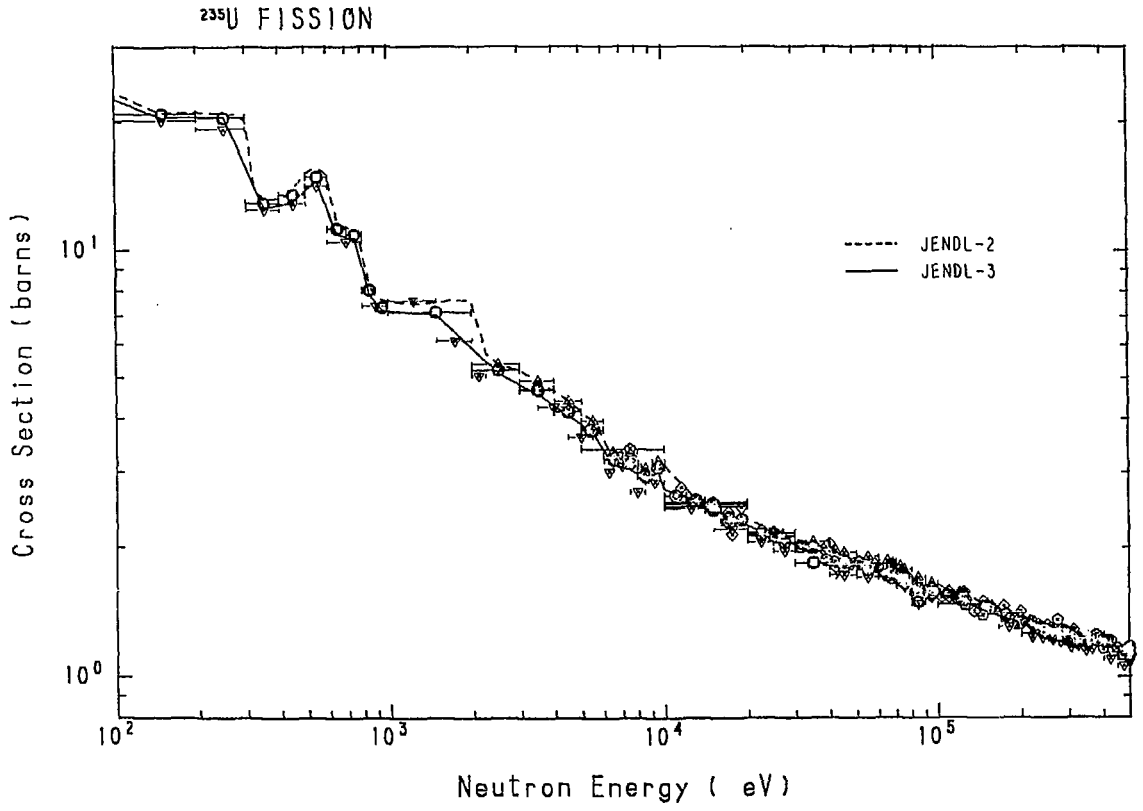

Fig. 9 ^{235}U fission cross section in the unresolved resonance region

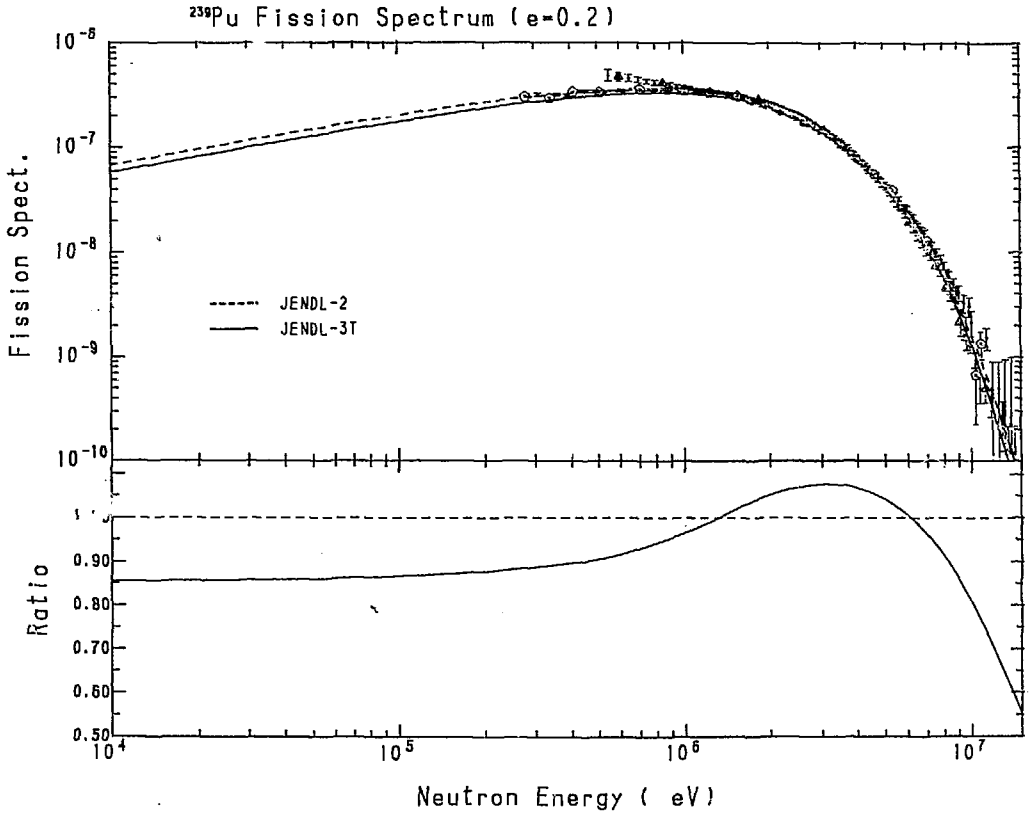

Fig.10 Neutron spectrum from 200-keV neutron induced fission of ^{239}Pu

2.1.3 Nuclear Data Evaluation for Medium and Heavy Nuclei

Motoharu Mizumoto
Japan Atomic Energy Research Institute
Tokai-mura, Naka-gun, Ibaraki-ken

Present status of nuclear data evaluation works for medium and heavy nuclei is described in this paper. These data are being prepared for JENDL-3 (Japanese Evaluated Nuclear Data Library - Version 3). At present, about a half of the data files, which are expected to be stored in the final library, has been brought into a temporary library called JENDL-3T. The remaining works and additional revisions are still needed to be made in order to finalize the data library as JENDL-3.

Special emphases have been put on the high energy neutron data for which the previous JENDL-2 had some inadequacies, and gamma-ray production cross sections have been newly evaluated. Systematic and consistent evaluations have been intended for the new evaluations.

1. Introduction

The sub-working group (SWG) on nuclear data evaluations for medium and heavy nuclei has been formed in April, 1987 by combining three sub-working groups, that is, the medium and heavy nuclei SWG, gamma-ray production nuclear data SWG and gas production nuclear data SWG. By taking over the preparatory efforts which these three SWG had been making for last several years, SWG on nuclear data evaluation for medium and heavy nuclei has been continuing to complete the JENDL-3 library. A list of the nuclei which this working group is responsible to evaluate is shown in Table 1, ranging from ^{23}Na to ^{209}Bi. The major important nuclei for structural and shielding materials for fission and fusion reactors are included in the list. Some nuclei for other applications such as medical and dosimetry purposes are also included.

In the course of the work, the special emphases have been put on the evaluations of high energy neutron data such as charged particle production cross sections, gas production cross sections, neutron emission cross sections and (n,2n) reaction cross sections. The energy-angle double differential cross sections (DDX data) of which previous evaluations in JENDL-2[1] had inadequacies, were also carefully investigated. Gamma-ray production cross sections, which were not included in JENDL-2, were newly

evaluated in the present works.

The data files for several nuclides (Na, Al, Si, P, S, K, Cr, Mn, Fe, Ni, Cu, Mo and Pb as for November 13, 1987) have been stored in the temporary data library called JENDL-3T[2] which is now supplied for the final checkup and integral tests.

Systematic comparisons between the evaluations and experiments have been made particularly for neutron emission DDX spectra taken at OKTAVIAN[3] and Tohoku Univ.[4] and for gamma-ray spectra by ORNL[5].

The evaluation works in this group have been carried out independently by individual evaluators. Common problems on the computer programs, systematics of parameters for calculations and the discrepancies in experimental data have been discussed in the group.

Since the number of the nuclei for the evaluations is large and a half of the data file is not still stored in JENDL-3T, only general outlines and typical examples in the evaluated quantities will be discussed in this paper.

2. Methods for evaluations

In order to maintain the energy balance and consistency among the various reaction channels, the large parts of data have been calculated by the comprehensive computer programs such as GNASH[6], TNG[7], DWUCK[8], ECIS[9], CASTHY[10] and ELIESE[11]. Several new computer programs were also developed to perform evaluations more efficiently; GAMFIL[12], PEGASUS[13] and LEVDENS[14]. Brief descriptions of these programs are shown in Table 2. The programs of GNASH and DWUCK were modified by changing the format of input parameters and adding some useful functions. The program CASECIS was also prepared by combining CASTHY and ECIS for simultaneous calculations of compound and direct reaction processes.

Fig.1 shows the flow chart for the typical scheme of the neutron cross section evaluation. For these evaluations, various quantities are necessary to be determined such as optical potential parameters, level density parameters and detailed information of nuclear level schemes. On the basis of experimental data, these parameters were surveyed consistently by individual evaluators. Calculations for preequilibrium processes were also carried out in the higher energy region. For the calculations of gamma-ray emission spectra, gamma-ray strength functions have been estimated to obtain good agreement with experimental data. Optical potentials for proton and alpha particle are necessary for the evaluations as well as those for

neutrons. The whole optical potentials for these calculations must be consistent in order to maintain the energy balance and data consistency.

The calculated results by one program are sometimes used as the input data for other programs as shown in the flow chart of Fig. 1. For example, direct reaction cross sections calculated by DWUCK code are used by GNASH in order to take into account these competitions in the compound reaction cross sections.

The reason to use these several programs is that each program has certain deficiencies. For example, GNASH can deal with many emission channels simultaneously but does not generate any outputs on total cross section and angular distributions of emitted particles. On the other hand, CASTHY can provide total cross section, elastic cross section and angular distribution of scattering neutrons from compound process by taking into account width fluctuation effects. This program, however, cannot deal with multi-particle emission processes. DWUCK can only calculate components of direct reaction processes.

Table 3. shows a list of the computer programs for evaluations which each evaluator used for his own evaluations. There have been no definite rules which code should be chosen for individual evaluations. Evaluators merely decided which computer programs are adequate for their evaluations depending on the properties of their nuclei. In general, GNASH has been most frequently used. Since this code cannot calculate angular distributions, JENDL-3T has some problems in the angular dependence of emitted neutron spectrum, except in the cases where the systematics proposed by Kalbach-Mann[15] was used for evaluations.

Fig. 2 shows a typical example of the calculated results for the ^{63}Cu neutron cross sections. In the low energy region, only a few reaction channels are necessary to be considered but, as the neutron energy increases, many reaction channels have to be considered as shown in the figure. Quantities to be evaluated such as file numbers(MF) and reaction types(MT) are shown in Table 4 as an example for a typical nucleus. In addition to these quantities, deuteron emission has to be considered in some nuclei.

The evaluated results are checked by several utility programs such as CHECKER, FIZCON and PHYCHE[16]. Almost all these evaluated quantities are also plotted by the plotting programs of SPLINT[17] and FAIRDDX/DDXPLOT[18] in order to compare with experimental data and make corrections for unreasonable values.

3. Evaluated results

3.1 Resonance parameters

The data in BNL-325 (4th ed.)[19] or new published resonance parameters data are used for the JENDL-3 evaluations whenever there are new data available. The resonance regions adopted in JENDL-3T are often expanded as listed in Table 5 in comparison with those in JENDL-2. Experimental data, however, are not sufficiently accurate in some cases. Fig. 3 shows the total cross sections of ^{28}Si in the resonance region. The calculated curves for the lowest two s-wave resonances are obtained from the values in BNL-325, which cannot reproduce the measured data points well. The new parameters had to be estimated to create the file as shown in the figure.

The evaluated data of the resonance integrals which are deduced by the utility programs are always checked with the recommended values given in the BNL-325.

3.2 Total, elastic scattering and capture cross sections

The total cross sections are usually most accurately known experimentally. These experimental values were adopted for the evaluations in most cases. Moreover, the total cross sections were used to obtain optical potentials by fitting the data. When angular distribution data of elastic scatterings were available, these values were also used to check the validity of the optical potentials.

Relatively accurate experimental capture cross sections are often available in the low energy region and they were adopted for the evaluations. In some cases, CASTHY program was used to calculate cross section shapes which were normalized to experimental data at a certain energy point. In the higher energy region, capture values calculated with CASTHY by taking into account only compound processes fall down very rapidly, which do not represent the actual situations. Direct capture components becomes dominant in the MeV region and the experimental or calculated results[20] are adopted in some cases.

3.3 Inelastic scattering cross sections

In the low energy region, inelastic scatterings are taken place mainly through compound processes. Therefore, CASTHY can reproduce cross section values and angular distribution with good accuracy when optical potentials and level information are accurately known. In the high energy region,

however, direct processes such as the collective motion and single particle transition become significant. Fig. 4 shows a comparison of calculated results of the direct reaction cross sections with DWUCK and compound cross sections with CASTHY in the case of the 1st 3^--octupole vibrational state and the 2nd 5^- state in the ^{208}Pb inelastic cross section. Experimental values for these inelastic channels increase very rapidly as the neutron energy increase as shown in the figure. Direct components are 10^3 times larger than the compound components at 14 MeV. In most cases of the JENDL-2 evaluations, direct components were not considered. This new approach gives significant improvements in the JENDL-3 evaluations for high energy neutron data.

3.4 Threshold reactions

Most laborious and difficult quantities to evaluate in JENDL-3 have been the threshold reactions. These values are especially important as nuclear data for fusion and dosimetry applications.

Fig. 5 shows the (n,2n) reaction cross section of ^{63}Cu. The previous experimental data disagree significantly each other as shown in the figure. The new adopted values for JENDL-3T were calculated based on the systematic parameters which were consistent with other quantities.

The (n,2n) reaction cross section of ^{nat}Pb is one of the most important quantity as the neutron multipliers for the fusion blanket. A discrepancy in the experimental values still seems to exist by as much as 20 % at 14 MeV as shown in Fig. 6.

Helium production cross sections (n,α) for structural materials are needed for the neutron damage calculations. Fig. 7 shows the He production cross sections for Cr, Fe and Ni which are used in stainless steel materials. Especially in the case of Ni nuclei, He production cross section is very large compared to the other nuclei.

Fig. 8 shows the proton emission spectrum in ^{55}Mn. These quantities are not stored as the JENDL-3 evaluations but are very useful to check the validity of the calculation.

Table 6 shows a list of cross section values for threshold reaction at 14 MeV. Relatively large changes have been made from JENDL-2 to JENDL-3T, and the new quantities such as deuteron emissions are included in JENDL-3T.

3.5 Double differential neutron cross sections

Neutron energy-angle double differential cross sections have been

recently measured at 14 MeV intensively at several laboratories including OKTAVIAN[3] and Tohoku Univ[4]. The quantities are sensitive to the values of various neutron emission cross sections such as elastic scattering, discrete inelastic scattering and continuum inelastic scattering and, in the low energy part, (n,2n), (n,3n), (n,pnx) and (n,αnx) reactions. The information on the angular dependence both for discrete and continuum components is also obtained from these DDX experiments. Fig. 9 shows a typical example of the case of ^{nat}Cu DDX data. The calculated results are obtained with GNASH calculations by taking into account the energy resolution of the experiments. In the figure, contributions from the individual reaction components are indicated separately.

In Fig. 10, the DDX data of ^{nat}Fe at three separate angles are shown. While the experimental data points in the continuum spectra exceed the calculated results at a forward angle, they gradually decrease as angles increase. The calculated results cannot reproduce this slight angular dependence. In the energy region between 10 and 12 MeV, calculated results does not include some inelastic levels for which direct effects still remain significantly. This discrepancy between experimental and calculated results often occurs due to the restriction of the ENDF format where the only limited number (40 levels as a maximum) of inelastic levels can be stored. In order to solve this problem, some of the levels have to be combined into one level.

There are some cases where the experimental DDX values from several laboratories do not agree each other. These discrepancies have been found in the works of SWG from the systematic comparison between experimental and evaluated data for many nuclei.

3.6 Gamma-ray production cross section

Calculated gamma-ray production cross sections are composite results from calculations of reaction cross sections and gamma-ray cascades. Information on nuclear level densities, level schemes and gamma-ray transition probabilities has to be known accurately as well as contributions from various reaction cross sections.

The experimental data for many elements have been available from ORNL experiments in the energy region up to 20 MeV, which used a continuous neutron source from the electron linac[5]. Systematic comparisons between calculated results and the ORNL data have been performed as mentioned previously.

Fig. 11 shows the ^{55}Mn gamma-ray production cross section at the neutron energy E_n = 11 MeV, which was calculated by the code TNG. Good agreement with the experimental data is obtained, though observed discrete gamma-rays seems much prominent. Fig. 12 shows ^{nat}Fe gamma-ray spectrum at 4.75 MeV calculated with GNASH, where the spectrum mainly consists of the discrete gamma-rays. In Fig.13, the gamma-ray spectrum of ^{nat}Mo is given at 4.75 MeV. Because the number of Mo isotopes is large to be 7, it is difficult and not reliable to calculate spectrum for each isotope separately and add up to construct the spectrum of natural isotope. In the evaluation, the empirical method proposed by Howerton[21] has been adopted, who assumed the systematic behavior of the gamma-ray spectrum to represent evaporation-like structure. The fitting parameters were based on the experimental data. This method may be useful in the cases where experimental data are available and calculational methods is not reliable.

4. Summary

The status of nuclear data of medium and heavy nuclei in JENDL-3T was briefly reviewed. Great improvements have been made in comparison with JENDL-2. Some modifications, however, are still necessary to obtain better agreement especially with DDX and (n,α) reaction data. Deficiencies are also remained in data for angular distribution of threshold reactions and continuum neutrons. Some works have to be made to supply data for special purpose file such as activation, gas production and dosimetry. "JENDL-4" will hopefully overcome these difficulties and enlarge the scope with respect to the energy range and type of reaction.

Acknowledgments

The author would like to thank all members of the sub-working group of the medium and heavy nuclei evaluations, the names of the members are listed in Table 1. He is also indebted to Messrs. T. Nakagawa and S. Chiba for helpful discussions.

References

1) Nakagawa T.: "Summary of JENDL-2 General Purpose File" JAERI-M 84-103 (1984)
2) JENDL Compilation Group (Nuclear Data Center, JAERI), JENDL-3T private communication (1987)
3) Takahashi A.: Private communication and will be reported in this meeting (1987).
4) Baba M. et al : Proc. Conf. on Nuclear Data for Basic and Applied Science, Santa Fe, 1985 vol p145 and private communication
5) Dickens K. et al.: Nucl. Sci. Eng. 62 (1977) 515
6) Young P.G., Arthur E.D.: "GNASH: A Preequilibrium, Statistical Nuclear Model Code for Calculation of Cross Sections and Emission Spectra" LA -6974 (1977).
7) Fu C.Y.: "A Consistent Nuclear Model for Compound and Precompound Reactions with Conservation of Angular Momentum" ORNL-TM 7042 (1980), Shibata K., Fu C.Y.: "Recent Improvements of the TNG Statistical Model Code" ORNL-TM 10093(1986)
8) Kunz P.D.: "DWUCK" Univ. Colorado (1974), unpublished.
9) Raynal J.: "ECIS" Unpublished, IAEA-SMR-9/8 & 9/9 p281 (1972)
10) Igarasi S.: J. Nucl. Sci. Technol., 12 (1975) 67
11) Igarasi S.: "Program ELIESE-3;Program for Calculation of the Nuclear Cross Sections by Using Local and Non-Local Optical Models and Statistical Model" JAERI 1224 (1972)
12) Hida K.: "GAMFIL A Computer Program for Generating Photon Production Nuclear Data File" JAERI-M 86-150 (1986) in Japanese
13) Iijima S. et al.: To be published in JAERI-M report, Private communication (1987)
14) Iijima S., Nakagawa T.: To be published in JAERI-M report, Private communication (1987)
15) Kalbach C., Mann F.M.:Phys. Rev. C23 (1981) 112
16) Programs are available from NEA Data Bank
17) Narita T. et al.: "SPLINT:A Computer Code for Superimposed Plotting of Experimental and the Evaluated Data" JAERI-M 5769 (1974), Nakagawa T.: "SPLINT: A Computer Program for Making Input Data of SPLINT",JAERI-M 9499 (1981) in Japanese
18) Minami K., Yamano N.: "FAIR-DDX:A Code for Production of Double Differential Cross Section Library" JAERI-M 84-022 (1984), Iguchi T., Yamano N.: "DDXPLOT A Program to Plot the Energy Angle Double

Differential Cross Sections" JAERI-M 84-033 (1984) in Japanese
19) Mughabghab S.F, Divadeenam M., Holden N.E.: Neutron cross sections, BNL -325 (4th ed.) (1981) Academic Press, New York
20) Kitazawa H. et al.: Nucl. Phys. A464 (1987) 61 and private communication
21) Howerton R.J., Plechaty E.F.: Nucl. Sci. Eng. 32 (1968) 178

Table 1 A list of evaluators for medium and heavy nuclei for JENDL-3

Nucleus	Evaluator
Na-23	H.Yamakoshi
Mg(Mg-24,-25,-26)	M.Hatchya
Al-27	Y.Harima
Si(Si-28,-29,-30)	H.Kitazawa
P-31	H.Nakamura
S(S-32,-33,-34,-36)	H.Nakamura
Cl(Cl-35,-37)	A.Zukeran
Ar-40	A.Zukeran
K(K-39,-40,-41)	H.Nakamura
Ca(Ca-40,-42,-43,-44,-46,-48)	M.Hatchya
Sc-45	T.Watanabe
Ti(T-46,-47,-48,-49,-50)	K.Kobayashi,H.Hashikura
V-51	T.Watanabe
Cr(Cr-50,-52,-53,-54)	T.Asami
Mn-55	K.Shibata,T.Hojuyama
Fe(Fe-54,-56,-57,-58)	S.Iijima,H.Yamakoshi, M.Igashira
Co-59	T.Watanabe
Ni(Ni-58,-59,-60,-61,-62,-64)	S.Iijima
Cu(Cu-63,-65)	K.Kawakita,N.Yamamuro
Zr	M.Sasaki
Nb(Nb-93,-94)	M.Kawai
Mo(Mo-92,-94,-95,-96,-97,-98,-100)	FP WG,M.Mizumoto
Hf(Hf-174,-176,-177,-178,-179,-180)	T.Yoshida
Ta-181	N.Yamamuro
W(W-180,-182,-183,-184,-186)	T.Watamabe,T.Asami
Pb(Pb-204,-206,-207,-208)	M.Mizumoto
Bi-209	A.Zukeran

Natural elements are always evaluated.

Table 2 A brief descriptions for computer codes for JENDL-3 evaluations

Program	Functions		
GNASH	Multi-step H.F.+Precomp	n-γ Spectra	no Angl.
TNG	Multi-step H.F.+Precomp	n-γ Spectra	Angl.
DWUCK	DWBA	no Spectra	Angl.
ECIS	C.C.		Angl.
CASTHY	H.F.		Angl.
ELIESE	H.F.		Angl.
PEGASUS	Evaporation+Precomp	n Spectra	no Angl.
GAMFIL2	Process code for generating ENDF data file from GNASH output		
LEVDENS	Determination of level density parameters		
CHECKER, FIZCON, PHYCHE	Codes for checking data file stored in ENDF format		
SPLINT	General purpose plotting routine		
FAIRDDX/DDXPLOT	DDX plot		

H.F. : Hauser-Feshbach statistical model calculation
Precomp : Precompound model calculation
DWBA : Distorted-Wave Born Approximation calculation
C.C. : Coupled-Channel calculation
Angl. : Angular distribution calculated
no Angl.: Angular distribution is not calculated
n-γ spectra : Emitted neutron or γ spectra calculated

Table 3 A list of computer programs used for evaluation.

Nucleus		Inela.		Threshold	Spectrum	
		Stat.	Direct		Neutron	Gamma-ray
1	Na-23	CASTHY	-	GNASH	GNASH	GNASH
2	Al-27	CASTHY	ECIS	GNASH	GNASH	GNASH
4	Si	CASTHY	ECIS	GNASH	GNASH	CASTHY+GNASH
5	P-31	CASTHY	-	GNASH	GNASH	-
6	S-32	CASTHY	-	GNASH	GNASH	-
9	K-39	CASTHY	-	GNASH	GNASH	-
14	Cr					
	Cr-52	CASTHY	DWUCK	GNASH	GNASH	GNASH
15	Mn-55	TNG	DWUCK	TNG	TNG	TNG
16	Fe					
	Fe-56	CASTHY	DWUCK	GNASH	GNASH	GNASH
18	Ni					
	Ni-58	CASTHY	DWUCK	PEGASUS	PEGASUS+GNASH	GNASH
19	Cu					
	Cu-63	CASTHY	DWUCK	GNASH	GNASH	GNASH
22	Mo	CASTHY		GNASH	Evaporation	CASTHY+ Howerton
26	Pb					
	Pb-208	CASTHY	DWUCK	GNASH	GNASH	GNASH

Table 4 An example of data types for evaluations

MT	Reaction type	MF1 Information	MF2 Res. parm.	MF3 σ(E)	MF4 $d\sigma/d\theta$	MF5 $d\sigma/dE$	MF12 mult(γ)	MF13 $\sigma(\gamma)$	MF14 $d\sigma/d(\gamma)$	MF15 $d\sigma/dE$
1	Total	○		○						
2	Elastic	○		○	○					
3	Nonelastic	○					○	○	○	○
4	Inelastic	○		○						
16	(n,2n)	○		○	○	○				
17	(n,3n)	○		○	○	○				
22	(n,n'α)	○		○	○	○				
28	(n,n'p)	○		○	○	○				
51-90	Discrete inela.	○		○	○					
91	Continuum inela.	○		○	○	○				
102	Capture	○		○						
103	(n,p)	○		○						
107	(n,α)	○		○						
151	Resonance	○	○							
251	Ave. cosine	○		○						

Table 5 A comparisson of resonance regions between JENDL-2 and JENDL-3T

	Nucleus	Resolved Region		Comment
		JENDL-2	JENDL-3T	
1	Na-23	500 eV - 150 keV	10^{-5} eV - 350 keV	new parameters
2	Al-27	3 keV - 140 keV	10^{-5} eV - 210 keV	BNL-325 4th
4	Si	no resonance	10^{-5} eV - 1.81 MeV	55, 180 keV levels
5	P-31	-	10^{-5} eV - 500 keV	BNL-325 4th
6	S-32	-	10^{-5} eV - 1.57 MeV	BNL-325 4th
9	K-39	-	10^{-5} eV - 200 keV	BNL-325 4th
14	Cr	10^{-5} eV - 300 keV	10^{-5} eV - 300 keV	new parameters
	Cr-52	10^{-5} eV - 300 keV	10^{-5} eV - 300 keV	
15	Mn-55	10^{-5} eV - 100 keV	10^{-5} eV - 100 keV	Macklin+85
16	Fe	10^{-5} eV - 250 keV	10^{-5} eV - 250 keV	
	Fe-56	10^{-5} eV - 250 keV	10^{-5} eV - 250 keV	1.15 kev level
18	Ni	10^{-5} eV - 600 keV	10^{-5} eV - 557 kev	
	Ni-58	10^{-5} eV - 600 keV	10^{-5} eV - 420 keV	new parameters
19	Cu	10^{-5} eV - 35 keV	10^{-5} eV - 153 keV	
	Cu-63	10^{-5} eV - 35 keV	10^{-5} eV - 153 keV	BNL-325 4th
26	Pb	10^{-5} eV - 500 keV	10^{-5} eV - 480 keV	Horen+84,86
	Pb-208	10^{-5} eV - 800 keV	10^{-5} eV - 800	

Table 6 A list of cross section values for threshold reactions at 14 MeV.

	Nucleus	Reaction	Cross section JENDL-2 (mb)	Cross section JENDL-3T (mb)	Other reaction JENDL-3T	(mb)
1	Na-23	(n,2n)	18.0	18.0	(n,n'α)	8
		(n,p)	44.7	43.7	(n,n'p)	8
		(n,α)	142.9	133.8		
2	Al-27	(n,2n)	10.5	0.	(n,n'α)	18.9
		(n,p)	77.5	71.7	(n,n'p)	285.4
		(n,α)	120.9	125.9		
4	Si	(n,2n)	8.03	30.0	(n,n'α)	26.5
		(n,p)	255.4	257.1	(n,n'p)	80.0
		(n,α)	160.1	167.0		
14	Cr	(n,2n)	324.4	300.5	(n,n'α)	0.31
		(n,n'p)	13.9	86.3		
		(n,p)	106.3	87.9		
		(n,α)	33.2	35.4		
15	Mn-55	(n,2n)	770.9	680	(n,n'α)	0.65
		(n,n'p)	9.51	37.5	(n,d)	4.3
		(n,p)	46.90	38	(n,t)	0.72
		(n,α)	24.60	32		
16	Fe	(n,2n)	422.4	426.2	(n,n'α)	0.78
		(n,p)	125.4	141.9	(n,n'p)	93.6
		(n,α)	105.2	43.1		
18	Ni	(n,2n)	162.0	155.8	(n,d)	8.94
		(n,n'α)	20.36	10.3	(n,2p)	8.05
		(n,n'p)	341.7	402.8		
		(n,p)	307.8	282.5		
		(n,α)	106.8	77.7		
19	Cu	(n,2n)	650.4	607.9	(n,n'p)	219.4
		(n,n'α)	11.99	11.6	(n,d)	6.3
		(n,p)	6.489	38.9		
		(n,α)	26.95	28.9		
26	Pb	(n,2n)	1921	2037		
		(n,n'α)	0.255	0.038		
		(n,n'p)	0.577	0.018		
		(n,p)	0.970	0.987		
		(n,α)	1.154	0.939		

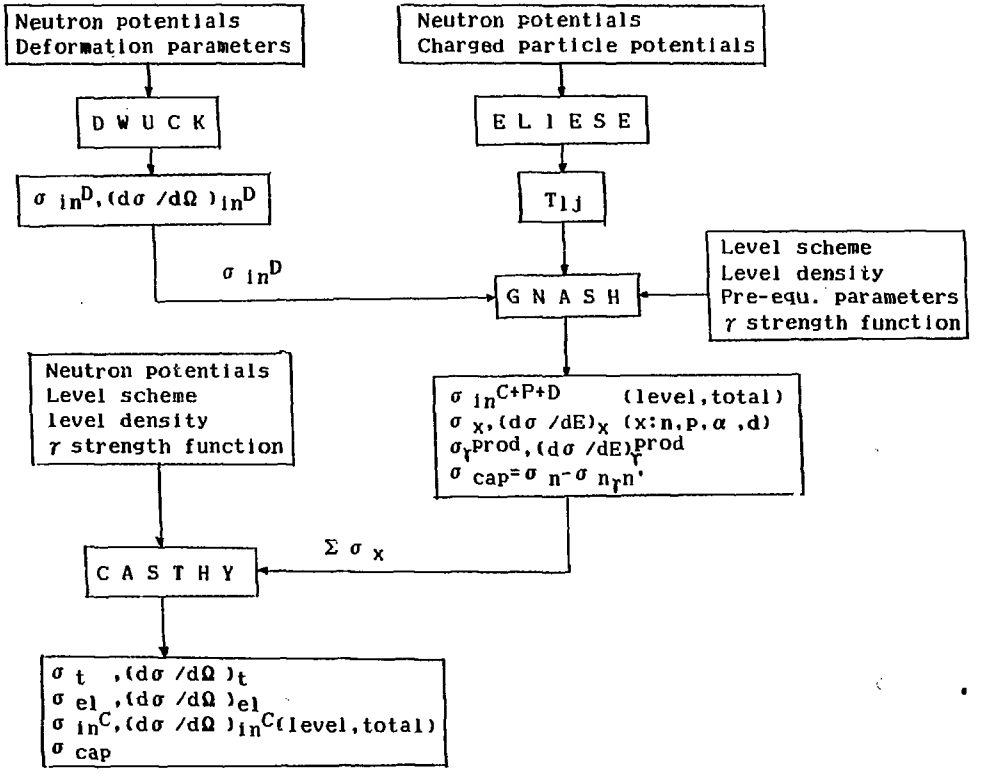

Fig. 1 A flow chart for the typical scheme of the neutron cross section evaluation

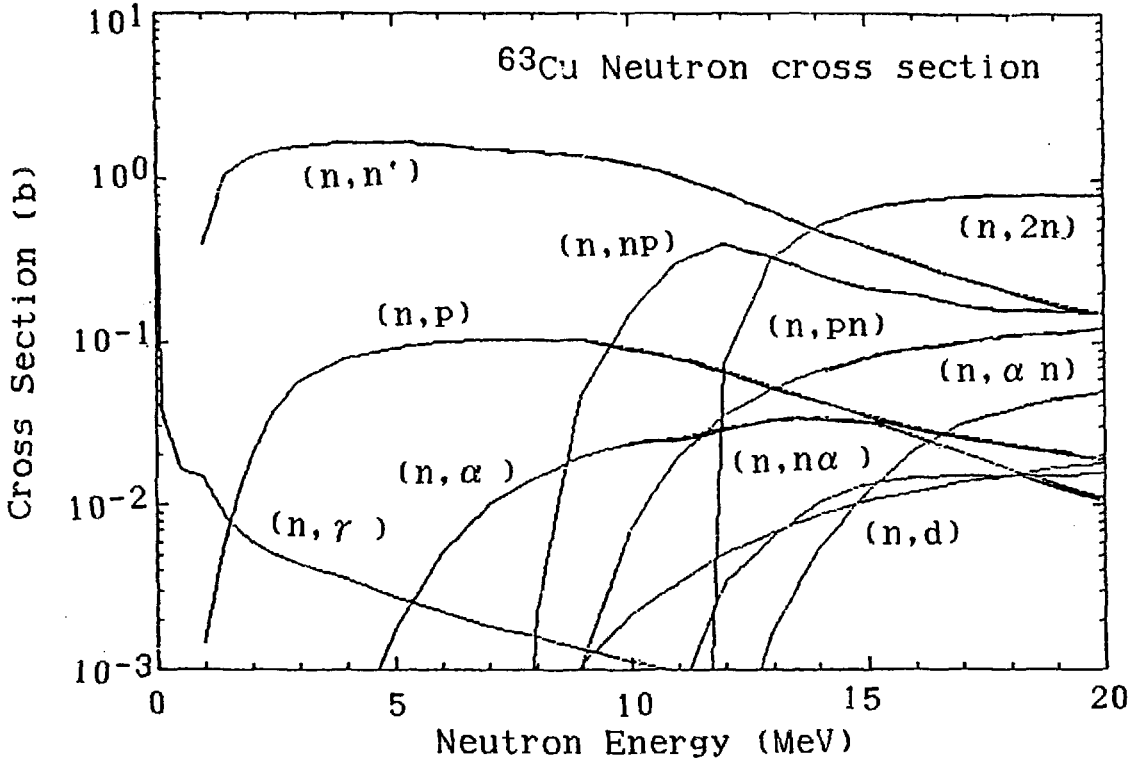

Fig. 2 A typical example of calculated results for the ^{63}Cu neutron cross sections calculated with GNASH.

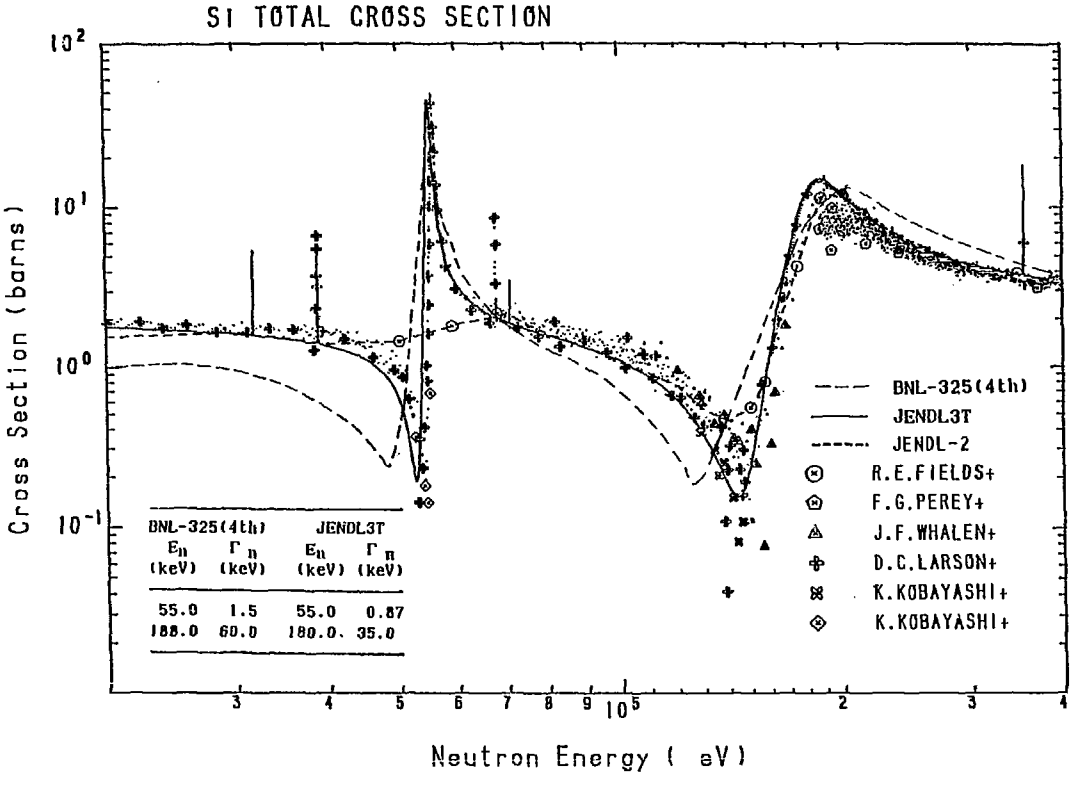

Fig. 3 Total cross sections of ^{28}Si in the resonance region. In the inset, resonance parameters in BNL-325 and JENDL-3T are indicated.

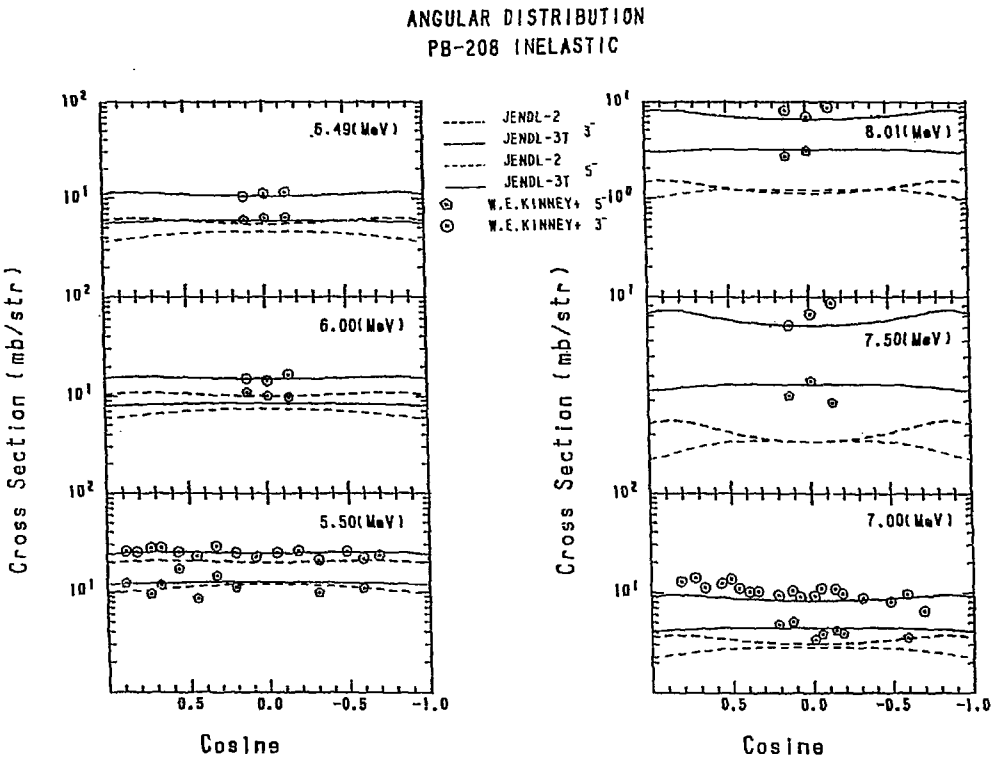

Fig. 4 Angular distributions of inelastic cross sections calculated with DWUCK (JENDL-3T) and CASTHY (JENDL-2) for the 1st 3^- and 2nd 5^- inelastic levels in ^{208}Pb.

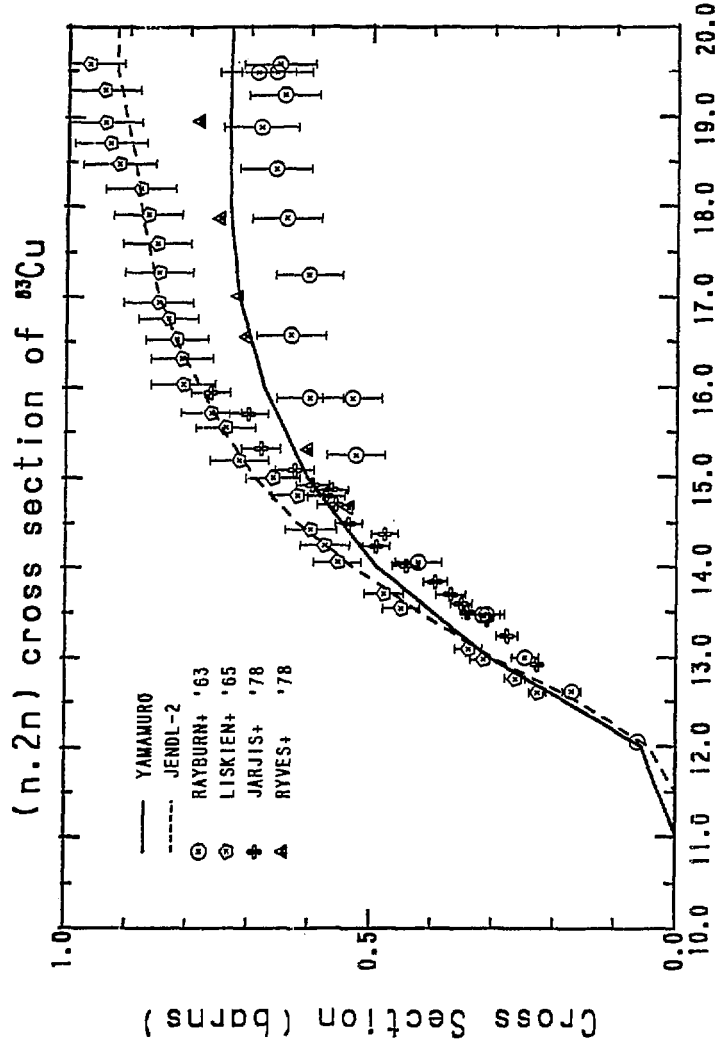

Fig. 5 (n,2n) reaction cross sections of ^{63}Cu calculated with GNASH.

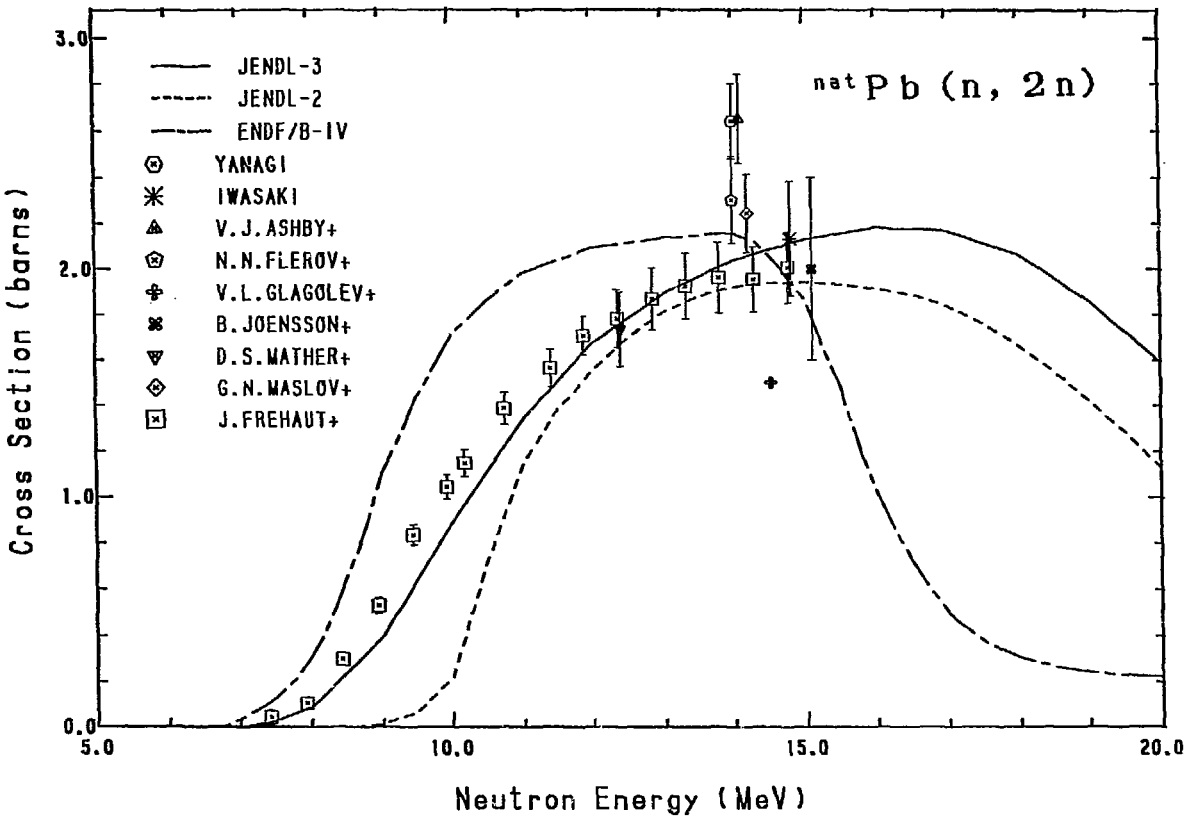

Fig. 6 (n,2n) reaction cross sections of ^{nat}Pb calculated with GNASH.

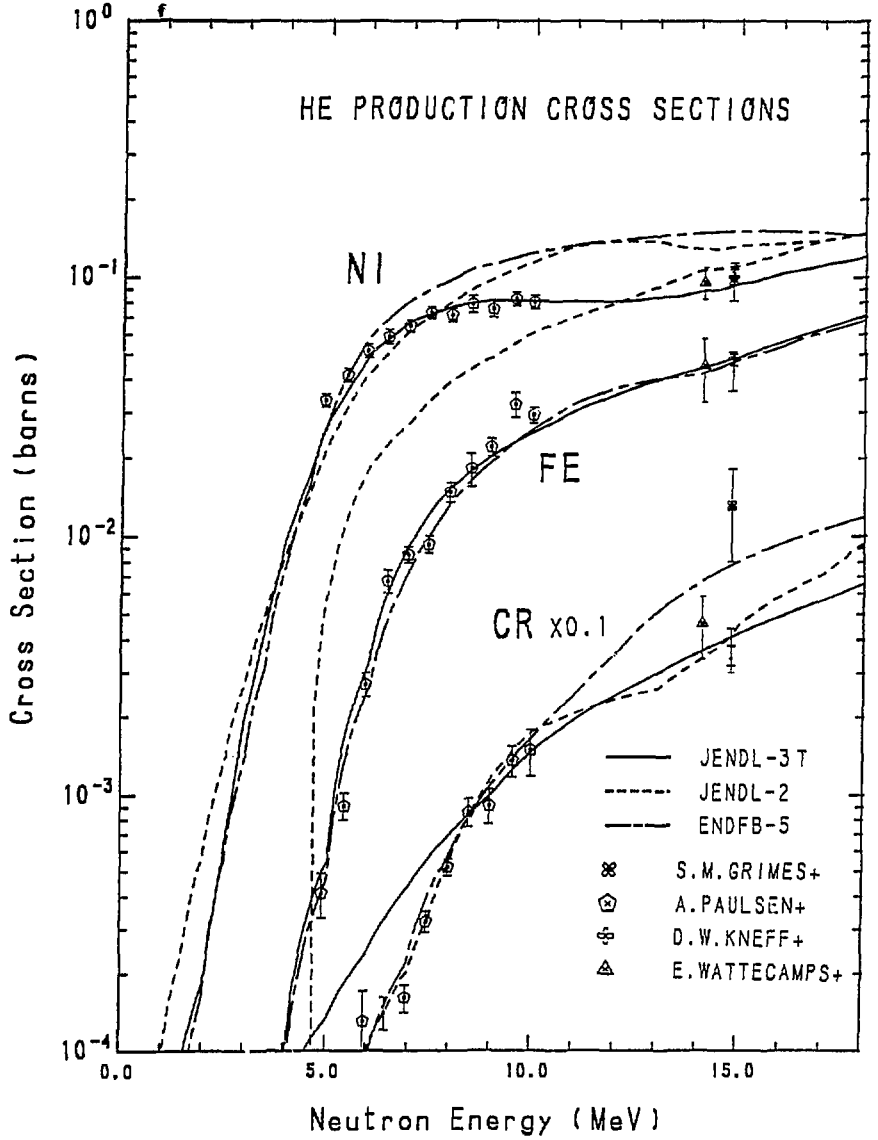

Fig. 7 Helium production cross sections of important structural materials Ni, Fe and Cr. Data of JENDL-3T were calculated with GNASH.

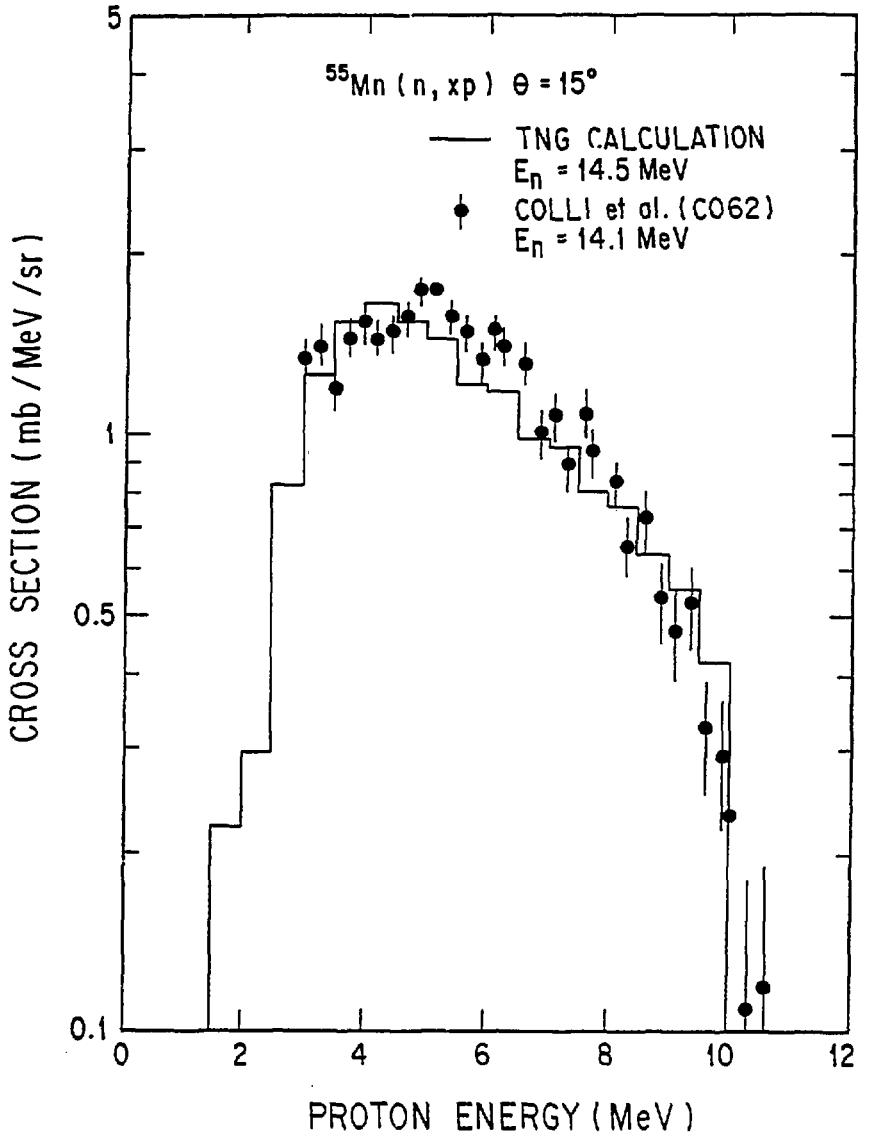

Fig. 8 Proton emission spectrum in ^{55}Mn calculated with TNG.

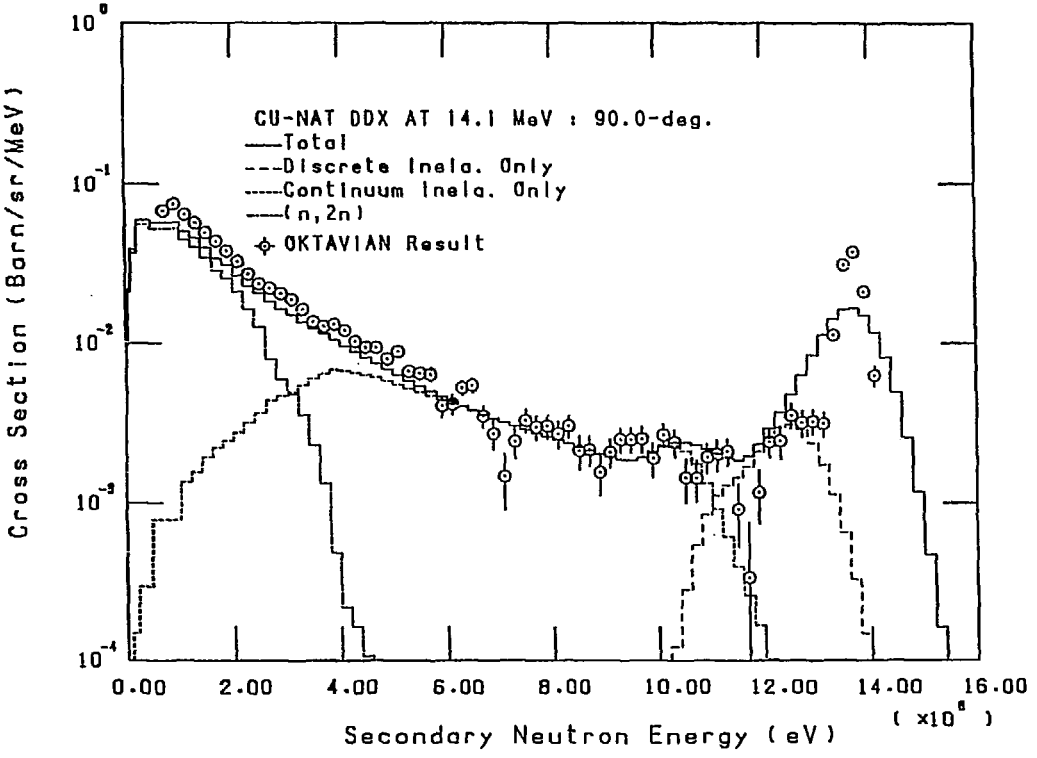

Fig. 9 Energy-angle double differential cross section of ^{nat}Cu calculated with GNASH

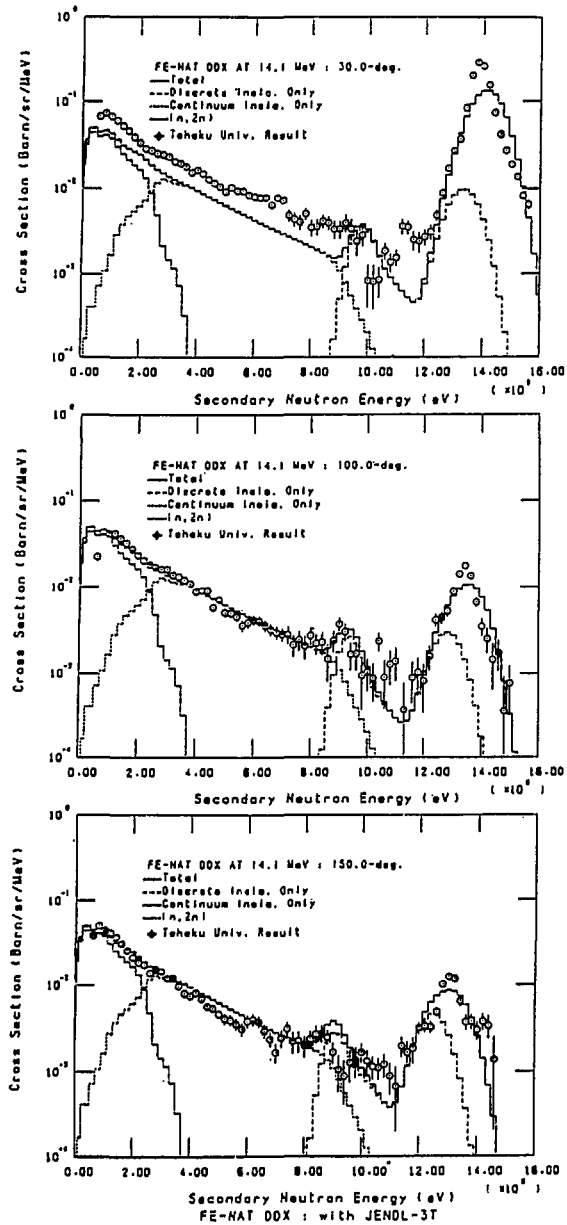

Fig. 10 DDX data of ^{nat}Fe at three separate angles of 30°, 100° and 150° calculated with GNASH. The angular dependence is observed in the continuum part of spectra in the experimental data.

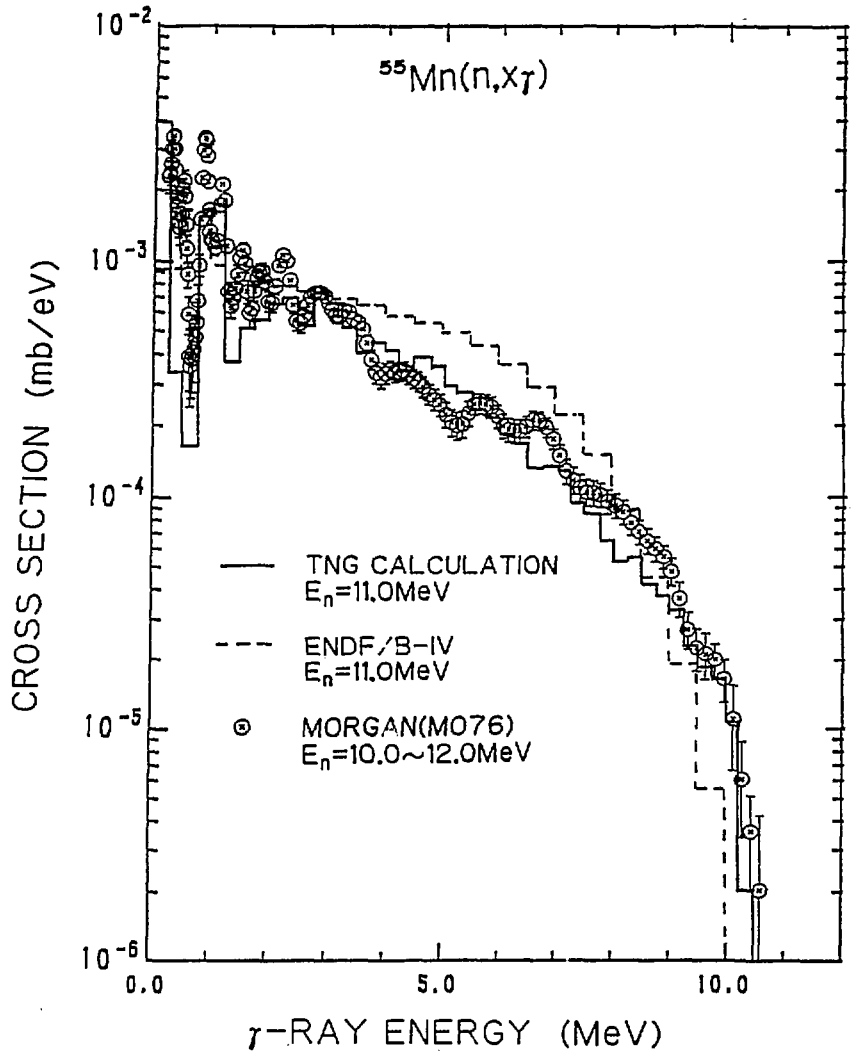

Fig. 11 The ^{55}Mn gamma-ray emission spectrum calculated with TNG at E_n = 10～12 MeV.

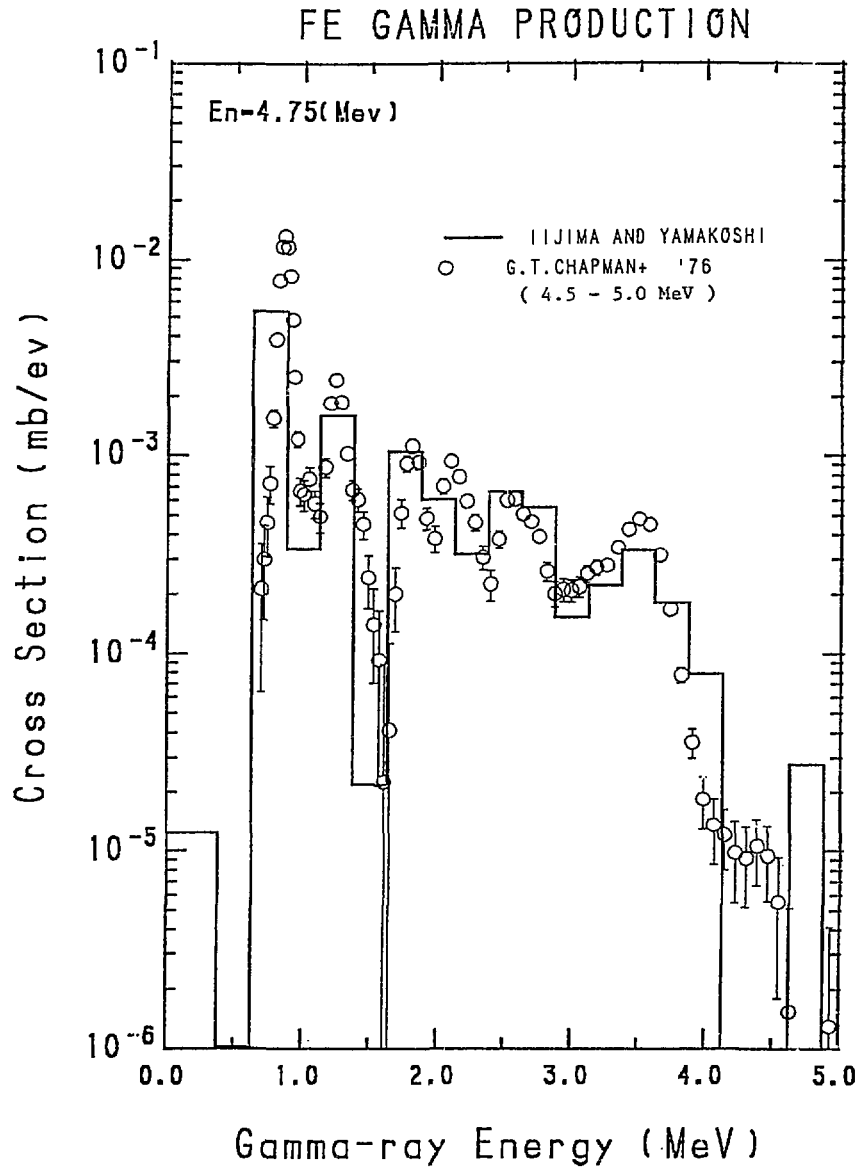

Fig. 12 The ^{nat}Fe gamma-ray emission spectrum calculated with GNASH at E_n = 4.5～5.0 MeV.

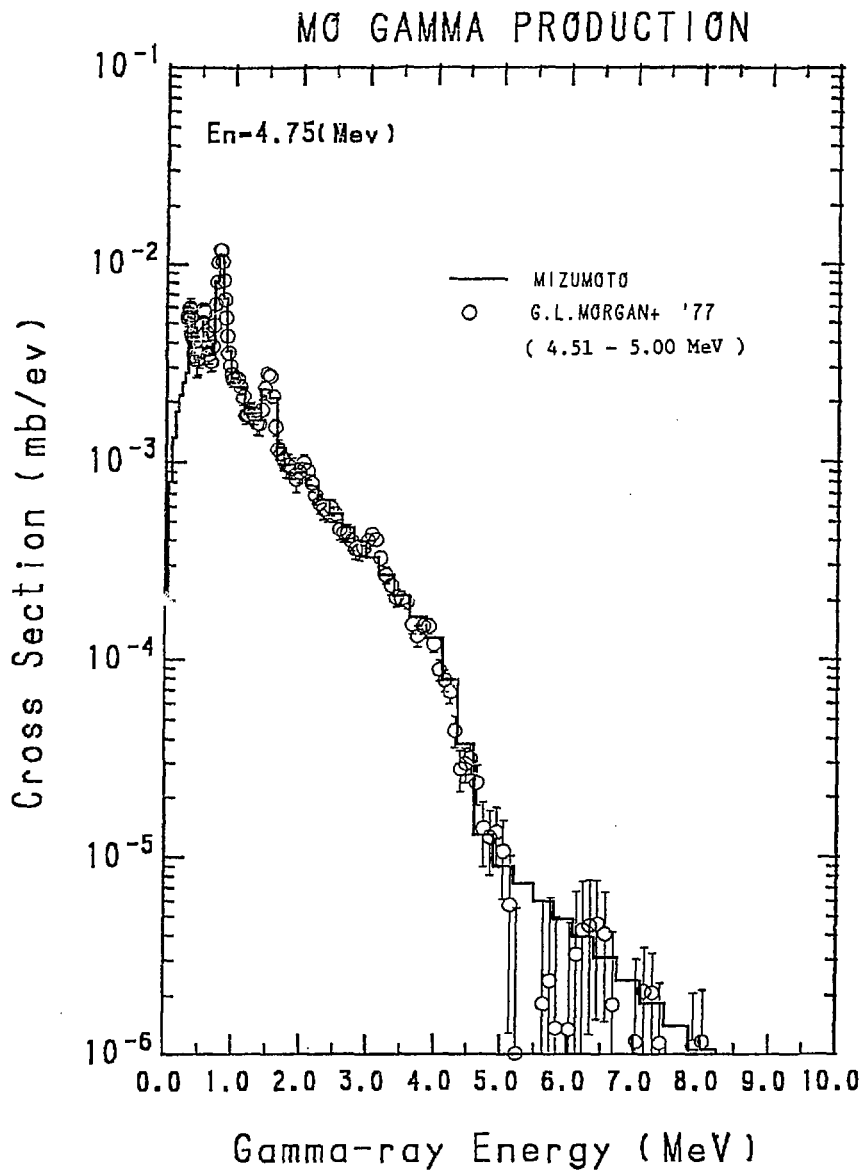

Fig. 13 The ^{nat}Mo gamma-ray emission spectrum calculated with Howerton's method at E_n = 4.51～5.0 MeV

2.1.4 Evaluation of FP Cross Sections for JENDL-3

Masayoshi KAWAI and FPND Sub-working Group*
Japanese Nuclear Data Committee

Abstracrt

Evaluation work of cross sections of fission product nuclides for JENDL-3 is in progress as an activity in JNDC FPND sub-working group. Compared to JENDL-2, the number of FP nuclides is extended to 172 by adding As, Se, Br, Sn and Te isotopes and short lived nuclides. Threshold reaction cross sections are also newly contained in the scope of genearal applications. Resonance parameters are evaluated by taking account of recent experimental data up to 1987. The nuclear model parameters are determined for calculating neutron cross sections with the spherical optical model and the statistical theory. The (n,2n), (n,p), (n,α), (n,np) and (n,nα) cross sections are evaluated for all FP nuclides by using the simple evaporation and preequilibrium model. In this paper, evaluation scope and its present status are described.

1. INTRODUCTION

JENDL-2 fission product cross section library[1] released in 1984 contains the data for 100 FP nuclides. It covers 99.6% captures and 195% yields for FBR burnup calculations. However, the number of FP nuclides is not enough to general applications[2,3] such as burnup calculations of various reactors, radiation dosimetry, diagnostics

---

N.B. *) JNDC FPND Sub-working group members:
M. Kawai (leader, NAIG), K. Hotta (MAPI), S. Iijima(NAIG),
H. Matsunobu(SAEI), T. Nakagawa(JAERI), T. Nishigori(Osaka Univ.)
M. Sasaki (MAPI), T. Watanabe (KHI), A. Zukeran (Hitachi)

and nuclear transmutation calculations in fission and fusion reactors. For thermal reactors, newly required[2] are the following nuclides: Nb-95, Rh-105, Ag-110m, Cs-134, Pm-148m, Pm-148g and Pm-149. For reactor dosimetry, Nb-93(n,n')Nb-93m, Rh-103(n,n')Rh-103m, In-115(n,n')In-115m, I-127(n,2n)I-126 cross sections are required. Cross sections of such reactions as (n,p) and (n,α) of Nb, Zr, Mo and Sn are needed for estimation of radiation damage of materials through atomic displacement and gas production. Reaction cross sections of Br, Kr, I and Xe isotopes are needed for estimating amounts of Kr and Xe isotopes which are used as tagging gases for detection of fuel failure. For estimation of induced activities of a fusion reactor, various kinds of activation cross sections are required[3]. The requirements are not satisfied for most cross sections except the capture cross sections up to JENDL-2.

For capture cross section, the accuracy of evaluated data is not always enough to satisfy the required accuracy of 10-30%. For example, capture cross sections for Cs-135 shows the discrepancy of factor of 2 between JENDL-2 and ENDF/B-IV in the keV energy region, where no experimental data were reported. Figure 1 compares the contributions of individual nuclides to total absorption in HCLWR[4], which were calculated with various nuclear data files. Large difference is observed even for important nuclides such as Cs-133, Xe-131, Tc-99, Ru-101, Nd-145, Pd-108, Pd-107, Cs-135, Eu-155, and Ru-103. The difference seems to have come from the discrepancy in the evaluated data of resolved resonance parameters. Additionally, neglecting competition with charged particle emission processes and direct processes in the statistical calculation for JENDL-2 has brought some ambiguities into capture and inelastic scattering cross

sections in the MeV energy region. Integral tests[5,6] of JENDL-2 also suggested the necessity of reevaluation of data for several isotopes.

Therefore, the evaluation for the fission-product data file of JENDL-3 started in 1985 with a new scope[7]. In the following sections, the scope and the main results are described.

2. Evaluation

2.1 General scope and evaluation method

JENDL-2 FP cross section file was made mainly for the purpose of FBR burnup calculations and it is not enough for general applications as mentioned in the previous section. Accordingly, evaluation of FP cross sections for JENDL-3 is made with the following scope:

(1) Number of nuclides is extended to 172 nuclides, ranging from As to Gd, by adding As, Se, Sn and Te isotopes and short-lived nuclides. Table 1 shows the list of FP nuclides for JENDL-3 FP cross section file. It is aimed that the file should be applicable to LWR, HCLWR and HTGR as well as FBR, and also to other possible general applications[3]. Threshold reaction cross sections are also newly considered in the file.

(2) Experimental data reported up to 1987 are taking into consideration for evaluation of resonance parameters and cross sections.

(3) The multi-level Breit-Wigner formula is employed to the resolved resonances. Unresolved resonance parameters in the energy region below 100 keV are determined with the ASREP code[8].

(4) The spherical optical model and the statistical theory are employed to estimate the capture, elastic and inelastic scattering and total cross sections above the unresolved resonance region with the CASTHY code[9].

(5) Threshold cross sections are evaluated for all FP nuclides by using the multistep evaporation and preequilibrium model calculation code, PEGASUS[10].

(6) For the capture cross sections of Xe-132, Xe-134, Eu-152, Eu-154 and Pm-147 for which no experimental data were reported, the results[5,6] of the integral test for JENDL-2 are reflected.

(7) Several auxilialy computer programs and parameter bases were newly generated[11] in order to promote the evaluation.

2.2 Auxiliary programs for assisting evaluation

The amount of nuclear data of FP nuclides is too much for us to perform their evaluation within the limited time. Accordingly, the evaluation method was nearly standardized and the auxilialy programs were developed[11] together with the data base to assist evaluation works. They are helpful for saving man power.

Figure 2 shows the schemes from evaluating level density parameters and resonance parameters to making a final file. Level density parameters are evaluated on the basis of the Evaluated Nuclear Structural Data File (ENSDF)[12]. The program ENSDFRET retrieves the level scheme data that consist of level energy, spin, parity and gamma transition data from ENSDF. LVLPLOT makes a staircase plot of level scheme. LEVDENS determins the parameters of level density formulas according to Gilbert Cameron's procedure so as to fit to the staircase plot of levels, observed level spacing

and so on. The determined parameters such as level density parameter, nuclear temperature, joint energy between gas model and constant temperature model, spin cutoff factor and normalization factor are compiled into the data base PARAMFL together with the level schemes and the optical model parameters. The optical model parameters were evaluated with the NDES[13] so as to fit the experimental data of total cross sections, neutron strength functions and nuclear radius.

These evaluated nuclear model parameters are used for calculations with CASTHY and PEGASUS. The input and the job control data of CASTHY for many nuclides are made one by one with the JOBSETTER code using PARAMFL as a data base. For the resolved resonances, a REPSTOR file is prepared and data are transformed into the ENDF/B format with REPSTOR. The REPSTOR file contains simultaneously the experimental and the evaluated data. Some kinds of programs are also generated to convert into the REPSTOR file from the data in EXFOR or ENDF/B format, and to calculate unknown parameters such as capture area and partial widths from the selected data set.

2.3 Evaluation of resolved resonance parameters

Resonance parameters for such nuclides as Cs-133, Xe-131, Tc-99, Ag-109, Pm-147, Sm-152, Ru-101, Eu-153, Pd-105, Pd-108, Nd-143, Pd-107, Cs-135, Eu-154, Sm-150, and Cs-134 are important to calculation of the effective resonance integrals in a HCLWR core, since resonance self-shieding effects on the absorption rates of these nuclides are prominent[4].

Evaluation was made for 46 nuclides among newly added 72 FP nuclides and for 15 nuclides out of 100 FP's in JENDL-2. The former

was mainly based on the data recommended by Mughabghab et al.[14,15] For the latter nuclides, new experimental data reported after the JENDL-2 evaluation were taken into cosideration. Particularly, it is noted that the experimental data for Zr-93, Kr-86 and Xe-136 are thoroughly new. Before compiling the final data file, calculated thermal cross sections and resonance integrals from the evaluated parameters will be compared with experimental data. In some cases, negative resonances will be artificially added so as to reproduce well the experimental data.

2.4 Evaluation of nuclear model parameters

The grobal fitting of optical potential parameters of FP nuclides was made by Iijima and Kawai[16] by taking acount of local systematics of measured total cross sections. Calculated cross sections showed a general agreement with the measured one for most nuclides. However, disagreement was observed for several elements such as Tc, Pr, Pm and Eu. Figure 3 shows an example of the poor case; Pm-147 total cross section. In such cases, reevaluation of optimum optical model parameters is made by using the NDES code.

Level density parameters of the Gilbert-Cameron's composite formula were determined with LEVDENS. Figure 4 shows a staircase plot of level schemes for Pd-107 and its family nuclides, as an example. For minor nuclides, the systematics[17] of 'a' parameter shown in Table 2 and the following systematics of nuclear temperature, T, are adopted:

$$T = 65/A, \qquad \text{for } A \leq 100,$$

$$= 0.65-0.00242(A-100), \qquad \text{for } A > 100,$$

where A is a nuclear mass number. Figure 5 shows the systematics of T.

Systematics of gamma-ray strength function was also investigated by using the ratios of radiation width to observed level spacing recommended by Mughabghab et al.[14,15] and the values determined in the evaluation for JENDL-2 FP data file so as to fit to the capture cross section. The values based on the Mughabghab's recommendation were generally consistent with those of JENDL-2, and their systematics was turned out to be different between even or odd mass nuclei.

2.5 Capture cross section

The capture cross section is estimated with CASTHY by adjusting gamma-ray strength function to reproduce well the experimental data in the keV energy region or by adopting its systematics. In the calculation, the competition with the threshold reactions, which were neglected for the previous evaluation[1], will be considered for all FP nuclides. For nuclides which have no experimental data, the result of the integral test will be reflected in the evaluation through the cross section adjustment method. The method can be expected to obtain a good cross section, as successfully obtained for Zr-93 of JENDL-2[1]. Accordingly, it will be applied to the evaluation for Xe-132, Xe-134, Pm-147, Eu-152 and Eu-154.

In the MeV energy region, contributions of semidirect and direct capture processes to cross section become larger. Therfore, the procedure of Benzi and Reffo[18] will be applied to the present evaluation.

2.6 Threshold reaction cross sections

The (n,2n), (n,p), (n,α), (n,np) and (n,nα) cross sections were evaluated for all nuclides by using the simple evaporation and preequilibrium model calculation code, PEGASUS. In PEGASUS calculation, the Kalbach's constant K, which represents the strength of the preequilibrium transition rate, was estimated as $K \sim 0.1/(g/A)^3$, where g is the single particle level density.

Figure 6 shows the experiment-to-calculation ratios of 14.5 MeV (n,2n) and (n,p) cross sections. The (n,2n) cross sections are predicted fairly well. The (n,p) cross sections are underestimated on the average by a factor of 2 ~ 3. The calculations are normalized to the experimental data or 14.5 MeV systematics.

3. Summary

Evaluation of neutron cross sections of 172 nuclides in the fission product nuclide mass region for JENDL-3 is in progress. In the work, the systematics of parameters of level density formulas and gamma-ray strength function were investigated. The calculations of threshold reaction cross sections have been nearly completed, and the efforts are concentrated to the evaluation for the resolved resonance parameters and to the cross section calculations with CASTHY.

References

1) T. Aoki, S. Iijima, M. Kawai, Y. Kikuchi, H. Matsunobu, T. Nakagawa, Y. Nakajima, T. Nishigori, M. Sasaki, T. Watanabe, T. Yoshida, A. Zukeran: Evaluation of FP Cross Sections for JENDL-2, Proc. Int. Conf. on Nuclear Data for Basic and Applied Science, May 1985, Santa Fe, Vol. 2, p.1627, Gordon and Breach Sci. Pub. (1985)

2) S. Iijima, T. Yoshida and T. Yamamoto: J. Nucl. Sci. Tecnol., 19, 96 (1982).

3) S. Iijima, J.Katakura, M. Nakazawa, M. Kawai, T. Asami, and T. Nakagawa: JENDL Special Purpose Data Files, Proc. of the 1986 Seminar on Nuclear Data, JAERI-M 87-025, p. 230 (1987)..

4) H. Takano, H. Ihara and H. Akie: Group Cross Sections of Fission Products and Minor Actinides, ibid., p. 121 (1987).

5) T. Watanabe et al.: Fission-Product Cross Section Evaluation, Integral Tests and Adjustment Based on Integral Data," Proc. of the 1985 Seminar on Nuclear Data, JAERI-M 86-080, p. 30 (1986).

6) T. Watanabe, et al.: presented at the present seminar.

7) S. Iijima: Plans for JENDL-3 Fission Product Data File, Proc. of the 1986 Seminar on Nuclear Data, JAERI-M 87-025, p. 205 (1987).

8) Y. Kikuchi, private communication.

9) S. Igarasi, J. Nucl. Sci. Technol. 12, 67 (1975) and private communication.

10) S. Iijima, T. Sugi, T. Nakagawa and T. Nishigori: "Program PEGASUS, A Precompound and Multi-step Evaporation Theory Code for Neutron Threshold Cross Section Calculation, Proc. of the 1986 Seminar on Nuclear Data, JAERI-M 87-025, p. 337 (1987).

11) T. Nakagawa, et al.: to be published in JAERI-M report.

12) J. K. Tuli: Evaluated Nuclear Structure Data File - A Manual for Preparation of Data Sets - BNL-NCS-51655, UC-34c [Phisics-Nuclear-TIC-4500]. see also, T. Tamura: JAERI-M 85-035, p. 330 (1986).

13) T. Nakagawa: J. At. Energy Soc. Japan, 22, 559 (1980).

14) S.F. Mughabghab, M. Divadeenam and N.M. Holden: Neutron Cross Cross Sections, Vol. I, Neutron Resonance Parameters and Thermal Cross Sections, Part A: Z=1 - 60, Academic Press, ISBN 0-12-509701-8 (1981).

15) S.F. Mughabghab: Neutron Cross Sections, Vol. I, Neutron Resonance Parameters and Thermal Cross Sections, Part B: Z=61 - 100, Academic Press, ISBN 0-12-509711-5 (V.1, Pt.B.) (1984).

16) S. Iijima and M. Kawai: J. Nucl. Sci. Technol., 20, 77 (1983).

17) S. Iijima, T. Yoshida, T. Aoki, T. Watanabe and M. Sasaki: ibid. 21, 10 (1984).

18) V. Benzi and G. Reffo: fast Neutron Radiative Capture Cross Sections of Stable Nuclei with $32 \leq Z \leq 66$ (A semi-empirical evaluation), CCDN-NW/10, p. 6 (1969).

Table 1 Fission product nuclides in JENDL-3.

Z	Nuclide
33	^{75}As
34	^{74}Se, ^{76}Se, ^{77}Se, ^{78}Se, ^{79}Se, ^{80}Se, ^{82}Se
35	^{79}Br, ^{81}Br
36	^{78}Kr, ^{80}Kr, ^{82}Kr, ^{83}Kr, ^{84}Kr, ^{85}Kr, ^{86}Kr
37	^{85}Rb, ^{87}Rb
38	^{86}Sr, ^{87}Sr, ^{88}Sr, ^{89}Sr, ^{90}Sr
39	^{89}Y, ^{91}Y
40	^{90}Zr, ^{91}Zr, ^{92}Zr, ^{93}Zr, ^{94}Zr, ^{95}Zr, ^{96}Zr
41	^{93}Nb, ^{94}Nb, ^{95}Nb
42	^{92}Mo, ^{94}Mo, ^{95}Mo, ^{96}Mo, ^{97}Mo, ^{98}Mo, ^{99}Mo, ^{100}Mo
43	^{99}Tc
44	^{96}Ru, ^{98}Ru, ^{99}Ru, ^{100}Ru, ^{101}Ru, ^{102}Ru, ^{103}Ru, ^{104}Ru, ^{106}Ru
45	^{103}Rh, ^{105}Rh
46	^{102}Pd, ^{104}Pd, ^{105}Pd, ^{106}Pd, ^{107}Pd, ^{108}Pd, ^{110}Pd
47	^{107}Ag, ^{109}Ag, ^{110m}Ag
48	^{106}Cd, ^{108}Cd, ^{110}Cd, ^{111}Cd, ^{112}Cd, ^{113}Cd, ^{114}Cd, ^{116}Cd
49	^{113}In, ^{115}In
50	^{112}Sn, ^{114}Sn, ^{115}Sn, ^{116}Sn, ^{117}Sn, ^{118}Sn, ^{119}Sn, ^{120}Sn, ^{122}Sn, ^{123}Sn, ^{124}Sn, ^{126}Sn
51	^{121}Sb, ^{123}Sb, ^{124}Sb, ^{125}Sb
52	^{120}Te, ^{122}Te, ^{123}Te, ^{124}Te, ^{125}Te, ^{126}Te, ^{127m}Te, ^{128}Te, ^{129m}Te, ^{130}Te
53	^{127}I, ^{129}I, ^{131}I
54	^{124}Xe, ^{126}Xe, ^{128}Xe, ^{129}Xe, ^{130}Xe, ^{131}Xe, ^{132}Xe, ^{133}Xe, ^{134}Xe, ^{135}Xe, ^{136}Xe
55	^{133}Cs, ^{134}Cs, ^{135}Cs, ^{136}Cs, ^{137}Cs
56	^{130}Ba, ^{132}Ba, ^{134}Ba, ^{135}Ba, ^{136}Ba, ^{137}Ba, ^{138}Ba, ^{140}Ba
57	^{138}La, ^{139}La
58	^{140}Ce, ^{141}Ce, ^{142}Ce, ^{144}Ce
59	^{141}Pr, ^{143}Pr
60	^{142}Nd, ^{143}Nd, ^{144}Nd, ^{145}Nd, ^{146}Nd, ^{147}Nd, ^{148}Nd, ^{150}Nd
61	^{147}Pm, ^{148g}Pm, ^{148m}Pm, ^{149}Pm
62	^{144}Sm, ^{147}Sm, ^{148}Sm, ^{149}Sm, ^{150}Sm, ^{151}Sm, ^{152}Sm, ^{153}Sm, ^{154}Sm
63	^{151}Eu, ^{152}Eu, ^{153}Eu, ^{154}Eu, ^{155}Eu, ^{156}Eu
64	^{152}Gd, ^{154}Gd, ^{155}Gd, ^{156}Gd, ^{157}Gd, ^{158}Gd, ^{160}Gd
65	^{159}Tb

Table 2 Neutron number dependence of parameter 'a' built in PEGASUS.

$$a = A \frac{C_1 (N-N_1) + C_2 (N_2-N)}{N_2 - N_1} + C_3 \quad (MeV^{-1})$$

N	N_1	N_2	C_1	C_2	C_3
$N \leq 17$	1	17	0.0	0.0	4.0
$18 \leq N \leq 27$	18	27	0.15	0.15	0.0
$28 \leq N \leq 41$	28	41	0.193	0.122	0.0
$42 \leq N \leq 49$	42	49	0.155	0.187	0.0
$50 \leq N \leq 59$	50	59	0.185	0.104	0.0
$60 \leq N \leq 81$	60	81	0.114	0.182	0.0
$82 \leq N \leq 88$	82	88	0.166	0.100	0.0
$89 \leq N \leq 98$	89	98	0.124	0.171	0.0
$99 \leq N \leq 116$	99	116	0.123	0.123	0.0
$117 \leq N \leq 126$	117	126	0.041	0.116	0.0
$127 \leq N \leq 139$	127	139	0.154	0.058	0.0
$140 \leq N \leq 146$	140	146	0.124	0.141	0.0
$N \geq 147$	147	200	0.120	0.120	0.0

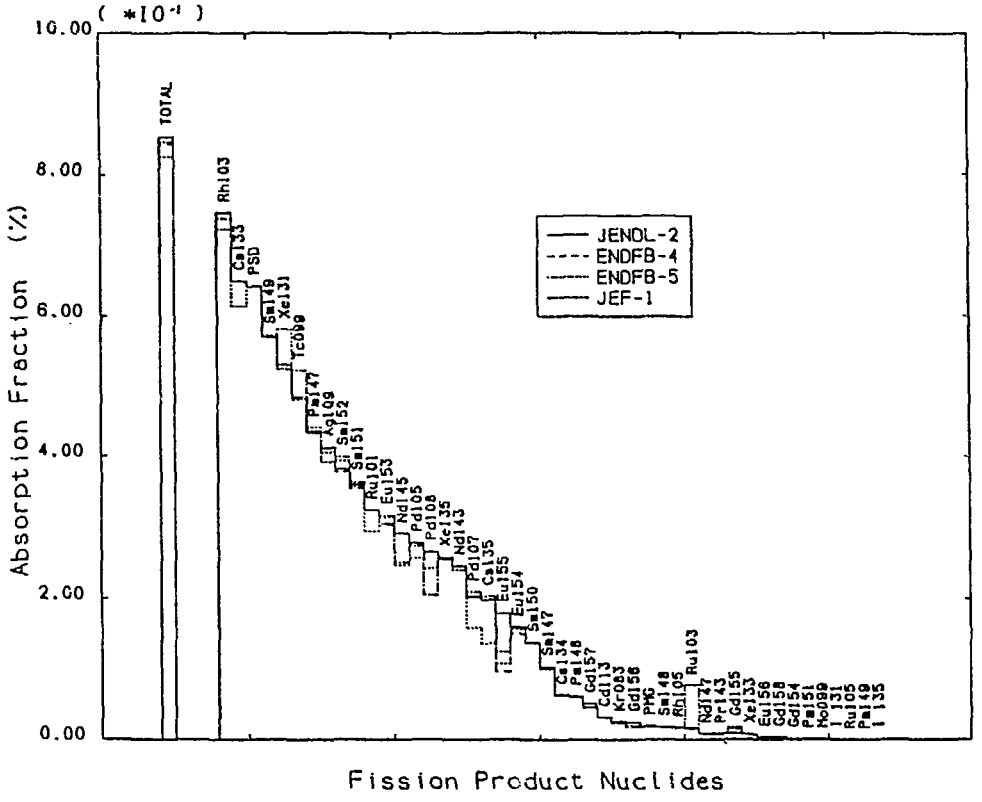

Fig.1 Contributions of individual nuclide to total absorption in HCLWR (42 GWD/t).

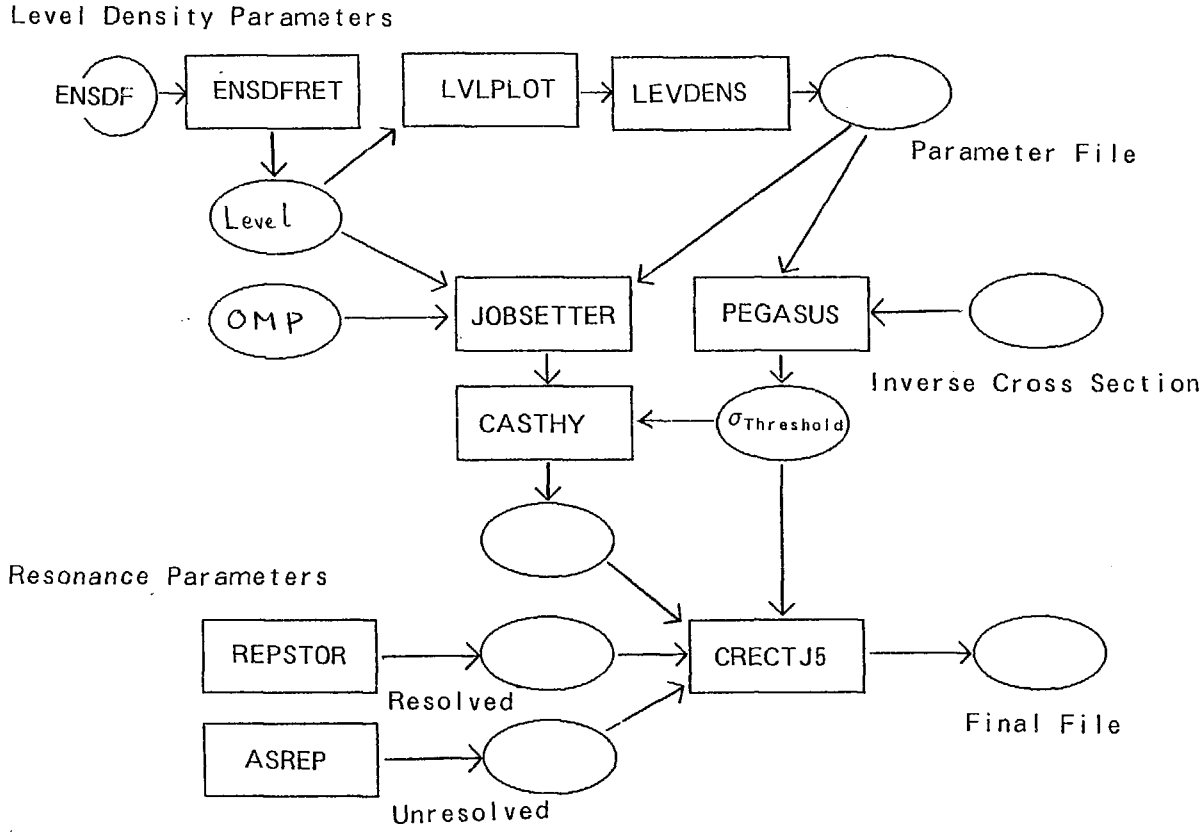

Fig. 2 Auxially evaluation programs and data flow.

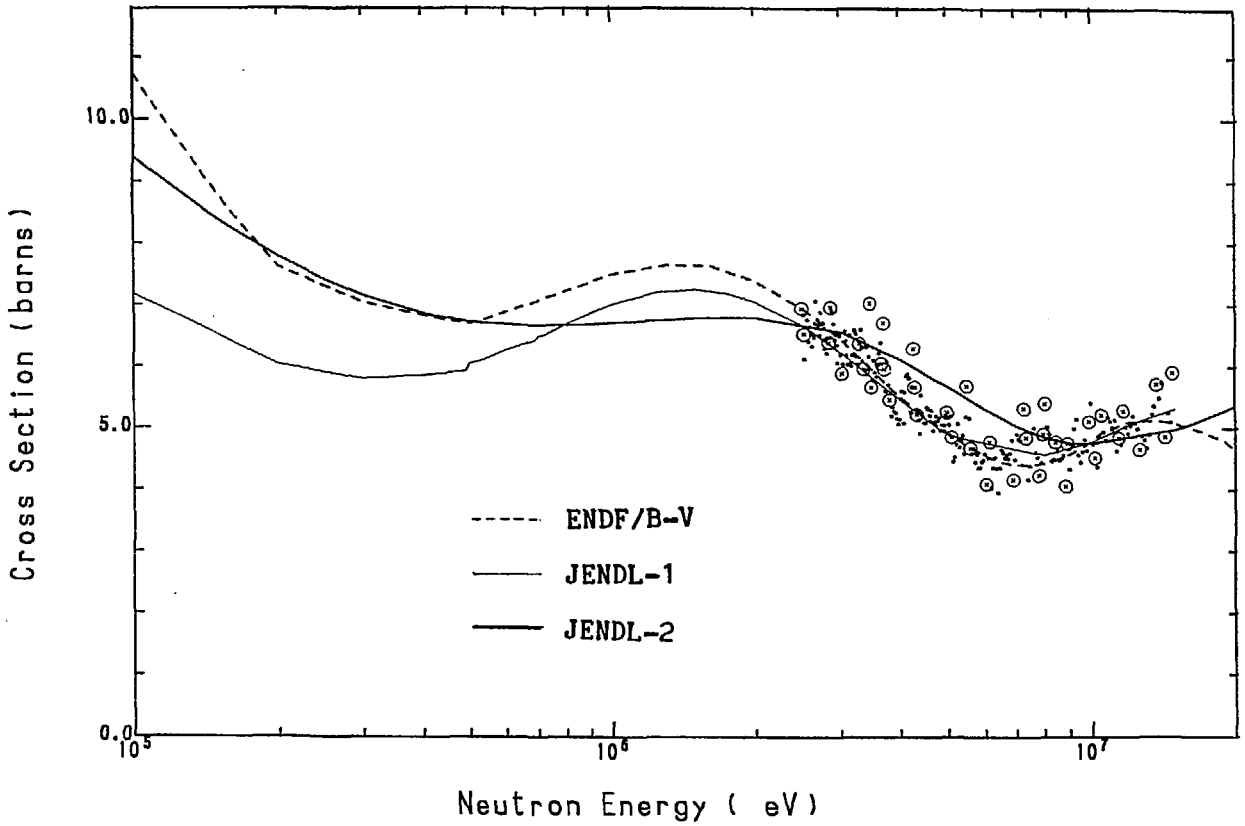

Fig. 3 Neutron cross sections for Pm-147.

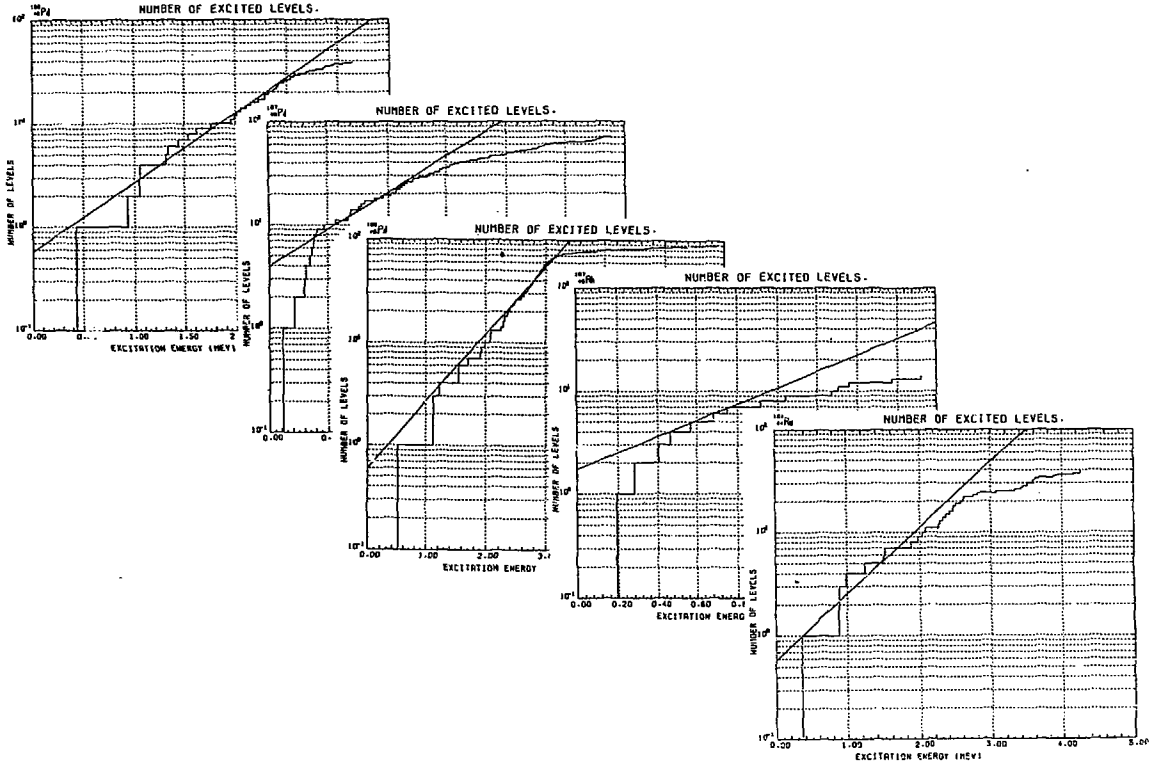

Fig. 4 Staircase plot of excited levels for Pd-107 and its family nuclides.

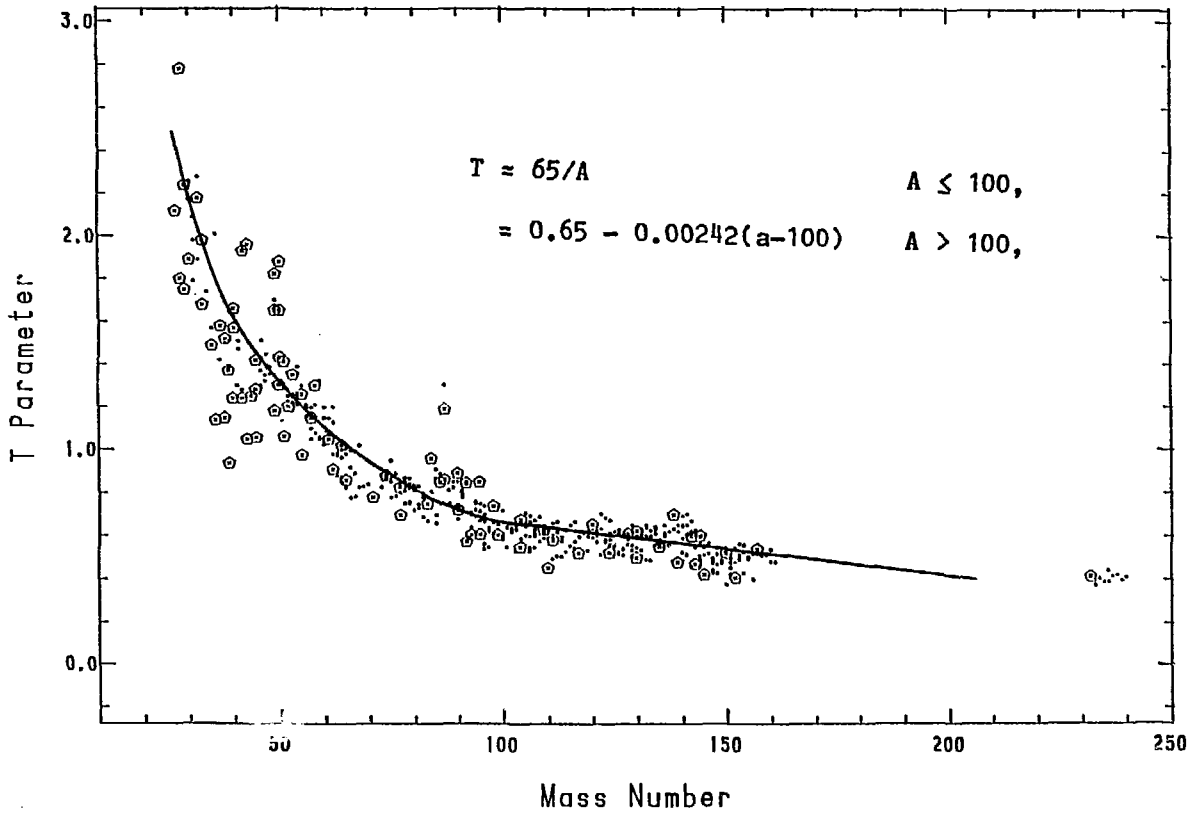

Fig. 5 Mass dependense of neutron temperature

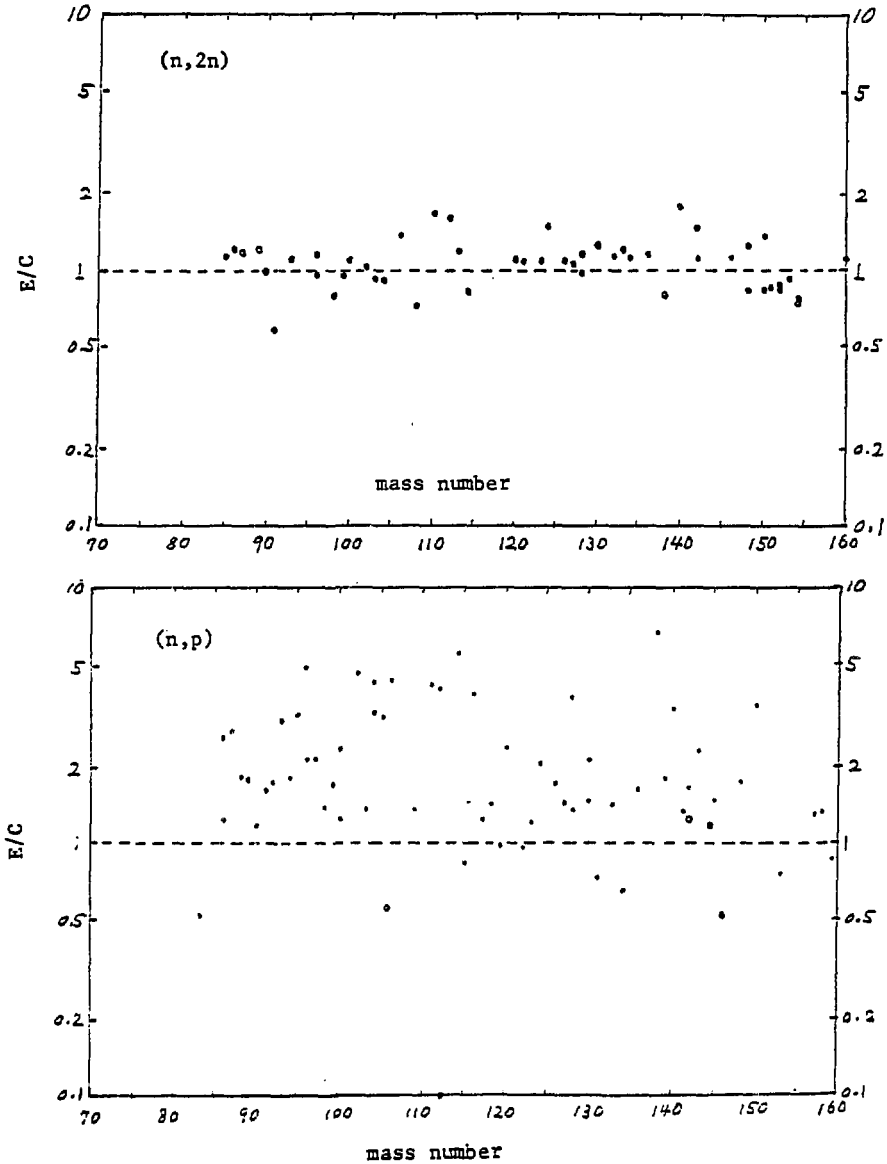

Fig. 6 Experiment-tocalculation ratios of (n,2n) and (n,p) cross sections at 14.5 MeV.

2.1.5 Evaluation of the Fusion-Related Neutron Nuclear Data for JENDL-3 － Nuclear Data in the Very Light Mass Region Stored in JENDL-3T －

Satoshi CHIBA

Japan Atomic Energy Research Institute
Tokai-mura, Naka-gun, Ibaraki-ken 319-11, Japan

Abstract

Status of the neutron nuclear data evaluations for JENDL-3 will be described for nuclides important in the development of D-T fusion reactors. In this article, however, only explanation of the evaluations for the very light mass region will be presented to avoid overlapping with what are given in another papers submitted to this seminar. Emphases are placed on the tritium production cross sections, inelastic scattering cross sections including the double-differential neutron emission spectrum (DDX), threshold reaction cross sections and photon production cross sections. The methods employed to prepare JENDL-3T library and their results will be summarized.

1. Introduction

Neutrons will play an important role in fusion reactors. They are produced in the plasma and transport the acquired energy to blankets to produce electricity and some useful materials which do not exist on the earth naturally, including tritium. In this sense, blankets are considered to be very active media which are essential to determine the characteristics of fusion reactors: it converts the large Q-value of the D-T fusion reaction to many useful forms through nuclear processes involving neutrons. The tritium breeding ratio, amount of energy deposition (nuclear heating) in a blanket, life-time and induced activities of the structural materials, gas production rates and shielding characteristics will be determined by those nuclear processes. The "evaluated" neutron nuclear data are necessary to estimate all these very important properties of fusion reactors.

Table 1 shows a list of fusion-related nuclides to be stored in JENDL-

3. They were selected referring literature on the studies of a D-T fusion reactor development. It is found from the table that the relevant mass region ranges from the very light nucleus (^{1}H) to very heavy one (^{209}Bi). The status for the medium-heavy nuclides ($^{23}Na \sim ^{209}Bi$) is, however, described in a paper presented by Mizumoto in this seminar. In this article, therefore, only the status of the evaluated neutron nuclear data for the very light nuclides ($^{1}H \sim ^{19}F$) stored in JENDL-3T will be described.

Historically, the JENDL-2[1], which was completed in April 1983, also aimed at using the design calculations of fusion reactors as well as the thermal and fast breeder reactors. The data in JENDL-2 were, however, found to be seriously inadequate in the energy range above several MeV which is essentially important for fusion neutronics. According to strong requests from the analysists of the Japan-US cooperative fusion experiment using the JAERI FNS (Fusion Neutronics Source) and the University jointed programs on fusion experiments using OKTAVIAN (Osaka University), a preliminary version for JENDL-3 named JENDL-3PR1 was prepared in the end of 1983 containing data for ^{6}Li, ^{7}Li, ^{9}Be, ^{12}C, ^{16}O, Cr, Fe and Ni[2-6]. Because some problems were still found in the JENDL-3PR1 data, a part of it was revised and a library called JENDL-3PR2 was made in 1986[7]. They are the bases of the presently compiled nuclear data for the very light mass region stored in JENDL-3T.

In evaluating the fusion-related neutron nuclear data, some quantities are considered to be of special importance. They are summarized as:

1)The tritium production cross sections,
2)The energy and angular distributions of secondary neutrons (DDX), including the direct reaction contribution to inelastic scattering processes,
3)Some threshold reaction cross sections,
4)The photon production cross sections, and
5)The activation cross sections.

The data in JENDL-3T were evaluated placing much emphasis on these quantities. Especially, the DDX and tritium production cross sections are of primary concern for the light elements. The activation cross sections are not so important in the very light mass region relevant in this article.

2. General description of the present evaluations

A list is presented in Table 2 of the evaluators and application uses, in the field of nuclear energy program, neutron physics and nuclear measurements, of the neutron nuclear data for each nuclide described in this paper. The main body in this mass region was evaluated by Shibata. The data for ^{14}N and ^{16}O were evaluated by the "fusion-related neutron nuclear data evaluation sub-working group (FRNNDESWG)" in JNDC, names of the members are given below the last line of the table.

A summary of the evaluated quantities, except for the total and elastic scattering cross sections, is given in Table 3. The $^{6}Li(n,t)\alpha$ and $^{7}Li(n,n't)\alpha$ reactions are two of the most important reactions in fusion neutronics. Besides the uses in fusion neutronics, some reactions in these nuclides are very important as the "standard" and "dosimetry" cross sections in nuclear measurements as shown in Table 2, i.e., the $^{1}H(n,n)$, $^{3}He(n,p)T$, $^{6}Li(n,t)\alpha$, $^{10}B(n,\alpha)^{7}Li$, $^{12}C(n,n)$ and $^{19}F(n,2n)$ reactions. For nuclides labeled with *, the photon production cross sections are also given. By 19 December, 1987, the data except for ^{19}F have been already compiled and stored in JENDL-3T.

Table 4 shows a list of nuclides included in various evaluated nuclear data libraries. The relation of the present evaluations with the previous JENDL libraries will be mentioned briefly here:

For ^{1}H and ^{2}H, the data stored in JENDL-2 were only slightly revised and most of them were transferred to JENDL-3T without any change. The data for $^{1}H(n,n)$ reaction above 100 keV had been taken from the evaluation of Hopkins and Breit calculated with the Yale phase shift[1]. The file 6 part in ^{2}H existed in JENDL-2[8] was removed in JENDL-3T.

The data for ^{3}He, ^{4}He, ^{11}B and ^{14}N were newly evaluated for JENDL-3.

The data for ^{6}Li, ^{7}Li, ^{9}Be, ^{12}C and ^{16}O were all included in JENDL-3PR1/2 evaluations[2]. These data were partly revised and transferred to JENDL-3T.

For ^{10}B, the data in JENDL-2 were mainly based on ENDF/B-IV. Hence, the data were newly evaluated for JENDL-3 taking account of up-to-date data and stored in JENDL-3T.

The evaluation for ^{19}F is now in progress and will be completed soon.

The evaluations in this mass region were mainly based on available experimental data, because for these nuclides theoretical calculations are difficult to be applied properly for some reasons. For example, the concept of "phenomenological optical potential" and "level density", which are widely used for heavier nuclides, would not be adequately applicable to this mass region. Moreover, theoretical treatments of such few-body break-up reactions as the $^{7}Li(n,n't)\alpha$ and $^{9}Be(n,2n)2\alpha$ are not well developed at present to be applied in nuclear data evaluation accurately enough. However, the proportion of theoretical calculation in the present evaluations was increased significantly compared with JENDL-2. This is partly because there were some progresses in the study of optical potential and other parameters in this mass region and also some new computer codes were developed after the evaluation of JENDL-2 was completed. These theoretical calculations will be superior to a simple adoption of experimental data in the sense of predictability in the region where there are only a few experimental data and to maintain the energy balance, consistency among the various reaction channels, and for future evaluation work for higher energy region when applied properly.

In Table 5, a list of computer programs used in the present evaluations is given for each nuclide. Those without parentheses are considered to be global programs. Some features are mentioned as:

1)In the low energy region, almost all nuclides are evaluated with the R-matrix theory and represented with the point-wise data. Only the ^{19}F file will have the resonance parameters,
2)In addition to the statistical models, some nuclides have the inelastic scattering cross sections calculated with DWBA or coupled-channel theory,
3)Some threshold reaction cross sections are calculated with the DWBA as well as the statistical model,
4)For ^{6}Li, ^{7}Li, ^{9}Be and ^{10}B, the continuum secondary neutron spectra were calculated by the three body model or sequential decay model in contrast to the simple evaporation spectra adopted in JENDL-2, and
5)The evaluation for deuterium was performed with the very sophisticated quantum mechanical three-body model based on the

Faddeev theory.

Among the codes listed in this table, those named ELIESE-3[9], CASTHY[10], RESCAL[11] and PEGASUS[12] were developed in Japan. The DWUCK4[13], GNASH[14] and TNG[15] codes were developed in other countries but were all modified in Japan for use in the evaluation for JENDL-3T.

Specific features of the presently evaluated data are summarized as follows:

1)The tritium production cross sections were updated taking account of the recently measured data with high precision tritium counting method,
2)The direct inelastic scattering contribution was taken into consideration for most nuclides,
3)For break-up reactions of the target nucleus, the three- and four-body break-up models were adopted,
4)Pseudo-level representation was adopted for continuum neutron spectra of ^{6}Li, ^{7}Li and ^{10}B to incorporate the energy-angle correlation approximately,
5)The threshold reaction cross sections were updated,
6)The photon production cross sections were newly evaluated for some nuclides, and
7)The R-matrix theory was applied for almost all nuclides below several MeV.

In the following sections, these features will be described with some typical examples according to this order.

3. Tritium production cross sections

In this section, status of the tritium production cross sections of ^{6}Li, ^{7}Li and ^{9}Be will be explained.

3.1 The $^{6}Li(n,t)\alpha$ reaction cross section

Fig. 1 shows the measured and evaluated $^{6}Li(n,t)\alpha$ reaction cross sections around the $P_{5/2}$ resonance at 250 keV. The solid line shows the values

stored in JENDL-3T. The present values were calculated with the R-matrix theory in this energy range (below 1 MeV), putting a weight on the data measured by Macklin et al.[16] A code named "RESCAL" was used for the calculation[11]. The peak value was calculated to be 3.364 barns at 239 keV. This is in very good agreement with one given in ENDF/B-V, 3.309 barns at 240 keV, which was calculated with the comprehensive R-matrix analysis including the data on the differential cross section and analyzing power of the $^{4}He(t,t)^{4}He$ reaction[17]. The calculated thermal cross section of 940.33 barns is also in good agreement with the evaluation of Mughabghab et al.[18], 940±4 [b].

In Fig. 2 shown are the $^{6}Li(n,t)\alpha$ reaction cross sections from 1 keV to 20 MeV. Above 1 MeV, the present evaluation was obtained by a least-squares fit to the data of Bartle[19] and Bartle et al[20].

3.2 The $^{7}Li(n,n't)\alpha$ reaction cross section

In the last several years, many experimenters have challenged to measure this cross section using the tritium accumulation and its β^{-}-ray counting method. With regard to the "integrated" cross sections, this method is superior to those which measure the spectrum of the secondary particles and integrate it over the secondary particles' energy and angle. As a result, the accuracy was significantly improved.

Fig. 3 shows this cross section in the entire energy range. Besides the very old data, Smith et al.[21], Liskien et al.[22], Maekawa et al.[23,24], Swinhoe et al.[25], Takahashi et al[26], Goldberg et al.[27] and Qaim et al.[28] all employed the tritium counting method. The dotted curve is the values stored in JENDL-3PR1/2. They are slightly smaller than the recent measured values around 14 MeV.

The $^{7}Li(n,n't)\alpha$ reaction cross sections around 14 MeV are plotted in Fig. 4. The JENDL-3PR1/2 evaluations were based on the data of Liskien et al. (1983)[22] in this energy range. However, all data measured after 1983 (except for the "revised" data of Swinhoe et al.[25]) were higher than their values and agreed very much with each other. The present evaluation curve was, therefore, drawn considering these up-to-date and consistent data sets. The present value is about 5% larger than that of the JENDL-3PR1/2 at 14 MeV.

3.3 The $^{9}Be(n,t)$ reaction cross section

The total tritium production cross section of ^{9}Be is shown in Fig. 5. This is a sum of the two reaction channels, i.e., the (n,t_0) and (n,t_1) reactions. The solid line shows the evaluation by Young[29] while the dashed line represents the data stored in JENDL-3T (= JENDL-3PR1/2 for this cross section). In the present evaluation, the "shape" of this cross section was calculated by the statistical model and it was normalized to the data of Boedy et al.[30] measured from 13.55 to 14.7 MeV. Triangles represent the data measured by Liskien et al.[31] in this year (1987) from 12.86 to 19.57 MeV. Although the applicability of the statistical model to this very light nucleus and the optical potential parameters for tritium will still be open questions, the newest data are in very good agreement with the JENDL-3T evaluation above 13.5 MeV. Below 13.5 MeV, the newest data exhibit a structure that could not be predicted by the statistical model.

4. Inelastic scattering cross sections

Evaluation of neutron emission spectra is important for transport calculations in fusion blanket materials. For the very light nuclides, it is especially important because there exists a strong angle-energy correlation in the secondary neutron spectra. In this section, the method employed to evaluate the inelastic scattering cross sections, including the energy-angular distributions of secondary neutrons, will be briefly reviewed for ^{2}H, ^{6}Li, ^{7}Li, ^{12}C, ^{9}Be and ^{16}O. After that, the DDX data will be compared with some experimental data.

4.1 Evaluation for ^{2}H

The data were taken from the JENDL-2 evaluation[8] except that the File 6 part was removed. In JENDL-2, the (n,2n) reaction cross section was evaluated based on the experimental data. As shown in Fig. 6, those values are also consistent with the recent measurement of Frehaut et al.[32]

The angular distribution of elastically scattered neutrons and the energy-angular distributions of the secondary neutrons emitted from the $^{2}H(n,2n)p$ reaction were calculated with the quantum mechanical three-body model based on the Faddeev equation[33]. The elastic and break-up T-matrix amplitudes were calculated by the method of Ebenhoh[34]. The results are

shown in Fig. 7 at 14.1 MeV. This figure indicates that a simple phase-space distribution, shown by the dashed lines, cannot reproduce the measured (n,2n) spectra. On the contrary, the three-body model calculation based on the Faddeev equation can reproduce the measured spectra very well. In the actual file, however, these spectra are given in File 5 as the angle-integrated spectra, which cannot incorporate with the energy-angular correlation.

4.2 The secondary neutron spectra emitted from ^{6}Li, ^{7}Li and ^{12}C

In JENDL-3T evaluation, the spectra of the secondary neutrons from the $^{6}Li(n,n'd)\alpha$ and $^{7}Li(n,n't)\alpha$ reactions were calculated by the three-body phase-space model corrected by the Coulomb penetrability[35]. In the center-of-mass system, this model is expressed by a very simple function;

$$d^2\sigma/dEd\Omega = 2\pi\eta/[\exp(2\pi\eta)-1]\cdot[E(E_{max}-E)]^{1/2}$$
$$\eta = Z_2Z_3e^2/(\hbar v_{23})$$

where E is the secondary-neutron energy in c.m. and E_{max} its kinematically allowed maximum value. The subscripts 2 and 3 correspond to two unobserved particles, and v_{23} is their relative velocity. The first factor gives the Coulomb penetrability between particles 2 and 3. This function gives a spectrum softer than one without the Coulomb correction and is in good agreement with the data measured in the 4～6 MeV region[36]. In order to incorporate kinematics into actual files, pseudo levels were used to express the above spectrum. This pseudo-level representation is adequate for preserving energy-angle correlation approximately.

The emission spectra from the $^{6}Li(n,2n)$, $^{7}Li(n,2n)$ and $^{12}C(n,n')3\alpha$ reactions were assumed to have the conventional evaporation shape. The values of nuclear temperatures θ were determined from the measured DDX data around 14 MeV[36,37]. For other energies (E_n) the following expression was assumed:

$$\theta = (E_n/a)^{1/2}$$

where a is a constant.

4.3 The emission neutron spectrum for ^{9}Be

The secondary neutron spectrum from the $^{9}Be(n,2n)2\alpha$ reaction was calculated with the sequential decay model. As the decay processes, two channels were considered:

$$^{9}Be + n \longrightarrow n' + {}^{9}Be^{*}$$
$$^{9}Be^{*} \longrightarrow n + {}^{8}Be$$
$$^{8}Be \longrightarrow 2\alpha \qquad (1)$$

and

$$^{9}Be + n \longrightarrow \alpha_1 + {}^{6}He^{*}$$
$$^{6}He^{*} \longrightarrow 2n + \alpha \qquad (2)$$

The energy spectra of secondary neutrons from these reactions were calculated with the analytical method of Beynon et al.[38] With regard to the excited states in ^{9}Be concerning the process (1), only four levels were incorporated (MT = 6 - 9) because in ENDF/B-V format that is the maximum allowed number for this type of reaction. In the real situation, however, more levels participate in this reaction. This might be one of the problems in the present evaluations.

For MT = 16, the spectrum was given by the evaporation model. The nuclear temperature was taken from the experimental data of Takahashi et al. This is considered as the simultaneous break-up process.

4.4 Inelastic scattering cross section of ^{16}O

In JENDL-3PR1/2, the inelastic scattering cross sections of ^{16}O were calculated by the statistical model for 29 discrete levels and a continuum state. For some low excited states, the contribution from the direct reaction process was given by the coupled-channel theory. For the (n,n_1+n_2) and (n,n_3+n_4) reaction channels, the γ-ray production cross sections measured by Nordborg et al.[39] were considered below 10 MeV. As shown in Figs. 8 and 9, the JENDL-3PR1/2 evaluations well follow their results. In the 14 MeV region, however, the JENDL-3PR1/2 evaluations apparently overestimate. In making the JENDL-3T evaluation, the JENDL-3PR1/2 curves were smoothed and renormalized to the data around 14 MeV. The results are shown by the solid lines.

The angular distributions for some levels were also inadequately given in JENDL-3PR1/2 evaluations. An example is shown in Fig. 10 for the (n,n_1+n_2) reaction. In the JENDL-3T file, a curve represented by the solid line is stored considering the experimental data.

4.5 The DDX data

In the present subsection, the DDX data reproduced from the JENDL-3T file are compared with the experimental data[36,37,40] except ^{2}H. The comparison here is mostly restricted to the 14 MeV region. Results are shown in Figs. 11 - 19. The DDX reproduced from the present evaluation is represented by the histograms.

^{6}Li, ^{7}Li and ^{12}C

As shown in Figs. 11 - 14, the present evaluation can reproduce the measured data very well. The agreement is especially good for ^{7}Li and ^{12}C. For ^{6}Li, however, there are some disagreements compared with the experimental data in the secondary neuron energy range of 8 - 12 MeV in the forward angles. There may be some effects of the final-state interactions not considered in the present evaluation. The status is, however, considered to be quite satisfactory for these nuclides.

^{9}Be

Results are shown in Fig. 15. The present evaluation cannot reproduce the spectrum in the 4 - 11 MeV region for forward angles at 14 MeV. At 7 MeV, the status is almost the same, as shown in the lower figure. This is partly because in the ENDF/B-V format, only four discrete levels are allowed to emit the second neutron in the (n,2n) reaction. For the (n,2n) reactions, the pseudo-level representation cannot be used, because it will count the cross section twice. Therefore, to incorporate the energy-angle correlation, there seems to be no other way than to use File 6.

^{14}N

Fig. 16 shows the results for ^{14}N. Apparently the present evaluation cannot reproduce the measured data well. Because the evaluation for this nuclide has been just finished, some revisions of the data will be performed in the near future.

^{16}O

In Fig. 17 shown are the results. The part just below the elastic scattering peak is due to experimental uncertainties, because there are no levels corresponding to that energy region. Besides the very low energy region, the present evaluation can reproduce the measured data very well.

^{10}B and ^{11}B

Status of the data for ^{10}B and ^{11}B are plotted in Figs. 18 and 19. Although there are some disagreements in the very low energy region, the situation seems to be satisfactory considering the roles of these nuclides in fusion neutronics.

5. Threshold reaction cross sections

Some examples are presented in this section of the threshold cross sections of ^{12}C and ^{16}O.

In Figs. 20 and 21, the $^{12}C(n,d)$ and $^{12}C(n,\alpha)$ reaction cross sections are displayed. The solid lines show the data stored in JENDL-3T. In the present evaluation, the $^{12}C(n,d)$ cross section was calculated by DWBA assuming the proton pick-up mechanism. The bound state wave function for the p + ^{11}B system was calculated by the separation-energy method. The calculation was normalized to 26 mb at 17.5 MeV, which was estimated from the inverse reaction cross section. The $^{12}C(n,\alpha)$ reaction cross section was evaluated by the spline-function fitting. This cross section is really the $^{12}C(n,\alpha_0)$ cross section. The $^{12}C(n,n')3\alpha$ reaction cross section was interpreted as the continuum inelastic scattering cross section.

The $^{16}O(n,p)$ and $^{16}O(n,\alpha)$ reaction cross sections are shown in Figs. 22 and 23. They were evaluated on the basis of experimental data with the least-squares function fitting method.

6. Photon production cross sections

For ^{1}H to ^{12}C, some discrete γ-rays were considered and their multiplicities were given. For ^{14}N, ^{16}O and ^{19}F, they were (will be for ^{19}F) calculated by the statistical model. Examples are shown in Figs. 24 and 25

for the secondary γ-ray spectrum from the $^{14}N(n,x)\gamma$ and $^{16}O(n,x)\gamma$ at En = 11.0 and 13.5 MeV, respectively. The experimental data were all measured at ORNL.

7. R-matrix calculations

In the present evaluations, many cross sections below several MeV were calculated with the R-matrix theory. A code named "RESCAL" was developed for this purpose[11]. Its features of it are summarized as:

1) Based on the Lane-Thomas formalism[42]. The U-matrix is calculated by the real eigenvalue expansion method,
2) Only neutron can be treated as the incident particle. On the other hand, n, p, d, t, ^{3}He and α particles are treated as emitted particles,
3) Up to 5 levels are considered for each $J\pi$,
4) Up to 10 partition channels are incorporated,
5) The maximum orbital angular momentum should be as much as 9,
6) Both the channel spin and j-j coupling schemes for spin coupling are incorporated,
7) Parameters can be searched automatically,
8) Calculated results are written on a disk file in the ENDF/B format, and
9) The background matrix is only diagonal. But it can be dependent on the incident neutron energy quadratically.

In Figs. 26 - 28 shown are some examples of cross sections calculated with RESCAL (solid lines).

Fig. 26 shows the total cross section of ^{11}B. The R-matrix calculation was performed up to 7.7 MeV. This cross section was calculated in the j-j coupling scheme. The initial parameters were taken from the paper of Koehler et al.[43], but were automatically searched for to give better agreement with the experimental data. In the whole energy region, the present calculation is closer than ENDF/B-IV to the experimental values.

Fig. 27 and 28 show the total cross section of ^{12}C and ^{16}O, respectively. They were calculated in the channel spin coupling scheme. As seen, the present calculations can reproduce the experimental results very well.

8. The thermal and 14-MeV cross sections

In this section, the thermal and the 14-MeV cross sections are summarized for some important reactions. Table 6 shows a list of cross sections for these reactions, compared with JENDL-2, ENDF/B-V (B-IV for some reactions) and BNL-325 (4-th edition)[18].

With regard to the thermal cross sections, the present evaluations are in good agreement with those given in JENDL-2 and BNL-325. The exception is the $^{10}B(n,t)$ cross section. The value in JENDL-2, which was taken from ENDF/B-IV, seems to have no foundation. The JENDL-3T value is based on a value reported by Cserpak et al.[44] However, the most recent value reported by Kavanagh after its evaluation is 7 ± 2 mb[45] and Qaim et al. obtained values somewhat higher than that preliminary[46]. The situation for this cross section is confusing at present.

For the 14-MeV cross section, they are updated in the present evaluations taking account of the up-to-date data.

9. Problems in JENDL-3T in this mass range

Although the JENDL-3T has been just compiled, there seem to be already some problems in it. A part of them will be reviewed here.

1) The total cross section of ^{7}Li might be larger than the JENDL-3T evaluation around 14 MeV by about 3 %. The situation is shown in Fig. 29.
2) The inelastic scattering cross section to the second 4.63-MeV state of ^{7}Li would be smaller than the present evaluation below 14 MeV, as shown in Fig. 30.
3) The (n,2n) reaction cross sections for some important nuclides, e.g., ^{6}Li, ^{7}Li and ^{9}Be, might have large errors because in 14 MeV region the experimental data are very scarce. The status is shown in Fig. 31 and 32.
4) Treatment of the emission neutron spectrum from ^{9}Be would be inadequate,
5) The DDX data for some nuclides will not be accurately enough,

6) For some of such important reactions as $^{1}H(n,n)$, $^{6}Li(n,t)\alpha$, $^{7}Li(n,n't)\alpha$ and $^{10}B(n,\alpha)$, covariance files should be necessary, and
7) From analysists of integral experiments, the total cross section of ^{16}O was pointed out to be too high in the 2 - 8 MeV region. The present evaluation was based on the high resolution data of Cierjacks et al.[47] above 3 MeV. However, as shown in Figs. 28 and 33, the present evaluation also follows other experimental data as well. Although a re-examination of the microscopic data might be needed, the reason is not clear at present.

9. Concluding remarks

Status of the light nuclides' neutron nuclear data stored in JENDL-3T was reviewed putting a weight on uses in the fusion neutronics. The present evaluations were performed taking account of the recently measured data. Improvements were achieved especially in the tritium production cross sections and the energy-angular distribution of the secondary neutrons. The photon production cross section was newly included for some important nuclides. Cross sections below several MeV were mainly calculated with the R-matrix theory.

Acknowledgment

The author would like to thank Dr. K. Shibata of JAERI Nuclear Data Center for fruitful discussion. He is also grateful to Dr. T. Fukahori of JAERI N.D.C. for offering many graphs, especially those of the DDX. He also acknowledges Drs. S. Igarasi, T. Nakagawa of JAERI N.D.C., M. Mizumoto of JAERI linac laboratory and K. Hasegawa of Tohoku University for helpful comments and discussions.

References

1) Nakagawa T.(ed.): "Summary of JENDL-2 General Purpose File", JAERI-M 84-103(1984).
2) Shibata K. and Kikuchi Y.: Radiation Effects, 96, 243(1986).
3) Shibata K.: "Evaluation of Neutron Nuclear Data of ^{6}Li for JENDL-3",

JAERI-M 84-198(1984).
4) Shibata K.: "Evaluation of Neutron Nuclear Data of ^{7}Li for JENDL-3", JAERI-M 84-204(1984).
5) Shibata K.: "Evaluation of Neutron Nuclear Data of ^{9}Be for JENDL-3", JAERI-M 84-226(1984).
6) Shibata K.: "Evaluation of Neutron Nuclear Data for ^{12}C", JAERI-M 83-221(1983).
7) Chiba S.: "Revision of the Neutron Nuclear Data of Lithium", JAERI-M 86-029, 32(1986).
8) Shibata K., Narita T. and Igarasi S.: "Evaluaion of Neutron Nuclear Data for Deuterium", JAERI-M 83-006(1983).
9) Igarasi S.: "Program ELIESE-3; Program for Calculation of the Nuclear Cross Sections by Using Local and Non-local Optical Models and Statistical Model", JAERI 1224(1972).
10) Igarasi S.: "CASTHY", private communication.
11) Komoda S., Shibata K., Chiba S. and Igarasi S.: "RESCAL", private communication.
12) Sugi T., Nakagawa T., Nishigori, T. and Iijima S.:"Calculation of Double Differential Cross Sections for Structural Materials by PEGASUS Code", presented in this seminar.
13) Kunz P.D.: "DWUCK4", private communication.
14) Young P.G. and Arthur E.D.: "GNASH: A Preequilibrium, Statistical Nuclear-Model code for Calculation of Cross Sections and Emission Spectra", LA-6947(1978); private communication.
15) Shibata K. and Fu C.Y.: "Recent Improvements of the Statistical Model Code", ORNL/TM-10093(1986).
16) Macklin R.L., Ingle R.W. and Halperin J.: Nucl. Sci. Eng., 71, 205(1979).
17) Hale G.M., Stewart L. and Young P.G.: "The ^{6}Li(n,t)^{4}He cross section", BNL-NCS-51619, 25(1982).
18) Mughabghab S.F., Divadeenam M. and Holden N.E.: "Neutron Cross Section", Vol. 1, Part A, Academic Press (1981).
19) Bartle C.M.: Nucl. Phys., A330, 1(1979).
20) Bartle C.M., Gebbie D.W. and Hollas C.L.: Nucl. Phys., A397, 21(1983).
21) Smith D.L., Meadows J.W., Bretsher M.M. and Cox S.A.: "Cross-section measurement for the ^{7}Li(n,n't)^{4}He reaction at 14.74 MeV",

ANL/NDM-87(1984).

22) Liskien H., Wolfle R. and Qaim S.M.: "Determination of $^{7}Li(n,n't)^{4}He$ cross sections", Proc. Int. Conf. on Nuclear Data for Science and Technology, Antwerp 1982, 349(1983).

23) Maekawa H., Tsuda K., Iguchi T., Ikeda Y., Oyama Y., Fukumoto T., Seki Y. and Nakamura T.: "Measurements of tritium production-rate distributions in a simulated blanket assemblies at the FNS", JAERI-M 83-196(1983).

24) Maekawa H.: private communication.

25) Swinhoe M.T. and Uttley C.A.: Nucl. Sci. Eng. 89, 261(1985).

26) Takahashi A., Yugami K., Kohno K., Ishigaki N., Yamamoto J. and Sumita K.: Proc. 13th Symp. Fusion Technology, Padua, Italy, September 1984, 1325, Pergamon Press, Oxford(1984).

27) Goldberg E., Barber R.L., Barry P.E., Bonner N.A., Fontanilla J.E., Griffin C.M., Haight R.C., Nethaway D.R. and Hudson G.B.: Nucl. Sci. Eng. 91, 173(1985).

28) Qaim S.M. and Wolfle R.: Nucl. Sci. Eng. 96, 52(1987).

29) Young P.G.: private communication.

30) Boedy Z.T., Cserpak F., Csikai J., Sudar S. and Mihaly K.: "Measurement and Evaluation of (n,t) Cross Sections", Proc. Int. Conf. on Nuclear Data for Science and Technology, Antwerp 1982, 368(1983).

31) Liskien H., Widera R., Wolfle R. and Qaim S.M.: to be published in Nucl. Sci. Eng.

32) Frehaut J., Bertin A., Bois R., Gryntakis E. and Philis A.A.: Radiation Effects, 96, 219(1986).

33) Faddeev L.D.: Sov. Phys.-JETP, 12, 1014(1961)

34) Ebenhoh W.: Nucl. Phys., A191, 97(1972).

35) Holland R.E., Elwyn A.J., Davids C.N., Lynch F.J., Meyer-Schutzmeister L., Monahan J.E., Mooring F.P. and Ray Jr. W.: Phys. Rev., 19, 592(1979).

36) Chiba S., Baba M., Nakashima H., Ono M., Yabuta N., Yukinori S. and Hirakawa N.: Jour. Nucl. Sci. Technol., 22, 771(1985).

37) Takahashi A., Yamamoto J., Murakami T., Oshima K., Oda H., Fujimoto F. and Sumita K.: Proc. Int. Conf. on Nuclear Data for Science and Technology, Antwerp 1982, 360(1983).

38) Beynon T.D. and Oastler A.J.: Ann. Nucl. Energy, 6, 537(1979).

39) Nordborg C., Nilsoon L., Conde H. and Stromberey L.G.: Nucl. Sci. Eng., 66, 75(1978).
40) Baba M., Ono M., Yabuta N., Kikuchi T. and Hirakawa N.: Radiation Effects, 92, 223(1986).
41) Takahashi A.: private communication.
42) Lane A.M. and Thomas R.G.: Rev. Modern Physics, 30, 257(1958).
43) Koehler P.E., Knox H.D., Resler D.A., Lane R.O. and Millener D.J.: Nucl. Phys., A394, 221(1983).
44) Cserpak F., Biro T, and Csika J.: "Measurement of Cross-Sections for /n,t/ Reactions on Light Nuclei", Proc. Int. Conf. on Neutron Physics and Nuclear Data for Reactors and other Applied Purposes, Harwell U.K., Sep. 1978, p.761(1978).
45) Kavanagh R.W. and Marcley R.G.: Phys. Rev., 36, 1194(1987).
46) Qaim S.M.: private communication.
47) Cierjacks S., Hinterberger F., Schwalz G., Erbe D., Rowwen P.V. and Leugers B.: Nucl. Instr. Methods, 169, 185(1980).

Table 1 A list of fusion-related nuclides to be stored in JENDL-3.

Atomic Number	Chemical Symbol	Mass Number*
1	H	1, 2
2	He	3, 4
3	Li	6, 7
4	Be	9
5	B	10, 11
6	C	12
7	N	14
8	O	16
9	F	19
11	Na	23
13	Al	27
14	Si	N, 28, 29, 30
19	K	N, 39, 40, 41
20	Ca	N, 40, 42, 43, 44, 46, 48
22	Ti	N, 46, 47, 48, 49, 50
23	V	51
24	Cr	N, 50, 52, 53, 54
25	Mn	55
26	Fe	N, 54, 56, 57, 58
27	Co	59
28	Ni	N, 58, 59, 60, 61, 62, 64
29	Cu	N, 63, 65
30	Zr	N
41	Nb	93, 94
42	Mo	N, 92, 94, 95, 96, 97, 98,100
74	W	N,180,182,183,184,186
82	Pb	N,204,206,207,209
83	Bi	209

* : N denotes the natural element

Table 2 A list of evaluator(s) and application uses of each nuclide.

Nuclide	Evaluator(s)	Uses in nuclear measurements and application fields
H-1	K.Shibata	Standard σ, Coolant, Shielding, Structural mat.
H-2	K.Shibata,T.Narita, S.Igarasi	Fuel, Cannon ball target
He-3	K.Shibata	Standard σ, T-breeder
He-4	K.Shibata	Coolant
Li-6	K.Shibata,S.Chiba	T-breeder, Standard σ, Coolant
Li-7	K.Shibata,S.Chiba	T-breeder, Coolant
Be-9	K.Shibata	Neutron multiplier, T-breeder, Coolant
B-10	S.Chiba	Standard σ, Shielding, Control rod, T-breeder
B-11	T.Fukahori	T-breeder, Shielding, First wall
C-12	K.Shibata	Standard σ, Structural m., Moderator, First wall
N-14	FRNNDESWG*(1)	Coolant, Air (Sky shine)
O-16	FRNNDESWG*(2)	Blanket component, Coolant, Air, Shielding
F-19	T.Sugi	Coolant, Thermal shield, Dosimetry

* : Fusion-related neutron nuclear data evaluation sub-working group organized in JNDC, whose members are ;
Y.Kanda(1,2), T.Murata(1,2), S.Tanaka(1), T.Asami(1,2), Y.Nakajima(1), K.Shibata(1,2), T.Fukahori and S.Chiba(1)

Table 3 A list of evaluated quantities for each nuclide (except for the total and elastic scattering cross sections).

Nuclide	Evaluated Quantities								
	(n,n')	(n,γ)	(n,2n)	(n,p)	(n,d)	(n,t)	(n,α)	(n,n'p)	(n,n'α)
^{1}H ＊		○							
^{2}H		○	○						
^{3}He				○	○	(○)			
^{4}He									
^{6}Li ＊	○	○	○	○		○	(○)		(○)
^{7}Li ＊	○	○	○		○	○			(○)
^{9}Be ＊	○	○	○	○	○	○	○		
^{10}B	○	○	○	○	○	○			
^{11}B	○	○	○	○			○	○	○
^{12}C ＊	○	○		○	○		○		
^{14}N ＊	○	○	○	○		○	○	○	○
^{16}O ＊	○	○	○	○	○		○		
^{19}F ＊	○	○	○	○	○	○	○	○	○

＊ : photon production data are included

Table 4 A list of nuclides included in various evaluated files.

Nuclide	JENDL-1	JENDL-2	JENDL-3RR1/2	JENDL-3T	ENDF/B-V
H-1	○	○		○	○
H-2		○		○	○
He-3				○	○
He-4				○	○
Li-6	○	○	○	○	○
Li-7		○	○	○	○
Be-9		○	○	○	○
B-10	○	○		○	○
B-11				○	○
C-12	○	○	○	○	○
N-14				○	○
O-16			○	○	○
F-19		○		○	○

Table 5 A list of computer programs used in the present evaluations.

Nuclide	Low energy region	Inelastic Stat.	Inelastic Direct	Threshold	Spectrum Neutron	Spectrum Gamma-ray
H-1						
H-2			(FADDEEV)		(FADDEEV)	
He-3	RESCAL					
He-4	RESCAL					
Li-6	RESCAL		ECIS79	RESCAL	(Three body model)	
Li-7	RESCAL		ECIS79	DWUCK4	(Three body model)	
Be-9	RESCAL	CASTHY		ELIESE-3	(Sequential decay model)	
B-10	RESCAL		DWUCK4	DWUCK4,GNASH	(Three body model)	
B-11	RESCAL,RESENDD	TNG	DWUCK4	TNG	TNG	
C-12	RESCAL			DWUCK4		
N-14	RESCAL	GNASH	DWUCK4	GNASH	GNASH	GNASH
O-16	RESCAL	CASTHY			GNASH	GNASH
F-19	RESENDD			PEGASUS	PEGASUS	

RESCAL --- R-matrix theory.
RESENDD --- Resonance calculation.
CASTHY,ELIESE-3 --- Statistical model with width fluctuation.
GNASH,TNG,PEGASUS --- Statistical and exciton models.
DWUCK4 --- DWBA.
ECIS79 --- Coupled-channel theory.

Table 6 A list of the thermal and 14-MeV cross sections for some important reactions.

Reaction	JENDL-2		JENDL-3T		BNL325(4-th)	ENDF/B-V*
	Thermal	14 MeV	Thermal	14 MeV	Thermal	14 MeV
$^{1}H(n,n)H$	20.44	0.6920	20.474	0.6920	20.491±0.0140	0.6929
$^{1}H(n,\gamma)^{2}H$	0.3320	2.983×10^{-5}	0.3320	2.983×10^{-5}	0.3326±0.0002	2.983×10^{-5}
$^{3}He(n,p)t$	---	----	5328	0.1397	5333 ±7	0.1220
$^{6}Li(n,t)\alpha$	936.3	0.02574	940.33	0.0280	940 ±4	0.0260
$^{7}Li(n,n't)\alpha$	---	0.3191	---	0.3029	----------	0.3350(IV)
$^{7}Li(n,2n)^{6}Li$	---	0.0550	---	0.07009	----------	0.0550(IV)
$^{9}Be(n,2n)2\alpha$	---	0.5140	---	0.5427	----------	0.5220(IV)
$^{9}Be(n,t)^{7}Li$	---	0.01547	---	0.0184	----------	0.0180(IV)
$^{10}B(n,\alpha)^{7}Li$	3836.5	0.06022	3837	0.0483	3837 ±9	0.06022
$^{10}B(n,t)2\alpha$	0.00057	0.08865	0.050	0.0888	----------	0.08865
$^{11}B(n,t)^{9}Be$	---	----	---	Not Yet	----------	0.0015(IV)
$^{12}C(n,n)^{12}C$	4.699	0.7379	4.746	0.7947	4.746 ±0.002	0.7379(IV)
$^{19}F(n,2n)^{18}F$	---	0.04294	Not	Yet	----------	0.0490(IV)
$^{19}F(n,t)^{17}O$	---	0.0150	Not	Yet	----------	0.00763(IV)

* : Values indicated with (IV) were taken from ENDF/B-IV, because for those nuclides ENDF/B-V is not available.

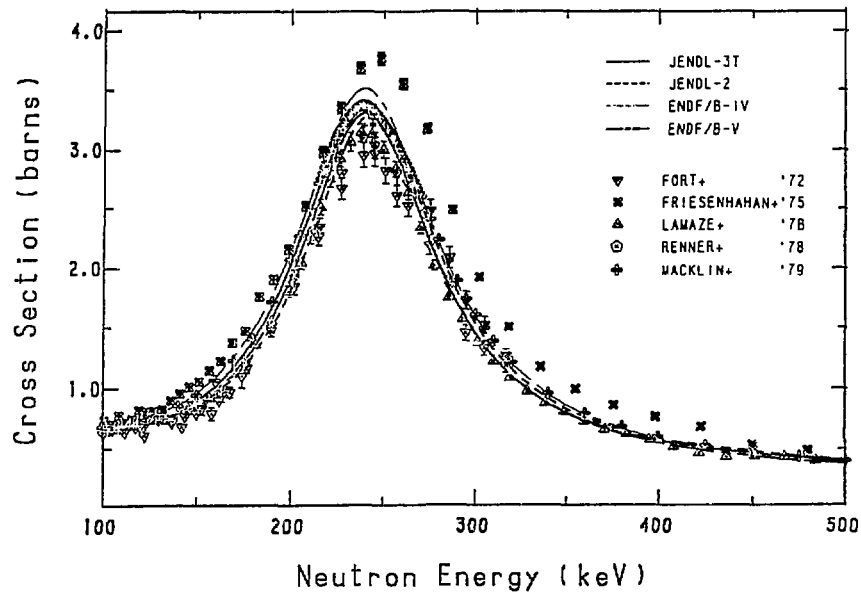

Fig. 1 The $^{6}Li(n,t)\alpha$ reaction cross section around the $P_{5/2}$ resonance.

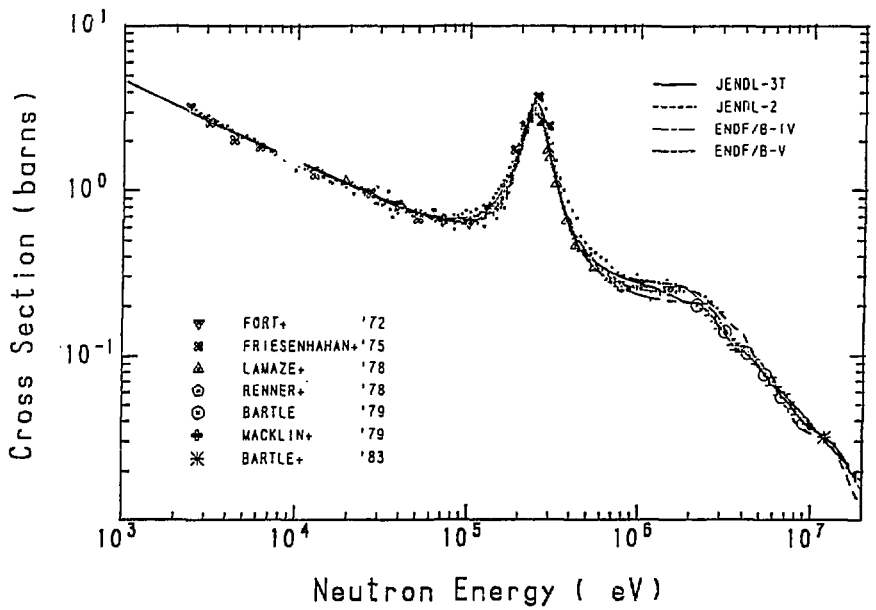

Fig. 2 The $^{6}Li(n,t)\alpha$ reaction cross section from 1 keV to 20 MeV.

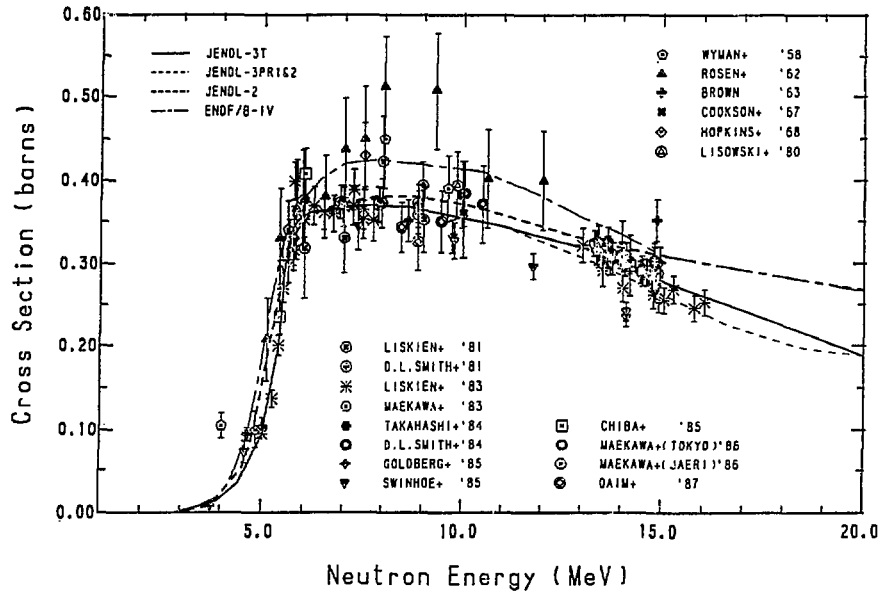

Fig. 3 The $^{7}Li(n,n't)\alpha$ reaction cross section.

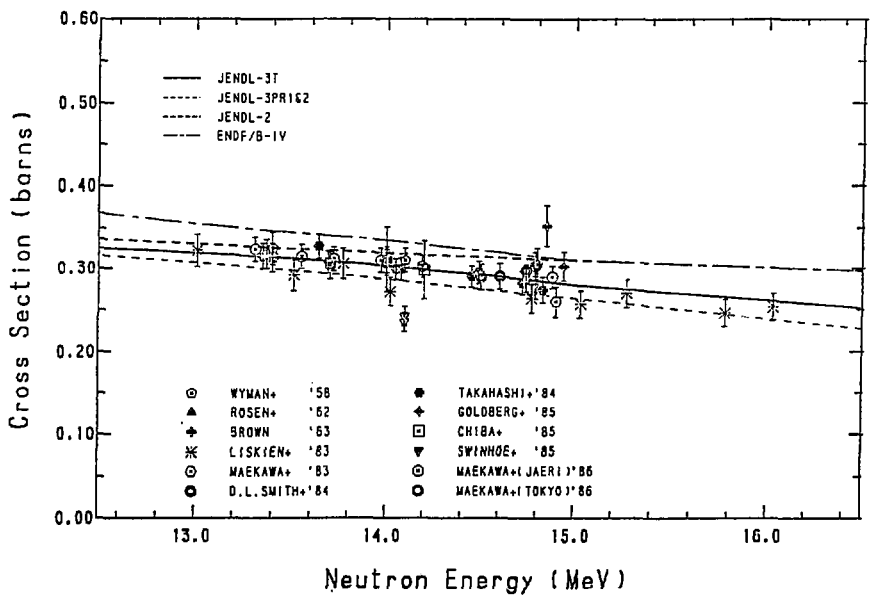

Fig. 4 The $^{7}Li(n,n't)\alpha$ reaction cross section from 12.5 to 16.5 MeV.

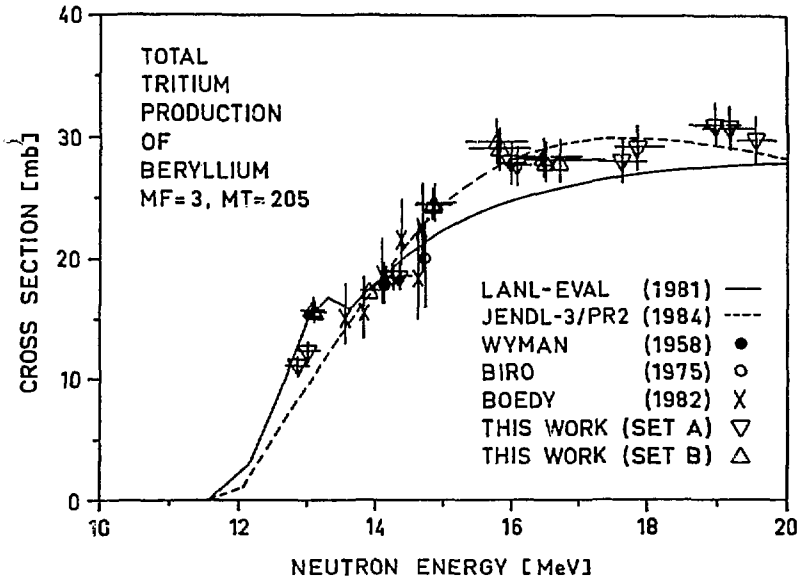

Fig. 5 The total tritium production cross section of ^{9}Be.

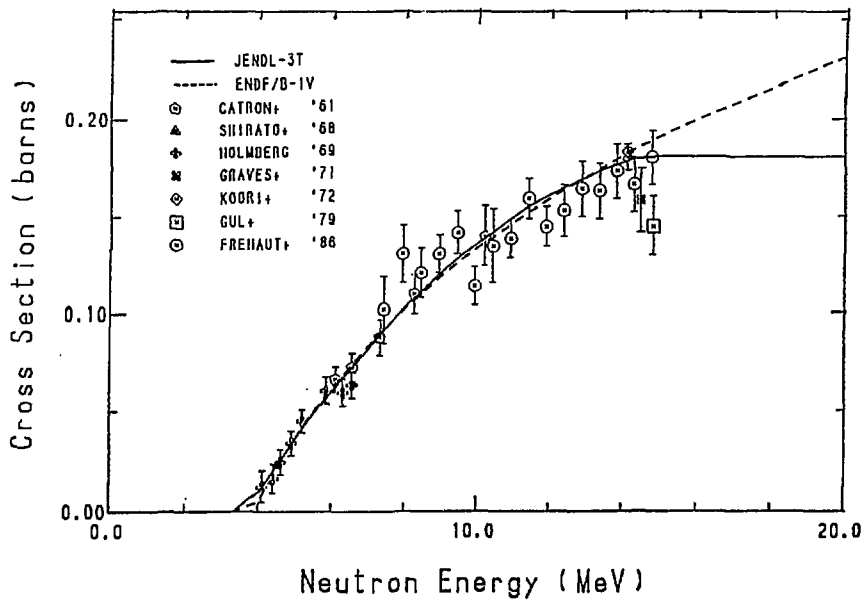

Fig. 6 The $^{2}H(n,2n)p$ cross section.

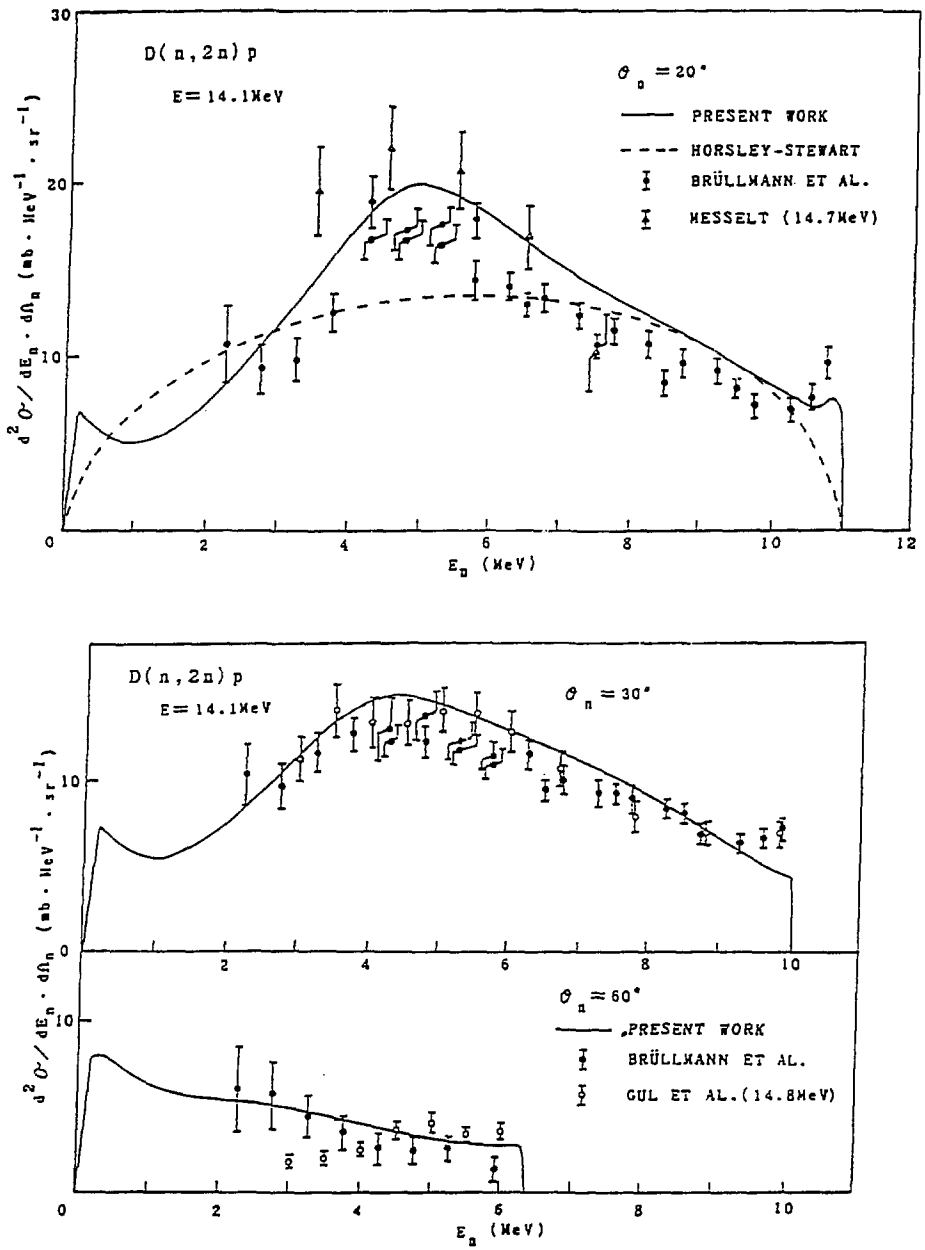

Fig. 7 Measured and calculated double-differential cross sections for the $^{2}H(n,2n)p$ reaction at 14.1 MeV.

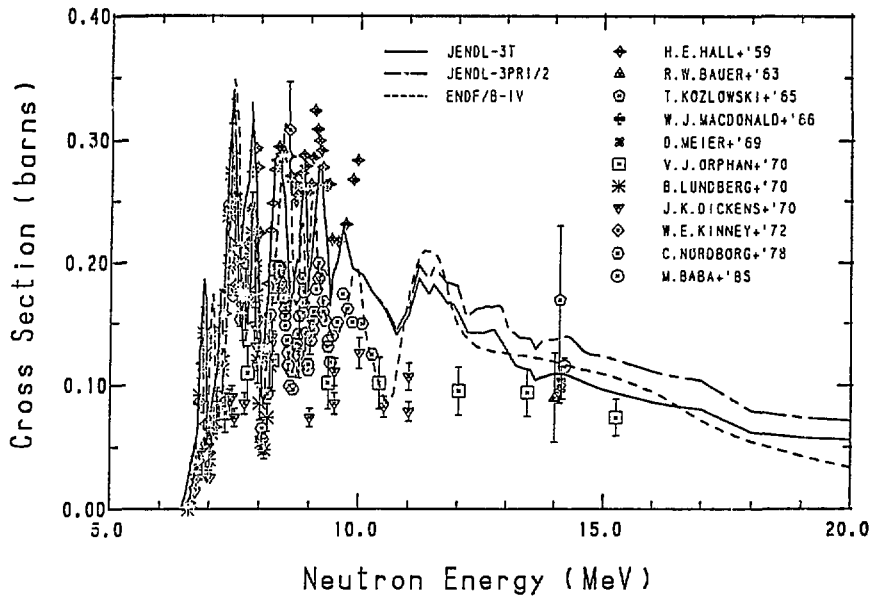

Fig. 8 The $^{16}O(n,n1+n2)$ reaction cross section (Q=-6.049, -6.130 MeV).

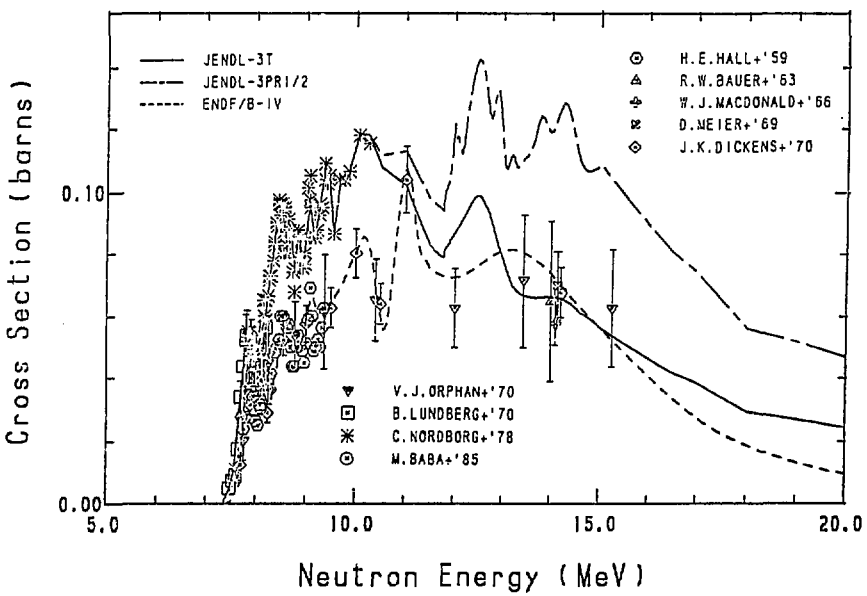

Fig. 9 The $^{16}O(n,n3+n4)$ reaction cross section (Q=-6.917, -7.117 MeV).

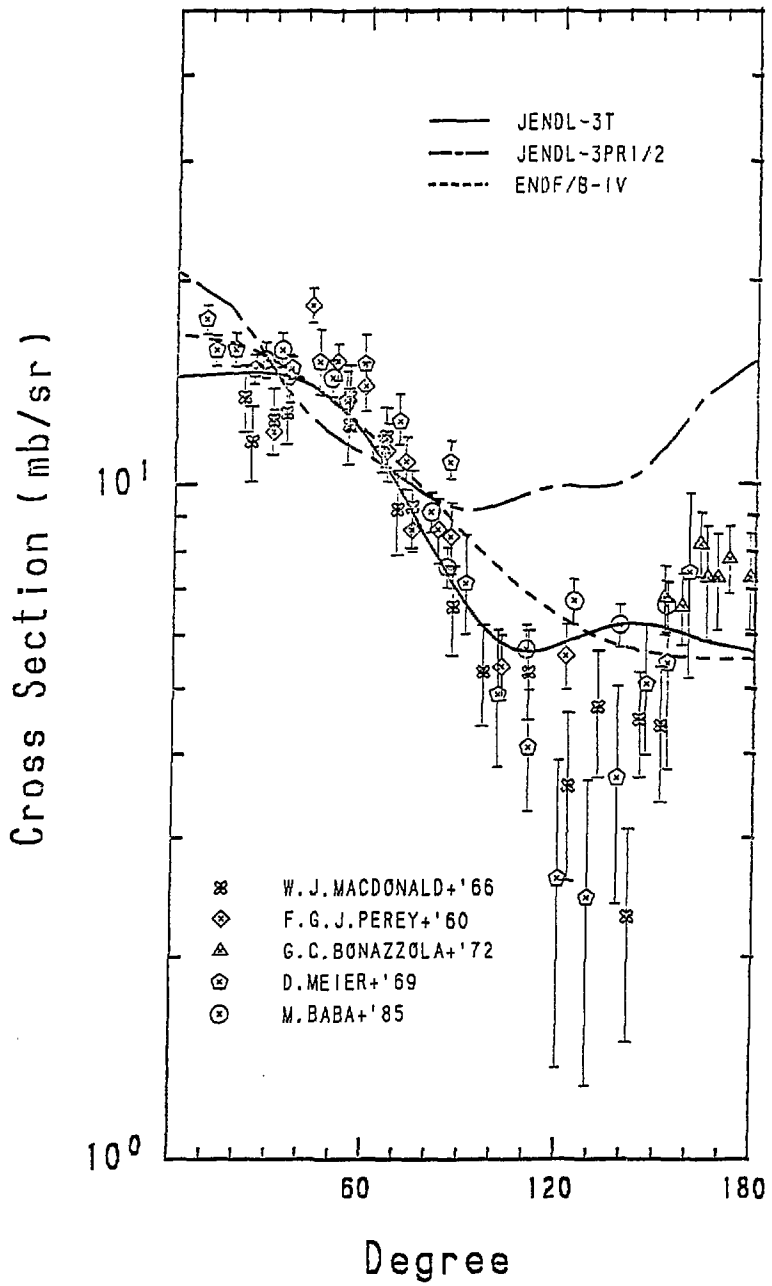

Fig. 10 The angular distribution of the $^{16}O(n,n1+n2)$ reaction.

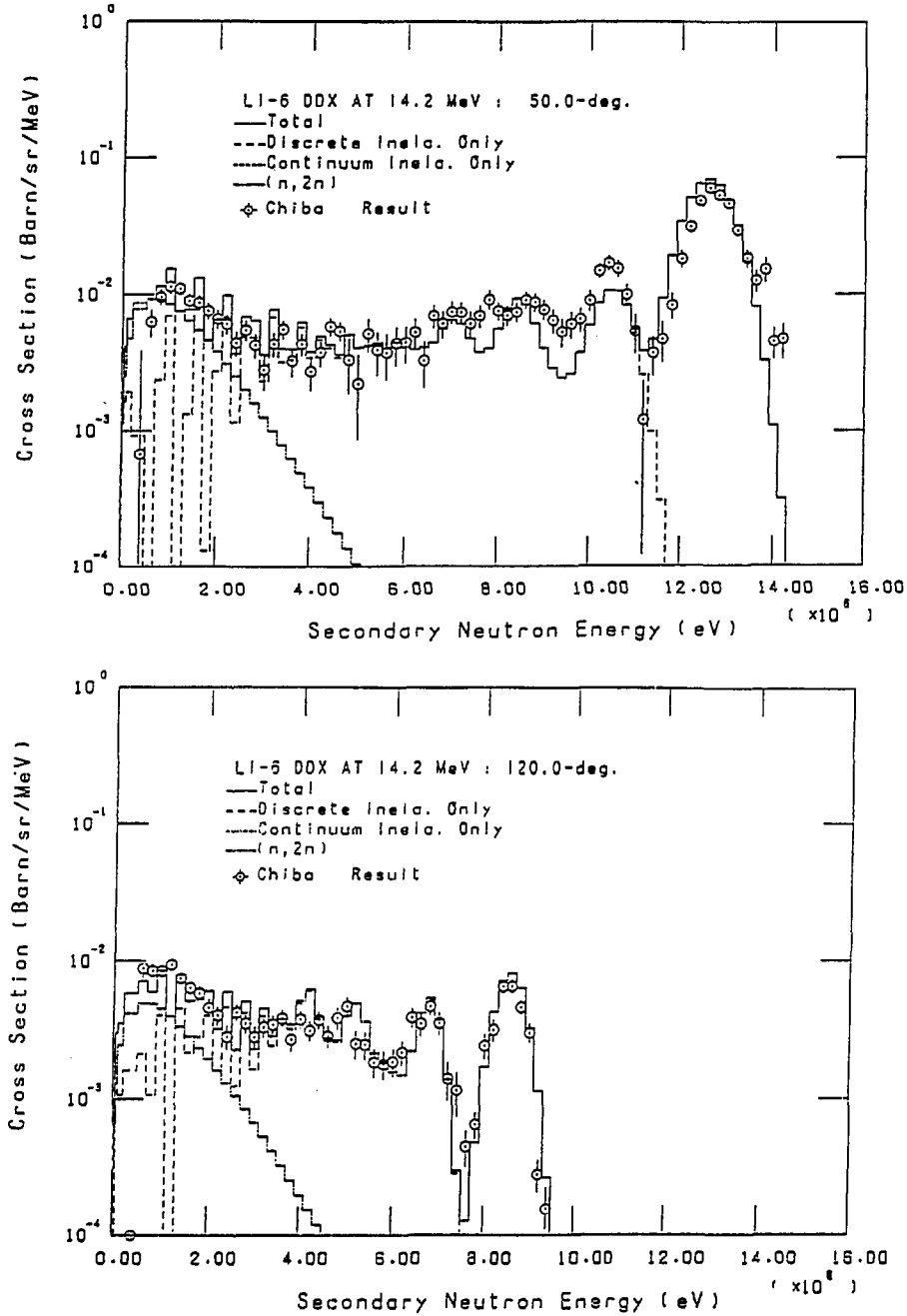

Fig. 11 Measured and evaluated DDX of ^{6}Li at 14.2 MeV.

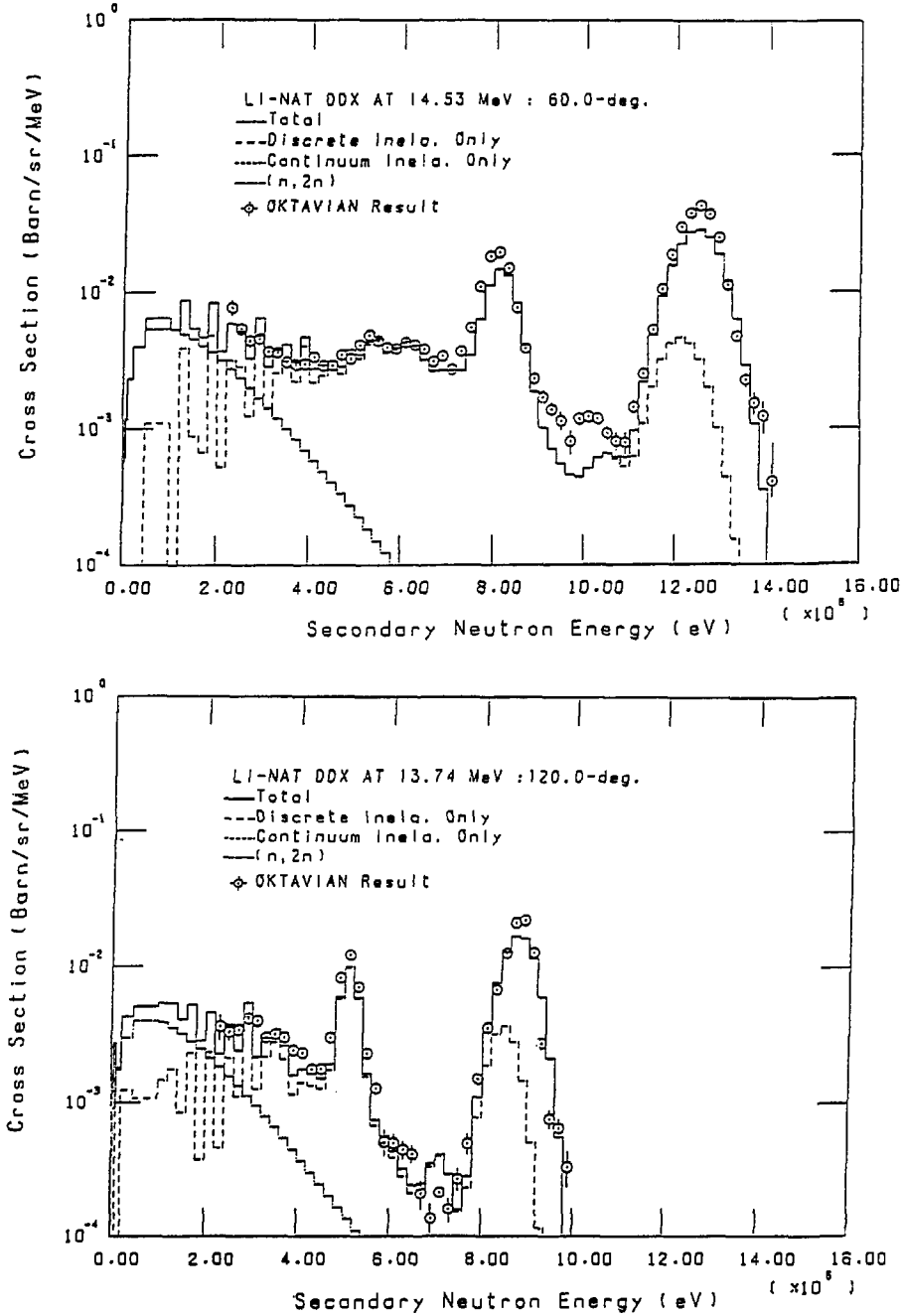

Fig. 12 Measured and evaluated DDX of ^{N}Li around 14 MeV.

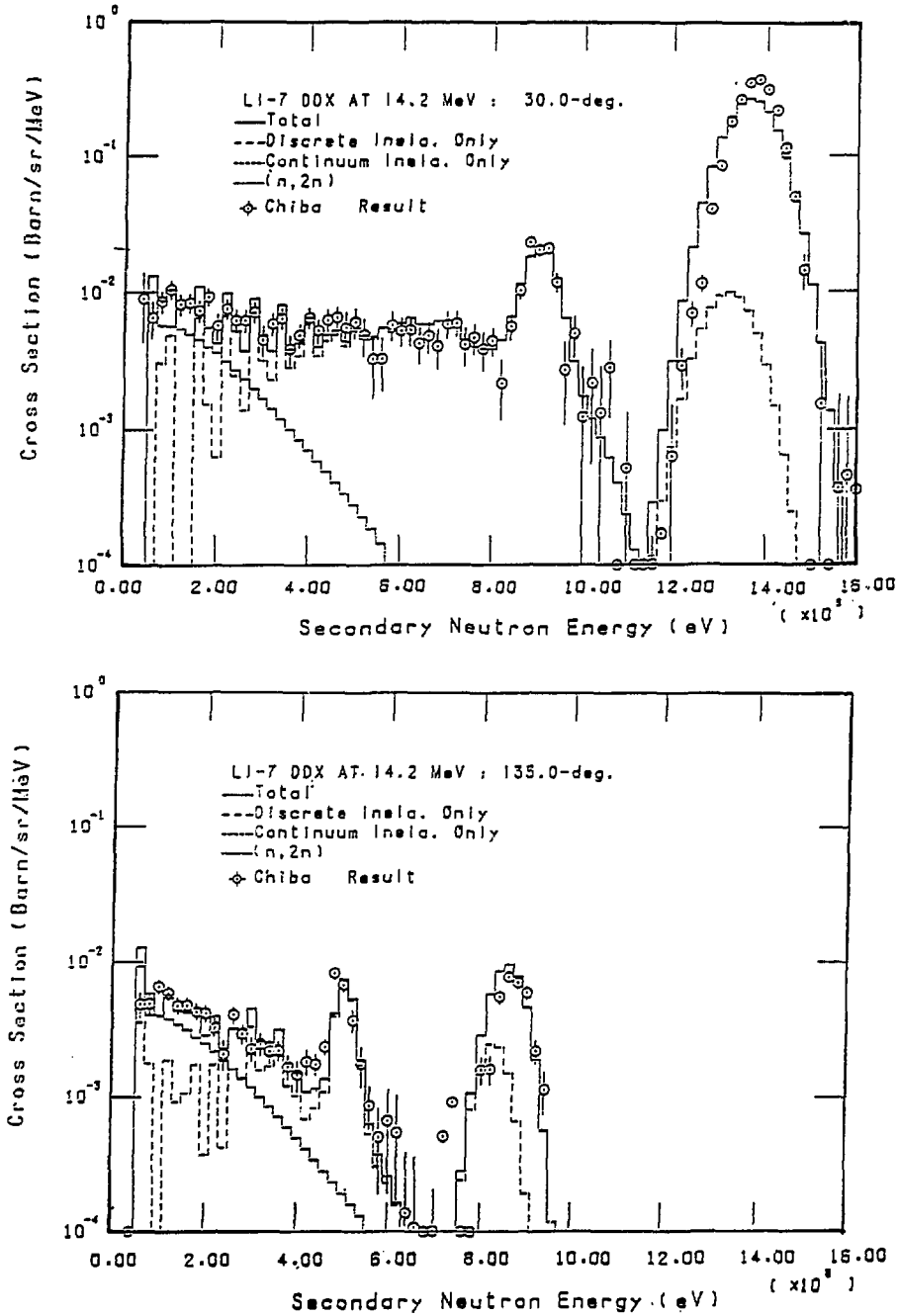

Fig. 13 Measured and evaluated DDX of ^{7}Li at 14.2 MeV.

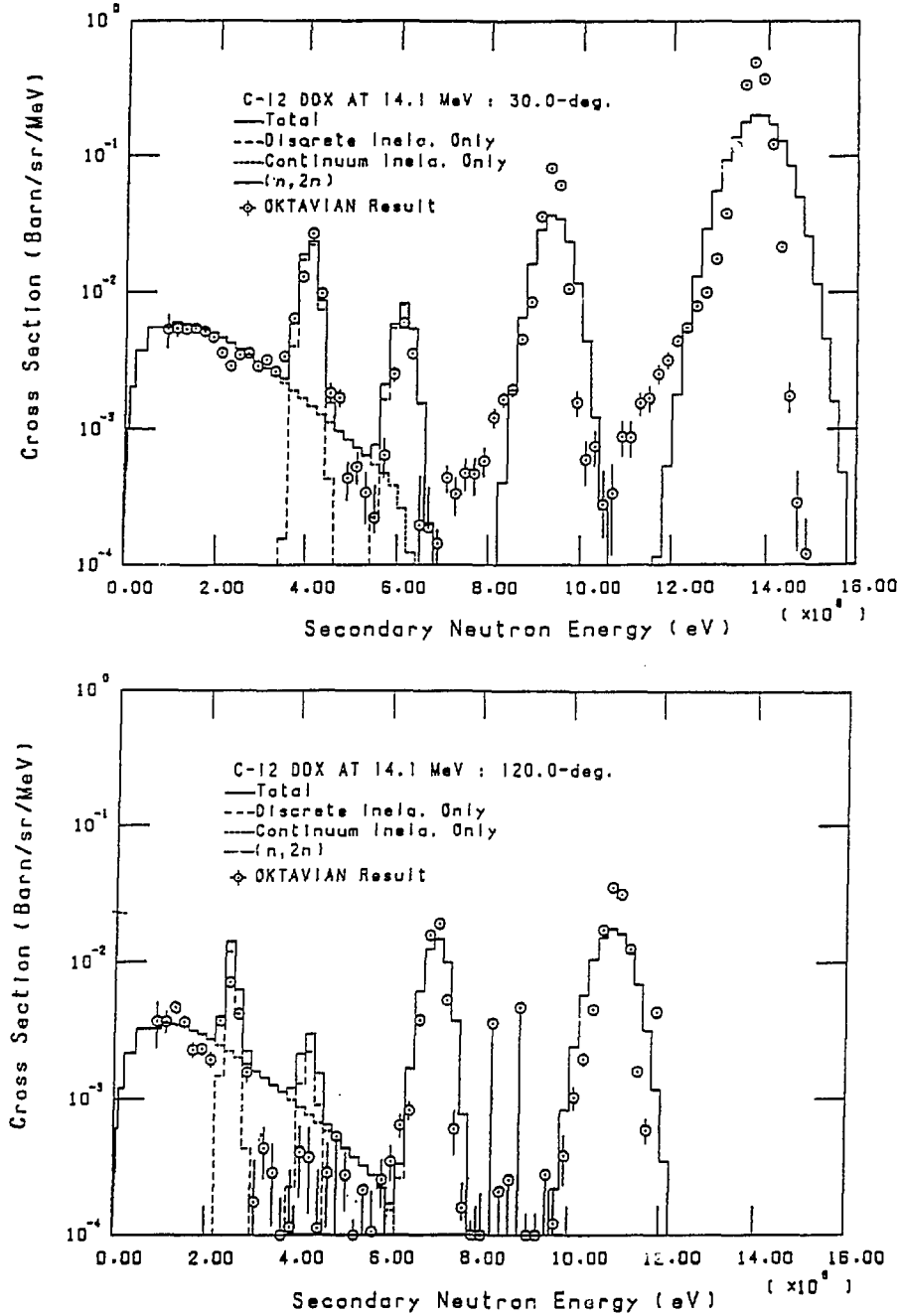

Fig. 14 Measured and evaluated DDX of ^{12}C around 14 MeV.

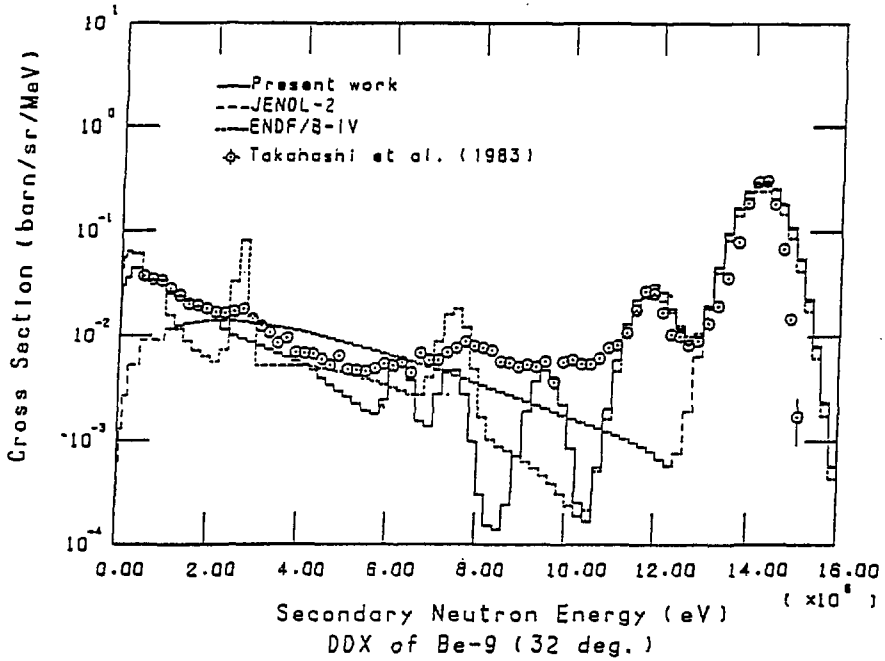

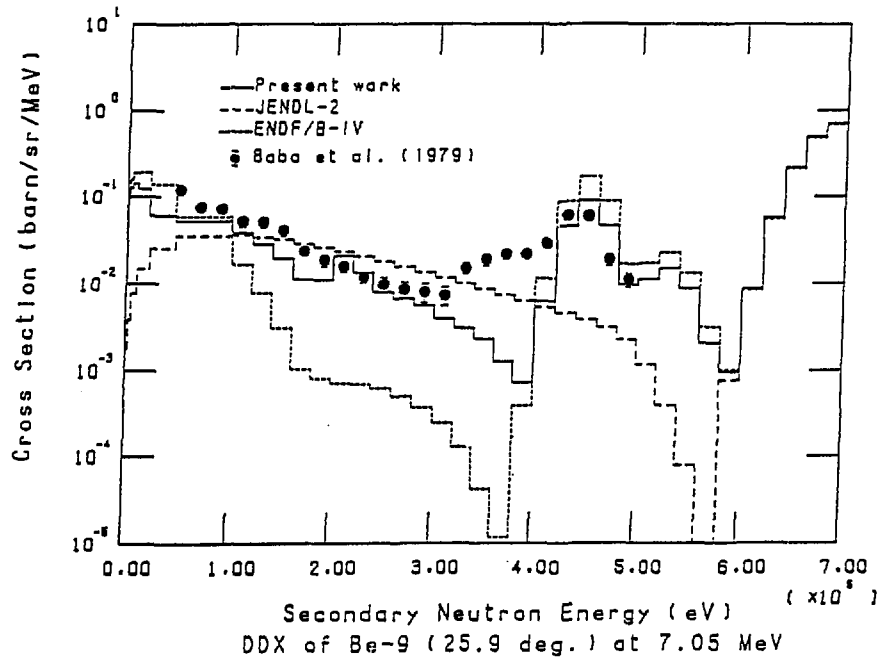

Fig. 15 Measured and evaluated DDX of ^{9}Be at 14 and 7 MeV.

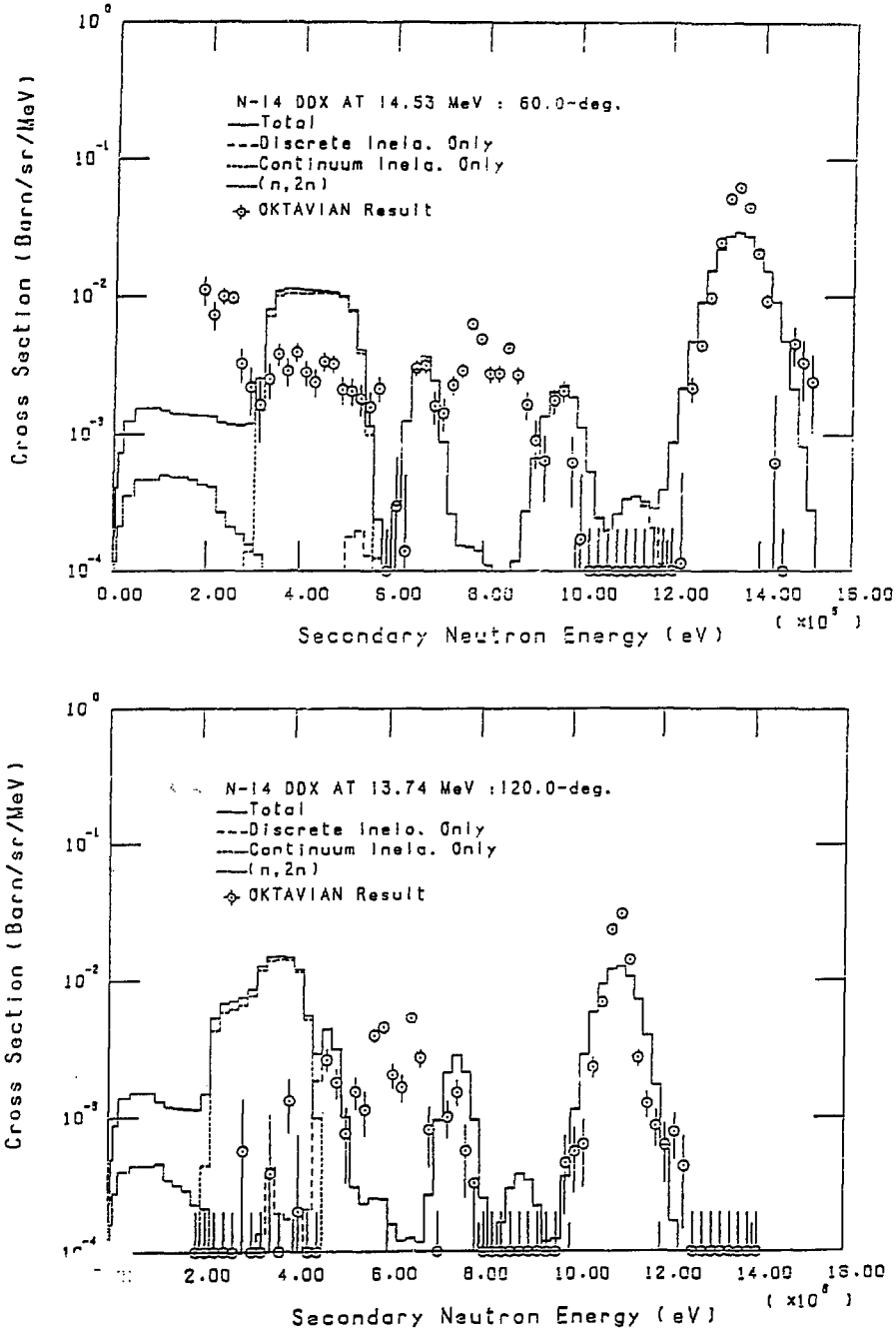

Fig. 16 Measured and evaluated DDX of ^{14}N around 14 MeV.

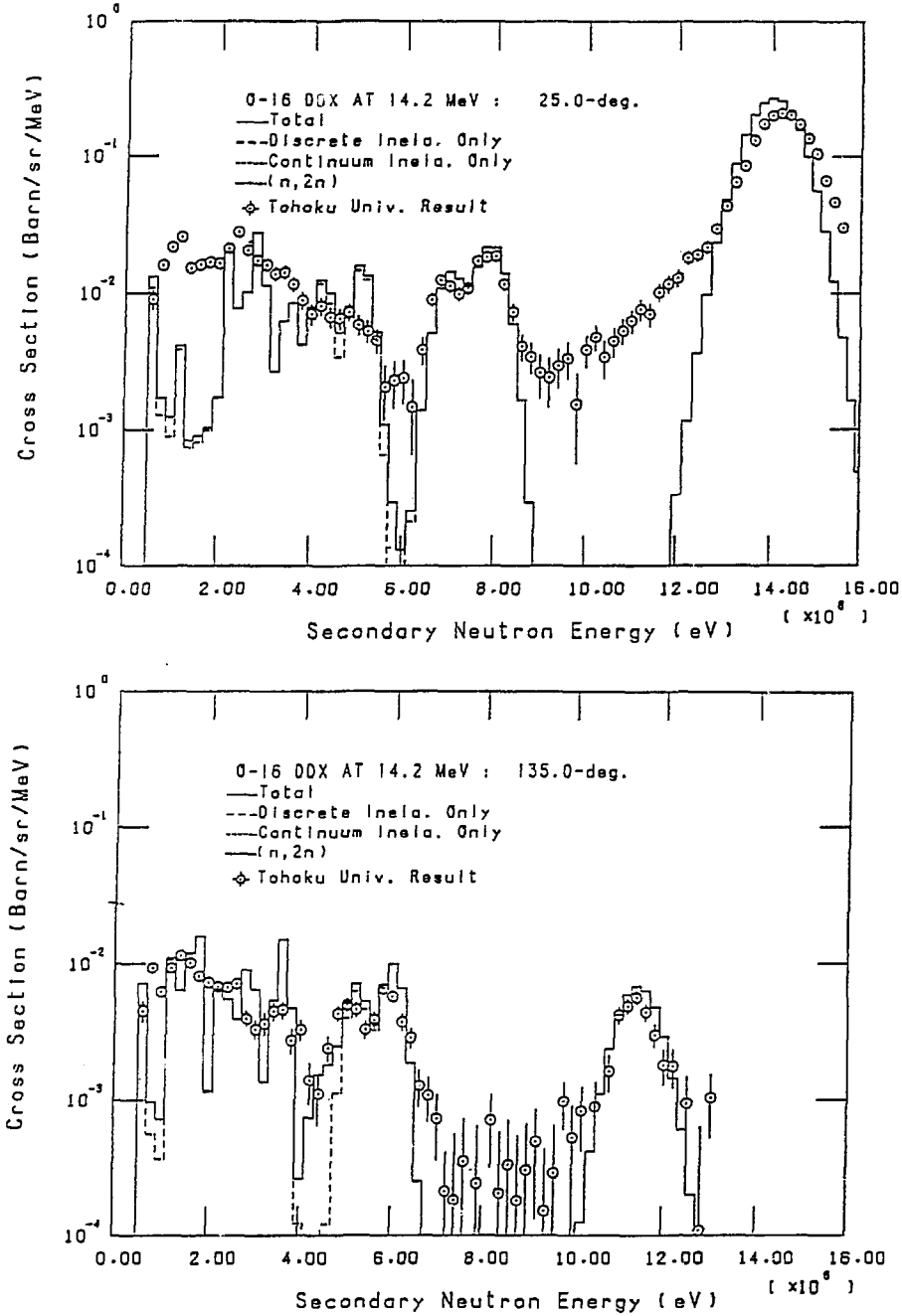

Fig. 17 Measured and evaluated DDX of ^{16}O at 14.2 MeV.

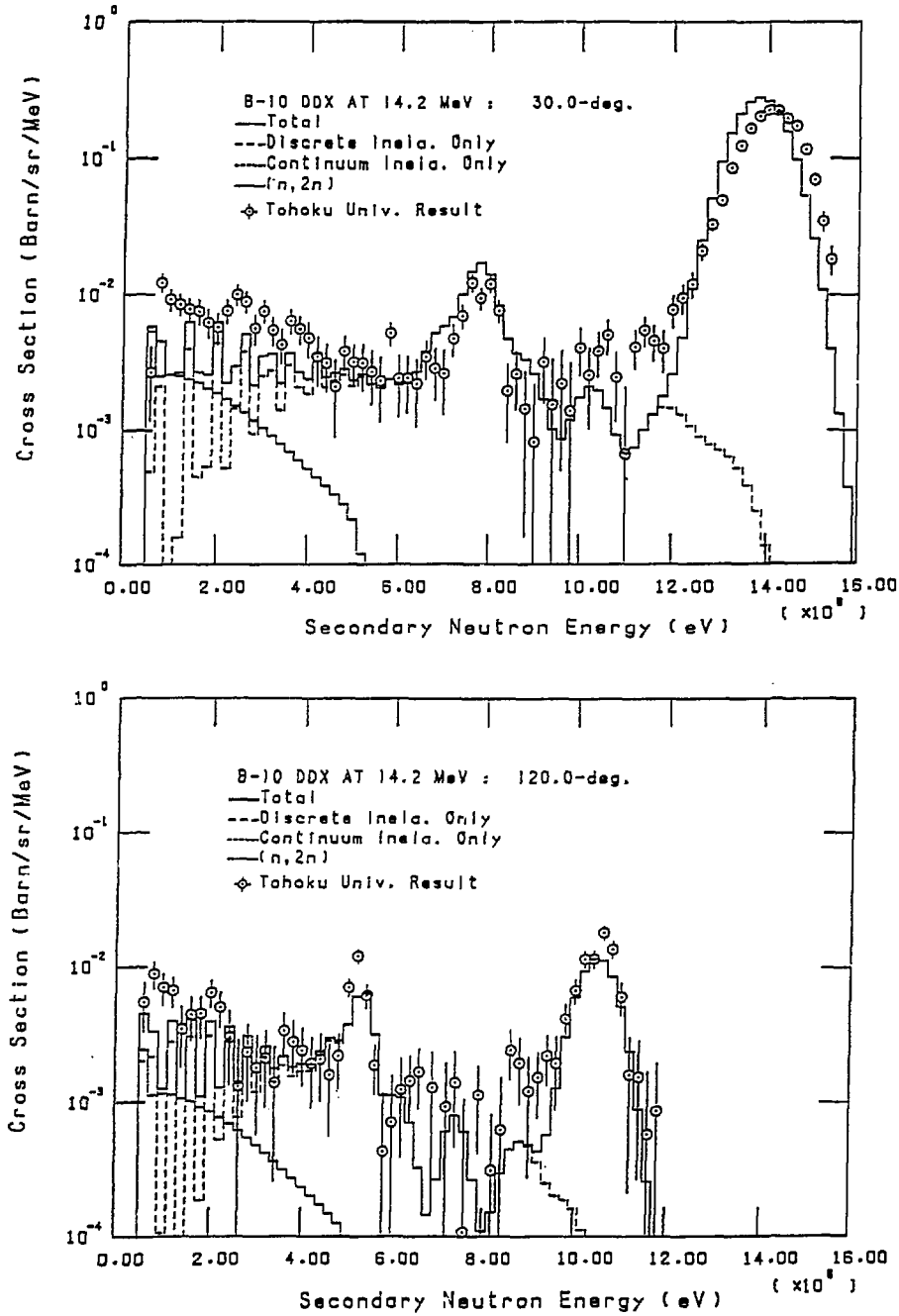

Fig. 18 Measured and evaluated DDX of ^{10}B at 14.2 MeV.

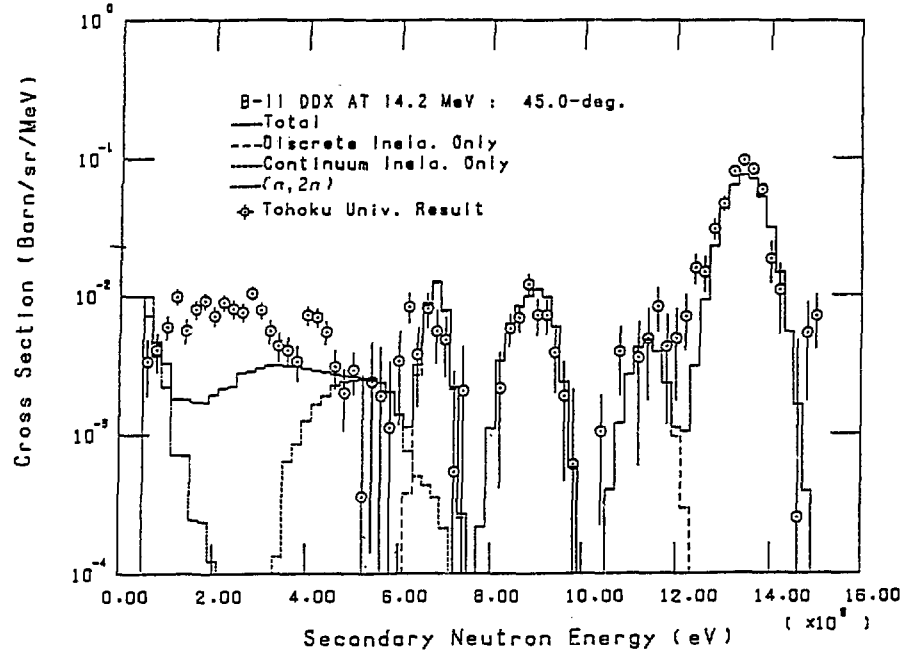

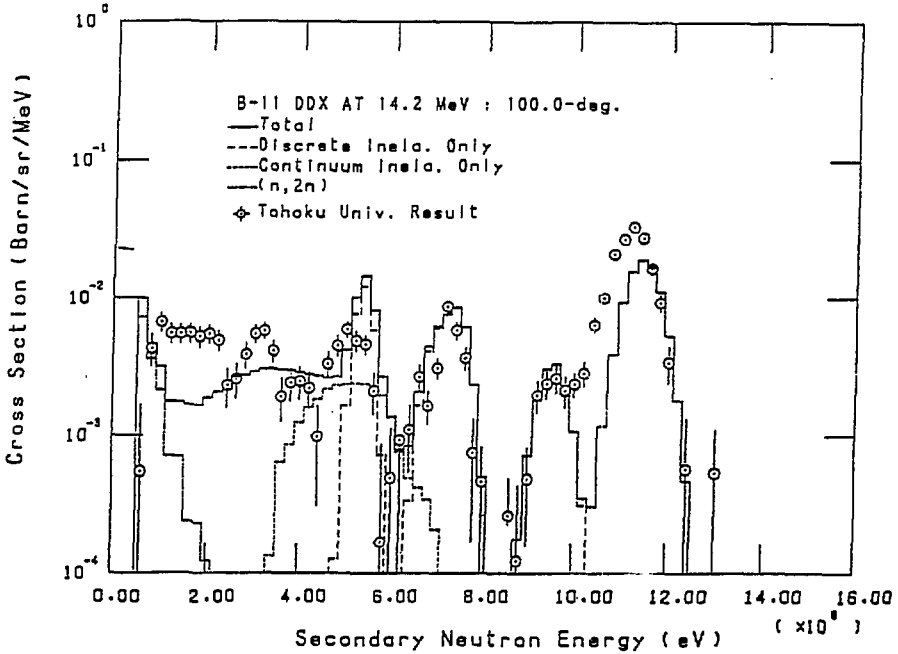

Fig. 19 Measured and evaluated DDX of ^{11}B at 14.2 MeV.

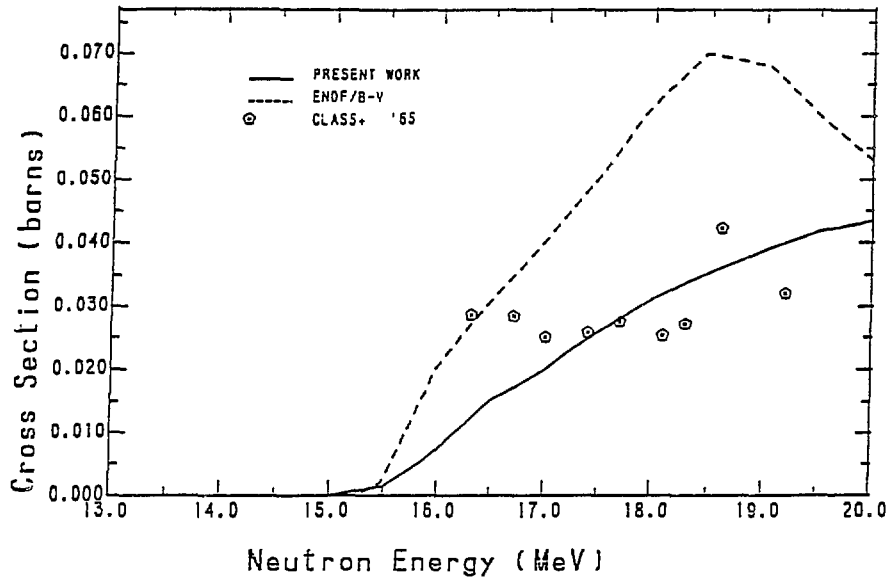

Fig. 20 The $^{12}C(n,d)$ reaction cross section.

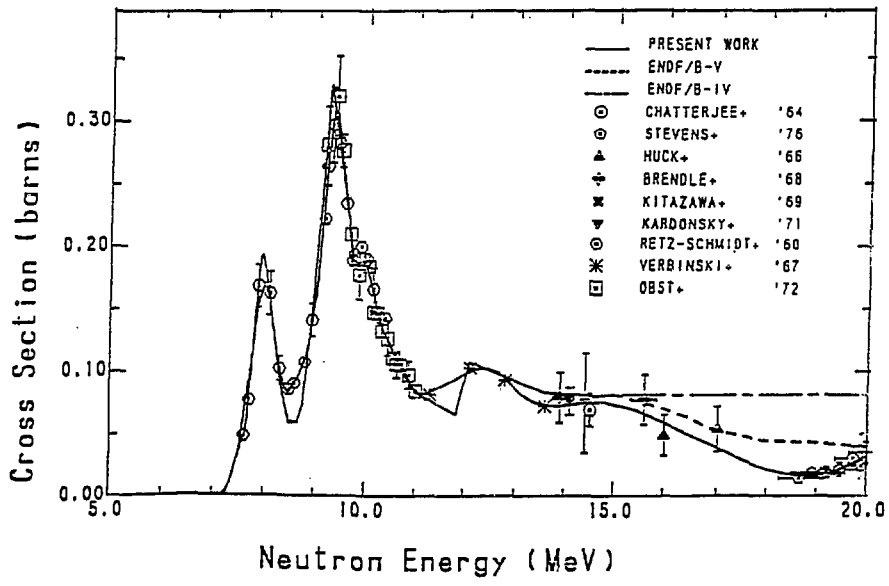

Fig. 21 The $^{12}C(n,\alpha)$ reaction cross section.

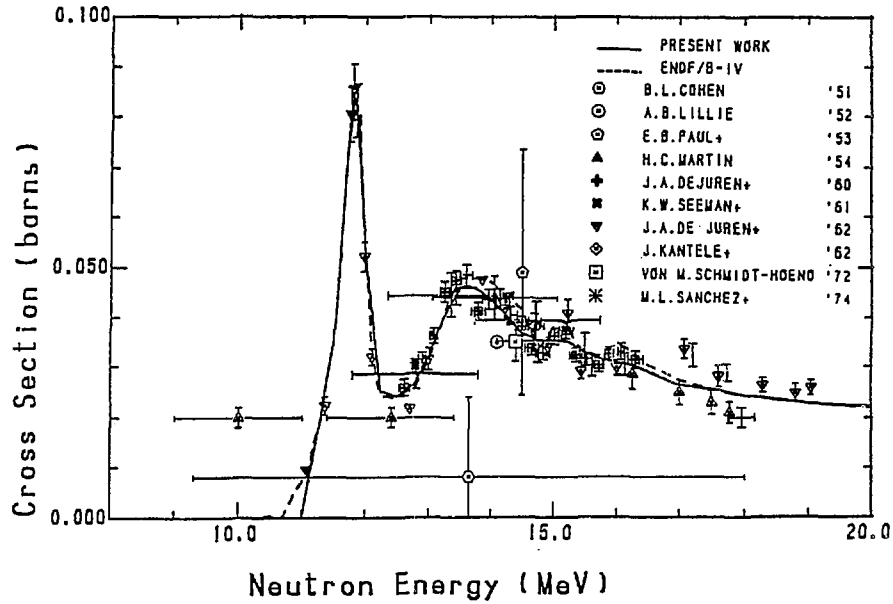

Fig. 22 The $^{16}O(n,p)$ reaction cross section.

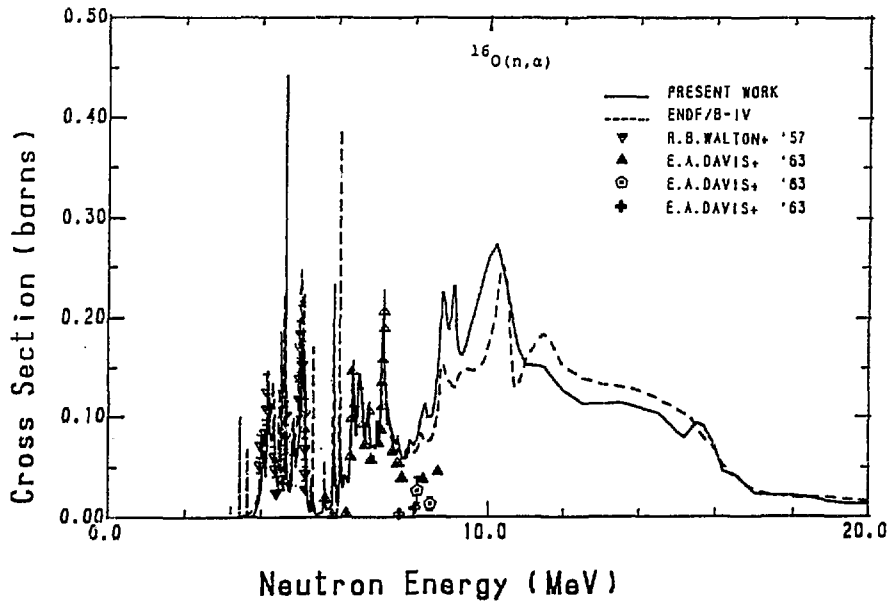

Fig. 23 The $^{16}O(n,\alpha)$ reaction cross section.

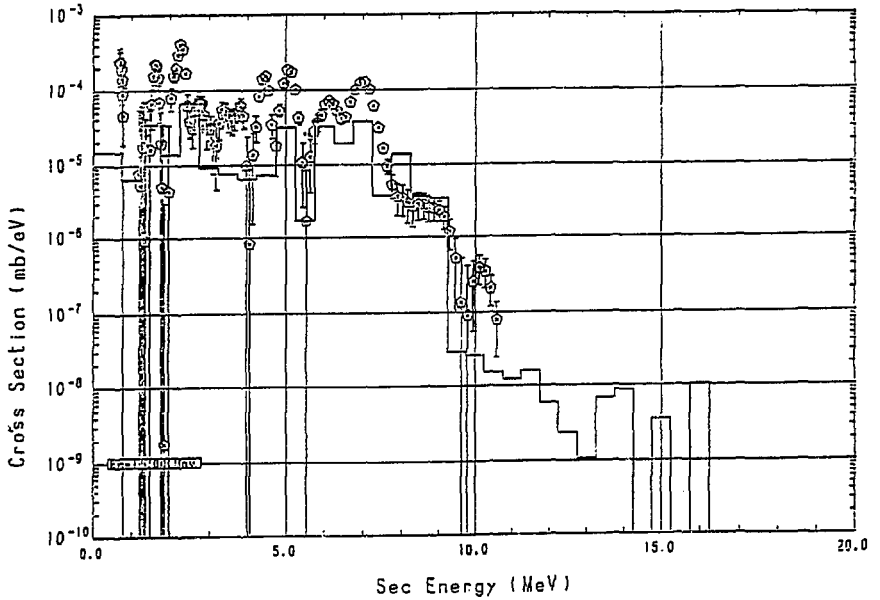

Fig. 24 The secondary γ-ray spectra from the $^{14}N(n,x)\gamma$ reaction at 11.0 MeV.

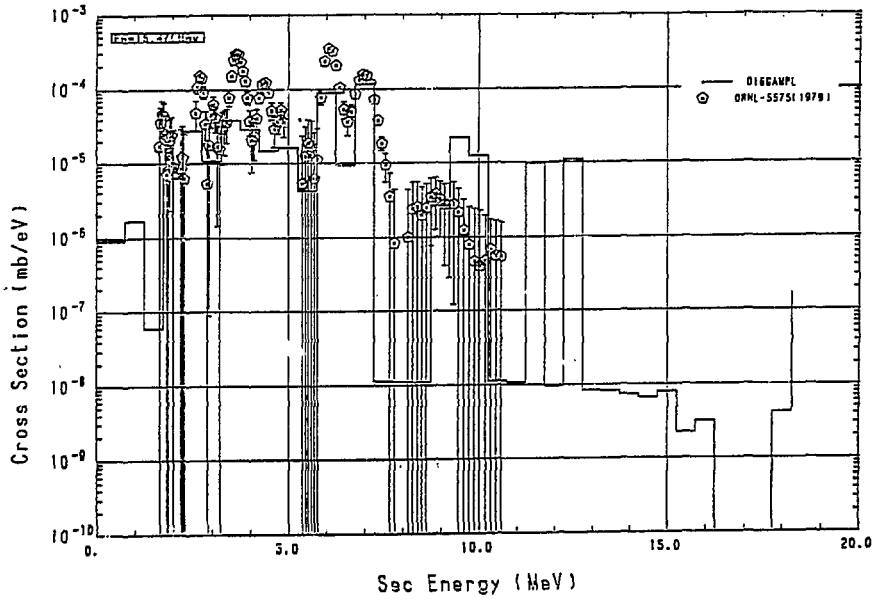

Fig. 25 The secondary γ-ray spectra from the $^{16}O(n,x)\gamma$ reaction at 15.5 MeV.

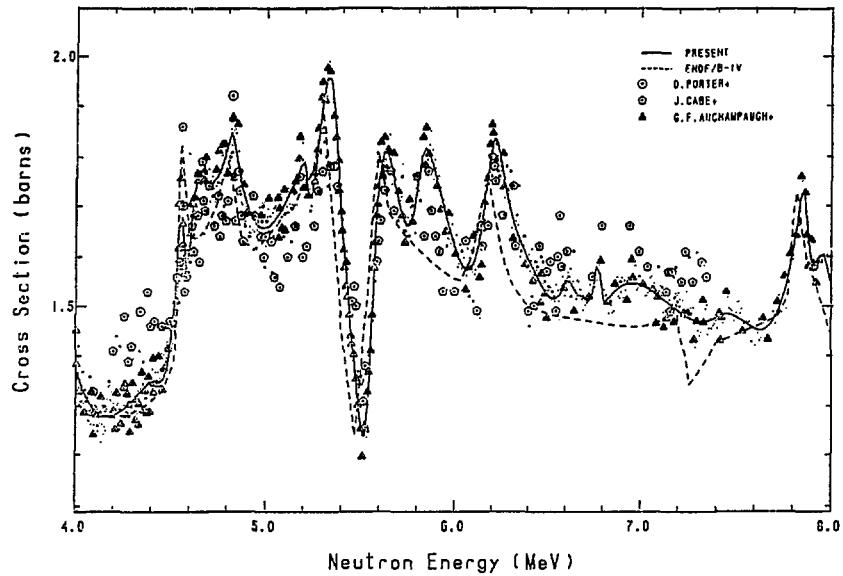

Fig. 26 The total cross section of ^{11}B from 4 to 8 MeV.

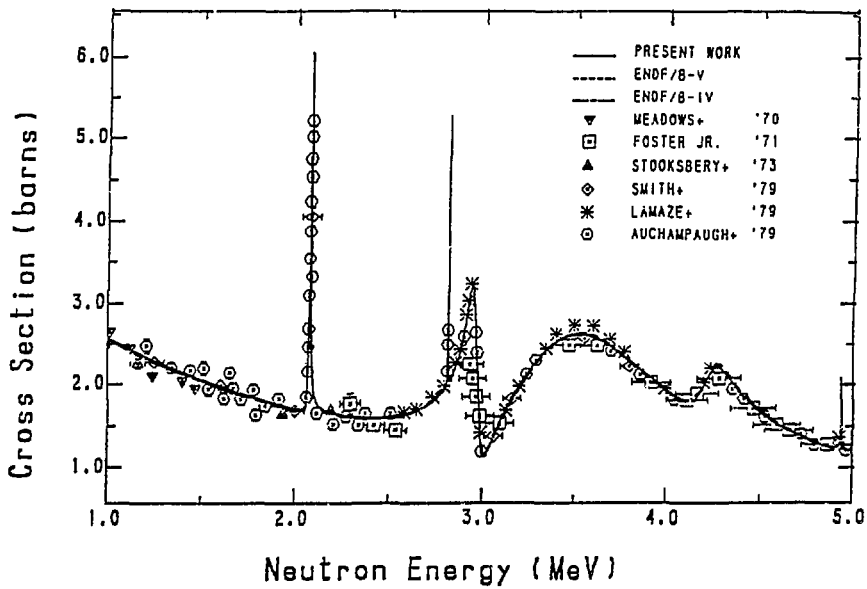

Fig. 27 The total cross section of ^{12}C from 1 to 5 MeV.

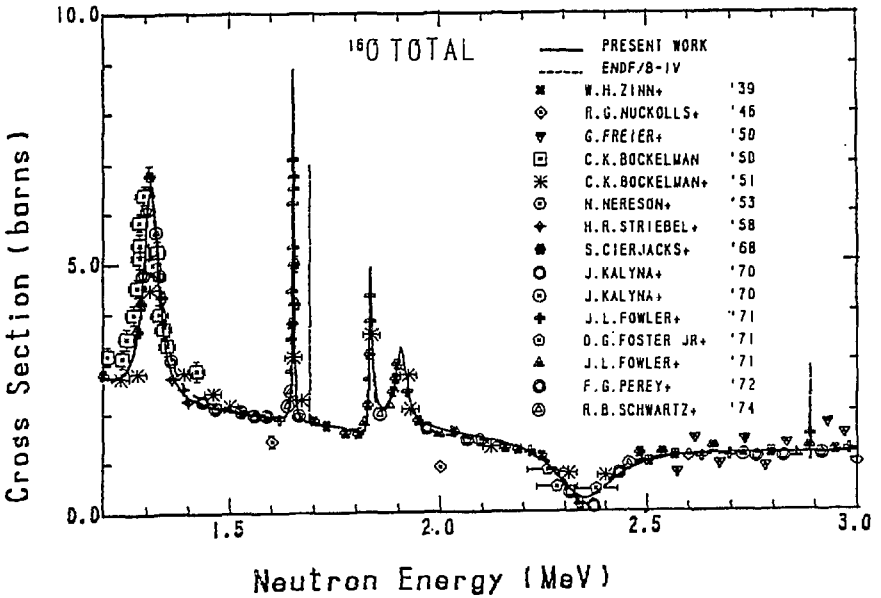

Fig. 28 The total cross section of ^{16}O from 1.3 to 3.0 MeV.

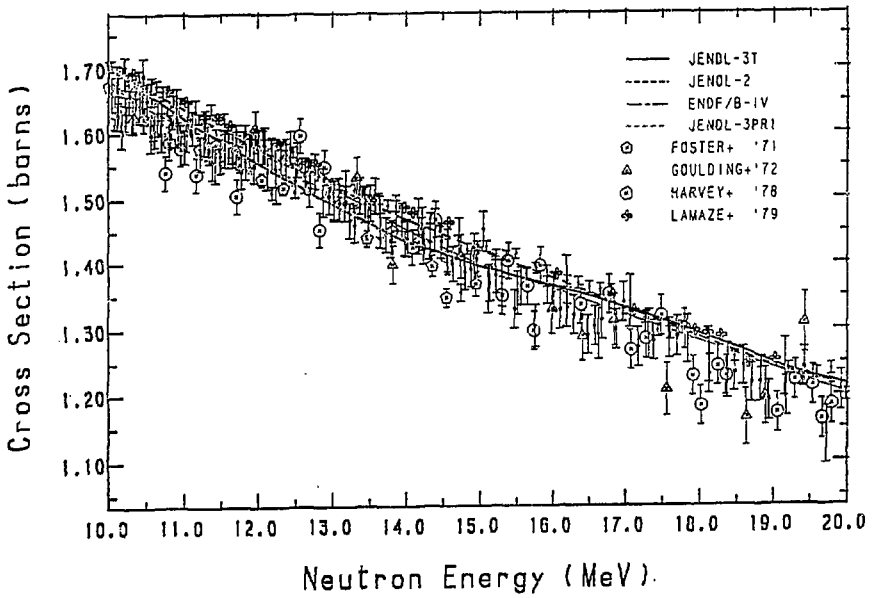

Fig. 29 The total cross section of ^{7}Li from 10 to 20 MeV.

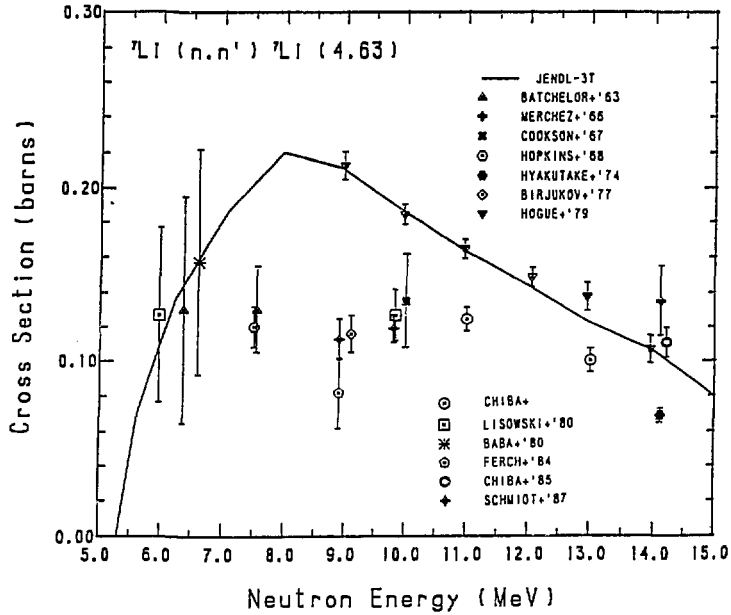

Fig. 30 The $^{7}Li(n,n2)^{7}Li^{*}(4.63MeV)$ reaction cross section.

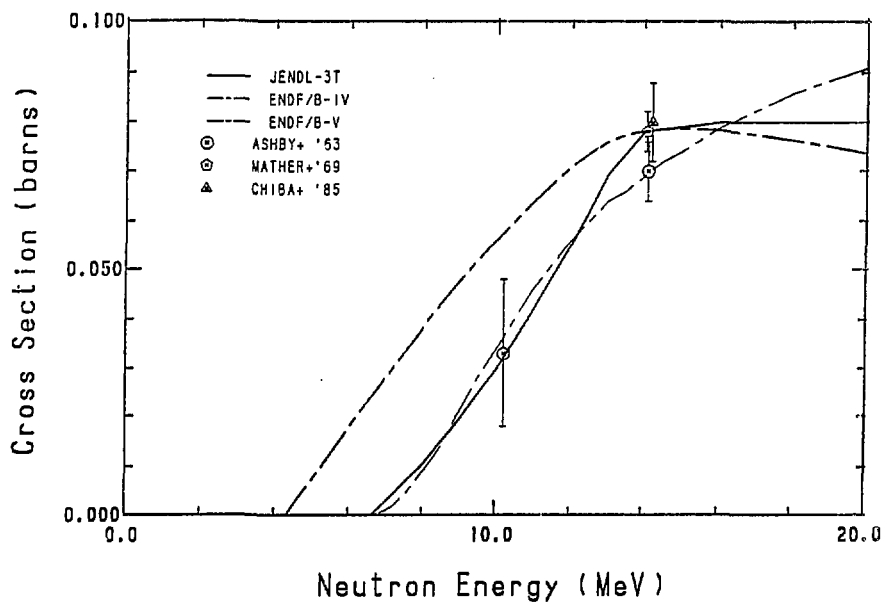

Fig. 31 The $^{6}Li(n,2n)$ reaction cross section.

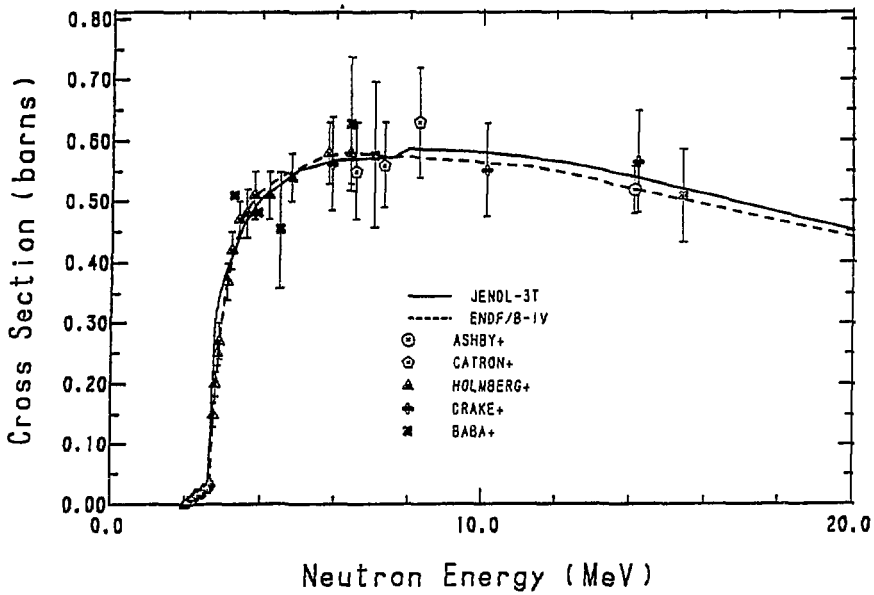

Fig. 32 The $^{9}Be(n,2n)$ reaction cross section.

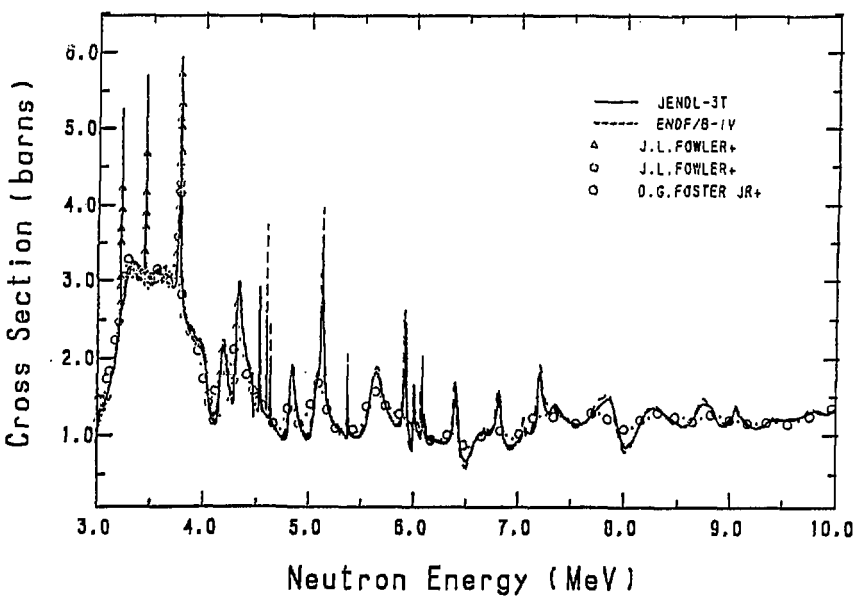

Fig. 33 The total cross section of ^{16}O from 3 to 10 MeV.

2.2 Benchmark Tests of JENDL-3T

2.2.1 Benchmark Tests of JENDL-3T for Thermal Reactor and High Conversion Light Water Reactor

Hideki Takano
Japan Atomic Energy Research Institute
Kunio Kaneko
Japan Information Service

Benchmark tests of JENDL-3T data were performed by analysing a lot of critical experiments, and the results were compared with those obtained using JENDL-2 data.

The benchmark calculations were performed with SRAC, a thermal reactor standard code system for reactor design and analysis. For these calculations, a SRACLIB-JENDL3T library was produced with the processing codes, TIMS-PGG and SRACTLIB.

The calculated results are summarized as follows:

(1) U-235 fuel cores : The k_{eff} calculated with JENDL-3T cross sections increased about 0.3 % with respect to the JENDL-2 based values. The increase reflects the 0.24 % increase in ν-235 at the 2200m/sec. However, for the case of the metal fuel core with a hard spectrum, the k_{eff} obtained with JENDL-3T increased about 2 % with respect to the JENDL-2 value. This is due primary to larger ν-235 values (2 %) in fast energy region and a hard Madland-Nix fission spectrum in JENDL-3T.

(2) Pu-239 fuel cores : The k_{eff} calculated with JENDL-3T data decrease about 0.6 % with respect to the JENDL-2 values . It is seemed that this is due to lower fission cross sections of Pu-239 in resolved resonance region. The lower fission cross sections cause a overestimation for conversion ratio in PROTEUS core of HCLWR.

(3) U-233 fuel cores : The k_{eff} obtained with JENDL-3T data decrease 0.5 - 2.5 % with respect to JENDL-2 values, excepting for the case of metal fuel core with hard neutron spectrum.

1. Introduction

A temporary nuclear data file JENDL-3T[1] has been generated for testing a evaluated data file of JENDL-3. To assess the adequacy of JENDL-3T data for use in nuclear reactor design and applications, benchmark calculations are required for a number of critical experiments for thermal and fast reactors.

In this report, the benchmark tests of JENDL-3T has been performed by analysing a lot of experiments for thermal and high conversion light water reactors (LWR and HCLWR). The present calculations were performed with SRAC[2], a thermal reactor standard code system for reactor design and analysis. For these calculations, a SRACLIB-JENDL3T library was produced with the processing codes, TIMS-PGG[3] and SRACTLIB[2]. This library contained 74-group constants for fast energy region and 48-group constants for thermal energy region. In resonance energy region, a ultra-fine group library was prepared for some important heavy resonant nuclides.

The selected benchmark cores are a number of critical experiments cores with different fuels of U-235, U-233 and Pu-239, two water-moderated lattice(TRX-1 and 2)[4], two heavy water-moderated cores (ETA-1 and 2)[5] and a large number of uniform water-moderated lattices collected by Strawbridge and Barry[6]. These benchmark cores are analysed with the SRAC system and the results are summarized in this report.

2. Benchmark Testing Cores

2.1 LWR Benchmark Cores

A variety of critical and lattice experiments were selected as seen in Tables 1 and 2. The ORNL series[4]are unreflected spheres of uranyl nitrate in H2O. The ratio-ranges of H/U-235 are from 972 to 1835. The critical experiments selected by McNeany and Jenkins[7] contain the high enriched U-235 and U-233 with the ratio-ranges of H/U from 0 to 1400. There are two experiments including U-233 and Th-232 fuels. The PNL 1 - 5 series[4] are homogeneous aqueous plutonium nitrate experiments with the H/Pu-239 ratio ranging from 131 to 1204.

The uniform water-moderated lattice experiments collected by Strawbridge and Barry[6] contain 61 U-metal and 55 UO2-rods lattices covering a wide range of parameters. The U-235 enrichment varied from 1.0 to 4.0 %. The ratio H2O/U ranges from 1 to 12. Fuel rod diameters

are from 0.445 to 2.35 cm and both stainless steel and aluminum clad are used. There are the lattice cores with heavy water-moderated.

Lattice parameters are measured in the TRX[4] and ETA [5] cores. The TRX- 1 and 2 represent fully reflected fuel rods of enriched 1.3 % uranium, aluminum-clad and H2O-moderated. The ETA-1 and 2 are tight Th-U235 and Th-U233 lattices moderated with heavy water.

2.2 HCLWR Benchmark Cores

The PROTEUS series[8] are tight lattice experiments with the moderator-to-fuel volume ratio of 0.5 for high conversion light water reactors. The fissile plutonium enrichments are about 6 and 8 % for the cores (1, 2 and 3) and (4, 5 and 6), respectively. Three different H2O-voidage states were measured , viz. 0. 42.5 and 100 % void, to check the void coefficient.

The FCA-XIV-1[9] is a plate fuel experiment with the enrichment 6.5 % U-235 and the moderator-to-fuel volume ratio of 0.6.

3. Benchmark Calculations

A number of critical and lattice experiments were analysed with SRAC using two group cross section libraries SRACLIB-JENDL2[10] and -JENDL3T based on JENDL-2 and JENDL-3T data, respectively. The cell spectrum calculations were performed by the collision probability method. The ultra-fine group method was used in the resonance region below 130 eV. Criticality calculations were performed with P_1-S_8 approximation by a one-dimensional S_n-transport code ANISN.

4. Results and Discussions

4.1 U-235 Fuel Assemblies

The multiplication factors calculated for 116 cases collected by Strawbridge and Barry are shown in Figs.1 and 2. The results obtained with JENDL-3T data are compared with those calculated with JENDL-2 data. Figure 1 shows the results obtained for UO2-rod lattices. The average $k_{e//}$ for JENDL-3T data is 0.991 and the standard deviation is 0.012. The average value increase 0.8 % with respect to the mean for JENDL-2. It is observed that the calculated $k_{e//}$ are underestimated with increase of the ratio H/U. Figure 2 shows the results calculated for U-metal rods. The average $k_{e//}$ for JENDL-3T data is 0.992 and 0.3 % larger than that obtained with JENDL-2 data. The calculated

k_{eff} are in good agreement with the experimental values in the cases of larger ratio H/U. Table 3 shows the comparison of average k_{eff} over different characteristics. An interesting observation from this table is that the average k_{eff} for JENDL-3T data is about 2 % larger than JENDL-2 data in the heavy water-moderated case. This is also seen for the case of H/U=0 with a hardening spectrum in Fig. 3.

Table 4 shows the comparison of ν-values at 2200m/sec. The ν-235 of JENDL-3T data is 0.24 % larger than JENDL-2 data, but it is not 2 %. This is observed in Fig.4 from the comparison of ν-values in the resonance and fast energy regions.

Integral lattice parameters calculated for TRX-1 and 2 cores are shown in Table 5. It is observed from this table that ρ_{28} and δ_{28} obtained using JENDL-3T data are overestimated.

4.2 U-233 Fuel Assemblies

Figure 5 shows the multiplication factors calculated as a function of the ratio H/U-233. The results obtained by JENDL-3T data become about 1.0 % smaller than those by JENDL-2 data and give good agreement with experiments.

Table 5 shows the integral parameters calculated for ETA-1 and 2 cores which are heavy water-moderated tight lattice with a hardening spectrum such as high conversion light water reactors. Hence, resonance energy region plays very important role for absorption calculations. The integral parameters ρ_{02}, CR, CR' and δ_{02} calculated using JENDL-3T data are significantly improved over corresponding analyses using JENDL-2 data. Figure 6 shows the comparison of Th-232 capture cross sections between JENDL-2 and 3T data. It is seen from this figure that Th-232 capture cross sections of JENDL-3T are significantly larger than JENDL-2 data in the resonance region below 200 eV.

4.3 Pu-239 Fuel Assemblies

The calculated multiplication factors are shown as a function of the ratio H/Pu-239. The k_{eff} obtained using JENDL-3T data are about 0.6 % smaller than those using JENDL-2 data, and the overprediction by JENDL-2 is improved. This is not due to the ν-value of Pu-239, because the value of JENDL-3T is 0.13 % larger than JENDL-2 data as seen from Table 4. Figure 8 shows the deviation of the Pu-239 fission cross

sections for JENDL-3T from those of JENDL-2. It is observed that the fission cross sections of JENDL-3T are significantly smaller than JENDL-2 data in many energy groups. This causes the decrease of k_{∞} obtained using JENDL-3T data.

4.4 HCLWR Benchmark Assemblies

4.4.1 FCA-XIV-1

Table 6 shows the infinite multiplication factors (k-infinity) and reaction rate ratios calculated using JENDL-2 and JENDL-3T data. The k-infinity obtained by JENDL-3T is about 3 % larger than that using JENDL-2. This is due to large discrepancy between ν-235 as shown in Fig.4. The overestimations for F8/F5 and C8/F5 obtained using JENDL-2 is not improved by using JENDL-3T data.

4.4.2 PROTEUS

The results calculated for PROTEUS cores 1 - 6 are shown as a function of the coolant void fraction (%) in Figs.9 - 12. The k-infinity using JENDL-3T gives very good agreement with experiments in the zero void state as seen in Fig.9. However, the k-infinity of JENDL-3T depend stronger than that of JENDL-2 on coolant voidage states.

Figure 10 shows the ratio of calculation to experiment (C/E) for the reaction rate ratio F5/F9. The results using JENDL-3T are slightly improved in the case of 100 % void state with a hard neutron spectrum such as fast breeder reactors.

Figure 11 shows the comparison of the spectral index (C8/F9) corresponding to conversion ratio. The results using JENDL-3T are about 3 % larger than those using JENDL-2 and overestimate significantly the experimental values.

Figure 12 shows the comparioson of the spectral index (F8/F9) for threshold fission reaction rate. The results using JENDL-3T increase still more the overprediction obtained by JENDL-2 for the experimental values.

5. Concluding Remarks

The benchmark calculation results using JENDL-3T are summarized as follows: For LWR benchmark tests,

U235-U238-H2O : Good k(0.992), C8/F5, but poor k for large ratio H/U-235 and poor F8/F5

U235-U238-D2O : Good k(0.997)

U233-U235-U238-H2O : Good k(0.99)

U233-Th232-H2O : Good k(0.99)

Pu239-Pu240-H2O : Good k(1.005)

U235-U238 metal : Poor k

U233-U235-U238 metal : Poor k(1.025)

For HCLWR benchmark tests,

Pu (PROTEUS) : Good k(1.00); Poor Void reactivity, C8/F9, F8/F9

U (FCA-XIV-1) : Good k(1.016) ; Poor F8/F5, C8/F5

The present benchmark tests of JENDL-3T showed that nuclear data to be reevaluated are ν, fission cross section and fission spectrum for U-235, fission cross section and fission spectrum for Pu-239, inelastic scattering cross section for U-238, capture and inelastic scattering cross sections for Pu-240, and capture and elastic scattering cross sections for aluminum and nickel.

References

1) JENDL Compilation Group(Nuclear Data Center, JAERI): JENDL-3T, Private communication (1987).

2) K. Tsuchihashi et al.:"SRAC: JAERI Thermal Reactor Standard Code System for Reactor Design and Analysis," JAERI 1285 (1983) and 1302 (1987).

3) H. Takano et al.:"TIMS-PGG: A Code System for Producing Group Constants," JAERI-M 82-072(1982).

4) "Cross Section Evaluation Working Group Benchmark Specifications ,"ENDF-202(BNL-19302), Brookhaven National Lab.

5) J Hardy et al.: Nucl. Sci. Eng., 55, 401 (1974).

6) L.E. Strawbridge and R.F. Barry: Nucl. Sci. Eng., 23, 58 (1965). 7) S. McNeany and D. Jenkins: Nucl. Sci. Eng., 65, 441 (1978).

8) R. Chawla et al.:" Comparison of Calculated and Measured Parameters for a Pu-Fueled LWHCR Lattice," Proc. ANS Meeting on Advanced in Reactor Physics and Core Thermal Hydraulic," Kiamesha Lake, N.Y., NUREG/CP-0034, 902 (1982).

9) T. Ousigi et al.:"Critical Experiment and Analysis at FCA," Proc. the Third Seminor Soft. Develop. Nuclear Energy Research, JAERI-M 86-178 (1986).

10) H. Takano et al.: to be published in JAERI-M report.

Table 1 LWR benchmark cores.

Critical experiment	Lattice parametr experiment
U-235 fuel	
ORNL － 1, 2, 3, 10	TRX-1,2(1.3 wt% U235 metal)
H/U-235 : 972 － 1835	V(H2O)/Vf : 2.35, 4.02
McNeany & Jenkins-Cores 1, 2, 3	ETA-1 (6.7wt%U235-ThO2)
H/U-235 : 0.0, 50, 1393	D2O (Driver TRX)
Strawbridge & Barry-Cores	
55 U-metal and 61 UO2-rods	
U-233 fuel	
McNeany & Jenkins-Cores 1 － 10	ETA-2 (3 wt% U233-ThO2)
H/U-233 : 0.0 － 381	D2O (Driver TRX)
McNeany & Jenkins -Cores 11, 12	
U-233 + Th-232	
H/U-233 : 1533, 1986	
PU-239 fuel	
PNL － 1, 2, 3, 4, 5	
H/Pu-239 : 131 － 1204	

Table 2 HCLWR benchmark cores.

PU-239 fuel
PROTEUS(pin) － cores (1, 2, 3) & (4, 5, 6)
Vm/Vf : 0.5
Void fraction(%) : 0, 42.5, 100
Two rod heterogeneity : UO-PuO + DUO
U-235 fuel
FCA-14-1 (plate, 6.5% E)
Vm/Vf : 0.6
Void fraction (%) : 0.0, 45

Table 3 Comparison of average k_{eff} and standard deviation.

CASE	REPORT		JENDL-2		JENDL-3T	
	AVERAGE K-EFF	STANDARD DEVIATION	AVERAGE K-EFF	STANDARD DEVIATION	AVERAGE K-EFF	STANDARD DEVIATION
ALL	0.99309	0.00860	0.98618	0.01079	0.99188	0.01015
FUEL - UO2	0.98991	0.00889	0.98336	0.01083	0.99145	0.01173
FUEL - METAL	0.99596	0.00728	0.98872	0.01019	0.99228	0.00856
CLAD - AL	0.99344	0.00790	0.98382	0.00992	0.98877	0.01011
CLAD - SUS304	0.99118	0.00827	0.98235	0.00685	0.99207	0.00830
CLAD - NONE	0.99527	0.01080	0.99998	0.00788	1.00121	0.00724
FUEL - UO2 CLAD - AL	0.98785	0.00965	0.98499	0.01531	0.99044	0.01600
FUEL - METAL CLAD - AL	0.99630	0.00488	0.98323	0.00564	0.98793	0.00507
LATTICE - SQUARE	0.98942	0.00953	0.98276	0.01160	0.99180	0.01265
LATTICE - HEXA	0.99560	0.00693	0.98850	0.00961	0.99194	0.00811
FUEL - UO2 LATTICE - HEXA	0.99279	0.00127	0.98687	0.00185	0.98937	0.00164
B-10	0.99369	0.00424	0.98290	0.00284	0.99363	0.00638
D2O	0.98110	0.00674	0.97901	0.00377	0.99757	0.00644
H/U < 3.0	0.99841	0.00453	0.98139	0.00620	0.98732	0.00602
3.0 < H/U < 9.0	0.99180	0.00870	0.98713	0.01032	0.99377	0.00935
9.0 < H/U	0.99072	0.01022	0.98946	0.01657	0.98967	0.01631

Table 4 Comparison of ν values (2200 m/s).

nuclide	JENDL-2	JENDL-3T	ENDF/B-IV	ENDF/B-V
U-235	2.4286	2.4345	2.4188	2.4367
Pu-239	2.8806	2.8843	2.8706	
U-233	2.4930	2.4930	2.4980	

Table 5 The C/E-values for lattice cell parameters.

assembly	parameter	JENDL-2	JENDL-3T
	ρ_{28}	1.057	1.081
TRX-1	δ_{25}	1.022	1.012
	δ_{28}	1.052	1.095
	C*	1.024	1.031
	ρ_{28}	1.040	1.063
TRX-2	δ_{25}	1.007	0.997
	δ_{28}	1.024	1.058
	C*	1.011	1.015
	ρ_{02}	0.977	1.011
ETA-1	δ_{25}	1.064	1.060
	δ_{02}	0.810	0.846
	CR	0.919	0.974
	ρ_{02}	0.958	0.982
ETA-2	δ_{23}	1.055	1.054
	δ_{02}	0.944	1.007
	CR*	0.895	0.938

ρ_{28} : U-238 capture epithermal to thermal
δ_{25} : U-235 fission epithermal to thermal
δ_{28} : U-238 fission to U-235 fission
C* : U-238 capture to U-235 fission
ρ_{02} : Th-232 capture epithermal to thermal
δ_{02} : Th-232 fission to U-235 fission
CR : Th-232 capture to U-235 fission
δ_{23} : U-233 fission epithermal to thermal
δ_{02}^{*} : Th-232 fission to U-233 fission
CR* : Th-232 capture to U-233 fission

Table 6 Benchmark calculation for FCA-XIV-1 assembly.
( ) shows the ratio of calculation to experiment

	EXPERIMENT	JENDL-2	JENDL-3T
< 0 % VOID >			
K-INFINITY	1.1759 ± 0.0015	1.16079	1.19407
		(0.987)	(1.015)
F 9/F 5	2.353 ± 3.1%	2.3603	2.3705
		(1.003)	(1.007)
F 8/F 5	0.00568± 6.0%	0.00673	0.00717
		(1.186)	(1.262)
C 8/F 5	0.03768± 2.8%	0.04293	0.04366
		(1.139)	(1.159)
<45 % VOID >			
K-INFINITY	1.0831 ± 0.0048	1.06579	1.10206
		(0.984)	(1.017)
F 9/F 5	2.083 ± 3.0%	2.0059	2.0184
		(0.963)	(0.969)
F 8/F 5	0.00798± 5.0%	0.00933	0.01006
		(1.169)	(1.260)
C 8/F 5	0.05489± 2.2%	0.06076	0.06225
		(1.107)	(1.134)

F9/F5 : Reaction rate ratio of Pu-239 fission to U-235 fission
F8/F5 : Reaction rate ratio of U-238 fission to U-235 fission
C8/F5 : Reaction rate ratio of U-238 capture to U-235 fission

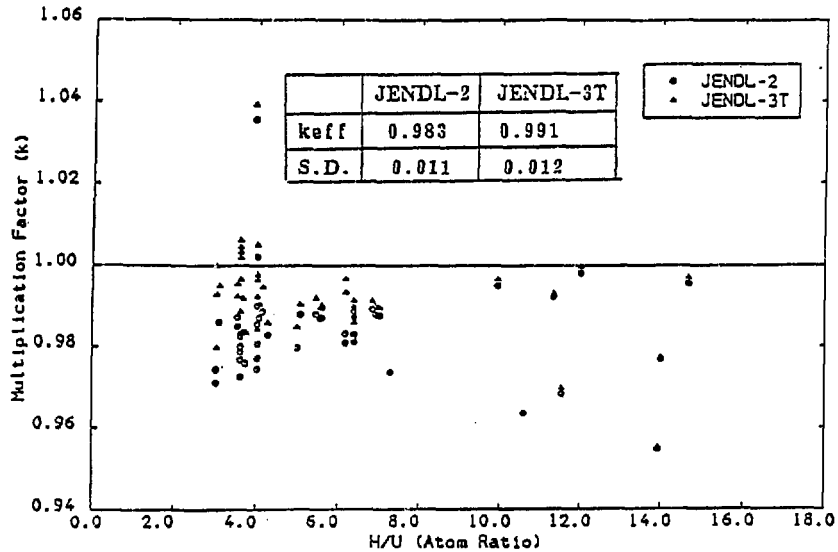

Fig. 1 Comparison of the multiplication factors calculated for Strawbridge and Barry UO_2-rod lattices.

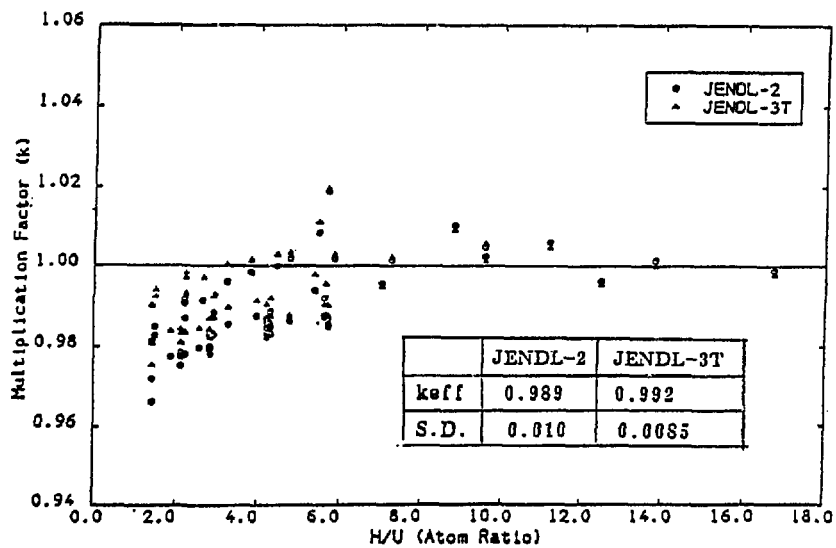

Fig. 2 Comparison of the multiplication factors calculated for Strawbridge and Barry U-metal lattices.

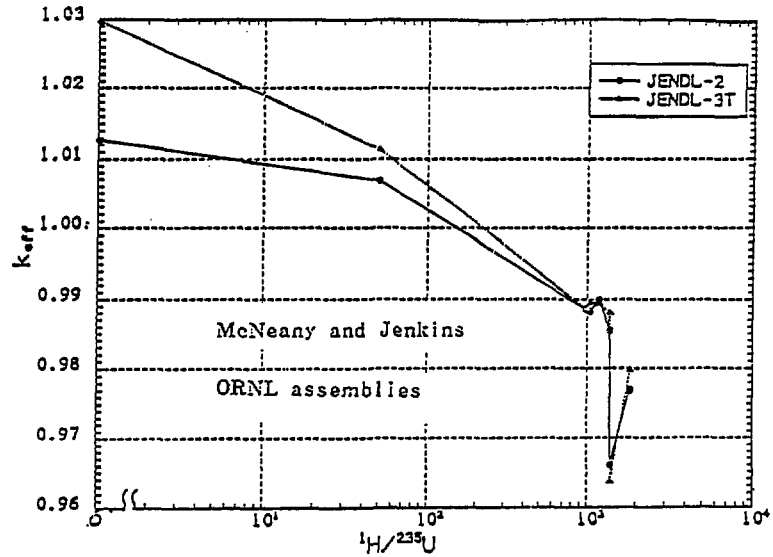

Fig. 3 k_{eff} for ^{235}U critical experiments (ANISN, P_1S_8).

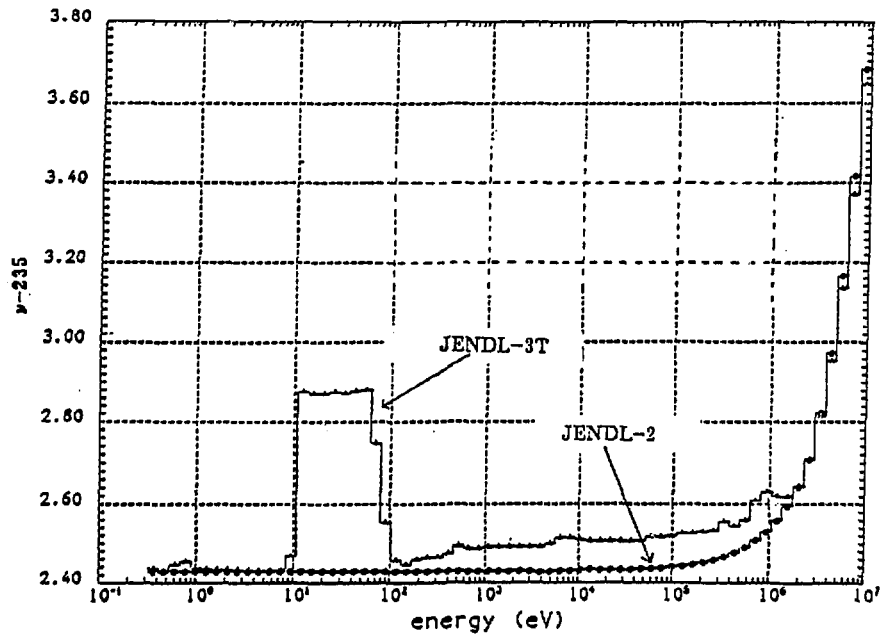

Fig. 4 Comparison of ν-235.

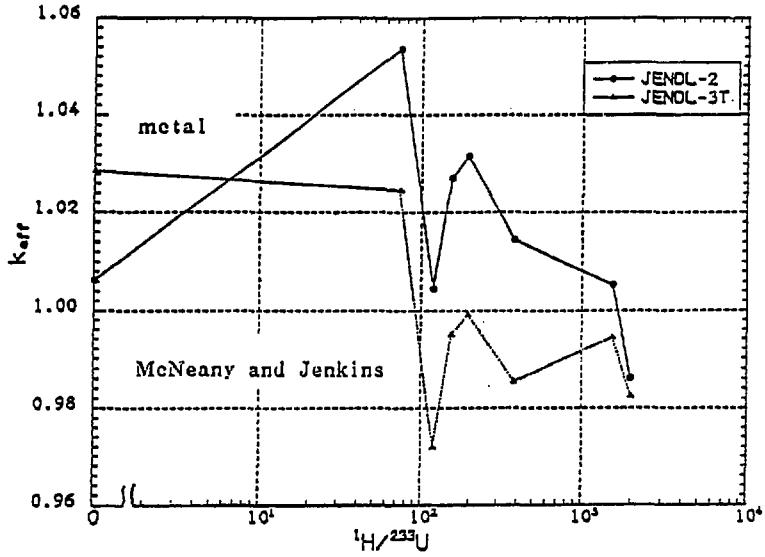

Fig. 5 k_{eff} for ^{233}U critical experiments (ANISN, P_1S_8).

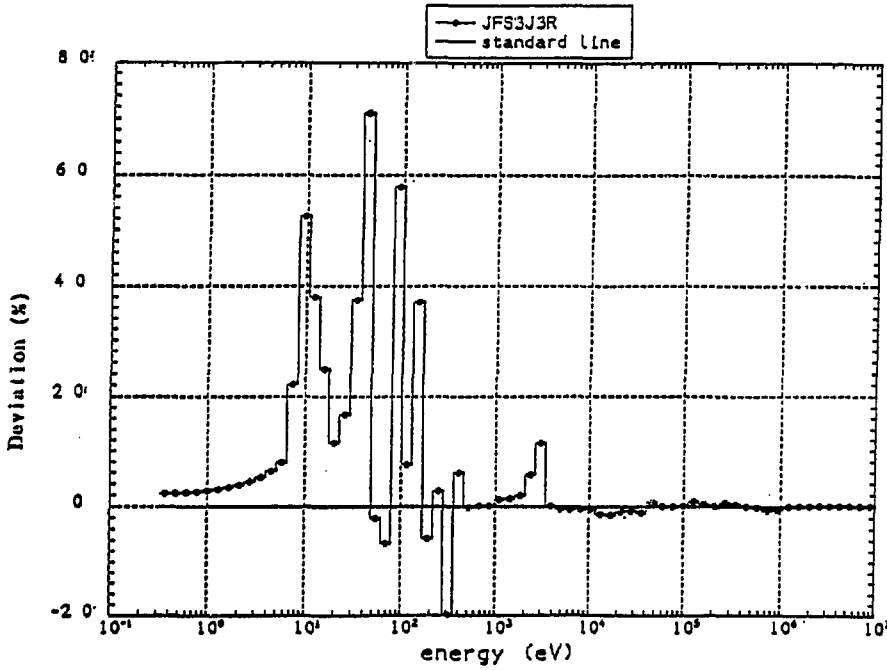

Fig. 6 Deviation for Th-232 capture cross sections of JENDL-3T from JENDL-2 data.

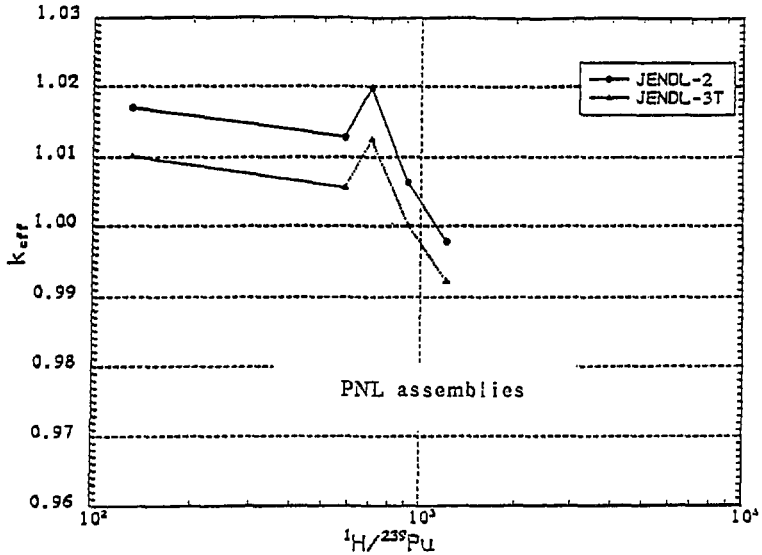

Fig. 7 k_{eff} for ^{239}Pu critical experiments (ANISN, P_1S_8).

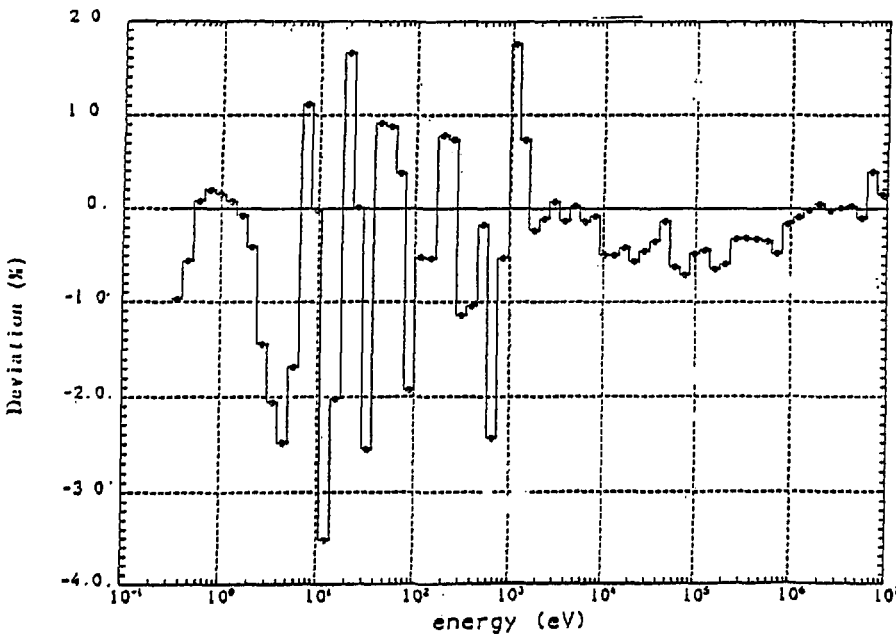

Fig. 8 Deviation for Pu-239 fission cross sections of JENDL-3T from JENDL-2 data.

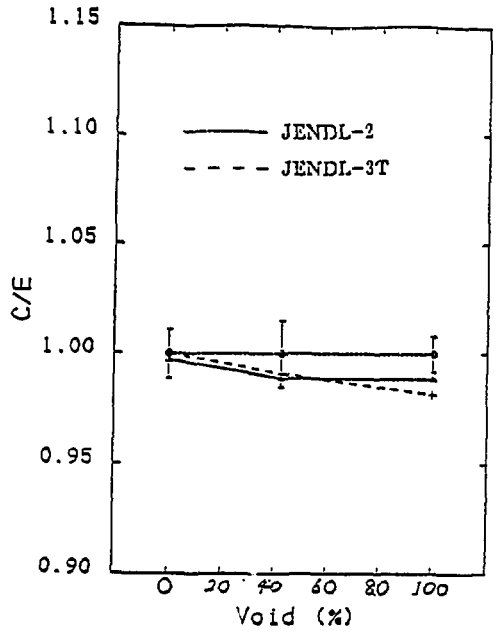

Fig. 9 The C/E values of infinite multiplication factors for PROTEUS cores 1, 2, and 3.

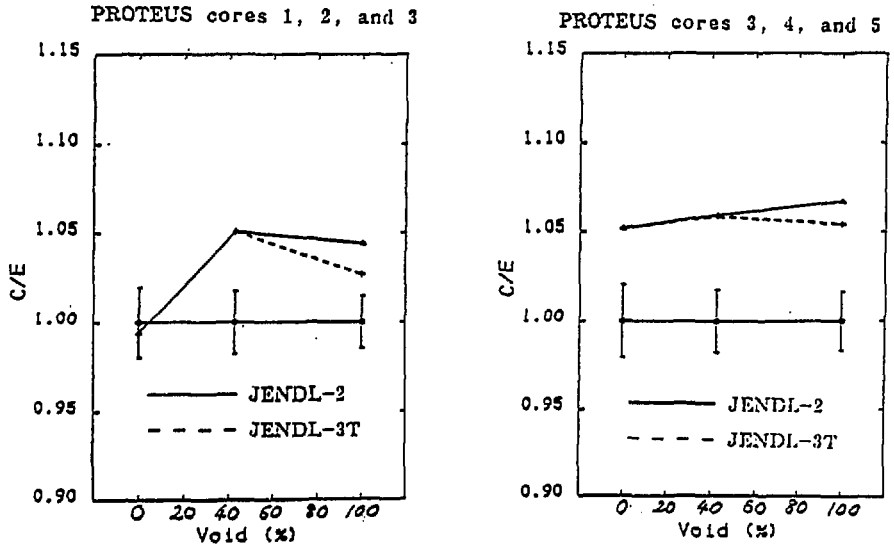

Fig. 10 Comparison of reaction rate ratios of U-235 fission to Pu-239 fission (F5/F9).

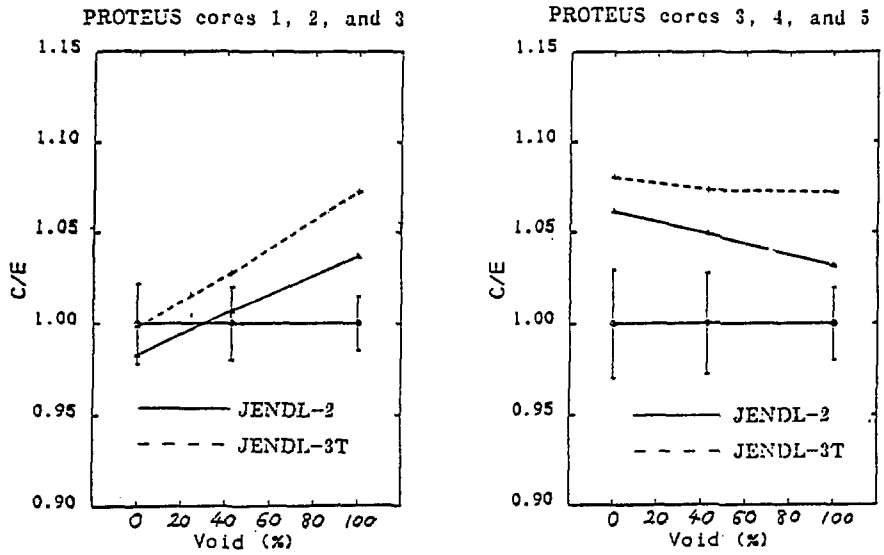

Fig. 11 Comparison of reaction rate ratios of U-238 capture to Pu-239 fission (C8/F9).

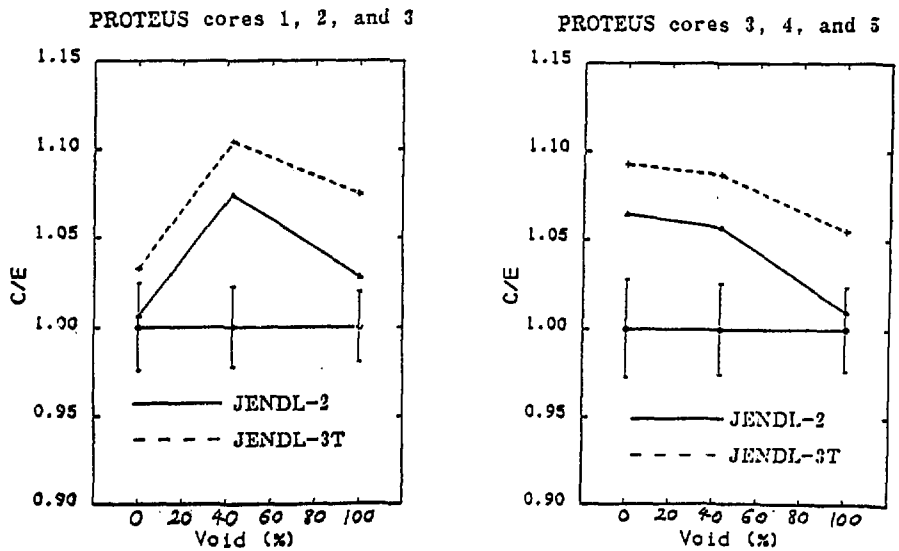

Fig. 12 Comparison of reaction rate ratios of U-238 fission to Pu-239 fission (F8/F9).

2.2.2 Benchmark Test of JENDL-3T on Fast Reactors

T.Takeda , M.Takamoto

Osaka University , Department of Nuclear Engineering ,
Faculty of Engineering

H.Takano and A.Hasegawa

Japan Atomic Energy Research Institute

Benchmark test of JENDL-3T[1] * has been performed using many 1-D and a few 2-D benchmark models of fast critical assemblies. The change in core parameters such as k_{eff}, reaction rate ratio , sodium void worth, Doppler reactivity worth calculated by JENDL-3T from those by JENDL-2 is investigated. We have analyzed the change using sensitivity coefficients calculated from two-dimensional generalized perturbation calculations based on diffusion theory, and investigated the effect of main heavy nuclides.

1. Introduction

The cross sections of main heavy nuclides of JENDL-3T vary remakably from JENDL-2. Thus, it is important to evaluate the effect of the cross section changes on core parameters such as k_{eff}, reaction rate ratio, sodium void worth, Doppler reactivity worth. As the benchmark models to evaluate the effect we choose the many 1-D benchmarks of fast critical assemblies and a few 2-D benchmarks, both of them were arranged for benchmark test by Takano[2].

---

* JENDL-3T is a temporary file for testing the evaluated data which are for JENDL-3. The data in JENDL-3T will be partly revised in JENDL-3.

We investigate the effect of the cross section change to see what nuclides have significant contributions to the core parameter changes. Furthermore, using the cross section sensitivity coefficients calculated by the SAGEP code[3], which is based on the two-dimensional generalized perturbation theory, we investigate the effect of the energy dependence of the cross section change on the core parameter changes. As the main nuclides with significant influence on fast reactor core parameters, we consider ^{235}U, ^{238}U and ^{239}Pu.

2. Benchmark Test

The JENDL-3T has been applied to the twenty-one 1-D benchmark cores of fast critical assemblies with Pu or U fuel. The k_{eff} values calculated by JENDL-2 and JENDL-3T based on diffusion theory are listed in Table 1. For the Pu fueled cores the JENDL-3T reduces k_{eff} by 2.0～0.3%dk/k depending on core size compared with JENDL-2 with an exception of ZPR3-56B which has a Ni reflector and is influenced by the Ni elastic cross section. The k_{eff} values of the U fueled cores increase by the use of JENDL-3T by about 0.8%dk/k.

The reaction rate ratios calculated by JENDL-3T and JENDL-2 are compared in Table 2. The ratio of the ^{238}U capture to ^{239}Pu fission rate, 28C/49F, which is an important parameter for the estimation of breeding ratio, is increased by 4% by the use of JENDL-3T for the Pu cores. The calculated to experimental value (C/E) of 28C/49F has been overestimated by about 6% for large Pu fueled fast critical assemblies. Therefore, the 28C/49F is overestimated by about 10% when one uses JENDL-3T. The ratios of the threshold reaction to ^{235}U fission such as 28F/25F and 40F/25F are also increased by 6% by the use of JENDL-3T.

The two-dimensional benchmark test was performed using the fast critical assemblies FCA VI-2 and ZPPR-9. The

Doppler reactivity worth, sodium void reactivity worth and reaction rate distribution were calculated. The UO_2 Doppler worth is increased by ~6% for JENDL-3T reactive to the JENDL-2 result, and the C/E value approaches unity as shown in Table 3. The overestimation of sodium void worth by JENDL-2 is improved remarkably by JENDL-3T. The C/E value of the sodium void worth for ZPPR-9 is shown in Fig. 1. The reaction distribution in ZPPR-9 is improved by JENDL-3T. The overestimation of the distribution in the outer core is improved by about ~1%.

3. Sensitivity Analysis

To investigate the effect of main heavy nuclides we calculate the change in FBR core parameters due to the change in each of fission, capture, scattering cross sections and ν and fission spectrum χ of the nuclide. Table 4 lists the percentage difference due to each cross section change from JENDL-2 to JENDL-3T for k_{eff} and 28C/49F, which had altered remarkably between JENDL-2 and JENDL-3T as shown in Tables 1 and 2. The k_{eff} of ZPPR-9 is decreased by 0.8% by the change of ^{239}Pu from JENDL-2 to JENDL-3T. Among the reduction, the ^{239}Pu fission cross section has the largest contribution. To study the contribution we show in Fig.2.1 and Fig. 2.2 the ^{239}Pu cross section change , the sensitivity coefficient of k_{eff}, and the product of the two quantities which corresponds to the energy-dependent contribution to the k_{eff} change. The ^{239}Pu fission cross section sensitivity is large in the energy range $10^4 \sim 10^6$eV,and the sum of sensitivity coefficient is 0.38. The JENDL-3T data is decreased by about 4.8% in this energy range from JENDL-2 to JENDL-3T. Therefore the ^{239}Pu fission cross section has an effect of -1.8%(=0.38x4.8) on k_{eff} in the energy range. The effect of the cross section increase just above 1keV is cancelled out by the cross section decrease just below 1keV. For the ZPPR-9 the fission

spectrum change has increased k_{eff} by 0.7% because of the spectrum hardening. The capture cross section is decreased by a few percent in the energy range 1~10^3keV, then k_{eff} has been increased by 0.2%. The change of ν value from JENDL-2 to JENDL-3T is shown in Fig. 3. The increase in the energy range 1~10^2keV has increased k_{eff} by 0.3%. Thus the each reaction of ^{239}Pu has a relatively large effect on k_{eff}.

The ^{238}U cross section change from JENDL-2 to JENDL-3T reduces k_{eff} for both Pu and U fueled cores by about 0.5%. The ^{238}U capture cross section above 50keV is increased from JENDL-2 to JENDL-3T, though increased in the energy range 3~50keV as shown in Fig. 4. The product of this cross section change with the sensitivity, which corresponds to energy-wise k_{eff} change, is shown in Fig. 4 also. The net change is about -0.3%.

The ^{238}U inelastic cross section largely changes from JENDL-2 to JENDL-3T as shown in Fig. 5. The JENDL-3T data is large than JENDL-2 by over 20% above 1MeV. This large change, however, leads to minor change in k_{eff} of about 0.2% as shown in Table 4. If we only change the inelastic cross section not the scattering matrix, the k_{eff} is reduced by 0.8%dk/k because of the neutron spectrum softening. However, when we consider the scattering matrix change, the effect becomes small

The ^{235}U cross section alteration has increased k_{eff} of FCA VI-2 core by 1.4%. The ^{235}U fission cross section is decreased by about 3% in the energy range 10keV~1MeV and by about 7% in the energy range 1keV~10keV as shown in Fig. 6. Then k_{eff} is decreased by ~1.0%. The energy dependence of this reduction is shown in Fig. 6. The ν value is tentatively largely increased from JENDL-2 to JENDL-3T by 2.5% in the energy range 100eV~1MeV. This increase has a remarkably contribution to k_{eff} of U fueled cores. But the JENDL-3T data of ^{235}U ν value may be revised.

For the 28C/49F, the change of the ^{239}Pu fission cross section has increased the ratio by about 3%, and that of the

^{238}U capture cross section has increased it by about 1.4%. Thus, the 28C/49F is increased by about 4% as shown in Table 2.

4. Concluding Remarks

From the 1-D and 2-D benchmark tests we have found that the core parameters estimated by JENDL-3T remarkably differ from those by JENDL-2. The k_{eff} for the Pu cores has decreased by about 0.7%dk/k in average, while that for the U cores has increased by about 0.7%dk/k . The reaction rate ratio has increased. The 28C/49F increased by about 4%, and the threshold reaction to 25F increased by about 6%. The UO_2 Doppler reactivity worth and the sodium void worth were improved.

To investigate the contribution to the change of core parameters, we have performed sensitivity analysis. For the k_{eff}, the ^{239}Pu fission cross section has an effect of -1.8%dk/kk' in the Pu cores. The ^{235}U fission cross section and the ν value have contributions of -1.5%, and 2.5%dk/kk' in the U cores. For the 28C/49F, the ^{239}Pu fission and ^{238}U capture cross sections have large contributions.

Therefore, we recommend to further investigate the above cross sections until the final compilation of JENDL-3.

Reference

1) JENDL Complication Group (Nuclear Data Center,JAERI):
JENDL-3T, private communication (1987)

2) H.Takano, Private Communication (1987)

3) A.Hara, T.Takeda, Y.Kikuchi
"SAJEP: Two-Dimensional Sensitivity Analysis Code Based on Generalized Perturbution Theory", JAERI-M 84-027 (1984)

Table 1 Comparison Between k_{eff} Values of 1-D Benchmark Cores Calculated by JENDL-2 and JENDL-3T

No.	ASSEMBLY	EXPERIMENTAL	JENDL-2	JENDL-3T
1	VERA-11A	1.00000	0.99496	0.97938
2	VERA-1B*	1.00000	0.99952	1.00648
3	ZPR-3-6F*	1.00000	1.01285	1.02642
4	ZEBRA-3	1.00000	0.99977	0.97954
5	ZPR-3-12*	1.00000	1.00630	1.01448
6	SNEAK-7A	1.00000	1.00578	0.99582
7	ZPR-3-11*	1.00000	1.00496	1.01269
8	ZPR-3-54	1.00000	0.96373	0.96285
9	ZPR-3-53	1.00000	0.99585	0.99214
10	SNEAK-7B	1.00000	1.00377	0.99200
11	ZPR-3-50	1.00000	1.00025	0.99547
12	ZPR-3-48	1.00000	1.00627	0.99636
13	ZEBRA-2*	1.00000	0.99247	0.99775
14	ZPR-3-49	1.00000	1.00896	0.99633
15	ZPR3-56B	1.00000	0.99622	0.99685
16	ZPR-6-7	1.00000	0.99919	0.99301
17	ZPR-6-6A*	1.00000	1.00408	1.00915
18	ZPPR-2	1.00000	1.00569	0.99866
19	MZA	1.01080	1.01080	0.99303
20	MZB(1)	1.00400	0.99651	0.99212
21	FCA-5-2	1.00000	1.99277	0.98993
Average of C/E in Pu core			0.99796	0.99023
Average of C/E in U core			1.00336	1.01116

* Uranium fuel core

Table 2 Results of Average Difference between Calculations and Experiments of Reaction Rate Ratio for 1-D Benchmark Test*

Reaction Rate ratio	Pu-core	U-core
49F/25F	-1.5*(3)**	-1.3 (-1.5)
28C/25F	5	1 (-4)
28C/49F	5 (1)	5 (-5)
28F/25F	13 (6)	11 (4)
40F/25F	13 (8)	10 (4)

* Deviation from experiments in unit of %

** Results for JENDL-2

Table 3 C/E value of ZPPR-9 Natural UO_2 Doppler Reactivity

Library	Temperature	C/E
JENDL-2	298K- 487.5K	0.879
	298K-1087.0K	0.888
JENDL-3T	298K- 487.5K	0.938
	298K-1087.0K	0.951

Table 4 Component-wise Change of k_{eff} and 28C/49F

Component		k_{eff} ZPPR-9 (Pu core)	k_{eff} FCA-6/2 (U core)	28C/49F ZPPR-9 (Pu-core)
^{239}Pu	fission	-1.8(%)	0.0(%)	3.1(%)
	capture	0.2	0.0	0.1
	ν	0.3	0.0	0.0
	χ	0.7	0.0	-0.7
Total		-0.6	0.0	2.5
^{238}U	fission	-0.2(%)	-0.3(%)	0.0(%)
	capture	-0.3	-0.4	1.4
	inelastic	0.2	----	----
Total		-0.3	-0.7	1.4
^{235}U	fission	0.0(%)	-1.5(%)	0.1(%)
	capture	0.0	0.1	0.0
	ν	0.0	2.5*	0.0
	χ	0.0	0.3	-0.1
Total		0.0	1.4	0.0

* This value may be revised

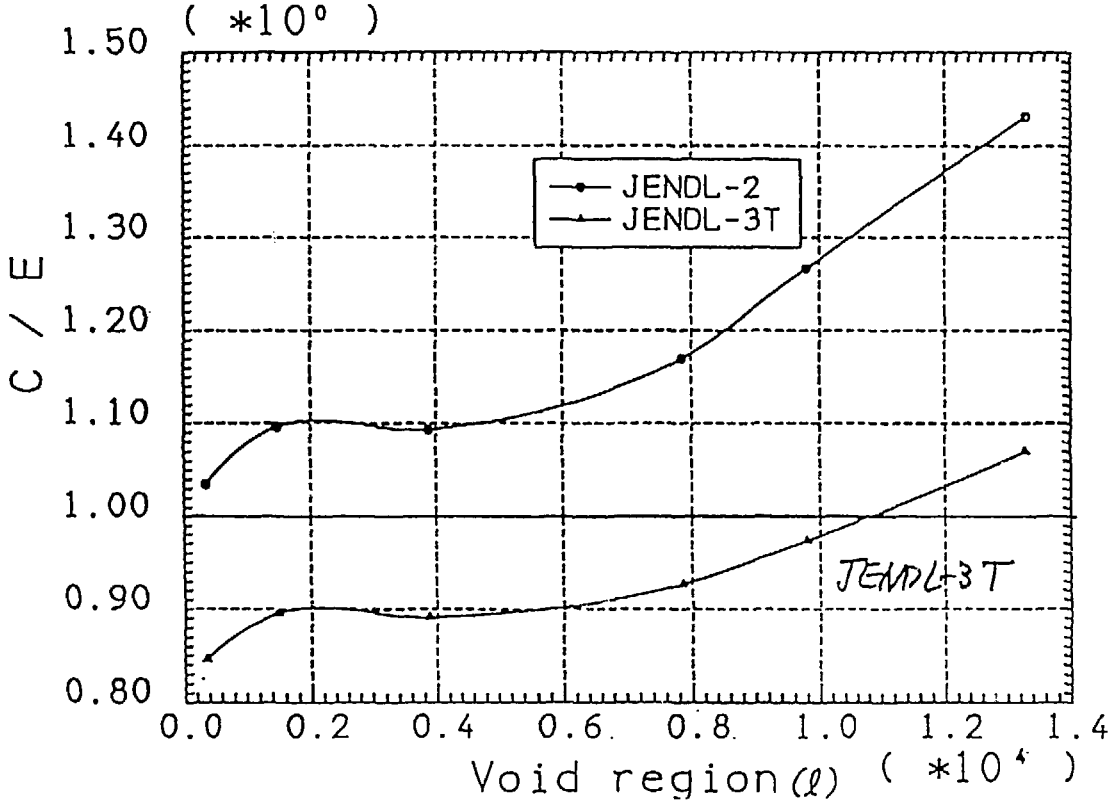

Fig. 1 Comparison of Na-void reactivity at ZPPR-9.

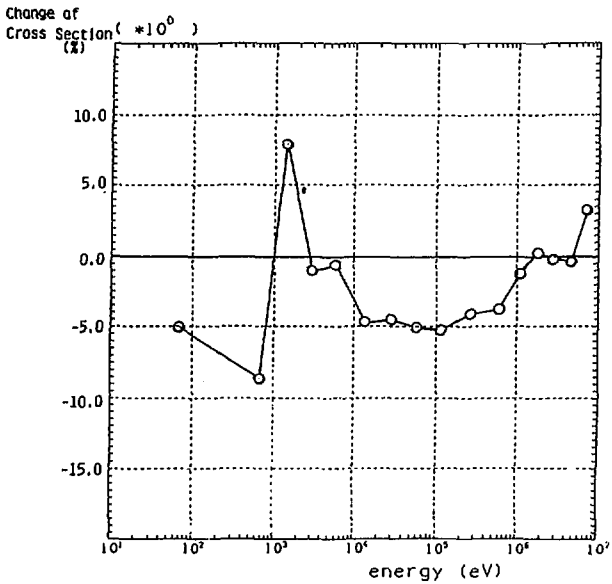

Fig. 2.1 Pu-239 fission cross section change from JENDL-2 to JENDL-3T (%).

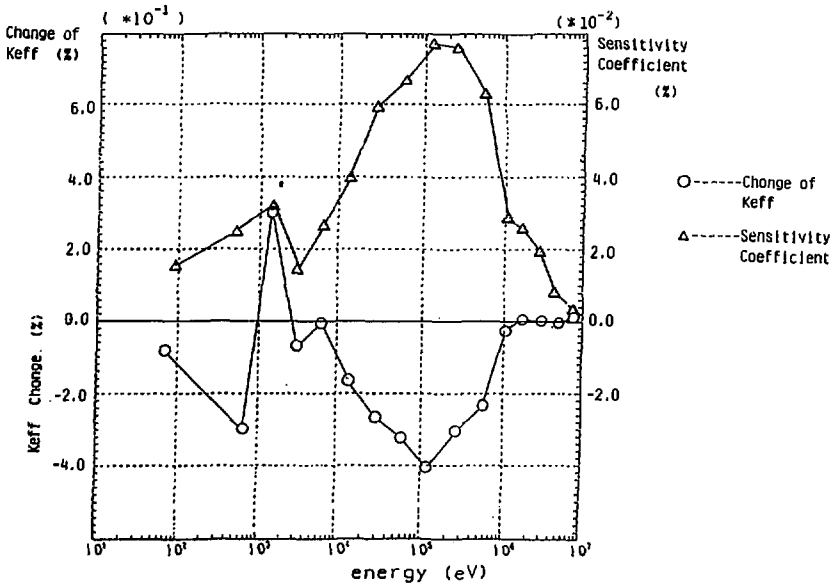

Fig. 2.2 Sensitivity coefficient and change of Keff with Pu-239 fission cross section in Pu-Core (ZPPR-9).

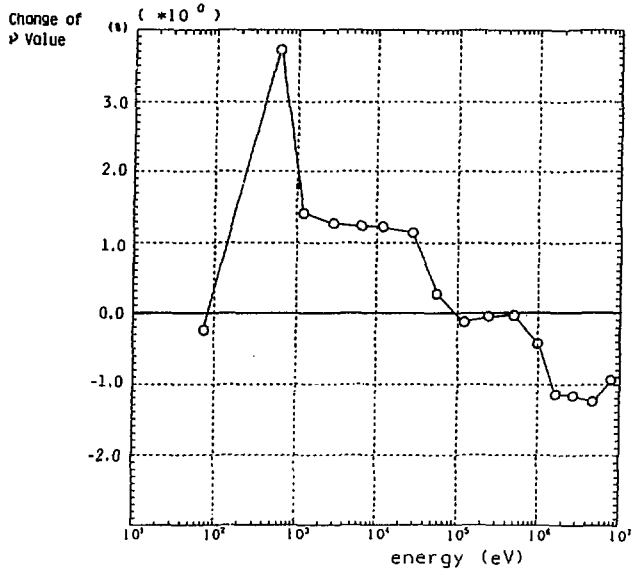

Fig. 3 Pu-239 ν value change from JENDL-2 to JENDL-3T (%).

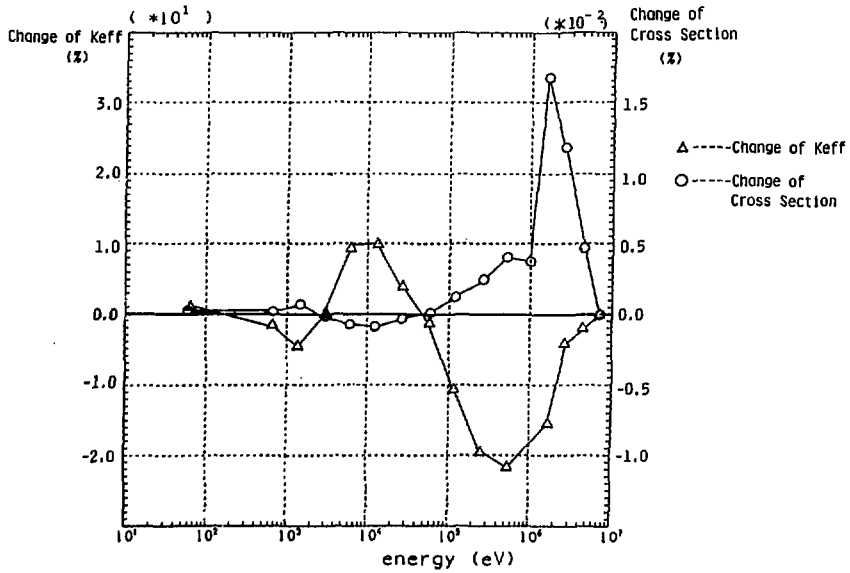

Fig. 4 Sensitivity coefficient and change of Keff with U-238 capture cross section in Pu-core (ZPPR-9).

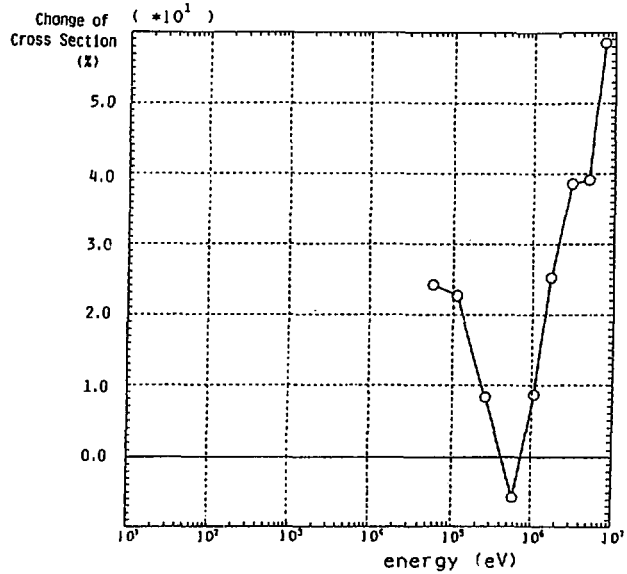

Fig. 5 U-238 inelastic cross section change from JENDL-2 to JENDL-3T (%).

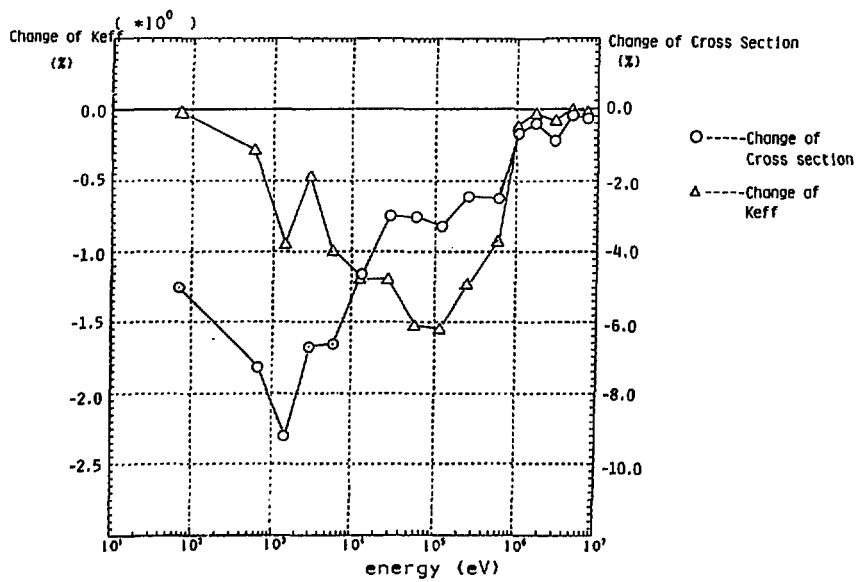

Fig. 6 Change of Keff and change of cross section with U-235 fission in U-core (FCA VI-2).

2.2.3 Fission-Product Cross Section Integral Tests and Adjustment Based on Integral Data

Fission-Product Nuclear Data Sub-Working Group
Japanese Nuclear Data Committee

T. Watanabe[1], T. Nishigori[2], S. Iijima, M. Kawai[3], M. Sasaki[4], T. Nakagawa[5], H. Matsunobu[6], A. Zukeran[7]

1) Kawasaki Heavy Industries, Ltd., Koto-ku, Tokyo, Japan.
2) Osaka University, Suita, Osaka, Japan.
3) Nippon Atomic Industry Group Co., Ltd., Minato-ku, Kawasaki, Japan.
4) Mitsubishi Atomic Power Industry Inc., Minato-ku, Tokyo, Japan.
5) Japan Atomic Energy Research Institute, Tokai, Ibaraki-ken, Japan.
6) Sumitomo Atomic Energy Industries, Ltd., Chiyoda-ku, Tokyo, Japan.
7) Hitachi, Ltd., Hitachi, Ibaraki-ken, Japan.

Abstract

The integral test of JENDL-2 fission product cross sections was carried out using EBR-II, CFRMF, and STEK data. For strongly absorbing fission-product nuclides, the flux depression corrections were approximately applied, and consistent results were obtained. Using these corrected results, integral test was evaluated on each nuclides again. To see overall consistency, bulk fission-product sample measurements in STEK were also investigated. Taking into account the moisture correction and standard deviations of experimental data, the C/E deviation from 1 are within 0.1.

The adjustment of cross sections based on the above integral test data were also performed using Bayesian least square method. The adjustment are made especially to the nuclides for which only integral data are available (e.g. Xe-132,134, Pm-147, Eu-152,154). Using adjusted cross section, the deviation of C/E from 1 will be within 0.2. Recommendations are given to the evaluation for JENDL-3.

1. Introduction

The objective of this representation is to give a brief review of the recent activities made by JNDC FPND Sub. WG. The review consists of the following two parts.

The first part is the integral test of JENDL-2 Fission-Product cross section data using EBR-II, CFRMF and STEK data.

The second part is the adjustment of cross section values to the above integral test results in order to reflect on the evaluation for JENDL-3, especially to the nuclides for which only integral data are available.

2. Integral test

At the beginning of 1987, the 70 group constants were regenerated with TIMS-PGG[1] together with self-shielding factor tables, and then integral tests were carried out again by comparing with the EBR-II[2] sample irradiation data and the STEK[3] and CFRMF[4] data. The normal and the adjoint fluxes of STEK cores were obtained by the third order B-spline interpolation (BINTFX program) of the values given in ref. (5). The flow diagram of the analysis is shown in Fig. 1.

After the previous analysis[6], the flux depression correction to the STEK experiments analysis was felt necessary, and the following approximate correction was applied when strongly absorbing samples were analyzed.

$$\Gamma \sim Pe(\Sigma a \ell)$$

Here

Γ ; flux depression correction factor defined as follows

$$\Gamma = \frac{\text{flux in sample}}{\text{flux without sample}}$$

Pe ; escape probabilities. The shape dependent approximate formula was adopted.

Σa ; macroscopic absorption cross section of the sample

ℓ ; mean chord length of the sample

The accuracy of these approximation to the cylindrical cell system is shown in Fig. 2. The error was evaluated to be within 10%.

For example, the epithermal flux depression of ^{103}Rh and ^{93}Nb samples are compared in Fig. 3.

The effect of the flux depression correction for Rh samples are shown in Figs. 4, 5, and for strongly absorbing elements almost the same results were obtained. From these results, it is clear that the systematic deviation of the calculation from experiment for strongly absorbing FP nuclides in soft spectrum core are drastically reduced enough to be used to the adjustment.

The sample averaged C/E of ρ/ρ_0 with and without flux depression correction are shown in Table 1. The upper and lower rows for each nuclide are the values of C/E with and without corrections, resp. However, as shown in Table 2, there remain some inconsistency between the results of analysis of different integral experiments.

To see overall consistency, integral sample measurement in STEK[7],[8] were also investigated. The tested samples were two HFR (-101 and -102) and one KFK (-101) measurement.

The two HFR samples are fission product samples produced in the HFR by thermal fission of ^{235}U, corresponding to a burn-up of about 60% and 30% FIMA respectively. The compositions of these samples are given in Refs. (7) and (8).

The KFK mixture is a fission product mock-up with known composition. This mixture consists of natural elements simulating a fission product mixture of a plutonium-fueled, steam-cooled, fast reactor having an average burn-up of 23 MWd/kg.

The C/E values of the analysis results are shown in Fig. 7. If moisture correction reported in ref. (8) and large uncertainty are taken into account, there remain no significant differences between the results on these samples and $|C/E-1|$ values are within 0.1.

3. Adjustment

The adjustment of main nuclide capture cross sections was carried out based mainly on the EBR-II and CFRMF integral test data using Bayesian least square method. The uncertainties of flux were taken into account as "method uncertainty" using flux covariance matrices (evaluated with COVERXCOVCOLPS program), and cross section covariance matrices were generated by the "strength function model" taking into account of the statistical model uncertainty[9]. The base data are those of JENDL-2 FP

values, and ref. (10), and are shown in Table 3. The covariance matrices are calculated with FPCOV program.

The adjustment of cross section values were performed with BAY-2 program, and the formula adopted were reported previously[6].

The adjustment were made especially to the nuclides for which only integral data are available e.g. ^{132}Xe, ^{134}Xe, ^{147}Pm, ^{152}Eu and ^{154}Eu.

The C/E of integral test before and after adjustment are compared in Table 4, and the recommended overall adjustment factors to the capture cross sections are shown in Table 5. Using these adjusted cross section values, $|C/E-1|$ seems to be within 0.2.

For ^{132}Xe, there is a giant resonance level below 1 Kev, and has large contribution to integral data. So uncertainties attributed to the resolved resonance parameters have large effect on the adjusted results as shown in Table 6 and Fig. 7. It will be desirable to review ^{132}Xe resolved resonance parameter before final capture cross section values are determined.

For ^{152}Eu and ^{154}Eu, there are inconsistency between C/E's of integral test in EBR51 and EBR52 spectrum. If we assume larger uncertainties in the strength function data, and permit more free change in the energy dependence of cross section, the adjusted cross section yields more consistent C/E as shown in Table 7 and Figs. 8 and 9.

From above results, the optical model parameters of these nuclide should be reevaluated before recommended capture cross section to JENDL-3 will be determined.

The present adjustment are carried out based on mainly EBR-II and CFRMF integral data. For ^{131}Xe and ^{147}Pm, the cross section adjustments using STEK integral data were tried and preliminary results are shown in Table 8. From these results, we can see that the weights or uncertainties attributed on integral data and the number of integral data of STEK adopted to the adjustment will have very important effect on adjusted cross section values.

4. Summary

As for integral test, much improvement was obtained with applying flux depression correction. However, there still remain some consistencies between integral data. Overall validity of JENDL-2 FP capture cross sections is shown by integral sample analysis and $|C/E-1|$'s are within 10%.

Capture cross section values were adjusted to the EBR-II and CFRMF data, and recommendation was obtained for JENDL-3 evaluation. However, some improvement, such as

(1) taking into account of scattering cross section uncertainties in case STEK experiments analysis

(2) simultaneous adjustment of plural nuclide capture cross sections. e.g., ^{131}Xe cross section simultaneously with ^{132}Xe and ^{134}Xe cross sections

(3) the check of the resolved resonance parameters and optical model parameters

will be necessary before JENDL-3 FP evaluation is finalized.

References

(1) Takano, H., et al., private communication
(2) Anderl, R.A., EGG-PHYS-5182 (1980)
(3) Veenema, J.J. et al., ECN-10 (1979)
(4) Harker, Y.D. et al., NEANDC(E)-209 "L" (1979)
(5) Dekker, J.W.M. et al., ECN-35 (1978)
(6) Watanabe, T., et al., JAERI M86-030 P.30 (1986)
(7) Gruppelaar, H., et al., RCN-205 (1974)
(8) Heijboer, R.J. and Jansen, A.J., ECN-11 (1976)
(9) Gruppelaar, H., IAEA-190 vol.II P.61 (1976)
(10) Mughabghab, S.F., Neutron Cross Section vol.1, part A & B Academic Press (1984)

Table 1 C/E of ρ/ρ_o with/without Flux Depression Correction

STEK-Nuclide	4000	3000	2000	1000	500	Average
Nb	1.028 1.048	1.075 1.098	1.066 1.089	1.106 1.132	1.197 1.222	1.074 1.096
Mo−95	0.972 1.021	1.034 1.066	1.073 1.094	1.111 1.121	1.071 1.074	1.029 1.060
Mo−97	0.959 0.997	1.044 1.052	1.028 1.035	1.082 1.088	1.110 1.115	1.038 1.045
Tc−99*	0.914 1.021	0.901 0.939	0.884 0.904	0.905 0.914	0.909 0.914	0.399 0.942
Ru−101	0.975 1.015	1.012 1.040	1.013 1.036	1.037 1.054	1.063 1.076	1.013 1.039
Rh−103*	1.016 1.813	1.085 1.345	1.065 1.147	1.107 1.136	1.142 1.154	1.060 1.350
Pd−104	1.594 1.605	1.308 1.315	1.065 1.070	1.289 1.293	2.086 2.089	1.381 1.388
Pd−105	0.971 0.996	0.968 0.988	0.987 1.002	0.995 1.006	0.991 1.003	0.978 0.996
Pd−107	0.942 1.971	0.969 0.991	0.969 1.989	1.007 1.021	1.043 1.056	0.971 0.993
Ag−109*	0.958 1.098	0.782 0.833	0.794 0.827	0.774 0.778	0.763 0.767	0.834 0.902
Cd−111	1.013 1.026	1.023 1.029	0.864 0.869	0.856 0.859	1.870 1.872	0.933 0.939
In*	0.916 2.306		0.914 1.056		0.900 0.918	0.909
Xe−131	0.926 0.979	1.077 1.112	1.176 1.197	1.171 1.175	1.179 1.180	1.045 1.082
Cs−133*	0.852 0.955	0.831 0.874	0.805 0.826	0.786 0.796	0.761 0.766	0.822 0.871
Cs−135*	0.899 0.981	0.875 0.908	0.840 0.857	0.870 0.877	0.841 0.844	0.877 0.915
Nd−143*	0.894 0.954	0.914 0.934	0.902 0.915	0.932 0.941	0.886 0.889	0.906

STEK-Nuclide	4000	3000	2000	1000	500	Average
Nd−145	0.836 0.869	0.865 0.881	0.894 0.905	0.943 0.950	1.171 1.176	0.876 0.895
Pm−147*	0.923 1.028	0.906 0.963	0.882 0.916	0.903 0.923	0.930 0.939	0.909 0.970
Sm−148	0.840 0.936	0.826 0.849	0.912 0.919	1.076 1.080	1.062 1.065	0.886 0.928
Sm−149*	0.916 1.828	1.000 1.171	1.012 1.087	1.043 1.097	1.051 1.084	0.999 1.327
Sm−150	0.895 0.972	0.857 0.881	0.831 0.842	0.876 0.880	1.048 1.050	0.881 0.914
Sm−151*	0.979 1.172	0.980 1.053	0.989 1.039	1.012 1.036	1.018 1.029	0.989 1.094
Sm−152*	0.874 1.258	0.845 1.045	0.782 0.861	0.812 0.827	1.088 1.093	0.836 1.010
Sm−154	0.873 0.892	0.871 0.880	0.836 0.843	0.978 0.982	0.523 0.525	0.865 0.877
Eu*	0.885 1.210	0.880 0.994	0.858 0.931	0.833 0.871	0.800 0.801	0.863 1.030
Eu−153*	0.950 1.053	0.961 1.018	0.936 0.975	0.904 0.928	0.887 0.900	0.939 0.995
Gd−156	1.238 1.262	1.112 1.124	1.194 1.204	0.756 0.760	0.918 0.920	1.606 1.070
Gd−157*	0.855 2.710	0.885 1.136	0.866 0.928	0.815 0.828	1.010 1.021	0.864 1.213
Tb−159	0.951 0.977	0.953 0.969	0.931 0.942	0.925 0.932	0.949 0.953	0.944 0.959

Table 2 Comparison Between Various Integral Test

Nuclide	S T E K		C F R M F	E B R － II	
	Average	500		core	Reflector
Tc-99	0.90	0.91	1.23(15)		
Ag-109	*0.83*	*0.76*	*0.67(10)*		
Cs-133	0.82	0.76	0.91(10)		
Nd-143	0.91	0.89		0.85(6)	0.86(14)
Pm-147	0.91	0.93	1.10(13)		
Sm-149	1.00	1.05		0.88(6)	0.97(14)
Sm-152	0.84	1.09	1.0 (6)		
Eu-151	0.86	0.80	0.83(6)	0.68(6)	0.68(15)
Eu-153	0.94	0.89		0.83(7)	0.87(14)

Table 3 Data to generate Covariance Matrices by Strength Function Model

Nuclide	S_0 ($\delta S_0/S_0$) 10^{-4}	S_1 ($\delta S_1/S_1$) 10^{-4}	S_2 ($\delta S_2/S_2$) 10^{-4}	P_r ($\delta S_r/S_r$) ev	D_0 ($\delta D_0/D_0$) ev	T Mev^{-1}
Xe-131	0.7 (0.3)	1.58(0.3)	0.99(0.3)	0.114 (0.15)	38(0.3)	0.65
132	1.04(0.3)	1.58(0.3)	0.99(0.3)	0.1055(0.15)	1070(0.2)	0.625
134	1.04(0.3)	1.58(0.3)	0.99(0.3)	0.11 (0.15)	2700(0.2)	0.557
Pm-147	3.1 (0.3)	0.68(0.3)	3.48(0.3)	0.066 (0.09)	4.6 (0.3)	0.43
Eu-151	3.7 (0.2)	1.0 (0.2)	3.5 (0.2)	0.13 (0.15)	0.11 (0.15)	0.41
152	2.48(0.33)	0.92(0.3)	3.2 (0.3)	0.1 (0.3)	0.462(0.1)	0.565
153	2.61(0.2)	1.4 (0.2)	2.95(0.2)	0.094 (0.15)	1.49 (0.15)	0.432
154	2.48(0.3)	0.92(0.3)	3.17(0.3)	0.13 (0.1)	1.13 (0.23)	0.496

Table 4 Results of Adjustment

Nuclide	Spectrum	C/E Before Adjust. (% error)	C/E After Adjust. (% error)
Xe-132	CFRMF	1.29 (15)	1.06 (5)
Xe-134	CFRMF	1.37 (19)	1.02 (5)
Pm-147	CFRMF	1.10 (19)	1.03 (10)
Eu-152	EBR51	0.64 (21)	0.80 (11)
	EBR52	0.90 (28)	1.12 (13)
Eu-154	EBR51	0.70 (18)	0.87 (10)
	EBR52	0.84 (22)	1.04 (12)

Table 5 Recommendation from Adjustment

Nuclide	Correction to σ_γ (77kev)	Rrmarks
Xe-132	0.72	If RRP changed, reevaluation necessary
Xe-134	0.74	
Pm-147	0.93	If STEK included, no correction will be necessary
Eu-152	1.21	If OMP changed reevaluation necessary
Eu-154	1.20	If OMP changed reevaluation necessary
...	...	...
Xe-131	0.61	Simultaneous adjustment with ^{132,134}Xe will be necessary
Eu-151	1.20	consistent to STEK data
Eu-153	1.11	consistent to STEK data

Table 6 Contribution of RRP to ^{132}Xe Adjustment

Nuclide	σ (RRP)	C/E (% error)	Correction to σ₀ (77kev)
Xe-132	———	1.29(15)	———
	0.1	1.06(5)	0.72
	0.3	1.04(6)	0.81
Eu-153	———	1.37(19)	———
	0.1	1.02(5)	0.74
	0.3	1.02(5)	0.74

Table 7 Effect of Strength function Uncertainty

Nuclide	σ (SI)	C/E		Correction to σ₀ (77kev)
Eu-152	———	0.64	0.90	———
	0.3	0.80	1.11	1.21
	0.5	0.85	1.12	1.35
Eu-154	———	0.69	0.84	———
	0.3	0.87	1.04	1.20
	0.5	0.94	1.05	1.36

Table 8 Preliminary Results of Adjustment using STEK Data

Nuclide	Spectrum	C/E Before Adjust (% error)	C/E After Adjust (% error)	Correction to σ₀ (77kev)
Xe-131	STEK500	1.18 (14)	0.96 (5)	0.61
	STEK1000	1.17 (10)	0.98 (1)	
	STEK2000	1.18 (8)	1.04 (2)	
Pm-147	CFRMF	1.10 (19)	1.13 (7)	1.10*
	STEK1000	0.94 (12)	0.97 (4)	

* It only CFRMF data used, correction is 0.93

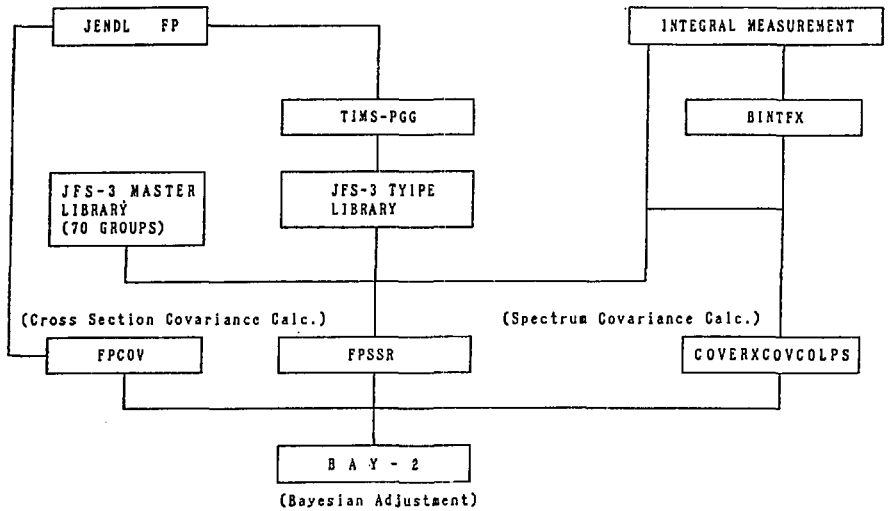

Fig. 1 Flow Diagram of Integral Test and Adjustment

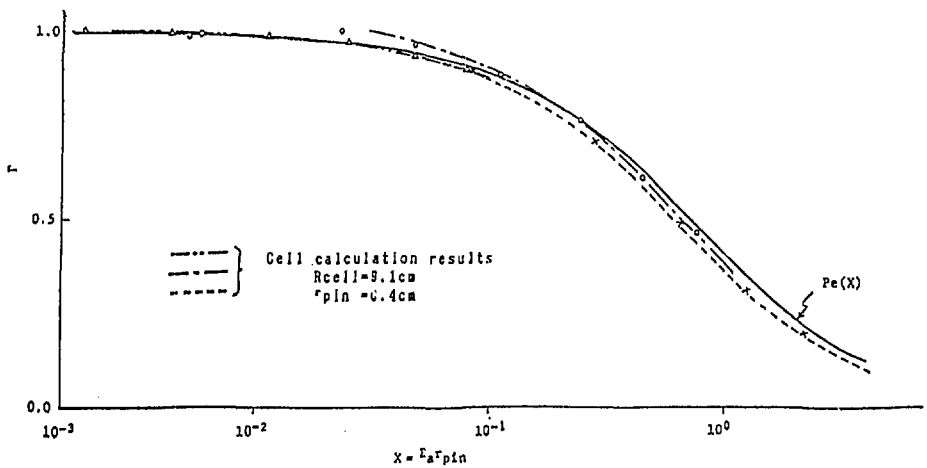

Fig. 2 Error of Approximation to the Flux Depression: Γ

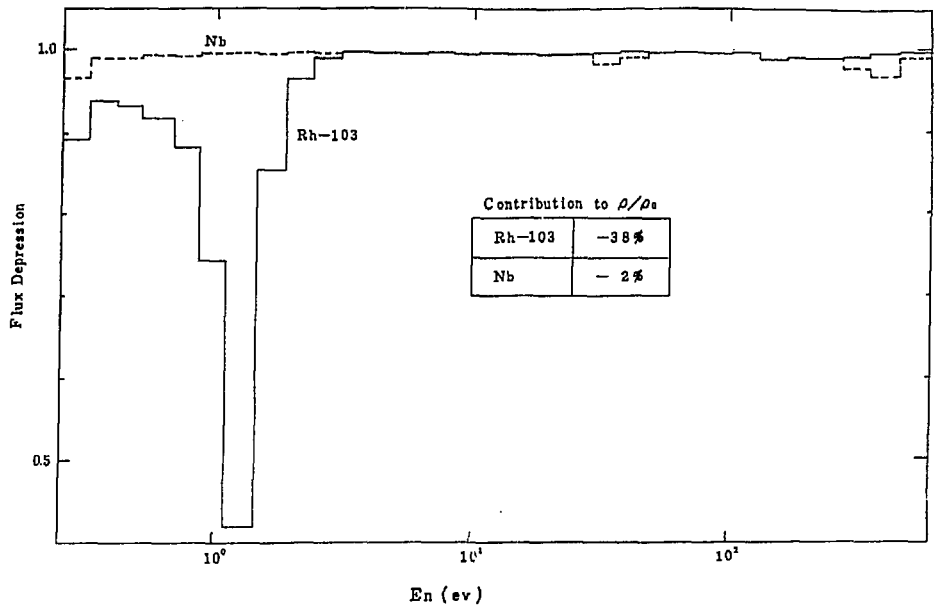

Fig. 3 Approximate Flux Depression in ^{103}Rh and ^{93}Nb Sample

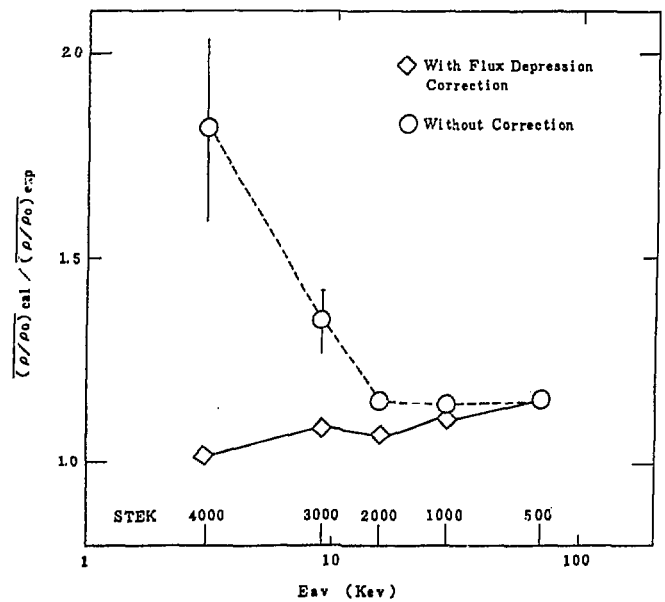

Fig. 4 C/E to ρ/ρ_0 of ^{103}Rh Sample in STEK

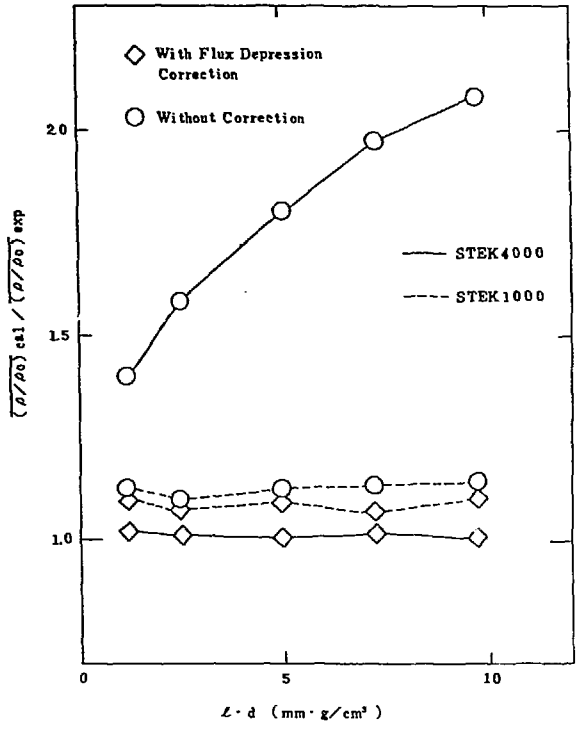

Fig. 5 Effect of the Flux Depression Correction to the ^{103}Rh Sample in STEK

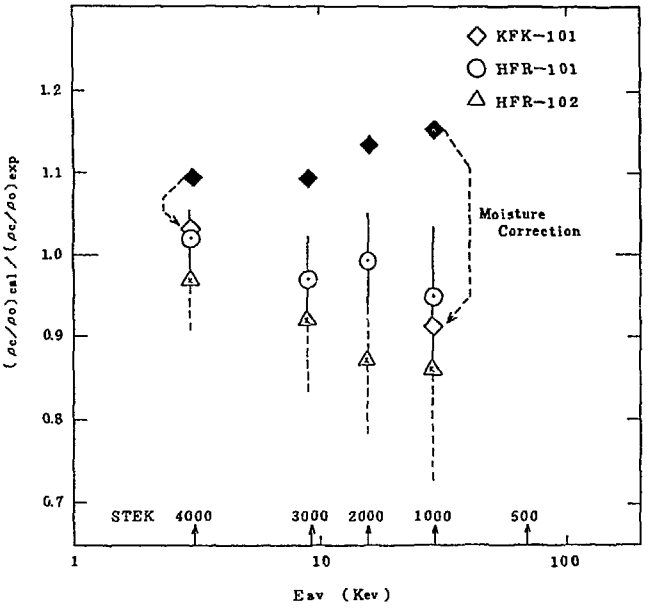

Fig. 6 C/E to ρ_c/ρ_o of Integral Samples in STEK

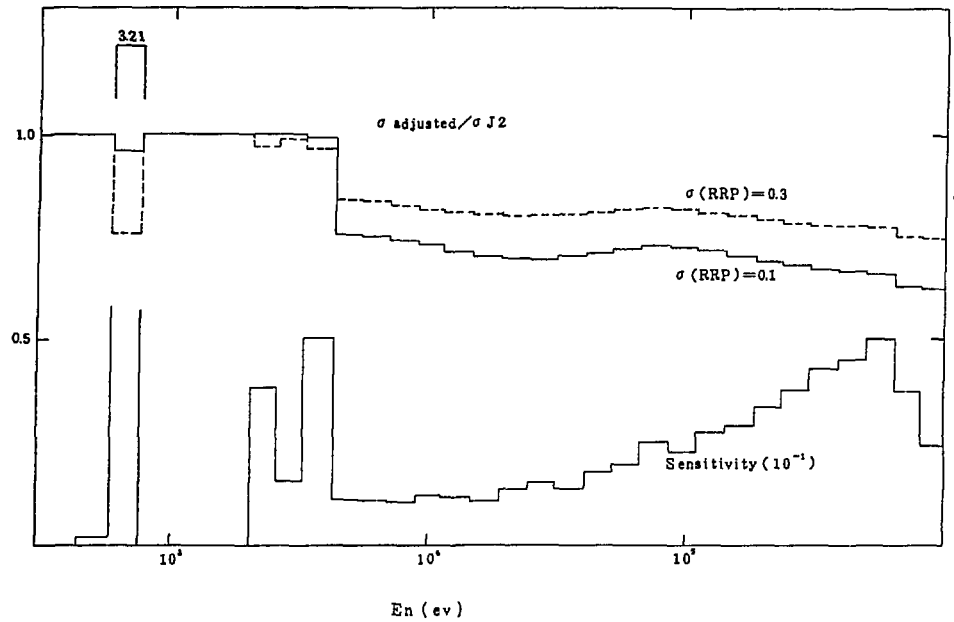

Fig. 7 Effect of σ(RRP) on ^{132}Xe Adjustment

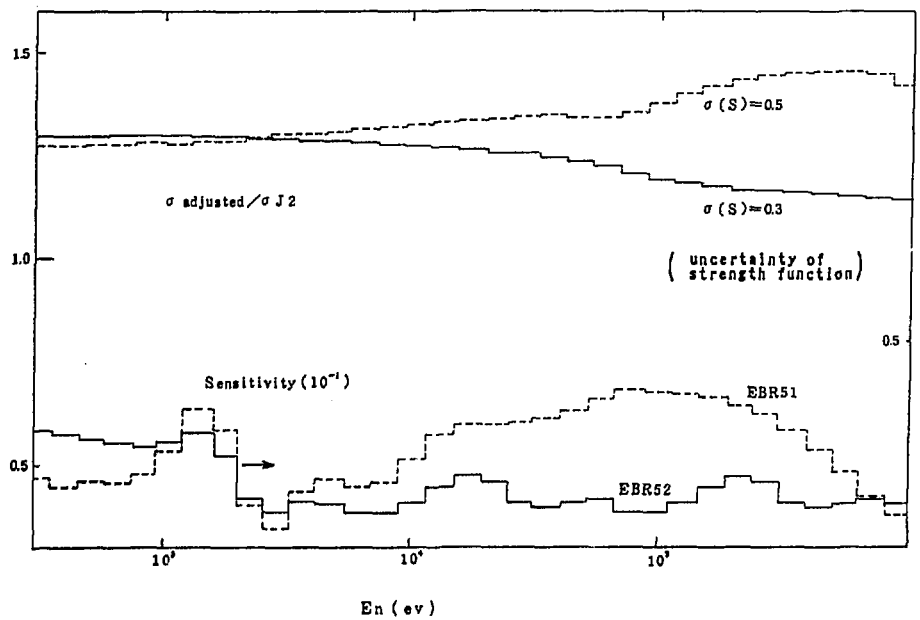

Fig. 8 Effect of Statistical Model Uncertainty on ^{152}Eu Adjustment

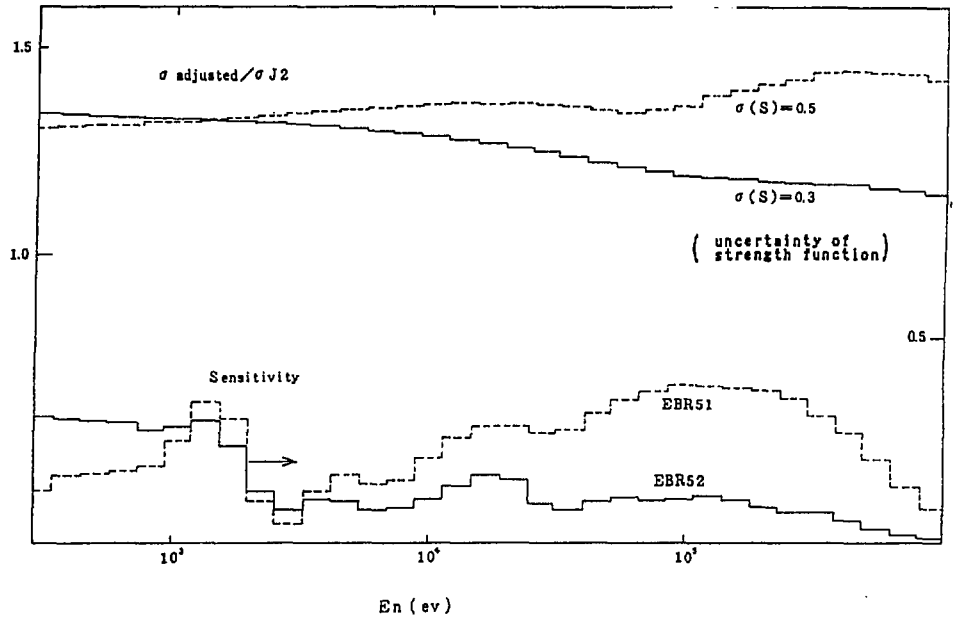

Fig. 9 Effect of Statistical Model Uncertainty on ^{154}Eu Adjustment

2.2.4 Shielding Benchmark Test for JENDL-3T

Akira HASEGAWA and JNDC Shielding Sub-working Group +

Japan Atomic Energy Research Institute
Tokai-mura, Naka-gun, Ibaraki-ken, Japan

Summary

The results of the shielding benchmark tests for JENDL-3T*(testing stage version of JENDL-3), performed by JNDC Shielding Sub-working group, are summarized. Especially, problems of total cross-section in MeV range for O, Na, Fe, revealed from the analysis of the Broomstick's experiment, are discussed in details. For the deep penetration profiles of Fe, which is very important feature in shielding calculation, ASPIS benchmark experiment is analysed and discussed.

From the study overall applicability of JENDL-3T data for the shielding calculation is confirmed. At the same time some problems still remained are also pointed out. By the reflection of this feedback information applicability of JENDL-3 , forth coming official version, will be greatly improved.

Key words: JENDL-3T, shielding, benchmark test, integral test, data applicability check, total cross-section, Broomstick experiment, ASPIS Fe experiment, deep penetration profile, iron cross-section, oxygen cross-section, sodium cross-section

---

* JENDL-3T is a temporary file for testing the evaluated data for JENDL-3. The data in JENDL-3T will be partly revised in JENDL-3.

+ JNDC Shielding Sub-working Group member
KAWAI Masayoshi(Leader,NAIG), OKA Yoshiaki (U. Tokyo), ITO Yasuyoshi (JAERI), TSUNODA Hirokazu (MRI), UEKI Kohtaro(Ship Res. Inst.), YAMANO Naoki (Sumitomo Atomic), SASAKI Kenji (MAPI), MATSUMOTO Nobuhiro (Mitsui Engng. Shipbldg.), SAKURAI Kiyoshi (Inst Nucl. Safety), UEMATSU Mikio (NAIG), TAKEMURA Morio (KHI), HASEGAWA Akira (JAERI)

1. Out-line of the shielding benchmark tests for JENDL-3T

(a) Shielding benchmark test in the frame work of JENDL-3T benchmarks

The project of the benchmark test for JENDL-3T /1/ is now in progress in Japanese Nuclear Data Committee(JNDC) organized by the Subcommittee on Reactor Constants with the cooperation between Nuclear Code Committee or Research committee of Reactor Physics.

JENDL-3T is a temporary version of JENDL-3, where 'T' stands for temporary or testing or tentative version, and it is destined to be the official version of JENDL-3. To confirm the applicability of the evaluated data delivered from the evaluater, benchmark testings are planned and performed for the primary nuclides important for the nuclear energy applications. The selected fields for the benchmark test covers following fields, i.e., LWR(Light water Reactor), HCLWR(High Conversion Light Water Reactor), FBR(Fast Breeder Reactor), Fusion Neutronics, Shielding, Dosimetry.

This benchmark test has a meaning of the testing prior to the fixing of the final version of JENDL-3. Thus the results from this benchmark test will be reflected to the final version.

To contribute to the JENDL-3T benchmarks in shielding applications, a sub-working group called Shielding Benchmark Test SWG was set up in the Working Group on Group Constants for Fusion and Shielding in the Subcommittee of Reactor Constants. The active members are 12, they are listed in the foot note on the top page. The results all presented in this article are the works performed by this SWG.

b) Selected problems as the shielding benchmark test and their status as of Nov '87.

As the shielding benchmark test, following experiments were selected as the benchmark problems. In the list, the name in the parenthesis represents the person contributing to the testing.

A. Total cross-section check by Broomstick's experiments/2-4/:
Uncollided spectrum measurements at ORNL using TSF-II reactor.
1) Oxygen (152.4cm),
2) Sodium (60.6cm),
3) Fe-natural (20.3 and 30.5cm) (A.Hasegawa).

The results are discussed in section 2.

B. Fe (& SUS) data:

1) ASPIS Fe deep penetration experiments (140 cm thick iron) using fission neutron source /5/, (A.Hasegawa & K.Ueki)

2) KfK leakage spectrum measurements from iron sphere (15 to 40 cm) using Cf-252 neutron source /6/, (N.Yamano)

3) ORNL neutron transmission experiment of iron (& SUS) block(30 to 90 cm thick) using collimated neutron beam of Tour Shielding Facility /7/. (M.Kawai)

The results for ASPIS are shown in section 3. The others, analysis is in progress.

C. Na data:

1) ORNL TSF Sodium deep penetration experiment (2.5 ft to 15 feet) /8/ (K.Sakurai & M.Kawai)

The results are presented as the poster session 10 /9/ in this seminar.

2) ISPRA EURACOS-II Sodium deep penetration experiment(400 cm thick) /10/ (A.Hasegawa)

The analysis is undergoing.

D. Carbon data:

1) ASPIS Graphite shielding experiment at WINFRITH /11/. (K.Sakurai & K.Ueki)

The results are presented as the poster session 12 /12/ in this seminar.

2) Profio experiment by RPI /13/ (N.Matsumoto)

The analysis is now going on.

E. Others: Light nuclides and structural materials relating for fusion neutronics

1) HANSEN experiment (Li-6, Li-7, C, O, Fe)/14/ (M.Kawai,M.Uematsu)

2) Linac TOF leakage spectrum experiment by KURRI (Li, Fe, Cr, Ni, SUS) /15/ (M.Kawai,M.Uematsu)

For these materials analyses are undergoing.

F. Fe secondary gamma-ray production cross-section data:

1) SUS-304 ORNL 14MeV neutron penetration experiment /16/
(K.Sakurai & K.Ueki)
The results are presented as the poster session 11 /17/
in this seminar.

In the above analyses, for comparisons, ENDF/B-4 /18/, JENDL2 /19/ and JENDL3-PR1 /20/ data are also used as well as JENDL-3T /1/. The analyses are performed by several neutron transport codes of Sn and Monte Carlo, such as ANISN-Jr(1-D)/21/ , DIAC(1-D) /22/ , DOT3.5(2-D) /23/, MORSE-CG(2-D) /24/ with more than 100 energy group calculations. Group constants are prepared by ourselves by PROF-GROUCH-G/B /25/ or RADHEAT-V4 /22/. Some analyses use JSSTDL library system /26/, which is a new library system for the sake of common use in the shielding calculations, it enables the user to provide proper group structure library he needs starting from the JSSTDL-295 common library. This library contains only major nuclides(25 nuclides) of JENDL-3T at this moment.

As already written for the comments in each benchmark items, some of them are now in progress for the analysis and some of them are presented in other sessions of this seminar. Here only the results of the analyses of A. and B. are presented in details.

2. Total cross-section check in MeV range by Broomstick experiments

a. General comments for the experiments

Broomstick experiments were performed by Straker to investigate the minima in the total neutron cross sections in MeV energy range for the typical shielding materials /27/.

Fig. 1 shows a schematic of the experiment. The sample was a cylinder form of 4 inch diameter and placed so that its axis coincided with the axis of the neutron beam. In order to reduce the effect of neutron inscattering in the sample, the distance from the neutron source (the Tower Shielding Reactor II) to the sample was 50 feet and the detector was 50 feet from the sample. The neutron beam was confined to a diameter of 3.5 inch by collimators placed between the reactor and sample near the sample position. To reduce air-scattering effects the reactor and detector were shielded with lead and water and the reactor beam and detector acceptance were tightly collimated.

The detector was a nominal 2 in X 2 in NE213 scintillator. The unfolding of the pulse-height distributions was accomplished using the FERDOR code.

b. Calculation method

As described above, this experiment is performed in good geometry. No transport calculation are needed for the analysis.

The calculation consists from two parts, the first one is to determine a transmitted uncollided spectrum, here we should not miss the minima of any kind in the total cross section and the second one is to fold the so calculated uncollided spectrum with the resolution function of the NE-213 spectrometer system which actually used. Source neutron spectrum and the detector resolution functions are given in a tabulated form. These calculation indications are given in the references /2/-/4/. The results are only presented in curves, we had to read the data from these reports to digital form.

To perform the calculation, we made a code system named WINDOW /28/ which accesses the ENDF/B format library and to calculate the value directly comparable to the experimental one.

c. Results

1) Oxygen

thickness : 154.2 cm

Testing Energy range : 800keV to 11 MeV

The results are given in Fig.2.1, where upper part shows transmitted spectrum of the experimental one and the calculated one by JENDL-3T and ENDF/B-IV data, and lower part shows the C/E value profiles of each evaluated data for the energy. In the Table 2.1, statistics of C/E is given for the each evaluated data. First column is the average of C/E, second is the absolute average of the deviation from C/E=1.0 ,third is standard deviation, i.e., root mean square.

From the figure and the table, we can see the C/E value by ENDF/B-IV is better than JENDL-3T. As the standard deviation(STD) is almost the same between the two, JENDL-3T data is 7 or 8 % underestimated from ENDF/B-IV. From this integral test, both ENDF/B-IV and JENDL-3T underestimate the experiment, i.e., total cross section in

the evaluated data file are relatively large. Because total cross section and the transmitted spectrum has the inverse proportional relation. JENDL-3T data are not superior to the ENDF/B-IV yet.

Table 2.1 Statistics of C/E values for Oxygen Broomstick experiment

	C/E	Abs(1.0-C/E)	STD
JENDL-3T	0.686	0.353	0.218
ENDF/B-IV	0.756	0.262	0.213

2) Sodium

thickness : 60.6 cm

Testing Energy range : 800keV to 11 MeV

The results are given in Fig.2.2, and Table 2.2. From the figure and the table, we can see the C/E value by all evaluations are overestimated systematically.There are no differences between JENDL-3T and JENDL-2 evaluations. On the other hand, there are clear differences between JENDL and ENDF/B-IV in the energy range 6 to 10 MeV. In this range, ENDF/B-IV has better agreement than JENDL.

From this integral test, both ENDF/B-IV and JENDL-3T overestimate the experiment about 20 % systematically , i.e., total cross section in the evaluated data file are suggested relatively small. No change was made from JENDL-2 to JENDL-3T for the total cross section of this energy range. JENDL-3T data are not superior to the ENDF/B-IV yet.

Table 2.2 Statistics of C/E values for Sodium Broomstick experiment

	C/E	Abs(1.0-C/E)	STD
JENDL-3T	1.243	0.243	0.189
JENDL-2	1.242	0.242	0.188
ENDF/B-IV	1.217	0.217	0.215

3) Iron

thickness : a) 20.3 cm b) 30.5 cm

Testing Energy range : a) 1.2-11. MeV b) 1.0-8. MeV

The results are given in Fig.2.3 - 2.4, and Table 2.3. From the figure and the table, we can comments following observations.

1. We can see no clear differences among JENDL evaluations, i.e., JENDL-3T, -3PR1, -2.
2. As to the standard deviation in the Table 2.3, the value by ENDF/B-IV (0.086) is much better than JENDL (0.160), about half the value of JENDL. Although the average of C/E is not so different between ENDF (0.954) and JENDL (0.958).
3. For the thick sample case, the agreement by ENDF/B-IV (C/E=0.986) is better than JENDL (0.937).
4. Especially in JENDL evaluations, C/E profiles has some systematic tendency i.e., C/E is increasing with energy. But not so much for ENDF case.
   The values of C/E of JENDL is too small (about 0.7) in 1 to 3 MeV, it suggests that the total cross section is too large. For 8 to 10 MeV, the values of C/E of JENDL is too large (about 1.2), i.e., total cross section is too small.

This time also JENDL-3T data are not superior to the ENDF/B-IV yet.

Table 2.3 Statistics of C/E values for Iron Broomstick experiment

	C/E		Abs(1.0-C/E)		STD	
	a	b	a	b	a	b
JENDL-3T	0.958	(0.937)	0.142	(0.219)	0.160	(0.254)
JENDL-3P1	0.959	(0.935)	0.144	(0.220)	0.163	(0.255)
JENDL-2	0.959	(0.938)	0.144	(0.219)	0.163	(0.254)
ENDF/B-IV	0.954	(0.986)	0.092	(0.130)	0.086	(0.176)

•The values in the parenthesis are for the thickness 30.5 cm

a: thickness 20.3 cm

b: thickness 30.5 cm

3. Applicability of natural iron data by the analysis of the ASPIS deep penetration experiments

a. General comments for the experiments

We selected this experiment because it was designed to provide information of benchmark quality for the testing of data and calculational methods for deep-penetration profiles by natural iron shielding material.

Experimental configuration is as follows, a low-power natural uranium converter plate, driven by the source reactor NESTOR, provided a large thin disc source of fission neutrons is placed at the interface of a graphite moderator and extensive iron shield (= 140 cm thickness).

Analyses are made for the axial attenuation measurements with three threshold detectors and one low-energy activation detector, and for the spectrometer measurements at four selected positions in the iron shield.

b. Calculational model and analysis

As for the calculational model, we closely follow the model in the report of M. D. Carter et al. /29/. However some modifications were made. Converter plate region is simulated rather in a straight way, i.e., it is composed from 5 regions as represented by Al-Fe-U-Fe-Al layers. Used configuration is shown in Fig.3.1 together with the detailed model of the converter plate in the upper part of the figure.

The volume distributed sources (equivalent radius is 59.3 cm and thickness 0.318 cm) were treated as cross products of energy and space(in radial direction only). For energy dependence of fission emitted neutrons, ENDF/B-V U-235 data was used. Average values of each functional data were calculated and inputted on each mesh points of the fuel region.

Cross-sections were prepared by PROF-GROUCH-G/B code /25/. For the energy groups, BERMUDA 121 /30/ group structure was adopted, which is defined as follows, from 16.487 MeV to 1.054 MeV (1-44 groups) lethargy increment(Δu) is 0.0625, from 1.054 MeV to 19.304 keV (45-76 groups) Δu is 0.125, for the rest of energy down to 0.32241 eV Δu is 0.250 and one thermal group down to 1.0E-5 eV. This energy

group structure is sufficiently detail for the ASPIS analysis.

Anisotropy were included up to P_5.

Weighting functions used for the generation of group cross-section were 1/E above 0.32241 eV and below Maxwellian.

For Fe natural cross-sections in the test region, which is thought as nearly pure material, fully shielded cross-sections including higher Pl matrices (1 / σt weight i.e., $\sigma_0 = 0.$) were calculated and used.

For the macro cross-section generation for DOT code, GLIB.MAKE -MACROX utilities /26/ were used.

Calculations were performed by DOT3.5 /23/ with S48 P_5 R-Z: 53x92 meshes. Typical running time was 140 minutes, required I/O exceeded 200,000 and used core memory was about 4 Mega-byte per one case by FACOM-M/380.

c. Results and discussion

To test the applicability of JENDL-3T data, JENDL-3 PR1 and ENDF/B-IV data are also used for comparisons.

c.1. Axial attenuation measurements

Measurements are made for the following 4 detectors.

Au(n,γ) Cd covered	<ENDF/B-V	MAT=1379 >
Rh-103(n,n') Rh-103m	<IRDF	MAT=4520 >
In-115(n,n') In-115m	<ENDF/B-V	MAT=6437 >
S-32(n,p) P-32	<ENDF/B-V	MAT=6439 >

Used detector cross-sections in the calculation of reaction rate are shown in the < > brackets. As to the Au detector, self-shielding correction of the foil was made by using Bethe's method /31/ and Cd-covered effect was also considered. Threshold detectors used in the analysis are shown in Fig.3.2 together with the sensitive energy range of each detector for shallow (=6cm) and deep penetration (=64cm) case.

The results are given in Fig.3.3 and 3.4. In the latter figure, C/E (calculated to experimental) values are plotted. From Fig.3.3, in general all results show good agreements for the axial attenuation profiles. But in Fig.3.4, for some detectors differences are clear between the results from JENDL-3T or -3PR1 and ENDF/B-IV. It reflects the differences of cross-sections of natural iron.

The C/E values for each detectors can be summarized as follows,

detector	JENDL-3T	JENDL-3PR1	ENDF/B-IV
Au(n,γ) Cd covered	1.2 - 1.0	1.2 - 0.9	1.1 - 1.0
Rh-103(n,n') Rh-103m	1.2 - 0.5	1.2 - 0.5	1.4 - 0.6
In-115(n,n') In-115m	1.1 - 0.6	1.1 - 0.6	1.1 - 0.9
S-32(n,p) P-32	1.3 - 0.8	1.1 - 0.6	1.1 - 0.6

A. S-32

The same tendency is observed both of ENDF/B-IV and JENDL-3PR1, i.e., C/E values are greatly underestimated along with the penetration depth. But for JENDL-3T, declining tendency with penetration depth is a little bit cured. As seen from Fig.3.2, this reaction is very sensitive of high energy spectra, from 2.0 MeV to 5.0 MeV. This suggests that for ENDF/ B-IV and JRNDL-3PR1 the inelastic cross-section of this energy range, which greatly contribute to the the formation of the spectra, is too high. Most of the neutrons generated in this energy range are slowed down by these high inelastic cross sections. For JENDL-3T, inelastic cross-section was changed to reduce the discrepancy.

B. Rh-103

This detector is sensitive to rather soft spectrum among the threshold detectors used in the experiments. C/E behaviors for both of the cross-sections are nearly same, no special conclusion are made.

C. In-115

A clear difference is observed between ENDF/B-IV and JENDL-3T & -3PR1. C/E of ENDF/B is almost flat along with the penetration depth, on the contrary JENDL profile is underpredicted considerably. This difference comes from the difference in the cross-sections. From 600 keV to 1.2 MeV energy, there is no clear difference in the total cross-section, but in the elastic and inelastic cross-sections some differences are found. As to the JENDL data, magnitude between elastic and inelastic scattering cross-section is attributed to this underprediction. This explanation is also supported from the results of the spectrum measurements described in section c.2.

D. Au-197 Cd covered

This is only one resonance detector used in the measurement. High energy sensitivity is attributed to only for a few Au resonances in the low energies, especially 4.9 eV resonance. As seen from Fig.3.4, C/E values of ENDF/B-IV data shows good results, no clear tendency is seen with the penetration depth. On the other hand, JENDL-3T and 3PR1 results have a tendency of underprediction with the penetration depth.

From the detailed cross-section check, we found that the JENDL 3PR1 data has errors for thermal values.

Table 3.1 Thermal value of Fe natural (2200 m/s value)

		JENDL-3 PR1	ENDF/B-IV	BNL-325 /32/
elastic	σ_e	12.55 (1.11)	11.50 (1.01)	11.35 (1.00)
capture	σ_a	2.52 (0.98)	2.56 (1.00)	2.56 (1.00)
total	σ_t	15.07 (1.08)	14.07 (1.01)	13.91 (1.00)

n.b. The values in the parenthesis are the ratio to the BNL-325 value.

Total and elastic cross section is 10 % higher than the normally recommended value. It was not sufficient to check the thermal values when the natural element data was build up from the elemental isotopes at the file editing stage of JENDL-3 PR1 data.

For JENDL-3T data, these errors are cleared. Although the difference is a little bit reduced, there still remains discrepancy.

c.2. Flux spectrometer measurements

Comprehensive spectrometer measurements at four selected positions within the iron shield are made, and measured spectra are obtained from unfolding of all these data using the RADAK code.

The results are shown in Fig.3.5 to Fig.3.8, in each figure comparison of experimental and calculated fluxes, and C/E values are displayed.

Over all agreements are rather good from these figures. For shallow penetration (=22.8 cm), all calculations are overpredicted, and underprediction proceeds with the penetration depth but not so much.

For JENDL-3T and -3PR1 data, as mentioned in c.1-C In-115 axial attenuation measurement, clear difference in fluxes from 600 keV to 1.2 MeV are seen, especially C/E values in this range of JENDL-3T and -3PR1 data are considerably lower than that of the ENDF/B-IV (see Fig.3.6).

On the other hand, the agreements by the JENDL-3T and -3PR1 data near the 24 keV Fe resonance range are superior to ENDF/B-IV data considerably. This means the 24 keV resonance data of JENDL-3T and -3PR1 is better than ENDF/B-IV.

Underprediction of fluxes in MeV range (2 -5 MeV) appeared in all evaluations JENDL-3T,-3PR1 and ENDF/B-IV (Fig.3.6 to 3.8), suggests that the inelastic cross- section in this energy range is rather high. This conclusion is also supported by the S-32 axial attenuation measurements result as described in section c.1-A.

4. Conclusion

From the study overall applicability of JENDL-3T data for the shielding calculation is confirmed. At the same time some problems still remained in JENDL-3T are also pointed out. Those are:

From Broomstick experimrnt;

Oxygen

total cross section for 2 to 8 MeV is rather large.

Sodium

total cross section for 2 to 10 MeV is rather small, especially for 6 to 10 MeV.

Iron-natural

total cross section for 1 to 3 MeV is rather large, contrarily for 8 to 10 MeV rather small.

For the several evaluations in JENDL, i.e., JENDL-2, -3PR1, -3T, no clear revision in total cross-section was found for the tested nuclides. Overall predictability of ENDF/B-IV is better than JENDL for this integral test.

From ASPIS analysis;

The agreement between calculation and experiment in the spectrum just after the 24 keV resonance is superior for JENDL evaluation, it means the evaluation of Fe 24 keV resonance is very good for JENDL.

From the evidence of C/E profiles in In-115 and the measured spectrum, some problems still remains in the assignments between elastic and inelastic cross-section in 600 keV to 1.2 MeV.

From axial attenuation profile of S-32 and the spectrum, JENDL-3T gives better results than ENDF/B-IV or JENDL-3PR1. However the declining tendency is still observed, i.e., underprediction proceeds with penetration depth. Inelastic scattering cross-section seems to be attributed.

From the attenuation profile of Au, the result by JENDL-3T is improved a little compared to that of JENDL-3PR1 but it does not yet reach to the level by ENDF/B-IV. Still some problems are remained.

By the reflection of these feedback information applicability of JENDL-3, forth coming official version, will be greatly improved.

References

/1/ JENDL compilation group (Nuclear Data Center, JAERI): JENL-3T private communication (1987).

/2/ Maerker R.E. : 'SDT1. Iron Broomstick Experiment -An Experimental Check of Neutron Total Cross Sections,' ORNL-TM-3867 (Revised), (1972).

/3/ Maerker R.E. : 'SDT2. Oxygen Broomstick Experiment -An Experimental Check of Neutron Total Cross Sections,' ORNL-TM-3868 (Revised), (1972).

/4/ Maerker R.E. : 'SDT4. Sodium Broomstick Experiment -An Experimental Check of Neutron Total Cross Sections,' ORNL-TM-3870 (Revised), (1972).

/5/ Carter M.D. and Packwood A. :'The Winfrith Benchmark Experimen in Iron -Experimental Results,' Proc. of the Specialists' Meeting on Sensitivity Studies and Shielding Benchmarks, p111-119, Paris, OECD, October 7-10 (1975).

/6/ Werle H., Kappler F. and Kuhn D. : 'Measurements of Neutron Leakage Spectra from Iron Spheres with a Cf-252 Source in the Center,' NEACRP-U-73, p8 (1976).

/7/ Maerker R.E., and Muckenthaler, F.J.: 'Final Report on a Benchmark Experiment for Neutron transport through Iron and Stainless Steel, ' ORNL-4892 (1974)

/8/ Maerker R.E., Muckenthaler, F.J., Childs R.L., and Gritzner M.L. : 'Final Report on a Benchmark Experiment for Neutron transport in Thick Sodium, ' ORNL-4880 (1974)

/9/ Sakurai K., Ueki K. and Kawai M. : 'Integral Test of Neutron Cross Sections of Sodium in the JENDL-3T through an Analysis on the Neutron Penetration Experiment at ORNL TSF,' Seminar on Nuclear Data, Poster Session No. 10 , Nov.12-13, Tokai, (1987).

/10/ Perlini G., Rief, H. : 'Neutron Penetration in Sodium at EURACOS II , ' NEA CRP Restricted Specialists Meeting on Shielding Benchmarks , Paris, 10/11 Sept,1984 Session B-1 (1984)

/11/ Carter M.D., Miller P.C. and Packwood A. :' The ASPIS Graphite Benchmark Experiment - Part 1 Experimental data and Preliminary Calculations,' NEACRP-A-630 (1984)

/12/ Ueki K. and Sakurai K. : 'Neutron Integral Test of Graphite Cross Sections in MeV Energy Region for the JENDL-3T through an Analysis of the Winfrith Shielding Experiment,' Seminar on Nuclear Data, Poster Session No. 12 , Nov.12-13, Tokai, (1987).

/13/ Profio A.E. : 'Fast Neutron Spectrum from a Point Fission Source in Infinite Graphite,' ORNL-RSIC-25 (1969).

/14/ Hansen L.F., Wong C., Komoto T. and Anderson J.D. :'Measurements of the Neutron Spectra from Materials Used in Fusion Reactors and Calculation Using the ENDF/B-III and -IV Neutron Libraries,'
Nucl. Sci. Eng.,60,27-35 (1976)
Benchmark models are summarized in the following reports.
Plechaty E.F. and Howerton R.J. :'Calculation Models for LLL Pulsed Spheres,' UCID 16372 (1973).
Tanaka S., Sasamoto N., Oka Y. et al.:'Shielding Benchmark Problems,' JAERI-M 7843 (1978) (in Japanese).
Tanaka S., Sasamoto N., Oka Y. et al.:'Shielding Benchmark Problems(II),' JAERI-M 8686 (1980) (in Japanese).

/15/ Kimura I., Hayashi S.A., Kobayashi K. et al. : 'The Integral Check of Neutron Cross Section Data for Reactor Structural Materials by Measurement and Analysis of Neutron Spectra,' Proc. of. Int. Conf. Antwerp, 6-10 Sept. 1982, K.H.Bockhoff(Ed.) Nuclear Data for science and Technology, 98-105,(1983).

/16/ Chapman G.T. et al. :'The ORNL Integral Experiment to Provide Data for Evaluating Magnetic Fusion Energy Shielding Concepts, Part I: Attenuation Measurements,' ORNL/TM-7356 (1982).

/17/ Sakurai K. and Ueki K. : 'Evaluation of Secondary Gamma-ray Production Cross-section of Iron in the JENDL-3T through an Analysis on the 14 MeV Neutron Penetration Experiment of SUS-304 at the ORNL ,' Seminar on Nuclear Data, Poster Session No. 11 , Nov.12-13, Tokai, (1987).

/18/ BNL : 'ENDF/B-IV: Evaluated Nuclear Data File, Version-IV' (1975), and its documentation: Garber D. : 'ENDF/B Summary Documentation ENDF-201 (2nd Edition) NNDC., BNL, (1975).

/19/ JAERI : 'JENDL-2: Japanese Evaluated Nuclear Data Library, Version-2' (1983), and its full documentation to be published.
Kikuchi Y. : 'Present Status and Benchmark Test of JENDL-2,'
Proc. of Int. Conf. Antwerp 6-10 Sept. 1982, K.H.Bockhoff(Ed.) Nuclear Data for science and Technology, 615-622,(1983).

/20/ JAERI : 'JENDL-3 PR1: Japanese Evaluated Nuclear Data Library, Version-3 PR1' (1984), and its full documentation to be published.

/21/ Koyama K., Minami K., Taji Y. and Miyasaka S. :'RADHEAT-V3, A Code System for Generating Coupled Neutron and Gamma-Ray Group

Constants and Analyzing Radiation Transport,' JAERI-M 7155 (1977).

/22/ Yamano N., Koyama K. and Minami K. : 'Development of Integrated Shielding Analysis Code System RADHEAT-V4,' Proc. of the Sixth Int. Conf. on Radiation Shielding, May 16-20, 1983, Tokyo, p331-340 (1983).

/23/ Rhodas W.A. and Mynatt F.R. :'The DOT-III Two Dimensional Discrete Ordinate Transport Code,' ORNL-TM-4280 (1973).

/24/ Straker E.A., Stevens P.N., Irving D.C. and Cain V.R. :' The MORSE Code - A Multigroup Neutron and Gamma Ray Monte Carlo Transport Code,' ORNL-4585 (1970).

/25/ Hasegawa A. : to be published.

/26/ Hasegawa A. : to be published.

/27/ Straker E.A. : 'Experimental Evaluation of Minima in Total Cross Sections of Several Shielding Materials,' ORNL-TM-2242 (1968).

/28/ Hasegawa A. : to be published.

/29/ Carter M. D., McCracken A.K. and Packwood A. : 'The Winfrith Iron Benchmark Experiment, A Compilation of Previously Published Results for use in the International Comparison of Shielding Data-Sets Sponsored by NEA,' AEE Winfrith (1982).

/30/ Suzuki T., Hasegawa A., Mori To. and Ise T. : ' BERMUDA-2DN : A Two -Dimensional Neutron Transport Code,' (in japanese), JAERI-M 82-190 (1982).

/31/ Reactor Physics Constants: ' Constants Related to Interpretation of Experimental Data,' Argonne National Laboratory , ANL-5800 (1963).

/32/ Mugahabghab S. F., Divadeenam M. and Holden N. E. : ' Neutron Cross Sections Volume 1 Neutron Resonance Parameters and Thermal Cross Sections,' Academic Press (1981).

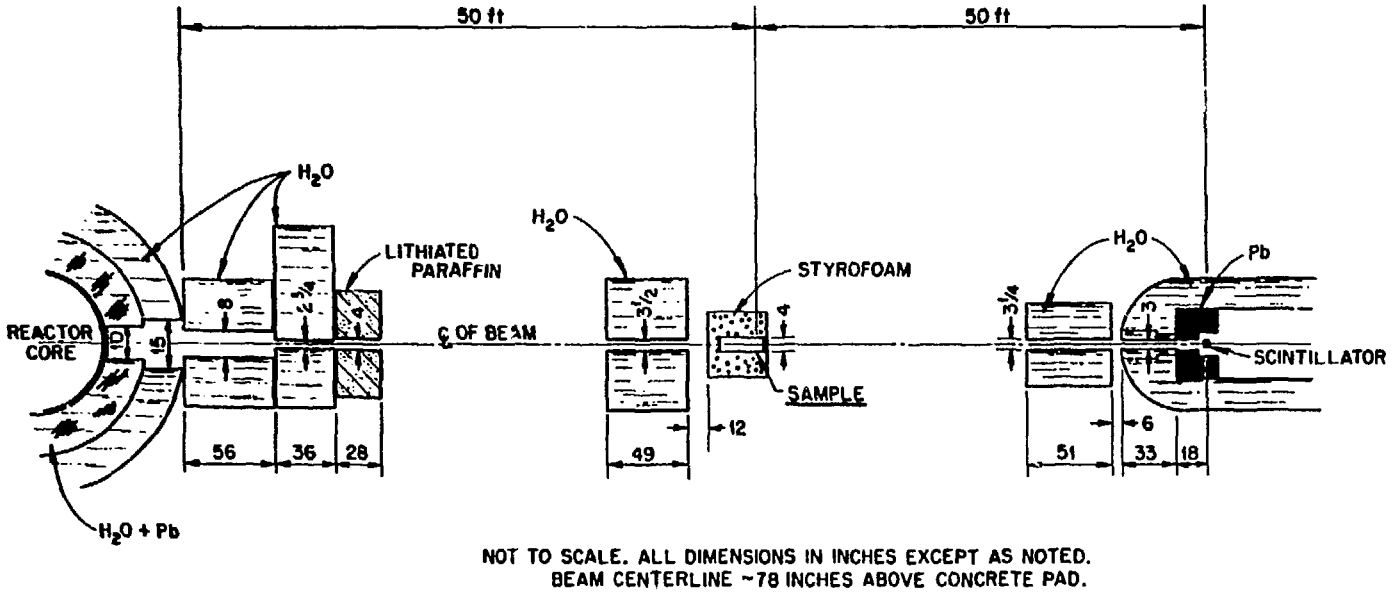

NOT TO SCALE. ALL DIMENSIONS IN INCHES EXCEPT AS NOTED.
BEAM CENTERLINE ~78 INCHES ABOVE CONCRETE PAD.

Fig. 1 Schematic of Broomstick experimental arrangement.

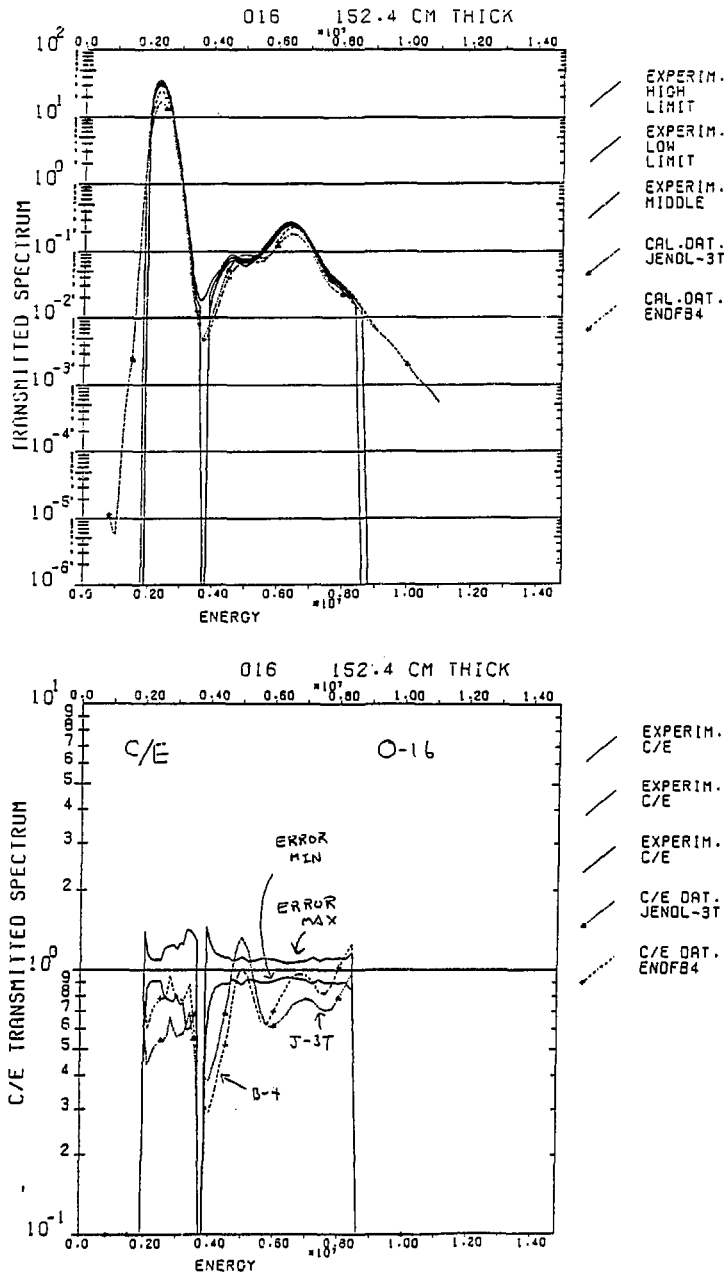

Fig. 2.1 Calculated and experimental transmitted spectrum and their C/E profiles for Oxygen sample.

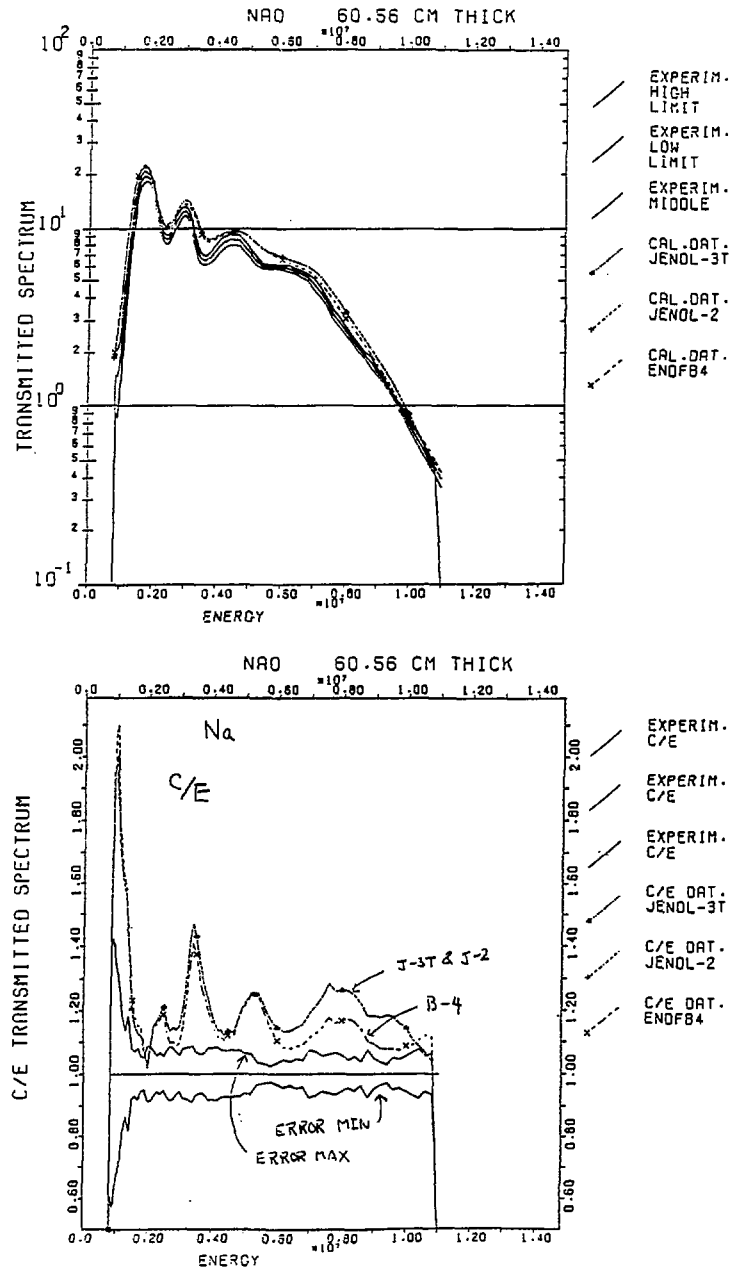

Fig. 2.2 Calculated and experimental transmitted spectrum and their C/E profiles for Sodium sample.

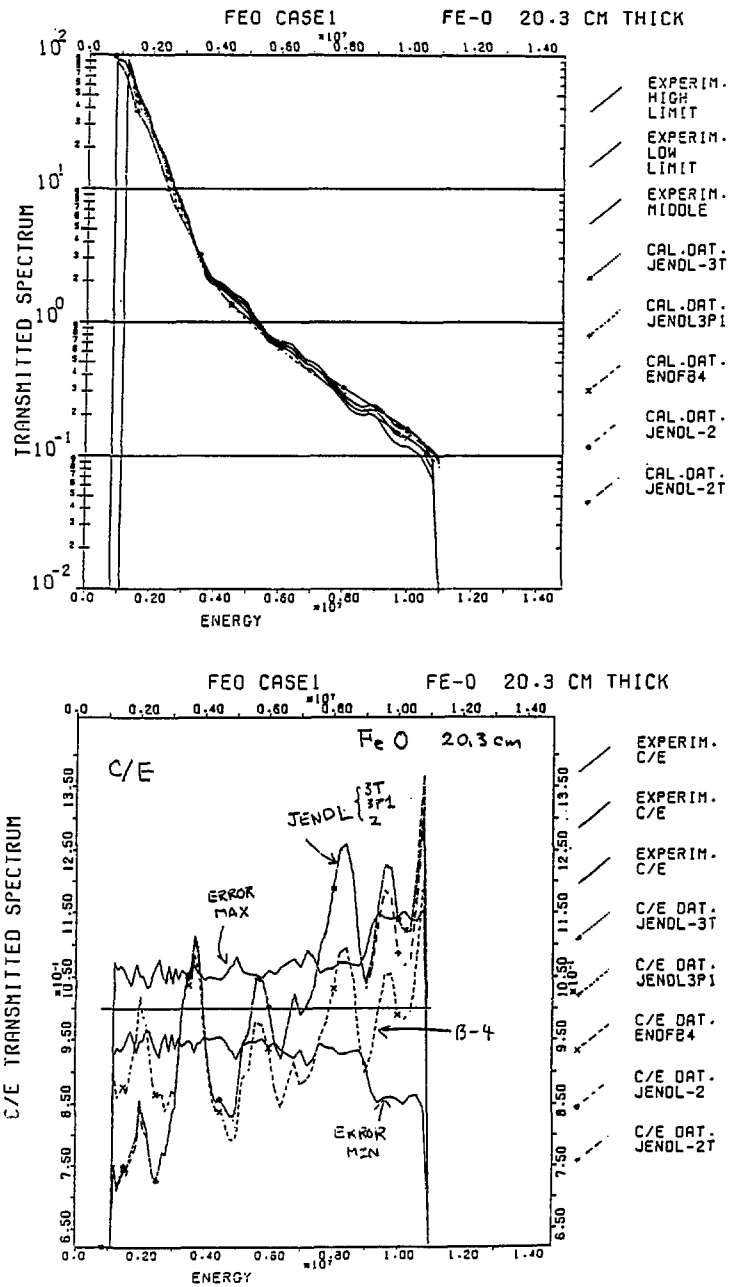

Fig. 2.3 Calculated and experimental transmitted spectrum and their C/E profiles for Fe sample (20.3 cm thick).

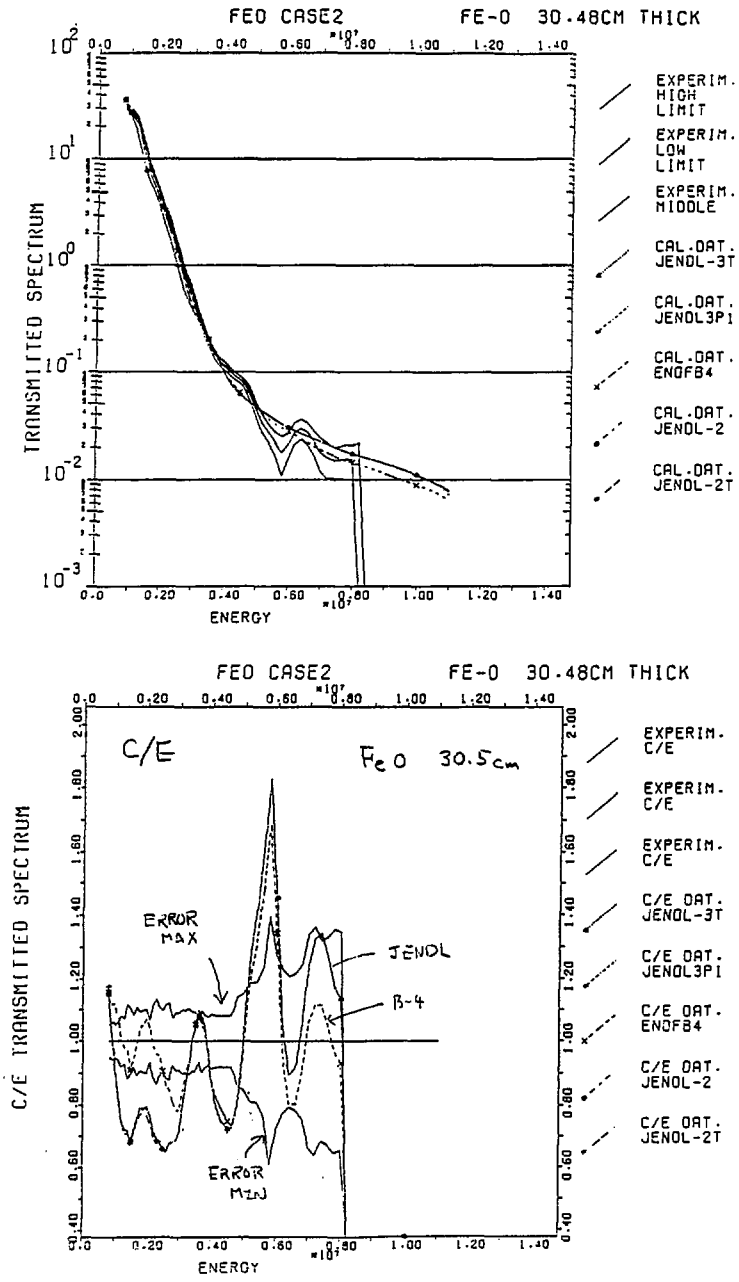

Fig. 2.4 Calculated and experimental transmitted spectrum and their C/E profiles for Fe sample (30.5 cm thick).

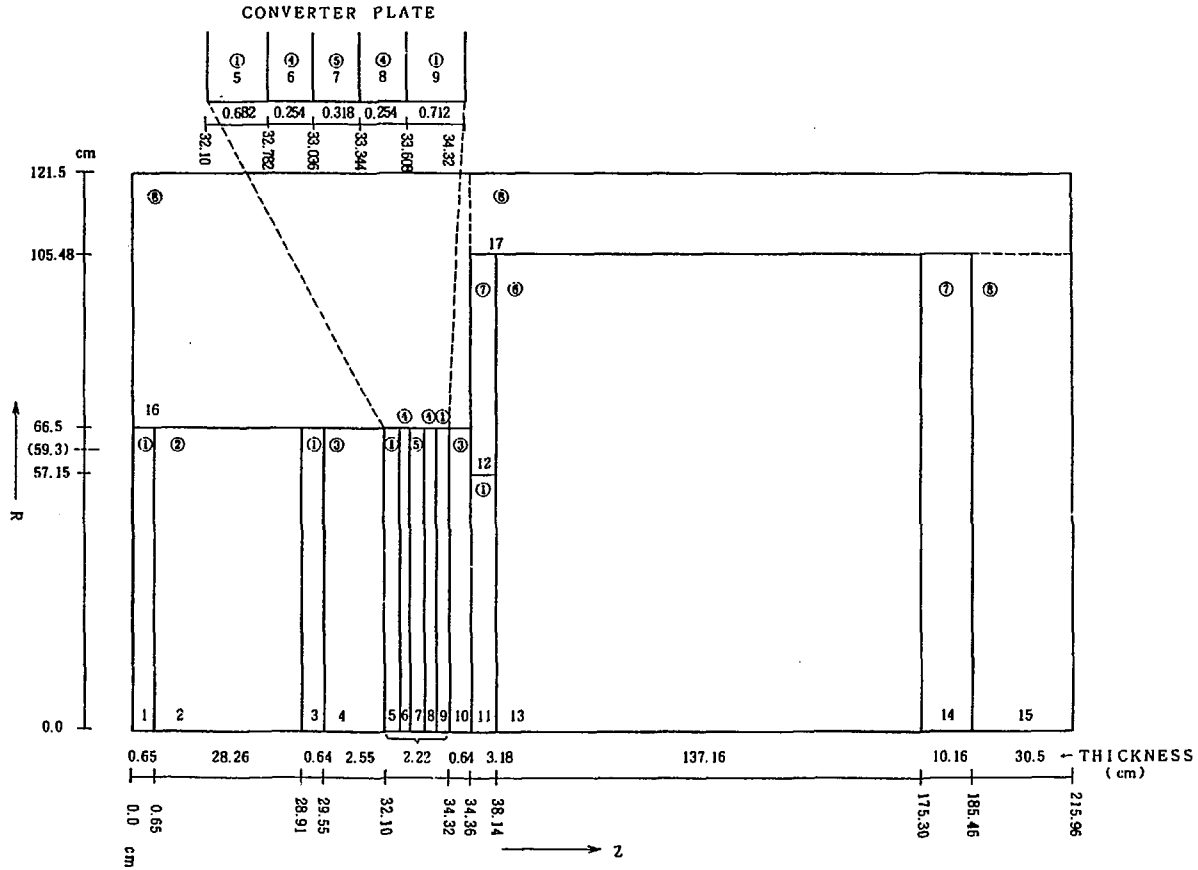

Fig. 3.1 Used R-Z geometrical model for the ASPIS analysis.

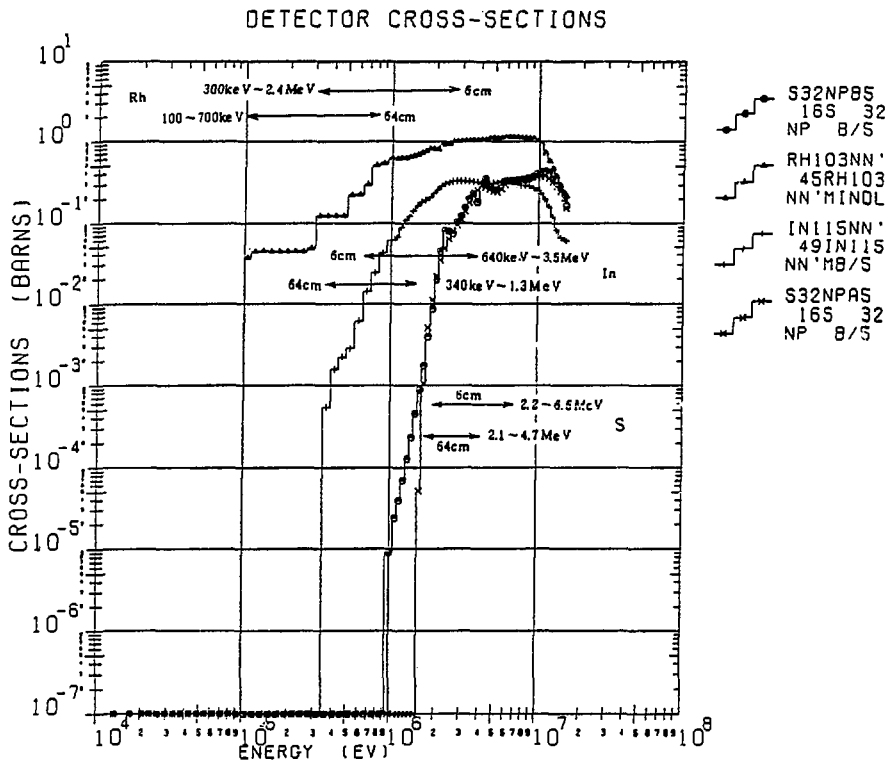

Fig. 3.2 Detector cross-section used in the analysis (group averaged data in BERMUDA 121 group structures and the sensitive energy ranges to each detectors for the reaction rate in the attenuation profile calculation).

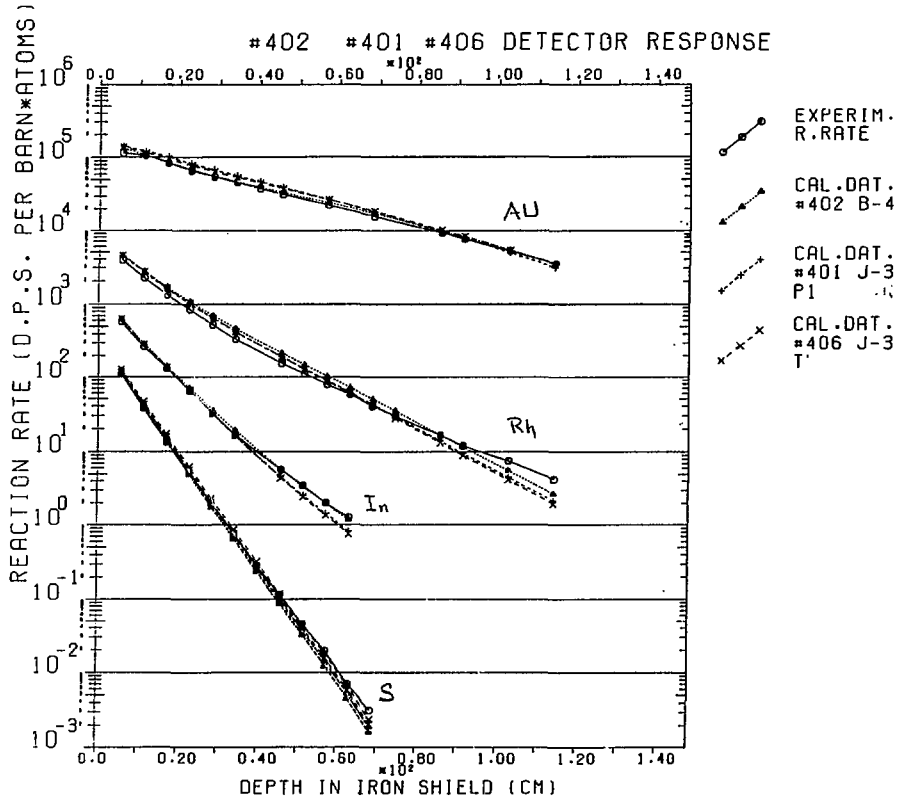

Fig. 3.3 Comparison of measured and calculated integral detector reaction-rate axial attenuation profile.

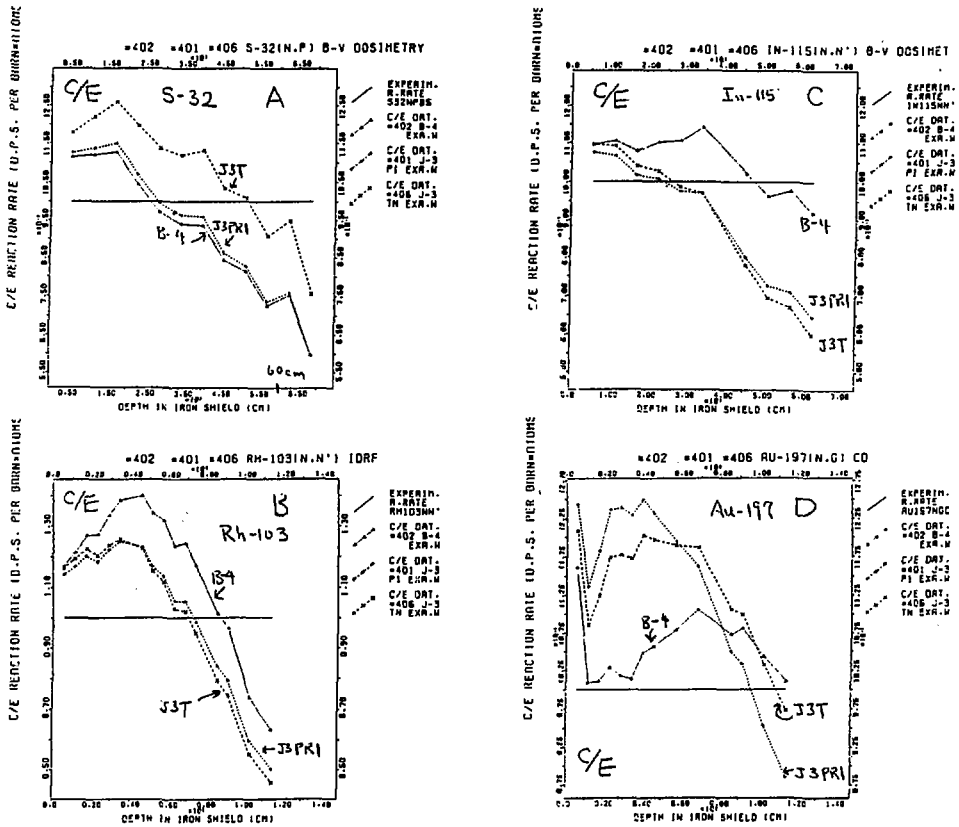

Fig. 3.4 Comparison of C/E values for the integral detector reaction-rate axial attenuation profile.

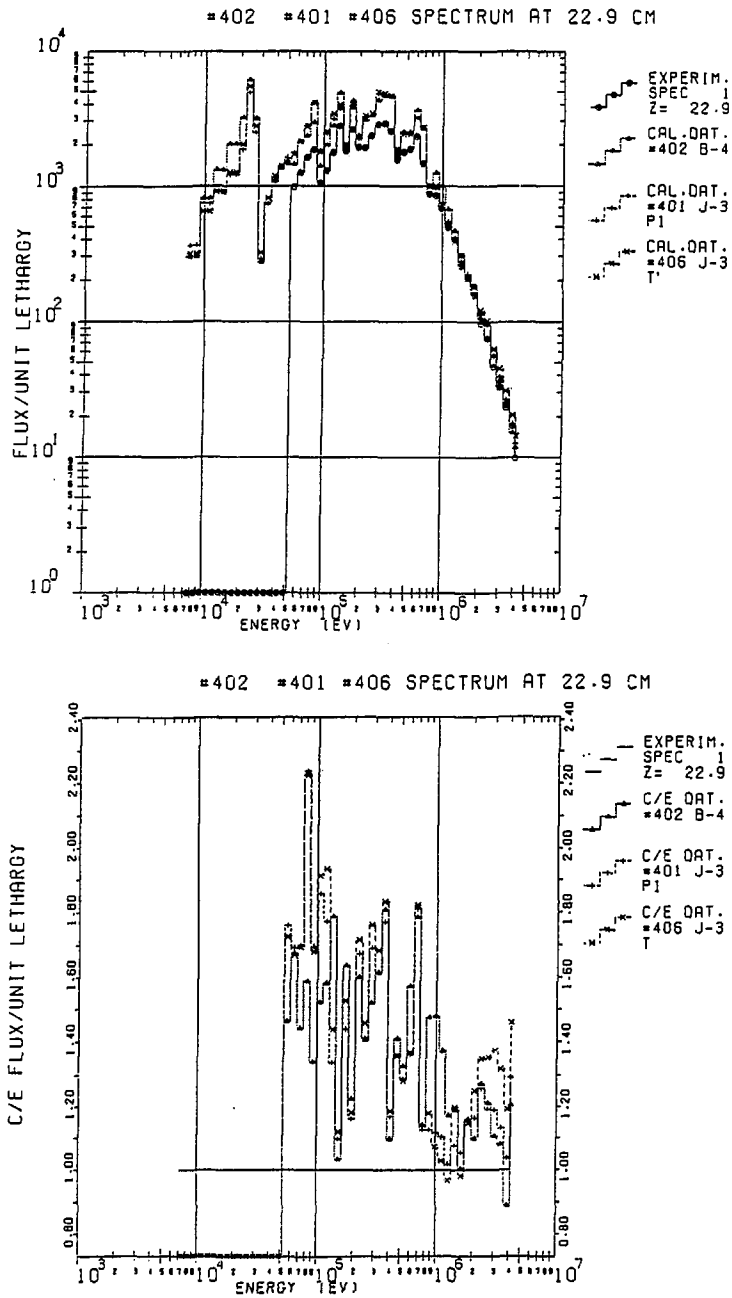

Fig. 3.5 Comparison of calculated flux profiles with RADAK unfolded spectrum measurement and C/E values at 22.8 cm position.

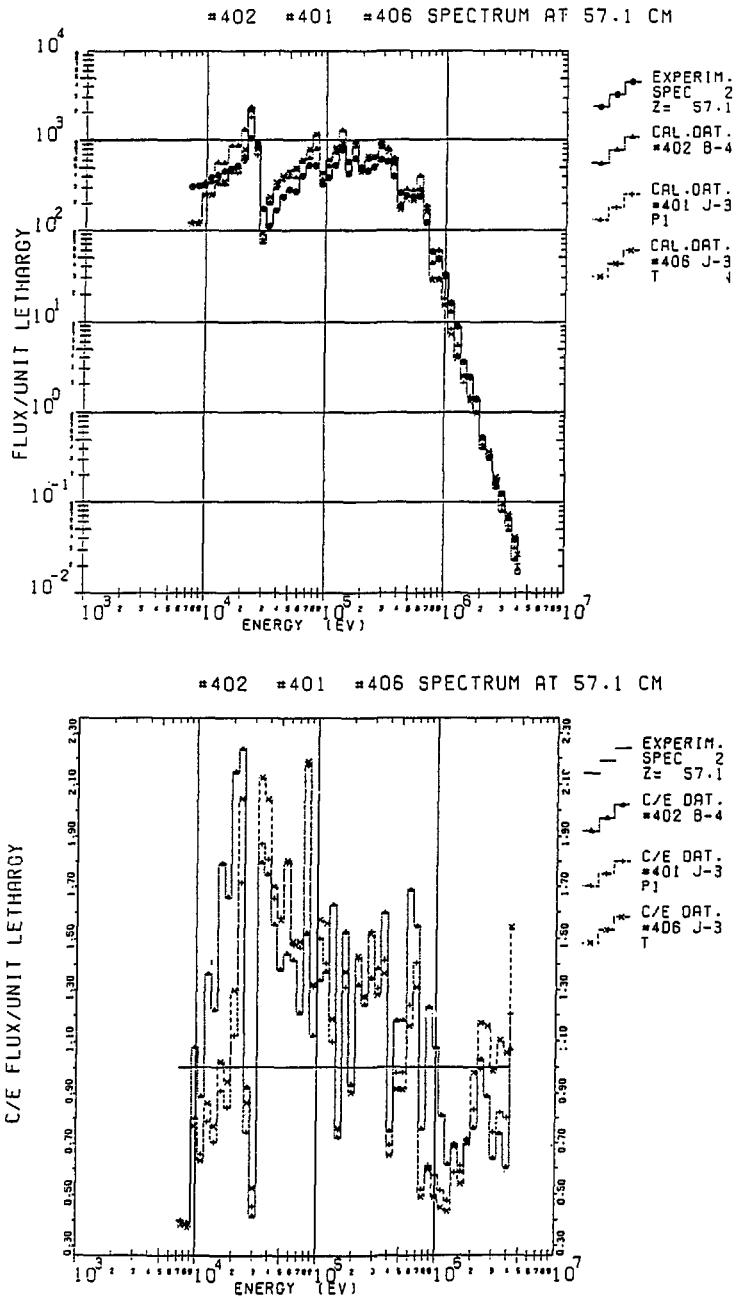

Fig. 3.6 Comparison of calculated flux profiles with RADAK unfolded spectrum measurement and C/E values at 57.1 cm position.

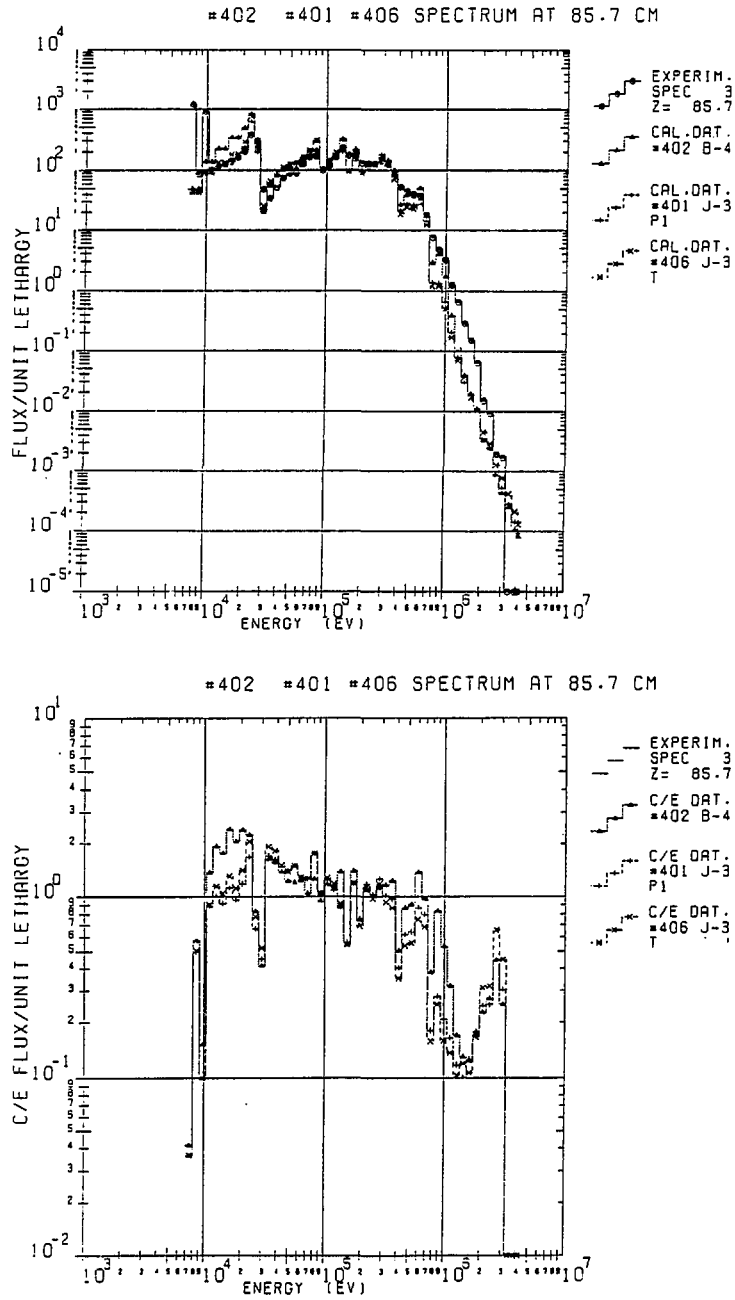

Fig. 3.7 Comparison of calculated flux profiles with RADAK unfolded spectrum measurement and C/E values at 85.7 cm position.

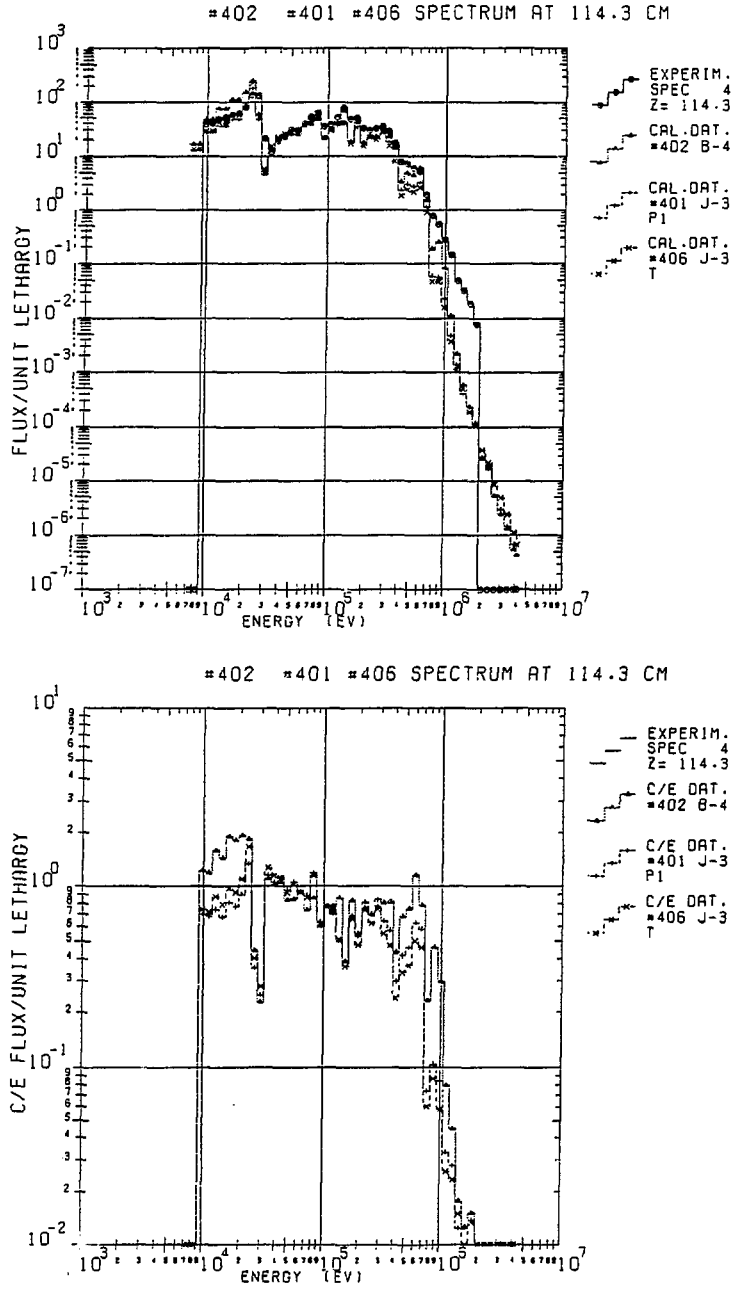

Fig. 3.8 Comparison of calculated flux profiles with RADAK unfolded spectrum measurement and C/E values at 114.3 cm position.

2.2.5 Dosimetry Benchmark Test of JENDL-3T

M. Nakazawa and Dosimetry Sub-WG,
University of Tokyo
7-3-1, Hongo, Bunkyo-ku, Tokyo

As a part of "Integral-Test Program of JENDL-3T", dosimetry benchmark test has been started in the dosimetry sub-working group, through which it is planed to produce the special purpose file for dosimetry from the JENDL-3. Presently, the 35 dosimetry reactions have been tested in the benchmark fields of Cf-252/U-235 fission spectra, CFRMF, YAYOI and JAERI-FNS 14MeV neutron. Several systematic discrepancies have been found in the following reactions of Al-27(n,α), S-32(n,p), Fe-54(n,p), Fe-58(n,γ), Ni-58(n,p), Ni-60(n,p), U-235(n,f) and U-238(n,γ).

1. Introduction

Several kinds of "Benchmark Test" of JENDL-3T are in progress in order to complete the JENDL-3 nuclear data libraly, in the fields of fast reactor physics, reactor shielding and so on. As a part of this integral-test program, dosimetry test has been started in the dosimetry sub-working group, and their final goal is toward the production of JENDL-3 dosimetry file.

The benchmark fields in this dosimetry test program are mainly selected from the IRDF-82, which are Cf-252 spontaneous fission spectrum , U-235 thermal fission spectrum, CFRMF and YAYOI. In order to test the apllicability to fusion reactor neutronics, another benchmark field of 14MeV neutron is added, which is JAERI-FNS 14 MeV neutron source.

2. JENDL-3T Dosimetry File

Table 1 shows the list of dosimetry reactions which are expected to be included in the JENDL-3 Dosimetry file, and presently 35 reaction cross-sections have been collected in its preliminal version of JENDL-3T dosimetry file. They are also shown in the Table 1.

In the production of JENDL-3T Dosimetry file at first point-wise data are obtained using RESENDD code for resonance paramete processing, then G20 group-wise cross section data, which is the same as the SAND-II code group structure, are calculated using the CRECTJ5 code to average the point-wise data with the weighting function of F(E)=1.0 .

Unfortunately, there is no uncertainty data in the present JENDL-3 library, so the covariance file of the IRDF-82 has been adopted tentatively in the present JENDL-3T dosimetry file.

3. Results and Discussion

Table 2 shows the typical results in the three neutron spectra, where it should be commented that the high threshold energy reactions such as Al-27(n,α), Ti-47(n,p), show a little overestimation in the Cf-252 spectrum field, because of the overestimation of the Maxwellian type fission spectrum representation of Cf-252 in the high energy region

Although generally better agreements are observed than the IRDF-82 data for many reactions except Fe-54(n,p) and Ni-58(n,p), additional comments should be made for each reactions like that;

S-32(n,p) reaction is 15 - 20 % high,

Al-27(n,α) reaction is 5 - 10 % high,

Ni-60(n,p) reaction is 50 % high,

U-235(n,f) reaction seems to be 2 -3 % high systematically,

and U-238(n,γ) reaction is 8 -10 % high.

Fig.1 shows the comparison of cross section curves in the 14 MeV energy region, and it can be guessed that the data evaluations in this

energy region are mainly based on the JAERI-FNS new data, because very good agreements are observed between the JAERI-FNS data and the JENDL-3T data.

The largest discrepancy has been found in the reaction of Fe-58(n,γ), which has been compared with the IRDF-82 data in Fig.2. Main difference has been observed in the resonance energy region, especially in the base cross section values between the resonances.

4. Conclusion

Present status on the JENDL-3T dosimetry benchmark test has been summarized, and several reactions for which re-check is requested, are pointed out. In order to complete the JENDL-3 Dosimetry -File, additional evaluations are required especially for (n,n') reactions of Nb-93,Rh-103,In-115 and Hg-199 nucleides which can not be obtained from the JENDL-3 library. And covariance data are requested for more quantitative comparison with experimental data, and for the neutron spectrum unfolding and/or adjustment application.

Member of Dosimetry sub-working group;

A.Hasegawa, Y.Ikeda, T.Nakagawa (JAERI), S.Iijima (NAIG),
K.Sakurai (RSAC), K.Kobayashi (KURI), S.Iwasaki (Tohoku Univ.)
T.Iguchi, M.Nakazawa (Univ.of Tokyo)

Table 1 Nuclear Reaction List to be included in JENDL-3 Dosimetry File (Underlined reactions are not included in the present JENDL-3T Dosimetry File).

1. Li- 6(n,t)α J3	18. Fe-58(n,γ) J3	32. U-235(n,f) J3
2. B-10(n,α) J3	19. Co-59(n,2n) J3	33. U-238(n,f) J3
3. F-19(n,2n) J3	Co-59(n,γ) J3	U-238(n,γ) J3
4. Na-23(n,2n) J3	Co-59(n,α) J3	34. Np-237(n,f) J3
Na-23(n,γ) J3	20. Ni-58(n,2n) J3	35. Pu-239(n,f) J3
5. Mg-24(n,p) J3	Ni-58(n,p) J3	36. Am-241(n,f) J3
6. Al-27(n,p) J3	21. Ni-60(n,p) J3	----------
Al-27(n,α) J3	22. Cu-63(n,2n) J3	37. Mn-55(n,γ) J3
7. P-31(n,p) J3	Cu-63(n,γ) J3	38. Nb-93(n,2n) J3
8. S-32(n,p) J3	Cu-63(n,α) J3	39. Rh-103(n,2n) J3
9. Sc-45(n,γ) J3	23. Cu-65(n,2n) J3	40. Eu-151(n,γ) J3
10. Ti-46(n,p) J3	24. Zn-64(n,p) —	41. W-186(n,γ) J3
11. Ti-47(n,p) J3	25. Zr-90(n,2n) J3	42. Ag-109(n,γ) J3
Ti-47(n,n'p) J3	26. Nb-93(n,n')-m —	43. Ta-181(n,γ) J3
12. Ti-48(n,p) J3	27. Rh-103(n,n')-m—	44. Hg-199(n,n') —
Ti-48(n,n'p) J3	28. In-115(n,n')-m—	45. Li- 7(n,n'α) J3
13. Mn-55(n,2n) J3	In-115(n,γ) J3	46. Al-27(n,t) —
14. Fe-DPA(ASTM) —	29. I-127(n,2n) J3	47. Ti-49(n,n'p) J3
15. Fe-DPA(EUR) —	30. Au-197(n,γ) —	48. Fe-57(n,n'p) J3
16. Fe-54(n,p) J3	31. Th-232(n,f) J3	49. Au (n,2n) —
17. Fe-56(n,p) J3	Th-232(n,γ) J3	

Note: Reactions from No.1 through No.36 are those included in IRDF. Reactions No.37 through No.49 are the new entries.

Table 2 Summary of Relative Deviations of Calculated Reaction-Rate Values from Experimental Data in three Benchmark Fields.

REACTION	FILE	Cf-252	U-235	CFRMF	AVERAGE	COMMENT
	IRDF	8.4%	10.4%	7.8%	9(1)%	
Al 27(n,p)	J-3T	4.6	6.5	8.8	7(2)	
	IRDF	14.4	2.1	10.6	9(6)	
Al 27(n,α)	J-3T	12.0	1.4	18.4	11(9)	check required
	IRDF	5.2	8.7	-	8(0)	
S 32(n,p)	J-3T	16.9	9.1	-	13(6)	check required
	IRDF	-2.1	-5.3	-5.7	-4(2)	
Ti 46(n,p)	J-3T	-3.8	-8.1	-5.2	-6(2)	
	IRDF	25.8	18.3	23.0	22(4)	
Ti 47(n,p)	J-3T	7.5	1.3	8.1	6(4)	improved
	IRDF	2.7	1.7	1.8	2(1)	
Fe 54(n,p)	J-3T	-4.8	-7.9	-6.9	-7(2)	
	IRDF	2.8	0.5	-	2(2)	
Fe 56(n,p)	J-3T	1.1	-2.2	-	-1(2)	
	IRDF	1(*)	1(*)	8.3		
Fe 58(n,γ)	J-3T	1.7	1.7	160	factor 2	check required
	IRDF	-0.7	-3.1	-2.5	-2(1)	
Ni 58(n,p)	J-3T	-2.9	-5.0	-3.5	-4(1)	
	IRDF	44.0	-	-		
Ni 60(n,p)	J-3T	44.1	-	-		check required
	IRDF	-11.8	-7.3	-	-10(3)	
Th232(n,f)	J-3T	-8.3	-2.4	-	-5(4)	improved
	IRDF	2.1	2.7	2.8	3(0)	
U 235(n,f)	J-3T	2.0	2.7	1.7	2(1)	systematic high
	IRDF	-1.7	-0.1	1.9	0(2)	
U 238(n,f)	J-3T	-0.9	2.0	3.0	1(2)	
	IRDF	1(*)	1(*)	7.8		
U 238(n,γ)	J-3T	6.4	6.3	8.8		systematic high
	IRDF	-0.7	-1.1	-0.3	-1(0)	
Pu239(n,f)	J-3T	-0.6	-0.6	-1.7	-1(1)	

note;Respective spectra of Cf-252 and U-235 are Maxwellian(T=1.42MeV) and Madland-Nix type. Mark "1(*)" means normalized to 1, and for the number of AVERAGE column, 9(1) means 9±1%.

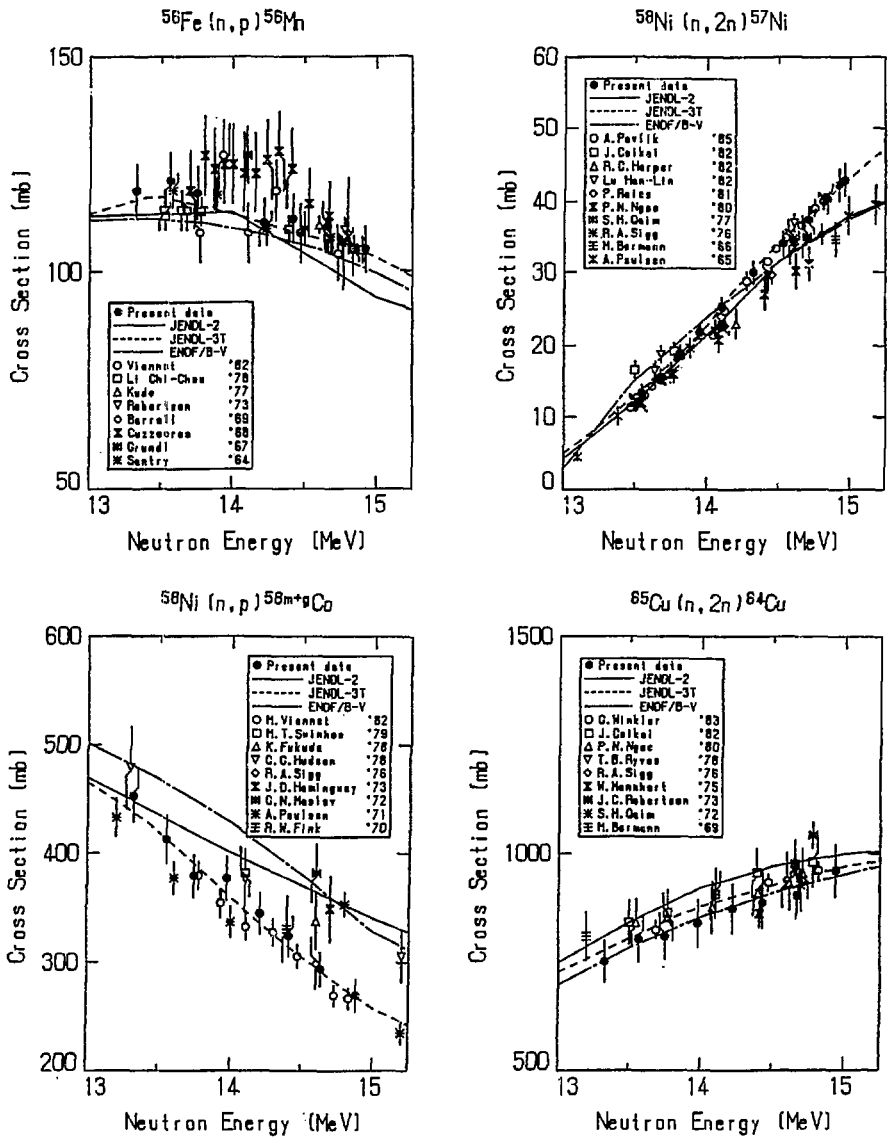

Fig. 1 Comparisons of Dosimetry Cross-Sections in 13 - 15 MeV Region. ("Present data" means experimental data of JAERI-FNS group.)

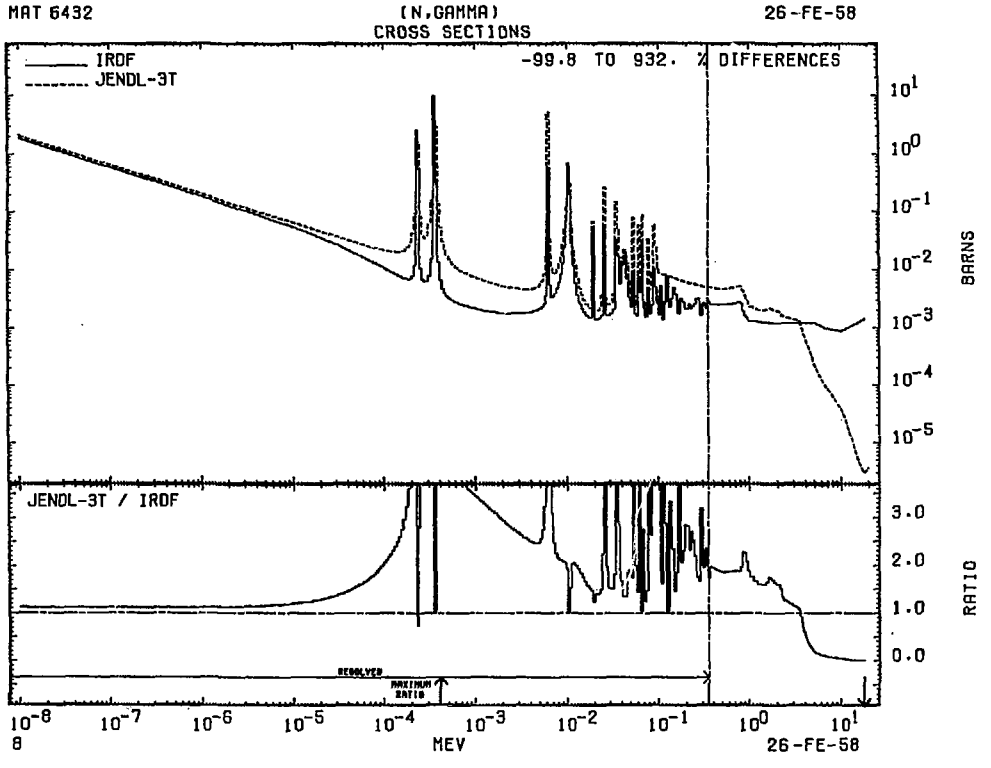

Fig. 2 Comparison of Fe-58(n,γ) Reaction between IRDF and JENDL-3T.

2.2.6 Fusion Neutronics Integral Test for JENDL-3T

Hiroshi Maekawa
Japan Atomic Energy Research Institute
Tokai-mura, Naka-gun, Ibaraki-ken, 319-11 Japan

Subworking Group on Fusion Neutronics Integral Test†

For the formal evauation of the JENDL series nuclear data files in fusion neutronics field, "Subworking Group on Fusion Neutronics Integral Test" was formed among the member of both the Subcommittee on Reactor Constants on the Japanese Nuclear Data Committee and the Subcommittee on Fusion Reactor of the Research Committee on Reactor Physics. The integral test was planned on the basis of results of an enquête. The results of integral tests were reported by seven groups at 24th meeting of Subcommittee on Fusion Reactor held on Oct. 30, 1987. This report is based on the presentations and discussions at the 24th meeting and made comments on the nuclear data of ^{1}H, ^{6}Li, ^{7}Li, ^{9}Be, ^{12}C, ^{16}O, Si, Cr, Fe, Mn, Cu and Pb.

KEYWORDS : JENDL-3, nuclear data, fusion neutronics, integral test, ^{1}H, ^{6}Li, ^{7}Li, ^{9}Be, ^{12}C, ^{16}O, Si, Cr, Fe, Mn, Cu, Pb

---

† Members of Subworking Group : H. Maekawa (Leader), A. Hasegawa, Y. Oyama, T. Mori, Y. Seki, S. Mori, C. Ichihara, A. Takahashi, J. Yamamoto, K. Shin, H. Sekimoto, T. Iguchi, S. Iwasaki, A. Zukeran, K. Maki, M. Kawai, M. Uematsu, K. Ueki, K. Sakurai

† Additional Contributors : M. Nakagawa, K. Kosako

1. Introduction

As JENDL-2 was evaluated for applying mainly to fission reactors, the accuracy of evaluated data above 5 MeV was pointed out to be insufficient for fusion neutronics study. In order to analyze the experiments at FNS, a new evaluated nuclear data file was strongly requested to the Japanese Nuclear Data Committee. Selected eight nuclei, ^{6}Li, ^{7}Li, ^{9}Be, ^{12}C, ^{16}O, Cr, Fe and Ni, had been evaluated as JENDL-3PR1 (JENDL-3 preliminary version one) by Dec. 1983.[1] A revised version JENDL-3PR2 was released in March 1985. The data of ^{6}Li, ^{7}Li and ^{12}C were modified taking into account of the result of Chiba et al.[2,3] Both files were used successfully for analyses not only the integral experiments at FNS and OKTAVIAN but of the double differential neutron emission cross sections (DDX) measured in the Universities. Many works related to the fusion neutronics experiments and analyses were reported in various meetings, such as Annual Meeting of Atomic Energy Society of Japan. Under this situation, a Specialists' Meeting on Nuclear Data for Fusion Neutronics was held in July 23-25, 1985 at Tokai Research Establishment of JAERI.[4] These results were applied to the evalation of JENDL-3.

For the formal evaluation of the JENDL-3 nuclear data files in the fusion neutronics field, an informal meeting was held during the 1987 Annual Meeting of Atomic Energy Society of Japan to discuss the plan of integral test. At the plenary meeting of Subcommittee on Reactor Constants held on Apr. 15, 1987, the integral test plan was also discussed. After then, "Subworking Group on Fusion Neutronics Integral Test" was formed among the members of both the Subcommittee on Reactor Constants of the Japanese Nuclear Data Committee and the Subcommittee on Fusion Reactor of the Research Committee on Reactor Physics. The first meeting of this Subworking Group was held on Sep. 11, 1987 to discuss the procedure of the integral test on the basis of results of an enquête regarding fusion neutronics integral tests. The proposed plan is summarized in Table 1. The breakdown of the standard group constants named "FSX125/J3T" is shown in Table 2. The first version, FSX125/J3T-1[5] processed from JENDL-3T[6]† by PROF-GROUCH-G/B[7], was distributed at the end of September; it includes 16

† JENDL-3T is a temporary file for testing the evaluated data for JENDL-3. The data in JENDL-3T will be partly revised in JENDL-3.

nuclides, namely, ^{1}H, ^{6}Li, ^{7}Li, ^{9}Be, ^{12}C, ^{16}O, ^{23}Na, ^{27}Al, Si, K, Cr, Fe, Ni, Mn, Cu and Pb. The results of integral tests were reported by seven groups at the 24th meeting of Subcommittee on Fusion Reactor held on Oct. 30, 1987 (See Table 1, marked by '*'). In the most of them, ANISN[8] and DOT3.5[9] were used with the standard group constants of FSX125/J3T-1. The MCNP code[10] was used by Oyama with the pointwise cross section set processed by NJOY[11] and the MORSE-DD code[12] was used by Nakagawa and Mori with the DDX-type group constants processed by PROF-DD. This report is based on the presentations and discussions at the 24th meeting. After the meeting, the results of integral tests were added by Shin and Sakurai.

2. Status of Nuclear Data in JENDL-3T relevant to Fusion Neutronics

The following comments on JENDL-3T are pertinent from the integral tests of seven groups:

^{1}H

The total and elastic scattering cross section below 100 keV are improved from JENDL-2. Good agreement is found for the analyses of experiments with water and polyethylene assemblies*c). The result is shown in Figs. 1 and 2. Hydrogen data seem to have reasonable accuracy.

^{6}Li, ^{7}Li

The data of ^{6}Li are the same as those in JENDL-3PR2. The calculated leakage spectrum*c) from a ^{6}Li sphere is deviated from the experiment between 7 and 12 MeV (See Fig. 3). Though there is some problem in it, the effect is not so large on the integral values in a assembly containing natural-lithium. Reevaluation is recommended when enriched ^{6}Li is essential for fusion blanket.

Good agreements are found for the TOF experiment on ^{7}Li sphere*c)(Fig. 4), the TOF experiment on Li_2O slabs*b)(Fig. 5) and the TOF experiment on Li-metal slab*f)(Fig. 6). Good agreements are also found within about 5 % for the tritium production rates in the Li_2O cylindrical assembly*a)(Fig. 7) and Li-metal sphere assembly*e)(Fig. 8). The data of ^{7}Li are almost reasonable. From the analyses of TOF experiments on the Li_2O and Li-metal slabs *b,*f), however, it is recommended that the $(n,2n)$ cross section is slightly increased; reevaluation is desirable for the total cross section.

^{9}Be

Though the inelastic cross section at 6.8 MeV in JENDL-3T are increased by a factor of two in comparison to that in JENDL-3PR2, discrepancies are still observed in the leakage spectra below 10 MeV from Be slabs*b)(Fig. 9) and Be sphere*c)(Fig. 10). Reevaluation is recommended, especially considering energy-angle correlation.

^{12}C

Agreement is very good on the whole for the TOF experiment on graphite slabs*b)(Fig. 11) and on graphite sphere*c)(Fig. 12). There are, however, some minor discrepancies in spectra corresponding to second and third levels.

^{16}O

From the analyses of the integral experiments on Li_2O and Li_2O-C*a), and TOF experiments on Li_2O*b), Oxygen*c)(Fig. 13), and concrete*f)(Fig. 14), ^{16}O data in JENDL-3T seem to be fairly good.

Si

The spectra calculated by JENDL-3T are almost the same as those calculated by ENDF/B-IV (See Fig. 15*g)). The C/E values vary by about ± 10 ∿ 30 %, however, the data are reasonably accurate for purpose of integral value estimation at the present time.

Cr

Agreement is fairly good for the leakage spectrum*g)(Fig. 16), however, there is discrepancy below 8 MeV due to the problem in the (n,2n) cross section.

Fe

Agreement is good for TOF experiments on Fe sphere*c,*d)(Fig. 17) and SS316 slab*f)(Fig. 18). The calculations, however, underestimate the leakage spectra around 8 ∿ 13 MeV. The same result is found in backscattered neutron spectra*h)(Fig. 19). There is no large problem in the nuclear data of Fe on the whole.

Mn

Agreement is fairly good on the whole for the leakage spectrum from Mn sphere*g)(Fig. 20). There is, however, some discrepancy around 10 MeV. Reevaluation is recommended, especially, for the elastic and (n,2n) cross sections.

Cu

Agreement is fairly good on the whole for the leakage spectrum from Cu sphere*g)(Fig. 21); however, there is large discrepancy near 10 MeV. This situation is almost the same as for Mn.

Pb

Large discrepancies are founded in the leakage spectra from Pb spheres (See Fig. 22*f) and Fig. 23*c)). Discrepancies are also observed in the neutron multiplication experiment*f)(Fig. 24). The calculated tritium production rates of ^{6}Li in Pb-Li sphere are a little lower than those of experiment (See Fig. 25*e)). From the analyses of integral and TOF experiments, reevaluation is strongly recommended.

3. Concluding Remarks

Using the nuclear data of JENDL-3T, we can estimate the tritium production rate in a typical fusion blanket without Be or Pb within 5 ∿ 10 %. Most types of reaction rates in it can be estimated within about 10 %. In the cases of fusion blankets with Be or Pb, rather large error is expected in a calculated result of tritium production rates and so on. Reevaluations are strongly recommended for the nuclear data of Be and Pb in JENDL-3T. A specialists meeting will be held on Dec. 25-26, 1987 to discuss the problem of nuclear data of Be, Pb and so on.

In the discussion at this 1987 Seminar on Nuclear Data, the problems of secondary neutron data due to the mismatch of energy-angle correlation are pointed out for light nuclei. The ENDF/B-6 format, i.e., the file-6 is essential for the nuclear data relevant to the fusion neutronics.

References

(1) Shibata K., Kikuchi Y.: "Evaluation of Nuclear Data for Fusion Neutronics," Proc. Int. Conf. Nucl. Data for Basic & Applied Science, Santa Fe, May 13-17, 1985, Vol. 2, pp1585-1588.

(2) Chiba S., et al.: "Interaction of Fast Neutrons with ^{6,7}Li," ibid., Vol. 1, pp227-230.

(3) Chiba S., et al.: J. Nucl. Sci. Technol. 22 [10] 771-787 (1985).

(4) Igarashi S., Asami T. (Ed.): "Proceedings of Specialists' Meeting on Nuclear Data for Fusion Neutronics," JAERI-M 86-029 (1986).

(5) Kosako K., et al.: "Neutron 125-Group Cross Section Library for Fusion Neutronics, FSX125/J3T," To be published in JAERI-M Report.

(6) JENDL Compilation Group (Nuclear Data Center, JAERI): JENDL-3T, Praivate communication (1987).

(7) Hasegawa A.: To be published in JAERI-M report.

(8) Engle W. W. Jr.: "ANISN : A User's Manual," Oak Ridge Gaseous Diffusion Plant, K-1693 (1967).

(9) Rhoades W. A., Mynatt F. R.: "The DOT-III Two DimensionalDiscrete Ordinates Transport Code," ORNL/TM-4280 (1979).

(10) Los Alamos Monte Carlo Group : "MCNP - A General Purpose Monte Carlo Code for Neutron and Photon Transport," LA-7396-M (Rev.) (1981).

(11) MacFarlane R. E., et al.: "The NJOY Nuclear Data Processing System: User's Manual," LA-9303-M ; ORNL/RSIC-41 (1978).

(12) Nakagawa M., et al.: "MORSE-DD, A Monte Carlo Code Using Multigroup Double Dofferential Form Cross Sections," JAER-M 84-126 (1984).

Table 1 Integral test plan of JENDL-3T for fusion neutronics.

Organization	Benchmark Problem	Personnel	Standard analysis	Additional analysis
JAERI	•Integral experiments on Li_2O, C & Li_2O-C assemblies	H. Maekawa K. Kosako	DOT 3.5*a	
	•TOF experiments on Li_2O, C, Li & Be slabs	Y. Oyama	DOT 3.5	MCNP*b MORSE-D
	•Pulsed Sphere Program (LLNL), ^6Li, ^7Li, C, O, Fe, Pb, P.E., H_2O, Be	T. Mori M. Nakagawa	MORSE	ANISN-DD DOT-DD MORSE-DD*c
	•Pulsed Sphere Program (LLNL), H_2O, Fe Fe sphere (Illinois Univ.)	S. Mori	ANISN*d DOT 3.5	MCNP
University Union	•Integral experiments on Li & Pb-Li spheres assemblies	T. Iguchi K. Sugiyama	ANISN*e	MCNP
Osaka Univ.	•TOF experiments on Li, Pb, SS316 & concrete assemblies	A. Takahasi J. Yamamoto	ANISN*f	NITRAN
Kyoto Univ.	•Backscattering experiments on concrete & SS304 assemblies	K. Shin	ANISN**h)	MCNP
KURRI	•Integral and TOF experiments on Si, Co, Mn, Cu, Nb & Cr sphere assemblies	C. Ichihara	ANISN*g	ANISN-DD NITRAN MCNP
TIT	•Spectra in LiF, C, H_2O & LiF-C assemblies	H. Sekimoto	MORSE	
Tohoku Univ.	•TOF experiments on P.E. & Pb slabs	S. Iwasaki		MCNP
	•Experiment on SS316 assembly at ORNL	K. Sakurai		MORSE MCNP**i)
NAIG	•Pulsed Sphere Program (LLNL)	M. Kawai M. Uematsu	ANISN MORSE	

* Results were available by the end of October, 1987 and refered in this report.
** Results were available by the end of November, 1987.

Table 2 Breakdown of standard group constant (FSX125/J3T)

Number of groups : 125 for neutron
Process code : PROF-GROUCH-G/B
Legendre coefficients : P-5

Group	Energy	ΔU	Weight
1 ∿ 32 (32)	16.5 ∿ 10 MeV	0.015625	1/E
33 ∿ 60 (28)	∿ 1.74 MeV	0.0625	1/E
61 ∿ 96 (36)	∿ 19.3 keV	0.125	1/E
97 ∿ 108 (12)	∿ 961 eV	0.25	1/E
109 ∿ 124 (16)	∿ 0.32 eV	0.5	1/E
125	∿ 0.00001 eV	10.38	Maxwell

* Gamma-ray group constant of about 21 groups will added on the standard set.

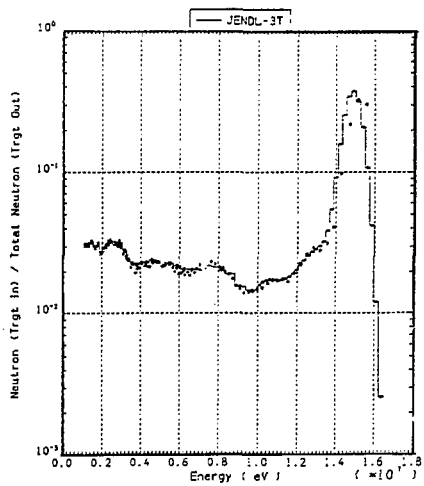

Fig. 1 Leakage spectrum from water sphere (1.1 mfp), 30°.

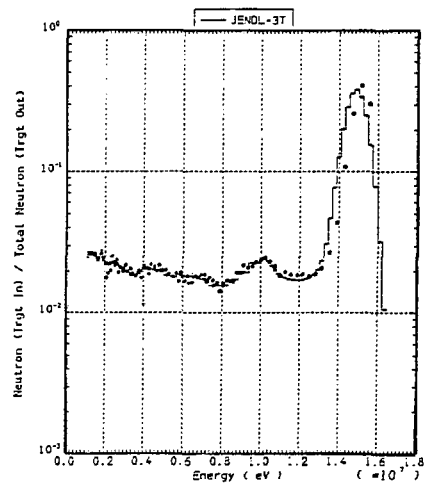

Fig. 2 Leakage spectrum from polyethylene sphere (0.8 mfp), 30°.

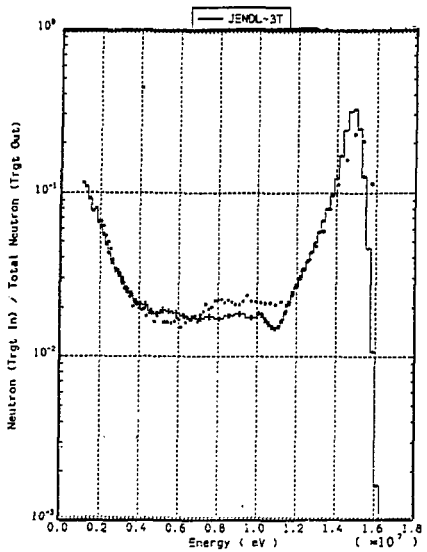

Fig. 3 Leakage spectrum from Li-6 sphere (1.6 mfp), 30°.

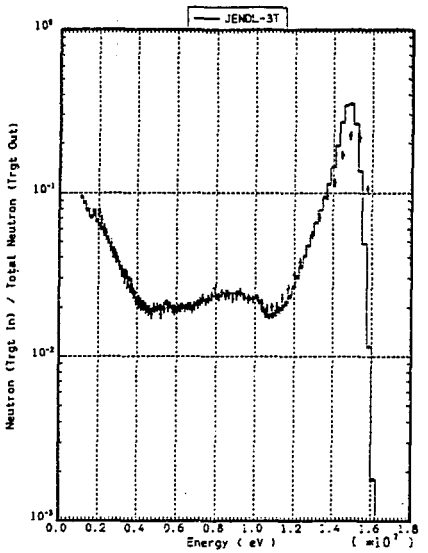

Fig. 4 Leakage spectrum from Li-7 sphere (1.6 mfp), 30°.

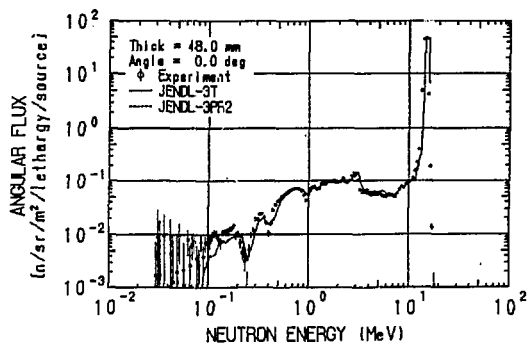

Fig. 5 Leakage spectrum from Li_2O slab.

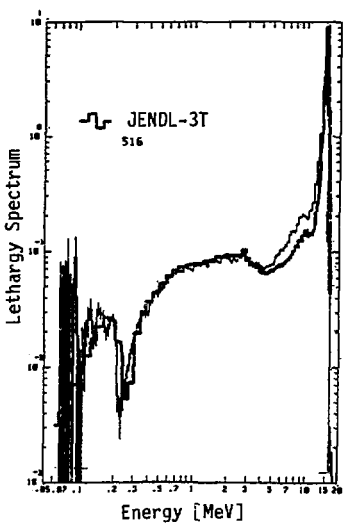

Fig. 6 Leakage spectrum from Li-metal sphere.

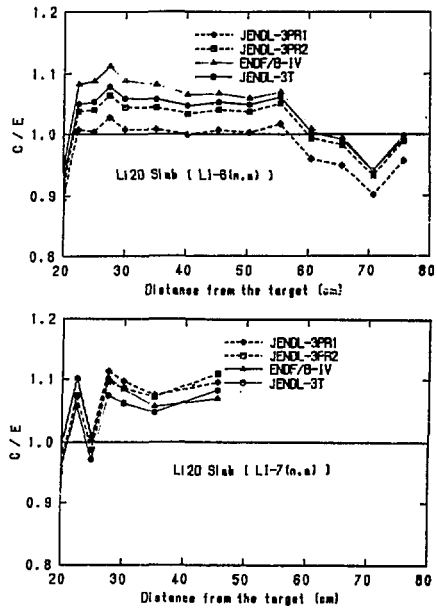

Fig. 7 C/E distributions of tritium production rates in Li_2O cylindrical assembly.

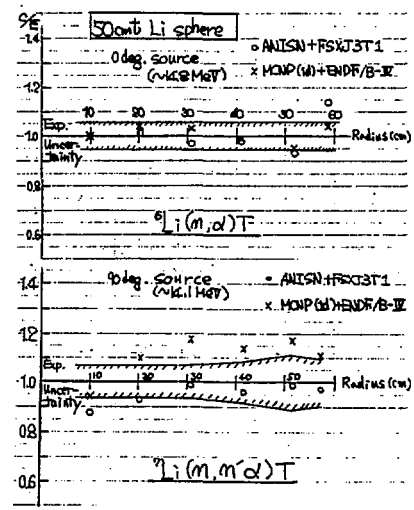

Fig. 8 C/E distributions of tritium production rates in Li-metal sphere assembly.

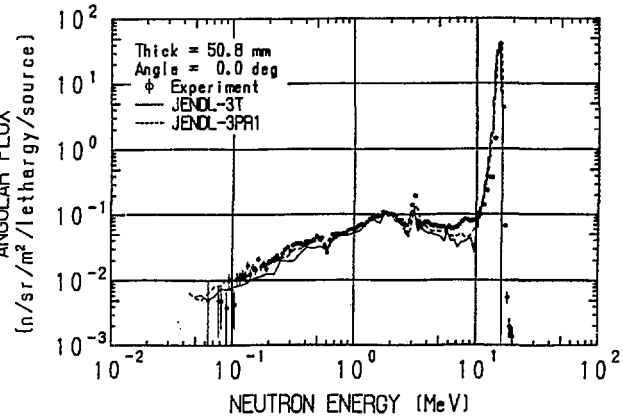

Fig. 9 Leakage spectrum from Be slab.

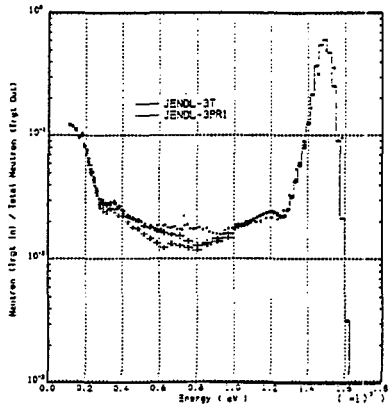

Fig. 10 Leakage spectrum from Be sphere (0.8 mfp), 30°.

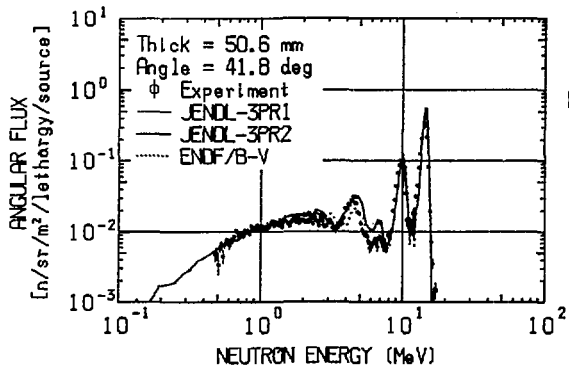

Fig. 11 Leakage spectrum from graphite slab.

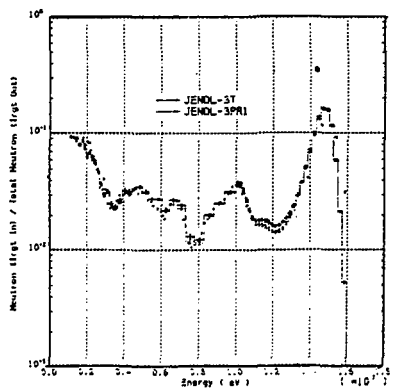

Fig. 12 Leakage spectrum from carbon sphere (2.9 mfp), 30°.

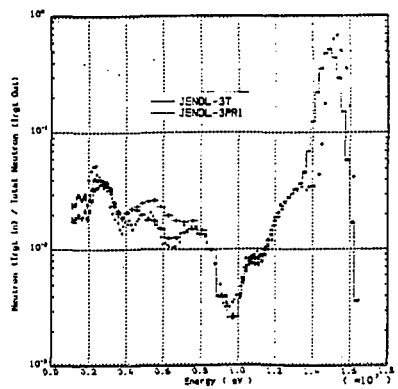

Fig. 13 Leakage spectrum from oxygen sphere (0.8 mfp), 30°.

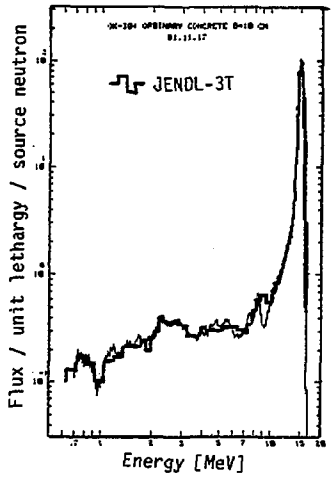

Fig. 14 Leakage spectrum from ordinary concrete slab.

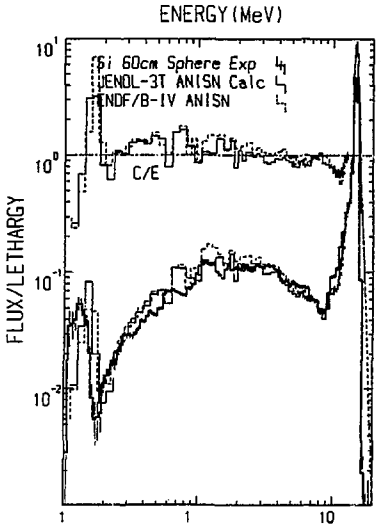

Fig. 15 Leakage spectrum from Si sphere.

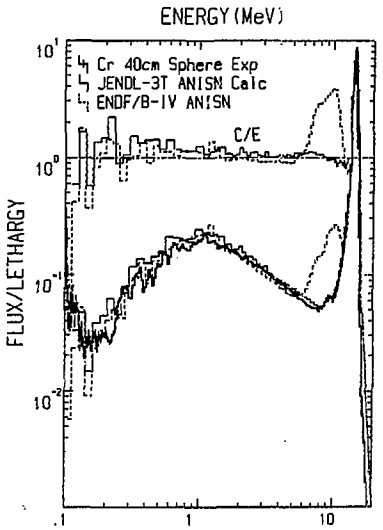

Fig. 16 Leakage spectrum from Cr sphere.

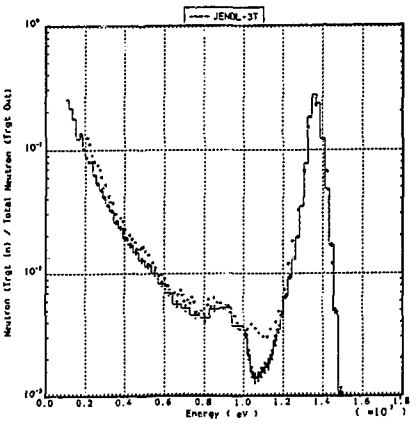

Fig. 17 Leakage spectrum from iron sphere (2.9 mfp), 120°.

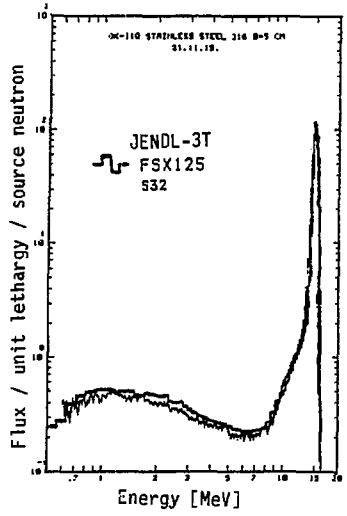

Fig. 18 Leakage spectrum from SS316 stainless steel slab.

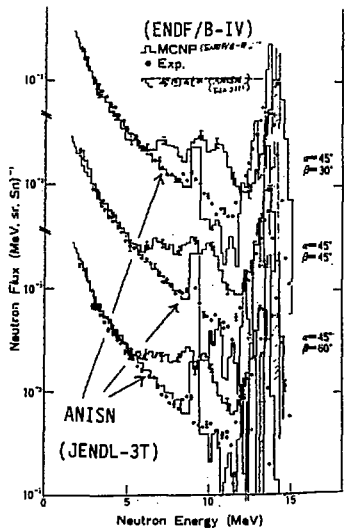

Fig. 19 Reflected spectrum from SS304 stainless steel slab.

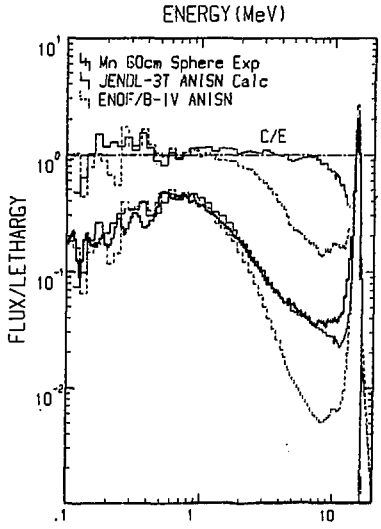

Fig. 20 Leakage spectrum from Mn sphere.

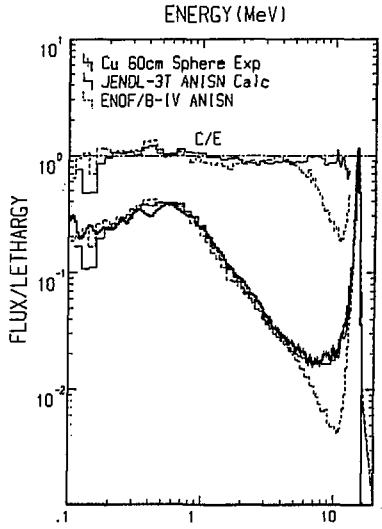

Fig. 21 Leakage spectrum from Cu sphere.

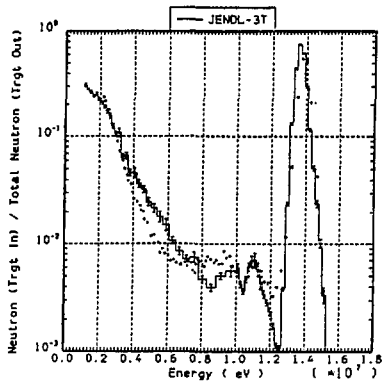

Fig. 22 Leakage spectrum from lead sphere (1.4 mfp), 120°.

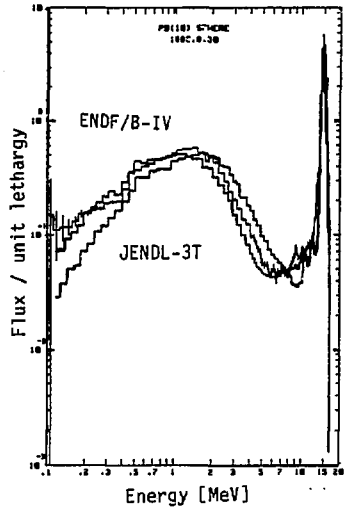

Fig. 23 Leakage spectrum from Pb sphere.

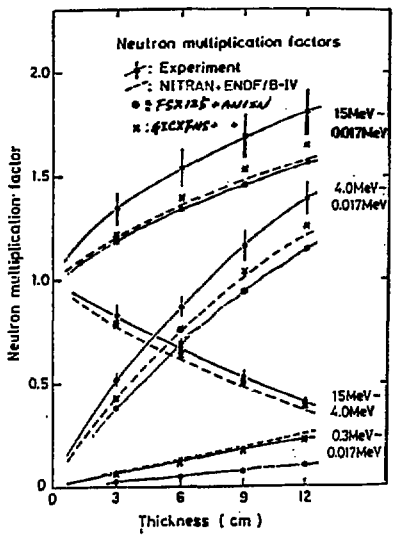

Fig. 24 Neutron multiplication factors of Pb spheres.

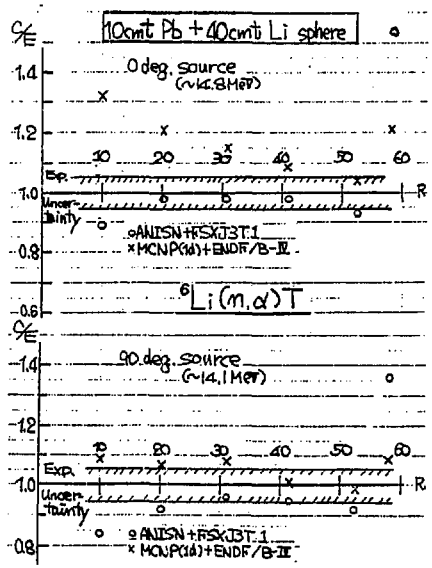

Fig. 25 C/E values of tritium production rates in Pb-Li sphere.

2.3 Topics

2.3.1 Energy Spectra of Particles Emitted from (p,n), (n,p), (p,α), (n,α), (p,p'), (n,n') and (p,d) Reactions on Nuclei around Magic Number

I. Kumabe, Y. Watanabe and N. Koori

Department of Nuclear Engineering, Kyushu University, Fukuoka 812

The energy spectra of particles emitted from (p, α) and (p,p') reactions on nuclei around magic number with 18 MeV protons were measured in order to clarify the shell and odd-even effects in the preequilibrium processes. From the experimental results, it was found that there exist no appreciable shell and odd-even effects in energy spectra for the preequilibrium (p, α) and (p,p') reactions. The energy spectra for (p,n), (n,p), (p, α), (n, α), (p,p') and (n,n') reactions were analyzed in terms of the preequilibrium exciton model introducing effective Q-values, the pairing correlation, and the modified uniform spacing model in which the uniform spacing model is modified so as to have a wide spacing at the magic number. The calculated spectra using the above model show good agreement with the experimental ones.

The fine structures of the energy spectra for the (p, α) reactions on nuclei around atomic number 50 can be qualitatively explained using the three-nucleon pickup model under the assumption that the states excited in the (p, α) reaction are formed by the coupling of two-neutron hole states excited in the (p, t) reaction and one-proton hole states excited in the (d, ^{3}He) reaction. The similar three-nucleon pickup model can explain qualitatively the fine structures of the energy spectra for the (n, α) reactions on nuclei around neutron numbers 50 and 82. The energy spectra for the (p,d) reaction on Mo isotopes were also measured and analyzed.

1. Introduction

It has been well known that the preequilibrium process plays an important role in reactions induced by 14 MeV neutrons.

Most of the important candidates for structural materials in a nuclear fusion reactor are metals or their alloys which contain atoms of the magic nuclei or nuclei around the magic number. Therefore studies of the shell effect in reactions are very important. Since available data for (n,n'), (n,p) and (n, α) reactions are relatively poor, detailed features

of the reactions such as the shell effect and the odd-even effect on target nuclei are not well known for the preequilibrium particle emission.

In general, accurate experimental data are available for the reaction induced by charged particles than those for neutron induced reactions because of better counting statistics for reactions related to the charged particles.

In the present study we have undertaken to measure systematically and accurately the double differential cross sections of the (p,p'), (p,n), (p,α) and (p,d) reactions, which are analogous to the (n,n'), (n,p), (n,α) and (n,d) reactions, respectively, in order to clarify the shell and odd-even effects on the reactions. By analogy with analyses of the reactions induced by protons, we expect to clarify the shell and odd-even effects on the reactions induced by 14 MeV neutrons.

Although the energy spectra of the particles emitted from reactions have been measured for nuclei in a wide mass-number range at various incident energies by several investigators, there exists no systematic study of the reactions on nuclei around the magic nuclei. Recently, the energy spectra of neutrons emitted form the (p,n) reactions on many nuclei at 25 MeV and 18 MeV were reported[1]. Therefore we have not measured the (p,n) reaction.

2. Experimental proceduce

Proton beams of 18 MeV from the tandem Van de Graaff accelerator at Kyushu University were analyzed by a beam analyzing magnet and brought into a scattering chamber. A detecting system mounted on a turntable inside the scattering chamber consisted of a ΔE-E counter telescope of two silicon surface barrier detectors. Emitted particles were identified and separated from other reaction products by means of a particle identifier.

3. Experimental results and analyses

3-1 (p,n) and (n,p) reactions

About ten years ago, we have analyzed[2] the 14 MeV (n,p) cross sections for nuclei with A > 90 in terms of the preequilibrium exciton model.

The ratios of the experimental to theoretical cross sections are plotted in the upper part of Fig. 1. A marked feature in this figure is that the ratios decrease suddenly near mass number A=120 (atomic number

Z=50) and increase suddenly near A=140 (neutron number N=82). The reason for these phenomena is considered to be whether there exists the shell effect in the experimental cross sections or in the calculated cross sections. The experimental 14 MeV (n,p) cross sections are plotted in Fig. 2 as a function of mass number. No appreciable shell effect appears near A=120 (Z=50) and A=140 (N=82). If the ground state Q-values for even-even nuclei are plotted, relatively large jumps of the Q-values are seen at Z=50 and N=82. The Q-values for odd Cd isotopes are about 2.5 MeV larger than those for corresponding even Cd isotopes. However no appreciable variation of the experimental cross sections between odd and even isotopes appears as is seen in Fig. 2. If the ground-state Q-values having the strong shell effect are used in the preequilibrium calculation, the calculated cross sections are expected to show the strong shell effect. Therefore a better agreement between the experimental and calculated cross sections is expected to be obtain using an effective Q-value which is a smooth function of mass and atomic numbers and is free from fluctuations near closed shells.

The ratios of the experimental to theoretical cross sections calculated using the effective Q-values are plotted in the lower part of Fig. 1. The deviations of the points from 1.0 are markedly reduced.

In order to solve the problem mentioned above, measurements and analyses of the energy spectra of particles emitted from the (n,p) or (p,n) reaction on nuclei around the magic number are needed.

Fortunately, Scobel et al.[1] reported the energy spectra of neutrons emitted from the (p,n) reactions on nuclei in the Cr-Ni and Zr-Mo regions at 25 MeV.

The neutron energy spectra for the (p,n) reaction on $^{90,91,92,94}Zr$, $^{92,94,95,96,97,98,100}Mo$ and ^{110}Pd with 25-MeV protons and $^{90,91,92,94}Zr$ with 18-MeV protons were analyzed[3] in terms of the preequilibrium exciton model introducing effective Q-values, the pairing correlation and the modified uniform spacing model in which the uniform spacing model was modified so as to have a wide spacing at the magic number.

It has been well known that large energy jumps of orbit spacing occur at the magic number in the usually adopted shell model with spin-orbit coupling as shown in Fig. 3(a). However, the uniform spacing model as shown in Fig. 3(c) is often used in the preequilibrium model, although it does not include the shell effect. In order to take the effect of the shell gap into account, therefore, we modified the single particle levels based on

the uniform spacing model so as to have a wide spacing at the magic number, as shown in Fig. 3(b). The energy gap at the magic number N=50 shown in Fig. 3(b) was chosen to be nearly equal to the energy gap between $1g_{9/2}$ and $2d_{5/2}$ states.

For (p,n) reactions on nuclei with a given atomic number the cross sections calculated with the preequilibrium exciton model increase with increasing Q value. It is seen from an inspection of the experimental 25 MeV (p,n) spectra for Zr isotopes that the cross sections in 12-18 MeV region of the emitted neutron energy increase smoothly with increasing mass number, in spite of large difference of the true Q values between the magic nucleus ^{90}Zr and the odd nucleus ^{91}Zr. This experimental trend is expected to be reproduced by the preequilibrium cross sections calculated by using the effective Q value which is a smooth function of mass number for a given atomic number.

The experimental angle-integrated energy spectra for Zr isotopes are shown by the histograms in Fig. 4. The energy spectra calculated using the true Q values and the uniform spacing model are shown by dotted-dashed curves in Fig. 4. It can be seen from these figures that the calculated spectra for ^{92}Zr and ^{94}Zr show fairly good agreement with the experimental ones except for the neutron energy higher than 18 MeV, but too small values for ^{90}Zr and large values for ^{91}Zr are given.

The energy spectra calculated using the effective Q values and the uniform spacing model are also shown by solid curves in Fig. 4. The calculated spectra show good agreement with the experimental ones for all the targets shown except for $E_n > 18$ MeV. In both calculations the K value was chosen to be 390 MeV.[3)]

As mentioned above, the energy spectra calculated using the effective Q values and the uniform spacing model show good agreement with the experimental ones for all targets except for high neutron energy region. As seen in Fig. 4, the contribution of the cross section in the high neutron energy region is rather small for the total cross section. Therefore, this fact can qualitatively explain that the deviations from 1.0 of the ratios of experimental total (n,p) cross sections to theoretical ones calculated using the effective Q values were markedly reduced[5] as compared with the use of the true Q values.

Next, we calculated the energy spectra by using the effective Q values, the modified uniform spacing model, and the pairing correlation. The leading term in preequilibrium spectra is particle emissions from

exciton number n=3 states in the composite nucleus. Therefore, energy spectra were calculated using the level densities obtained from the modified uniform spacing model for only n=3 and the level densities obtained from the uniform spacing model for $n \geq 5$ for the sake of simplicity.

The energy spectra calculated using the effective Q values, the modified uniform spacing model, and the pairing correlation are shown by the dashed curves in Fig. 4. As is seen in Fig. 4, the calculated spectra show good agreement with the experimental ones, not only on the absolute cross sections in the energy region of E_n = 12-18 MeV, but also on the observed spectra with pronounced structures in the energy region of E_n > 18 MeV.

The same model was applied to the analysis of 14-MeV (n,p) reaction, which is the inverse reaction of the (p,n) reaction, on nuclei in the Zr-Mo region, and the calculated energy spectra show good agreement with the experimental ones[4] as shown in Fig. 5.

Next, the energy spectra from the (p,n) reaction on nuclei in the Cr-Ni region and the (n,p) reaction on nuclei in the Ti-Cu region were analyzed in terms of the preequilibrium exciton model introducing effective Q values, the pairing correlation and modified uniform spacing model. For nuclei in the Cr-Ni region both the neutron and proton shells are near the magic number 28. Therefore the modified uniform spacing model was used for both the neutron and proton shells. The calculated neutron energy spectra are shown by the solid curves in Fig. 6. The experimental angle-integrated energy spectra[1] are shown by the histograms in Fig. 6. It is seen from these figures that the shapes of the calculated spectra show fairly good agreement with the experimental ones except for the odd-mass target nuclei in which the calculated peak positions shift slighly from the experimental ones.

In the calculation of the preequilibrium process, the same method as the (p,n) reaction was applied to the 14 MeV (n,p) reactions on nuclei in the Ti-Cu region. The experimental angle-integrated energy spectra[5] are shown by the open circles in Fig. 7. The calculated neutron energy spectra for the preequilibrium process are shown by the dotted-dashed curves in Fig. 7. The calculated energy spectra for the statistical evaporation process and the (n,np) process are shown by the dashed and dotted curves, respectively. The sum of these is shown by the solid curves in Fig. 7. As can be seen from Fig. 7, the calculated energy spectra are in fairly good

agreement with the experimental ones within the large experimental errors although some calculated spectra are slightly larger than the experimental ones.

3-2 (p, α) and (n, α) reactions

The measured cross sections of 14 MeV (n, α) reaction for nuclei with mass number larger than 100 were analyzed[6] in terms of the preequilibrium exciton model.

The ratios of the experimental to theoretical cross sections are plotted in the upper part of Fig. 8. In this figure a similar gross mass-number dependence to that for the (n,p) reaction is seen. The experimental 14 MeV (n, α) cross sections are plotted in Fig. 9 as a function of mass number. Appreciable shell effect appears near A=120 (Z=50) and A=140 (N=82).

The ratios of the experimental to theoretical cross sections calculated using the effective Q-values are plotted in the middle part of Fig. 8. The A-dependence of the points seems to be just opposite to that using the true Q-values. The use of the average cross section $(\sigma_t+\sigma_e)/2$ is expected to achieve good results, where σ_t and σ_e are the cross sections calculated using the true and effective Q-values, respectively. The ratios of the experimental to average cross sections are plotted in the lower part of Fig. 8. The deviations of the points from 1.0 are markedly reduced.

In order to solve the problem mentioned above, measurements and analyses of the energy spectra of α-particles emitted from the (n, α) or (p, α) reaction on nuclei around the magic number are needed.

Therefore we have measured[7] systematically and accurately the double differential cross sections of the (p, α) reaction for 18 and 15 MeV protons, which is analogous to the (n, α) reaction, and have clarified the shell effect and the odd-even effect on the (p, α) reaction. By analogy with the (p, α) reaction, we expect to clarify the shell effect and the odd-even effect on the 14 MeV (n, α) reaction.

Energy spectra of α-particles integrated over angle are shown by the histograms in Fig. 10. The energy specra for ^{90}Zr and ^{92}Mo, which are magic nuclei, fall sharply to zero near 16 MeV. The energy spectra for ^{94}Mo and ^{96}Mo, which are near magic nuclei with a few nucleons outside the magic shell, fall sharply near 16 MeV and have some pronounced structures above 16 MeV which seem to correspond to discrete levels or groups of levels of

the residual nuclei. Features similar to those for ^{94,96}Mo are also seen for ^{98}Mo and ^{100}Mo, but the integrated cross sections above 16 MeV increase slightly with increasing mass number. In spite of the large Q-value difference, the shape and magnitude of the energy spectrum for Ag are almost similar to those for ^{106}Pd, if some structures at the high energy spectrum for ^{106}Pd are neglected. Moreover, the cross sections above 20 MeV for Ag are very low. In other words, the levels of the residual nuclei ^{104}Pd and ^{106}Pd in energies smaller than 3 MeV are very weakly excited. On the contrary, low lying levels of the residual nucleus ^{103}Rh are strongly excited. A similar feature is also seen for an odd-even pair, ^{93}Nb and ^{94}Mo. Thus, it may be concluded that the unpaired proton acts as a spectator in the process.

The experimental energy spectra have been analyzed in terms of the statistical evaporation model and the preequilibrium exciton model. We calculated the (p,α) cross sections for the preequilibrium process under the following assumptions. The incident proton interacts with a preformed α particle in the nucleus and $1p\text{-}1\alpha$ hole states are excited. In the case of α-particle emission the excited states in the residual nucleus are formed by the combination of α-cluster hole states and proton particle states. For the α shell the uniform spacing model is modified so as to have a wide spacing at the magic number. We calculated the energy spectra, using the knockout model introducing the effective Q values, the modified uniform spacing model, and the pairing correlation.

The calculated energy spectra for preequilibrium process are shown in Fig. 10. The shell effect of the gross structure of the energy spectra for the nuclei near the magic nuclei can be explained very well in terms of the present knockout model, although the fine structure of the spectra above 16 MeV which corresponds to the low lying states or groups of the states of the residual nuclei cannot be explained so well.

In conclusion, although the shell and odd-even effects for the energy spectra in the energy region larger than 16 MeV exist, there exist no appreciable shell and odd-even effects for the energy spectra of the preequilibrium process in energy regions smaller than 16 MeV.

As described above, for the (p,n) reaction the contribution of the cross section in the high neutron energy region is rather small for the total cross section, but as is seen in Fig. 10, for the (p,α) reaction on nuclei in the Zr-Mo region the contribution of the cross section in the high α energy region (> 16 MeV) is considerably large for the total cross

section except for the magic nuclei. Therefore, this fact can explain that there is appreciable shell effect for the total cross section of the (n, α) reaction as is seen in Fig. 9. The reason why there exist large peaks in α energy region larger than 16 MeV in the (p, α) reaction will be explained later.

Under the assumption of the three-nucleon pickup mechanism, the (p, α) reactions on proton-magic nuclei and near proton-magic nuclei are analogous to the (n, α) reactions on neutron-magic nuclei (N=50 or 82) and near neutron-magic nuclei, because for both reactions one nucleon is picked up from magic or near magic shell states and two nucleons are picked up from BCS states. In the present experiment, therefore, we have measured systematically and accurately the double differential cross sections of the (p, α) reactions on ^{112}Cd, ^{118}Sn, ^{120}Sn, Sb, ^{128}Te and ^{130}Te in order to clarify the shell and odd-even effects on the (p, α) reactions on nuclei around atomic number 50.

Energy spe a of α particles integrated over angle are shown by the histograms in Fig. 11. The figure indicates clearly a shell effect. The energy spectra for ^{112}Cd, ^{118}Sn and ^{120}Sn fall sharply to zero near 20 MeV. The energy specra for Sb, ^{128}Te and ^{130}Te, which are near magic nuclei with a few nucleons outside the magic shell, also fall sharply near 20 MeV and have some weak structures above 20 MeV which correspond to discrete levels or groups of levels of the residual nuclei.

The energy spectrum for an odd-mass nucleus Sb is compared with that for even-even nucleus ^{128}Te in Fig. 11. The ground state Q-values on ^{121}Sb, ^{123}Sb and ^{128}Te are 6.92, 6.74 and 4.16 MeV respectively. In spite of the large Q-values difference, the shape and magnitude of the energy spectrum for Sb are almost similar to those for ^{128}Te, except for some weak structure above 22 MeV and the evaporation region below 15 MeV in the spectrum for Sb.

As shown in Fig. 12, we found that the energy spectrum from the ^{120}Sn (p, α) reaction shows a striking resemblance in shape to that from the ^{120}Sn (p, t) reaction[8], both spectra have sharp peaks near 0 and 1.2 MeV and broad peaks near 2.5-5 MeV of excitation energies of the residual nuclei. This feature can be qualitatively explained by using a pickup model as follows.

Removal of a proton from the Z=50 closed proton shell leads to a simple proton-hole spectrum as observed in (d, ^{3}He) experiments[9] on tin isotopes. The two-neutron tranfer strength is concentrated in a few

collective states due to the superconductivity of the neutron core as exhibited in the Sn(p, t) reactions. Therefore we expect that the states populated in the Sn(p, α) reaction are formed by combining these two excitations in a weak-coupling scheme. The (d, ^{3}He) reaction[7] on Sn isotopes can only excite pure hole components (J^π= $9/2^+$, $1/2^-$, $3/2^-$ etc.). Among them the $1g_{9/2}$ strength is known to be dominant. Therefore the states excited in Sn(p, α) reaction are mainly formed by combining one proton hole state $1g_{9/2}$ and two-neutron hole state. Thus the energy spectrum for the ^{120}Sn(p, α) reaction shows a striking similarity in shape to that for the ^{120}Sn(p, t) reaction.

The (p, t) reaction on even tin isotopes excites zero-quasiparticle state (J^π=0^+) and two-quasiparticle states (J^π=2^+, 3^-, 4^+, 5^-, 6^+, 7^-, 8^+, 9^- and 10^+) in the major shell. The 0^+ state and one of the 2^+ states correspond to the ground and the first excited states, respectively, of the residual nucleus. Other two-quasiparticle states are considered to distribute in the energy region of 2.5-5 MeV, where a broad peak is observed in ^{120}Sn(p, t) reaction as shown in Fig. 12.

The situation of three-nucleon pickup process is shown schematically in Fig. 13. The excitation energies and strengths of the states excited in Sn(p, t) and Sn(d, ^{3}He) reactions are shown schematically in Figs. 13(a) and 13(b), respectively. Fig. 13(c) shows the excitation energies and strengths of the states excited in Sn(p, α) reaction which are formed by combining these two excitations (Figs. 13(a) and 13(b)) in the weak-coupling scheme. Fig. 13(c) corresponds to the energy spectrum from the Sn(p, α) reaction and shows the similar shape to the measured energy spectra from the (p, α) reactions on ^{112}Cd, ^{118}Sn and ^{120}Sn. Thus the fine structures of the energy spectra from the (p, α) reactions on ^{112}Cd, ^{118}Sn and ^{120}Sn can be qualitatively explained by using the pickup model.

For Sb or Te, one or two protons are added in $1g_{7/2}$ orbit outside the Z=50 closed proton shell. The excitation energies and strengths of the states excited in Te(d, ^{3}He) and Te(p, α) reactions are shown schematically in Figs. 14(b) and 14(c), respectively.

The energy spectra above 20 MeV from the (p, α) reaction on Sb, ^{128}Te and ^{130}Te correspond to one-proton pickup from $1g_{7/2}$ orbit. The energy spectra below 20 MeV are due to mainly the one-proton pickup from Z=50 closed proton shell and show structures duller than those in the cases of Cd and Sn because of the proton pickup from the deep states ($1g_{9/2}$, $2p_{1/2}$, $2p_{3/2}$) which produces the fragmentation[10] of single-particle levels. Thus

the fine structures of the energy spectra from the (p, α) reactions on Sb, ^{128}Te and ^{130}Te can be qualitatively explained.

Glowacka et al[11]. have reported the energy spectra of α particles emitted from the ^{147}Sm(n, α) reaction at neutron energies of 12.4, 14.1, 18.2 and 19.5 MeV. The energy spectrum for ^{147}Sm(n, α) reaction is shown in Fig. 15. Since the energy spectra for the ^{147}Sm(n, α) reaction show a striking similarity in shape to that from the Sb(p, α) reaction, a following explanation of the energy spectrum is possible. Peaks near 29 MeV and near 27.5 MeV of the α-particle energy correspond to one-neutron pickup from unpaired and paired neutrons in $2f_{7/2}$ orbit outside the N=82 core, respectively. The energy spectra below 26 MeV correspond mainly to the one-neutron pickup from the N=82 core, and show similar structures to those from the (p, α) reaction on nuclei around Z=50. Namely, the (n, α) spectrum has two large peaks near 25.5 and 24.5 MeV and a broad peak around 22 MeV.

Haight et al[5]. have reported the energy spectra of α particles from the 14 MeV (n, α) reaction on nuclei around N=50. Although these energy spectra are very poor, these spectra are not inconsistent with those predicted by analogy with the present (p, α) reaction.

3-3 (p,p') and (n,n') reactions

Energy spectra of protons emitted from (p,p') scattering were measured[12] for ^{90}Zr, ^{93}Nb, ^{92,94,96,98,100}Mo, ^{106}Pd, and Ag at an incident energy of 18 MeV. It was shown that there were no appreciable shell and odd-even effects on the preequilibrium proton spectra corresponding to excitations higher than 4 MeV of the residual nucleus. The experimental results were interpreted on the basis of the state densities generated from two sets of single particle levels using the recursion method by Williams et al.; one is based on the spherical Nilsson model, and the other on the modified uniform spacing model in which a shell gap is introduced into the uniform spacing model.

The energy spectra of neutrons emitted from 14 MeV neutron induced reactions on Ag, Cd, In, Sn, Sb, and Te were measured[13] at 70° in order to investigate the shell and odd-even effects in the preequilibrium (n,n') process. As a result, it was found that there are no appreciable shell and odd-even effects in the preequilibrium (n,n') process that leaves the residual nucleus in the continuum region.

These results for the (p,p') and (n,n') scattering are presented in

detail in poster No. 14 in this seminar by Y. Watanabe.

3-4 (p,d) reaction

Energy spectra of deuterons emitted from (p,d) reactions were meaured for ^{92,94,96,98,100}Mo at an incident energy of 19 MeV. The measured energy spectra at θ=50° are shown in Fig. 16. The energy spectrum for the ^{92}Mo(p,d) reaction has three sharp peaks which correspond to the neutron pickup in orbits of $1g_{9/2}$, $2p_{1/2}$ and $2p_{3/2}$. For other Mo isotopes, the energy spectra below the energy indicated by the arrow correspond mainly to the one-neutron pickup from the N=50 core and show structure duller than that for ^{92}Mo, because of the neutron pickup from the deep states ($1g_{9/2}$, $2p_{1/2}$, $2p_{3/2}$) which produces the fragmentation[8] of single particle levels.

Cross sections integrated over the deuteron energy below the energy indicated by the arrow, which correspond to the core excitation, are shown in Fig. 17. The cross sections increase monotonically with increasing mass numbers. The Q values of the (p,d) reactions on Mo isotopes increase monotonically with increasing mass numbers. Therefore if the corrections of the cross sections by the penetrability of deuterons are carried out, each of the corrected cross sections is nearly equal between the measured isotopes. Thus it was found that there is no appreciable shell effect in the (p,d) cross section corresponding to the excitation of the N=50 core.

References

(1) SCOBEL, W., et al.: Phys. Rev. C 30, 1480 (1984), Lawrence Livermore National Laboratory Report No. UCID-20101, 1984 (unpublished).
(2) KUMABE, I.: J. Nucl. Sci, Technol. 18, 563 (1981).
(3) KUMABE, I., WATANABE, Y.: Phys. Rev. C 36, 543 (1987).
(4) GRIMES, S.M., et al.; Nucl. Sci. and Eng. 62, 187 (1977), Phys. Rev. C 17, 508 (1978), Phys. Rev. C 19, 2127 (1979).
(5) HAIGHT, R.C., et al.: Phys. Rev. C 23, 700 (1981).
(6) KUMABE, I.: Proc. Europhys. Topical Conf. on Neutron Induced Reactions, 1982, Smolenice, Czechoslovakia, p. 305.
(7) KUMABE, I., et al.: Phys. Rev. C 35, 467 (1987).
(8) BASSANI, G., et al.: Phys. Rev. 139 B830 (1965).
(9) WEIFFENBACH, C.V. and TICKLE, R.: Phys. Rev. C 3, 1668 (1971).
(10) BERTSCH, G.F. et al.: Rev. Mod. Phys. 55, 287 (1983).

(11) GLOWACKA, L., et al.: Nucl. Phys. A 329, 215 (1979), DALMAS, J., et al.: Can. J. Phys. 61, 1013 (1983).
(12) WATANABE. Y., et al.: Phys. Rev. C 36, 1325 (1987).
(13) WATANABE, Y., et al.: To be published in Phys. Rev. C.

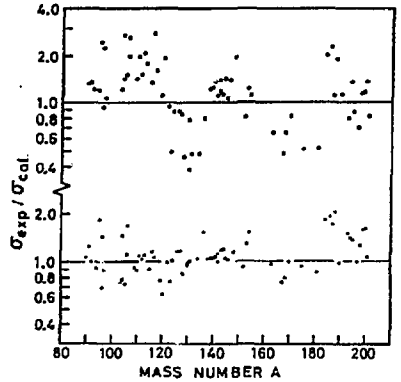

Fig. 1 Ratios of experimental to theoretical cross sections calculated using true Q-values and effective Q-values plotted in upper and lower parts, respectively.

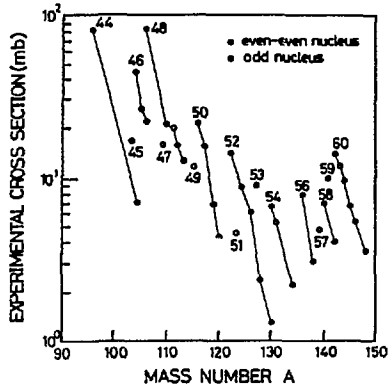

Fig. 2 Experimental cross sections of 14 MeV (n,p) reaction as a function of mass number. Numbers in the figure represent atomic numbers.

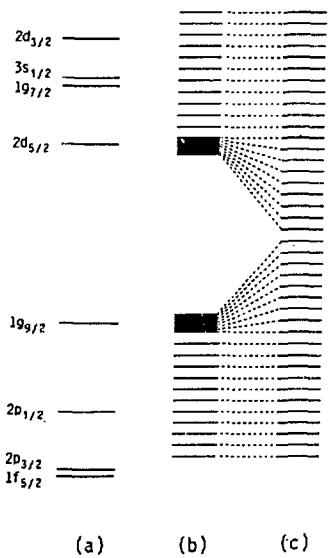

Fig. 3 (a) Shell model with spin-orbit coupling;
(b) modified uniform spacing model;
(c) uniform spacing model.

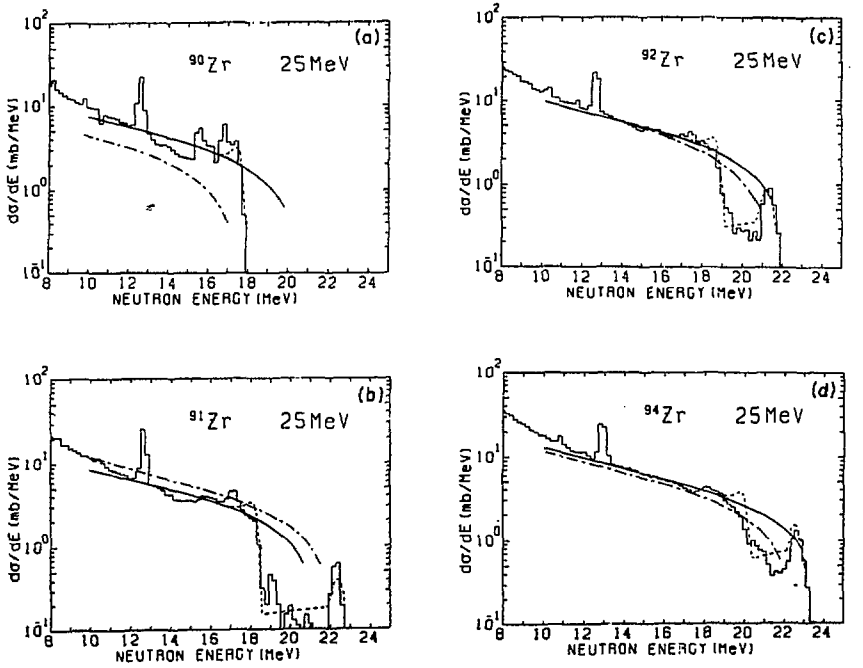

Fig. 4 Calculated and experimental angle-integrated energy spectra of neutrons for 25 MeV (p,n) reaction on Zr isotopes. (Histograms: experimental spectra, dotted-dashed curves: uniform spacing (US) model using true Q values, solid curves: US model using effective Q values (Q_e), and dashed curves: modified uniform spacing model using Q_e plus pairing correlation.)

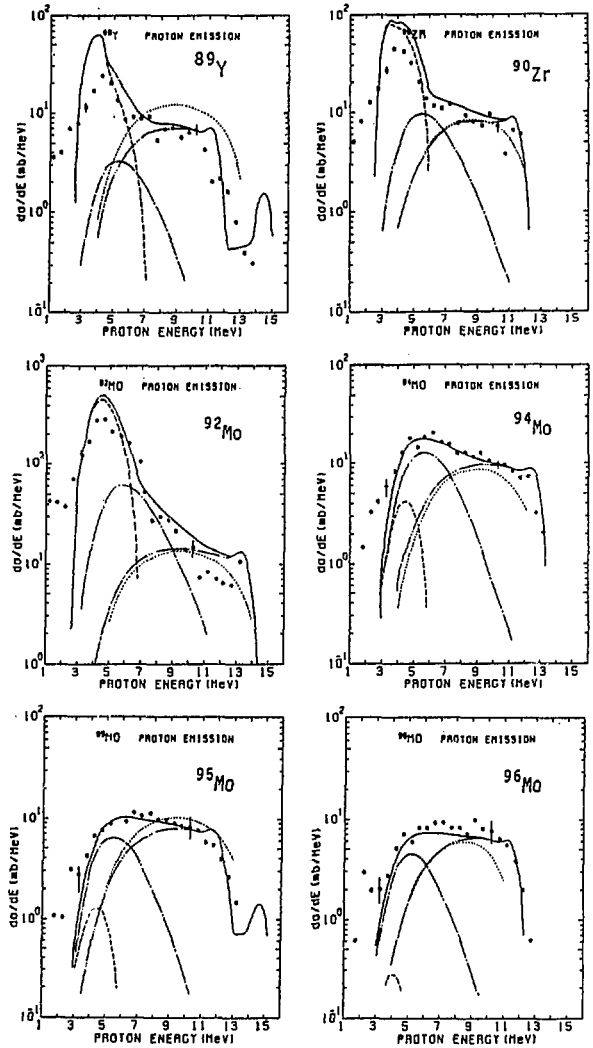

Fig. 5 Calculated and experimental angle-integrated energy spectra of protons for 14 MeV (n,p) reaction. The closed circles show the experimental energy spectra. The double-dotted-dashed curves are the calculated preequilibrium energy spectra using the modified uniform spacing model, effective Q values and the pairing correlation; the dotted-dashed curves are the calculated evaporation spectra; the dashed curves are the calculated energy spectra for the (n,np) reaction; the solid curves are the sum of these. The dotted curves are the calculated preequilibrium energy spectra using true Q values.

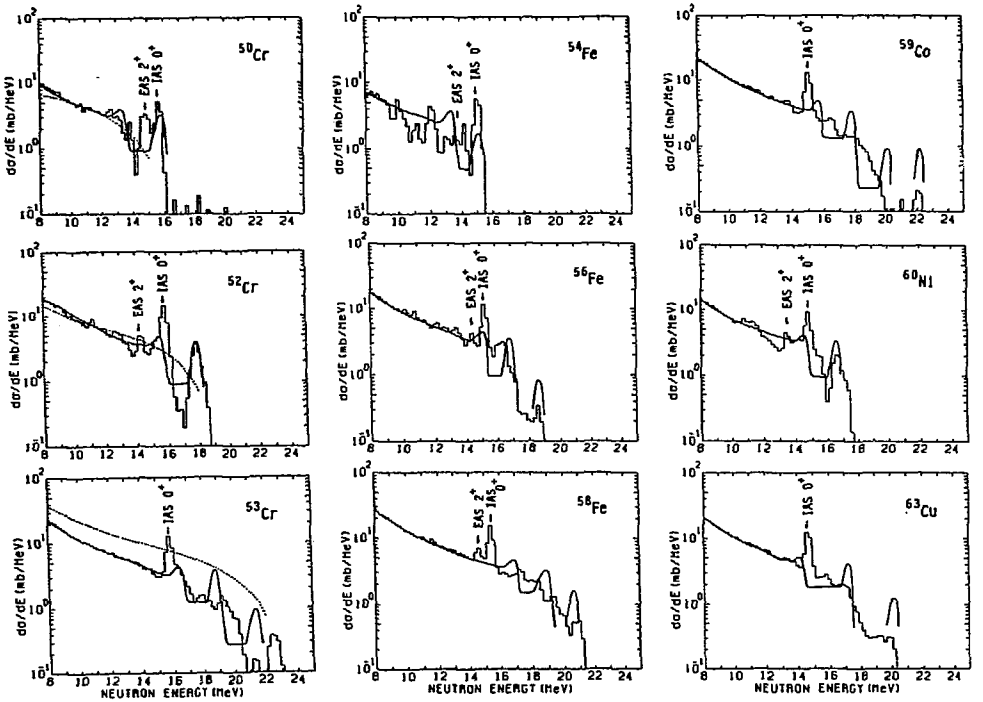

Fig. 6 Calculated and experimental angle-integrated energy spectra of neutrons for 25 MeV (p,n) reaction. The histograms show the experimental energy spectra. The solid curves are the calculated preequilibrium energy spectra using the modified uniform spacing model, effective Q values, and the pairing correlation. The dotted curves are the calculated preequilibrium energy spectra using the Q values.

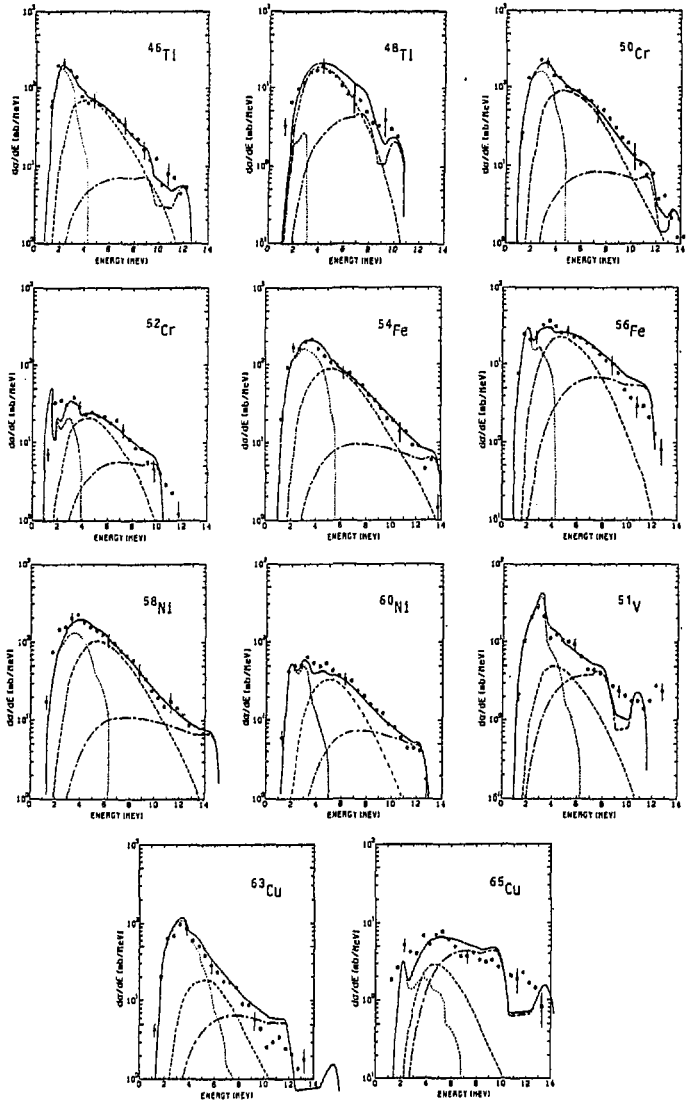

Fig. 7 Calculated and experimental angle-integrated energy spectra of protons for 14 MeV (n,p) reaction. The open circles show the experimental energy spectra. The dotted-dashed curves are the calculated preequilibrium energy spectra using the modified uniform spacing model, effective Q values and the pairing correlation; the dashed curves are the calculated evaporation spectra; the dotted curves are the calculated energy spectra for the (n,np) reaction; the solid curves are the sum of these.

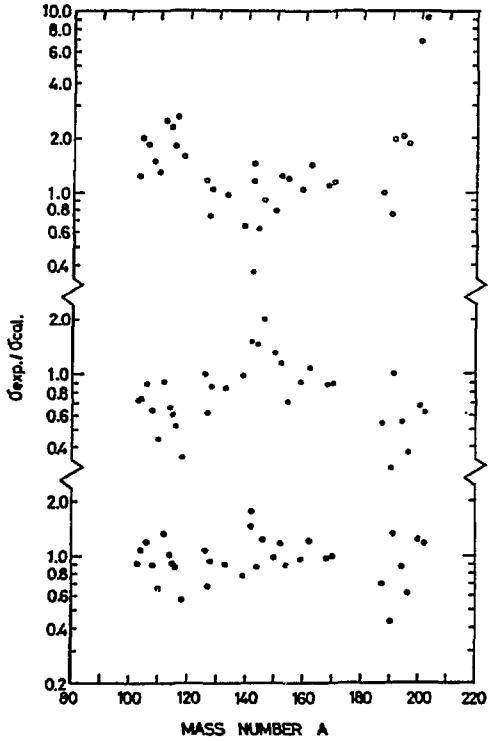

Fig. 8 Ratios of experimental to theoretical (n,α) cross sections.

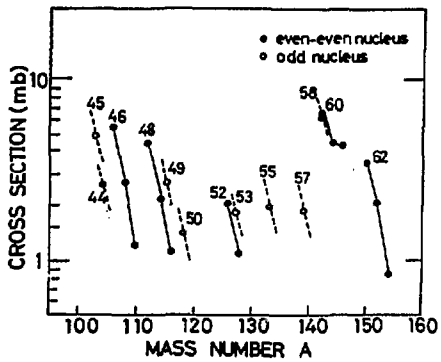

Fig. 9 Q-values of the (n,α) reaction as a function of mass number.

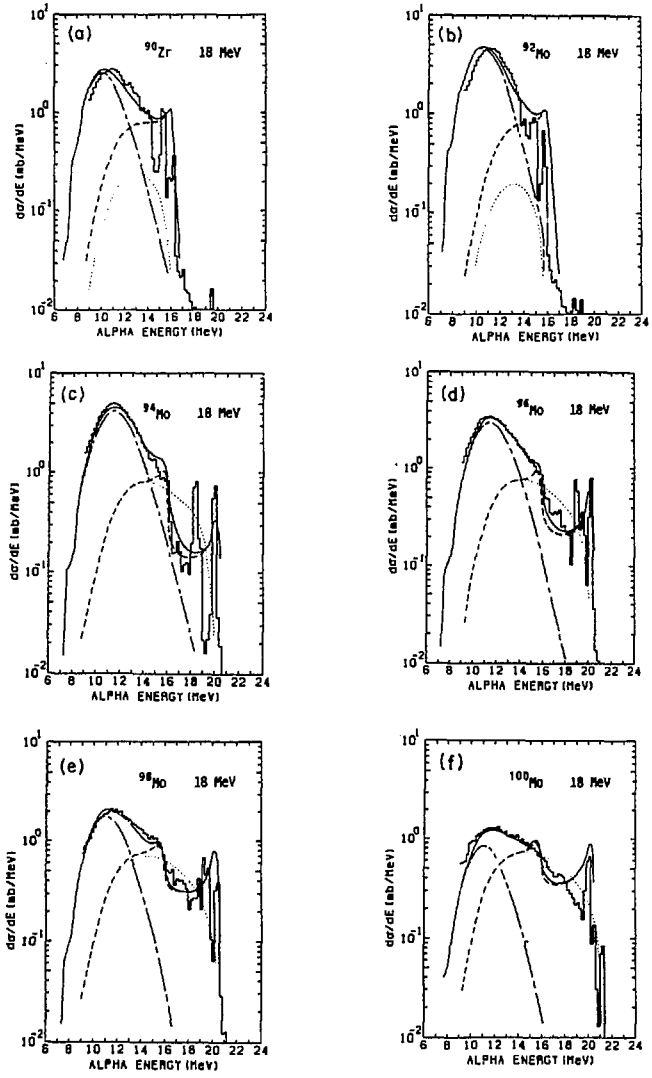

Fig. 10(1) Energy spectra of α particles for ^{90}Zr and ^{92,94,96,98,100}Mo. The histograms show the experimental energy spectra. The dashed curves are the calculated preequilibrium energy spectra using the modified uniform spacing model, effective Q values, and the pairing correlation; the dotted-dashed curves are the calculated evaporation spectra; the solid curves are the sum of these. Dotted curves show the calculated preequilibrium energy spectra using the uniform spacing model and the true Q values.

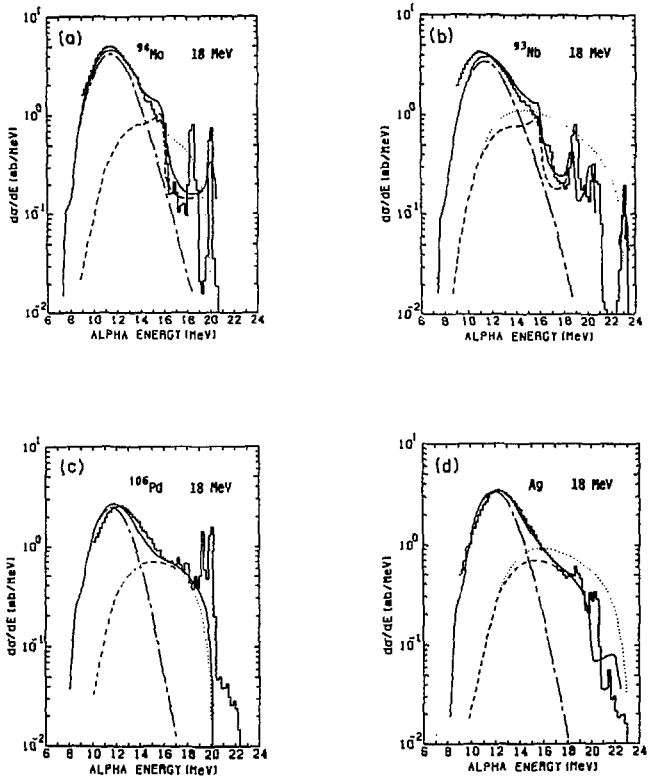
(a)
^{96}Mo 18 MeV
(b)
^{93}Nb 18 MeV
(c)
^{106}Pd 18 MeV
(d)
Ag 18 MeV
dσ/dE (mb/MeV)
ALPHA ENERGY (MeV)

Fig. 10(2)

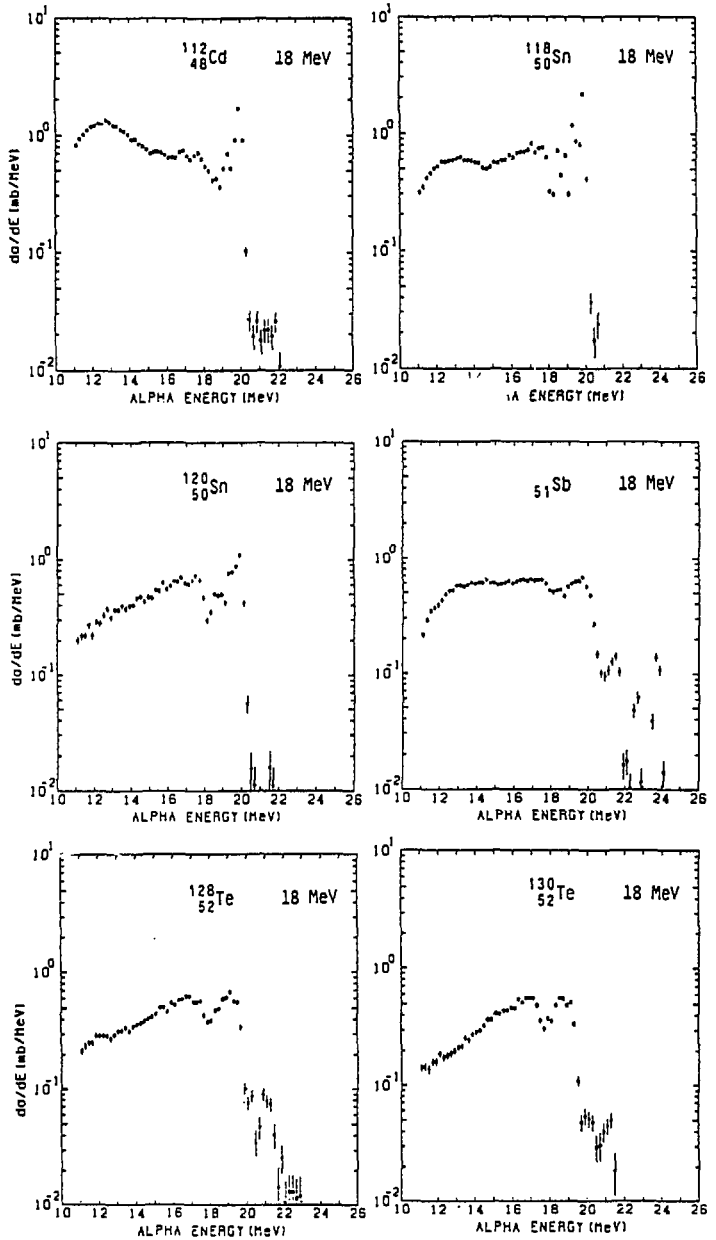

Fig. 11 Energy spectra of α particles for ^{112}Cd, ^{118,120}Sn, Sb and ^{128,130}Te. The histograms show the experimental energy spectra.

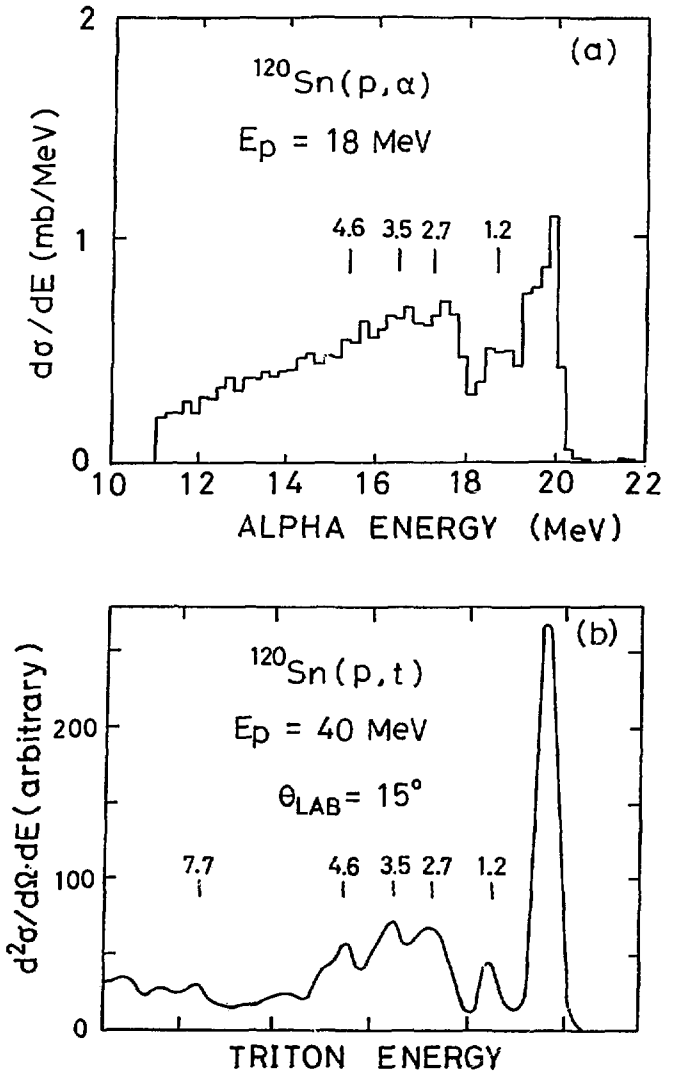

Fig. 12 Measured energy spectra of particles emitted from the ^{120}Sn(p,t) and ^{120}Sn(p,α) reactions.

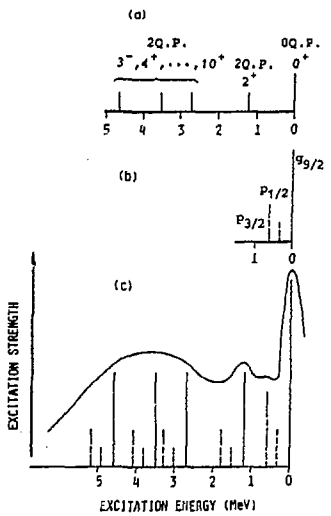

Fig. 13 Schematic illustrations of the excitation energies and strengths of the states of the residual nuclei.
(a): Sn(p,t) reaction.
(b): Sn(d,^{3}He) reaction.
(c): Sn(p,α) reaction from which the states are formed by combining two excitations ((a) and (b)).

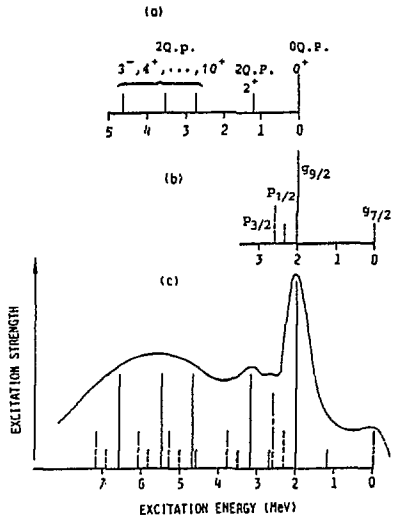

Fig. 14 Schematic illustrations of the excitation energies and strengths of the states of the residual nuclei.
(a): Te(p,t) reaction.
(b): Te(d,^{3}He) reaction.
(c): Te(p,α) reaction from which the states are formed by combining two excitations ((a) and (b)).

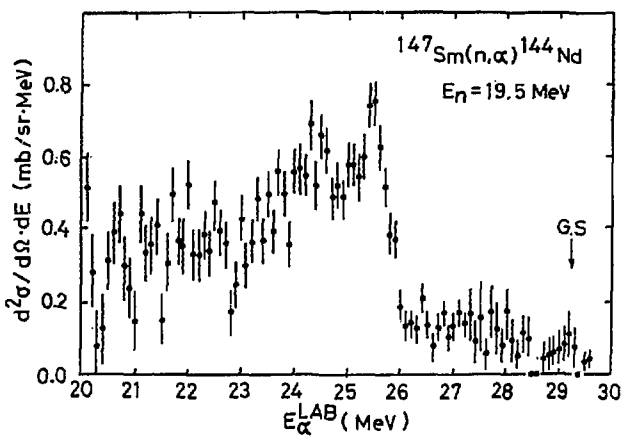

Fig. 15 Energy spectrum of α particles from the ^{147}Sm(n,α) reaction at the neutron energy of 19.5 MeV.

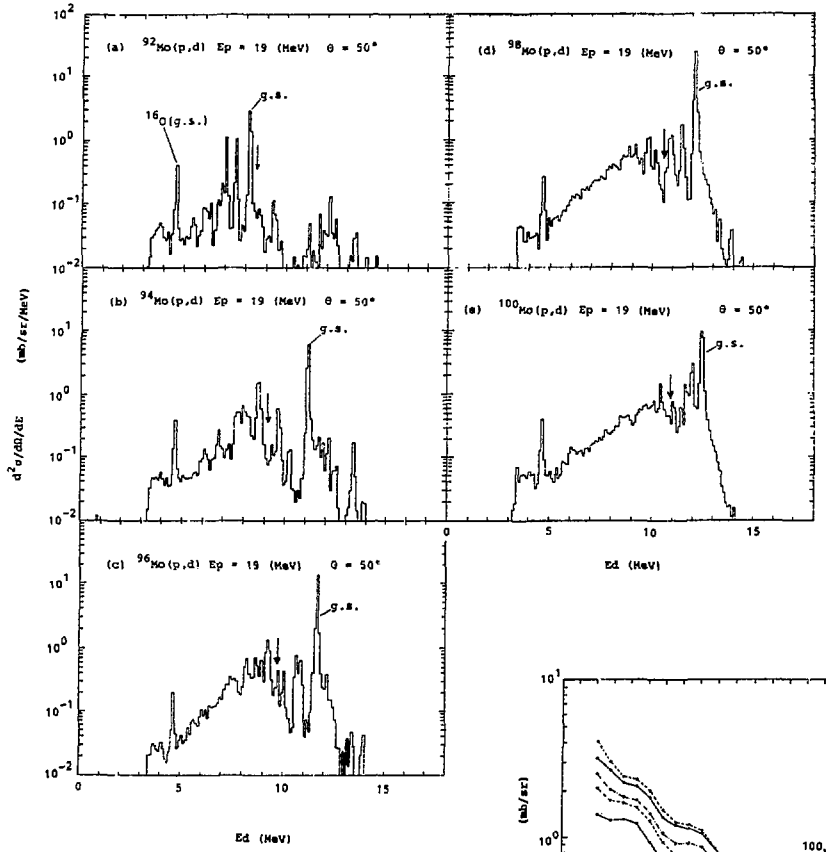

Fig. 16 Energy spectra of deuterons from the (p,d) reaction at θ_L=50°.

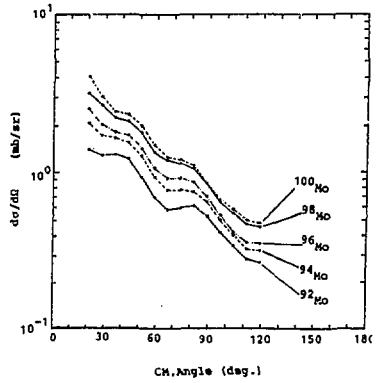

Fig. 17 Cross sections integrated over the deuteron energy below the energy indicated by the arrow in Fig. 16, which correspond to the core excitation.

2.3.2 Activities on Atomic and Molecular Data for Fusion

Toshizo Shirai
Japan Atomic Energy Research Institute
Tokai-mura, Naka-gun, Ibaraki 319-11

Recent data compilation and evaluation work in the Nuclear Data Center is introduced briefly.

1. Introduction

For fusion research and development, such as in JT-60, a large number of atomic and molecular (A&M) data are needed not only for diagnostic purposes of high temperature plasmas but also for plasma-modellings. Since 1977, compilation and evaluation have been made of them in the Nuclear Data Center in cooperation with the Research Committee on A&M Data consisting of the members in and outside JAERI. Under the Research Committee, we have two subcommittees: One is for planning and the other is for three working groups concerning atomic collision data, particle-material interaction data, and atomic structure data.

Bibliographic informations can be obtained from the International Bulletin on A&M Data for Fusion published quarterly by IAEA and from publications by NBS and ORNL. For numerical data compilation, we survey a large number of papers with use of them, and collect experimental data to be needed. These experimental data are stored in the A&M Data Storage and Retrieval System (AMSTOR)。 For comprehensive data sets, we evaluate them to produce the Evaluated A&M Data Library (JEAMDL).

2. Progress Report

Brief summary of the activities in each working group is given below.

I。 Atomic collision working group

1) Total cross section for charge changing processes in collisions of atomic and molecular hydrogen and helium with atoms/molecules
2) Total cross section for electron capture of multiply-charged ions in collisions with atomic and molecular hydrogen and helium

An analytic semiempirical formula as a function of collision energy is available at present for each cross section.

II. Particle-material interation (PMI) working group

1) Data on elementary processes for hydrogen-isotope recycling in fusion device, such as trapping and detrapping processes, diffusion, and particle impact desorption
2) Radiation effects through atomic collision cascade in fusion materials by ion beam and fast neutron bombardments
3) Compilation of bibliographic informations on PMI published in Japan for the contribution to the IAEA Bulletin

III. Atomic structure working group

1) Evaluation of spectroscopic data (atomic wavelengths, energy levels, and transition probabilities) for highly ionized ions of Ti, Cr, Fe, Ni and Mo
2) Grotrian diagrams for the evaluated spectroscopic data

This work is partially supported by the US-Japan fusion cooperation program between NBS and JAERI.

3. Recent Publications

1) K. Mori, W.L. Wiese, T. Shirai, Y. Nakai, K. Ozawa, and T. Kato, "Spectral Data and Grotrian Diagrams for Highly Ionized Titanium, Ti V - Ti XXII", Atomic Data and Nuclear Data Tables 34, 79-184 (1986).

2) T. Shirai, Y. Nakai, K. Ozawa, K. Ishii, J. Sugar, and K. Mori, "Spectral Data for Highly Ionized Molybdenum Ions, Mo VI - Mo XLII", J. Phys. Chem. Ref. Data 16, 327-377 (1987).

3) Y. Nakai, T. Shirai, T. Tabata, and R. Ito, "Cross Sections for Charge Transfer of Hydrogen Atoms and Ions Colliding with Gaseous Atoms and Molecules", Atomic Data Nuclear Data Tables 37, 69-101 (1987).

4) T. Shirai, K. Mori, J. Sugar, W.L. Wiese, Y. Nakai, and K. Ozawa, "Spectral Data and Grotrian Diagrams for Highly Ionized Nickel, Ni IX- Ni XXVIII", Atomic Data and Nuclear Data Tables 37, 235-332 (1987).

5) Y. Funatake, T. Shirai, and Y. Nakai, "Grotrian Diagrams for the Hydrogen I Isoelectronic Sequence, H I through Kr XXXVI", JAERI-M Report 87-053 (1987).

2.3.3 Free-Electron Laser: Brief Review and Topics

Yuuki KAWARASAKI

Linac Laboratory, Department of Physics
Japan Atomic Energy Research Institute
Tokai-mura, Ibaraki-ken 319-11, Japan

Abstract

The birth and the recent topics of FEL researches are briefly reviewed in connection with the change of a research objective.

1. Introduction

Even research themes can never be free from the social trends surrounding us. This year should be remembered as a turning point in the atomic energy era, dawned some 30 years ago in Japan. The Atomic Energy Commission of Japan has issued its revised long-term plan[1] this june. In this issue, the study of free-electron lasers(FELs) is brought out as one of the new research fields and its application to the isotope separation is considered among others with much expectation.

2. Beginning of FEL

The root of an FEL can be traced back to H. Motz's works[2]: theoretical calculation of radiation emissions from the wiggled electron beam and experimental confirmation of this process using a Stanford linear accelerator in 1950s. As was announced at the 9th International FEL Conference he has died very recently (June).

In 1960s, R.M. Phillips of General Electric Microwave Lab., Palo Alto, Calif. invented a high-power traveling-wave tube based on a periodic field-electron beam interaction in an unloaded waveguide "Ubitron"(undulated beam interaction)[3], which utilized the very undulator magnet, though the electron energy was much lower than in the FELs. He is now a vice president of STAR MICROWAVE Inc. and gave an invited talk "History of the Ubitron" at the 9th Intl. FEL Conf. Ubitron is the living ascendant of FEL and still offers us much to learn.

In 1970s, J.M.J. Madey, a student of Stanford University has completed his doctoral thesis on FELs[4]。 A group in High Energy Physics Lab.(HEPL), Stanford Univ., headed by Prof. H。 Alan Schwettman, has begun to challenge an experimental FEL study using HEPL's superconducting linac(SCL), the construction of which had presumably been initiated in late 1960s[5]。 In 1975, they have succeeded in the observation of the stimulated emission of radiation at a wavelength of 10.6 μm, the same wavelength as that of a dominant spectral line in CO_2 gas laser. This experiment has been published by L.R. Elias et al. in 1976[6]。 Next year they have successfully demonstrated the first operation of a FEL in the world at a wavelength of 3.4 μm, using the same SCL[7]. This success has eventually given a great impetus to the related research in other institutions in the world. In this summer, the first workshop on "Novel Source of Coherent Radiation" has been held, being followed by the Intl. FEL Conf. in very year, besides other Conf.s on laser and microwave has already continuously been held.

In 1983, a visible FEL oscillation has been achieved at the Orsay storage ring ACO by the collaboration team of LURE(Orsay) and HEPL (Stanford)[8]. In 1984, L. Elias has shown a unique FEL system using a van de Graaff accelerator at a far-infrared wavelength at Santa Barbara of Univ. of Calif. (UCSB)[9]. This scheme can be characterized by use of genuinely continuous electron beams and by implementing the facility of beam energy recovery.

3. Recent Topics

The superiority of FELs over conventional lasers is in: 1) tunabilty, 2) high-efficiecy and 3) high-power[10]. Academic interest in FELs with enthusiastic view for science and technology is the main incentive of FEL peoples, while it can not be denied that some expectations have recently been cast on the potentiality of the FELs as "space shield" by the proponents of the Strategic Defense Initiative (SDI)。

This situation is offering a number of FELs' topics. They are in chronological order[11]: 1) 3 μm operation of the Stanford Univ. FEL driven by their room-temperature, Mark-III RF linac, 2) 2 % energy extraction from tapered-wiggler oscillator experiments at 10 μm at Los Alamos National Lab.(LANL), 3) 40 % energy extraction from a tapered-

wiggler FEL amplifier at 8.6 mm at Lawrence Livermore National Lab.(LLNL), 4) first visible-wavelength operation (528 nm) of an RF-linac driven FEL by a Stanford Univ./TRW team using the SCL, 5) coherent harmonic FEL production in the vacuum-ultraviolet at 177 and 106 nm by bunching the electrons in the ACO ring with an external 532 nm laser, and 6) 3 % spectral tuning at 4 μm by use of a H_2-gas-loaded wiggler in the Mark 111 FEL.

To attain high-efficiecy FEL operation, two experiments were conducted to test the feasibility of energy recovery from a recycled electron beam. At HEPL, a racetrack configuration first accelerated and then decelerated the electrons in the same SCL structure. Energy-recovery experiments at LANL used separate standing-wave structure(room temperature) to accelerate and decelerate the electrons with an RF coupling element between the two to return the recovered energy to the accelerator cavities. While lasing at 10 μm with beam energy of 20 MeV and 0.1 A average current, 70 % of the residual electron energy passing through the wiggler was recovered.

Recent major advances in accelerator components is the RF-injectors that produce low-emittance beams of unprecedented brightness. With the Mark 111 Stanford Univ. (Stanford Photon Research Lab.; SPRL) injector, normalized emittance values as low as 4 π mm•mrad were measured with 20A peak current by use of a fieled-emission gun with a LaB_6 cathode. At LANL, a laser-driven photocathode injector also produced beams with normalized emittance as low as 10 π mm•mrad with substantial micropulse charge of as large as 5 nC. Peak currents to 400 A and average current 3 A were reported for the latter injector. These new injectors will lead to operations in vacuum-ultraviolet region, as well as operation in the visible region with higher powers and enhanced extraction efficiency.

The FEL research conducted at UCSB has led to the first FEL user facility dedicated to scientific experiments in the far infrared region (130-800 μm). Also at HEPL and at SPRL, the FEL facilities are now being prepared for the same kinds of researches even in shorter wavelength region. LANL's FEL is also in the same direction for applications.

The Boeing Aerospace Company/Spectra Technology Incorporation visible-wavelength FEL experiments have had a success within less than

two and half years after the initiation of the construction. The U.K. FEL Project, started in 1982 has been stopped financially in a half way to the full oscillation experiments. The U.K.'s linac has similar specifications to the JAERI's. The difficulty lies in the too short width of the macropulse (2.5 μs).

4. Our Planning

The linac lab., JAERI has started the FEL study which includes first to develop a high-quality electron beam linear accelerator with superconducting Nb cavities. JAERI's Tandem Booster[12] (an energy-boosting linac of heavy ions from the Tandem van de Graaff) now under construction is much influential to the choice of type of the FEL linac. A large-scale SCL of the CEBAF[13] (Continuous Electron Beam Accelerator Facility) also under construction at Newport News, Virginia, may indicate forthcoming linac feathers.

Recent discovery of [14] and developments in high temperature superconducting materials seem to be encouraging us, though it will take some years to put them into practical use.

K. Sasaki is greatly acknowledged for his valuable comments.

Reference

1) 原子力委員会；原子力開発利用長期計画，昭和６２年６月２２日
2) H. Motz; J. Apple. Physics 22 (1951) 527
H. Motz, W. Thon and R.N. Whitehurst; J. Appl. Physics 24 (1953) 826
3) R.M. Phillips; IRE Transactions on Electron Devices (1960) 231
4) J.M.J. Madey; J. Appl. Physics 42 (1971) 1906
5) J.P. Turneaure and Nguyen Tong Viet; Appl. Phys. Letters 16 (1970) 33
6) L. Elias, W. Fairbank, J.M.J. Madey, H.A. Schwettman and T. Smith; Phys. Rev. Lett. 36 (1976) 717
7) D.A.G. Deacon, L.R. Elias, J.M.J. Madey, G.J. Ramian, H.A. Schwettman and T.I. Smith; Phys. Rev. Lett. 38 (1977) 892
8) M.Billardon, P. Elleaume, J.M. Ortega, C. Bazin, M. Bergher, M. Velghe, Y. Petroff, D.A.G. Deacon, K.E. Robinson and J.M.J. Madey; Phys. Rev. Lett. 51 (9183) 1652
9) L.R. Elias; Phys. Rev. Lett. 42 (1979) 977,
L.R. Elias, G. Ramian, J. Hu and A. Amir; Phys. Rev. Lett. 57 (1986) 424

10) There are now many references and reviews available; as a text-book of FEL theory and experiment by G. Dattori and A. Renieri in "Laser Hand book", Elsevier Science Publishers B.V., 1985

11) from Proceedings of FEL Conference (1986) and Abstract of FEL Conference (1987)

12) S. Takeuchi et al. Annual Report of Department of Physics, JAERI (1986)

13) H.A. Grunder, J.J. Bisognano, W.I. Diamond, B.K. Hartline, C.W. Leeman, J. Mougey, R.M. Sundelin, R.C. York; CEBAF-PR-87-017

14) J.G. Bednorz and K.A. Müller; Zeitschrift fur Physik B 64 (1986) 189-193

2.3.4 A Basic Study on the Transmutation of Radioactive Wastes by Photonuclear Reactions

Takashi Nakamura, Akira Yamadera and Takeshi Kase
Cyclotron and Radioisotope Center, Tohoku University
Aoba, Aramaki, Sendai 980, Japan

The mass yield distributions and the nuclear transmutation ratios of ^{237}Np and ^{238}U by photofission were measured by using the bremsstrahlung beam of 20-, 30- and 60-MeV energies.

Introduction

As a basic study on the transmutation of high level radioactive wastes by using photonuclear reactions, we have started to measure the mass yield distributions of ^{237}Np and ^{238}U by photofission, which are the main transuranium components in the wastes. Several studies have already been published on the relative yields of the mass distribution of fission products for the photofission of ^{237}Np and ^{238}U with bremsstrahlung of various energies. Here in our study, we obtained the absolute yields of the mass distribution of fission products and the amounts of transmutation of ^{237}Np and ^{238}U nuclides.

Experimental

The bremsstrahlung beam with the 20-, 30- and 60-MeV end-point energies was produced from a 0.5-mm or 1.0-mm thick platinum converter bombarded by 20-, 30- and 60-MeV electron beam from the electron linear accelerators of Nuclear Engineering Research Laboratory, University of Tokyo and of Laboratory of Nuclear Science, Tohoku University. Figure 1 shows the schematic diagram of the experimental arrangement. Only for the linac of Tohoku University, the electrons penetrated through a converter were sweeped out by the beam cleaning magnet as shown in Fig. 1.

The ^{237}Np target is about 50 μg/cm^2 in thickness of 99.3% enriched ^{237}Np deposited on a nickel metal and the ^{238}U target is 0.025-mm thick metal enriched up to 99.959% ^{238}U. These targets were covered with a 0.1-mm thick aluminum catcherfoils to collect fission products. The bremsstrahlung flux injected on the target was measured from the $^{197}Au(\gamma, n)$ reaction with a 0.1-mm thick gold foil attached on the target.

Figure 2 exemplifies the cumulative mass yield distributions obtained for the ^{238}U target by 30- and 60-MeV bremsstrahlung irradiation, together with the experimental data by Jacobs et al.[1] Our experimental results show good agreement with Jacobs' data, except some fluctuated data points. By summing up this distribution curves, the total amounts of transmutation, Δm, of ^{238}U nuclides into fission products by photofission reaction could be estimated.

Discussion

The transmutation ratio, Δm/m, where m is the initial amounts of the relevant nuclide in the target, can also be calculated as follows,

$$\Delta m/m = \int_0^{E_0} \sigma(\gamma, f)\ \phi(E)\ dE,$$

where $\sigma(\gamma, f)$ = photofission cross section,
$\phi(E)$ = bremsstrahlung flux,
E_0 = electron energy.
The results calculated by the above formula give good agreement with our experimental results.

We are now continuing this work for other transuranium targets. This work is a cooperative work with the Power Reactor and Nuclear Fuel Development Corporation.

Reference

1) E. Jacobs et al., Phys. Rev. C19, 422 (1979).

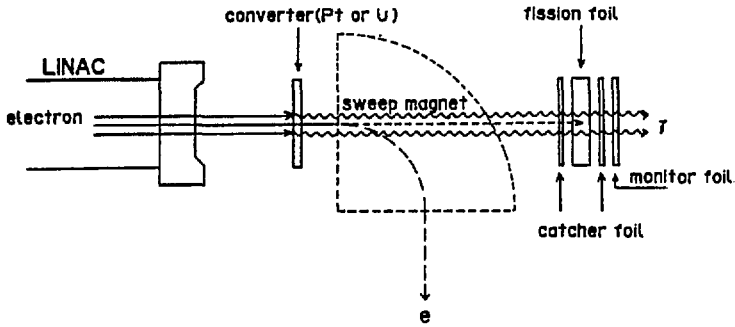

Fig. 1 Schematic diagram of experimental arrangement

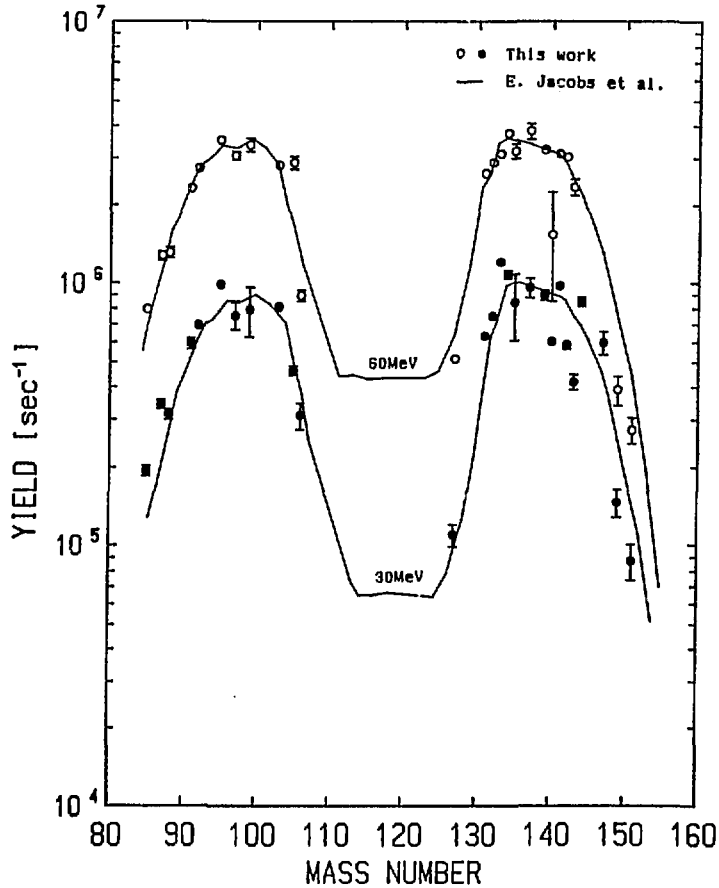

Fig. 2 Mass yield distribution of fission products of ^{238}U photofission induced by 30- and 60-MeV bremsstrahlung radiation

2.3.5 Analysis of Transmutation of Transuranic Wastes by Nuclear Spallation Reactions

Takahiko Nishida and Yasuaki Nakahara

Japan Atomic Energy Research Institute

For applying the proton spallation reaction to the transmutation of transuranic products and evaluating its feasibility by a Monte Carlo simulation, preliminary analyses of spallation product yields have been performed by using the NUCEUS code for the proton induced reactions of TRU nuclides. A simulation code NUCLEUS has been developed at JAERI to calculate the nuclear spallation reaction (intranuclear cascade + evaporation and/or fast fission) between a nucleus and a projectile. The results obtained by our code can be compared directly with measured nuclear data obtained by thin foil experiments, in which internuclear multiple collisions have little effects on the data, and will serve to upgrade the calculational methods and the values of nuclear parameters currently used in the calculations.

The computational results obtained by using NUCLEUS are reported. Mass and half life distributions of reaction products as well as the number of emitted neutrons have been calculated for the spallation reactions of U, Np and Am with a proton of the energy from 0.5 to 3 GeV. After spallation reactions, a variety of nuclei, especially many neutron-deficient nuclides with nuclear charges not far from that of a target nucleus, are produced as the results of many neutron emissions. From our calculated results that most of them have half lives less than one year, it seems that this transmutation method is promising and has additional merits due to the neutron production also.

1. Introduction

In order to obtain the public acceptance of nuclear energy, the security against the risk of accumulating radioactive wastes with long half-lives, produced in a nuclear plant, is one of the most crucial problems. It is known that the annual TRU(Trans Uranirum) production rate is about 250 kg/y in ten units of 1000 MWe LWR. The protection against the hazard due to these products is currently being planned by reducing their volumes, putting them in time-enduring strong containers and cooling them for a long time in the spots isolated from our life environments, in such places as deep strata. Recently the alternative methods, which transmute long-life waste nuclides to short-life and/or stable ones in a short process time by the irradiation with a radiation beam, have been proposed to alleviate the burden of the waste management. These are the followings:

a) transmutation of transuranic products with the nuclear spallation reaction by using a intense beam proton linac,

b) transmutation of waste actinides with the fast neutron flux in Actinide Burning Fast Reactor,

c) disintegration of fission products with the photo-nuclear reaction around a giant resonance by using a high current electron linac.

These methods have their own practical advantages and technical difficulties to be solved. As for the TRU transmutation, it seems to us that the method (a) is not only most interesting from the scientific point of view but most practical from the technical point of view.

Our basic idea is to transmute TRU in a target directly by the proton beam and to breed fissile nuclides simultaneously in a balanket by the use of spallation neutrons coming from the target. One incident proton can destroy a number of target nuclides. The reason why it can is as follows. Since the spallation cross section is proportional to $A^{2/3}$ where A is the mass number of a target nuclide, the spallations are frequent reactions in a TRU target composed of heavy nuclides. Moreover, the high energy secondary particles emitted by the proton induced reactions make spallation reactions further in cascade. Since the spallation reactions are very effective as described above, the feasibility of the TRU transmutation seems quite promising. In order that the transmutation has the practical meaning, it is necessary to make sure that very little amounts of long life hazadous nuclides are produced in the transmutation processes. On the other hand, the possibility may be pointed out of the production of scarce

stable nuclide or short-life RI useful for special purposes as the residual nuclides of the transmutation. Since many high energy neutrons are also emitted as byproducts in this transmutation process, they can be used for other applications such as the breeding of fissile nuclides and the creation of very intense neutron source.

A computational study program has been being carried out at JAERI to develop the idea mentioned above to a realistic engineering concept. In order to make feasibility studies of the concept, we have been developing a computer code system, the principal code of which is the Nucleon Meson Transport Monte Carlo Simulation Code NMTC/JAERI[1], revised at JAERI to incorporate nuclear fissions from highly excited states into the computational flow. From the transmutation point of view, the reliable estimate of spallation ptoduct yields and the determination of their half-life distribution are very important. Their reliabilities critically depends on the computational model used in the NMTC/JAERI code.

In order to examine in detail the computational model of the nuclear spallation reaction a simulation code NUCLEUS[2] has been developed at JAERI for calculating only the nuclear spallation reaction of one nucleus. As the results obtained by this code can be compared directly with nuclear data measured by thin foil experiments, the code is useful for evaluating and improving the computational methods and upgrading the values of nuclear parameters currently used in the calculations. Some results of evaluation studies were compared already with experimental data[3].

In the present paper some computational results obtained by NUCLEUS are presented. The mass, isotope and half-life distributions of reaction products are examined in some detail for the nuclear spallations of TRU nuclei, such as U, Np-237 and Am-241 in the energy range from 0.5 to 3.0 GeV. Cross section data for charged particles and neutrons in the intermediate and high energy range up to 3 GeV are important in the evaluation of our computational results. As the experimental data are scarce at present, comparisons between calculated and measured values can be made only for a few examples.

2. Calculational method

A nucleus bombarded by a sufficiently energetic particle, such as a proton with the energy of hundreds to thousands MeV, undergoes a complicated destruction process, i.e., the so-called spallation. The theoretical models

used in NUCLEUS are essentially the same as those in NMTC[4] and HETC[5] except the fission model which has been incorporated at JAERI. A brief description of the theoretical models and computational method is given in the following.

We use the two step model which consists of intranuclear cascades and competing decays of a highly excited residual nucleus by the high energy fission and particle evaporations. At the first step after a high energy particle has been injected into a nucleus, the intranuclear cascades of nucleons and pions are computed.

In the present model a nucleus is assumed to be a sphere of a degenerate Fermi gas, in which the two body collision model gives a good approximation to the collision process in the intranuclear cascade in the energy range higher than 100 MeV. The characteristics of nuclear matter are determined by the distributions of nucleon density, momentum and potential energy. At each nucleon-nucleon collision event the relativitistic conservations in particle's energy and momentum are checked and it is examined also if Pauli's exclusion principle admits the scattered Fermions. Pion production cross sections are calculated using the Isobar model.[6]

At the second step after the intranuclear cascade has ceased, a highly excited residual nucleus decays selecting the path to the evaporation or the nuclear fission as the subsequent process according to the fission probability based on the Bohr-Wheeler theory and a semi-empirical mass distribution of fission fragments. The evaporation calculation is carried out for neutron, proton, deuteron, triton, helium 3 and alpha particle by the Weisskopf statistical model. The Cameron's mass formula[7] and Uno & Yamada's mass formula[8] are used to calculate binding energies of particles to be emitted.

3. Results and discussions

It is generally known that the products yielded in the nuclear spallation reaction consist mainly of residual nuclei in the evaporation stage of nuclear reaction, where the precision of the mass formula is crucial in getting good results. Comparisons, using two mass formulas, i.e., Cameron's and Uno & Yamada's, have been made with measured data for the spallation of a uranium nucleus bombarded by protons from 0.38 to 2.9 GeV[9]. These results have shown that Uno & Yamada's mass formula reproduce those better

than Cameron's one. In the recent calculations we have used the former formula in preference to the latter one. In this section, main results of our calculations are summarized and discussed.

All the residual nuclides and particles produced from a Np-237 nucleus bombarded by protons were calculated with energies from 0.5 to 3.0 GeV. Figure 3.1 (a) shows the mass yield distribution of residual nuclei for the incident proton energy of 500 MeV. The first peak near the target nucleus and the second peak apart from it seen around A $\simeq$ 200 correspond to intranuclear cascade and non-fission evaporation products, respectively, which are characterized by neutron-excess and neutron-deficient nuclides. The spires in the light mass region correspond to the evaporated α, ^{3}He + t and d. A flat region in the intermediate mass range represents products due to the high energy fission. As the proton energy increases from 0.5 GeV to higher energy, the hill of non-fission product yield (A = 190 - 240) transforms to the one with a milder slope. The mass distributions of reaction products were examined in some detail for the nuclear spallation reactions of other nuclei, such as Nat. U, ^{241}Am, Pb and Ag in the same energy range. These results show that the distribution of reaction products ceases to change its form and the yields decreases slightly as the proton energy increases over about 2 GeV. The same tendency is seen in the energy variation of the number of particles emitted from a nucleus. Table 3.1 summarizes the number of emitted neutrons per an incident proton and a nucleus. It is apparent that the maximum yield of neutrons emitted from transuranic nuclides, Nat. U, ^{237}Np, ^{241}Am, is about 17 at 2 GeV, while it decreases also slightly over 2 GeV probably because of an increase of nuclear transparency for incident protons. But we can expect larger neutron yields in a bulk target due to subsequent internuclear cascades. The same tendency is seen in cases of lead and silver nuclei.

The computations by NUCLEUS show that after nuclear spallation reactions, a variety of nuclei, especially many neutron-deficient nuclides with nuclear charges not far from the one of a target nucleus, are produced. In Fig. 3.2 mass distributions of isotopes produced in the nuclear spallation reaction by a 1 GeV proton bombarding a neptunium-237 nucleus are shown for atomic numbers Z = 91 - 37. It is aparrent that the maximum in each distribution with Z = 91 - 71 appears on the neutron deficient side on the A-axis except for Np (neutron excess peak : ^{236}Np), since the stable nuclide of each element exists in the right tail of each peak. However the isotope distribution becomes symmetric with respect to the position of a stable

isotope for elements with Z = 67 - 53, and neutron excess isotopes become asymmetrically dominant in the distributions for Z = 49 - 37.

On the other hand, the actual accumulation of residual nuclide to a specific nuclide due to build-up and decay processes may be roughly estimated from product yields on the $\beta^{\pm}$ decay chain leading to it and their half-lives. In the transmutation of ^{237}Np product yields on β^{+} and β^{-} decay chains leading to the stable isotope ^{203}Tl, which is known as useful materials for semiconducter, and superconducter and scarce in the earthen resources, are shown by open rectangles together with the direct yield indicated by the closed rectangle in Fig. 3.3. Most of them are produced mainly from the non-fission processes on the β^{+} chain just after intranuclear cascades and build up to ^{203}Tl in due time due to their short half-lives. Similarly the product yields on the Z-axis with mass numbers of 235 and 233 are expected to accumlate in due time to ^{235}U and ^{233}U, respectively, as shown in Fig. 3.4. It is very interesting that not a small amount of fissile materials ^{235}U and ^{233}U are produced also. The spallation reaction producing a nuclide at the first peak in the non-fission product region is virtually equivalent to "one neutron emission" reaction. There is a flow scheme producing a fissile nuclide from a TRU nucleus by the suitable combination of two "one neutron emission" and one short life β decay. Two production routes to ^{235}U from ^{237}Np and to ^{239}Pu from ^{241}Am are shown in Fig. 3.5. Product yields on β^{-} decay chains leading to ^{90}Sr and ^{137}Cs are shown by open rectangles in Fig. 3.6. Most of them are produced mainly from the fission processes just after intranuclear cascades. These product yields are smaller by about an order of magnitude than those of non-fission products and the accumulations from the decay chains are seen also to be small. It is advantageous in the transuranic waste transmutation that the production of harmful FP nuclides such as ^{90}Sr is small.

Figure 3.7 illustrates half-life distributions of product yields in the transmutation of three transuranic nuclei bombarded by a 2 GeV proton, where 9 decay classes represent the time ranges of half lives of nuclides as described in this figure. It is desired from the transmutation point of view that yields in the 7th (1 y - 100 y) and the 8th (>100 y) classes are as small as possible. As seen from the figure, these yields are very small except triton.

From results of calculations for a target model (cylinder, length 60 cm, radius 10 cm) of Nat. U, it is possible that about five nuclei are transmuted per an incident proton of 1.5 GeV in internuclear cascades of

high energy particles above 15 MeV. The value implies that the annual products of TRU from four units of 1000 MWe LWR can be transmuted by using this method. It should be noted, however, that the contribution of the spallation neutrons with energies below 15 MeV is not taken into consideration in estimating the transmutable amount of TRU. If all those spallation neutrons are used also to transmute TRU, it is estimated that it is possible to transmute the amount of TRU from 10 units of 1000 MWe LWR.

In order to make technical assessments of the transmutation process from the practical point of view, the calculations of build-up and decay processes of spallation products should be performed by solving the exact time evolution equations. However, it is very difficult in the actual computation to follow the time evolution of all the nuclides in the target irradiated continuously by protons, due to the enormous number of kinds of produced nuclides. At present we have no means to do it, because there are no available computer codes and nuclear data files for performing the build-up and decay calculations for nuclides including spallation products. We are deveolping a computer code by extending the one-point depletion code DCHAIN[10], which was developed by Tasaka at JAERI for the calculation of build-up and decay of fission products, to include the spallation products and TRU nuclides.

4. Conclusion

A nuclear spallation simulation code NUCLEUS was used to evaluate the spallation product yields from TRU nuclides from the transmutation point of view. We can summarize the present results as follows:

(1) Results of calculations of all the produced nuclei and number of emitted neutrons show that an energy brought into a TRU nucleus by an incident proton saturates around 2 GeV, independent of the mass of a target nucleus.

(2) In the nuclear spallation reaction, more neutron deficient nuclides are produced than in the fission and most of them have half-lives shorter than 100 y. Few harmful nuclides such as ^{90}Sr are produced.

(3) From these results it seems that the transmutation of TRU using the spallation reaction is promising.

(4) Moreover, we can expect the feasibility of producing fissile

materials with the proton irradiation of a TRU target by employing a suitable processing technique.

The main study program in the near future will include the following:

(a) upgrading the precision of simulation calculations of nuclear reactions in the high and intermediate energy region.

(b) developing a computer code and compiling a nuclear data file for the calculations of destruction, decay and build-up processes of nuclides during the transmutation process under the continuous proton irradiation.

(c) design analysis of a transmuter (a proton beam target/branket for the TRU transmutation)

Acknowledgements

The authors wish to express their hearty thanks to Dr. Y. Ishiguro for his continued interests and encouragements, and to Mr. T. Tsutsui for program improvements.

References

(1) Nakahara Y., Tsutsui T.: "NMTC/JAERI: A Simulation Code System for High Energy Nuclear Reactions and Nucleon - Meson Transport Processes," JAERI-M 82-198 (1982) (in Japanese).

(2) Nishida T., Nakahara Y., Tsutsui T.: "Development of a Nuclear Spallation Simulation Code and Calculations of Primary Spallation Product," JAERI-M 86-116 (1986) (in Japanese).

(3) Nishida T., Nakahara Y.: Kerntechnik, 50, 3(1987).

(4) Coleman W.A., Armstrong T.W.: "The Nucleon-Meson Transport Code NMTC," ORNL-4606 (1970).

(5) Chandler K.C., Armstrong T.W.: "Operating Instructions for High Energy Nucleon-Meson Transport Code HETC," ORNL-4744 (1972).

(6) Sternheimer R.M. and Lindenbaum S.J.: Phys. Rev., 105, 1874 (1957); 109, 1723 (1958); 123, 333 (1961).

(7) Cameron A.G.W.: Canad. J. Phys., 35, 1021 (1957).

(8) Uno M., Yamada M.: "Atomic Mass Formula with Constant Shell Terms," Prog. Theor. Phys., 65, No.4, 1322 (1981).

(9) Nishida T., Nakahara Y., Tsutsui T.: "Analysis of the Mass Formula Dependence of Spallation Product Distribution," JAERI-M 87-088 (1987).

(10) Tasaka K.: "DCHAIN: Code for Analysis of Buildup and Decay of Nuclide," JAERI 1250 (1977).

Table 3.1 Number of neutrons emitted from a single nucleus of some actinides, lead and silver

Energy of protons (MeV)		500	1000	2000	3000
(1)	Ag	5.18	6.15	6.59	5.33
(2)	Pb	10.64	13.09	14.31	12.20
(3)	Nat. U	13.01	16.05	17.32	14.91
(4)	Np 237	12.34	15.30	16.46	14.24
(5)	Am 241	12.41	15.39	16.48	14.28

(1),(2) : Cameron's mass formura, (3),(4),(5) : Uno's mass formula

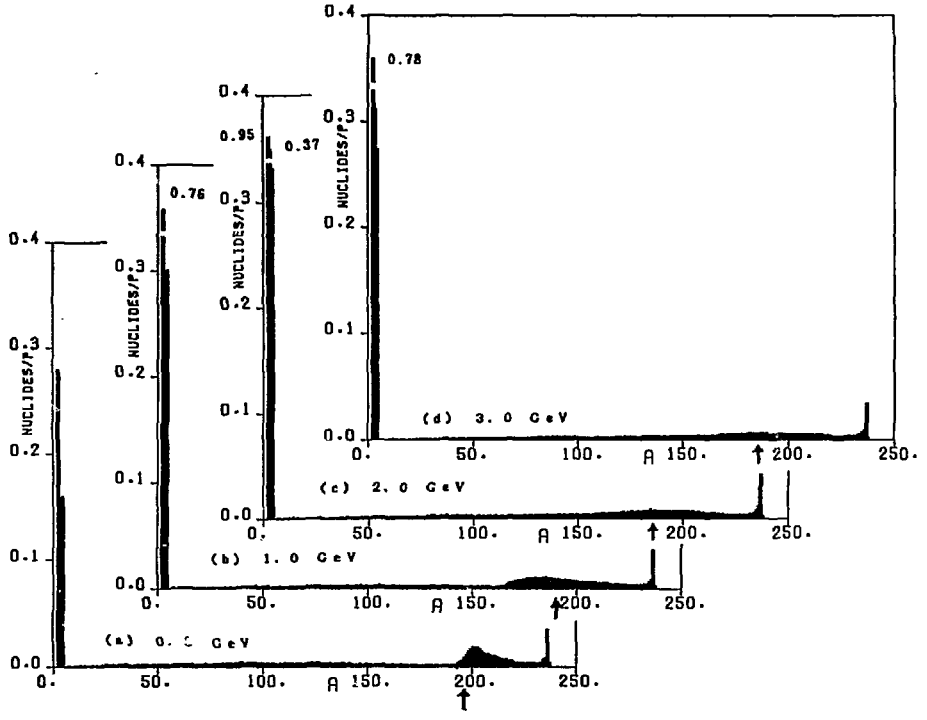

Fig. 3.1 Mass yield distributions of products in the proton induced nuclear spallation of a Neptunium-237 nucleus
Proton energies:
a) 0.5 GeV, b) 1.0 GeV, c) 2.0 GeV and d) 3.0 GeV

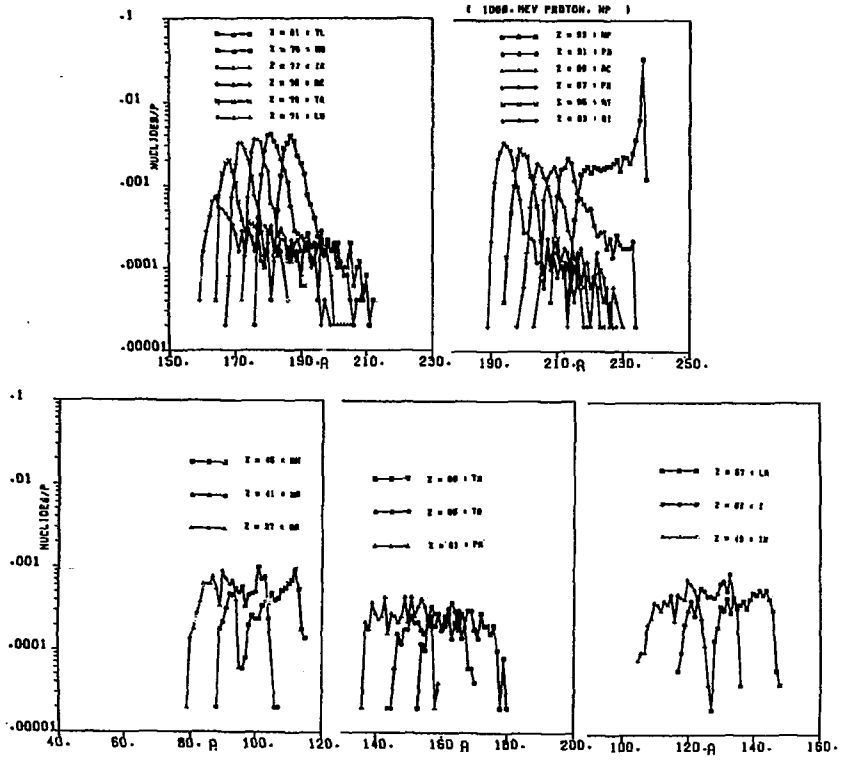

Fig. 3.2 Isotope yield distributions of products with Z = 93 - 37 in the nuclear spallation reaction of a Neptunium-237 nucleus with a 2 GeV proton

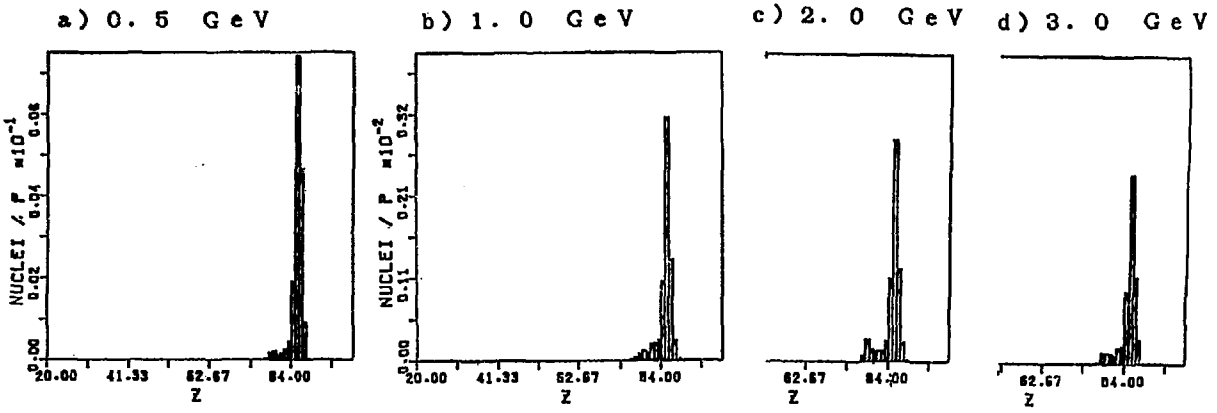

Fig. 3.3 Product yields on the β decay chain leading to ^{203}Tl for the nuclear spallation of a Neptunium-237 nucleus
Proton energies:
a) 0.5 GeV, b) 1.0 GeV, c) 2.0 GeV and d) 3.0 GeV

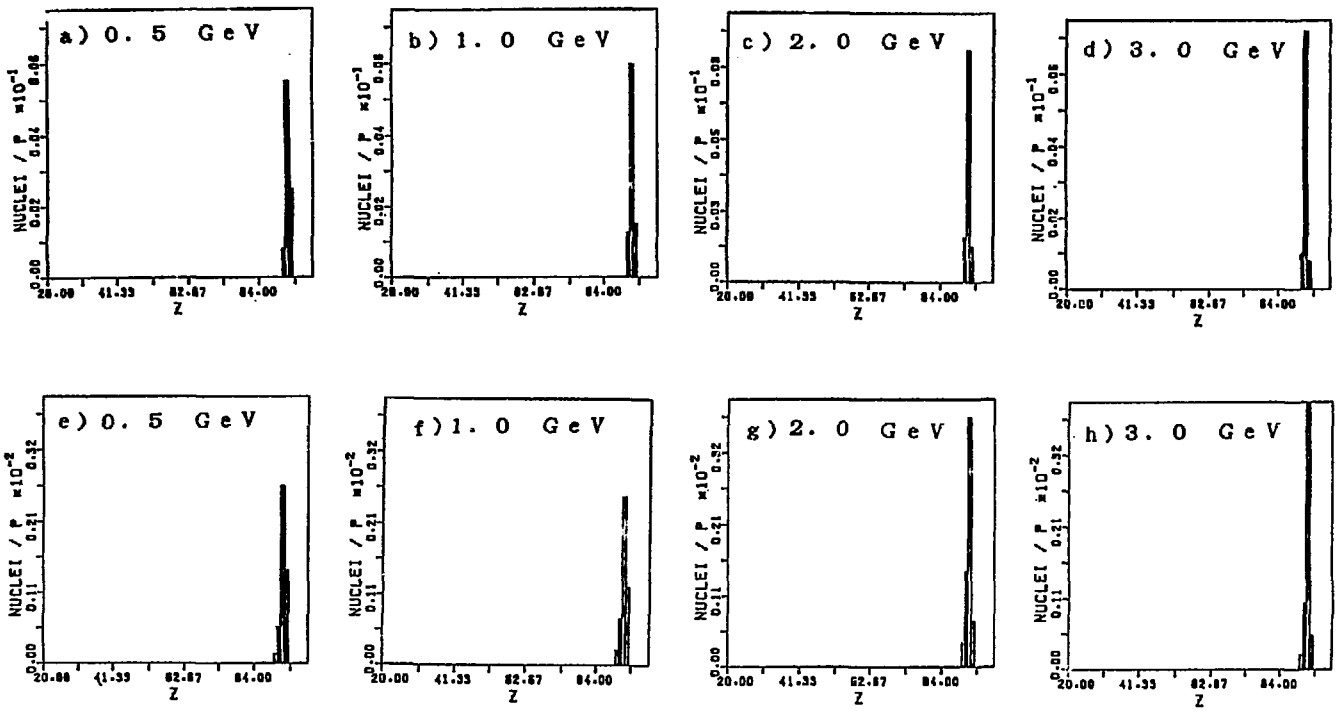

Fig. 3.4 Product yields on the β decay chain leading to ^{235}U and ^{233}U for the nuclear spallation of a Neptunium-237 nucleus

Proton energies:

(a)~(d) for ^{235}U ; (e)~(h) for ^{233}U

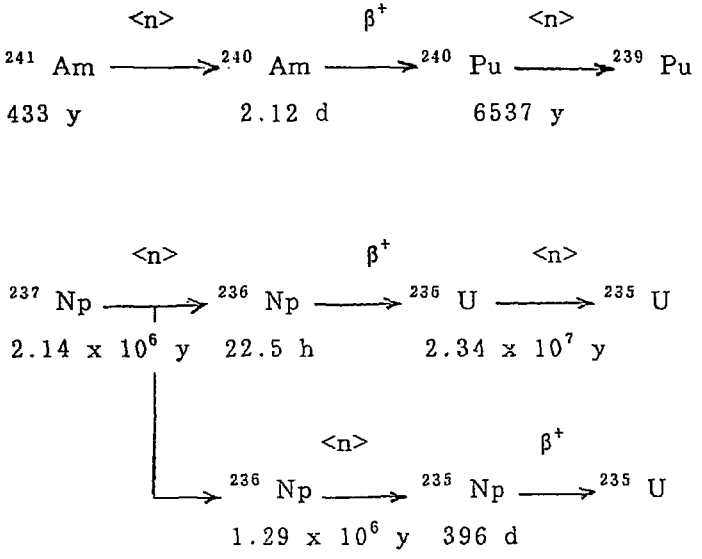

<n> : main peak in the spallation reaction

Fig. 3.5 Reaction chain leading to fissile production from TRU due to the suitable combination of neutron emissions and β^+ decays

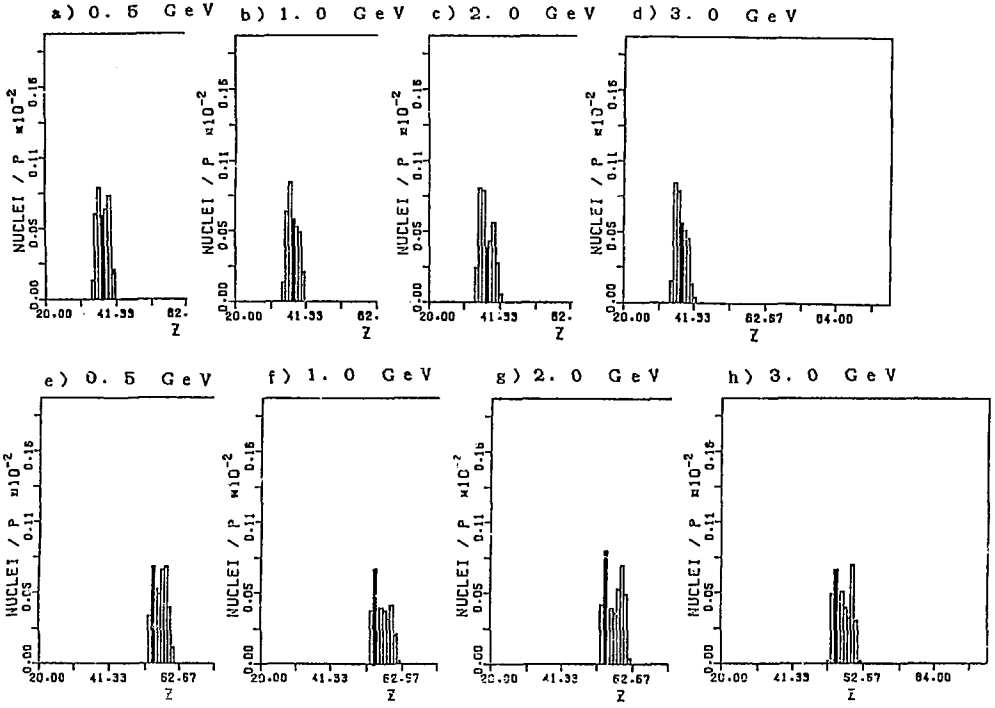

Fig. 3.6 Product yields on the β decay chain leading to ^{90}Sr and ^{137}Cs for the nuclear spallation of a Neuptunium-237 nucleus
Proton energies:
(a)~(d) for ^{90}Sr ; (e)~(h) for ^{137}Cs

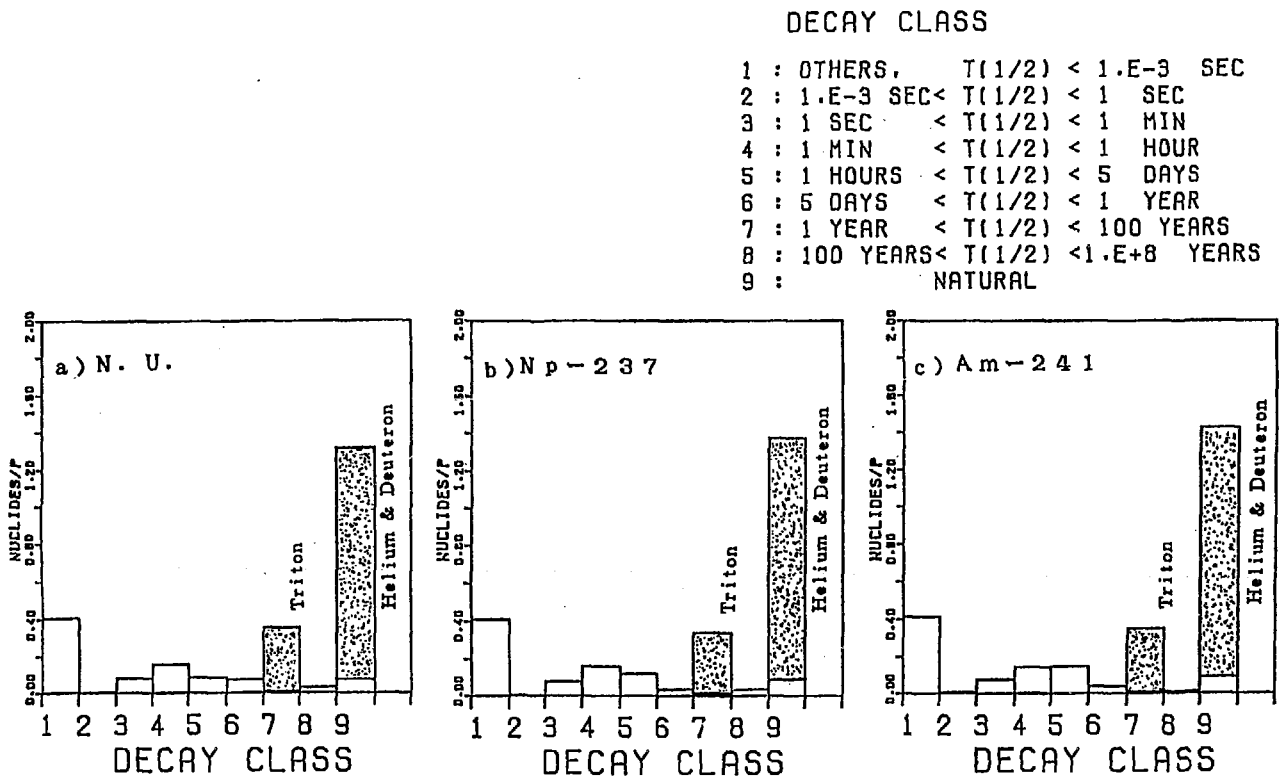

Fig. 3.7 Half-life distribution of product yields in the spallation reaction of a 2 GeV proton with a target nucleus
a) natural Uranium, b) Neptunium 237 and c) Americium 241

2.3.6 Measurement of Leakage Neutron Spectra from Various Sphere Piles with 14 MeV Neutrons

Chihiro ICHIHARA, Shu A. HAYASHI,
Katsuhei KOBAYASHI, Itsuro KIMURA

Research Reactor Institute, Kyoto University, Osaka, Japan

Junji YAMAMOTO, Akito TAKAHASHI, and Mikio IZUMI

Faculty of Engineering, Osaka University, Suita, Japan

Abstract

A series of experiment to measure neutron leakage spectra from six different piles is reported. Measured samples include silicon, chromium, manganese, cobalt, copper and niobium. The experiments were performed by using an intense 14 MeV pulse neutron facility OKTAVIAN [1] and a time-of-flight (TOF) technique in the energy range between 100 keV and 15 MeV. The piles were constructed by filling the powder in spherical shells made of stainless steel or ordinary steel.

The results were compared with theoritical calculation using one-dimensional transport codes to check the existing data files, ENDF/B-IV and/or JENDL-3T. Generally speaking, JENDL-3T data gave much preferable calculated spectrum to ENDF/B-IV ones did, while ENDF/B-IV data contains several primitive mistakes as to the inelastic-level scattering or (n,2n) cross sections of chromium, manganese, copper and niobium. For copper pile, the calculated spectrum using

JENDL-3T data gave satisfactory prediction. However, for silicon and chromium case, the calculated spectra gave overestimation provably due to the error of (n,2n) cross sections. For manganese case, the problem observed in ENDF/B-IV calculation still remained unimproved to some extent.

1 Introduction

An integral experiment is useful to check nuclear data files and calculation methods. We have measured the angular neutron fluxes in various sphere piles by using a time-of-flight(TOF) technique and photoneutrons from the electron linear accelerator at the Research Reactor Institute, Kyoto University and to verify the cross section data for fast reactor candidate materials [2] to [11]. The results were analyzed using one-dimensional discrete ordinates transport codes, mainly ANISN and several multi-group constant derived from either JENDL-2 or ENDF/B-IV nuclear data.

The present experiment was intended to extend the information about various nuclear data files to higher energy region. The part of the present experiment has been also performed as the integral bench mark test for the JENDL-3T data file which is the test version of the JENDL-3 data file being prepared.

2 Experiment

2.1 Sample Piles

Sample piles were formed as sphere so as to make it easy to compare with one-dimensional calculations. The samples include silicon, chromium, manganese, cobalt, copper and niobium. Those sample elements were packed into spherical shells made of stainless steel or normal steel. Table-1 shows the list of the measured sample piles, where atomic weight, pile diameter, sample thickness (in unit of cm and in mean free paths for 14 MeV neutrons), packing density and atomic density of each pile are given. The geometries of the piles are given in Fig.1.

2.2 Experimental Arrangement

The experiment have been performed with a TOF technique at the intense 14 MeV neutron source facility OKTAVIAN at Osaka University. The experimental arrangement in the OKTAVIAN facility is shown in Fig.2. The energy of the incident deuterons was about 250 keV. A tritium target of the OKTAVIAN was set at the center of each pile.

An NE-213 cylindrical liquid scintillator (5 in-diam × 2 in-long) was used as a neutron detector. The detector was located at the angle of 55 with respect to the incident deuteron beam. Neutron flight path was about 10.5 m from the center of the pile to the surface of the detector. A pre-collimator system made of polyethylene-iron multi layers was set between the pile and the detector to reduce the neutron background. The aperture size of this collimator is variable and was determined so that the whole surface of the piles facing to the detector could be viewed.

2.3 Data Processing

The detector efficiency was determined by combining the theoritical calculation by using the O5S code and the relative efficiency derived from TOF measurements of well-known ^{252}Cf spontaneous fission spectrum and the neutron leakage spectrum from a graphite sphere.

Several sort of the activation foils (aluminum, niobium and zirconium) were irradiated to monitor the source neutron strength between the measurements. By using this monitor value, the absolute neutron energy spectra can be measured with the method stated in [12].

3 Calculations

The calculation was performed by using one-dimensional transport codes, ANISN [13] and NITRAN [14]. The NITRAN code treats anisotropies of inelastic scatterings with the P_i-method and utilizes DDX(double differential cross section) type scattering kernel.

Nuclear data library used were JENDL-3T and ENDF/B-IV and ENDF/B-V. For the ANISN calculation, 135-group neutron cross section sets (P5S16) processed from ENDF/B-IV file with NJOY code were used. A 125-group

constant sets, FSX125/J3T-1 (P5S16) [15] produced from JENDL-3T file were also used for the ANISN calculation. For the NITRAN calculation, DDX type group constants with 135-group energy structure and 19 angular meshes were derived from ENDF/B-IV.

4 Results and concluding remarks

The measured leakage spectra are shown in Figs.3 to 8 together with the calculated ones and the comparisons between calculation and experiment. The calculation for silicon, chromium, manganese and copper includes the results from both ENDF/B-IV and JENDL-3T nuclear data. As JENDL-3T does not include cobalt and niobium data, only ENDF/B-IV calculation are given for these two piles.

4.1 Silicon

Fig.3 shows the experimental and calculated leakage spectrum from the silicon pile. Both calculations show pretty large discrepancies for almost whole energy region, especially for energy region 0.2 MeV$< E_n <$2 MeV. This implies existing two nuclear data have problems as to the cross section data of (n,2n) reaction and/or continuum-level reactions. The difference between ENDF/B-IV and JENDL-3T data files are small.

4.2 Chromium

Quite different result from the experiment was obtained by the calculation using ENDF/B-IV data (Fig.4). This problem is consistent with the differential measurement [16] carried out by Takahashi et al.. They showed that the DDX derived from ENDF/B-IV data gave quite different value for the energy region between 7 MeV and 12 MeV, which meant an existence of serious problems as to inelastic-level scattering cross section of chromium [16]. JENDL-3T dat give much better calculation as to this problem. However, for the energy region 0.2 MeV$< E_n <$2 MeV, both data file give overestimation to the experiment similar to the silicon result.

4.3 Manganese

The ENDF/B–IV prediction gives quite different spectrum for energy region 1 MeV< E_n <14 MeV (Fig.5). This is consistent with DDX measurement by Takahashi et al. [16]. The JENDL–3T data seems to have been much improved, but there still exists some problems as to the inelastic-level scattering cross sections.

4.4 Cobalt

The calculated spectrum shows some amount of underestimation of the experiment almost uniformly (Fig.6). The cause of this underestimation is not clear from present analysis.

4.5 Copper

The ENDF/B–IV calculation considerably underestimates the spectrum around 10 MeV (Fig.7). However, other part of the calculation seems fair. The calculation using JENDL–3T data predicts the experiment pretty well. It can be concluded that JENDL–3T data are satisfactory.

4.6 Niobium

Though the calculation using ENDF/B–IV data predicts well the elastic scattering peak, the shape of the spectrum under 10 MeV differs from the experiment (Fig.8). As the (n,2n) reaction is dominant in this case, there should be some problem as to this reaction either in excitation function or energy distribution of the secondary neutrons. Similar behavior was obtained in [16] by Takahashi et al..

5 — Acknowledgement —

Part of this work has been suported by a Grant-in-Aid for Scientific Research of the Ministry of Education, Science and Culture, Japan, and undertaken with in the framework of the co-operative research program of OKTAVIAN facility.

References

[1] SUMITA, K., et al.: *Proc. 12-th Fusion Technol.*, 1, 687(1982).

[2] KIMURA, I., et al.: *NBS Sp. Publ.* 425, Vol. 1, 184(1977).

[3] KIMURA, I., et al.: *J. Nucl. Sci. Technol.*, 15[3], 183(1978).

[4] KIMURA, I., et al.: *Proc. Conf. of Nuclear Cross Sections for Technology*, NBS Sp. 598, p.265(1980).

[5] KIMURA, I., et al.: *Nuclear Data for Science and Technology*, p.98(1983), D. Reide Publ.

[6] MORI, T., et al.: *J. Nucl. Sci. Technol.*, 19[6], 427(1982).

[7] MORI, T., et al.: *ibid.*, 20[12], 991(1983).

[8] SELVI, S., et al.: *Atomkernenerg. -Kerntech.*, 45[3], 183(1985).

[9] MORI, T., et al.: *J. Nucl. Sci. Technol.*, 22[9], 708(1986).

[10] HAYASHI, S. A., et al.: *Ann. Nucl. Energy*, 13[3], 131(1986).

[11] HAYASHI, S. A., et al.: *J. Nucl. Sci. Technol.*, 24[9], 702(1987).

[12] TAKAHASHI, A., et al.: *OKTAVIAN Report*, C-83-02(1983).

[13] ENGLE, W. W. Jr.: *K*-1693, (1967).

[14] TAKAHASHI, A.,RUSCH D.: *KfK*-2822/1, (1979).

[15] KOSAKO, K., et al.: *JAERI-M* (in preparation).

[16] TAKAHASHI, A., et al.: *OKTAVIAN Report*, A-83-01(1983).

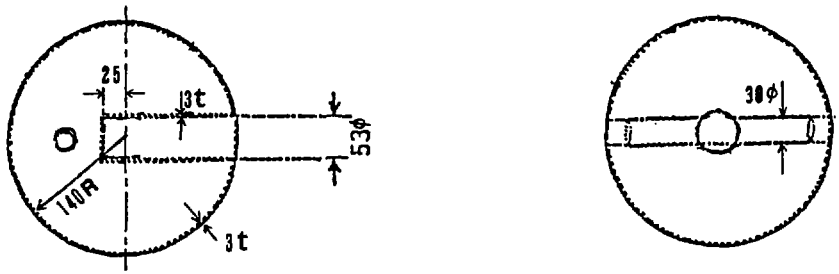

(a) 28 cm diameter sphere for use with niobium pile.

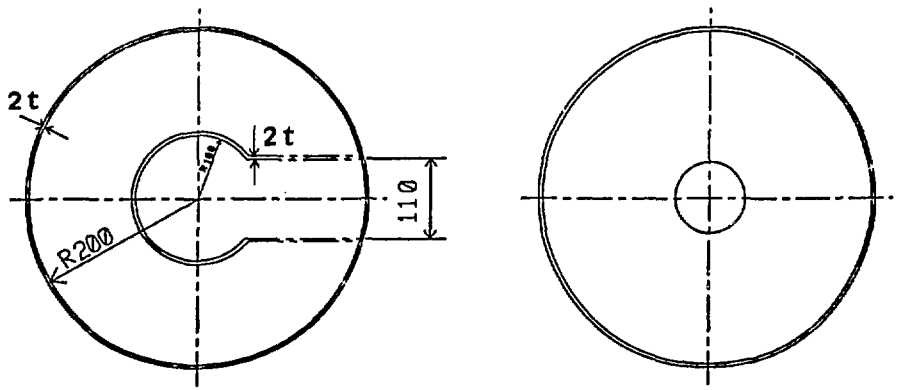

(b) 40 cm diameter sphere for use with chromium and cobalt pile.

Fig.1 The geometries of the sample piles.

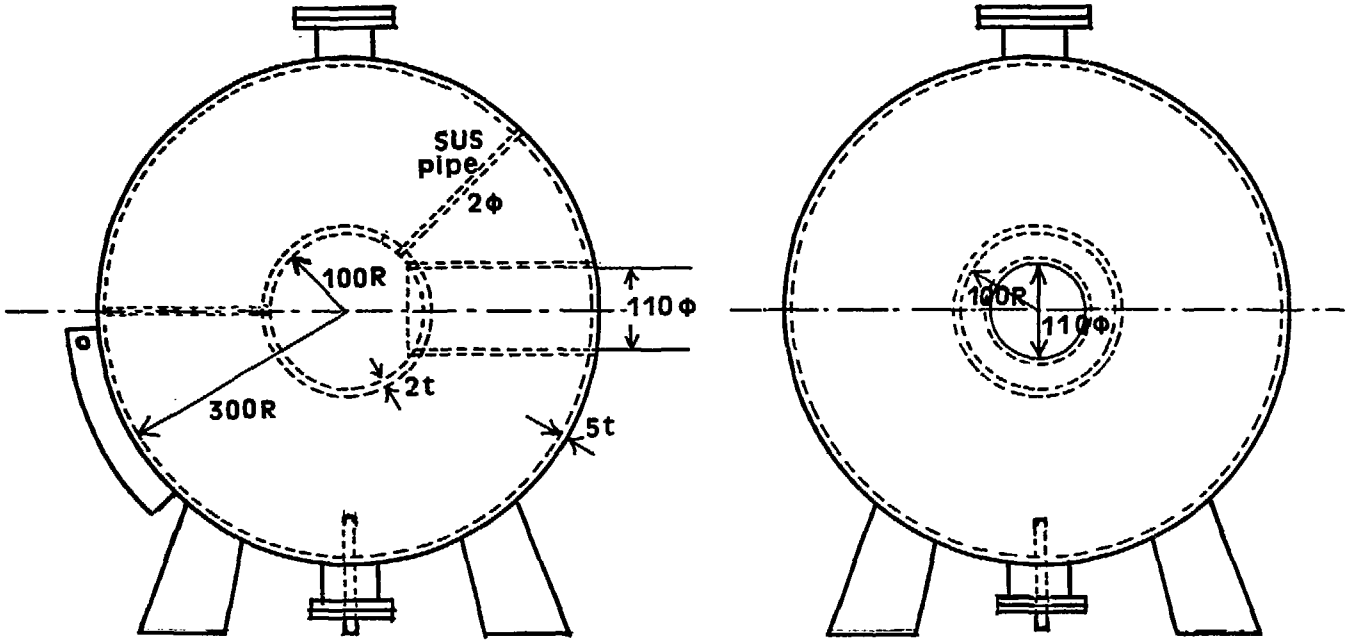

(c) 60 cm diameter sphere for use with silicon pile.

Fig. 1 (continued)

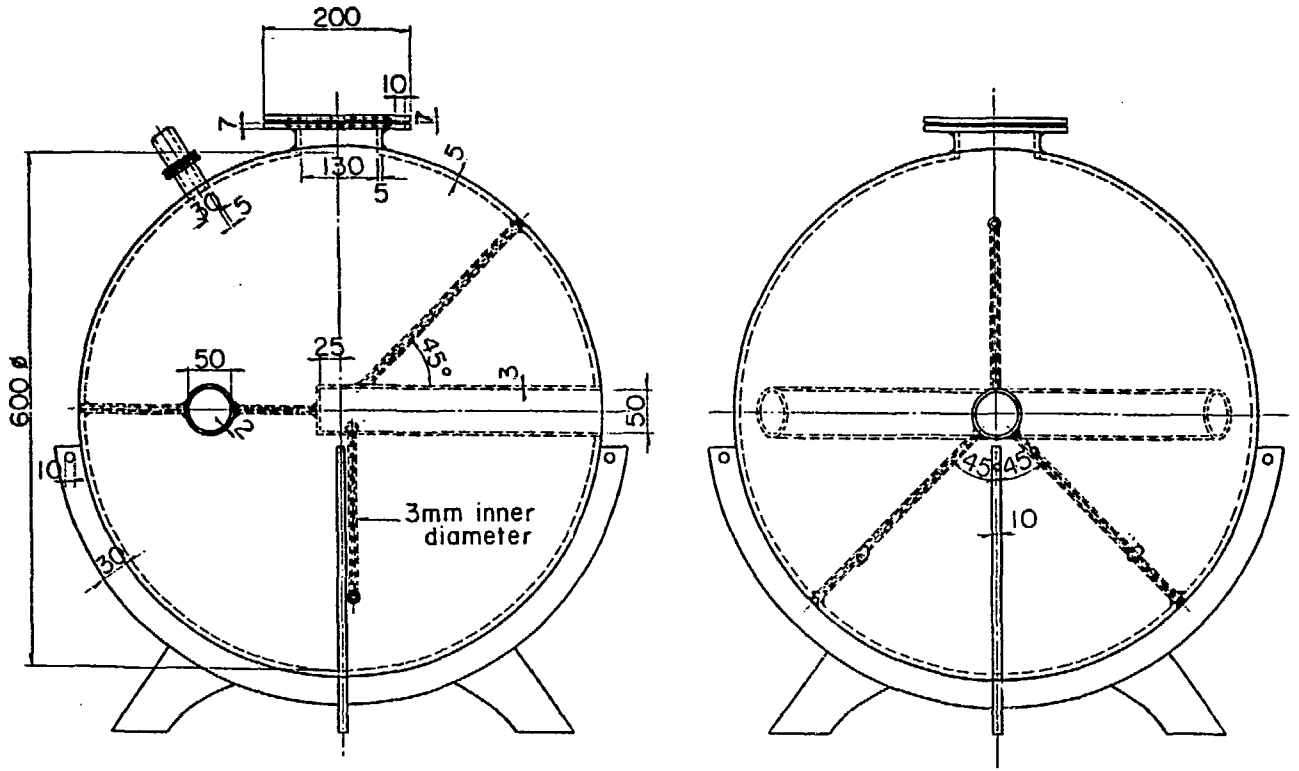

(d) 60 cm diameter sphere for use with manganese and copper pile.

Fig. 1 (continued)

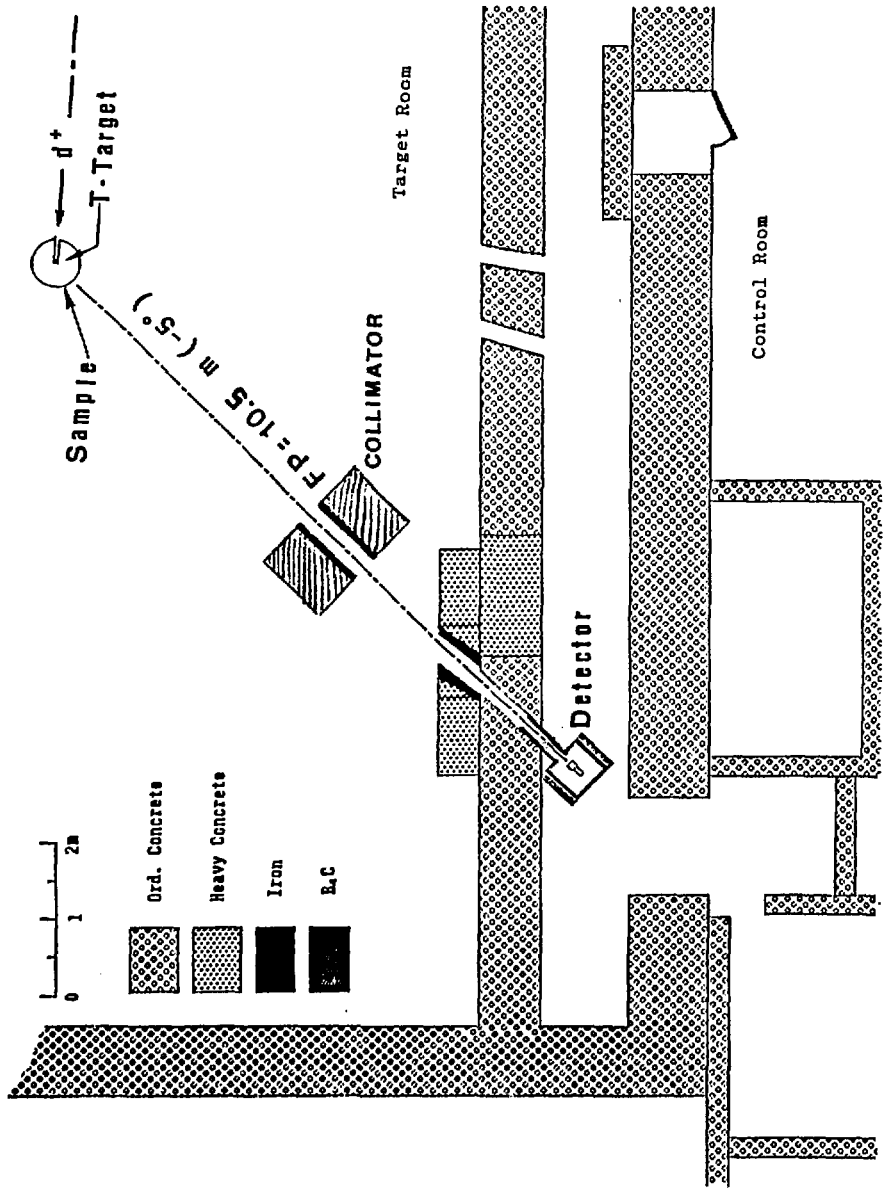

Fig.2 Experimental arrangement in OKTAVIAN facility.

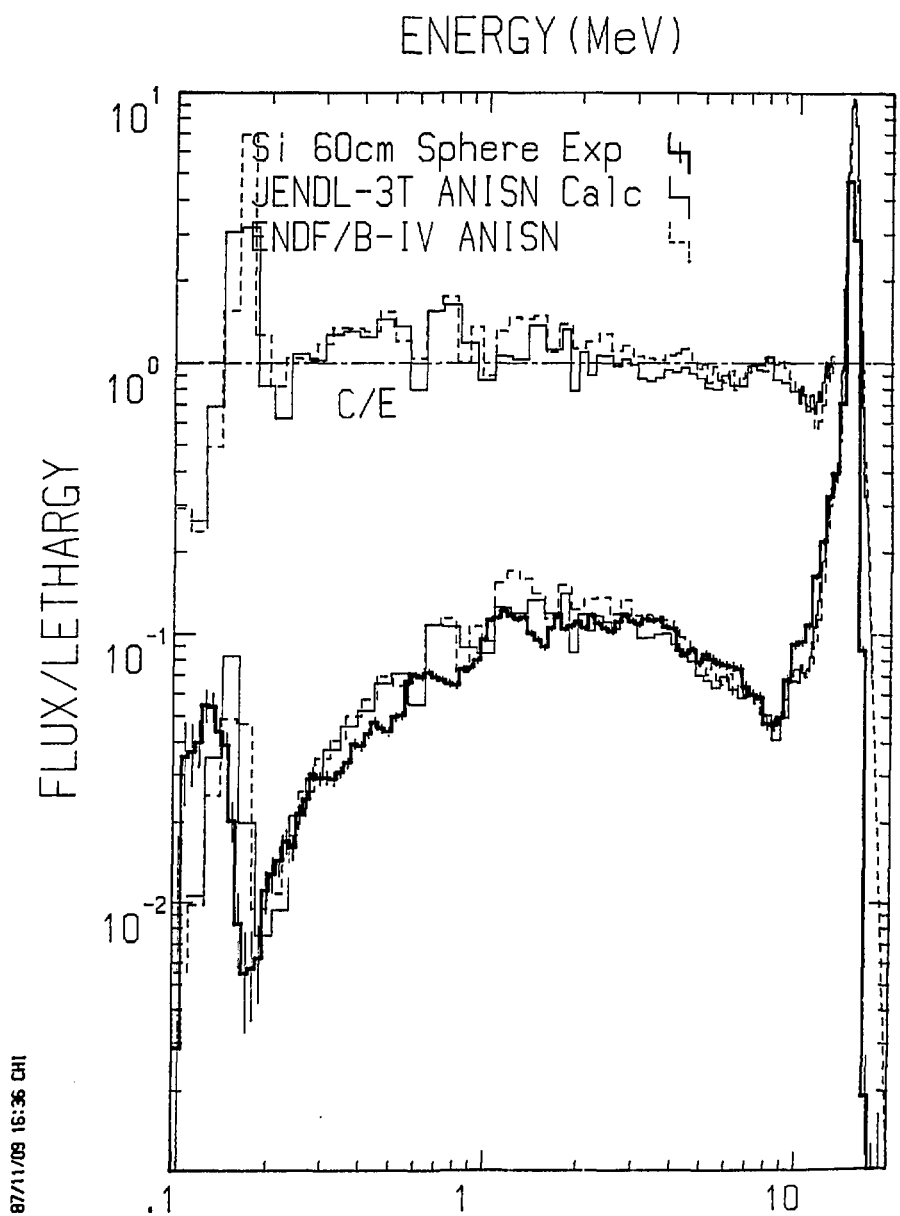

Fig.3 Experimental and calculated spectra from silicon pile calculated with ANISN-ENDF/B-IV and JENDL-3T.

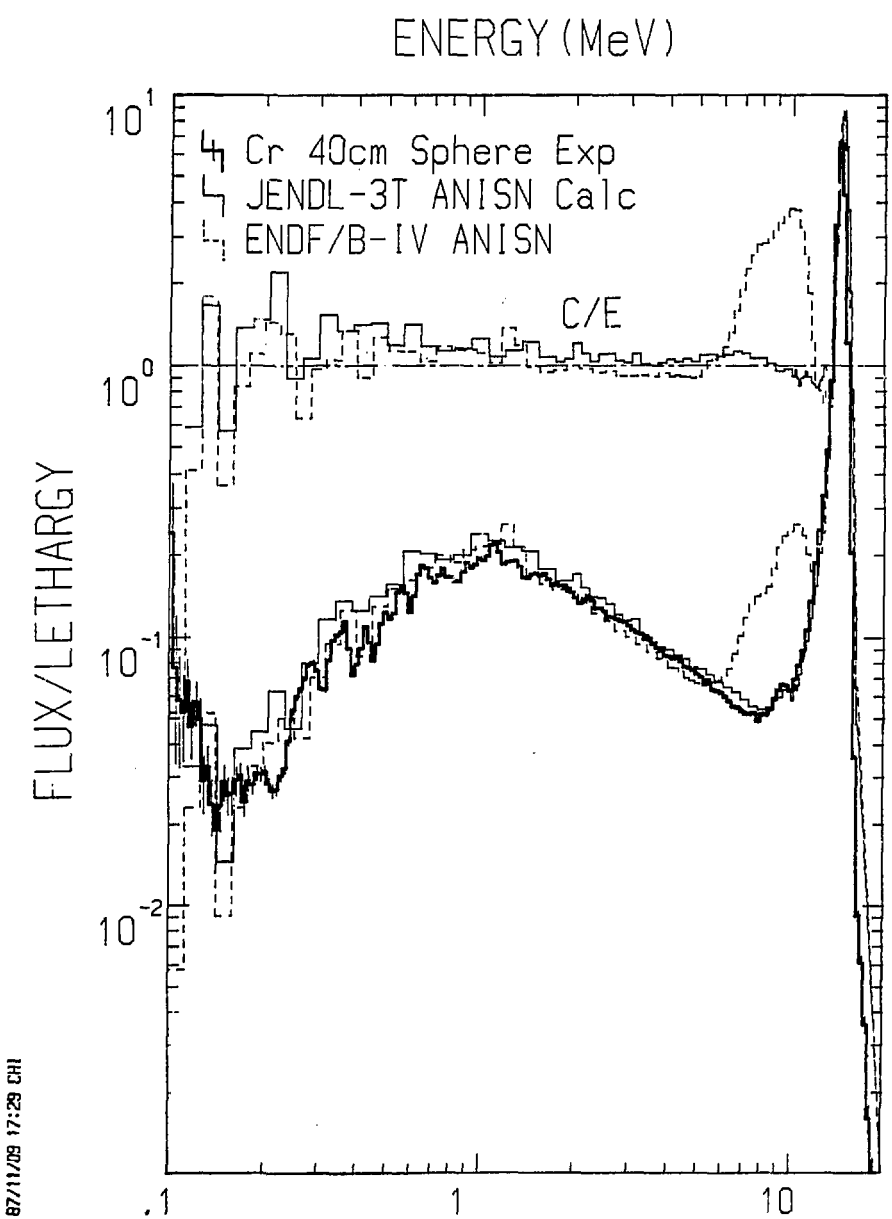

Fig.4 Experimental and calculated spectra from chromium pile calculated with ANISN-ENDF/B-IV and JENDL-3T.

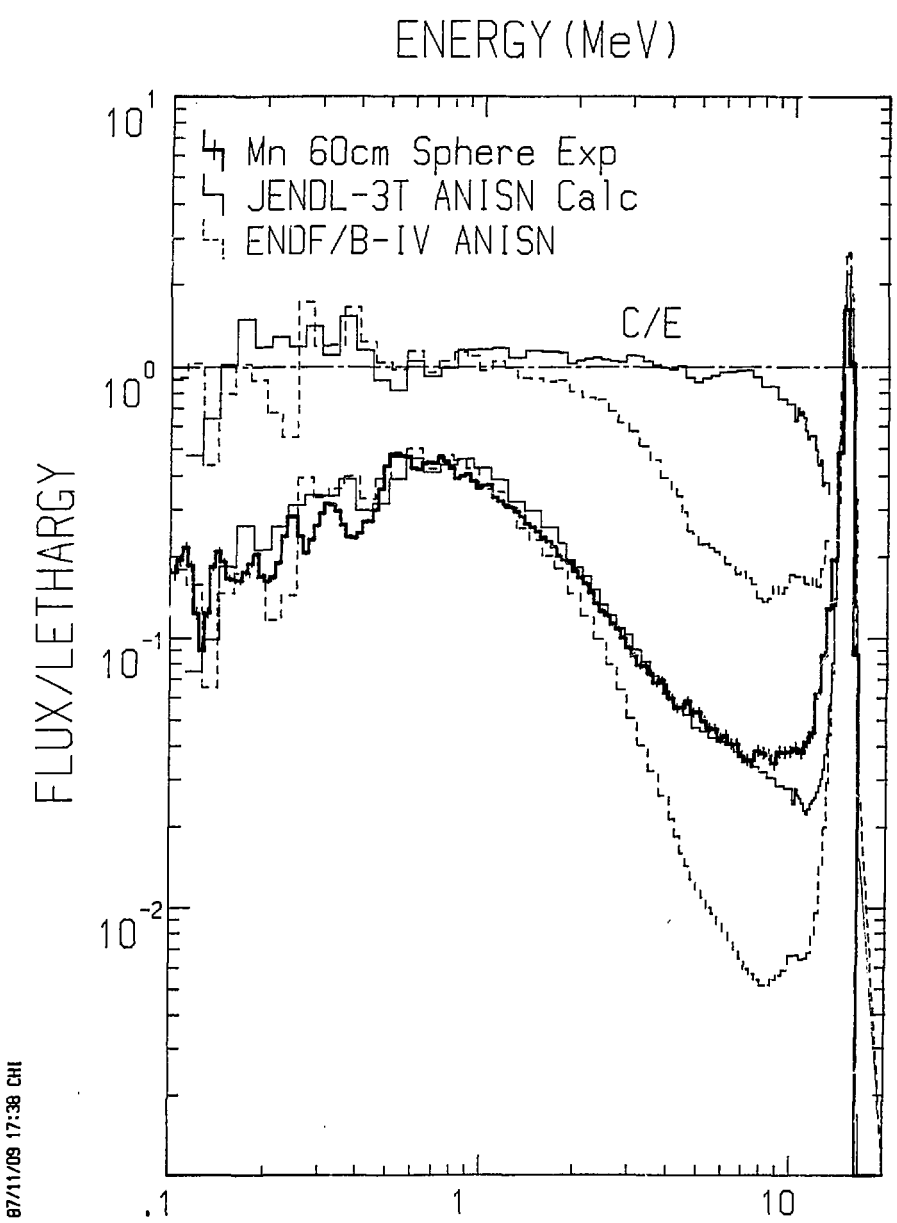

Fig.5 Experimental and calculated spectra from manganese pile calculated with ANISN-ENDF/B-IV and JENDL-3T.

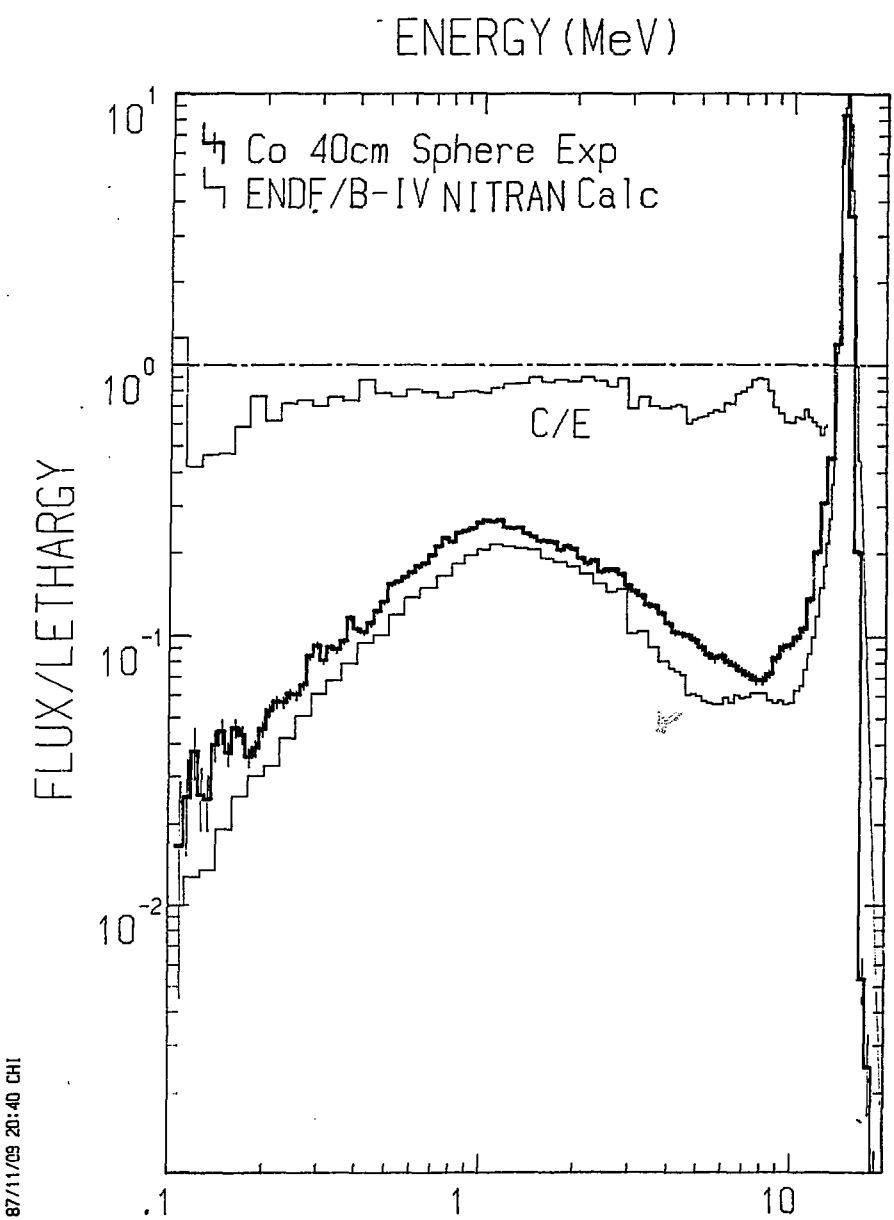

Fig.6 Experimental and calculated spectra from cobalt Pile calculated with NITRAN-ENDF/B-IV.

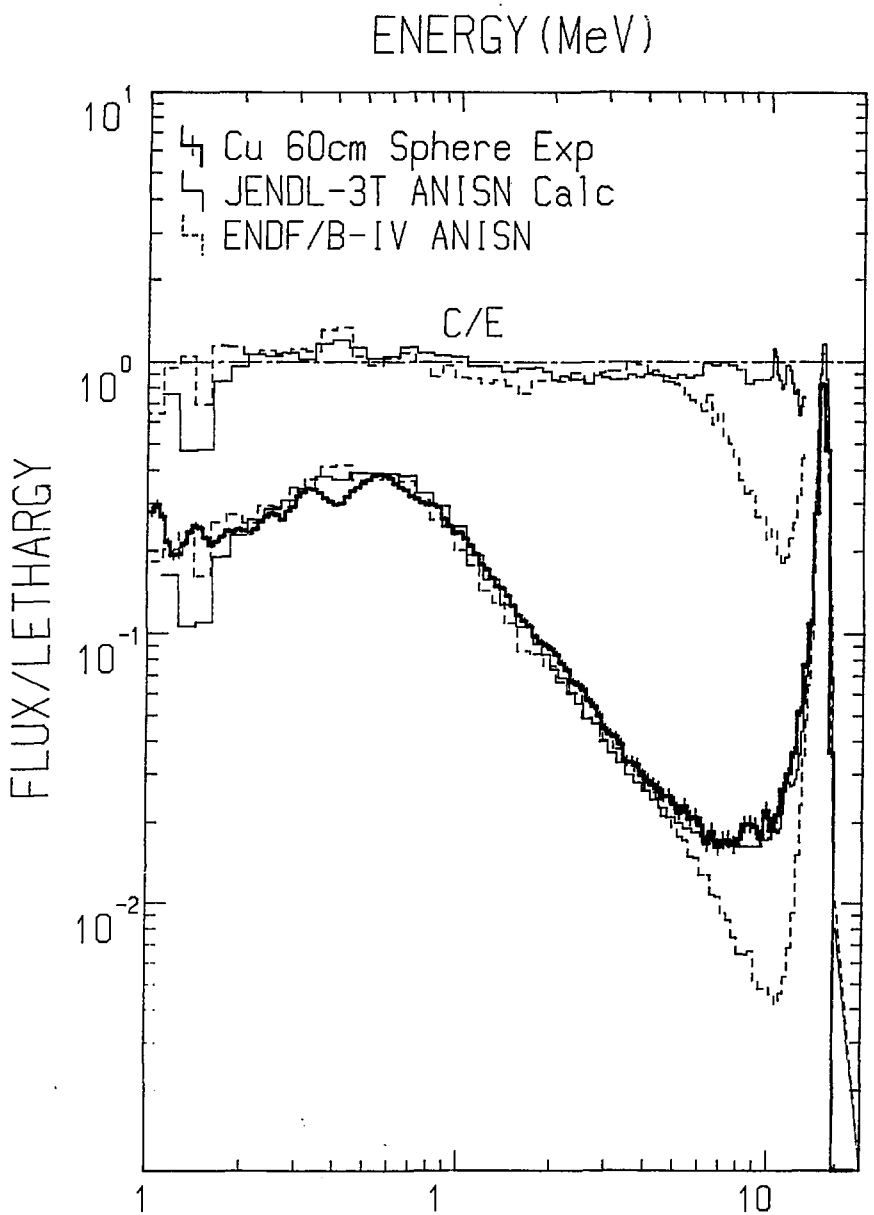

Fig.7 Experimental and calculated spectra from copper Pile calculated with ANISN-ENDF/B-IV and JENDL-3T.

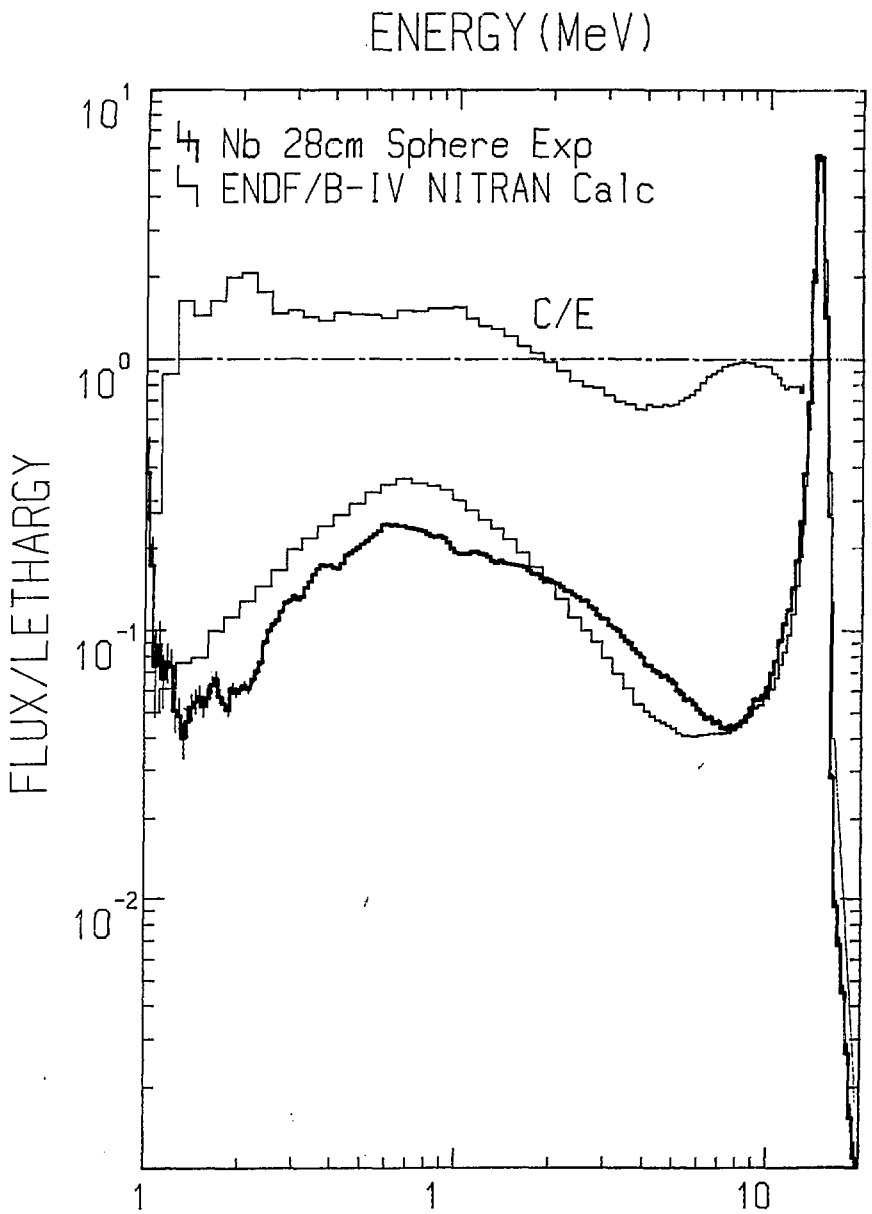

Fig.8 Experimental and calculated spectra from niobium Pile calculated with NITRAN-ENDF/B-IV.

2.3.7 Angle-integrated Neutron Emission Spectra at 14 MeV for Be, C, F, Mg, Al, Si, V, Fe, Cr, Cu, Pb and Bi

Akito Takahashi, Yasuhiro Sasaki and Hisashi Sugimoto
Department of Nuclear Engineering, Osaka University
Yamadaoka 2-1, Suita, Osaka 565, Japan

Using measured double differential neutron emission cross sections at 14.1 MeV for 15 to 16 angle-points, angle-integrated neutron emission spectra in the center-of-mass system were deduced for Be, C, F, Mg, Al, Si, V, Fe, Cr, Cu, Pb and Bi. These angle-integrated data are useful to assess partial emission cross sections of elastic, discrete inelastic, continuum inelastic scattering and other reaction channels like (n,2n) given in evaluated nuclear data libraries, e. g., JENDL-3 and ENDF/B-IV. Through comparison between experimental and evaluated emission data, status of JENDL-3T or ENDF/B-IV at 14 MeV has been made clear in this report. Significant improvement has been made by JENDL-3T for most elements except Be and Pb. For Be and Pb, further investigation is needed to improve JENDL-3T. Generally, improvement is needed to reproduce the forward-enhancement of neutron emission in double differential data.

1. Introduction

Differential neutron emission cross sections for the incident neutron energy region of 10 to 15 MeV are important nuclear data of current interest in fusion neutronics application[1], since the neutron transport phenomenon in a D-T fusion reactor becomes very transient in forming spatial, angular and energy distribution of neutrons, and many threshold reactions of interest take place in competition in the energy region of several MeV to 15 MeV. In last years (1980-1987), double differential neutron emission cross sections have been measured in several laboratories [2, 3, 4, 5, 6] for many elements of fusion reactor materials, and been utilized for assessing evaluated nuclear data, e. g., ENDF/B-IV and JENDL-2, and newly evaluating updated nuclear data libraries, i. e., JENDL-3, ENDF/B-VI and EFF-1. Accumulation of accurate data of differential neutron emission cross sections are required still for many elements.

In Japan, the new evaluation of JENDL-3 is about to be finished in March 1988 and a temporary file JENDL-3T[7] *) has been provided to limited members in Japan for preliminary test. During the JENDL-3 evaluation work, latest (hottest) data of double differential neutron emission cross sections (DDX), which have been measured at Osaka[8] and Tohoku[9] Universities, have been provided by private communications. At the OKTAVIAN facility of Osaka University, DDX data at En = 14.1 MeV (fixed incident energy) have been measured[8, 10] with high energy resolution and good counting statistics comparable to the previous ring geometry experiments[6, 11].

To test the JENDL-3T data, DDX data at each scattering angle can be compared between experiment and calculation with JENDL-3T, directly. However, it introduces a lot of figures to be compared. To see an overall trend, comparison of angle-integrated neutron emission spectra is simpler and useful, and afterwards we can discuss on a trend of angular dependence using only typical DDX data at forward and backward angles. In this way, a comparison and discussion is made in this report to assess JENDL-3T from the view point of neutron emission spectrum. To make contrast with JENDL-3T, comparison with ENDF/B-IV[12] is parallelly done.

In this report, angle-integrated neutron emission spectra and some of DDX data for En = 14.1 MeV are shown for neutron multiplier elements (Be, Pb and Bi), breeder elements in chemical compounds (F, Al and Si) and first wall - structure elements (C, Mg, Al, V, Fe, Cr and Cu).

Since the experimental method is written elsewhere briefly[13, 14] and in detail[10] and the data processing method of DDX from evaluated nuclear data libraries is also given elsewhere in detail[15, 16], only short explanations are given in the following and major part of the report is shared for comparison and discussion of neutron emission spectra for 12 elements. Comparison and discussion will be done using, mostly, angle-integrated neutron emission spectra in the center-of-mass system (CMS), since the secondary neutron energy in the CMS can directly correspond to excitation energy of inelastic scattering, if at all, and we can make direct assessment of partial cross sections for many excited states which are given in JENDL-3T. For F, Mg and V, comparison are shown only for ENDF/B-IV, since

*) JENDL-3T is a temporary file for testing the evaluated data which are for JENDL-3. The data in JENDL-3T will be partly revised in JENDL-3.

no data are available in JENDL-3T for these elements in time of the present work. For Bi, data are not given in both of ENDF/B-IV and JENDL-3T, and comparison is done only with ENDL86 and a trial calculation with GNASH86.

2. Neutron Emission Spectra by Experiment

2.1 Measurement of DDX[10]

The experimental arrangement is shown in Fig.1. An 8.3 m long time-of-flight facility was constructed in an 85° direction against the Pulse Beam Line[6] of OKTAVIAN. A cylindrical scattering sample of 3 cm in diameter and 5-7 cm in length was used. As a neutron detector at 8.3 m point of flight path, an NE213 liquid scintillator of 25.4 cm in diameter and 10 cm in thichness was prepared. To discriminate γ-ray background, two parallel pulse shape discrimination circuits were set and a relatively wide dynamic range (0.5 to 15 MeV or 0.3 to 15 MeV) could be covered by setting gain ratio of the two circuits to be 1/10. Incident neutron energy can be almost fixed to 14.1 MeV, by moving a sample along an arc drawn in the insert of Fig.1 to change scattering angle. Pulsed neutron source by D-T reaction was operated with 2 ns pulse width and 1 MHz repetition. Time-dependent background was measured by removing a sample. Overall energy resolution of the present TOF system is ± 0.2 MeV.

Double differential cross sections were measured for 15-16 angle-points from 15° to 160° with 10° interval, for each element. For multiple scattering correction, a computer code MUSCC3[10] which is based on a multipoint collision probability method is used. For the correction by MUSCC3, DDX-type data set processed from JENDL-3T or ENDF/B-IV was used. Correction for the parasitic low energy neutrons of incident neutron spectrum is included in MUSCC3, together with the multiple scattering correction for a 1.5 cm diam. 5 cm long polyethylene cylinder which was used for determination of absolute DDX values and calibration of the neutron detector efficiency. To show quality of the present experiment, comparison of DDX data for carbon with other experiments, by Baba[3] and Drosg[2], is shown in Fig.2. Energy resolution of the present experiment is the best of three experiments. Except difference in energy resolution, agreement between experiments is good as a whole. However, in the lower energy region than about 6 MeV, both of Baba's and Drosg's data are higher

than the present result, presumably due to their neglection of the correction for the parasitic low energy neutrons which would be contained in incident neutron spectra.

2.2 Angle-integrated neutron emission spectra

Angle-integrated neutron emission spectrum in the LAB system (EDX-in-LAB) can be deduced by directly integrating DDX data over scattering angles in the LAB system. For integration, a fitting code to the Legendre polynomials was used and the P_0 term is an integrated value. An example is shown in Fig.3 for carbon. The Legendre fitting some times causes a problem in the higher energy tail of elastic scattering peak, for some elements, since data values are zero for backward angles in the LAB system, as seen in figures of Ref.8.

To obtain angle-integrated neutron emission spectrum in the center-of-mass system (EDX-in-CMS), conversion of DDX data from the LAB system to the CM system was carried out, by supposing the kinematics of inelastic scattering to be valid for pseudo-excitation levels which were defined by discretizing the secondary energy region of 0.0-14 MeV with 0.2 MeV interval. An example is shown in Fig.4, which shows the conversion is reasonable. Note that EDX-in-CMS is deduced by integrating DDX-in-CMS over scattering angles in the CM system using the Legendre polynomial fitting, which does not cause a problem at elastic peak because the secondary energy is fixed in the CM system. It was checked by comparing with a total neutron emission cross section, which is obtained by direct double integration of DDX over angle and energy in the LAB system, that the LAB to CMS conversion causes 1-2 % error in total neutron emission cross section. However, this error is well within experimental error of total neutron emission cross section.

The Legendre fitting for integrating DDX-in-CMS is successful, since the outgoing energy with a specified excitation is fixed as expressed by the following equation,

$$E_{n'cms} = E_n/(1 + 1/A)^2 - Q_i/(1 + 1/A) \qquad (1)$$

where $E_{n'cms}$ is the outgoing neutron energy in the CM system, E_n the incident neutron energy (14.1 MeV), Q_i the discretized excitation energy and A the relative mass of target nucleus, respectively.

Some of resolved peaks in EDX-in-CMS can correspond to elastic scatt-

ering and low-lying states of discrete inelastic scattering, as shown typically in Fig.4. Since the secondary neutron energy in the CM system can correspond to excitation energy through Eq.(1), EDX-in-CMS can be used to compare experimental and evaluated neutron emission cross sections to particular excited states. Thus it will become clear in the comparison of EDX-in-CMS whether the evaluation of partial cross section to particular reaction channel is underestimated, satisfactory or overestimated.

Numerical data tables of DDX and EDX are given elsewhere for elements except Fe and Bi[8].

3. DDX and EDX from JENDL-3T and ENDF/B-IV

To produce groupe-wise DDX data from JENDL-3T and ENDF/B-IV, a processing code DDXS[15, 16] was used. Group-wise DDX data with 64 angle points and 135 energy groups were generated and stored on a computer permanent-file. For elastic and discrete inelastic scattering, DDX data are generated using angular differential cross sections and their scattering kinematics. For continuum neutron emission, i. e., inelastic continuum, (n,2n), etc., isotropic emission in the LAB system was assumed unless angular distribution data were given in the evaluated nuclear data files. In case that angular distribution data were given, DDX data were calculated using product of energy distribution and angular distribution data. Therefore, the energy-angle correlation was not taken into account. (In JENDL-3T, File-6 data, i. e., DDX-type data are not given.)

To obtain angle-integrated neutron emission spectra, DDX data in the LAB system which are stored in a computer file are directly integrated to get emission spectra in the LAB system. To deduce EDX-in-CMS, DDX data in the LAB system are converted once to DDX-in-CMS using the scattering kinematics of inelastic scattering for pseudo-discrete states, in the same way with the conversion for experimental data, and integration of DDX-in-CMS is done over scattering angles in the CM system.

To compare experimental data with either DDX or EDX by calculation, a spectrum-broadening technique with the Gaussian resolution function was used for calculated data. To realize close resolution function to experimental one, a broadened DDX spectrum of calculation, with use made of the experimentally given resolution ($\pm$ 0.2 MeV), was displayed once on a computer graphics to be compared with an experimental DDX at same angle,

and for the next trial a small change was given to the resolution, if necessary. Usually, a very close resolution or broadening to an experimental one was attained by the second trial.

4. Results and Discussions

4.1 Beryllium

In Fig.5 are shown angle-integrated emission spectra in the CM system. Discrete excited states of ^{9}Be, i. e., 2.429, 4.7, 6.8 and 7.9 MeV states by inelastic scattering are indicated in the figure. The excitation of 1.65 MeV state has not been observed in experimental spectra[11].

JENDL-3T shows a significant improvement, but not sufficient enough as discussed later, in the low energy region of 0-5 MeV, where ENDF/B-IV draws quite a different curve from the experiment. In the higher energy region of 5-11 MeV, JENDL-3T gives significant overestimation at discrete peaks, and on the contarary it gives distinct underestimation between the peaks. It has been pointed out[17, 18] that the reaction model of time-sequential neutron emission for the first and second neutrons of ^{9}Be(n,2n), adopted in JENDL-3T and ENDF/B-IV, can not produce the experimental shape of spectrum. By taking account of the processes of simultaneous direct break-up to four (2n + 2α) and three (n + α + ^{5}He) bodies, the experimental spectral shape and angular dependence can first be explained[17, 18]. In Fig.6 is shown the result of a Monte Carlo simulation calculation of the simultaneous multi-body break-ups, compared with the experiment in the LAB system. The simulation agrees very well with the experiment.

By integrating EDX-in-CMS of ^{9}Be over secondary neutron energy region except the 10-13 MeV region where we have an elastic scattering peak, we can obtain total neutron emission cross section of ^{9}Be(n,2n) and half of that value becomes (n,2n) cross section that is important value to use beryllium as a multiplier of fusion reactor blanket. In Table-1 is shown the ^{9}Be(n,2n) cross section of this experiment, compared with evaluated cross sections and our previous estimation[25]. The ENDL86 evaluation[23] gives a very close value to the present experiment, while the JENDL-3T evaluation gives 13 % higher value than the experimental one. This overestimation by JENDL-3T comes from a significant overestimation of differential (n,2n) cross sections in backward angles, as shown in Fig.7, although

it gives good agreement in forward angles. This fact is commonly seen in the comparison of DDX, as shown in Figs.8-a and b. It is notified that no discrete inelastic scattering peaks, except that of the 2.43 MeV state, are observed in backward angles.

4.2 Carbon

Comparison of angle-integrated neutron emission spectra in the CM system is shown in Fig.4. Agreement between the present experiment and JENDL-3T looks good in the secondary neutron energy region except the 3.5-6 MeV region. Inelastic scattering cross section for the 7.65 MeV state in JENDL-3T is too high, and the data for continuum inelastic scattering in the 3.5-6 MeV region are also overestimated. For the evaluation of the 7.65 MeV state cross section in JENDL-3T, our old data by the ring geometry [11] and the data by Tohoku University[3], both of which gave much higher cross sections than the present experiment, have been referred. Through the present experiment, however, it was found that the correction for the parasitic low energy tail of incident neutron spectra gave drastic effect on low energy side of emission spectra for light elements[10] and this correction was ignored in both of the previous experiments. As a consequence, differential emission cross sections in the region less than 6 MeV are given significantly smaller in the present experiment and also in the new result of Tohoku University[19].

Comparison of partial cross sections between the present experiment and evaluated data is reshown[10] in Table-2, for elastic, 4.44, 7.65, 9.63 MeV state inelastic scattering, continuum inelastic scattering and (n,n'3α) reaction. JENDL-3T underestimates cross sections for elastic and inelastic scattering to the 4.44 MeV state, by about 10 % for both, while overestimates cross sections for inelastic scattering to the 9.64 MeV state, continuum inelastic scattering and (n,n'3α) reaction, respectively by 12 %, 14 % and 16 %. It is therefore suggested that improvement of JENDL-3T is needed to meet the required accuracy for blanket reflector and first wall material.

4.3 Fluorine

Angle-integrated neutron emission spectrum of the present experiment is shown in Fig.9, in comparison with that of ENDF/B-IV. In the ENDF/B-IV spectrum, four peaks of inelastic scattering, i. e., 1.554, 2.780, 4.683

and 5.618 MeV states, are seen and those are corresponding to peaks in experiment. For 1.554 and 4.683 MeV states, agreement between the present experiment and ENDF/B-IV is good. However, at the 2.780 MeV state, ENDF/B-IV underestimates largely the experiment, while it overestimates at the 5.618 MeV state. In the continuum region of 0-7 MeV, the experiment gives a slightly fluctuated spectrum different from the evaporation-like spectrum of ENDF/B-IV. ENDF/B-IV overestimates the experiment in the region of 1-5 MeV. Comparison of DDX spectra[8, 10] shows a significant overestimation by ENDF/B-IV in the region of 1-7 MeV, where consideration of direct and precompound effects shall be taken into account in new evaluations.

4.4 Magnesium

Angle-integrated neutron emission spectrum of the present experiment is shown in Fig.10, compared with that of ENDF/B-IV. We can see 6 peaks of experiment which correspond to the 1.37, 4.12, 5.23, 6.00, 7.62 and 8.44 MeV states of discrete inelastic scattering, as indicated in the figure. In the whole region of secondary neutron energy, agreement between the present experiment and ENDF/B-IV is good. However, if we see the detail, ENDF/B-IV underestimates cross sections at the 1.37, 4.12, 6.00 and 7.62 MeV sates of discrete inelastic scattering, as well as in the continuum region of inelastic scattering. For elastic scattering, agreement is very good. The underestimation by ENDF/B-IV in the continuum region is mainly attributed to underestimation of DDX in forward angles[8, 10].

4.5 Aluminum

Experimental angle-integrated neutron emission spectrum is shown in Fig.11, in comparison with those of JENDL-3T and ENDF/B-IV. The JENDL-3T data reproduce the experimental emission spectrum very well for the elastic and two discrete inelastic scatterings of 2.21 and 3.00 MeV states. However, JENDL-3T largely underestimates the experiment at the 1.10, 4.64 and 5.54 states of inelastic scattering. The discrete state of 5.54 MeV is not given in JENDL-3T. In the lower energy part less than 5 MeV, JENDL-3T significantly overestimates the experiment.

Comparison of DDX data are shown in Figs.12-a and b, for 35° and 150°. At forward angle (35°), JENDL-3T drastically underestimates the experiment in the region of 6-10 MeV and at the elastic scattering and 1.10 MeV state

peak of inelastic scattering. However, it overestimates significantly the experiment at the 3.00 MeV state of inelastic scattering and also in the low energy region of 1-5 MeV. The present experiment shows enhancement of neutron emission in forward angle even in such low energy region. Therefore, a reasonable nuclear theory should be applied to explain this forward-enhancement, presumably based on an precompound model with angular dependence.

4.6 Silicon

Experimental emission spectrum (EDX-in-CMS) is shown in Fig.13, in comparison with those of JENDL-3T and ENDF/B-IV. Agreement between the present experiment and JENDL-3T is good, while ENDF/B-IV significantly overestimates the experiment in the low energy region of 0-4 MeV. If we see the detail, JENDL-3T overestimates cross sections for the elastic and 1.779 MeV state inelastic scattering and underestimates in regions around 4 and 6 MeV of secondary neutron energy. In Figs.14-a and b are shown DDX data for 30° and 150°. At 30°, JENDL-3T underestimates the experimental spectrum, significantly in the low energy region. At backward angle (150°), agreement is however good for JENDL-3T while ENDF/B-IV overestimates in the low energy region of 0-5 MeV. The evaluation of JENDL-3T for silicon is close to be satisfactory.

4.7 Vanadium

In Fig.15 is shown experimental EDX-in-CMS compared with those of ENDF/B-IV. As a whole, distinct disagreement between the experiment and ENDF/B-IV is obvious. Especially in the region of 3-13 MeV, ENDF/B-IV drastically underestimates the experiment, since necessary treatment of direct and precompoud processes is not included yet in the ENDF/B-IV evaluation for vanadium. In the experimental spectrum, three peaks of discrete inelastic scattering, i. e., 1.8, 3.8 and 5.0 MeV states as shown in the figure, can be resolved. Inelastic scattering to excite these three states shall be treated by direct reaction theories (DWBA or coupled channel). The experimental spectral shape of 2-7 MeV can tell us the effect of precompound process is significant. A bump is seen at about 7 MeV and it may be explained by the low energy octupole resonance[20].

In the low energy region of 0-3 MeV where emission of (n,2n) neutrons is dominant, ENDF/B-IV overestimates the cross section by about 15 %.

Improvement of this cross section value is important, since vanadium-chromium alloy is candidated as a fusion first wall material.

4.8 Iron

Neutron emission spectrum of iron has been well studied, since iron ia a primarilly important element as structural material for various purposes. In Fig.16 is shown EDX-in-CMS of the present experiment, in comparison with those of JENDL-3T and ENDF/B-IV. Very good agreement is seen between the experiment and JENDL-3T for the energy regions of 0-9 MeV and 13-15 MeV. Improvement of JENDL-3T is seen in the region of 5-9 MeV. However, disagreement is obvious in the region of 9-12 MeV where neutron emission by direct inelastic scattering would be dominant. The 3.23 MeV state peak observed in the experiment is not appeared in JENDL-3T.

Three discrete excited states, i. e., the 0.81 (2+), 3.23 and 4.40 (3-) MeV states are indicated in the figure. Since an angle-integrated spectrum in the CM system can show emission cross sections at respective excitation energies, if we convert the secondary neutron energy to the excitation energy by using Eq.(1), we can assess partial cross sections for respective excited states given in JENDL-3T. In Table-3 are shown partial cross sections for various excited states, given in JENDL-3T. Partial cross sections are given for discrete states (Q-values) from 0.0144 to 4.949 MeV. By comparing this table with Fig.16, we can say the following. Cross sections for excited states from 2.075 to 4.033 MeV shall be greatly increased, by several times depending on state-energy. Numerical values of factors for increment can be obtained from ratios of the experimental[8] and evaluated angle-integrated emission spectra in the CM system. The cross section for the 4.40 MeV state in JENDL-3T should be decreased by about 50 %. After these improvements will be done, almost complete agreement will be attained.

After attaining a complete agreement in EDX-in-CMS, a problem will be left for angular dependence. In Figs.17-a, b and c are shown DDX data at 30°, 70° and 150°. In the region of 0-9 MeV where we have had an almost complete agreement between the experiment and JENDL-3T, JENDL-3T can not thoroughly reproduce the forward-enhancement of experimental emission spectra. To meet further agreement in DDX, treatment by a precompound model with angular dependence shall be considered. Forward-enhancement of discrete inelastic scattering is more in experiment than JENDL-3T.

4.9 Chromium

Situation of neutron emission spectrum for Cr in JENDL-3T is somewhat similar to that for iron. Experimental EDX-in-CMS is shown in Fig.18 in comparison with that of JENDL-3T. Calculated spectrum from ENDF/B-IV is very much different from the experimental one, as already pointed out[11].

Agreement between the experiment and JENDL-3T is relatively good. However, as a whole, JENDL-3T underestimates the experimental emission spectrum. Especially, underestimation is obvious in the region of 1-4 MeV and 10-12 MeV. In the 10-12 MeV region, emission cross sections for discrete states in JENDL-3T shall be increased as is the case of iron. In the 6-8 MeV region, we have a bump in the experimental spectrum which may be attributed to the low energy octupole resonance[20]. Underestimation of JENDL-3T in the 1-4 MeV region is attributed to significant underestimation of DDX around 90° as shown in Fig.19-b, although overestimations are obvious in both of forward and backward angles. In JENDL-3T, angular distributions in this region are given as symmetric around 90°, for continuum spectrum by precompound process. From the experiment, it is noticed that the angular dependence for the continuum part looks much milder than that of JENDL-3T and has a slight forward-enhancement of neutron emission.

4.10 Copper

Almost complete agreement is seen between the experimental and JENDL-3T emission spectra, as shown in Fig.20, while ENDF/B-IV drastically underestimates the experiment in the region of 6-12 MeV. Improvement of JENDL-3T, by treating direct and precompound processes in the 6-12 MeV region, is drastic. Slight underestimation of JENDL-3T is seen around the 3.7 and 0.962 + 1.33 MeV states. The peak appeared at the 3.7 MeV state for JENDL-3T is treated in the inelastic continuum, and therefore its discrete cross section is not given. In Figs.21-a and b, experimental DDX data of Cu are shown in comparison with those of JENDL-3T and ENDF/B-IV. The JENDL-3T data underestimate the forward-enhancement of emission spectra in the whole energy region except the elastic scattering region around 14 MeV.

4.11 Lead

Lead is one of important candidate materials for neutron multiplier

and therefore accurate neutron emission data are required. In Fig.22 are shown angle-integrated neutron emission spectra, comparing the present experiment with JENDL-3T and ENDF/B-IV. It has been pointed out[11] that ENDF/B-IV gives softer emission spectrum for (n,2n) neutrons in the region of 0-6 MeV. However, JENDL-3T gives much harder emission spectrum than both of the experiment and ENDF/B-IV. Locally, JENDL-3T significantly underestimates emission spectrum in the energy region of 0.5~2 MeV and overestimates in the region of 3-6 MeV.

Using the Q-value 6.74 MeV of Pb(n,2n) reaction, (n,2n) cross section at 14.1 MeV was deduced by integrating EDX-in-CMS within the region of 0-7.3 MeV. The result is shown in Table-4, in comparison with evaluated values in JENDL-3T, ENDF/B-IV, EFF-1[26] and ENDL86[23]. The present experiment again[21] gives about 10 % larger (n,2n) cross section than that of ENDF/B-IV. In JENDL-3T, smaller cross section, by about 15 % than the experiment, is given. This difference should be further investigated to meet agreement, because (n,2n) cross section value is most sensitive[22] to neutron multiplication factors.

In the higher energy region than 7.3 MeV, JENDL-3T significantly underestimates the experimental emission spectrum in the region of 7-10 MeV, although very good agreement is seen in the region of 10-15 MeV. Component of direct inelastic scattering should be added in the 7-10 MeV region.

The recent analysis at Dresden[5] shows a very good agreement with our experiments[11] for the Pb(n,2n) emission spectrum, as well as the case of EFF-1[26] in spectral shape. Parameters in precompound and compound calculations should be chosen to be deviated from empirical systematics, as discussed for Bi later.

As for the angular dependence of emission spectra, comparison of DDX is shown in Fig.23. Slight forward-enhancement seen in the experimental spectrum is better to be considered in theoretical analysis, by using a precompound model with angular dependence.

Accuracy of obtained Pb(n,2n) cross section by the present experiment shall be checked by comparing with other experiments and, if necessary, further refined measurement. Typical DDX data of the present experiment are compared with those of Elfurth et al.[5] in Fig.24, for 60° at which DDX spectrum in the low energy region of (n,2n) neutrons is near to the angle-integrated one. Agreement between the two experiments is very good,

considering difference in energy resolutions. In the lower energy region than 3 MeV, the present experiment agrees with that of Vonach[4].

4.12 Bismuth

In Fig.25 is shown measured angle-integrated neutron emission spectrum in comparison with that of ENDL86[23]. Disagreement is obvious in the whole energy region. Emission spectrum of Bi(n,2n) neutrons distributes in the region of 0-6.5 MeV, where ENDL-86 overestimates spectrum significantly and gives harder spectrum than the experiment. Underestimation of ENDL86 in the region of 6.5-13 MeV is due to ignoring direct inelastic scattering components, i. e., to excite the 2.68, 4.28 MeV and some higher states. As shown in Fig.26 for DDX, the ENDL86 evaluation gives good agreement at forward angles, but largely overestimates spectrum at backward angles. Experimental DDX shows significant angular dependence, i. e., forward-enhancement of emission for Bi(n,2n) neutrons.

To obtain good agreement between the experimental emission spectrum and calculated one, a trial calculation with GNASH86[23] was made and the result is shown together in Fig.25. Used parameters of level density and precompound process are shown in Table-5. Usually, the a-parameter for level density is chosen to be from A/6 to A/7, where A is the relative mass of target nucleus. In the present calculation, the a-parameter was chosen to be A/14. The Kalbach constant in usual calculation is from 130 to 160, but it was changed to 4000 in the present calculation. The reason why we had to use very deviated parameters from usual ones so as to meet agreement with the experimental spectrum is not clear, and further investigation is needed to explain the present result.

5. Conclusion

Using measured double differential neutron emission cross sections at En = 14.1 MeV for 15-16 angle-points from 15° to 160°, angle-integrtated neutron emission spectra in the center-of-mass system have been deduced for Be, C, F, Mg, Al, Si, V, Fe, Cr, Cu, Pb and Bi. Since the secondary neutron energy in the CM system directly corresponds to excitation energy, assessment of partial neutron emission cross sections given in JENDL-3T and ENDF/B-IV can be easily made by comparison of emission spectra in the

CM system between experimental and evaluated ones. This kind of comparison work has been done in this report for all of the above elements.

Through comparisons and discussions, status of JENDL-3T or ENDF/B-IV for neutron emission data at 14 MeV has become clear and summaried in Table-6 and Table-7, respectively for JENDL-3T and ENDF/B-IV. Significant over- or under-estimations of ENDF/B-IV in local energy regions of emission spectra (see Table-7) have been eliminated or improved in JENDL-3T for most elements except Be and Pb. Especially, evaluations of ENDL-3T for Si, Fe and Cu are close to be satisfactory. For Be and Pb, however, disagreements with experimental data are still large and should be resolved by further improvements in evaluation work, since these two elements are essential to thermal blankets for breeding tritium by $^{6}Li(n,t)$ reaction. Some of local disagreements in emission spectra can be improved by adding direct inelastic scattering components for higher excited states and improving precompound model calculations. As for angular dependence of emission spectra, general trend of underestimation by ENDF/B-IV for forward enhancement of emission is not resolved in the new evaluation of JENDL-3T, and the use of precompound model calculation with angular dependence is expected.

Acknowledgment

The experiment for vanadium and bismuth was carried out under the financial support of the Japan Atomic Energy Research Institute. The authors are grateful to Drs. T. Asami and T. Fukahori for their discussions on calculated results.

References

1) Constantine, G., IAEA-TEC-DOC-223, (1979)
2) Drosg, M., et al., Proc. Conf. Nuclear Data for Basic and Applied Science, Santa Fe, 1985, Vol.1, p.145-149, Gordon and Breach (1986)
3) Baba, M., et al., ibid., p.223-226
4) Vonach, H., et al., BNL-NCS-51245, INDC(USA)-84/L, (1980)
5) Elfurth, T., et al., INDC(GDR)-044/GI, INT(86)-12, (1986)
6) Takahashi, A., et al., J. Nucl. Sci. Technol., 21, 577-598, (1984)
7) JENDL Compilation Group (Nuclear Data Center, JAERI), JENDL-3T, private communication

8) Takahashi, A., et al., OKTAVIAN Rep. A-87-03, Osaka Univ., (1987)
9) Baba, M., et al., NETU-49, Progress Rep. FNL Tohoku Univ., (1987)
10) Takahashi, A. et al., 'Measurement of Double Differential Neutron Emission Cross Sections for Incident Neutrons of 14 MeV', to be pub. in J. Nucl. Sci. Technol.
11) Takahashi, A., et al., Proc. Conf. Nuclear Data for Science and Technology, Antwerp, 1982, p.360-367, Reidel Pub., (1983)
12) ENDF/B-IV Summary Documentation, BNL-NCS-17451, (1975)
13) Takahashi, A., et al., Proc. Conf. Fast Neutron Physics, Dubrovnik, 1986, p.219-223, Ruder Boskovic Institute Pub., (1986)
14) Takahashi, A., et al., JAERI-M-86-080, p. 393-406, (1986)
15) Yamamoto, J., et al., J. Nucl. Sci. Technol., 19, 276-288, (1982)
16) Takahashi,A., Rusch, D., KfK-2832/I, II, (1979)
17) Ferenc, D., et al., Ref.13, p.183-185
18) Sasaki, Y., et al., Trans. 1987 JAES Annual Meet., D-27, (1987)
19) Baba, M., private communication
20) Watanabe, Y., et al., 'Preequilibrium (n,n') Cross Sections on Nuclei around Atomic Number 50 at En = 14.1 MeV', to be published in Physical Review C
21) Takahashi, A., Ref.2, Vol.1, p.59
22) Oda, H., et al., OKTAVIAN Rep. A-83-06, Osaka Univ., (1983)
23) Howerton, R. J., UCRL-50400 Vol.25, (1983), and private communication
24) Yamamuro, N., JAERI-memo 61-260 (1986), private communication
25) Yanagi, Y., Takahashi, A., OKTAVIAN Rep. A-84-02, Osaka Univ., (1984)
26) EFF-1, the European Fusion File, private communication by H. Gruppelaar

Table-1 $^{9}Be(n,2n)$ cross sections at En = 14.1 MeV

	$^{9}Be(n,2n)$ cross section (b)	error (b)	C/E
Present Exp.	0.478	± 0.014	
ENDF/B-IV	0.536		1.12
JENDL-3PR2	0.521		1.09
JENDL-3T	0.542		1.13
ENDL-86	0.485		1.01
Ring Exp.[25]	0.485	± 0.030	

Table-2 Partial cross sections of ^{12}C at En = 14.1 MeV

	JENDL-3T (b)	ENDF/B-V (b)	Present Exp. (b)	ENDL86
Elastic	0.794	0.795	0.890 ± 0.032	0.811
4.44 MeV st.	0.183	0.186	0.207 ± 0.008	0.227
7.65 MeV st.	0.0195	0.0129	0.0081±0.0015	0.0198
9.64 MeV st.	0.0780	0.0634	0.0694±0.0054	0.0148
Continuum	0.163	0.163	0.143 ± 0.016	0.180
(n,n'3α)	0.261	0.239	0.225 ± 0.020	0.214
σ-total	1.24	1.22	1.320 ± 0.047	1.25

Table-3 Content of iron partial cross sections in JENDL-3T

********** IRON INFORMATION FROM JENDL-3T **********

MT	SEQ	JMAX	Q-VALUE	XSEC AT 14.10(MEV)
1	540	4471	0.0000E+00	2.5120E+00
2	2035	4414	0.0000E+00	1.0596E+00
3	3511	225	1.0044E+07	1.4524E+00
4	3590	149	-1.4400E+04	7.3003E-01
16	3644	19	-7.6435E+06	4.3918E-01
22	3655	18	-7.3225E+06	9.9282E-04
28	3665	16	-8.8600E+06	9.9009E-02
51	3675	54	-1.4400E+04	1.4810E-05
52	3697	48	-1.3650E+05	1.9912E-05
53	3717	45	-3.6680E+05	1.6657E-05
54	3736	42	-7.0640E+05	5.1599E-05
55	3754	66	-8.1080E+05	7.4148E-02
56	3780	40	-1.0072E+06	9.0197E-05
57	3798	37	-1.2654E+06	4.0990E-05
58	3815	41	-1.4082E+06	2.4912E-03
59	3833	47	-1.6273E+06	9.3279E-05
60	3853	30	-1.9893E+06	4.6602E-05
61	3867	68	-2.0765E+06	1.2884E-03
62	3894	37	-2.2189E+06	9.0473E-05
63	3911	43	-2.4560E+06	2.6841E-04
64	3930	57	-2.6000E+06	1.1565E-03
65	3953	68	-2.8764E+06	9.0528E-04
66	3980	62	-3.0840E+06	1.1525E-03
67	4005	57	-3.2330E+06	2.1685E-03
68	4028	37	-3.4454E+06	9.5316E-04
69	4045	35	-3.6009E+06	2.4337E-03
70	4061	42	-3.8320E+06	1.7277E-03
71	4079	38	-4.0330E+06	3.3678E-03
72	4096	32	-4.2632E+06	4.0481E-03
73	4111	27	-4.4010E+06	2.7909E-02
74	4124	21	-4.6550E+06	1.2437E-03
75	4135	17	-4.9490E+06	4.4616E-04
91	4145	32	-2.7600E+06	6.0385E-01
102	4160	153	1.0044E+07	9.3030E-05
103	4215	29	8.7770E+04	1.3970E-01
107	4229	25	2.3952E+06	4.3405E-02
251	4242	119	0.0000E+00	8.0622E-01

Table-4 Pb(n,2n) cross sections at En = 14.1 MeV

	Pb(n,2n) cross section (b)	error (b)	C/E
Present Exp.	2.43	±0.10	
JENDL-3T	2.04		0.84
ENDF/B-IV	2.15		0.885
EFF-1	2.10		0.864
ENDL-86	2.15		0.885
Ring Exp.[25]	2.33	±0.12	

Table-5 Parameters used in GNASH calculation for Bi

Level Density Parameters

Nucleus	a MeV^{-1}	Δ MeV	T MeV	E_x MeV	$\sigma^2(0)$
^{205}Tl	14.643	0.41	0.810	3.642	21.24
^{206}Tl	14.710	0.00	0.946	3.228	21.34
^{204}Pb	14.857	1.21	1.798	4.431	21.56
^{205}Pb	14.920	0.83	1.105	3.458	19.91
^{208}Bi	14.857	0.00	0.915	3.221	21.56
^{209}Bi	14.920	0.38	1.394	3.598	21.67
^{210}Bi	15.000	0.00	0.872	3.214	21.78

Pre-compound Process Parameters

state density constant $g=6a/\pi^2$

Kalbach constant K=4000

Table-6 Status of JENDL-3T for neutron emission data at En = 14.1 MeV

	n-emission spectrum ; region (MeV)	DDX forward-enhancement ; region (MeV)	(n,2n) cross section
Be	(+); 0.3-5 (-); 6.5-9	(-); 0.3-5	(+), 13%
C	(+); 3, 5 (-); 8, 12	(-); 0.5-4	(+);(n,n'3α)
Al	(+); 0-5	(-); 2-8	(+)
Si	(-); 4-5, 6-7	(-); 1-13	
Fe	(+); 9-10 (--); 10-12	(-); 4-12	(0)
Cr	(-); 1-5	(-); 3-13	(0)
Cu	(0)	(-); 2-10	(0)
Pb	(--); 7-9 (-); 0.5-1.5 (+); 3-7	(-); 3-10	(-), 15%

(++), (+); overestimation
(0); satisfactory
(-), (--); underestimation

Table-7 Status of ENDF/B-IV for neutron emission data at En = 14.1 MeV

	n-emission spectrum ; region (MeV)	DDX forward-enhancement ; region (MeV)	(n,2n) cross section
Be	(+); 0-1.5 (--); 1.5-5	(-); 0.3-7	(+), 10% [(0); ENDL86]
F	(+); 1-5 (-); 6-7, 9-10	(-); 2-13	
Mg	(-); 1-12	(-); 2-11	(-)
Al	(+); 1-9	(-); 6-10	(+)
Si	(+); 1-6 (-); 6-7	(-); 2-10	
V	(+); 1-3 (--); 3-13	(-); 1-3 (--); 3-13	(+)
Fe	(+); 5-9 (-); 1-13	(-); 3-12	(-)
Cr	(++); 6-12 (--); 10-13	(-); 5-11	(-)
Cu	(--); 5-12	(-); 5-12	(0)
Pb	(-); 0.5-5	(-); 3-9	(-), 10%
Bi [ENDL86]	(++); 2-7 (--); 7-13	(--); 6-13 (-); 2-6	(+)

(++), (+); overestimation
(0); satisfactory
(-), (--); underestimation

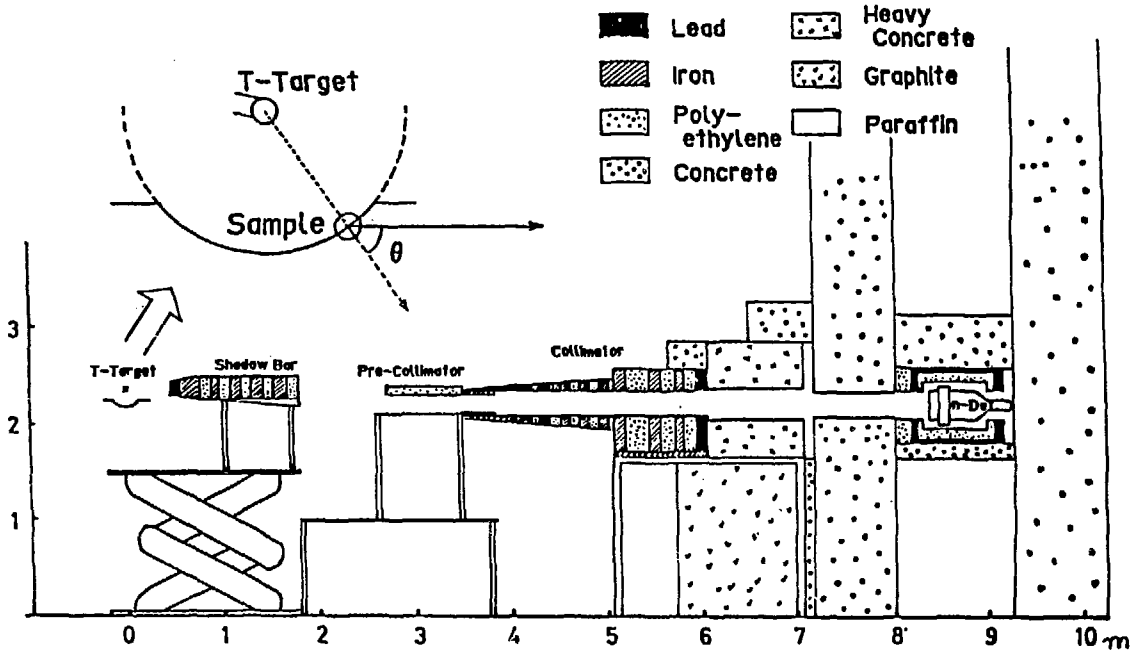

Fig.1 Experimental arrangement of double differential neutron emission cross section measurement, with En = 14.1 MeV

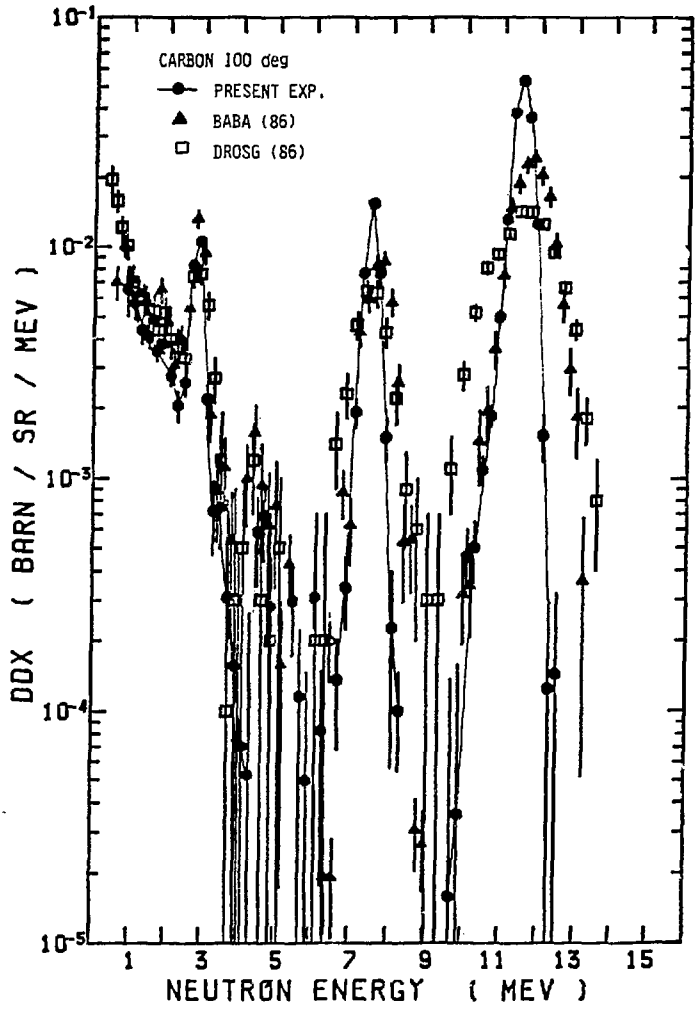

Fig.2 Comparison of the present DDX data with others

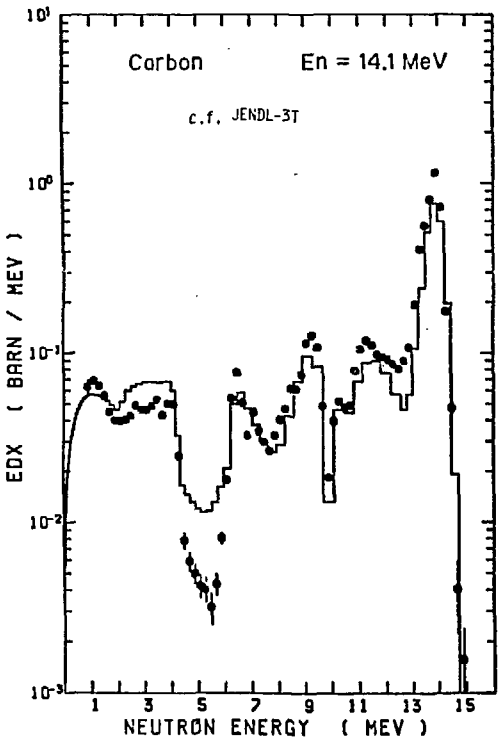

Fig.3 Angle-integrated n-emission spectrum of carbon in the LAB system

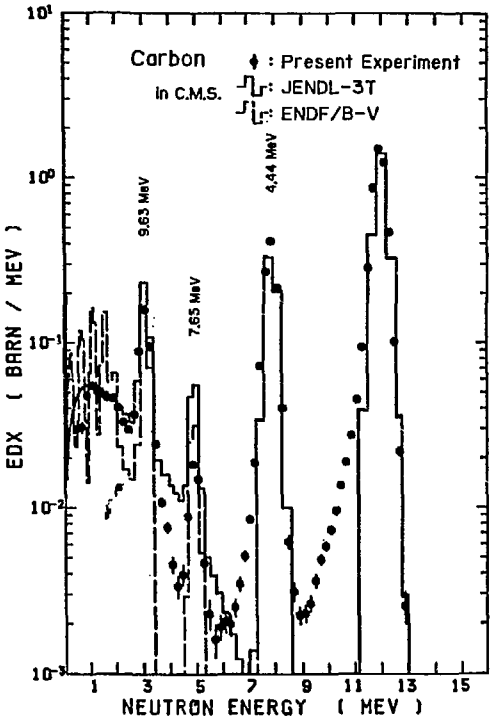

Fig.4 Angle-integrated n-emission spectrum of carbon in the CMS

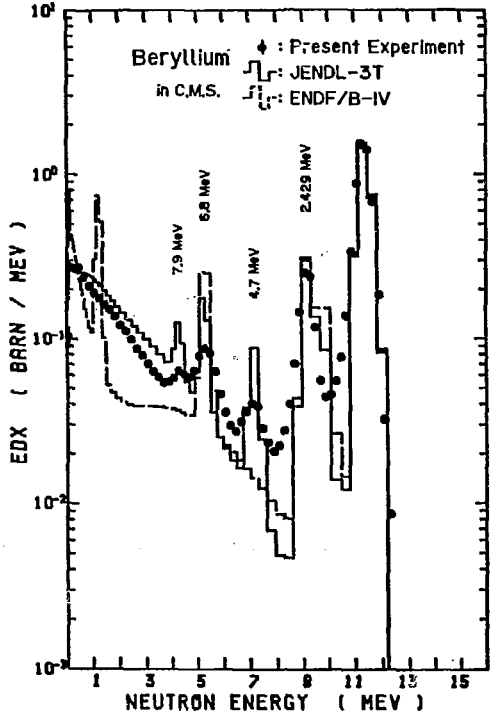

Fig.5 Angle-integrated n-emission spectrum of beryllium, in the CMS

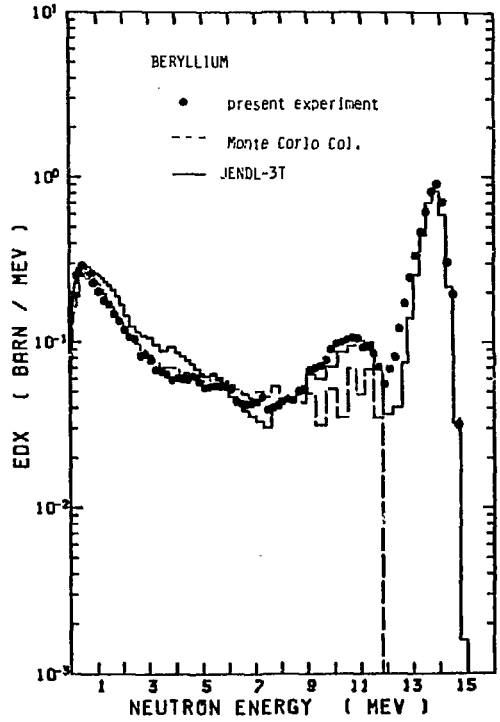

Fig.6 Angle-integrated n-emission spectrum of beryllium, in the LAB system

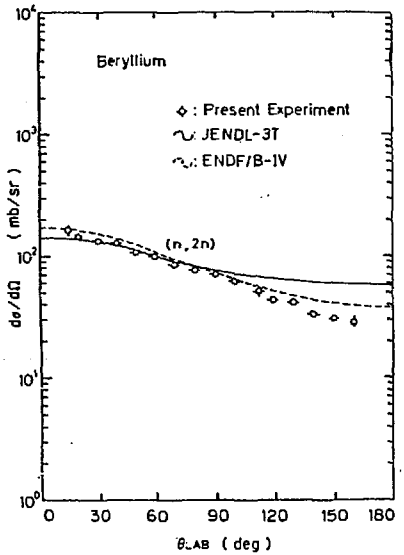

Fig.7 Angluar distribution of $^{9}Be(n,2n)$ cross sections

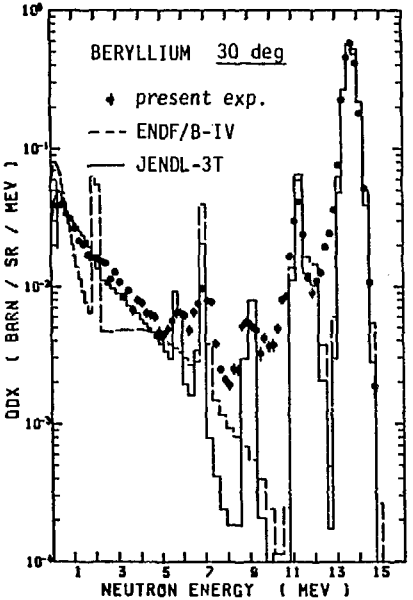

Fig.8-a DDX of Be at 30°, En = 14.1 MeV

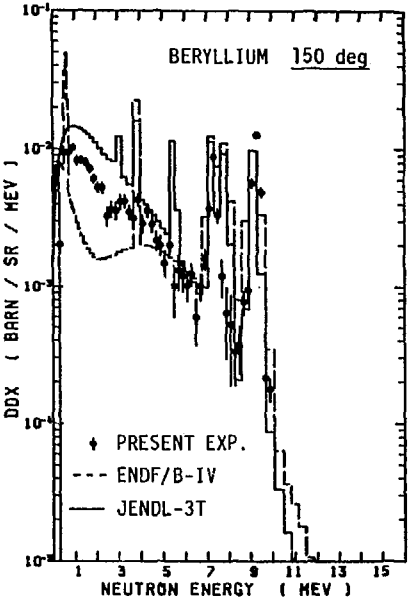

Fig.8-b DDX of Be at 150°, En = 14.1 MeV

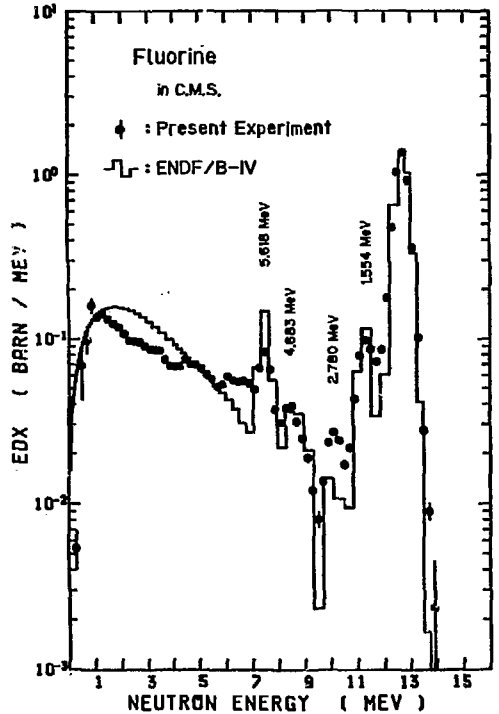

Fig.9 Angle-integrated n-emission spectrum of fluorine in the CMS, En = 14.1 MeV

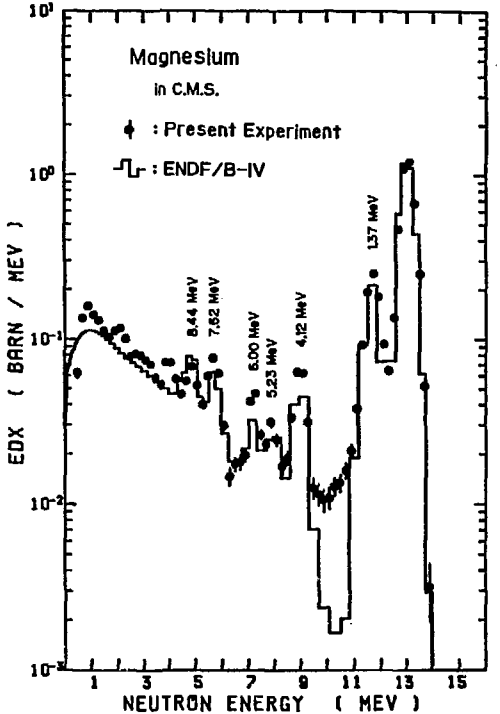

Fig.10 Angle-integrated n-emission spectrum of Mg in the CMS, En = 14.1 MeV

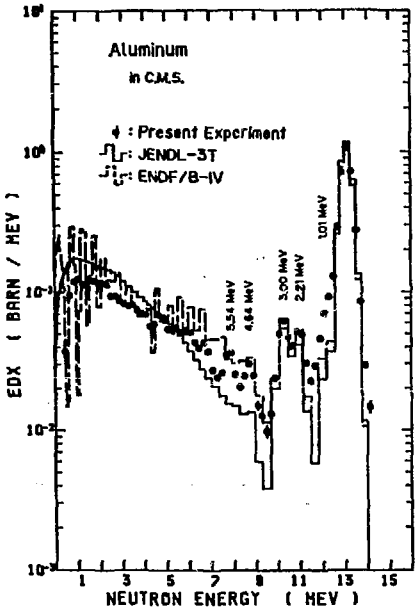

Fig.11 Angle-integrated n-emission spectrum of Al in the CMS, En = 14.1 MeV

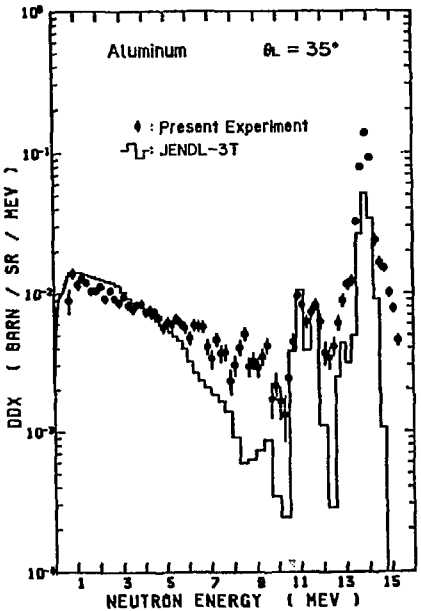

Fig.12-a DDX of Al at 35°, En = 14.1 MeV

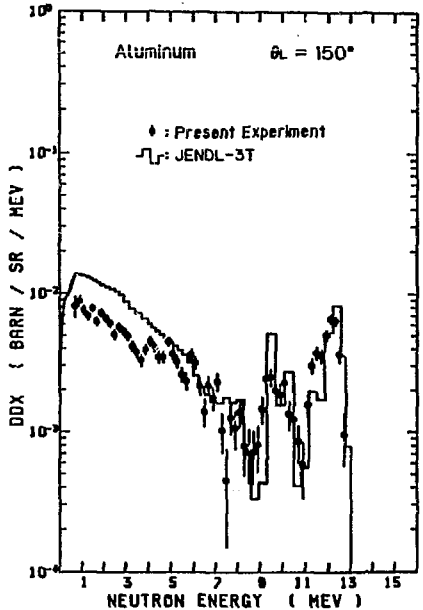

Fig.12-b DDX of Al at 150°, En = 14.1 MeV

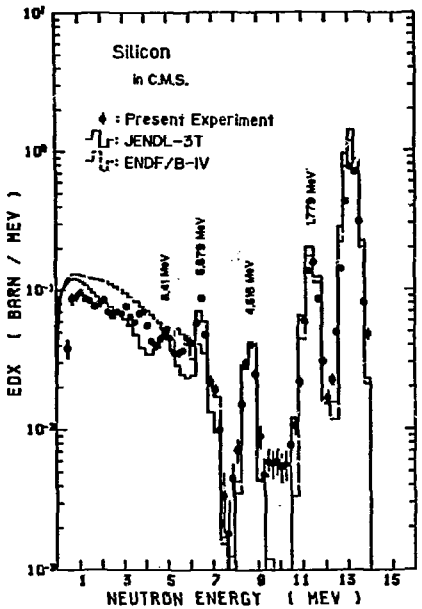

Fig.13 Angle-integrated n-emission spectrum of Si, En = 14.1 MeV

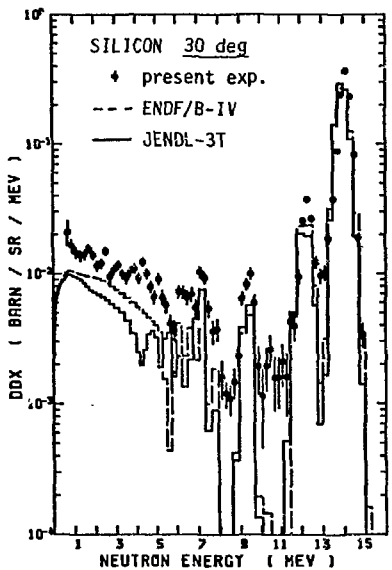

Fig.14-a DDX of Si at 30°, En = 14.1 MeV

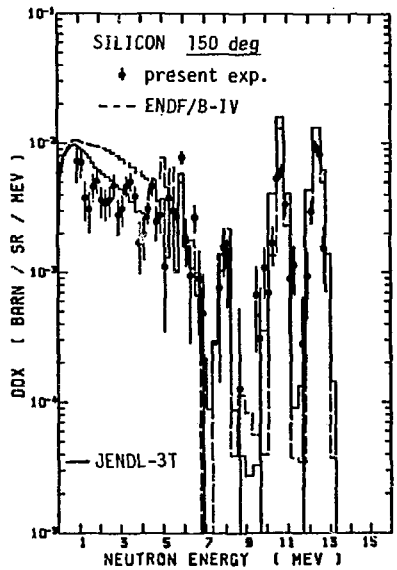

Fig.14-b DDX of Si at 150°, En = 14.1 MeV

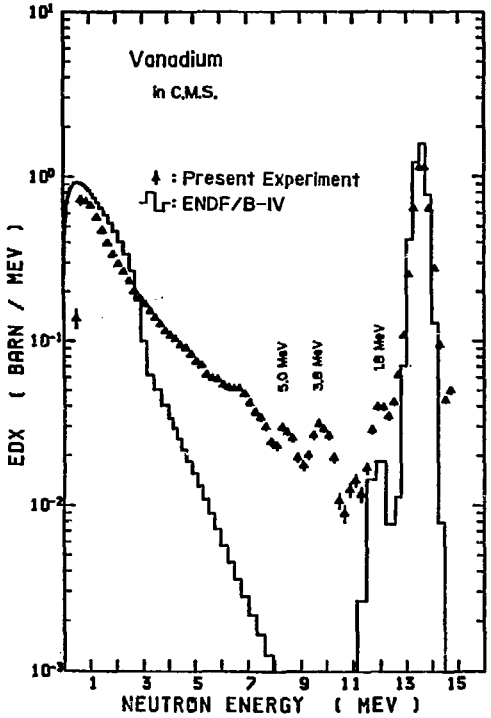

Fig.15 Angle-integrated n-emission spectrum of V, En = 14.1 MeV

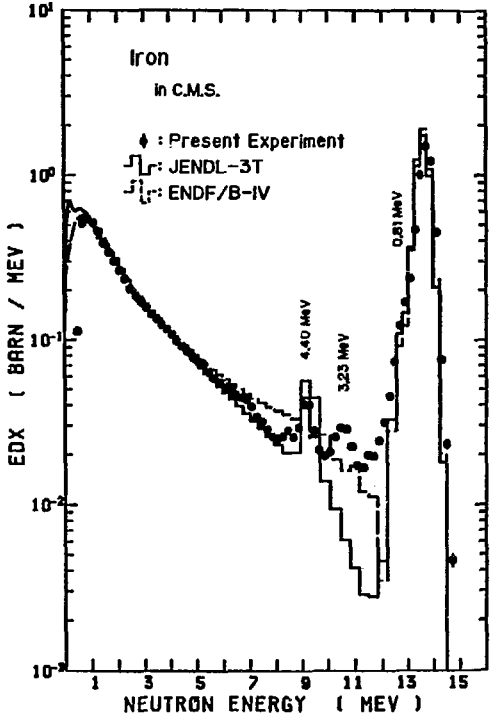

Fig.16 Angle-integrated n-emission spectrum of Fe, En = 14.1 MeV

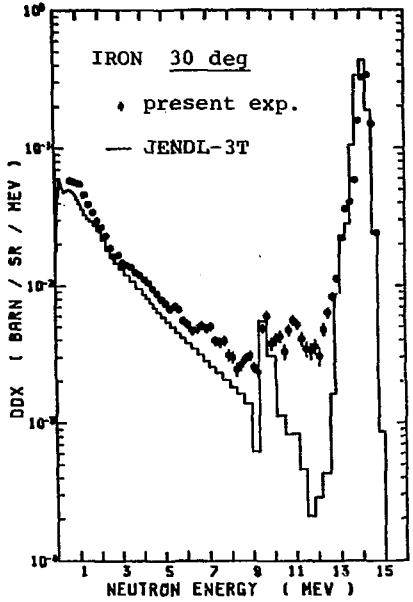

Fig.17-a DDX of Fe at 30°, En = 14.1 MeV

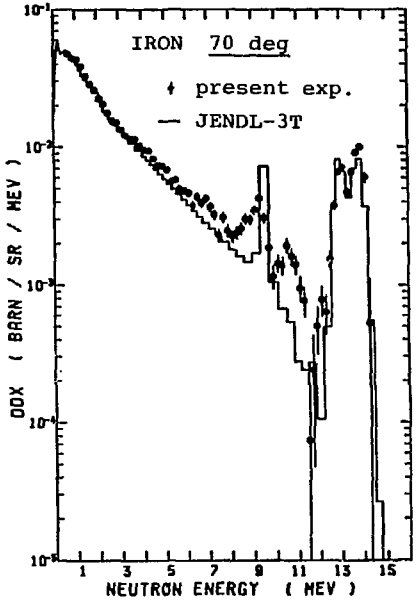

Fig.17-b DDX of Fe at 70°, En = 14.1 MeV

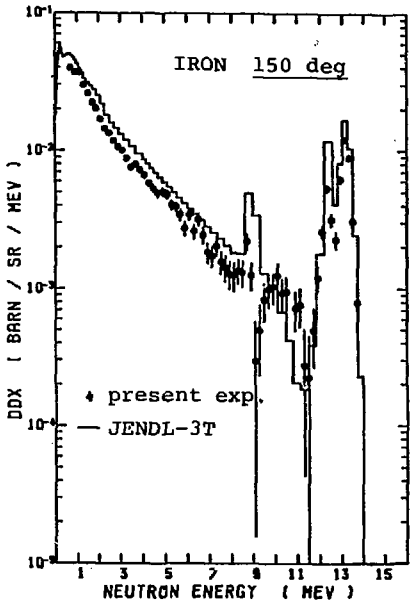

Fig.17-c DDX of Fe at 150°, En = 14.1 MeV

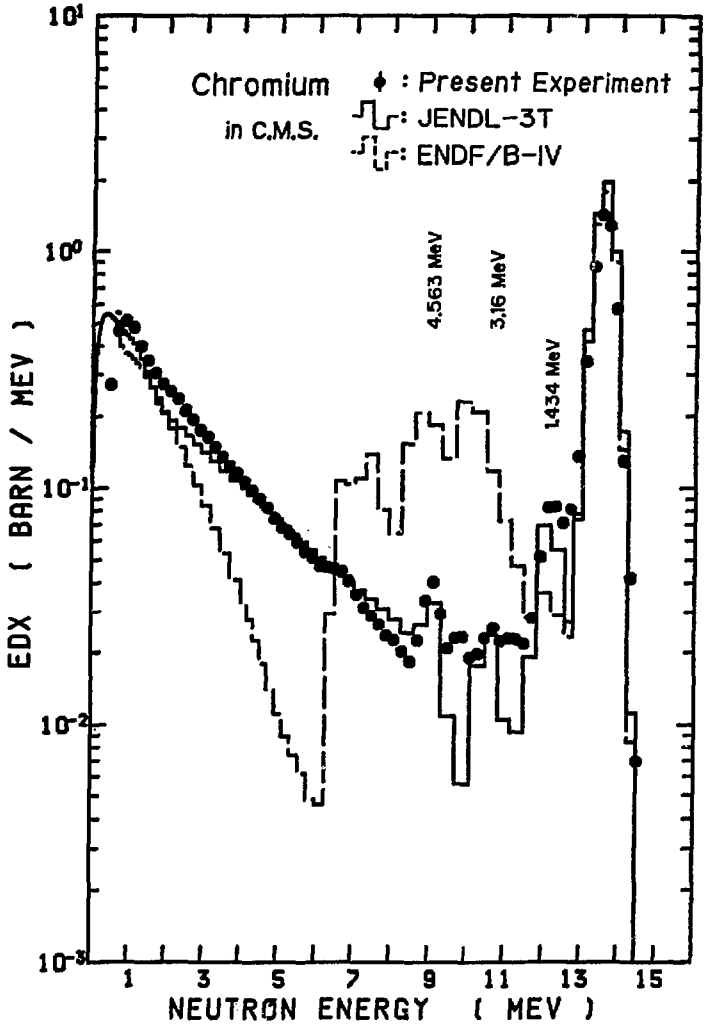

Fig.18 Angle-integrated neutron-emission spectrum of chromiu
En = 14.1 MeV

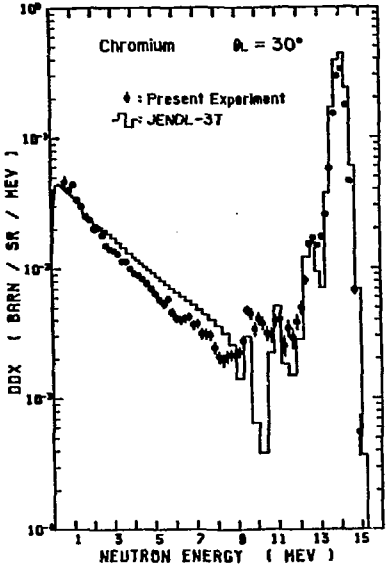

Fig.19-a DDX of Cr at 30°,
En = 14.1 MeV

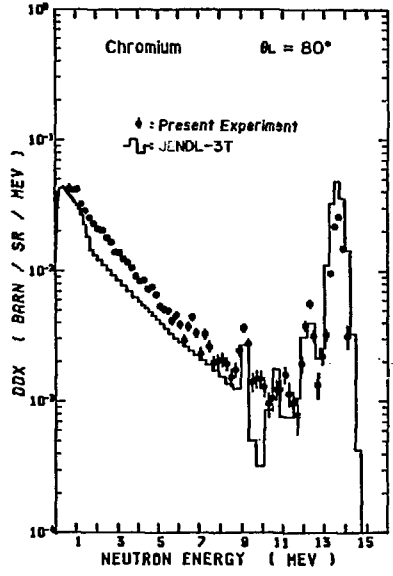

Fig.19-b DDX of Fe at 80°,
En = 14.1 MeV

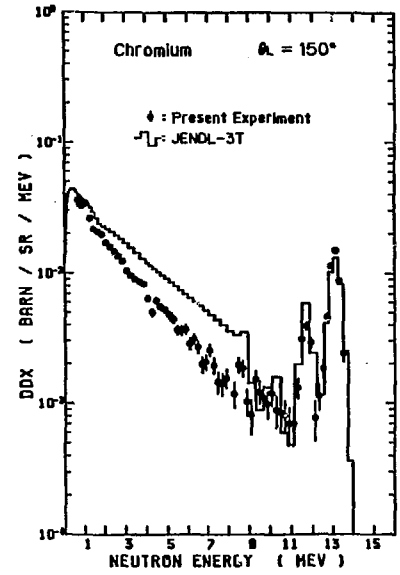

Fig.19-c DDX of Fe at 150°,
En = 14.1 MeV

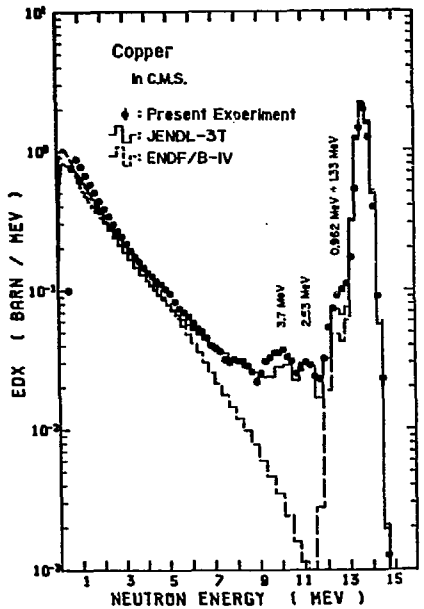

Fig.20 Angle-integrated n-emission spectrum of Cu, En = 14.1 MeV

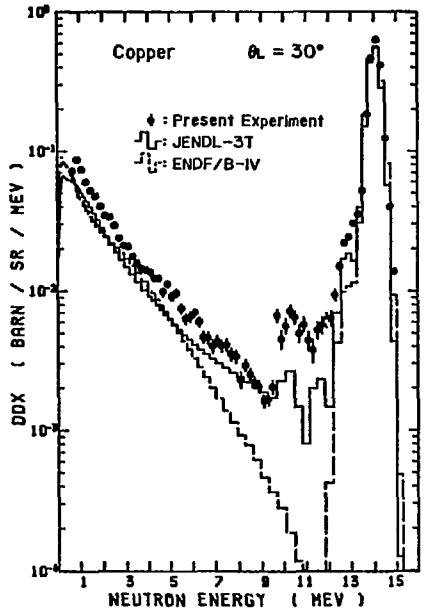

Fig.21-a DDX of Cu at 30°, En = 14.1 MeV

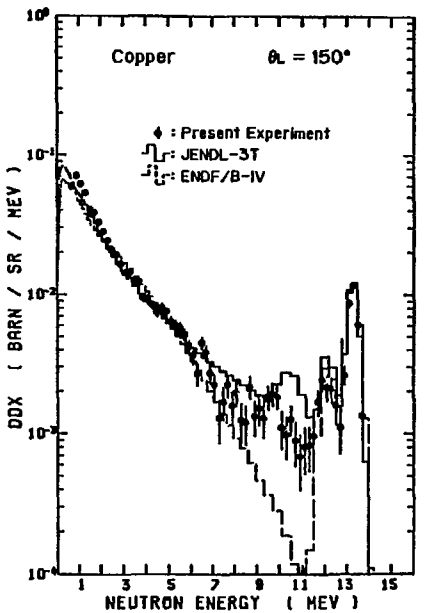

Fig.21-b DDX of Cu at 150°, En = 14.1 MeV

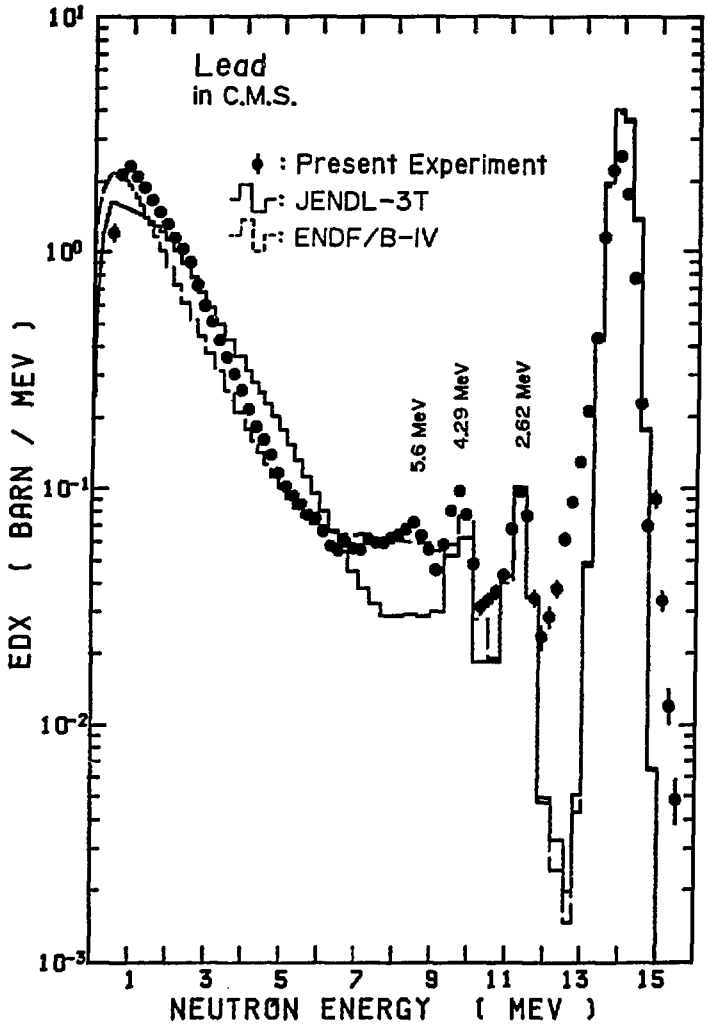

Fig.22 Angle-integrated neutron-emission spectrum of lead in the center-of-mass system, En = 14.1 MeV

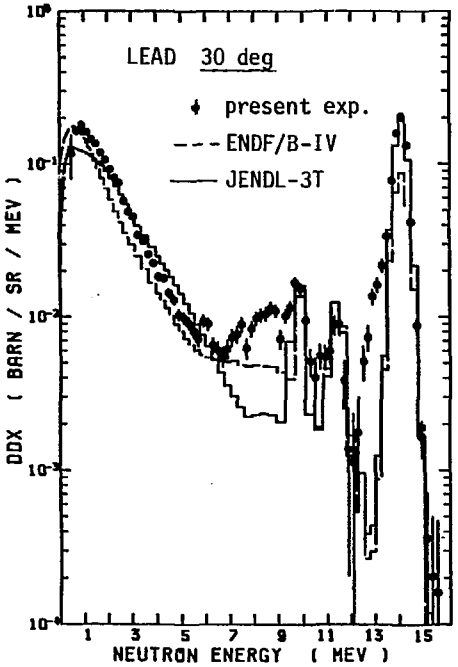

Fig.23-a DDX of Pb at 30°, En = 14.1 MeV

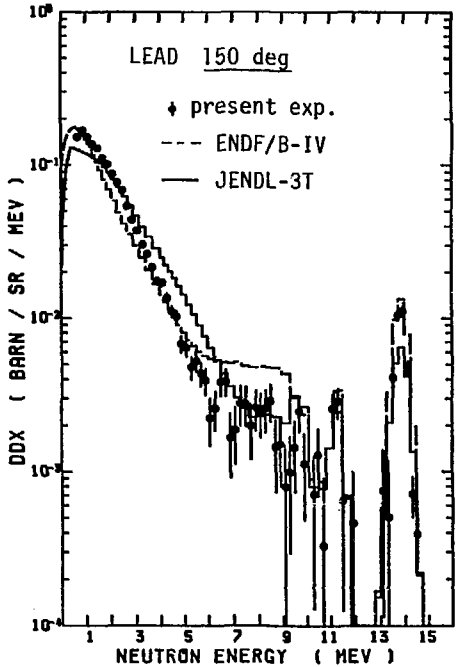

Fig.23-b DDX of Pb at 150°, En = 14.1 MeV

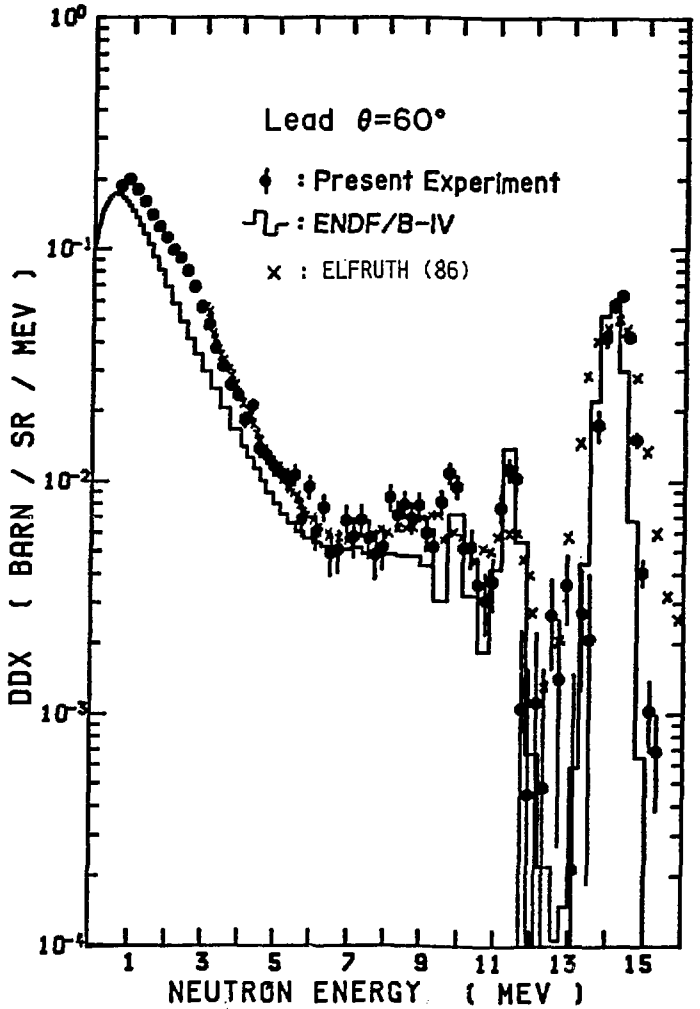

Fig.24 Comparison of DDX data between the present experiment and that of Elfurth et al.[5]

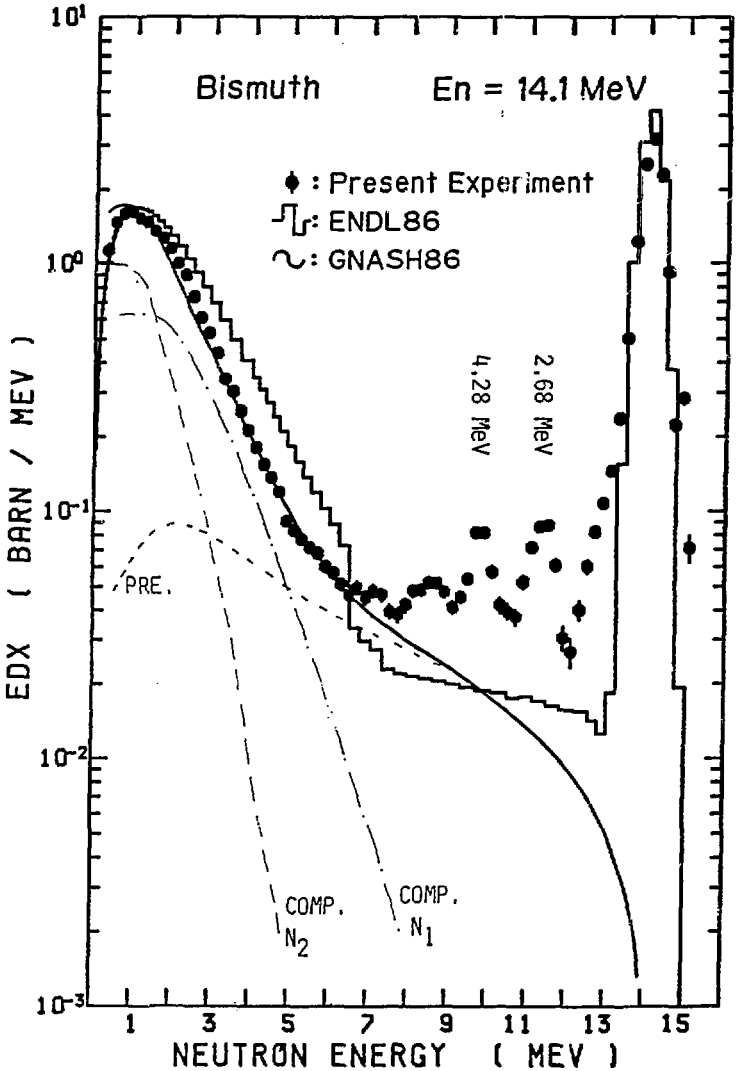

Fig.25 Angle-integrated neutron-emission spectra of bismuth at En = 14.1 MeV, compared with ENDL86 and GNASH calculation

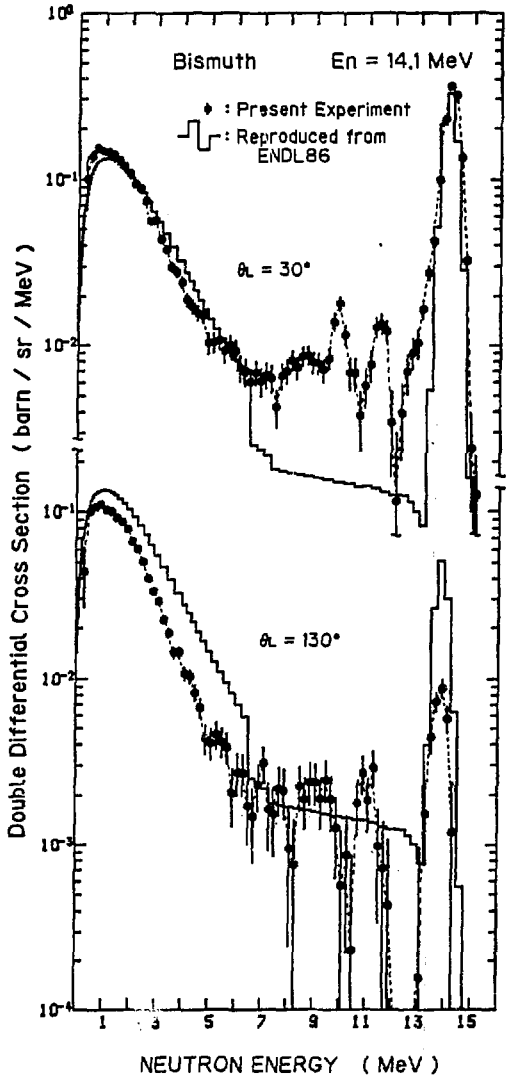

Fig.26 DDX of Bi at 30° and 130°, compared with ENDL86

3. Papers Presented in Poster Session

3.1 Evaluation of the Fission Cross Section for U-233 and Comparison with that for U-235

Hiroyuki MATSUNOBU
Sumitomo Atomic Energy Industries, Ltd.
2－6－1 Kaji-cho, Chiyoda-ku, Tokyo 101

The fission cross section for U-233 was reevaluated in the energy range from 10 keV to 20 MeV, as a part of works for JENDL-3. This revise was performed on the basis of the recent experimental data published after 1982 in which JENDL-2 was released, and using the fission cross section of U-235 which was obtained by simultaneous evaluation for JENDL-3. Especially, the data of fission cross section ratio of U-233 to U-235 which were measured in Tohoku University in 1985 and 1987, were taken into account in the energy range from 200 keV to 7 MeV.

1. Introduction

U-233 is a main nuclide in thorium series fuel cycle, and the fission cross section plays an essential role in determination of the characteristics of reactors and fuel burn-up. Therefore, it is necessary to known the values of fission cross section as accurate as possible, in order to obtain the reliable characteristics by calcuration.

Measurements of the fission cross section for U-233 have been actively perfomed, and a number of data were accumulated up to the present. The measurements are classified broadly into two categories of relative measurement and absolute mesurement. Most of the data by relative mesurement are given in the form of the ratio to the fission cross section of U-235, and have been measured at so many energy points that the energy dependence (sharp) can be easily seen. On the other hand, the data by absolute mesurement are used to normalize the relative data, though the data points are scarce.

As to the measurement of fission cross section for U-233 after JENDL-2 was released in December, 1982, two relative measurements were performed with the Dynamitron accelerater at Tohoku Univercity in the energy ranges from 490 keV to 6.97 MeV and from 218 to 849 keV, and the ratio data to U-235 were published by Kanda et al[1] in 1985 and by Manabe et al.[2] in 1987, respectively. In the high energy region around 14～15 MeV, the absolute data were published by Dushin et al.[3] in 1983 and by Zasadny et al.[4] in 1984, and the ratio data to U-235 were also presented by Meadows[5] in 1987.

In the present work, the fission cross section of U-233 was reevaluated on the basis of the latest experimental data and the fission cross section of U-235 obtained by a simultaneous evaluation of heavy nuclides.

2. Comparison of the Recent Experimental Data

In this section, the latest experimental data are compared with the previous data which were partially used in the evaluation[6] for JEDAL-2. At first, the domestic data by Kanda et al.[1] and Manabe et al.[2] are compared with the ratio data by meadows[7], by Fursov et al.[8], and by Carlson and Behrens[9] in the energy range from 200 keV to 7 MeV. These ratio data are shown in Fig.1 (200 keV ～ 1 MeV) and Fig.2 (0.5 ～ 8 MeV). which were offered from the authers,[2),1)] respectively.

The data by Meadows show the highest values in 200 to 800 keV. Although the data by Carlson and Behrens agree very well with those by Meadows in 200 to 300 keV, their data are about 3 % lower than his data in 300 to 800 keV. The data by Fursov et al. show the lowest values in 200 to 700 keV, though their data agree very well with those by Carlson and Behrens between 700 and 800 keV. Although the data by Manabe et al. are 2.9 ～ 4.7 % lower than those by Meadows and by Carlson and Behrens in 200 to 300 keV, their data distribute between those by Meadows and by Carslon Behrens in 300 to 800 keV. The energy dependence (shape) of the data by Manabe et al. is similar to that by Fursov et al. The data by Kanda et al. which overlap with those by Manabe et al. in 490 to 860 keV, distribute between the data by Manabe et al. and by Carlson and Behrens. The difference between the data by Kanda et al. and by Manabe et al. is 0.6 to 4.4 %.

The data points of each measurement are abundant in the energy region from 800 keV to 2 MeV. In this energy region, a part of the data by Kanda et al. show the highest values and agree well with the data by Meadows. The other data by Kanda et al. lie between the data by Meadows and by Carlson and Behrens. The data by Fursov et al. agree very well with those by Carlson and Behrens in this energy region, though their data show slightly lower values than those by Carlson and Behrens. The energy dependence of the data by Kanda et al. which show low values, is quite similar to those of Carlson and Behrens and of Fursov et al. in 1.2 to 2.0 MeV.

In the energy region from 2.0 to 2.5 MeV, the data by Kanda et al. show high values with those by Meadows. Both data show good agreement within the experimental errors. On the other hand, the data by Carlson and Behrens and by Fursov et al. show low values and agreement of both data is also excellent except the data aronud 4 MeV. However, the discrepancies between high value and low value groups become maximum (～ 6 %) in this energy region. The energy dependence of the data by Kanda et al. is roughly similar to that of Carlson and Behrens.

In the energy region from 5.5 to 7.0 MeV, the data by Meadows show again the highest values. The data by Kanda et al. are 1 ～ 2 % lower than those by Meadows and 2 ～ 6 % higher than those by Carlson and Behrens. Although the data by Fursov et al. show the lowest values in 5.5 to 6.2 MeV, the data by Carlson and Behrens become the lowest values in 6.4 to 7 MeV. The difference between the data by Fursov et al. and by Kanda et al. is 3 to 5 %. The discrepancies among the data are comparatively small in this energy region. The energy dependence of the data by Kanda et al. is similar to that of Fursov et al.

Next, the data by absolute mearsurements around 14 MeV were peblished in 1983 by Dushin

et al.[3] and by Zasadny et al.[4] in 1984. The data given by Dushin et al. are 2.254 b (measured in Khlopin Radium Institute) and 2.244 b (measured in Technical University) at 14.7 MeV, and the weighted mean value of both data is 2.248 b. On the other hand, the cross section measured by Zasadney et al. (University of Michigan) is 2.43 b at 14.62 MeV. This value is 8.1 % higher than the mean value by Dushin et al.

The relative measurement to U-235 was also performed by Meadows[5] in 1987. This ratio value is 1.132 at 14.74 MeV, and is 3.7 % higher than that (1.092) at 14.904 MeV measured by Carlson and Behrens[9]. The cross section derived from this ratio value and the fission cross section of U-235 at 14.74 MeV is 2.40 b and close to the data by Zasadny et al.

3. Evaluation and Results

In the present work, the fission cross sections of U-235 obtained by simultaneous evaluation of the heavy nuclides for JENDL-3 were used to derive those of U-233 from the ratio data. This simultaneous evaluation was performed in the energy range from 50 keV to 20 MeV. Accordingly, the present evaluation in the energy range from 10 to 50 keV was performed on the basis of the absolute data by Gwin et al. (1976)[10]. Their data were adopted in order to keep the consistency with the simultaneous evaluation, because their data were used in the evaluation of Pu-239, and their ratio data agree well with the data by Carlson and Behrens around 50 keV. The fission cross section in the energy range from 50 to 200 keV were evaluated on the basis of the data by Carlson and Behrens and by Poenitz[11),12]. The data of absolute measurement by Poenitz[11] show good agreement with the evaluated values derived from the ratio data by Manaba et al.[2] around 200 keV.

As mentioned in the previous section, the data by Manaba et al. and Kanda et al.[1] agree well with those by Meadows[7] except a few point, and the energy dependence of the fission cross section shows good agreement with that of Fursov et al.[8] in the entire energy region except around 4 MeV. Therefore, in the present evaluation, the fission cross section in the energy region from 200 keV to 7 MeV was evaluated on the basis of the ratio data by Manabe et al. and by Kanda et al. The fact that they are the first and latest domestic data, is also a reason of adoption. The data by Fursov et al. were also used to determine the detailed shape of the ratio data, because their data points are abundant compared with those of Manabe et al. and Kanda et al.

The results of evaluation in the energy range from 100 keV to 7 MeV are shown in Fig.3 and Fig.4 with the experimental data and previous evaluation (JENDL-2). The difference between the present and previous evaluations is considerably large in this energy range. This is due to the differences of the adopted ratio data and of the fission cross sections of U-235. This problem is discussed in the next section.

Finally, the fission cross section in the energy range above 7 MeV was evaluated on the basis of the ratio data by Carlson and Behrens[9] except around 14 ～ 15 MeV. As mentioned in

the previous section, large discrepancies exist between the absolute measurements by Dushin et al.[3] and by Zasadny et al.[4], and also between the relative measurements by Carlson and Behrens and by Meadows[5] around 14 MeV. The latest data by Meadows support the measurement by Zasadny et al., though the data by Carlson and Behrens lie between both absolute measurements. In addition, the accuracy of the data by Meadows is very good (0.7 %). Therefore, in the present work, the data by Meadows at 14.74 MeV were adopted instead of the data by Carlson and Behrens at 14.180 and 14.904 MeV.

The result of evaluation in the energy range from 7.5 to 20 MeV is shown in Fig.5 with the experimental data and previous evaluation (JENDL-2). As seen in this figure, the energy dependence (sharp) of fission cross section was determined on the basis of the data by Carlson and Behrens except around 14 ～ 15 MeV. The difference between the present and previous evaluations is due to the effect taking into the structure of cross section in 8 to 13 MeV, because this structure was ignored in JENDL-2. The data by Arlt[13] plotted in Fig.5 are the same data as those presented in the paper of Dushin et al.

4. Comparison with the Fission Cross Section for U-235

As seen in Fig.4, the present results show considerably high value compared with the JENDL-2 data and the absolute measurements by Poenitz[11] in the energy range from 2 to 5.5 MeV. The maximum difference between the present results and the data by Poenitz attains to 13.5 % at 4 MeV. This difference is composed of two factors. That is, the first factor is due to the fact that the ratio data adopted in the present work are higher than the other ratio data except those by Meadows in this energy range. The second factor is due to the fact that the fission cross sections of U-235 used to derive those of U-233 are also higher than the absolute measurements of U-235 by Poenitz[14] in the same energy range.

These relations are shown in Fig.6 in the energy range from 1 to 7 MeV. In this figure, the solid line shows the ratios of the present result (JENDL-3T) to the data by Poenitz[11]. The long dashed line shows the ratios of the relative measurements by Kanda[1] (Tohoku Univ.) to those by Poenitz. These ratio data by Poenitz were calcurated on the basis of his absolute measurements for U-233[11] and U-235[14]. The short dashed line shows the ratios of the simultaneously evaluated fission cross sactions (JENDL-3T) to the absolute measurements by Poenitz[14] for U-235. As seen in this figure, the short dashed line ($^{235}\sigma_f$(J-3T)/$^{235}\sigma_f$(Poenitz)) shows the highest values in the energy region from 3 to 4.25 MeV. This is based on the following reason. Roughly speaking, the simultaneously evaluated data are the weighted averages of the recent experimental data which are largely scattered in the above energy region, where as the data by Poenitz belong to the lowest group of the experimental data in this ehergy region. This situation is shown in Fig.7. Although the ratios of the relative measurements (R(Tohoku)/R(Poenitz)) are also large in the energy region from 3.5 to 5.25 MeV, the effect of the above systematic discrepancy of U-235 has been strongly reflected in the present results.

5. Concluding Remarks

The present evaluation of the fission cross section for U-233 in the energy range from 10 keV to 20 MeV was carried out on the basis of the latest and domestic data. As shown in Fig.3 and Fig.4 the results show high values of a few % compared with JENDL-2 and the other experimental data except those by Meadows in the energy region above 325 keV except around 800 keV. In particular, the difference between the present results and JENDL-2 data increases to 8.5% in the energy region from 4 to 5 MeV. This large discrepancy depends on two reasons that the simultaneously evaluated fission cross sections of U-235 are 5 ～ 6 % hegher than the absolute data by Poenitz in this energy region, and the ratio data by Kanda et al. are also 2.5 ～ 6 % higher than the ratios obtained from the absolute data of U-233 and U-235 by Poenitz. We can not decide at present that the high value data including the present results are coreect or not. It should be expected to future experiments.

References

1) Kanda, k., Imaruoka, H., Yoshida, K., Sato, O., and Hirakawa, N. : "Nuclear Data for Basic and Applied Science" , Proc. Int. conf., Santa Fe, 13 ～ 17 May, 1985, A Special Issue of Radiation Effects, Vol. 1, P.569 (1985)

2) Manabe, F., Iwasaki, T., Karino, Y., Matsuyama, S., Baba, M., and Hirakawa, N. : "Measurements of Neutron Induced Fission Cross Sections of U-233 at Several Thousands keV", 1987 Annual Meeting of the Atomic Energy Society of Japan, Nagoya, April 1 ～ 3, Abstracts Vol. I, P.167 (1987) (in Japanese)

3) Dushin, V.N., Fomichev, A.V., Kovalenko, S.S., Petrzkak, K.A., Shpakov, V.I., Arl't, R., Iosh, M., Muziol', G., Ortlepp, Kh. -G., and Vagner, V. : Atomnaya Energiya, 55, 218 (1983)

4) Zasadny, K.R., Agrawal, H.M., Mahdavi, M., and Knoll, C.F. : American Nucl. Soc. 47, 425 (1984)

5) Meadows, J.W. : "The Fission Cross Sections of ^{230}Th, ^{232}Th, ^{233}Th, ^{233}U, ^{234}U, ^{236}U, ^{238}U, ^{237}Np, ^{239}Pu and ^{242}Pu Relative to ^{235}U at 14.74 MeV Neutron Energy", Actinide Newsletter, Issue 10, P.27 (1987)

6) Asano,N., Matsunobu, H., and Kikuchi, Y. : J. Nucl. Sci. Tech., 19, 1037 (1982)

7) Meadows, J.W. : Nucl. Sci. Eng., 54, 317 (1974)

8) Furusov, B.I., Kupriyanov, V.M., and Smirenkin, G.N. : Atomnaya Energiya, 44, 236 (1978)

9) Carlson, G.W. and Behrens, J.W. : Nucl Sci. Eng., 66, 205 (1978)

10) Gwin, R., Silver, E.G., Ingle, R.W., and Weaver, H. : Nucl Sci. Eng., 59, 79 (1976)

11) Poenitz, W.P. : "Absolute Measurements of the ^{233}U (n,f) Cross Section between 0.13 and 8.0 MeV", ANL/NDM-36 (1978)

12) Poenitz, W.P. : Nucl. Sci. Eng., 53, 370 (1974)

13) Arl't, R. et al. : ZFK-491, P.135 (1982)

14) Poenitz, W.P. : Nucl. Sci. Eng., 64, 894 (1977)

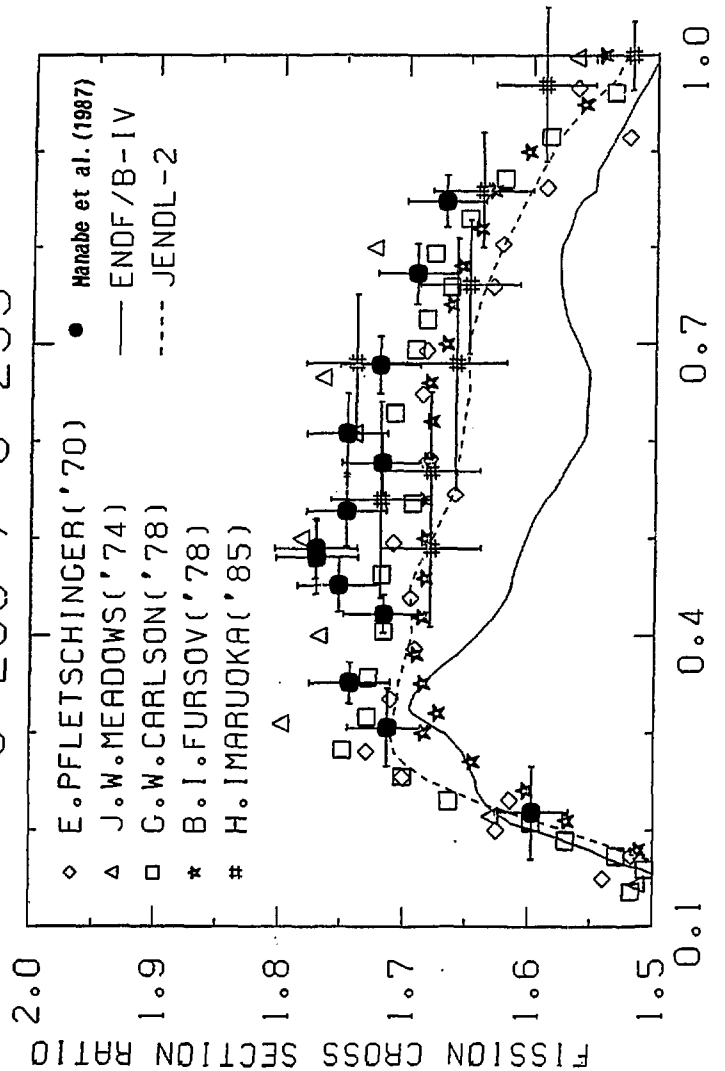

Fig. 1 The Ratios of Fission Cross Section for U-233 to U-235 in the Energy Range from 100 keV to 1 MeV.

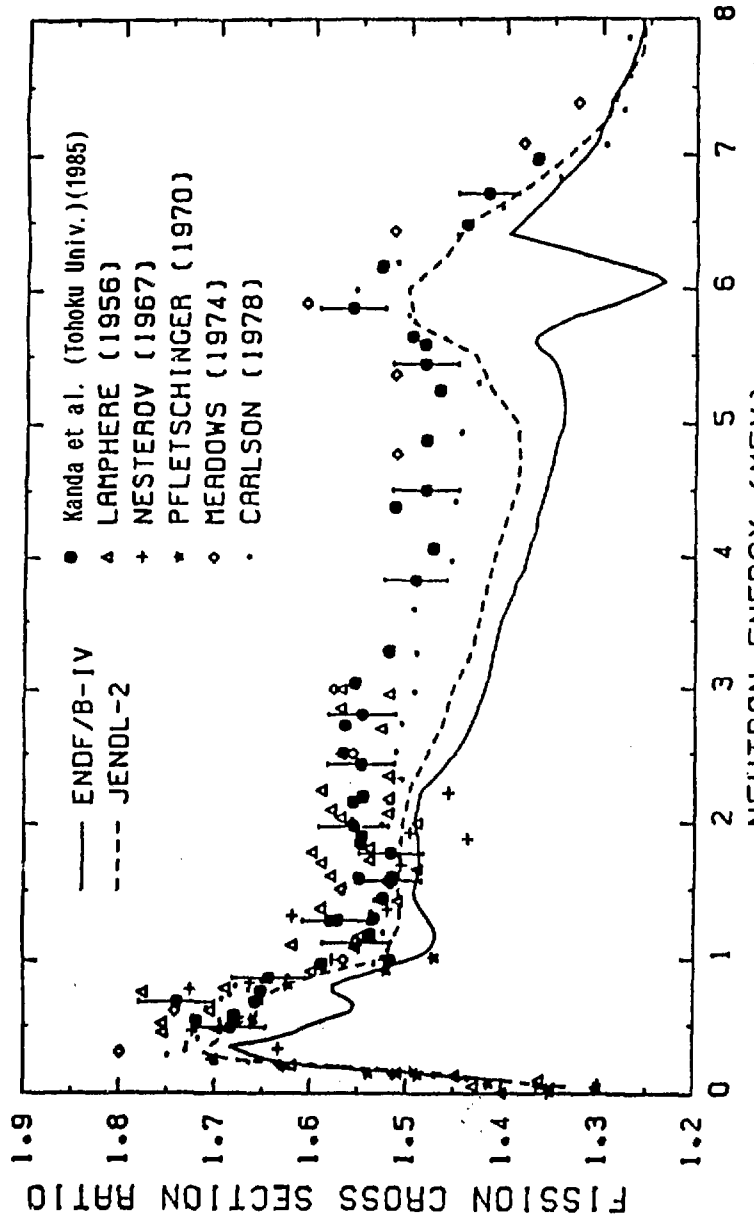

Fig. 2 The Ratios of Fission Cross Section for U-233 to U-235 in the Energy Range from 0.1 to 8 MeV.

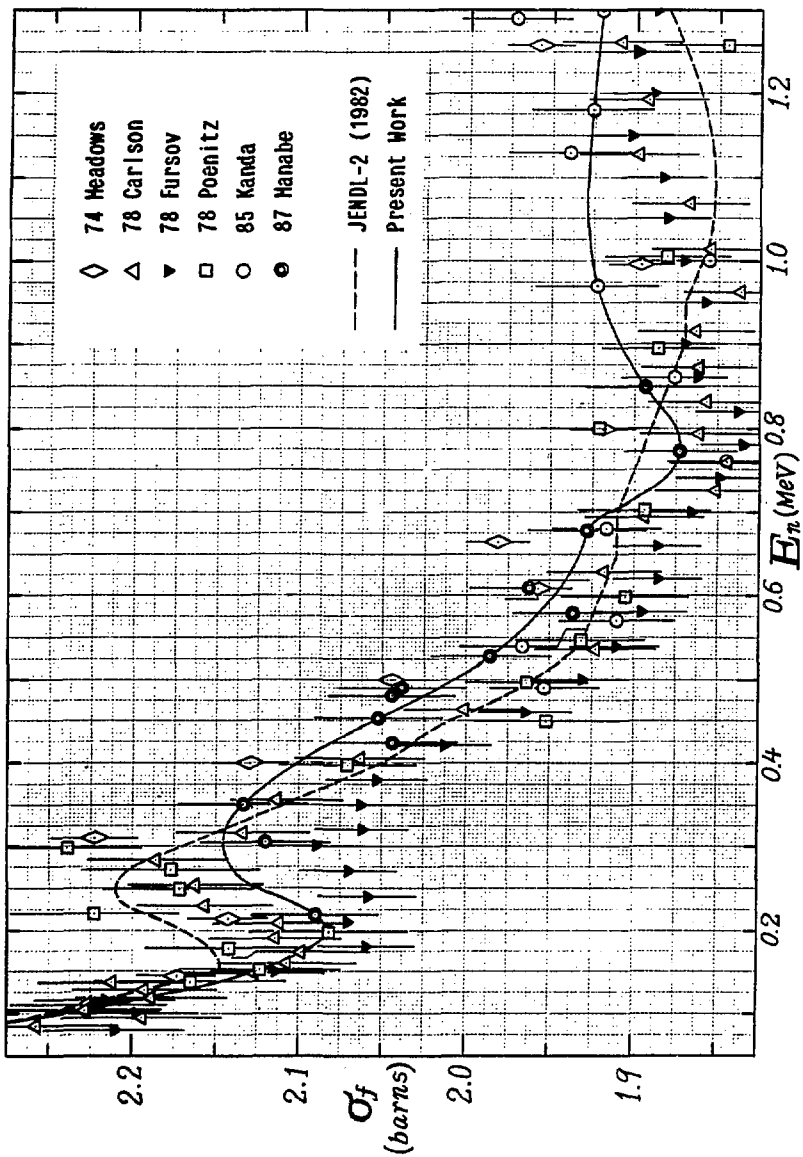

Fig. 3 The Evaluated and Experimental Fission Cross Sections for U-233 in the Energy Range from 100 keV to 1.3 MeV.

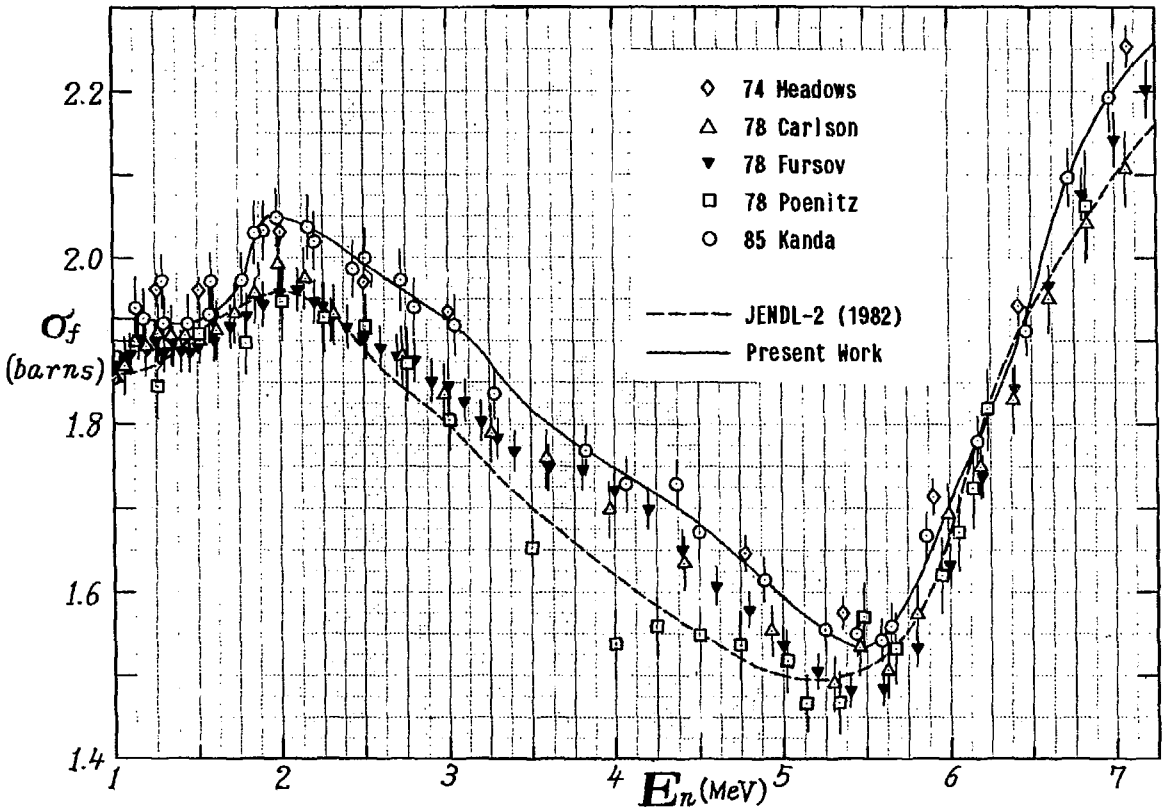

Fig. 4 The Evaluated and Experimental Fission Cross Sections for U-233 in the Energy Range from 1 to 7 MeV.

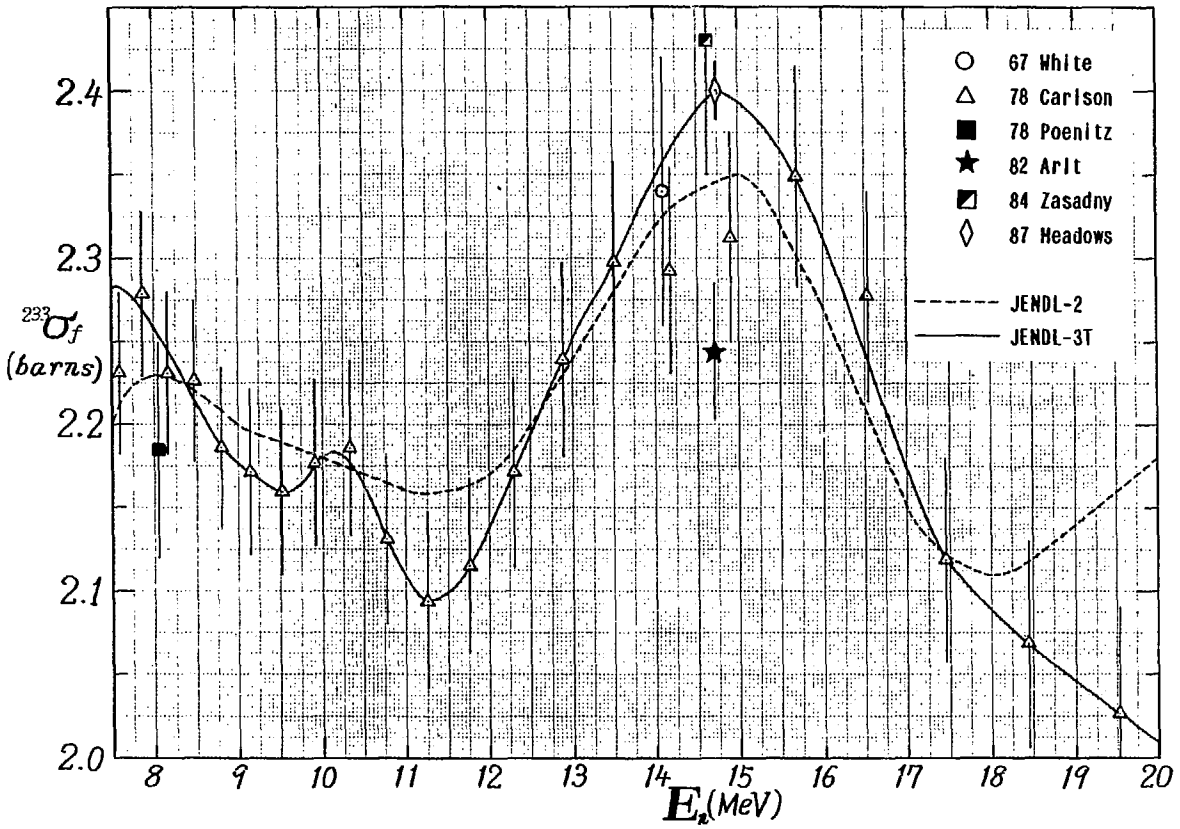

Fig. 5 The Evaluated and Experimental Fission Cross Sections for U-233 in the Energy Range from 7.5 to 20 MeV.

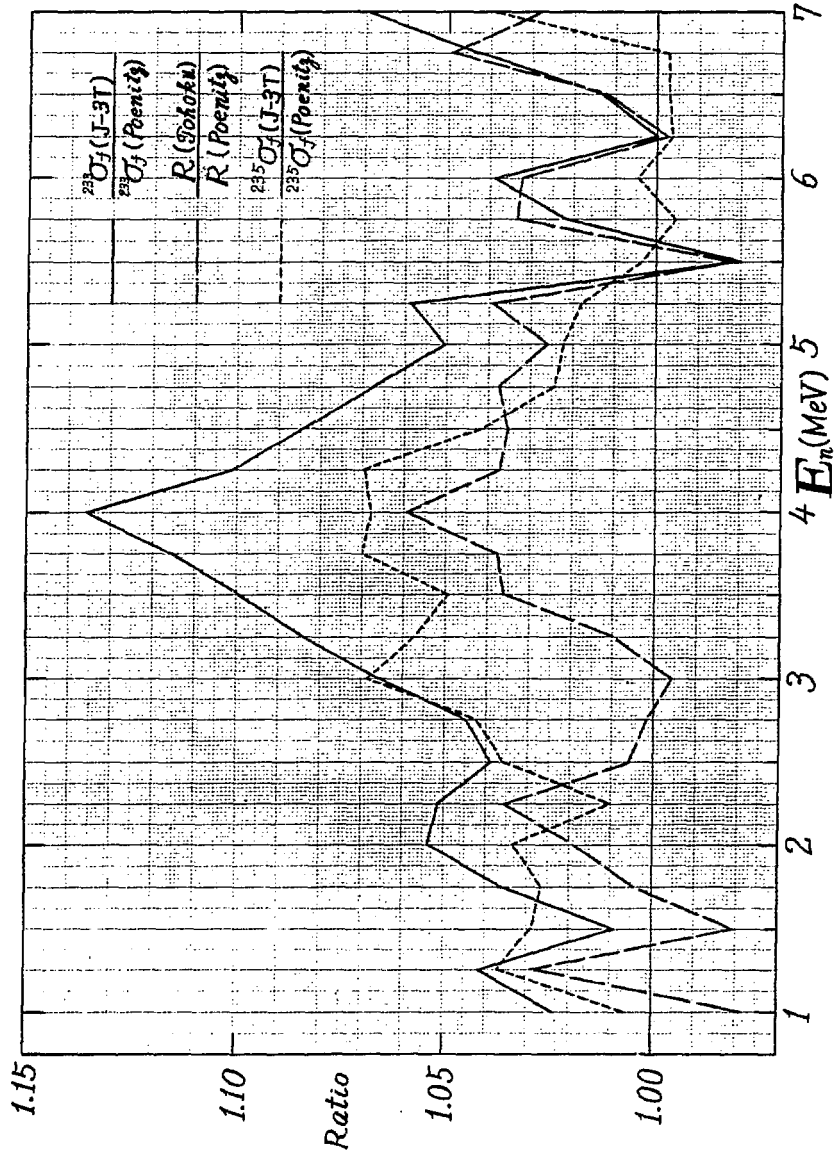

Fig. 6 The Ratios of Fission Cross Sections for U-233 and U-235 to the Data by Poenitz in the Energy Range from 1 to 7 MeV.

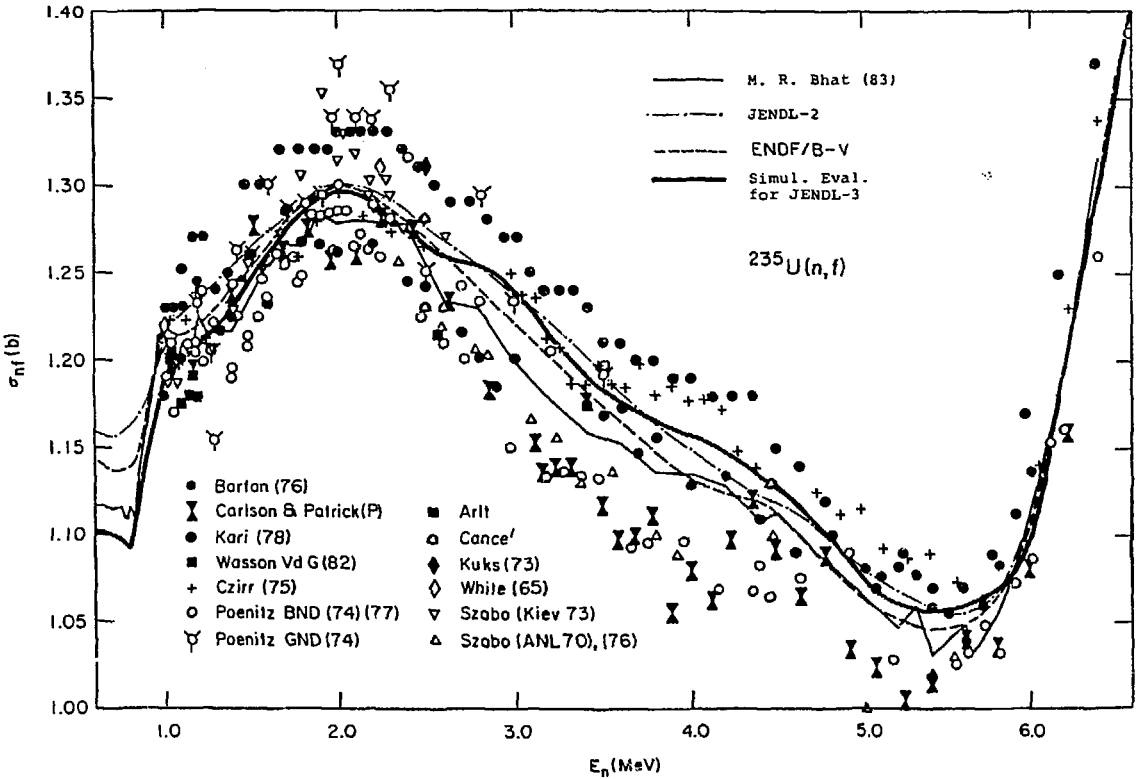

Fig. 7 Comparison of the Experimental and Evaluated Data of the Fission Cross Section for U-235 in the Energy Range from 0.6 to 6.6 MeV.

3.2 Activation of Structural Materials due to Recoil Protons in Light Water Reactor

M. Takahashi, Y. Yuasa, S. Iijima and T. Murata

NAIG Nuclear Research Laboratory
Nippon Atomic Industry Group Company, Ltd.
4-1, Ukishima-cho, Kawasaki-ku, Kawasaki, 210 Japan

The long-lived radioactivities of structural materials induced by recoil protons in BWR were estimated for land disposal of low level waste after reactor decommisioning. Reactions of interest are listed. Method of calculation of the proton spectrum in materials was developed. A program PEGASUS-P was developed by modifying PEGASUS to calculate proton induced reaction cross sections. The proton-induced activities are shown as not exceeeding 1/1000 of that of a typical neutron induced nuclide, Ni-63, for cooling up to 1000 years after irradiation of 40 years.

1. Introduction

It is important to estimate precisely the radioactivities of the low level waste for land disposal after the decommissioning of reactor. The activities have been evaluated hitherto based mostly on the neutron induced reactions. However, in the core of Light Water Reactor(LWR), high energy recoil protons are produced via scattering of neutrons with water molecules, which, by chance, impinge on the fuel cladding or other structural materials and induce proton reactions. We note here an early work by Tagami et al.(1) to evaluate the N-13 production in coolant water by reaction of recoil protons with O-16 atoms.

In the present work, the radioactivities of structural materials induced by proton reactions are evaluated. The long-lived isotopes of interest are Mn-53, Nb-91, Nb-94, Tc-97, Sb-125, Lu-173 and Lu-174, which will be produced by proton reactions with stainless steel, inconel or zircaloy. The results are compared with the Ni-63 activity (half-life

of 100y) which is a typical long-lived isotope produced by the neutron reaction with the structural materials.

2. Method of Calculation

Figure 1 shows a BWR lattice configuration. Fission neutrons born in fuel, escaping from fuel and colliding with water, give rise to the high energy recoil protons which eventually impinge on the structural materials and cause nuclear reactions. The long-lived nuclides of interest induced by proton reactions are listed in Table 1.

The recoil proton source spectrum is expressed by,

$$Q(E_p) = \int_{E_p}^{\infty} dE \sum_{SH}(E)\ \phi_n(E)/E \qquad (1)$$

where $\sum_{SH}$ is the macroscopic scattering cross section of hydrogen in water and ϕ_n the neutron flux. Neglecting the neutron absorption and slowing down by the collision with oxygen atoms we obtain,

$$\sum_{SH} \phi_n(E) = \nu \sum_f \phi_{th} f \left[\chi(E) + \frac{1}{E}\int \chi(E')\, dE'\right] \qquad (2)$$

Here ϕ_{th} is the thermal neutron flux in fuel, χ is the normalized thermal fission neutron spectrum, and f the fraction of neutrons that escape from fuel and make collisions with water. The factor f may be taken as the order of magnitude of 0.5.

The protons attenuate mostly within water, but that are born near material surface impinge on the structural materials. Assuming that the protons are born uniformly and isotropically in water, it is shown that the average proton flux spectra in water and structural material are given by,

$$\phi_W(E) = \int_E^\infty dE_p \, Q(E_p) / S_W(E_p), \tag{3}$$

$$\phi_M(E) = \frac{S}{4V} \frac{1}{S_M(E)} \int_E^\infty dE_p \, Q(E_p) \left[R_W(E_p) - R_W(E) \right] \tag{4}$$

Here, S_m and S_w are the proton stoping powers of the material and water, respectively, and R_w the proton range in water. S and V are the surface area and volume of the material.

The proton reaction rate in material is then,

$$R = \int_0^\infty \sigma(E) \, \phi_M(E) \, dE \quad \text{(reactions/atom/s)}. \tag{5}$$

Since ϕ_M is proportional to thermal neutron flux, the reaction rate is conviniently expressed in terms of the effective thermal cross section defined by,

$$\sigma_{eff} \equiv R / \phi_{th} \tag{6}$$

This can be compared directly with the effective thermal neutron cross section for production of Ni-63 by neutron capture rection with Ni-62 :

$$\sigma^* = (\pi T_0 / 4 T_n)^{1/2} \sigma_{2200} + r I \tag{7}$$

Here, T_0=293K, T_n the neutron temperature, r the epithermal index, and I the resonance integral. Taking T_n=1123K, r=0.165, σ_{2200} =14.5 b and I=6.6 b, we obtain σ^* = 7.7 b.

The activity after irradiation and cooling is,

$$A = N (1 - e^{-\lambda t_1}) e^{-\lambda t_2} \int \sigma(E) \, \phi_M(E) \, dE, \tag{8}$$

where N is the initial total number of parent nuclides, t_1 the irradiation time taken as 40 y, and t_2 the cooling time.

The proton cross sections were calculated with PEGASUS-P described in section 3. The compositions of core structural materials were taken from the report ORNL/TM9591. The U-235 thermal neutron fission spectrum was adopted from the NBS recommendation. The proton stopping powers in water, SUS and Zircaloy-2 were constructed from the elemental stopping power data of Ziegler(2). The void volume fraction of 40 % was assumed for water. For other parameters, $\nu\Sigma_f$ was taken as 0.075 cm^{-1} and S/4V as 1.0 (equivalently the fuel radius or channel box thickness of 0.5 cm). Thermal neutron flux value was taken as $6x10^{14}$ n/cm^2 /s. These values are typical of the operating BWR's.

The calculated proton source spectra Q(Ep), and the average spectra in water and structural materials are depicted in Fig. 2. It is seen that the protons of energy grerater than about 10 MeV will not contribute significantly to reactions. The integrated fluxes relative to thermal neutron flux are $2.15x10^{-4}$, $5.7x10^{-7}$, and $3.9x10^{-7}$ in water, Zircaloy-2 and SUS, respectively, showing a considerable reduction of proton reactions compared with neutron reactions.

3. Proton Reaction Cross Sections

Since the proton flux is of significance up 10 MeV, the reactions considered are restricted to the thresholds less than 10 MeV. The proton reaction cross sections were calculated with a micro-computer program PEGASUS-P, a version of PEGASUS(3). which is a preequilibrium and multistep evaporation theory code. It calculates proton reaction cross

sections involving the emission of gamma-rays, neutrons, protons, alphas and deuterons up to the second stage. The gamma-ray spectrum is not calculated. The preequilibrium cluster particle emission is treated by using the theory of Iwamoto and Harada(4). In the present calculation, however, the preequilibrium effect was ignored since it is not effective for proton energy below 10 MeV.

The neutron inverse cross sections were taken as the non-elastic cross sections given by the Pearlstein's formula(5). Inverse cross sections for charged particles were calculated from the optical potential of Perey (6) for protons, Huizenga and Igo(7) for alpha, and Lohr and Haeberli(8) for deuterons.

The parameters of Gilbert-Cameron type composite level density formula were determined from the slow neutron resonance data and the lowlying level scheme data. A systematics consideration was used whenever necessary.

Figure 3 shows the comparison of the calculated (p,n) cross sections for Cu-63 and Cu-65 with experimental data after adjusting the level density parameters to some extent. Without experimental data, the uncertainties of the factor of 2 - 3 have to be allowed in the calculated cross sections.

4. Resutls and Discussions

In Fig. 4(a) and 4(b) are shown the total response functions versus proton energy for production of Nb-91 and Lu-173 in Zircaloy-2, respectively, together with the average proton spectrum relative to thermal neutron flux (dot and dash line) and the main contributing reaction cross sections

(dotted line). The effective activation cross sections are given in Table 2. The induced activities per gram of materials are also given in the rightmost column of Table 2 for irradiation of 40 years. At the bottom of Table the Ni-63 activity induced by neutron reaction is given with the same condition.

As seen from Table 2, the Nb-91 activity produced in Zircaloy-2 is dominant among proton induce activities. It is still by a factor of 1/10,000 smaller than that of Ni-63.

Figure 5 shows the activity per gram of parent materials as a function of cooling time after irradiation of 40 years. For cooling time up to 1000 years, the proton induced activities are less than 1/1000 of the Ni-63 activity. It is concluded that the activities due to recoil protons may be safely ignored by the land disposal of low level waste. The conclusion is believed to be applicable also to the case of PWR.

Acknowledgement

We are thankful to T.Sugi and T.Nakagawa of Japan Atomic Energy Research Institute for use of the charged particle inverse cross section file. H. Mizuta at NAIG Nuclear Research Laboratory provided us with the nuclear calculational results on operating BWR's. A pioneering work in this field by T. Tagami, late M. Yamamoto and T. Osawa at Hitachi was very instructive to the present study.

References

(1) Tagami,T., Yamamoto,M., Osawa,T. : J. Atom. Energy Soc. Japan 17 12(1964) (in Japanese)

(2) H.H. Anderson and J.F. Ziegler : Hydrogen, Stopping Powers and Ranges in All Elements, vol.3 of the Stopping and Ranges of Ions in Matter, organized by J.F.Ziegler, Pergamon Press (1977)

(3) Iijima,S., Sugi,T., Nakagawa,T., Nishigori,T.: Program *PEGASUS*, *JAERI-M* 87-025 (1987) 337

(4) Iwamoto,A., Harada,K.: Phys. Rev. C26 1821 (1982), Sato,K.,Iwamoto,A.,Harada,K.:Phys. Rev. C28 1527 (1983)

(5) Pearlstein, S.: J. Nucl. Energy 27 88 (1973)

(6) Perey, F.G. : Phys. Rev. 181 745 (1963)

(7) Huizenga,J.R., Igo,G. : Nucl. Phys. 29 462 (1962)

(8) Lohr,J.M., Haeberli,W. : Nucl.Phys. A232 381 (1974)

Table 1 List of radioactive nuclides of interest produced by proton reactions ($T_{1/2}$ > 1y).

product nuclide	production mode			
Al-26g	^{27}Al (p, pn)	^{29}Si (p, α)	^{30}Si (p, αn)	^{27}Al (p, d)
Cl-36	^{36}S (p, n)			
Mn-53	^{52}Cr (p, γ)	^{53}Cr (p, n)	^{56}Fe (p, α)	^{57}Fe (p, αn)
Fe-55	^{55}Mn (p, n)	^{56}Fe (p, pn)	^{59}Co (p, αn)	^{56}Fe (p, d)
Co-60	^{64}Ni (p, αn)			
Ni-59	^{59}Co (p, n)	^{60}Ni (p, pn)	^{63}Cu (p, αn)	^{60}Ni (p, d)
Ni-63	^{64}Ni (p, pn)	^{64}Ni (p, d)		
Zr-93	^{94}Zr (p, pn)	^{94}Zr (p, d)		
Nb-91	^{90}Zr (p, γ)	^{91}Zr (p, n)	^{92}Zr (p, 2n)	^{93}Nb (p, dn)
	^{94}Mo (p, α)	^{95}Mo (p, αn)		
Nb-92	^{91}Zr (p, γ)	^{92}Zr (p, n)	^{93}Nb (p, d)	^{94}Mo (p, dp)
	^{95}Mo (p, α)	^{96}Mo (p, αn)		
Nb-93	^{92}Zr (p, γ)	^{94}Zr (p, 2n)	^{95}Mo (p, dp)	^{96}Mo (p, α)
	^{97}Mo (p, αn)			
Nb-94	^{94}Zr (p, n)	^{96}Mo (p, dp)	^{97}Mo (p, α)	^{98}Mo (p, αn)
Mo-93	^{93}Nb (p, n)	^{94}Mo (p, pn)	^{95}Mo (p, pn)	^{94}Mo (p, d)
	^{95}Mo (p, d)			
Tc-97	^{96}Mo (p, γ)	^{97}Mo (p, n)	^{98}Mo (p, 2n)	
Tc-98	^{97}Mo (p, γ)	^{98}Mo (p, n)		
Tc-99	^{100}Mo (p, 2n)			
Ag-108m	^{110}Cd (p, dp)	^{111}Cd (p, α)	^{112}Cd (p, αn)	
Cd-109	^{110}Cd (p, pn)	^{111}Cd (p, dn)	^{110}Cd (p, d)	
Cd-113m	^{114}Cd (p, pn)	^{114}Cd (p, d)		
Sn-121m	^{122}Sn (p, pn)	^{122}Sn (p, d)		
Sb-125	^{124}Sn (p, γ)			
Hf-172	^{174}Hf (p, dn)			
Hf-178m	^{179}Hf (p, pn)	^{180}Hf (p, dn)	^{179}Hf (p, d)	
Lu-173	^{176}Hf (p, α)	^{177}Hf (p, αn)		
Lu-174g	^{176}Hf (p, dp)	^{177}Hf (p, α)	^{178}Hf (p, αn)	
Ta-179	^{178}Hf (p, γ)	^{179}Hf (p, n)	^{180}Hf (p, 2n)	^{182}W (p, α)
	^{183}W (p, αn)			
Re-186m	^{186}W (p, n)			

Table 2 The effective cross sections and induced radioactivities in materials after irradiation of 40 year in BWR.

structual material	nuclide (half life)	production mode	Q-value (MeV)	effective cross section (barn)	radioactivity (μCi/g)
zircaloy-2	Nb-91 (6.8×10^{2} y)	^{90}Zr (p,γ)	+5.17	4.9×10^{-10}	6.1×10^{-5}
		^{91}Zr (p,n)	-2.04	1.2×10^{-8}	
		^{94}Mo (p,α)	+3.10	1.5×10^{-10}	
		^{92}Mo (p,2p)	-7.46	1.1×10^{-16}	
	Nb-94 (2.0×10^{4} y)	^{94}Zr (p,n)	-1.67	1.3×10^{-8}	3.1×10^{-4}
	Sb-125 (3.2 y)	^{124}Sn (p,γ)	+7.31	4.9×10^{-11}	3.4×10^{-6}
	Lu-173 (1.4 y)	^{176}Hf (p,α)	+7.18	4.6×10^{-13}	9.1×10^{-11}
	Lu-174 (3.3 y)	^{177}Hf (p,α)	+7.76	2.2×10^{-13}	1.6×10^{-10}
inconel 718	Mn-53 (3.7×10^{6} y)	^{52}Cr (p,γ)	+6.57	6.8×10^{-10}	2.0×10^{-7}
		^{53}Cr (p,n)	-1.36	9.8×10^{-9}	
		^{54}Cr (p,2n)	-11.1	7.2×10^{-12}	
		^{56}Fe (p,α)	-1.05	7.4×10^{-11}	
		^{54}Fe (p,2p)	-8.86	7.8×10^{-16}	
	Tc-97 (2.6×10^{6} y)	^{96}Mo (p,γ)	+5.73	3.0×10^{-10}	1.3×10^{-8}
		^{97}Mo (p,n)	-1.09	7.8×10^{-9}	
		^{98}Mo (p,2n)	-9.74	1.1×10^{-10}	
zircaloy-2	Ni-63 (1.0×10^{2} y)	^{62}Ni (n,γ)	+6.84	7.7	2.6×10^{3}

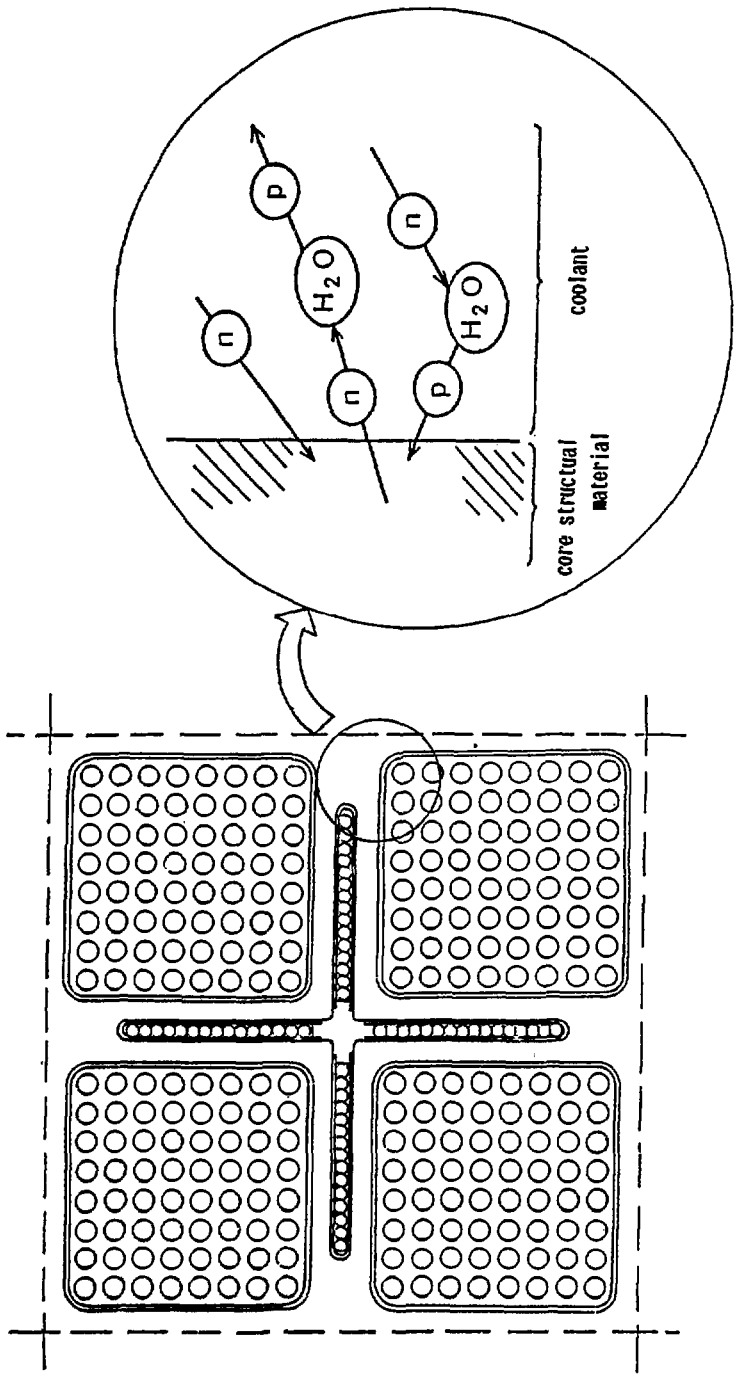

Fig.1 Production of recoil protons in BWR lattice.

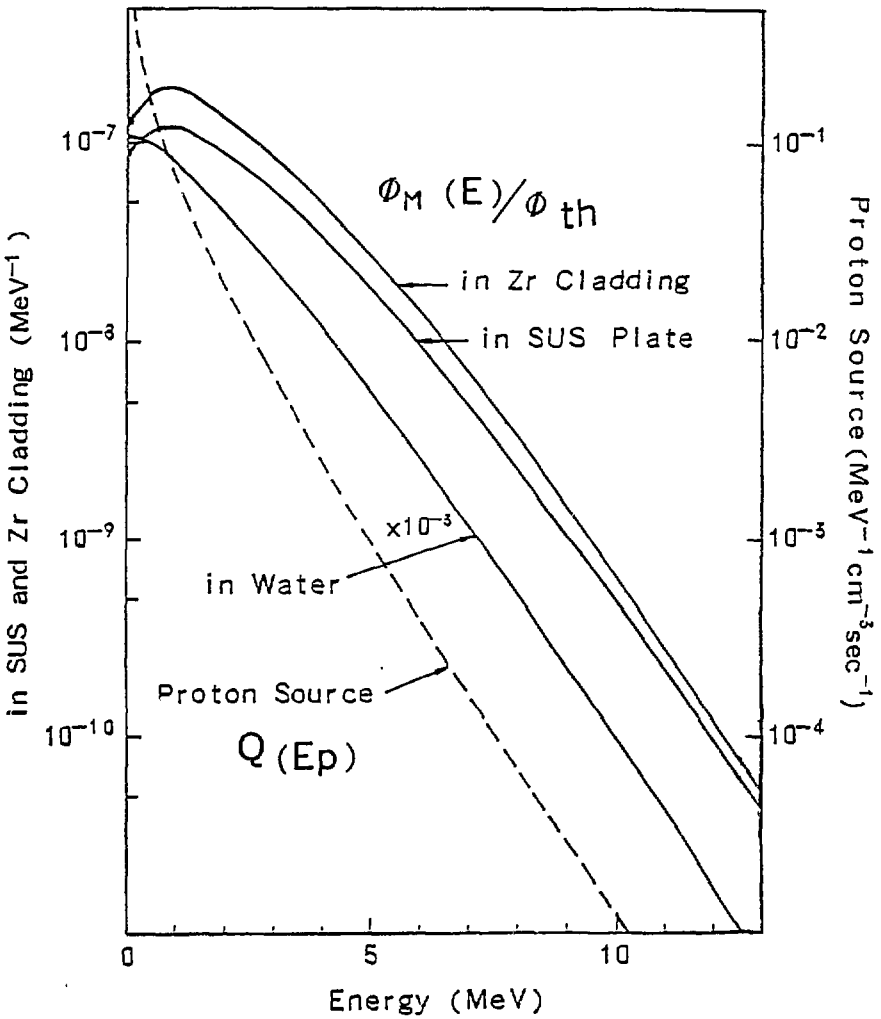

Fig.2 Proton source spectrum in water and the average proton spectra in water and structual materials.

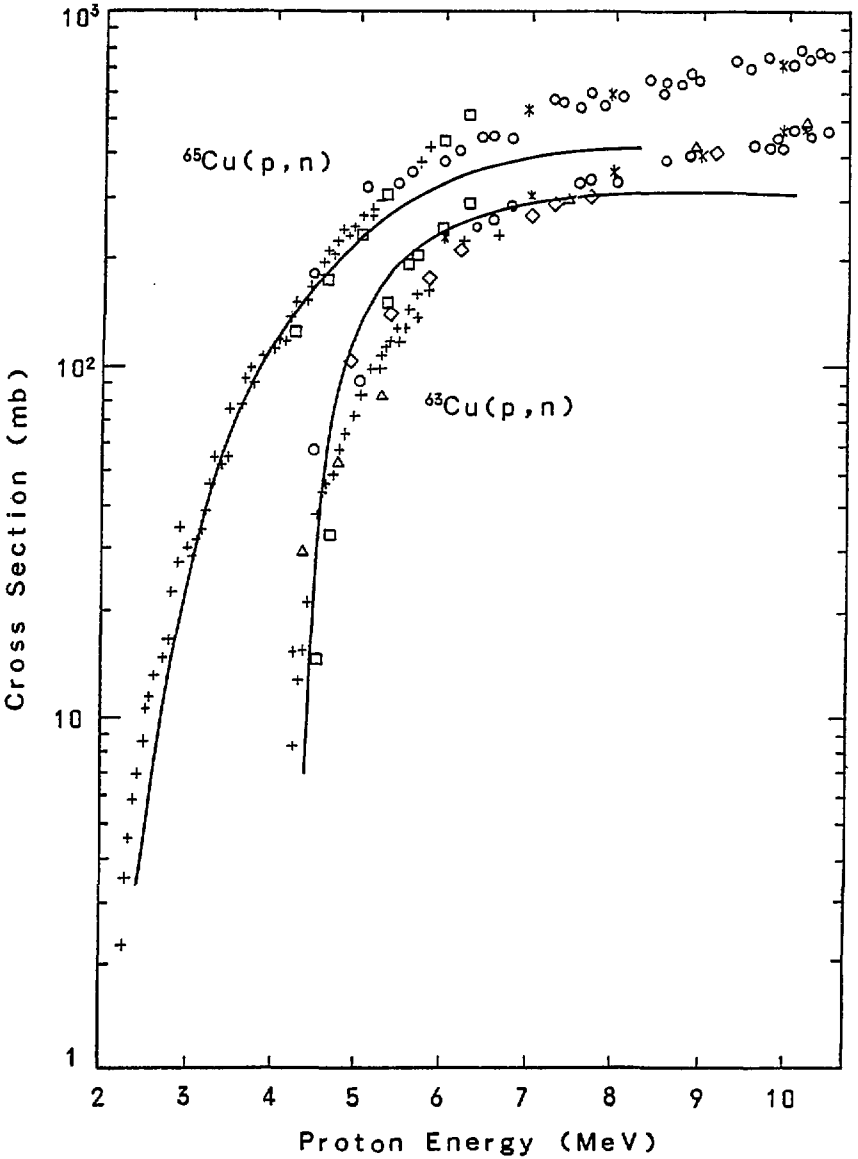

Fig.3 ^{63}Cu(p,n) and ^{65}Cu(p,n) cross sections. Comparison of caluculation with experiment. Solid curves are the result of calculated with PEGASUS code, and the marks of +, *, ○, △, □ and ◇ are experimental data.

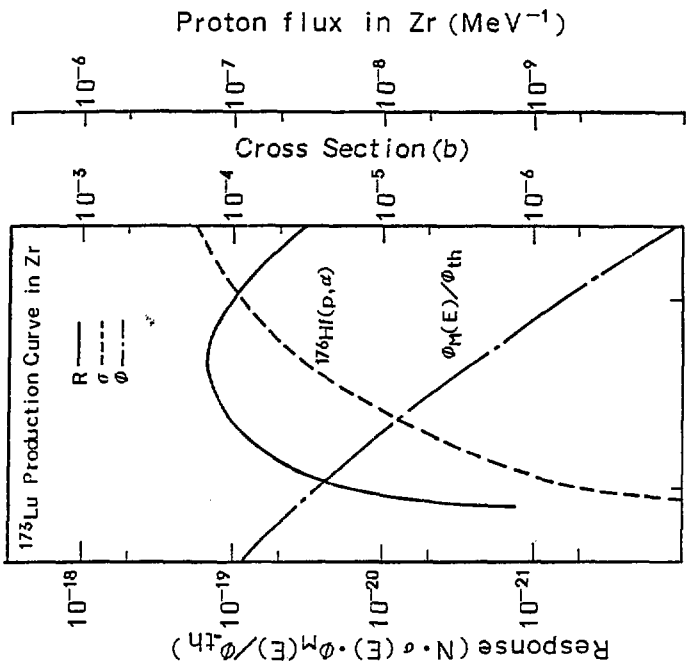

Fig.4 (a) Total response function for production of ^{91}Nb in zircaloy-2. Proton spectra and dominant contributing reaction cross sections are also depicted.

(b) Total response function for production of ^{173}Lu in zircaloy-2. Proton spectra and dominant contributing reaction cross section are also depicted.

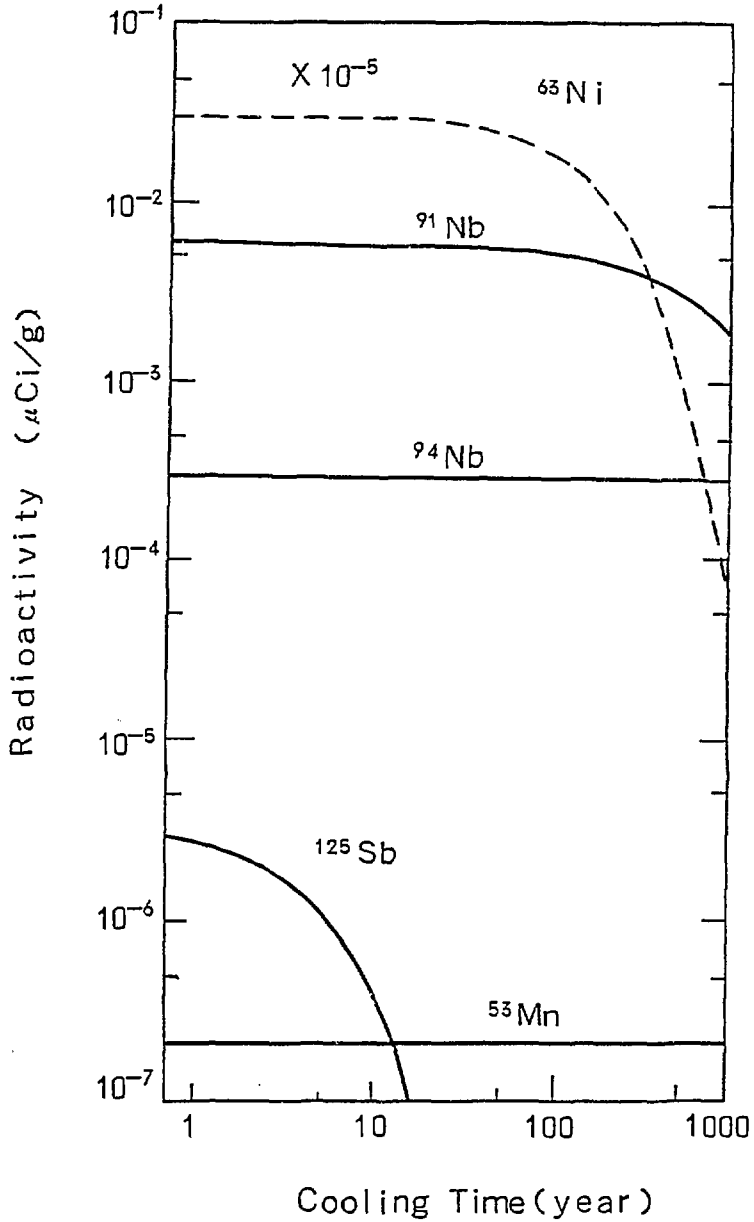

Fig.5 Proton induced radioactivities of main long-lived isotopes as a function of cooling time after irradiation of 40 years in BWR in comparison with neutron-induced ^{63}Ni activity.

3.3 Cross Section Measurement and Integral Test for Several Activation Reactions Using T+d and Thick-Li+d Sources

J. R. Dumais, S. Tanaka, N. Odano
S. Iwasaki, and K. Sugiyama
Department of Nuclear Engineering, Tohoku University
Aramaki-Aza-Aoba, Sendai 980, Japan

Recent activities on the area of the cross section measurement for several activation reactions at Department of Nucl. Eng., Tohoku Univ. are described. The first subject is the cross section measurement for (n,2n) reaction on aluminum using the RTNS-II neutron source. Cross sections with rather small error band were obtained for the incident neutron energies from 14 to 14.7 Mev. The second one is the status of the program for the integral experiments on several reactions using the thick Li+d source at Tohoku Fast Neutron Lab. The experimental results showed the usefullness of the source as a tool for the cross section assessment.

I. Introduction

In this paper, we will briefly describe our recent activities on the area of the cross section measurement for several activation reactions. The first subject is the cross section measurement for (n,2n) reaction on aluminum using the RTNS-II neutron source and the second one is the integral experiment for several reactions using the thick Li+d source.

II. Measurement of the Cross Section for $^{27}Al(n,2n)^{26}Al(T_{1/2}=7.16\times10^{5}Y)$ with Activation Technique around 14 Mev.

II-1 Introduction

As well known, the structural material activation is one of the

most important issues in the material development for the fusion energy[1]. Aluminum has been considered one of the low activation materials among the structural material candidates, because of the short lives of their main activities. However, the (n,2n) reaction on aluminum leaves the very long activity of about 10^6years. The cross section for this reaction has not been measured because of its long life and small cross section. Very recently, Smither et al.[2] of ANL, measured the cross section using the RTNS-II neutron source and accelerator mass spectroscopy technique. Sasao et al.[3] of PPRI, Nagoya University, also measured the cross section using activation technique at Oktavian of Osaka University. Their cross section data were smaller than those of an evaluated cross section file of the ENDF/B-IV by about factor of two or three, and also disagree with each other.

Aim of the resent papar is to obtain the highly reliable cross section data of the reaction than above two by using the maximum fluence irradiation condition among the experiments performed at RTNS-II.

II-2 Samples Preparation and Irradiation

According to the results of the previous experiments, we have chosen rathar large size of the aluminum samples. The aluminum disc samples of 2cm-diameter and 0.5cm-thickness were machined from the high purity aluminum metal ingot. The total 21 samples were grouped to make 7 sets by three samples, lapped by Kapton tape, and fixed on an aluminum arch frame. The samples with the frame were set beside the HEDL's material container with two-temperature furnace of the main irradiation experiment around the rotating target to span their angles from 25 to 85 deg. with respect to the incident deuteron beam. The main experiment was planed so that the samples would be irradiated upto the maximum fluence of $10^{19}(n/cm^2)$. The geometrical configuration of the present experiment is shown in Fig. 1.

Twenty-one iron dosimetry foils were inserted in front of

each aluminum disc to evaluate the neutron fluence on the sample through the irradiation term. In addition, seven sets of zirconium and niobium foils were attached in front of the each aluminum set to measure the average energies of the incident 14-MeV neutrons, using so called Zr-Nb ratio method, and were taken out after first 4-days of the irradiation.

The irradiation was continued from March 26 to November 3 of 1985. Through the term, the irradiation was stopped totally 41 times. The irradiation history was recorded by accumulating the output signals from the two calibrated proton recoil counters and two proportional counters in the target room into a computer system. These counters were checked and calibrated every month.

II-3 Activity Measurement

The irradiated samples were cooled for three months and then shipped to Tohoku University. Activity measurement was initiated after additional cooling for eight months using a 70cc Ge(Li) detector at Cyclotron Radio Isotope Center of the University. The distance of the samples from the surface of the detector was 20mm. The measurement times were about 75 to 120 hours per sample, and total peak counts of the 1809keV gamma-rays associated to the decay of the aluminum-26 were between 1500 and 6000. Many peaks of the gamma-rays from impurities in the samples were observed besides the natural back ground. However, there was no significant interference on the 1809KeV peak. One of the sample was remeasured at 100mm from the detector surface in order to certify the validity of the corrections applied on the 20mm-point measurments.

The activities of the iron dosimetry foils were also measured in the same detector system. The activities for the zirconium and niobium foils had already been measured at RTNS-II by using a 80cc HpGe detector in the two or three days after the taking-out the foils.

II-4 Fluence Determination

The determination of the fluence of the 14MeV neutrons were done as follows. The dosimetry reaction was the $^{54}Fe(n,p)^{54}Mn$ ($T_{1/2}$=312.2days). The cross section of this reaction was taken from the ENDF/B-V dosimtry file.

The half life of the residual nucleus was not so long enough to neglect the effect of the flux fluctuation during the irradiation. This effect was corrected using the data of the irradiation record previously mensioned.

In the present case, the most important correction on the fluence calculation is that on the effect of the scattered neutrons from the surrounding materials. The scattered neutron spectra have been estimated by simulating the scattering process taking account the neighbouring materials, such as, the rotating target copper disc, cooling water and the specimen container of the main experiment. The calculation was performed using a Monte-Carlo code, MCNP[4] with a NJOY[5] processed cross section set. In order to get the correction factors, the calculated flux at each smple position was multiplied by the cross section curve from the ENDF/B-V. The amount of the factors was ranging from 8 to 11%.

The neutron fluence of a given sample was simply calculated by averaging the two data for the front and back side dosimetry data of each sample. The average fluence was about 5×10^{16} (n/cm^2).

II-5 Mean Energies of the Irradiated Neutrons.

Because of the steep variation character of the cross section to be measured with the incident neutron energy, it is important to determine the mean energy of the source neutrons at each sample position, unambiguously. We have adopted the so called the method of zirconium-niobium reaction rate ratio[6].

The mean energies were calculated using a formula of Ref 6. of which coefficients were derived by a least squares fitting

method with a lot of reliable cross sections from 13.5 to 15MeV. The validity of the formula was confirmed[7] by them at various intense 14MeV neutron fields.

The present results are summarized in Table 1. In the calculation, the effect due to the scattered neutrons, similarly as mensioned in II-4 were also corrected by 0.5 to 3%.

II-6 Results and Discussion

The results for the cross secitions and energies are summarized in the Table 1. The cross section for each energy is given as an average of the two front side samples' data. Major corrections applied in deriving the cross sections, and not mensioned before were those on the sum-coincidence loss effect, on the gamma-ray self-absorption effect, on the finite solid angle in the measurement process of the gamma rays, and on the effect of the large variation of the energy width of the source neutrons with the emmission angles to the reaction rate of the steep cross section. The corrections for the sum-coincidence loss effect and finite solid angle were certified by comparing the experimental data for the sample remeasured at 10cm where these corrections were almost negligible.

The half life and gamma-ray branching ratio data of aluminum-26 with their errors (4.5 and 3.6%, respectively) were taken from Table of Isotopes[8].

Other main error sources of the cross section given in Table 1 are due to a statistical errors of peak areas (1-3%), the uncertainty of the gamma ray sources (2.5%) for efficiency calibration, the uncertainty of the neutron fluence (7%), and uncertainties due to the various corrections (5%). Total errors are 10.3 -11.1%.

The present results are compared with previous experiments and those given in the evaluated cross section files in Fig. 2. The present ones give the smallest error band among the experiments. Three experimental data differ by a factor of two or more above 14.4MeV. Both evaluations do not reproduce any

experimental data.

III. Integral Experment for Several Activation Cross Sections Using the Thick Li+d Neutron Source.

III-1 Introduction

Accessment of the activation (dosimetry) cross section has been done mainly by the integral experiment using fission neutron sources such as reactor fields and the Cf-252[9]. These integeral experiments played important roles for the establishment of the reactor dosimetry technique.

These neutron sources, however, are relatively low intensity in the high energy region, and also the uncertainty of the spectrum of the region is not small[10] even now. Therefore these neutron fields have some limitation in the cross section assessment of the reactions which have relatively high threshold energies.

In contrast to this, the neutron sources based on the accelerators have large advantage in the intensity of the high energy regions and the source spectra can be measured accurately by the time-of-flight technicque. Only the accelerator source have less stability of the spectra than fission sources. Greenwood et al[11] of ANL did the first integral experiment using thick-Be+d neutron source produced by the tandem-Dynamitron accelerator, and showed the usefullness of the source.

In the second subject, we report the status of the integral experiment program at the Tohoku University Fast Netron Laboratory (TUFNL). We have chosen the neutron source of the thick-Li+d reaction because the higher energy component of this reaction is stronger than the Be+d in the accelerated deuteron energy range by the single-ended Dynamitron.

III-2 Neutron Source

A thick lithium metal plate was melted on the copper backing plate by heating in the vacuum. Then the surface of the metal was coated by thin gold layer in order to prevent the oxidization of the lithium surface. The target plate was mounted on the end of the beam duct. The backing plate was cooled by air blow. The source neutron was produced by bombarding a deuteron beam of 2MeV on the target.

The angular distributon of the source neutron spectrum was measured from 0 to 25deg. by the time-of-flight technique using a 5inx 2in thick NE213 scintillator (main detector) set in a heavy shield-goniometer. Neutron fluence was monitored by two detector systems; one was a 2"x2" NE213 and the other a BF_3 counter.

The relative efficiency of the main detector was measured using a Cf-252 source from 0.4 to 5MeV. The efficiency was calculated by Monte-Carlo code, O5S[12] in the region from 2 to 20 MeV. The two efficiency curves were joined smoothly at 4 to 5MeV. Validiy of this curve was certified by the scattering cross section measurement for H(n,n)H [13] from 0.4 to 12MeV.

III-3 Irradiations

Irradiated samples were thin foils of Al, Ti, Fe, Ni, Zr, Nb, In, and Pb. The sample foils were tightly packed and set on a thin styroform bar in front of the target at 5cm in 0 deg. Two independent irradiation experiments were done according to the length of half lives. The souce neutrons were produced using a DC deuteron beam of 10micro-amp. Output of the monitor detectors were recorded in a MCS.

In the same arrangement, another irradiation experiment for aluminum using the T+d neutron source was made too in order to obtain the absolute flux of the neutrons at 15MeV at the irradiation position using the standard cross section of $^{27}Al(n,\alpha)^{24}Na$ reaction.

III-4 Activity Measurement

Gamma-ray measurement was made using a HPGe detector of 80cc at 11cm from the surface of the detector canning. The efficiency of the detector was calibrated by a set of standard source of their accuracy about 2.5%.

III-4 Result and Discussion

Average cross section is defined as follows,

$$\langle \sigma \rangle = \frac{\int \phi(E_n)\sigma(E_n)dE_n}{\int \phi(E_n)\,dE_n}$$

where $\phi(E_n)$ is the source neutron flux and $\sigma(E_n)$ is the cross section to be studied. The flux was measured by the experiment. In the calculation, the cross sections were taken from the evaluated nuclear data files. In the experiment, the numerator of above equation is replaced by the reaction rate. Absolute value of the average cross section is not so important, and usually the ratio between the experiment to the calculation (E/C) is discussed.

Obtained results for Al, Fe and Ni are summarized in Table 3. The cross sections were taken from three data files; ENDF/B-V dosimetry file[14,15,16], and JENDL-3T*,[17]. In Fig. 3,the measured neutron flux at zero deg. and cross sections for ^{27}Al (n,α) ^{24}Na taken from both cross section files. The error analysis of the present experiment have not been completed, however, the preliminary error band is estimated to be about 5-8%. The ENDF/B-V cross sections are in good agreement with the present experiment, whereas the JENDL-3T file shows some discrepancy. As shown in Fig. 3, the source neutron spctrum show a broad peak from 8 to 15MeV where the above cross sections have maximum responces. Therefore the discrepancy of the JENDL-3T file means the existence of inadequate cross sections in the energy region.

As seen above, the present technique with the thick Li+d neutron source produced by the Dynamitron showed very useful tool for the dosimetry cross section assessment, especially for the reactions with high threshold energies.

---

*) JENDL-3T is a temporary file for testing the evaluated data which are for JENDL-3. The data in JENDL-3T will be partly revised in JENDL-3.

References

1) E.T. Cheng, et al., GA-A17754/UC-20, GA Technologies (1984).
2) R.K. Smither and L.R. Greenwood, J. Nucl. Mat., 122&123 1071 (1984).
3) M. Sasao et al., IPPJ-805, Inst. Plasma Phys., Nagoya Univ. (1987).
4) "MCNP-A General Monte Carlo Code for Neutron and Photon Transport," Los Alamos Laboratory report LA-7396-M, Revised (Nov. 1979).
5) R.E. MacFarlane, et al., "The NJOY Nuclear Data Processing System, Vol I: User's Manual," Los Alamos National Laboratory report LA-9303-M (ENDF-324) (May 1982).
6) M. Nakazawa et al., JAERI-M 86-080, P116 (1986).
7) M. Nakazawa et al., 1985 Ann. Res. Rep. Jap. Contri. for Japan-US Collab. on RTNS-II Util., Monbusho (1986).
8) C.M. Lederer and V.S. Shirley, Ed., Table of Isotopes, 7th. ed., John Willey & Sons, Inc. (1978).
9) Proc. of a Consultants' Meeting on Integral Cross Section Measurements in Standard Neutron Fields for Reactor Dosimetry, Vienna, 15-19 Nov., 1976, IAEA-208 (IAEA Vienna 1978).
10) Proc. IAEA Consult. Meet. on The U-235 Fast-Neutron Fissionn Cross Section, and the Cf-252 Fission Neutron Spectrum, INDC(NDS)-146, Smolenice, (July 1983).
11) L.R.Greenwood et al., Nucl. Tech., vol. 41 p109 (1978).
12) R.E. Textor and V.V. Vervinsky, ORNL-4160, ORNL (1968).
13) L. Stewart, R.J. LaBauve and P.G. Young, ENDF/B-V Cross Section Measurement Standards, A.D.Carlson and M.R.Bhat Ed., BNL-NCS-51619/ENDF-301 (BNL Upton 1982).
14) P.G. Young and D.G. Foster, Jr., ENDF/B-V Dosimetry Cross Section file,(1977).
15) C.Y. Fu, ibid.(1978).
16) M. Divadeenam, ibid. (1977).
17) JENDL Compilation Group (Nuclear Data Center, JAERI): JENDL-3T, private communication (1987).

Table 1 Present results of the cross sections for the $^{27}Al(n,2n)^{26}Al$ reaction around 14 MeV.

average incident energy (MeV)			cross section (mb)		
14.08	±	0.04	11.6	±	1.2
14.16	±	0.05	14.3	±	1.5
14.32	±	0.07	21.4	±	2.2
14.37	±	0.07	27.8	±	2.9
14.47	±	0.08	32.0	±	3.4
14.56	±	0.10	36.1	±	3.9
14.68	±	0.11	40.6	±	4.5

Table 2 The average cross sections for $^{27}Al(n,\alpha)^{24}Na$, $^{56}Fe(n,p)^{56}Mn$ and $^{58}Ni(n,p)^{58}Co$ reactions in the thick-Li+d neutron source field compared with calculations using two evaluated cross section files, ENDF/B-V and JENDL-3T.

Reaction		Average CS (b) Calc.	Exp.	Ratio (C/E)
$^{27}Al(n,\alpha)^{24}Na$	ENDF/B-V	4.15(-2)	4.04(-2)	1.03
			4.12(-2)	1.01
	JENDL-3T	4.35(-2)	"	1.08
			"	1.05
$^{56}Fe(n,p)^{56}Mn$	ENDF/B-V	3.67(-2)	3.76(-2)	0.97
	JENDL-3T	3.77(-2)	"	1.00
$^{58}Ni(n,p)^{58}Co$	ENDF/B-V	0.303	0.312	0.97
	JENDL-3T	0.284	"	0.91

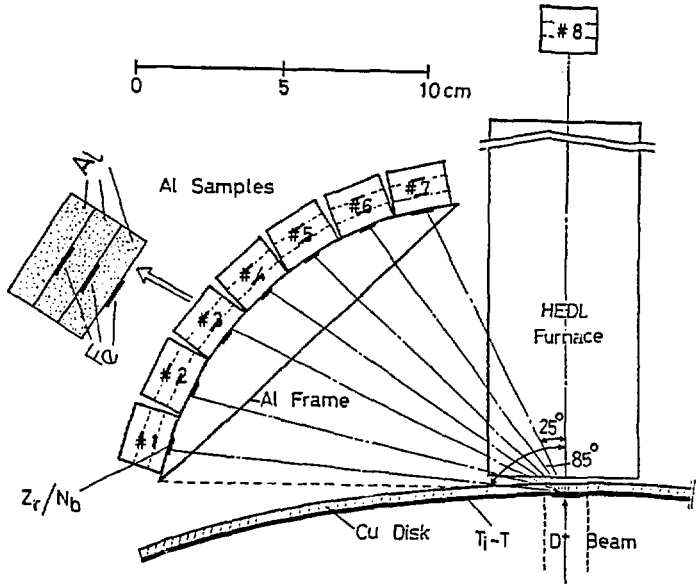

Fig. 1 Experimental set up of the present irradiation.

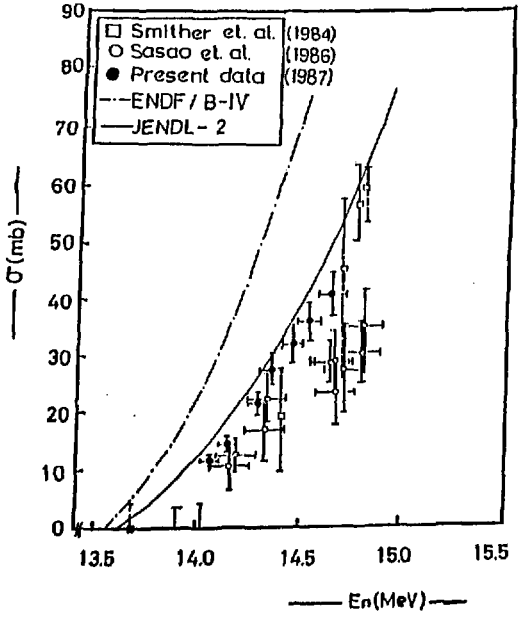

Fig. 2 Comparison of the experimental and evaluated data for the $^{27}Al(n,2n)^{26}Al$ reaction cross section around 14MeV.

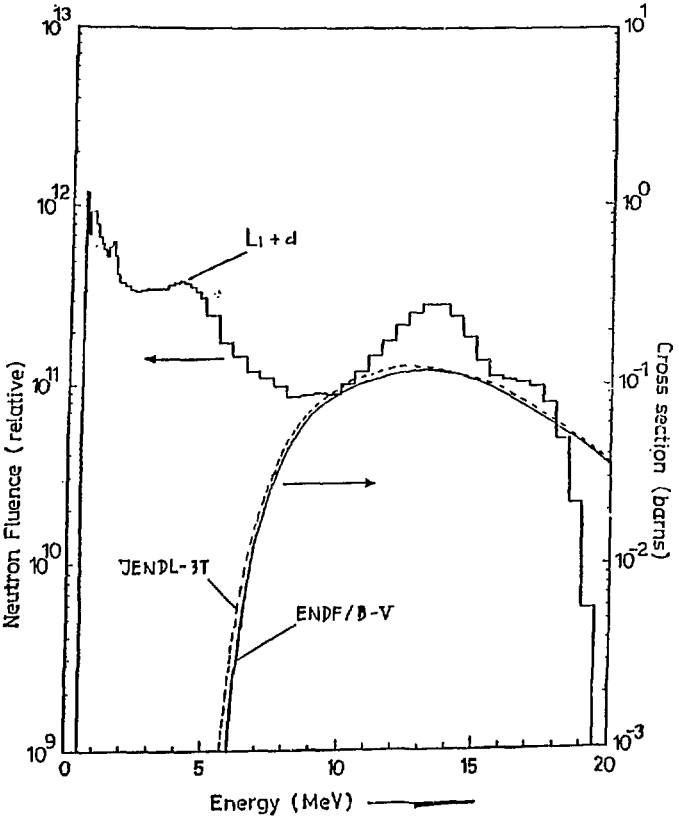

Fig. 3 The thick-Li+d source spectrum and cross section curve for $^{27}Al(n,\alpha)^{24}Na$ reaction.

3.4 Measurements of Fast Neutron Induced Fission Cross Sections of Actinide Nuclides

T.Iwasaki, Y.Karino, F.Manabe, M.Baba, S.Matsuyama and N.Hirakawa
Department of Nuclear Engineering, Tohoku University

A short introduction is given for recent works on fission cross section measurements at Tohoku University. The technical developments and the measurements using the techniques are described for

1. absolute fission cross sections of ^{235}U, and
2. fission cross section ratio of ^{233}U and $^{239,240,242}Pu$ relative to ^{235}U

1. Introduction

The neutron induced fission cross sections are the basic nuclear data for reactor design and assessment of nuclear fuel cycle including nuclear transmutation system. At present, however, there existing marked disagreement between the experimental data even for the major nuclides of uranium and plutonium isotopes.

A series of measurements of fast neutron induced fission cross sections has been conducted for variety of actinide at Dynamitron facility of Tohoku university. Previous studies and results have been reported in ref.1 to 3. In these years, the measurements are in progress for absolute fission cross section of ^{235}U [3] and fission cross section ratio of ^{233}U [4] and plutonium isotopes relative to ^{235}U. This report describes the experimental method and results thus far obtained.

2. Fission cross section measurement of ^{235}U [3]

Among the current techniques for absolute fission cross section measurements, the time-correlated associated particle (TCAP) method is the most reliable one. This technique, however, is applicable only in limited energy region around 14 and 3 MeV. Thus, we adopted a technique of fission rate measurements relative to hydrogen scattering cross sections using a

recoil-proton counter that has been calibrated with the TCAP method. As shown in Fig.1, the counter system is composed of an ionization fission chamber and a recoil-proton counter-telescope coupled in back to back form and is enclosed in a thin walled housing. This configuration enables determining the neutron fluence on fission foil with minimal uncertainty. The recoiled protons are detected through three-hold coincidence among the signals from two proportional counters and a CsI(Tl) scintillator with sufficient signal to background ratio.

The neutron sensitivity of the recoil-proton counter was calibrated for 14.7 MeV neutrons using the TCAP method for d-T reaction; the counter-telescope was irradiated with the neutron flux whose intensity and spatial distribution were defined tightly by the associated alpha particles which were detected by a silicon surface-barrier detector. Fig.2 and 3 show the experimental arrangement and measured neutron cone, respectively. The use of a virgin Ti-T target eliminated the background events due to the D(d,p) and ^{3}He(d,p) reactions. The measured neutron sensitivity of the counter, corrected for the effects of neutron attenuation, countloss of protons due to scattering by counter wire and counter gas and for radiator-out backgrounds, was in agreement within 1% with the calculated one on the basis of analytical formula by Bame et al.[5] (Fig.4); this fact proved the validity of the method in experiment and data analyses, and applicability of the counter-telescope to reliable neutron fluence determination.

The fission cross section measurements were carried out for five energy points from 13.5 to 14.9 MeV, using the primary neutrons obtained by the T(d,n) reaction at the emission angles between 0- to 135-deg. relative to the incident beam. The measured fission rate data were corrected for the effects of 1) room returned neutrons which was measured by shadowing the direct beam, 2) pulse height bias, 3) anisotropy and kinematic effects of fission fragments, and 4) neutron attenuation and multiple scattering. The overall experimental uncertainty was estimated to be 2.5 to 2.8%.

The result is shown in Fig.5, compared with the evaluated and other experimental data. The present result is in good agreement in magnitude with that by Wasson et al.[6] using the TCAP method, and in energy dependence with the white neutron measurements by Czirr and Sidhu[7].

3. Fission cross section ratio of ^{233}U and ^{239,240,242}Pu relative to ^{235}U

The fission cross section ratio were measured at hundred keV region for

^{233}U and 0.7 to 7 MeV for plutonium isotopes. The experimental method[1,2] was upgraded to reduce the background caused by room-returned neutrons and alpha-particles which is serious for these nuclei. The timing resolution of the back to back fission chamber was improved to 5 - 10 nano-second in FWHM, by optimizing the closer electrode spacing (6mm) and adopting the fast timing electronics. The electrode spacing was chosen as the compromise between the timing and pulse height resolution. This improved timing resolution enables the measurements in time-of-flight (TOF) method for background reduction. By using the dual parameter data storage, pulse height versus TOF, the background due to room-returned neutrons, alpha-particles and spontaneous fission, was drastically reduced and could be determined from the foreground data. Figure 6 illustrates typical examples of the spectrum for TOF and pulse height distribution.

The fission rate measurements were carried out using the monc-energy neutrons produced via the Li(p,n), T(p,n), D(d,n) reactions employing LiF, tritium-titanium and deuterium gas targets, respectively. The background due to the $^{7}Li(p,n)^{7}Be^{*}$ reaction was evaluated by the calculation. For the D(d,n) reaction, the measurements with the deuterium gas replaced with hydrogen gas were also performed to remove the backgrounds due to parasitic neutrons produced via the C(d,n) and O(d,n) reactions. In each neutron energy, two measurements were done with the chamber turned by 180-deg.[1,2]. The fission cross section ratio was derived from the geometric average of two measurements to cancel out the effects of fission fragment anisotropy and flux attenuation[1,2]. In addition, the data were extrapolated to zero pulse height and corrected for the effects of 1) sample impurity, 2) self-absorption of fission fragments, 3) neutron scattering in target and chamber,and for 4) nonuniformity of fission layer. The experimental uncertainty was evaluated considering the correlation among the error sources and are presented in the form of covariance matrix.

The results for ^{233}U and ^{242}Pu are presented in Fig.7 and 8, together with the evaluated and other experimental data. The data analyses for ^{239}Pu and ^{240}Pu are now in progress. The present results for ^{233}U are higher by several % than both evaluation, JENDL-2 and ENDF/B-IV, but agree with the experimental values by Meadows[8] and Carlson & Behrens[9], while the latter are slightly lower. For ^{242}Pu, the present results are in general agreement with other experiments and JENDL-2 evaluation; however, the present values are slightly higher than JENDL-2 around 1 MeV and above 5 MeV.

The fission samples were provided by JAERI through the cooperative study between the universities and JAERI.

References

1. K.Kanda et al., J.Nucl.Sci.Technol., 24(6) 423 (1987)
2. K.Kanda et al., Radiation Effects 92~96 569(1986)
3. Y.Karino et al., NETU-49 (Department of Nuclear Engineering, Tohoku Univ.) pp.76 (1987)
4. F.Manabe et al., ibid., pp.64, and to be published in Technol. Report, Tohoku University
5. S.J.Bame et al., Rev.Sci.Instr.,28 997(1975)
6. O.A.Wasson et al., Nucl.Sci,Eng.,81 196(1982)
7. J.B.Czirr and G.S.Sidhu, Nucl.Sci.Eng.,57 18(1975)
8. J.W.Meadows, Nucl.Sci.Eng., 54 317(1978)
9. G.W.Carlson and J.W.Behrens, Nucl.Sci.Eng.,66 205(1978)

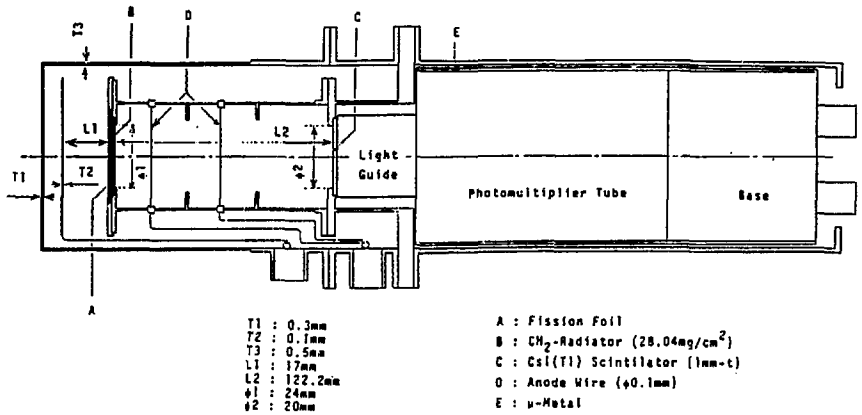

Fig.1 Schematic view of fission chamber and counter-telescope system.

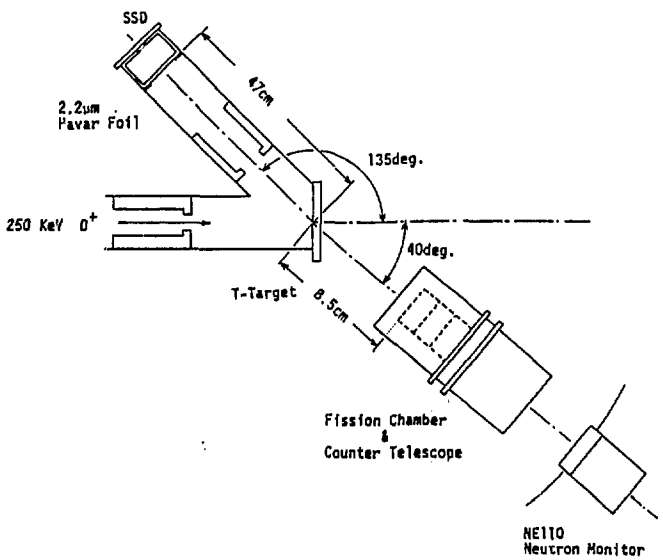

Fig.2 Experimental arrangement for counter telescope calibration.

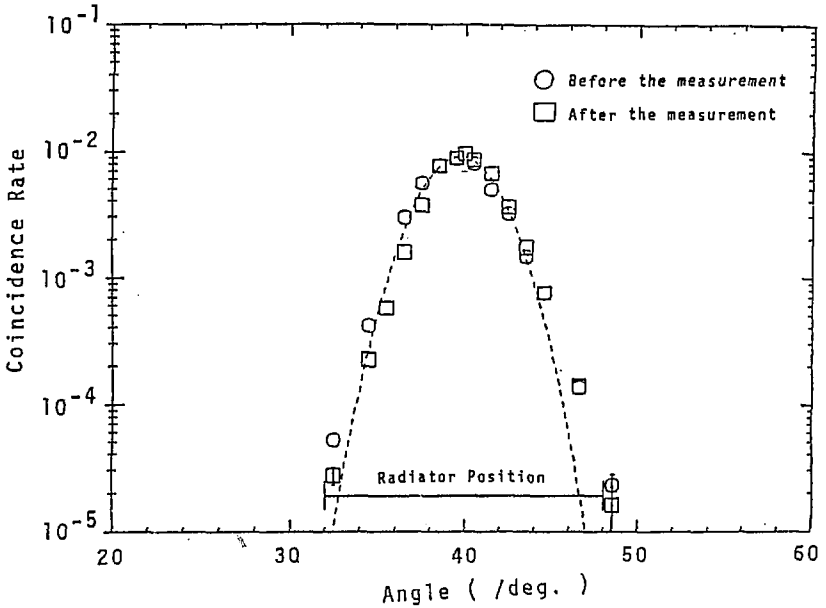

Fig.3 Neutron beam profile for telescope calibration.

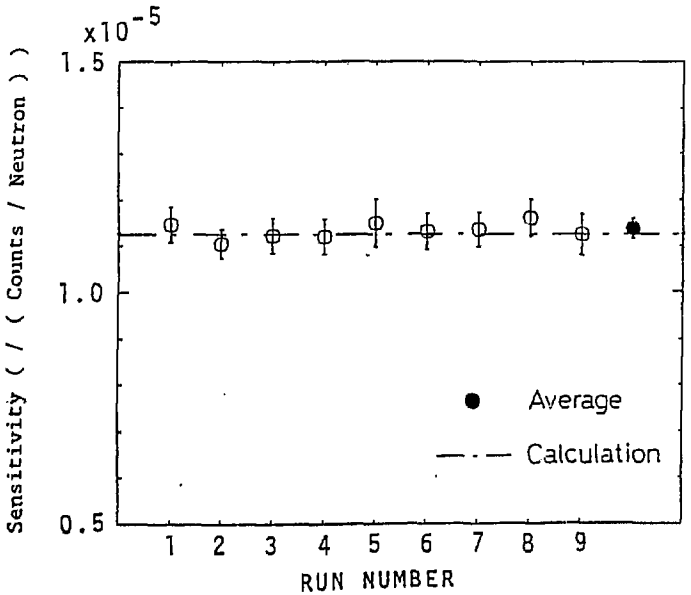

Fig.4 Neutron sensitivity of the counter-telescope.

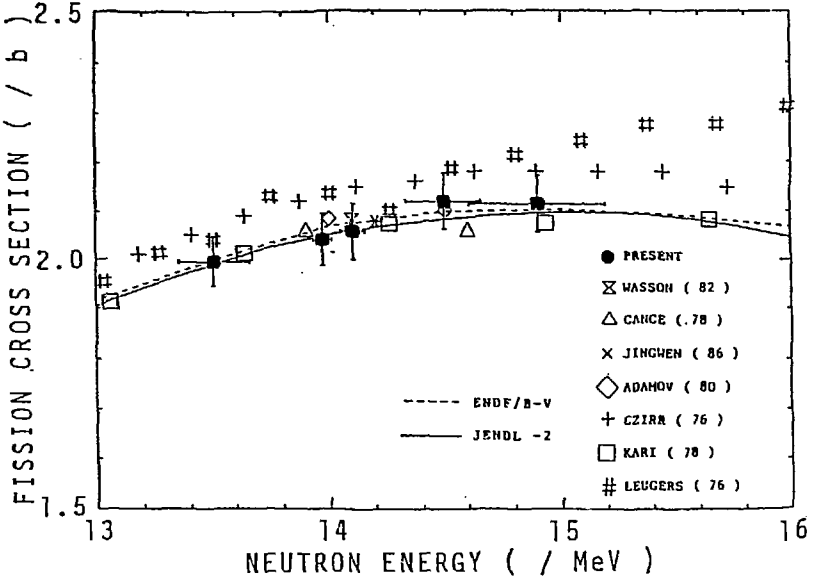

Fig.5 Fission cross section of ^{235}U around 14 MeV.

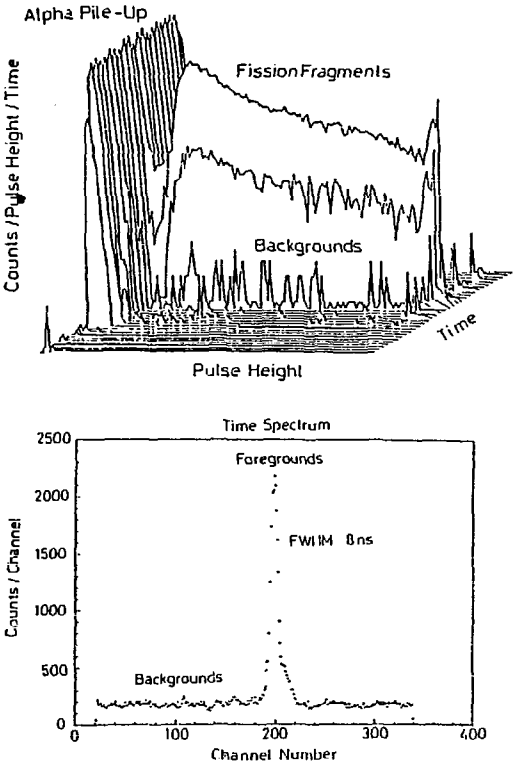

Fig.6 TOF and Pulse height distribution of the fission chamber.

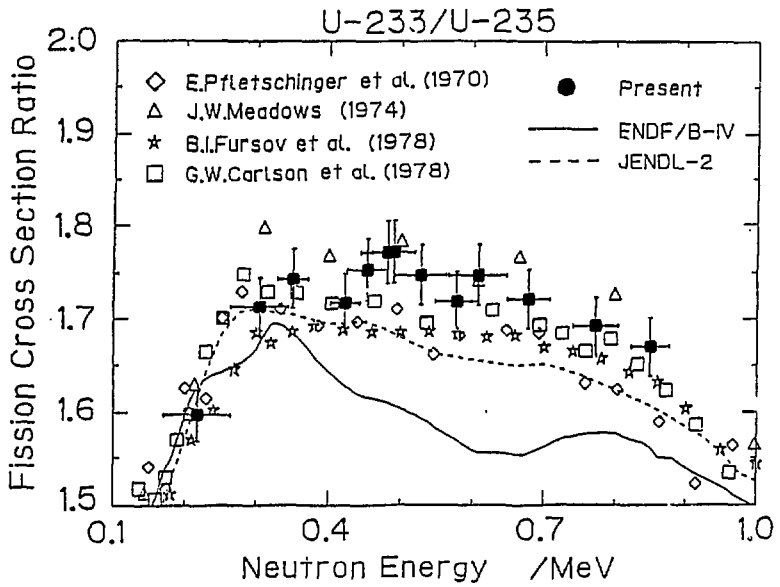

Fig.7 Fission cross section ratio of ^{233}U to ^{235}U.

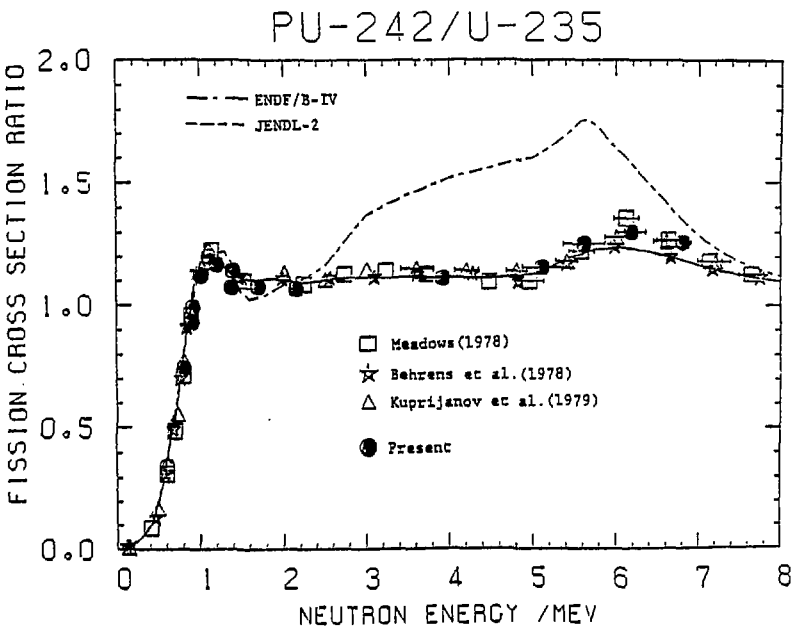

Fig.8 Fission cross section ratio of ^{242}Pu to ^{235}U.

3.5 Measurements of Double-differential Neutron Emission Cross Sections

M.Baba, M.Ishikawa, T.Kikuchi, H.Wakabayashi and N.Hirakawa
Department of Nuclear Engineering, Tohoku University

A brief description is presented on recent works of double-differential neutron emission cross sections measurements at Tohoku university Dynamitron accelerator facility. Typical results of measurements and analyses are shown as well as the method of experiment and data analyses.

1. Introduction

We have been carrying out a series of double-differential neutron emission cross sections (DDX) measurements at 14 and 18 MeV for fusion reactor materials using Tohoku university Dynamitron T-O-F spectrometer[1-3]. The neutron DDX data are of importance not only as the practical data but also as the reference data for the evaluation of high energy neutron cross sections. Therefore, the 18 MeV data will be of interest as well since the experimental data on neutron reactions are very scant above 15 MeV.

Recently we have measured the DDX for beryllium, carbon, oxygen, vanadium, manganese and zirconium at 14.1 MeV, and for beryllium, carbon, oxygen, aluminum, copper and zirconium at 18 MeV. The measurements for beryllium, carbon and oxygen were performed again to check and improve the data quality of our previous measurements[3,4] by employing better energy resolution and refined data analyses method. The measured results are compared with the current evaluation and with model calculations based on the multi-particle decay scheme for beryllium and carbon, and Kalbach-Mann systematics[4] for medium weight nuclides.

2. Experiments and Data Analyses

The experiments have have been performed using the primary neutrons produced via the T(d,n) reaction with a solid tritium target at the emission angles of 90- or 97.5-deg. and 0-deg. for 14.1 and 18 MeV measurements respectively. The target is contained in a thin walled chamber to reduce the neutron degradation. A NE213 liquid scintillator, 14 cm in dia. and 10 cm

thick, was used to detect secondary neutrons adopting two bias technique. The detector was housed in a massive shield and rotated around the scattering samples to vary the scattering angle. The flight path length was chosen between 4 and 7 m depending on the energy resolution required. The scattering samples were right cylinders, 2 to 3.5 cm in dia. and 4 to 5 cm long. The powder samples of MnO_2 and Al_2O_3, which were used to obtain oxygen data, were canned in aluminum cans with 0.3 mm wall thickness. The measurements were made at 7 to 12 laboratory angles and for secondary neutrons above 0.4 MeV. An iron sample was measured occasionally during the experiments as the standard reference to check the experimental system.

The raw data were corrected for 1) sample-out background, 2) detector efficiency, 3) background due to parasitic and degraded neutrons, and for 4) sample size effects. The corrections 3) and 4) were made concurrently by use of Monte-Carlo simulation on the basis of evaluated nuclear data. In the cases that the evaluated data were unacceptably discrepant from the measured one, the neutron emission data were revised to be consistent with the experimental results.

From the DDX obtained, partial cross sections were extracted for elastic and discrete inelastic scattering processes. The angular distribution of continuum neutrons and angle integrated energy spectra were derived as well for nuclei heavier than aluminum.

3. Results and Discussion

Here presented are only the typical results and more details will be published later.

Figure 1 presents the DDX results for beryllium at 14.1 MeV, compared with the evaluated values. The present results are in fair agreement with those at LANL by Drake et al.[5] at higher energy region, but are substantially lower at the energy range below a few MeV, and result in smaller value in (n,2n) cross section by about 15%. The present results are generally consistent with those at OKTAVIAN[6] in DDXs and (n,2n) cross section. On the other hand, as seen from Fig.1, the DDX derived from JENDL-3T[7]* differs substantially from the experimental data in both spectral shape and anglular dependence. It is noted that the discrete levels observed

---

* JENDL-3T is a temporary file for testing the evaluated data for JENDL-3. The data in JENDL-3T may be partly revised in JENDL-3.

experimentally are much less than assumed in the evaluation; this fact suggests the importance of simultaneous break up process in the neutron emission. Therefore, we tried a model calculations by assuming the contribution of simultaneous four-body break up process as well as the sequential decays from the excited 2.43, 4.6, and 6.7 MeV levels and $^{6}He^{*}$ nuclide. As shown in Fig.2, the presently calculated DDXs trace the measured ones fairly well. The present results for cross sections of the elastic scattering and 2.43 MeV level excitation are in agreement with the evaluation.

Figure 3 shows the DDX for carbon at 14.1 MeV. The present values of partial cross sections are in good agreement with our previous ones[3,4] except for those of the second level and neutron continuum. The alpha production cross section is about 30 % lower than previous one as a result of considering the background due to degraded neutrons. The present lower value is close to other recent measurements.[6,8] In the low energy continuum part, systematic differences are observed among the experimental and evaluated data, while the experimental data are not so definitive because of smaller cross sections. As in the case of beryllium, the four-body phase space distribution shown by the solid line in the figure reproduces fairly well the spectral shape and angular dependence.

In Fig.4 illustrated are the DDXs of oxygen at 14 MeV. General agreement is seen between the experiment and evaluation. However, the present data for the inelastic scattering cross section of 8.8 MeV level is much lower than JENDL-3T and close to ENDF/B-IV.

Figure 5 and 6 show the DDX and neutron angular distribution for vanadium and manganese. The experimental data show marked angle dependence and are not followed by the evaluated data at higher energy region where the pre-compound and/or direct process dominates the neuron emission; such a trend is seen generally for medium-weight and heavy nuclei but is not reproduced so well by the theoretical calculations[9].

Therefore, the angular distribution of these continuum neutrons were compared with that expected from Kalbach-Mann systematics[4] which will be convenient for practical purposes. The pre-compound ratio necessary for the calculation, was found from the fitting of the angle integrated neutron spectra with the superposition of evaporation and exciton spectrum. The results of the fitting and calculated angular distributions are shown in Fig.7,8,9 for aluminum, iron and zirconium. The angular distributions are

reproduced fairly well in whole the energy region, except for the high energy region where direct process will have certain contribution. The comparison will be extended to other nuclei measured in this study including 18 MeV results.

References

1. M.Baba et al., Proc.Int.Conf.Nuclear Data (Harwell,1978) pp.198
2. S.Chiba et al., J.Nucl.Sci.Technol.,22 10 (1985)
3. M.Baba et al., Radiation Effects 92-96 223(1986) and JAERI-M 86-029 (1986) pp.119
4. C.Kalbach and F.M.Mann, Phys. Rev.,C23 112(1981)
5. D.M.Drake et al., Nucl.Sci.Eng., 63 401(1977)
6. A.Takahashi et al., OKTAVIAN REPORT A-87-03 and JAERI-M 86-080(1986) pp.191
7. JENDL Compilation Group (Nuclear Data Center, JAERI); JENDL-3T, private communication
8. B.Antolkovic et al., Proc.Int.Con.Neutron Physics.,(Dubrovnik 1986) pp.137
9. P.E.Hodgson et al., Radiation Effects 92-96 1033(1986)

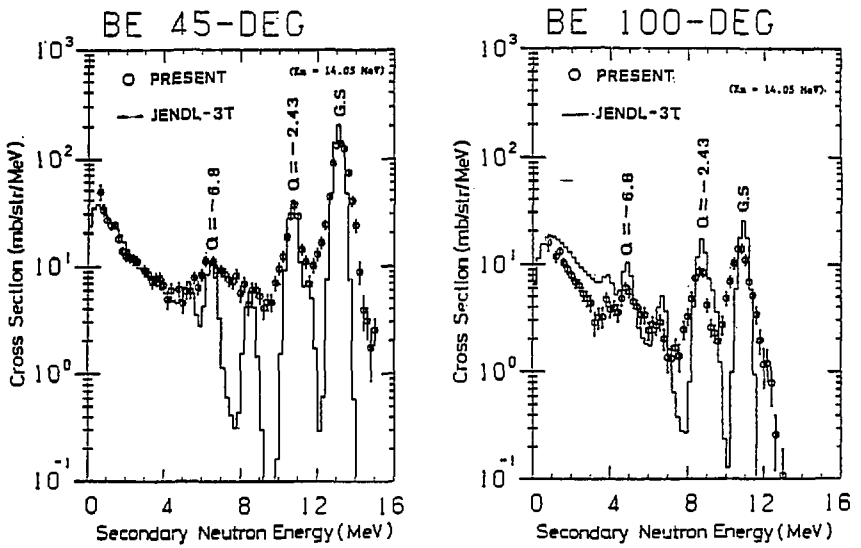

Fig.1 Beryllium DDX for 14.1 MeV neutrons. The present results are compared with the Those derived from JENDL-3T.

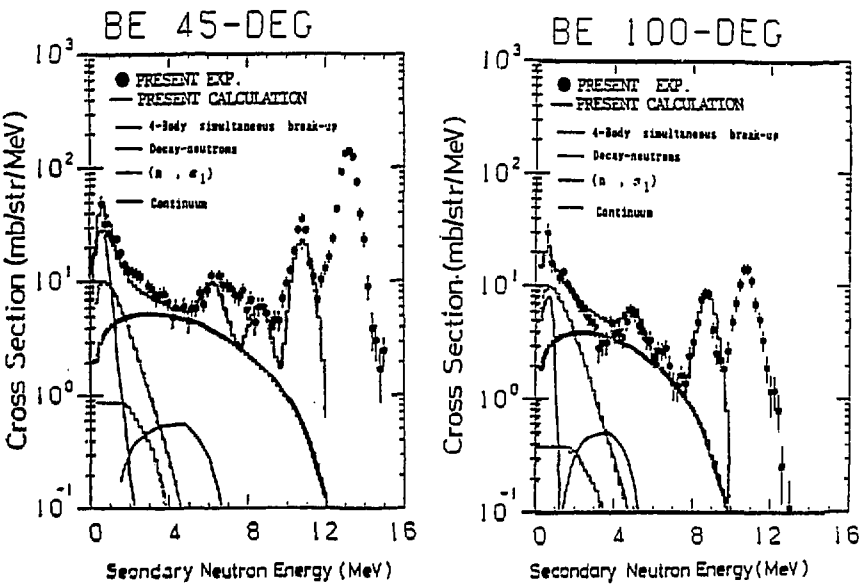

Fig.2 Beryllium DDX for 14.1 MeV neutrons. The experimental data are compared with the present calculation.

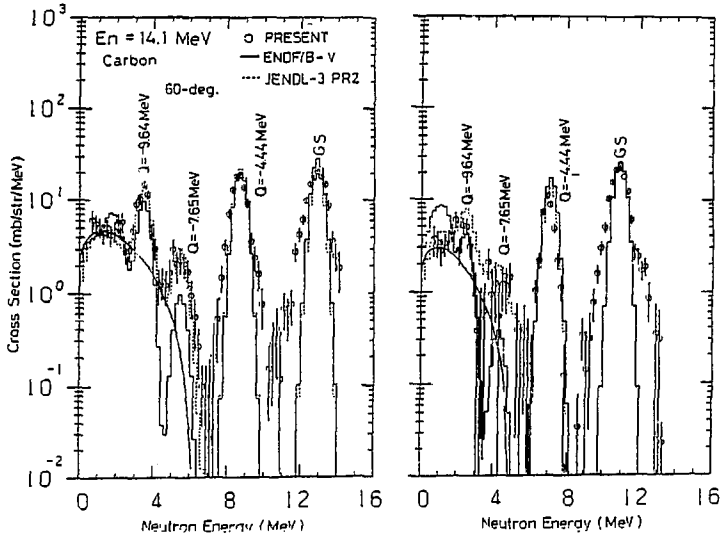

Fig.3 Carbon DDX for 14.1 MeV neutrons. The present results are compared with the evaluated data. The solid line shows the 4-body phase space in the laboratory system.

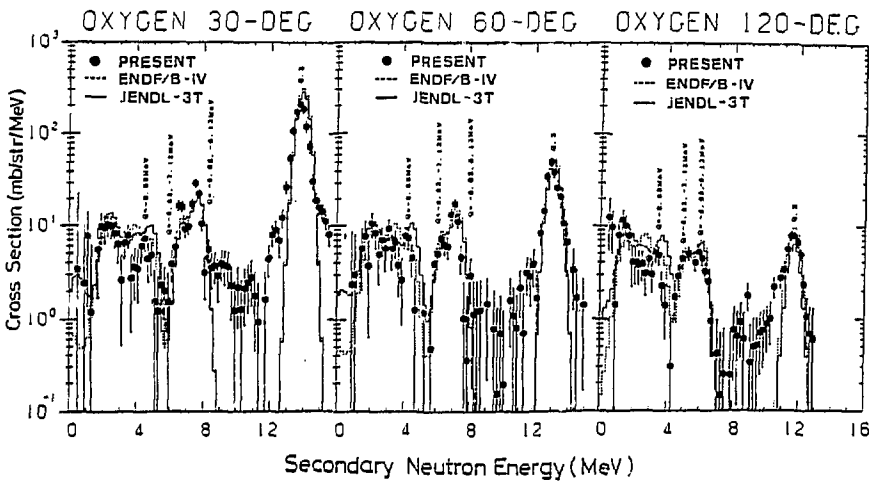

Fig.4 Oxygen DDX for 14.1 MeV neutrons. The present data are compared with the evaluated data.

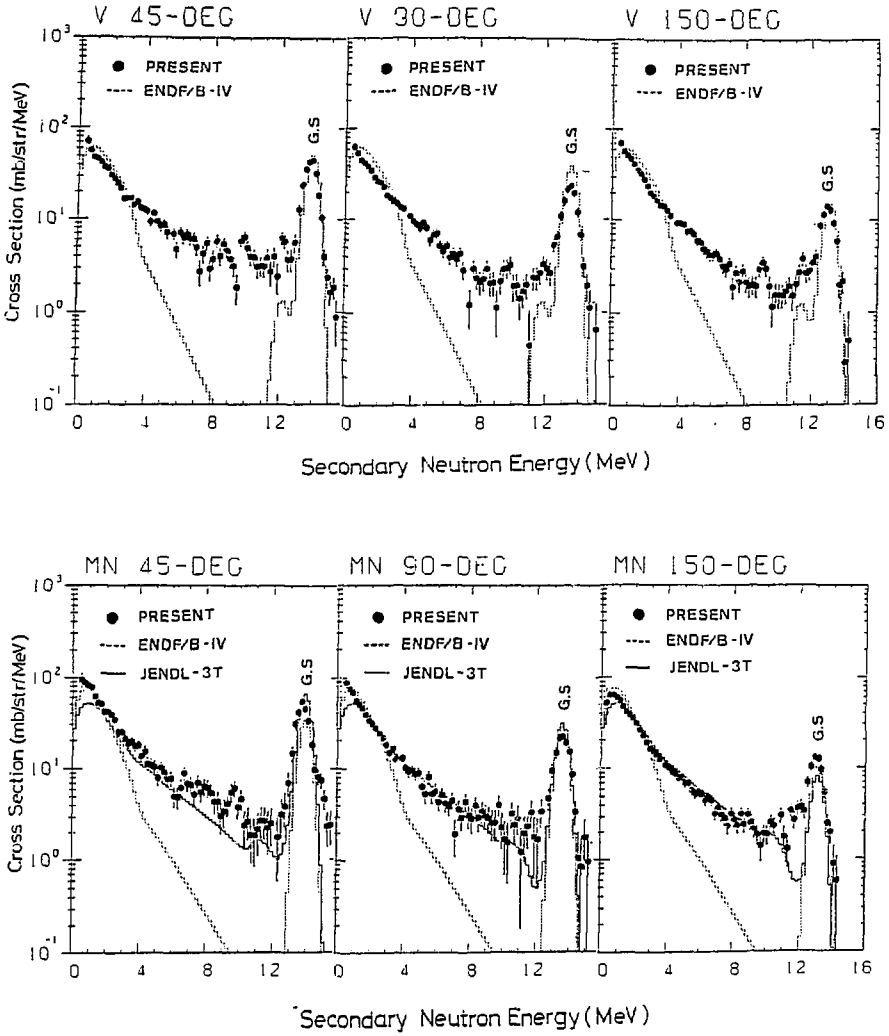

Fig.5 Double-differential neutron emission cross sections of vanadium and manganese at 14.1 MeV.

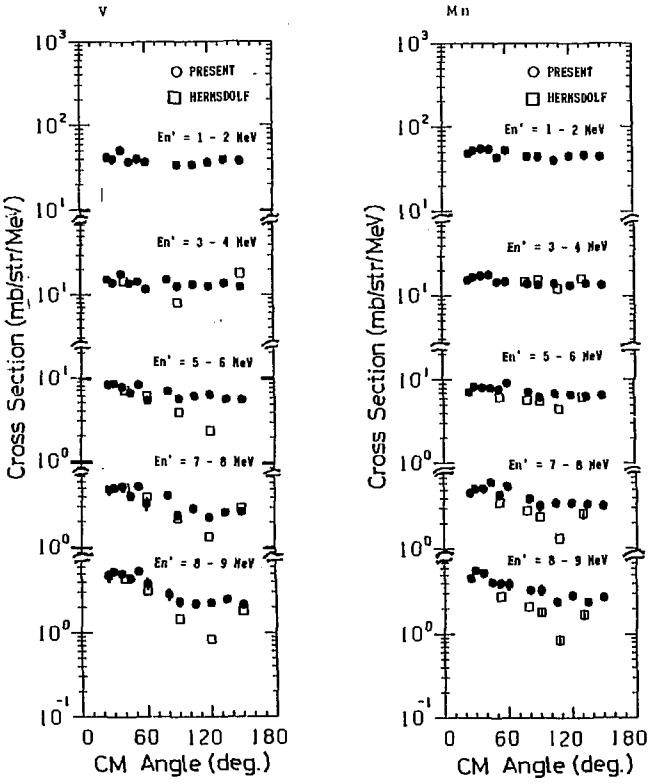

Fig.6 Angular distributions of emission neutrons of vanadium and manganese at 14.1 MeV

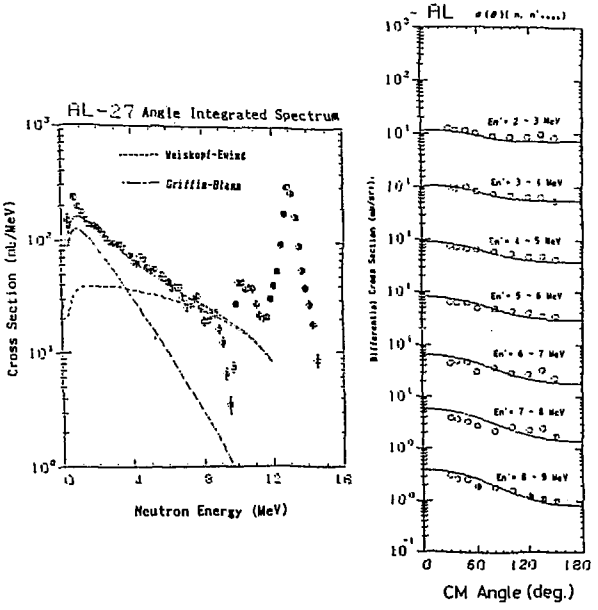

Fig.7 Angle integrated neutron spectrum (left) and angular distributions of emission neurons for aluminum at 14.1 MeV incident energy.

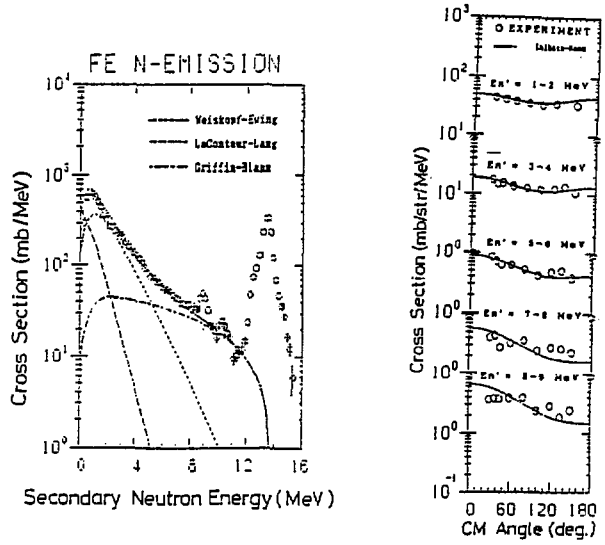

Fig.8 Angle integrated neutron emission spectrum (left) and angular distribution of emission neutrons (right) for iron at 14.1 MeV incident energy.

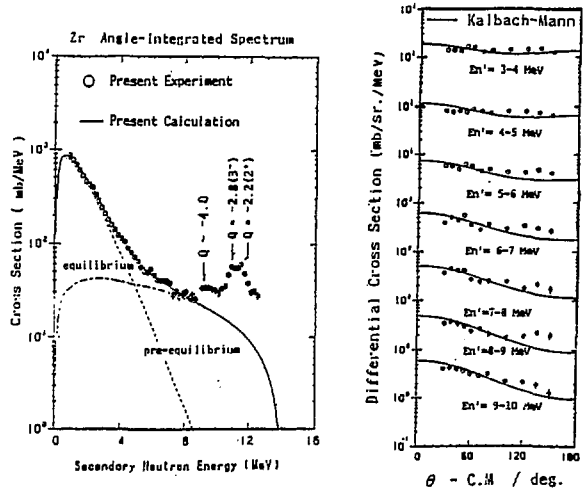

Fig.9 Angle integrated neutron emission spectrum (left) and angular distribution of emission neutrons (right) for zirconium at 14.1 MeV incident energy.

3.6 Differential Cross Sections for Gamma-Ray Production by 14 MeV Neutrons

Junji Yamamoto, Isao Murata, Akito Takahashi and Kenji Sumita

Department of Nuclear Engineering, Osaka University
2-1 Yamada-oka, Suita, Osaka 565, Japan

Gamma-ray production cross sections were measured for (n,xγ) reactions by 14 MeV neutrons using the D-T neutron source OKTAVIAN of Osaka University. Energy differential cross sections are given for five samples of aluminum, silicon, chromium, iron and nickel over the energy region from 0.5 to 10 MeV. Angular distribution of discrete gamma-rays is also presented for 4.44 MeV gamma-rays from (n,n') reaction in ^{12}C. Measured cross sections were compared with the differential data evaluated in currently used nuclear data files of JENDL-3T and ENDF/B-IV.

1. Introduction

Nuclear data for gamma-rays produced by interactions of high energy neutrons around 14 MeV are one of the important data in the desigh work of D-T fusion reactors. The present work has been initiated to accumulate the differential data for gamma-rays emitted from 14 MeV neutron induced-reactions with elements in structural materials and to check the gamma-ray production data in current nuclear data files.

The experimental program consists of two types of cross section measurements: (a) to obtain the energy differential cross sections and (b) to provide the production cross sections of discrete gamma-rays from individual reactions of (n,n'), (n,n'p), (n,2n) and so on. The secondary gamma-ray spectra have been observed at three angular points at most in forward and backward scattering angles, since the energy spectra have not in general so sharp angular dependence as those of secondary neutrons from non-elastic scattering by 14 MeV neutrons. A large NaI crystal was used as a spectrometer to cover the energy range from 0.5 to 10 MeV with good counting statistics. To obtain the production cross sections of discrete gamma-rays, angular distributions were measured by a Ge detector with high energy-resolution. In this paper, some results of the energy differential cross sections are presented for the elements of aluminum, silicon,

chromium, iron and nickel. The present data were compared with the evaluations in two nuclear data files of JENDL-3T[1] * and ENDF/B-IV[2].

2. Experimental method and data reduction

An experimental method was a conventional one. Energies of gamma-rays emitted from a sample material were analyzed with an NaI crystal. Time-of-flight technique using a pulsed neutron source was applied to the discrimination of the desired prompt gamma-rays from the neutron background. Figure 1 shows a schematic of the experimental layout. The NaI detector of 5" in diameter and 5" in length was surrounded by a lead-block shield with additional shield of boron carbide, paraffin and heavy concrete to eliminate the neutron background. In order to suppress Compton component on a pulse height spectrum in the detector, the incident photons were collimated within 7.2 cm in diameter by the lead blocks. The ratio of a full energy peak to a Compton component was 11.3 for 6.1 MeV gamma-ray with the collimator and 5.8 without one.

Samples were either disks of 10 cm in diameter or squares of 10 cm by 10 cm with thickness of 5 to 10 mm. As shown in Fig.1, the plate sample was placed at the angles between incident neutrons and emitted photons of 45, 90, 125 and 135 degrees. The measurement of angular dependences of discrete gamma-rays has been also made at several angles of 30 to 135 degree using the NaI detector. The samples in this measurement were hollow cylinders of 1.4 cm inner diameter x 4.0 cm outer diameter x 5 cm long. The distance between the sample and the neutron source was long enough to separate the desired gamma-rays from the time-dependent background of gamma-ray events, which were generated at the source position by interactions of the D-T neutrons with materials of a target support and then scattered in the sample toward the detector.

The energies of the incident neutrons varied slightly depending on the sample positions due to the kinematics of D-T reaction. The mean-energy of incident D-T neutrons was 14.4 MeV at the 135 degree measurement. The difference in mean-energy was 400 keV between the sample positions at 90 and 135 degree measurements. The neutron fluence at the sample position was determined with aluminum and niobium foils activated by $^{27}Al(n,\alpha)^{24}Na$ and $^{93}Nb(n,2n)^{92}Nb$ reactions, respectively. The yield of source neutrons in each run was monitored with 1.5" diameter x 1.5" long NE213 liquid scintillator.

---

* JENDL-3T is a temporary file for testing the evaluated data which are for JENDL-3. The data in JENDL-3T will be partly revised in JENDL-3.

The pulse height spectra were unfolded by using the FERDOR[3] code. In this data processing, the response functions of the NaI detector were provided for monoenergetic sources in the gamma-ray energy region from 0.3 to 11 MeV with a 100 keV interval. The detector efficiency and response functions were determined with calculations by the Monte Carlo method. The following two events were estimated in the response calculations: (a) In-scattered photons in the collimator and (b) Back-scattered photons from the lead shield surrounding the detector. Figure 2 and 3 show the calculated response functions for 1.78 and 6.13 MeV, respectively, in comparison with the measured functions[4]. MCRF in the figures denotes the calculations of only energy-deposit of photons in the crystal and MCNP[5] denotes the calculations with corrections for the events of in-scattered and back-scattered photons. It was confirmed for some monoenergetic sources that the calculated functions were in good agreement with the experimental results.

The Monte Carlo calculations were also applied to the corrections both of gamma-ray attenuation and multiple scattering of incident neutrons in the sample.

3. Data presentation and comparison

Angular distributions are given in Fig.4 for 4.44 MeV gamma-ray from the first excited level of ^{12}C. Figure 5 to 9 show the experimental results for five samples of aluminum to nickel, comparing with the energy differential cross sections constructed from the photon production data in the nuclear data files in use. The photon production data consist of continuous energy distributions and discrete photon data of multiplicity and transition probability. Brief discussion for each element is as follows.

Carbon

The present values were close to the values in ENDF/B-V[6], which is available only for carbon. The production cross section for this discrete gamma-ray was estimated to be 180 mb from a Legendre polynomial least-squares fit to the present data, though the neutron energies varied depending on the sample positions as previously mentioned. The values of the cross sections were 169 mb in JENDL-3T and 185 mb in B-V.

Aluminum

Four discrete gamma-rays of 1.0, 1.8, 2.2 and 3.0 MeV were observed in the energy spectrum. A 1.8 MeV discrete gamma-ray results from the transition in (n,n'p) channel and the other lines result from the (n,n') channel. As shown in Fig.5, the measurement fairly agrees with the differential data in B-IV in the whole energy region. The JENDL-3T evaluation overestimated the measurement

in the energy range over 7 MeV and the discrete line of 1.8 MeV was not distinguished from the 2.2 MeV line.

Silicon

No discrepancy can be seen in comparison of the measued spectrum with the energy distribution in B-IV. The photon spectrum in JENDL-3T agreed with the measured spectrum, though the energy structure given in the file had the coarse intervals. Problem may still remain for the discrete photon data in JENDL-3T at the energies of 0.5, 1.0 and 4.5 MeV.

Chromium

The emission of 1.434 MeV gamma-rays from (n,n') reaction appears sharply on the energy spectrum of natural chromium. A line of 1.334 MeV gamma-rays, which were the transition from 2.676 to 1.434 MeV excited level, contributed to the peak at 1.4 MeV in the measured spectrum. At the peak, the cross section values in the present data were larger than the values in JENDL-3T. The B-IV data could not give the correct spectrum of secondary gamma-rays for natural chromium.

Iron

Agreement appears to be good between the measurement and the evaluations in both of JENDL-3T and B-IV. In the continuous region from 2 to 6 MeV, however, the overestimation with 60 % in maximum can be seen in the secondary photon spectrum of JENDL-3T.

Nickel

A peak around 1.3 MeV attributed to the competition of transitions among levels in ^{58}Ni and ^{60}Ni. The energy bins presently available in JENDL-3T were not appropriate to the tabulated energy distributions for the discrete photons because of coarse energy intervals.

4. Concluding remarks

Differential cross sections have been measured for the gamma-ray production from (n,xγ) reactions by 14 MeV neutrons. With the use of a large NaI crystal to measure the energy spectra of secondary gamma-rays, the data for six elements of C, Al, Si, Cr, Fe and Ni could be obtained with good accuracy in statistics. The following remarks were derived from the comparison work between the measured and evaluated data in two nuclear data files. In JENDL-3T, some disagreements still remain in the production cross sections for discrete gamma-rays. The ENDF/B-IV data agreed well with the present data except natural chromium.

References

(1) JENDL Compilation Group (Nuclear Data Center, JAERI): JENDL-3T, private communication (1987)

(2) ENDF/B summary documentation, BNL-NCS-17541 (ENDF-201), 2nd Edition (1975)

(3) Kendrick, H. et al.: An introduction to the principle and use the FERDOR unfolding code, GA-9882, Gulf Radiation Technology (1970)

(4) Murata, I., et al.: Preprint 1987 Fall Meeting of the Atomic Energy Society of Japan, C-10(1987)

(5) Los Alamos Radiation Transport Group (X-6): MCNP-A general Monte Carlo code for neutron and photon transport, LA-7396-M, Rev.(1981)

(6) ENDF/B summary documentation, BNL-NCS-17541 (ENDF-201) 3rd Edition (1979), C(MAT 1306, MOD 1), evaluated by C. Y. Fu and F. G. Perey (ORNL)

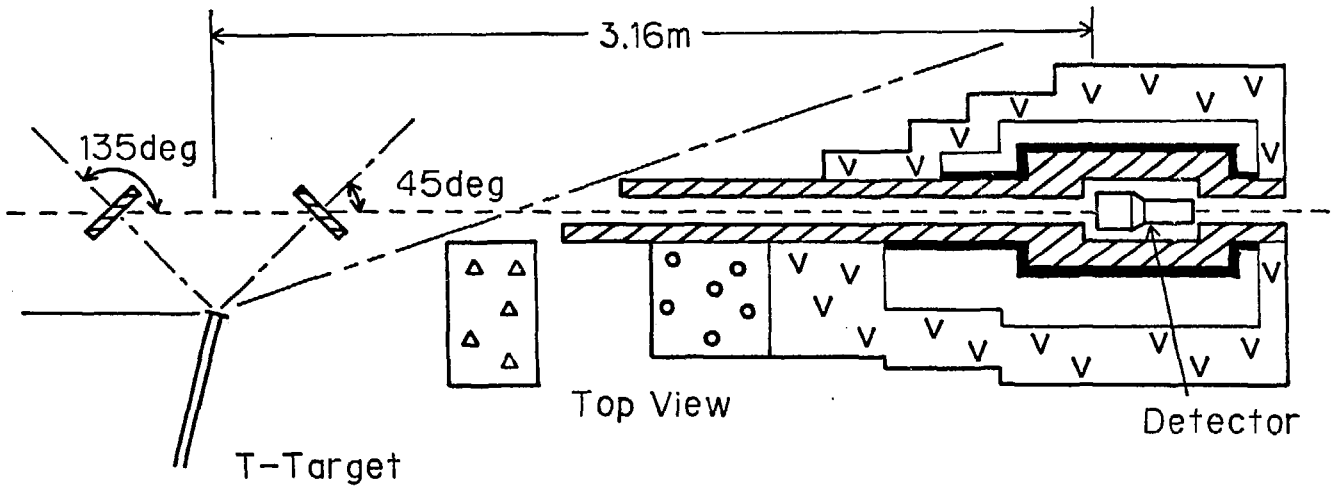

Fig. 1 Experimental arrangement.

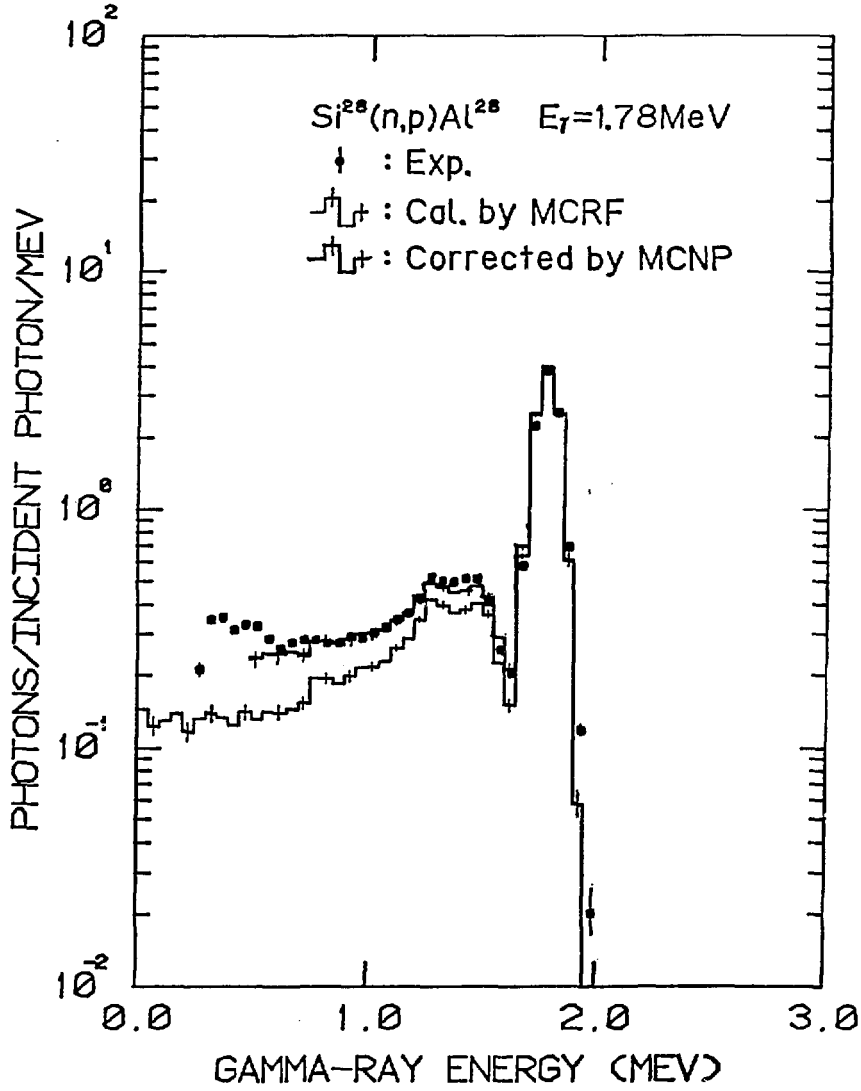

Fig. 2 Response function of the NaI detector for 1.78 MeV gamma-ray.

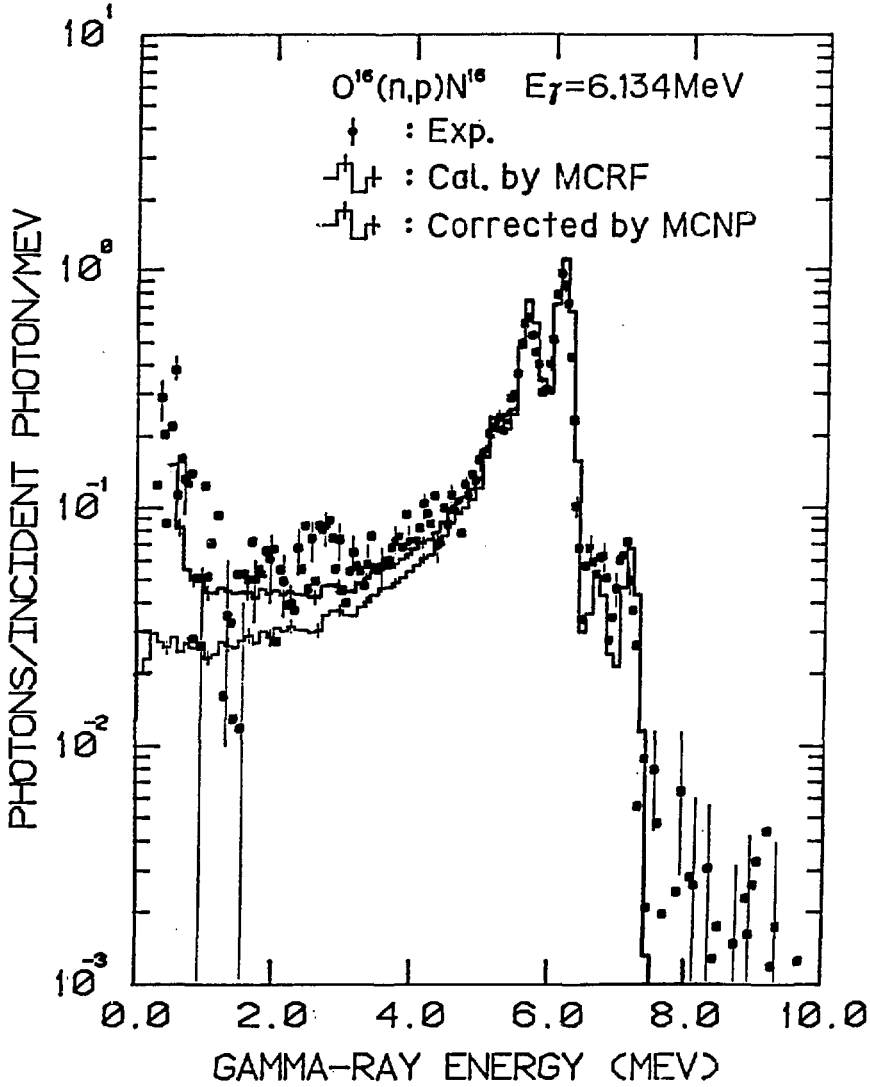

Fig. 3 Response function of the NaI detector for 6.134 MeV gamma-ray.

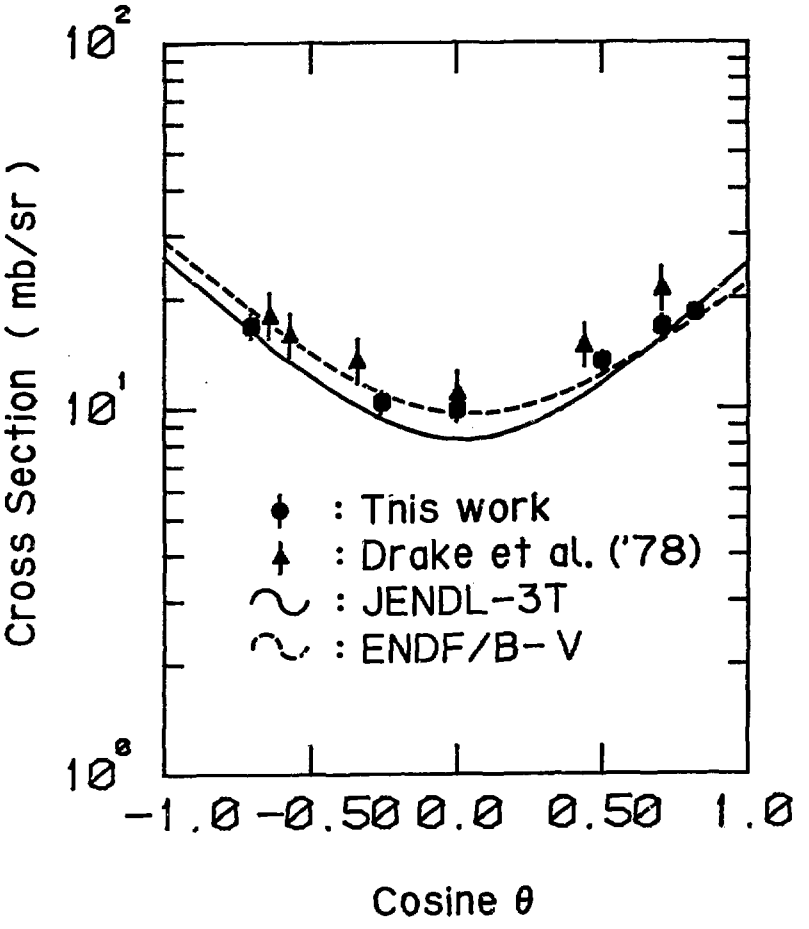

Fig. 4 Angular distribution of 4.44 MeV gamma-ray in ^{12}C.

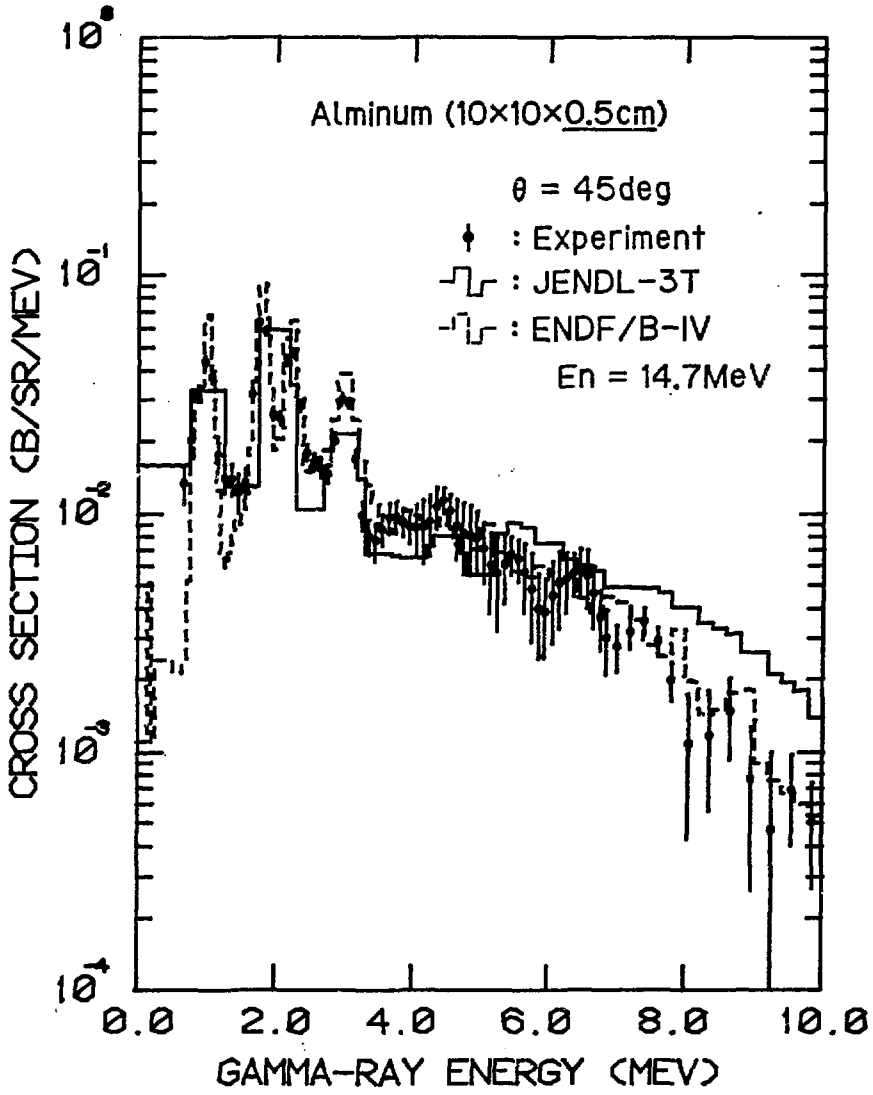

Fig. 5 Energy differential cross sections for gamma-rays from aluminum at 45 deg.

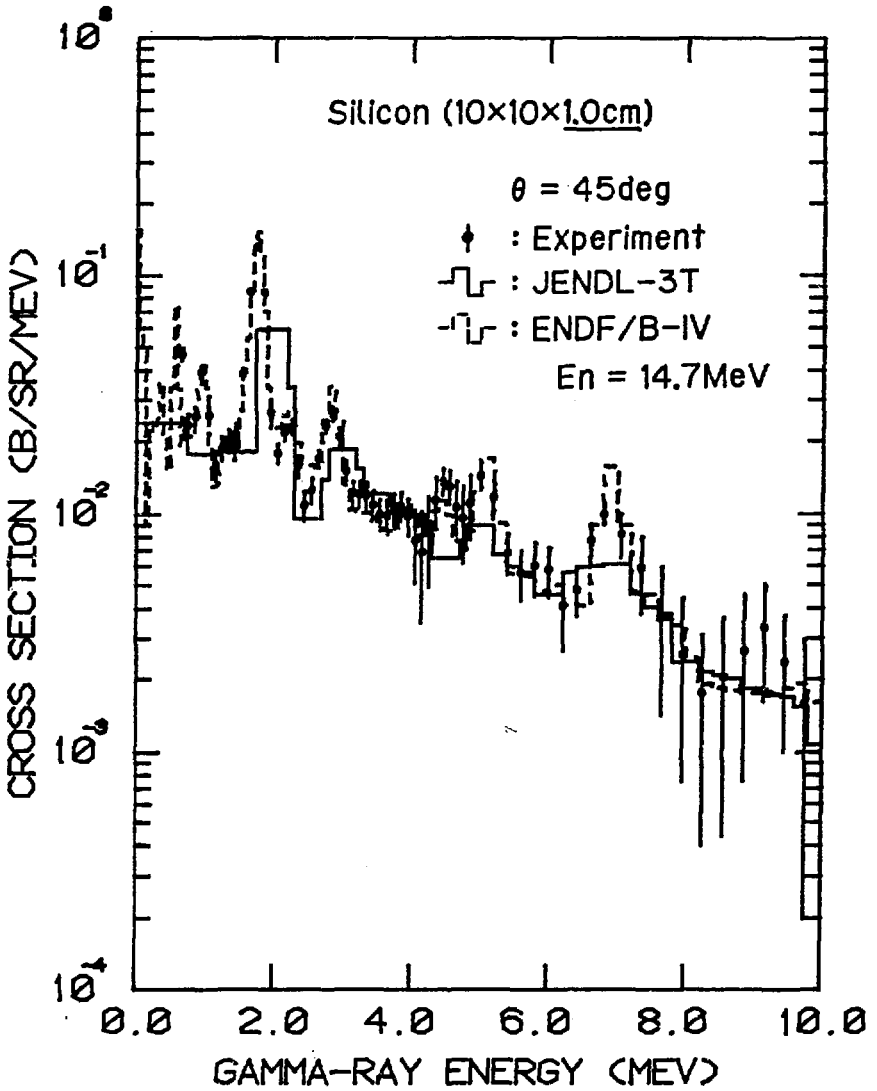

Fig. 6 Energy differential cross sections for gamma-rays from silicon at 45 deg.

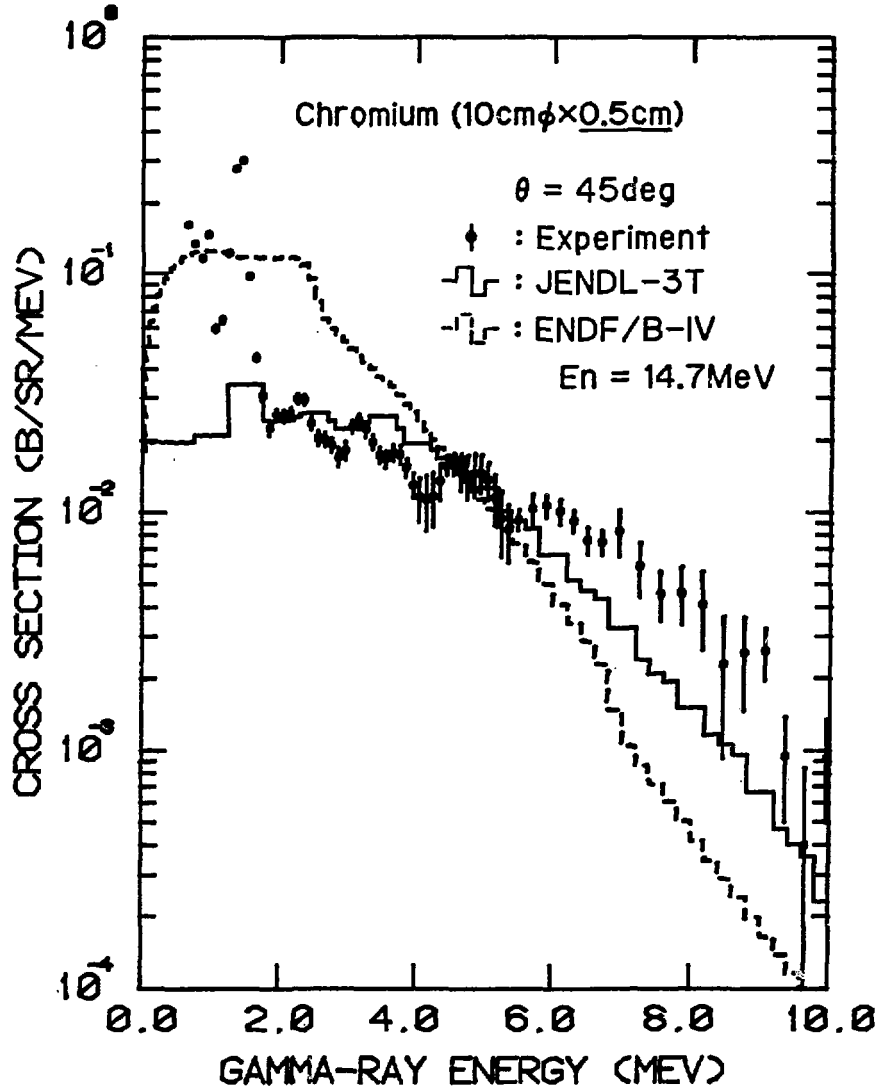

Fig. 7 Energy differential cross sections for gamma-rays from chromium at 45 deg.

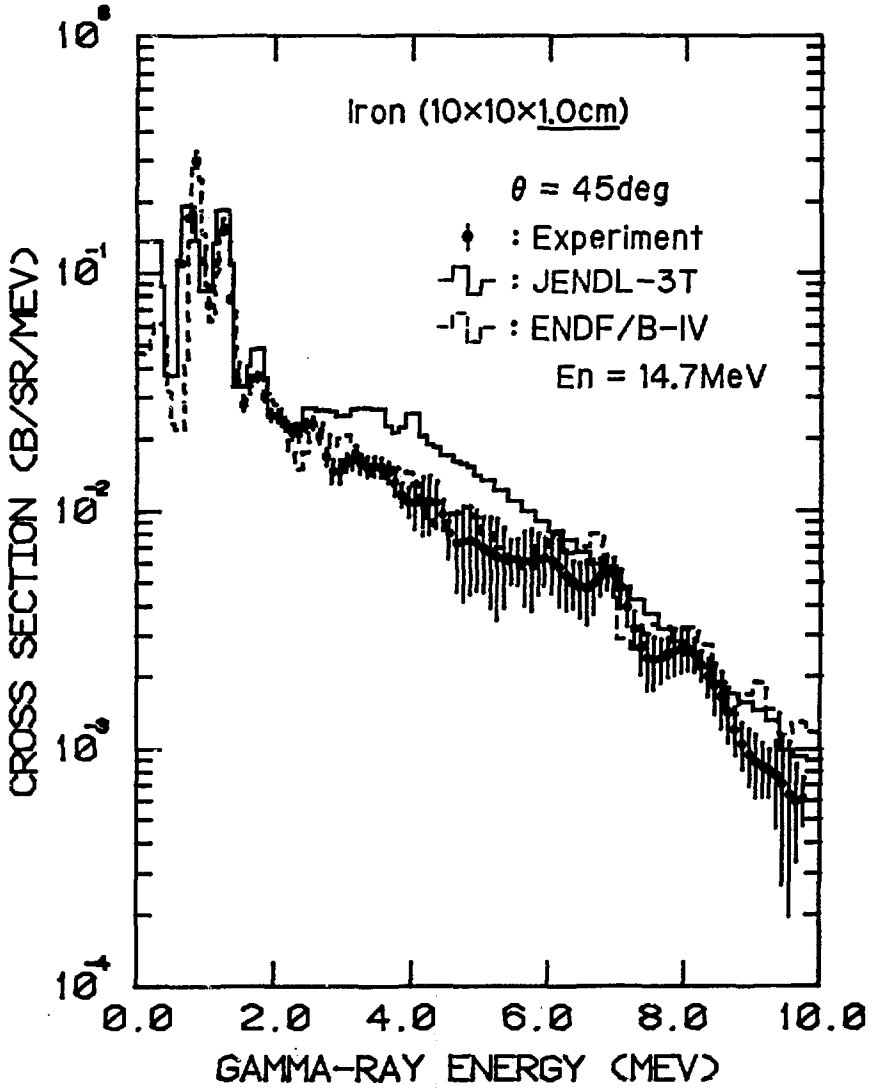

Fig. 8 Energy differential cross sections for gamma-rays from iron at 45 deg.

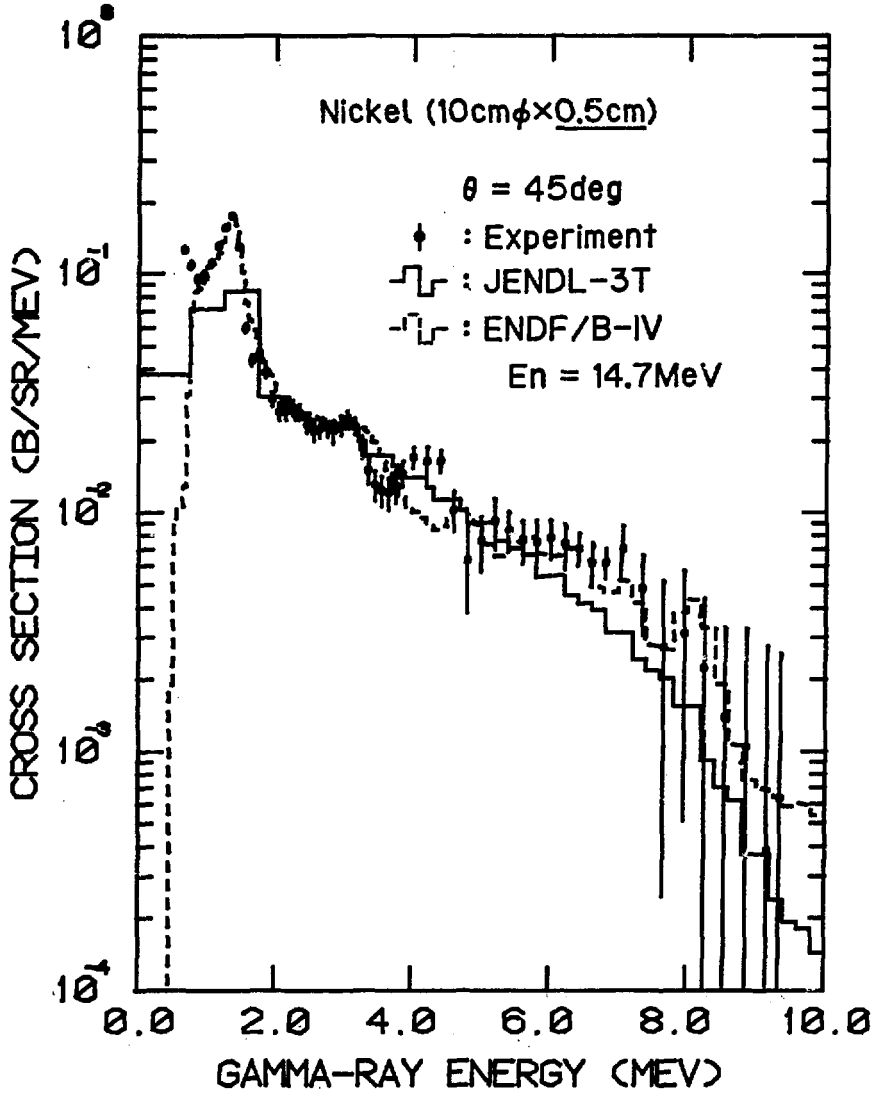

Fig. 9 Energy differential cross sections for gamma-rays from nickel at 45 deg.

3.7 Analysis of Neutron Spectra Measurement in Concrete Assembly Using JENDL-3T

Koji Oishi[1], Yujiro Ikeda, Kazuyuki Tomioka[1] and Tomoo Nakamura

Japan Atomic Energy Research Institute, Tokai-mura, Ibaraki-ken
Institute of Technology, Shimizu Corporation, Etchujima, Koto-ku, Tokyo[1]

For the verification of JENDL-3T (test version of JENDL-3), the analysis of neutron spectral measurement in concrete using that new data library was applied to the experiment. Comparison with JENDL-2 was also performed as a reference. The result obtained using JENDL-3T was in approximate agreement with experiment in the higher neutron energy range En ≧7.3MeV, but in the lower energy range there remained much room for further investigation.

1. Introduction

Concrete is one of the most practical shielding materials for the future design of fusion facilities. For the proper design of the shield, the measurement of neutron spectra in concrete is indispensable to estimate nuclear data libraries and transport codes, which supplies an important information not only for shielding of fusion facilities, but for the proper prediction of induced activities in the shield. In this study the result of calculations for neutron spectrum based on JENDL-3T have been compared with that of experiment to verify that new test version.

2. Experiment

2.1 Experimental procedure

Experiments have been performed at the Fusion Neutronics Source (FNS)[1] of Japan Atomic Energy Research Institute (JAERI). Deuterium-Tritium neutrons were produced by bombarding the T-Ti target with the 330KV deuteron beam. The concrete cylindrical assembly, 600mm in diameter and 600mm thick, was set at 200mm from the target, in the direction of d beam. Experimental layout is shown in Fig.2.1. Two physical quantities, reaction rates and neutron spectra, were obtained using foil detectors and NE213 spectrometer, respectively. In

case of foil activation method seven sets of foils Fe, In, Al, Ni, Au, Zr, Nb were placed along the central axis of the assembly. Detector positions were 0, 25, 50, 100, 200, 400, and 550mm from the front surface of the assembly. After irradiation for 10 hours, reaction rates were deduced from the gamma-ray counts using Ge detectors with necessary corrections. Used reactions are listed in Table 2.1.1 with their nuclear data. To measure neutron spectra in the assembly, miniature spherical NE213 spectrometer[2] was adopted. The detector was placed at 16, 41, 66, 116, 216, 416, and 616mm from the surface of the assembly. Neutron spectra at each position were obtained through unfolding the pulse height spectra by the unfolding code FORIST[3].

2.2 Experimental result

In Fig.2.2.1 and 2.2.2, reaction rates for each foil and neutron spectra measured using NE-213 are shown, respectively. To prove whether those two experimental methods were consistent, neutron spectra were deduced from the result of reaction rates for each foil using unfolding code SAND II[4]. Integrated neutron flux, in the several neutron energy range are shown in Fig.2.2.3. We could conclude that the results of those two experimental methods agreed well within the experimental errors.

3. Analysis

3.1 Calculational Code and Nuclear Data

Calculation was performed using two dimensional transport code DOT3.5 with P5-S16 approximation. Nuclear data libraries used were 125 group independent cross section libraries FSXJ3T[5] and JACKEX[5] processed using JENDL-3T and mainly JENDL-2, respectively. The evaluated nuclear data files of each library are listed in Table 3.1.1. with every material.

3.2 Calculational model

The result of calculation using the Monte Calro code simulating the structure of the target assembly (see Fig.3.2.1.) was used as the D-T neutron source spectrum. The composition of the concrete assembly, listed in Table 3.2.1, was analized by chemical analysis. Some elements, which were not included in the nuclear data libraries, were replaced by the main component of the assembly (see Table 3.1.1). It could be considered that there was no effect of that operation on the transport calculation, because the fraction of those rare elements was less than 0.3wt%.

3.3 Calculational Results

The values of calculational result based on JENDL-3T to that based on JENDL -2 (C/C) for several neutron energy range are shown in Fig.3.3.1. Those two calculational results agreed within －5% to ＋10% except neutron energy range En ≧7.3 MeV. For all neutron energy range C/C values inclined to increase as the distance increased from the front surface. JENDL-3T overestimated JENDL-2 by about 10% deeper than 40 cm position for neutron energy range En≧7.3 MeV, but in the neutron energy range E≧1.05 MeV those two calculational results agreed very well.

4. Comparison between Experiment and Calculations

To verify JENDL-3T, comparison between experiment and calculations based on JENDL-3T and JENDL-2 have been performed. Comparisons between experimental spectrum and calculational one measured by NE213 and multi-foil activation method at several position are shown in Fig.4.1 and Fig.4.2, respectively. From those figures, calculations overestimated experiments in the lower energy range En ≦7.3 MeV, but in the higher energy range good agreement between experiment and calculation was ovserved except at the deeper position d≧400㎜. For the further examination in detail, comparison between experiment and calculation was done for several energy ranges. The calculational to experimental (C/E) values for several energy ranges are shown in Fig.4.3 ～Fig.4.6.

1) En≧11.5 MeV

This energy range corresponds to the D-T neutron peak. Good agreement between calculations and experiments were obtained within±10% except at the deeper position d ≧550 ㎜ for JENDL-3T and at the position d ＝615 ㎜ for JENDL -2.

2) En≧7.3 MeV

There were some differences between the calculaional result based on JENDL-3T and JENDL-2, but those two calculational results agreed well with experimental ones within ±10% except at the detector position d ＝ 616㎜. The underestimation of the calculational result based on JENDL-2 was caused by the discripancy of neutron spectrum around neutron energy between 9 MeV and 12 MeV.

3) En≧2.5 MeV

Both calculations based on JENDL-3T and JENDL-2 overestimated experiment by

more than 10% at the detector position deeper than 200 mm.

4) En≧1.05 MeV

Good agreement between calculational result based on JENDL-3T and JENDL-2 was obtained, but C/E values increased up to 1.4 as the distance increased from the front suface.

Those discrepancies in the neutron energy range 1.05 ≦En≦ 7.3 MeV was probably caused by the overestimation of inelastic cross sections of silicon and oxygen in the nuclear libraries, because those two elements were the main components of concrete. (see Table 3.2.1)

5) En<1.05 MeV

In the energy range lower than 1.05 MeV verification could only be done using $^{197}Au(n, \gamma)$ reaction. The calculational to experimental ratio of $^{197}Au(n, \gamma)$ reaction rate is shown in Fig.4.7. There was much deference between experiment and calculations. C/E values varied from 0.6 to 1.4. Calculations underestimated experiment by about 40% at the detector position 100 mm where the lower energy flux showed maximum value.

5. Conclusion

The analyses of neutron spectral measurement in concrete assembly irradiated by 14 MeV neutrons were performed using DOT3.5 transport code with cross section library based on JENDL-3T and that based on mainly JENDL-2. The analysis lead to the conclusion that JENDL-3T proved very effective for the analysis of neutron spectral measurement in concrete in the neutron energy range higher than 7.3 MeV except at the position deeper than 550 mm, but in the lower energy range there still remained much room for further investigation in the same manner as JENDL-2. Further study for the containment of H_2O in concrete assembly will be necessary.

References

1. Nakamura, T.: JAERI-M-86-080, (1986)
2. Oyama, Y. et al.: Nucl.Instr.and Meth, A256, (1987) 333
3. Johnson, R.H.: Nucl.Sci.Eng, 73, 93 (1980)
4. Simons, R.L. et al.: BNWL-1312, Battelle-Northwest Laboratories (1970)
5. Kosako, K.: Private Communication

Table 2.1.1 Used reactions and their nuclear data

Reaction	Half life	Q-value(MeV)
$^{54}Fe(n, p)\ ^{54}Mn$	2.579h	－ 2.9129
$^{115}In(n, n')^{115m}In$	4.3 h	－ 0.3360
$^{27}Al(n, \alpha)\ ^{24}Na$	15.02 h	－ 3.1303
$^{58}Ni(n, 2n)\ ^{57}Ni$	1.50 d	－ 12.1967
$^{197}Au(n, \gamma)^{198}Au$	2.696d	6.5124
$^{90}Zr(n, 2n)\ ^{89}Zr$	3.27 d	－ 11.9765
$^{93}Nb(n, 2n)\ ^{92m}Nb$	10.15 d	－ 8.9674
$^{58}Ni(n, p)\ ^{58}Co$	70.8 d	0.4021

Table 3.1.1 Evaluated nuclear data files of each library

	FSXJ3T	JACKEX
Si	JENDL3T	JENDL2
Al	JENDL3T	JENDL2
Fe	JENDL3T	JENDL3PRI
Ca	JENDL2	JENDL2
Mg	ENDF/B-Ⅳ	ENDF/B-Ⅳ
S	→ Si	→ Si
Na	JENDL3T	JENDL2
K	JENDL3T	ENDF/B-Ⅳ
Ti	→ Fe	→ Fe
P	→ Si	→ Si
Mn	JENDL3T	JENDL2
Ba	→ Si	→ Si
V	→ Fe	→ Fe
Co	→ Fe	→ Fe
Zn	→ Fe	→ Fe
Cu	→ Fe	→ Fe
Ni	→ Fe	→ Fe
C	JENDL3T	JENDL3PRI
H	JENDL3T	JENDL2
O	JENDL3T	JENDL3PRI

Table 3.2.1 Composision of the concrete assembly analized by chemical analysis

	Atomic density
Si	1.1370+22 *
Al	2.4650+21
Fe	7.0330+20
Ca	5.2209+21
Mg	5.3073+20
S	1.1689+20
Na	6.5574+20
K	4.3714+20
Ti	7.0278+19
P	2.4489+19
Mn	3.0154+19
Ba	1.0463+19
V	5.249 +18
Co	2.27 +17
Zn	1.43 +18
Cu	6.52 +17
Ni	2.73 +17
C	2.1264+20
H	9.3507+21
O	3.9484+22

*read as 1.1370×10^{22}

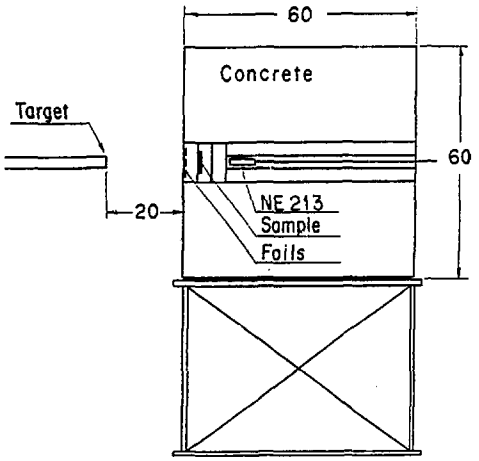

Fig. 2.1 Experimental layout

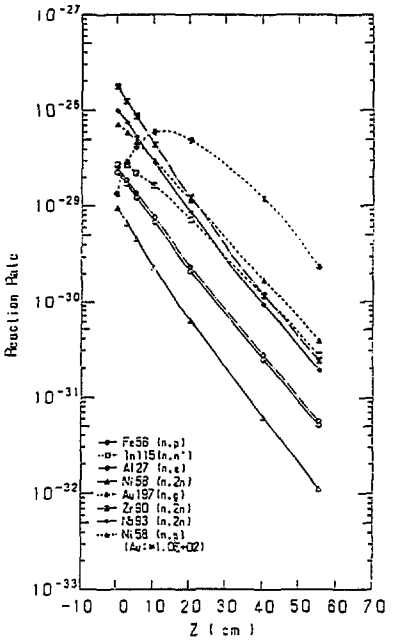

Fig. 2.2.1 Distribution of reaction rate for each foil

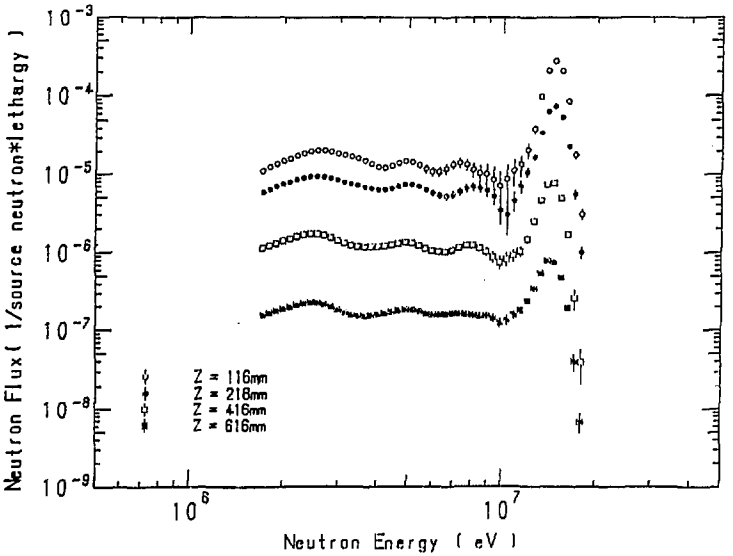

Fig. 2.2.2 Neutron spectra measured by NE213 spectrometer

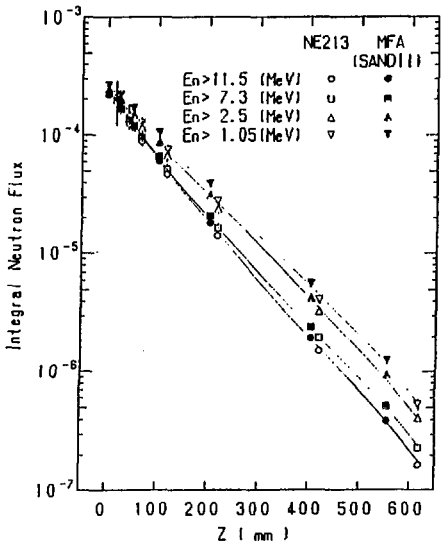

Fig. 2.2.3 Integrated neutron flux for several energy range

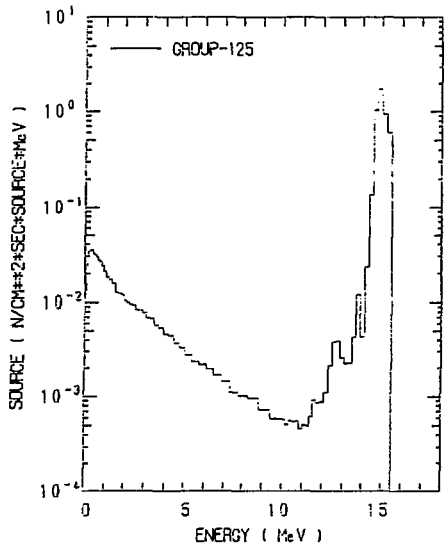

Fig. 3.2.1 D-T neutron source spectrum used for calculations

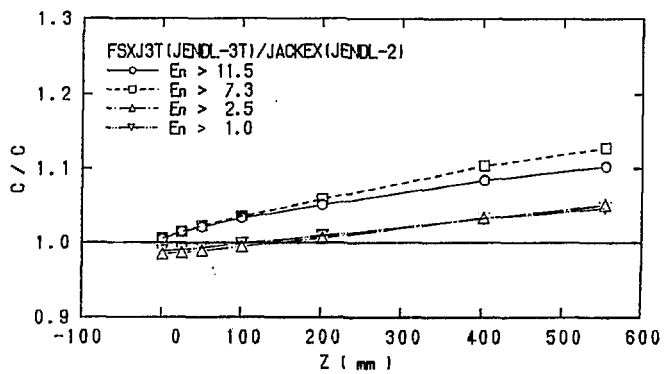

Fig. 3.3.1 The C/C values between JENDL-3T and JENDL-2 for several energy range

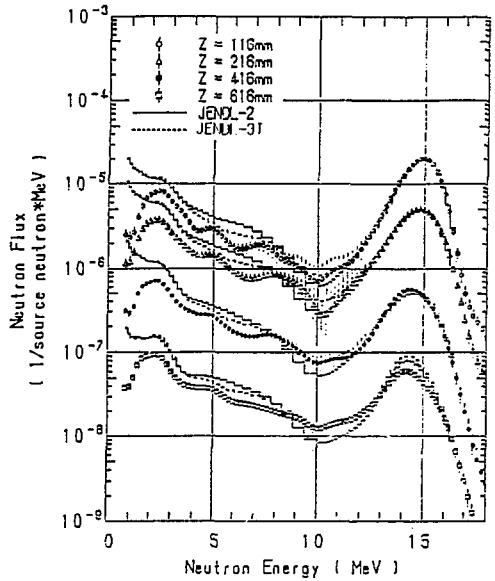

Fig. 4.1 Comparison between calculated neutron spectra based on JENDL-3T and experimental ones measured using NE213 spectrometer

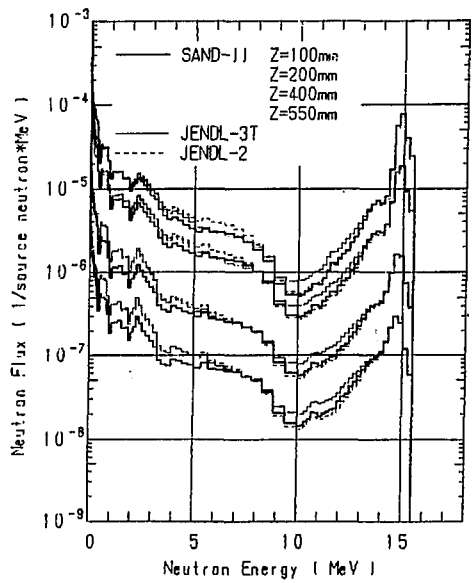

Fig. 4.2 Comparison between calculated neutron spectra based on JENDL-3T and exprimental ones obtained using multi-foil method (SANDII)

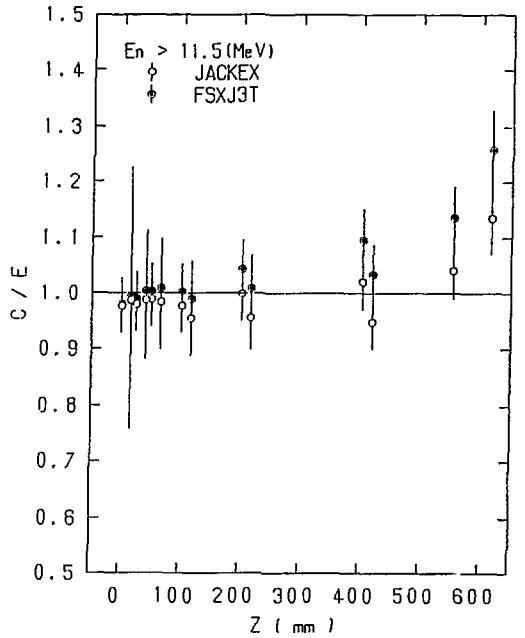

Fig. 4.3 C/E value of integrated spectrum for neutron energy range En≧11.5 MeV

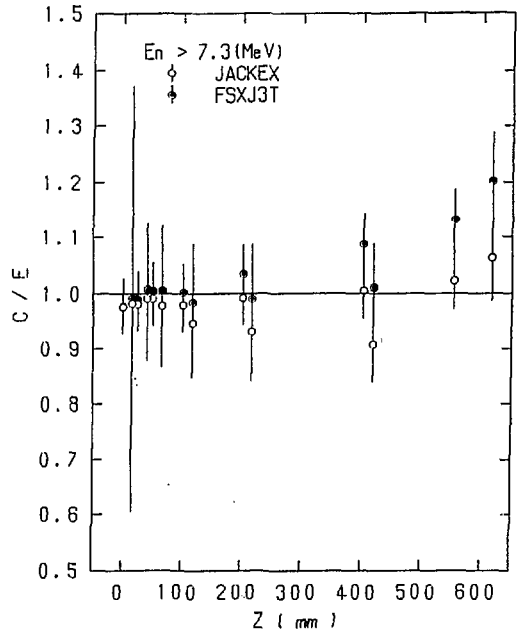

Fig. 4.4 C/E value of integrated spectrum for neutron energy range En≧7.3 MeV

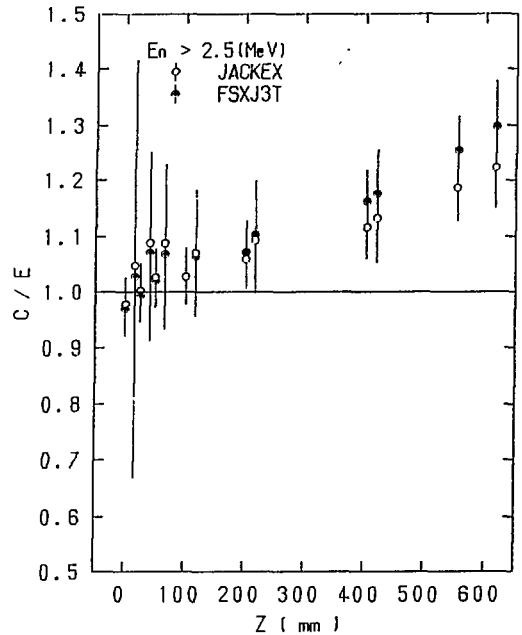

Fig. 4.5 C/E value of integrated spectrum for neutron energy range $E_n \geq 2.5$ MeV

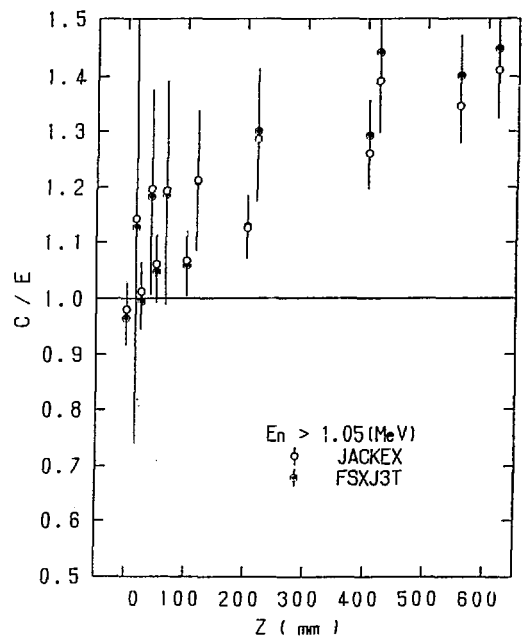

Fig. 4.6 C/E value of integrated spectrum for neutron energy range $E_n \geq 1.05$ MeV

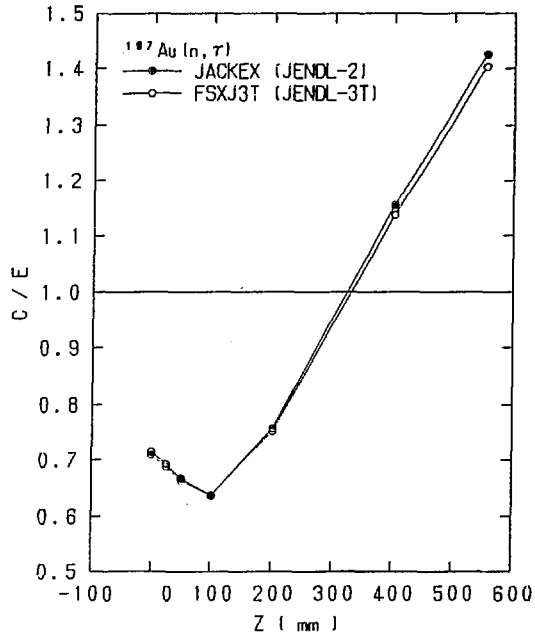

Fig. 4.7 C/E value of reaction rate for $^{197}Au(n,\gamma)$ reaction

3.8 Si-PKA Spectra in a Si-SSD Bombarded by 14 MeV Neutrons

K. Yageta, S. Iwasaki, K. Sugiyama
Department of Nuclear Engineering, Tohoku University
Aramaki-Aza-Aoba, Sendai 980, Japan

An atempt to measure the PKA's energy spectra for silicon was made using a method in which a silicon detector was used as a sample too. The Si-SSD was bombarded by 14MeV neutrons and the resulting spectra have been measured in order to compare with the calculated ones using a code developed in this study for the PKA's and charged particles (CP's) with evaluated neutron nuclear data library, ENDF/B-IV.

The calculated one globally reproduced the experimental one. However, in detailed inspection, the present conventional model was too simple to compare both spectra.

It is necessary to adopt more realistic nuclear models, especially for two-body continuum and three-body reactions, and include some effects such as penetration of the energetic particles and energy loss process of the PKA's at low energy regions, etc.

I. Introduction

Recently it is pointed out that the reliable energy and angular distributions of the primary knock-on atoms (PKA's) are very important nuclear data in the field of the radiation damage study, especially in the microscopic simulation calculation[1]. In spite of this demand, there have been no experimental data for the PKA's because of their extremely short range in a target materials.

In this study, an atempt to measure the PKA's energy spectra for silicon was made using a method in which a silicon was used

as a sample, too. The Si-SSD was bombarded by 14MeV neutrons and the resulting spectra have been measured in order to compare with the calculated ones using a code developed in this study for the PKA's and charged particles (CP's) with evaluated neutron nuclear data library, ENDF/B-IV.

II. Experiment

The employed Si-SSD was a surface barrier type one of 100-mm^2 active area and a depletion layer of 300mm at maximum bias voltage of 100V. The energy resolution of the detector was about 15keV. This detector (PKA-SSD) was put in a small SUS vacuum chamber of cyrindirical shape. A flat surface of the chamber (neutron entrance side) was made by niobium thin plate, and the inside of the lateral surface was covered by molibdenum foil. These were the high Z materials and used for preventing the incidence of the energetic CP's from the wall mateials.

A neutron beam of 14MeV was produced by the T+d reaction on a titanium-tritium target of about 1mg/cm^2 thickness. The associated alpha particles were detected by another surface barrier SSD (α-SSD) which was mounted at 25 cm from the target in a 165 deg. direction. The PKA-SSD was positioned at the place inside the neutron cone corresoponding to the α-particles around 15 deg. The coincidence signals between the two timing signals from the detctors opened gate for the pulse height signals from the PKA-SSD. This coincidence technique remarkably reduced background level in the low pulse height range, mainly due to the gamma-rays emitted from surrouding materials.

The experimental layout and block diagram of the electronics are shown together in Fig. 1. The obtained typical spectrum is shown in Fig. 2. The ordinate of the spectrum was calibrated by an alpha-source of Am-242.

III. Calculational Model

At present, recoil energy distributions of the PKA's are not

included in the ENDF files, so they have to be estimated using models. Considering the present experimental method, all light charged particle (CP's) as well as the PKA's should be taken into account, because the light particles are emitted simultaneously with the PKA's and obtained spectra in the SSD should be a coherent sum of the corresponding two contributions. We are now developing a spectial code for the CP's and PKA's spectra in the SSD. In the primary stage of the code developing, we adopt one of the simple models used in the analysis codes of the radiation damage which have been developed by many authors[2,3,4,5]. Present model is essentially the same as the ref. 5, as follows.

For elastic and two-body discrete-level scattering (ENDF/B designations MT=2 and MT=51 through 90), recoil energy can be calculated accurately using the relation,

$$E_R(E,\mu_C) = AE(1 - 2M\mu_C + M^2)/(A+1)^2,$$

where $M = (1-(A+1)(-Q)/AE))^{1/2}$, A is the target mass number, E is the incident neutron energy, and μ_C is the center-of-mass scattering cosine. The angle integrated PKA's spectrum is given as,

$$\phi_R(E) = \sigma(E) \int_{-1}^{1} f(E,\mu_C)E_R(E,\mu_C)d\mu_C,$$

where f is the angular distribution of the scattered neutrons from the ENDF/B file 4. Discrete-level reaction with ENDF "LR flag" -- for example, (n,n') reations--- are treated in the same way. The effect of the additional emitted particle on the recoil spectrum is ignored.

Continuum reactions, such as the ENDF MT91 for (n,n'_c), give a recoil spectrum,

$$E_R(E,E',\mu_L) = (E - 2(EE')^{1/2}\mu_L + E')/A$$

where E' is the secondary neutron energy, and μ_L is the laboratory cosine. The PKA's spectrum becomes,

$$\phi_R(E,E') = \sigma(E) \int_{-1}^{1} d\mu_L f(E,\mu_L) g(E-E') E_R(E,E',\mu_L)$$

where g is the secondary-neutron energy distribution from ENDF/B file 5. The angular distribution is taken to be isotropic.

The same procedure is used for (n,2n), (n,np), etc., with no account being taken of any extra charged particle emitted. The treatment used above implicitly neglected the effects of photon momentum.

Finally, the (n,charged particle) reactions such (n,p) (MT=103) and (n,) (MT=107) are computed using

$$E_R = (E^* - 2(aE^*E_a)^{1/2}\mu + aE_a),$$

where a is the atomic mass ratio of the emitted particle to the neutron, E^* is given by,

$$E^* = (A+1-a)E/(A+1),$$

and the particle energy E_a is approximated being equal to the smaller of the available energy,

$$E_{av} = Q + AE/(A+1),$$

or the Coulomb energy,

$$E_c = (1.029 \times 10^6)\ zZ/\ (a^{1/3} + Z^{1/3})\ \text{(in eV)},$$

where z is the charge number of the emitted particle and Z is the charge number of the target atom. This "delta-function approximation" represents the most important feature of the charged-particle spectrum. The angular distribution for the emitted particles is assumed to be isotropic in the lab.

The calculated spectra by the code V.1 was shown in Fig .2 and compared with that of the present experiment. In the figure, we

can see the existence of the three distinctive regions; the high energy region, where there are many sharp line spectra which are considered to be the contribution of sum of the PKS's and charged particles from the (n,p) and (n,α) reactions for the discrete levels of the final nuclei; the medium energy region less than 6MeV, where a plateau seemed to be due to the (n,p) (n,α) (n,n) contiuum components and also partially penetrated discrete protons, which will be discussed later; and the lowest energy region less than 1MeV, in which the (n,n) and (n,n') are the main components.

The present calculatinal model roughly reproduce the total behavior of the experimental spectrum. In the high energy region, the line spectra of the protons and alpha-particles are almost reproduced. In the low energy region, the broad peaks due to the kinematical effect of the elastic scattering angular distribution is shown in both spectra around 1MeV.

In contrast, in the middle energy region, there is no peak in the experimental one as shown in the calculational one. Also, the plateau in the middle of the experimental spectrum increase with decreasing the energy, whereas the calculational one shows rather flat. This is because that the energetic protons penetrated through the depletion layer and deposited the small portion of their original energies in the sensitive layer. Therefore the contribution of these protons would build up in the lower energy side from the standared pulse height region. The last effect was not included at present.

The former three peaks is obviously due to the unrealistic model for the three-body reactions in the present calculation, which shows the inadequacy of the conventional damage calculational model at least from the microscopic view point.

IV. Concluding Remarks

Using the method that the solid state silicon detector was used as detector and also target simultaneously, the PKA's spectrum could be measured as the mixed one with charged

particles. The measured spectrum was compared with that of the calculated one using a code which was developed in the present study. The calculated one globally reproduced the experimental one. However, in detailed inspection, the present conventional model was too simple to compare both spectra.

It is necessary to adopt more realistic nuclear model[5,6,7], especially for two-body continuum and three-body reactions, and include some effects such as penetration of the energetic particles and energy loss process[8] of the PKA's at low energy regions, etc.

The first observed PKA's spectra is very useful to assess the nuclear data file, from the aspects of the charged particles and PKA's, which have been developed mainly for the neutron transportation problem.

References

1) Proc. of seminar on the elementary damage processes due to 14MeV neutrons and their simulation (in Japanese), Mar. 25, 1987, General Steering Group for Special Study on Energy Development (Nuclear Fusion) Ed., Monbusho (1987).

2) JJ.D.Jenkins, "Primary-Recoil Atom Spectra from ENDF/B Data" Nucl. Sci. Eng. 41, 158-163 (1970).

3) D.G.Doran "Neutron Displacement Cross Sections for Stainless Steel and Tantalum Based on a Lindhard Model, Nucl. Sci. Eng. 49, 130-144 (1972).

4) T.A.Gabriel, J.D.Amburgey, and N.M.Greene, "Radiation-Dameage Calculations: Primary Knock-On Atom Spectra, Displacement Rates, and Gas Production Rates", Nucl. Sci. Eng., 61, 21-32 (1976).

5) R.E. MacFarlane et al., D.W. Muir, and F.M. Mann, "Radiation Damage Calculations with NJOY," Jour. Nucl. Mat.,122 &123 1041 (1984).

6) R.E. MacFarlane et al., D.G. Foster, Jr., "Advanced Nuclear Data for Radiation Damage Calculations," ibid., 122 & 123,1047 (1984).

7) K. Takahashi, Private communication.

8) J. Lindhard, V. Nielsen, M. Scharff, and P.V. Thomsen, Kgl. Dansk. Vidensk. Selsk. Mat-Fys. Medd.,33 (1963).

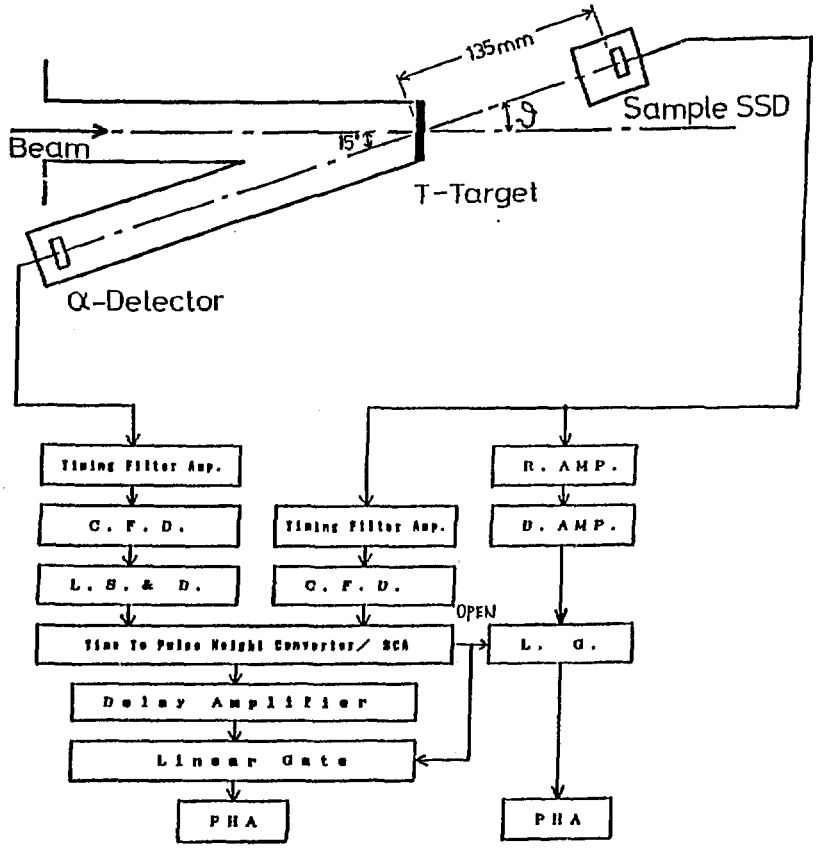

Fig. 1 Present experimental layout and block diagram of electronics.

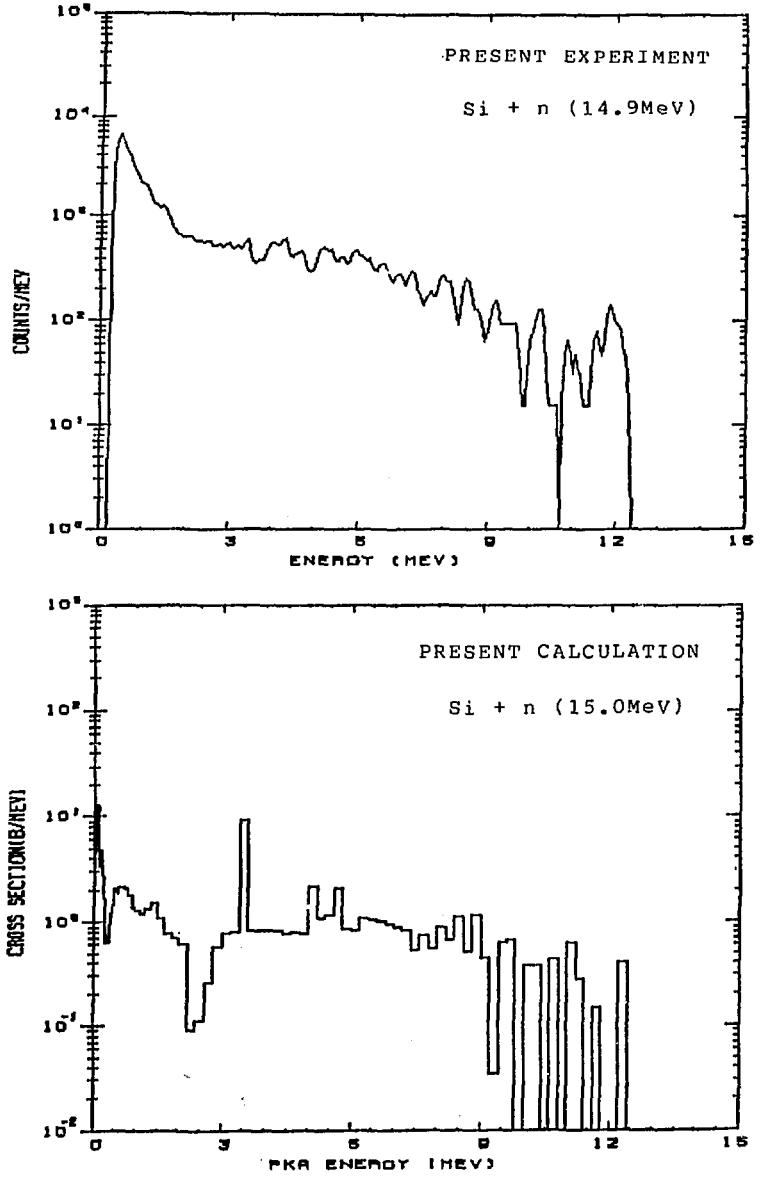

Fig. 2 Present experimental (upper) and calculational (lower) spectra for silicon PKA's and charged particle's bombarded by 14 MeV neutrons.

3.9 Measurement of Formation Cross-sections of Short-lived Nuclei Produced by 14 MeV Neutron

Toshio Katoh, Hiroyuki Yoshida, Akihiko Osa, Yu Gotoh,
Masahide Miyachi, Hiroe Ukon, Michihiro Shibata,
Hiroshi Yamamoto, Kiyoshi Kawade
Toshyuki Iida* and Akito Takahashi*
Department of Nuclear Engineering, Nagoya University

Abstract:

Measurements of formation cross-sections of short-lived nuclei produced by 14 MeV neutron were made by using the Intense Neutron Source(OKTAVIAN) for the energy range of 13.40 MeV and 14.87 MeV. Measured reactions were ^{92}Mo(n, 2n), ^{92}Mo(n, α), ^{63}Cu(n, 2n), ^{65}Cu(n, α), ^{90}Zr(n, 2n), ^{55}Mn(n, α) reactions.

1. Introduction

Measurements of formation cross-sections of short-lived nuclei produced by 14 MeV neutron have been done by the activation method. The measurements are not easy because of the half-lives of the product nuclei are short and reliable data are scarce. Then, we made measurements of reaction cross-sections of short-lived nncleus(with half-lives of 1 - 15 min) formation.

2. Experiment

Experiments were performed at the Intense 14 MeV Neutron Facility(OKTAVIAN) of Osaka University. Cross-sections were obtained by the activation method. Pneumatic tubes were set at 6 directions(between 0° and 155°) for the incident deuteron beam direction as is shown in Fig. 1 for the purpose

*Department of Nuclear Engineering, Osaka University

of transportation of samples. The distances between the T-target and the irradiation points were 15 cm. The neutron flux at the irradiation points were monitored by using aluminum foils (purity: 99.2 %, 1 cm x 1 cm x 0.2 cm^t). Samples of natural molybdenum, zirconium, manganese and copper were irradiated together with the monitor foils. The amount of each sample was about 100 mg. The neutron flux at the sample was about 1 x 10^8 n/cm^2 s, and determined for each irradiation by using the $^{27}Al(n, p)^{27}Mg$($T_{1/2}$ = 9.46 m) reaction (see Fig. 2) as a reference. The irradiation times were nearly same as the half-lives of nuclei to be measured. Gamma-rays of induced short-lived nuclei were measured by a Ge detector at the distance of 5 cm equivalent, immediately after the irradiation. The neutron energies at the irradiation points were determined by the Zr-Nb method.

3. Results

Cross-sections of reactions of $^{92}Mo(n, 2n)^{91m}Mo$($T_{1/2}$ = 65 s), $^{92}Mo(n, \alpha)^{89m}Zr$($T_{1/2}$ = 4.18 m), $^{63}Cu(n, 2n)^{62}Cu$($T_{1/2}$ = 9.74 m), $^{65}Cu(n, \alpha)^{62m}Co$($T_{1/2}$ =13.91 m), $^{96}Zr(n, 2n)^{89m}Zr$($T_{1/2}$ = 4.18 m), and $^{55}Mn(n, \alpha)^{52}V$($T_{1/2}$ = 3.75 m) were measured.

Measured cross-sections are shown in figures(Fig. 3 through Fig. 8) together with previous results[1)-23)].

The use of the Intense Neutron Source(OKTAVIAN) and the $^{27}Al(n, p)^{27}Mg$ reaction as a reference results in successful measurements of cross-sections of short-lived nucleus formation reactions. Next measurements will be done by using separate isotpes.

REFERENCES

(1) JARJIS, R. A.: J. of Physics G: Nuclear Physics, 4, 445 (1978).

(2) RYVES, P. B., KOLKOWSKI, P., ZIEBA, K. J.: J. of Physics G: Nuclear Physics, 4, 1783 (1978).

(3) CSIKAI, J.: Nuclear Data for Sci. & Technol., 414 (1982).

(4) HARPER, R. C., ALFORD, W. L.: J. of Physics G: Nuclear Physics, 8, 153 (1982).

(5) LU, W.-D., RANAKUMAR, N., FINK, R. W.: Phys. Rev. C, 1, 350 (1970).

(6) QAIM, S. M.: Nuclear Physics, A185, 614 (1972).

(7) KANDA, Y.: Nuclear Physics, A185, 177 (1972).

(8) RAO, C. V. S., DAS, N. L., RAO, B. V. T., RAO, J. R.: Physica Scripta, 24, 935 (1981).

(9) AMEMIYA, S., ISHIBASHI, K., KATOH, T.: J. Nucl. Sci. Technol., 19, 781 (1982).

(10) MARCINKOWSKI, A., STANKIEWCS, K., GARUSKA, U., HERMAN, M.: Z. f. Physik, A -Atomic Nuclei, 323, 91 (1986).

(11) SIGG, R. A., KURODA, P. K.: J. inorg. nucl. Chemistry, 37, 631 (1975).

(12) LISKIEN, H., PAULSEN, A.: J. Nucl. Energy A/B, 19, 73 (1965).

(13) GHANBARI, F., ROBERTSON, J. C.: Annals of Nuclear Energy, 13, 301 (1986).

(14) PREISS, I. L.: A-ARK-60, 2 (1960).

(15) KANTELE, J., GARDNER, D. G.: Nucl. Phys., 35, 353 (1962).

(16) BRAMLITT, E. T., FINK, R. W.: Phys. Rev., 131, 2649 (1963).

(17) BORMANN, M.: EANDC(E)-66, 4 (1966).

(18) CLATOR, I. G.: private communication to JNDC (1969), see JENDL-2

(19) HUSAIN, L., BARI, A., KURODA, P. K.: Phys. Rev. C, 1, 1233 (1970).

(20) FUJINO, Y., HYAKUTAKE, M., KUMABE, I.: NEANDC(J)-51/U (1977).

(21) TURKIEWICS, J.: private communication to JNDC (1975), see JENDL-2.

(22) GARUSKA, U., DRESLER, J., MALECKI, H.: ZfK-376, 51 (1978).

(23) ZUPRANSKA, E., RUSEK, K., TUREKIEWICS, J., ZUPRANSKA, P.: Institute of Nuclear Research-182/I/PL 20, 37 (1980).

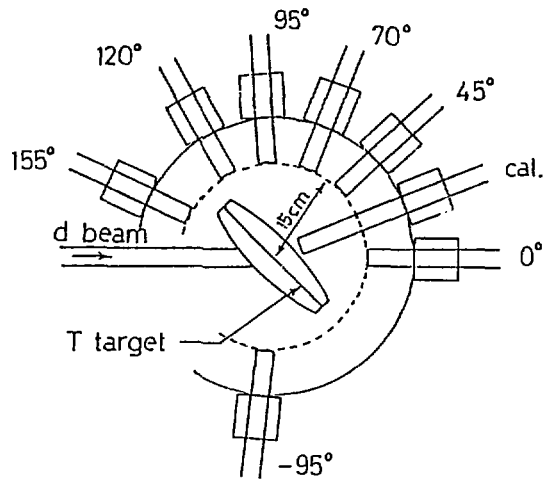

Fig. 1 The arrangement of the T-target and the pneumatic tubes

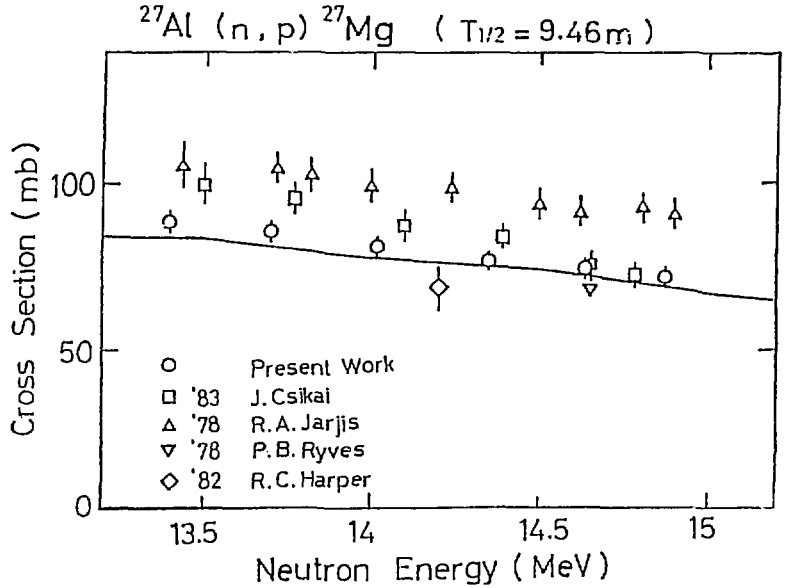

Fig. 2 Cross-sections of the $^{27}Al(n, p)^{27}Mg$ reaction measured in the present experiment. The reference reaction of this measurement was the $^{27}Al(n, \alpha)^{24}Na$ reaction.

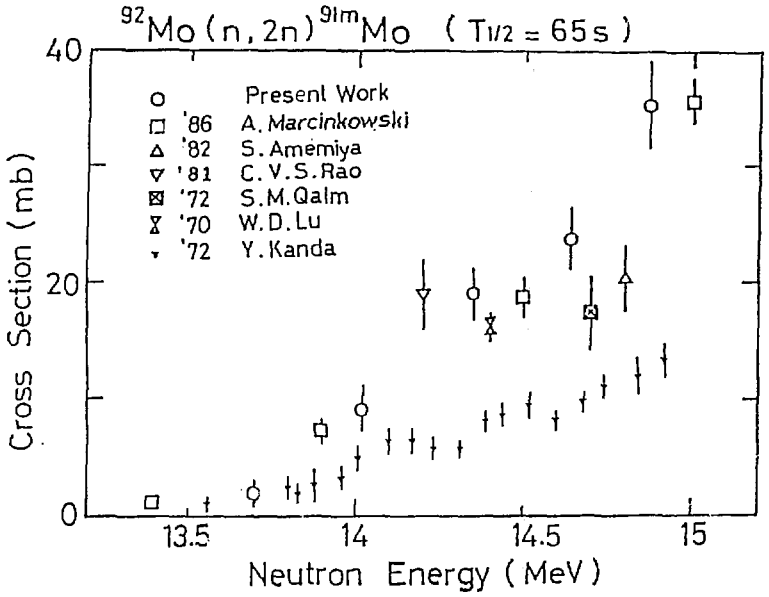

Fig. 3 Cross-sections of $^{92}Mo(n, 2n)^{91m}Mo$ reaction. The reference reaction for this measurement and the following 5 reactions was the $^{27}Al(n, p)^{27}Mg$ reaction.

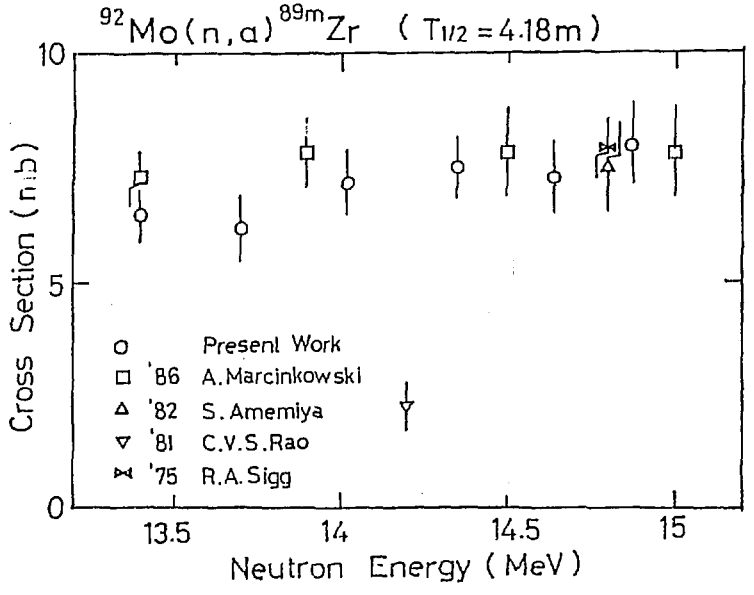

Fig. 4 Cross-sections of $^{92}Mo(n, \alpha)^{89m}Zr$ reaction.

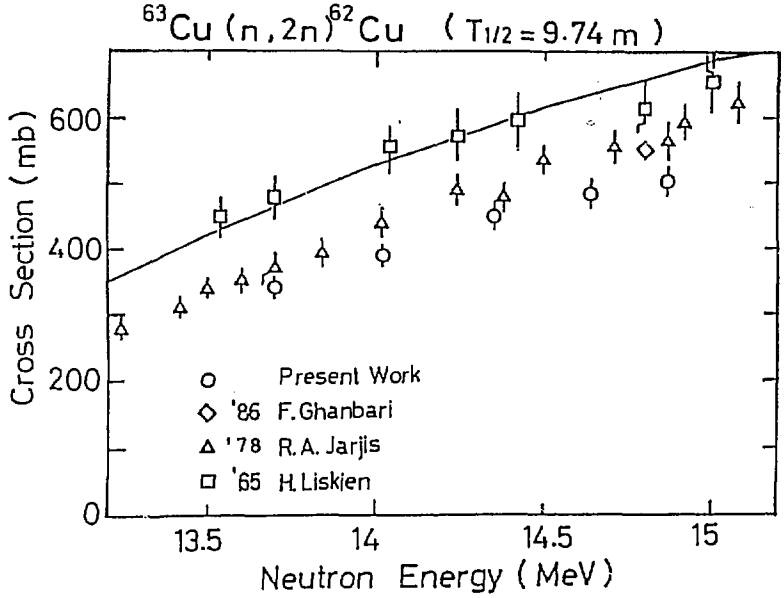

Fig. 5 Cross-sections of $^{63}Cu(n, 2n)^{62}Cu$ reaction.

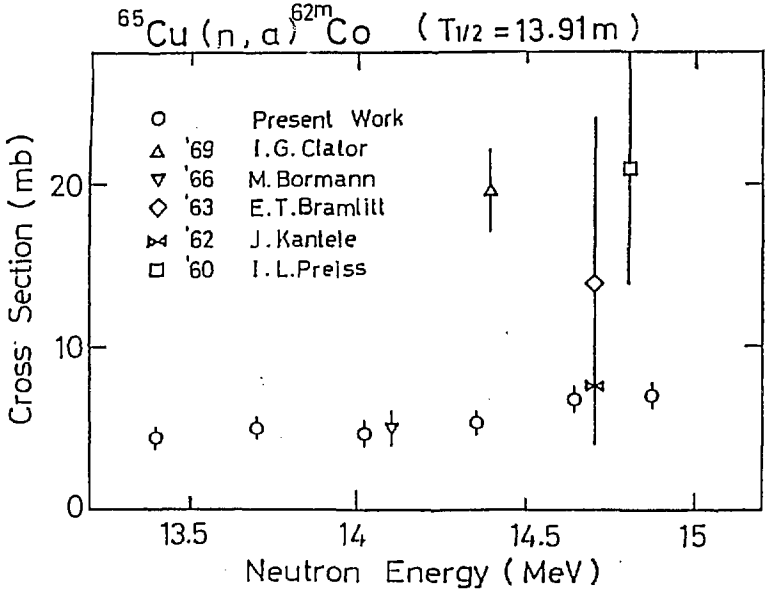

Fig. 6 Cross-sections of $^{63}Cu(n, \alpha)^{62m}Co$ reaction.

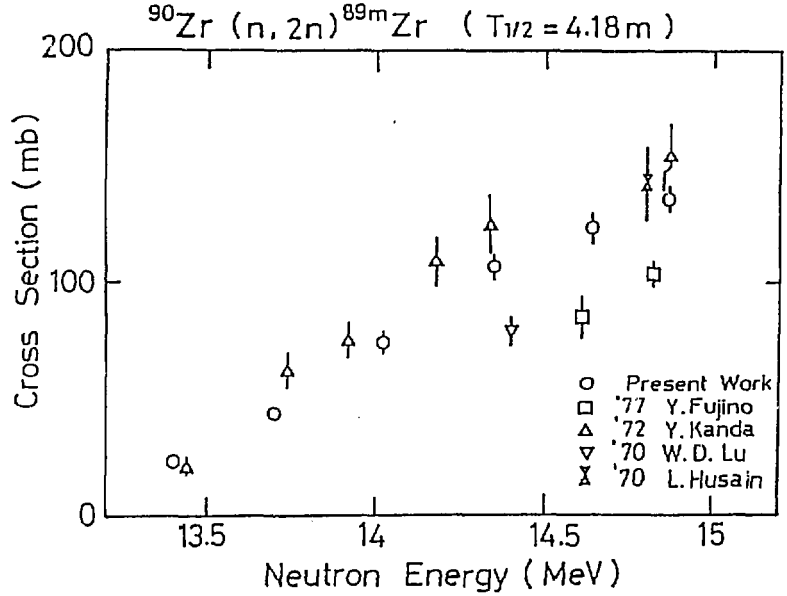

Fig. 7 Cross-sections of $^{90}Zr(n, 2n)^{89m}Zr$ reaction.

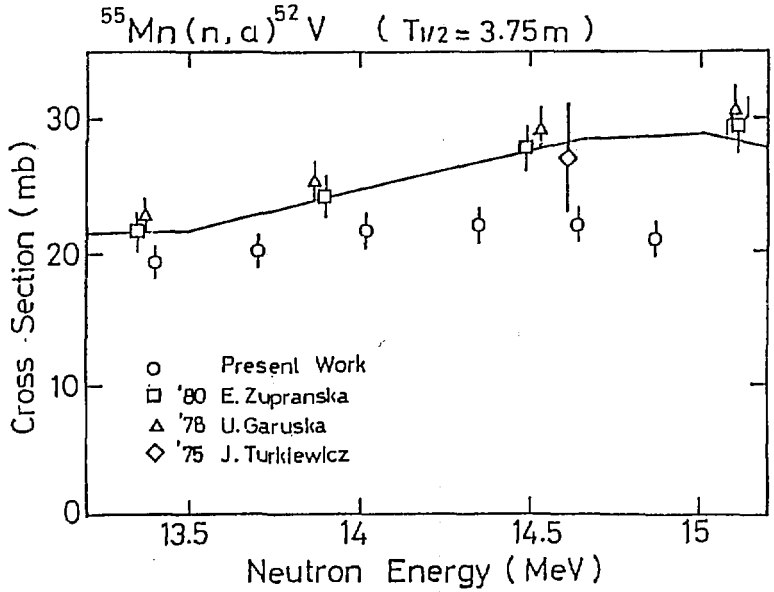

Fig. 8 Cross-sections of $^{55}Mn(n, \alpha)^{52}V$ reaction.

3.10 Integral Test of Neutron Cross Sections in the JENDL-3T through an Analysis on the Neutron Deep Penetration Experiment at the ORNL TSF

Kiyoshi Sakurai†, Kohtaro Ueki†† and Masayoshi Kawai†††

† Japan Institute of Nuclear Safety, Minato-ku, Tokyo
†† Ship Research Institute, Mitaka, Tokyo
††† Nippon Atomic Industry Group, Co., Ltd., Kawasaki, Kanagawa

ORNL TSF sodium neutron deep penetration benchmark experiment is analysed for integral test of neutron cross sections in JENDL-3T. C/E's of Bonner ball reaction rates are about 1.0 - 1.1. As for neutron spectrum in the energy range 0.1 - 10 MeV, the JENDL-3T slightly overestimates neutron fluxes as like ENDF/B-IV. It is concluded that the JENDL-3T is the most applicable to shielding analysis.

1. Introduction

As one of activities of JNDC, an integral test of the evaluated nuclear data has been made for shieldind application. Recently, applicability of the sodium neutron cross sections in the ENDF/B-IV and JENDL-2 has been clarified by analysing the shielding benchmark experiment concerning deep penetration in sodium[1] which was conducted at the Tower Shielding Facility of the ORNL[2]. In the present work, the reliability of the JENDL-3T[3]* neutron cross sections is examined through analysis of the experiment. The calculated results are compared with the experimental data and those for the ENDF/B-IV and JENDL-2.

2. Benchmark experiment system

The experiment was performed with large diameter samples of sodium from 2.5 ft to 15 ft thick and a collimated neutron source extracted from the TSR reactor. Integral measurements of neutron fluence were

* JENDL-3T is a temporaly file for testing the evaluated data which are for JENDL-3. The data in JENDL-3T will be partly revised in JENDL-3.

made with Bonner ball detectors (BB) behind sodium and neutron spectra were with NE-213 and Benjamin type spectrometers. The experiment is suitable for integral test, since its arrangement can be exactly expressed with a cylindrical model.

3. Analysis method

The analysis is made for 10 ft thick sodium sample with the two-dimensional Sn transport code DOT-3.5. The benchmark system is modeled as shown in Fig. 1. Calculations are carried out in 100 energy groups with P3-S48 approximation, using first collision source and the resonance self-shielded 100 energy group neutron cross sections which are generated from JENDL-3T by the shielding analysis code system RADHEAT-V4[4]. The ENDF/B-IV cross sections are also adopted for materials except sodium, so as to ascertain in effect of only sodium cross section difference between JENDL-3T and the other libraries such as ENDF/B-IV and JENDL-2. Neutron fluence and spectra behind the sodium sample are calculated with the SPACETRAN code which treats neutron transmission in air from sodium to the detectors. In calculation of BB reaction rates, there are two points which are different from the former analysis[1] : adoption of revised detector response functions and effective detection center instead of actual detector center. In this condition, calculations are carried out with JENDL-3T, -2 and ENDF/B-IV.

4. Results

The C/E's of BB reaction rates are thus obtained. The C/E's are shown in Figs. 2, 3, 4 and 5 for Cd-BB, 3" BB, 6" BB and 10" BB, respectively. The average C/E's are summarized as shown in Table 1. Agreement of JENDL-3T calculation with the measurement is better than those of ENDF/B-IV and JENDL-2.

As for neutron spectrum in the energy range 0.1 to 1 MeV, JENDL-2 result shows the best agreement with the data measured by Benjamin detector, as shown in Fig. 6, while JENDL-3T result slightly overestimates neutron fluxes as like ENDF/B-IV. In the energy range from 1 to 10 MeV, JENDL-3T and ENDF/B-IV results go along the upper limit of the error band of unfolded neutron spectrum measured by NE-213 spectrometer and JENDL-2 result goes along the lower limit.

5. Discussion and conclusion

The difference between JENDL-3T and -2 results of integral test come from the following cross section fifferences : (1) total cross sections of JENDL-3T are about 5 % smaller than JENDL-2 in the energy range below 1 eV, (2) it is about 2 % smaller from 1 to 100 eV, shown in Fig. 7, (3) in the energy range from 3 to 10 MeV, elastic scattering cross sections of the former are about 15 % larger and reversely inelastic scattering cross sections are about 15 - 20 % smaller, while total cross sections are nearly equal.

The reason of larger values of BB reaction rates for JENDL-3T is attributed mainly to an decrease of total cross sections, i.e. items (1) and (2) and partially to an increase of slowing-down neutrons due to item(3). Spectrum hardening in the energy range from 0.1 to 10 MeV can be explained by decrease of inelastic scattering, item (3), which slow down within the wider energy range than elastic scattering. Agreement of the calculated spectrum with the measured data is not enough, but it is acceptable with consideration of very deep penetration of 10 ft thick sodium. It is concluded that the JENDL-3T is the most applicable to shielding analysis, compared with JENDL-2 and ENDF/B-IV.

References

1) K. Sakurai, et al. : private communication (1986).
2) K. E. Maerker : ORNL-4880 (1974).
3) JENDL Compilation Group (Nuclear Data Center, JAERI) : JENDL-3T, private communication (1987).
4) N. Yamano, K. Koyama and K. Minami : Proc. 6th Conf. on Radiation shielding, vol. 1, 331 (1983).

Table 1 Average C/E's of BB reaction rates

Detector	JENDL-3T	ENDF/B-IV	JENDL-2
Cd-BB	1.0	0.8	0.7
3" BB	1.1	0.9	0.8
6" BB	1.05	0.9	0.9
10" BB	1.0	0.85	0.9

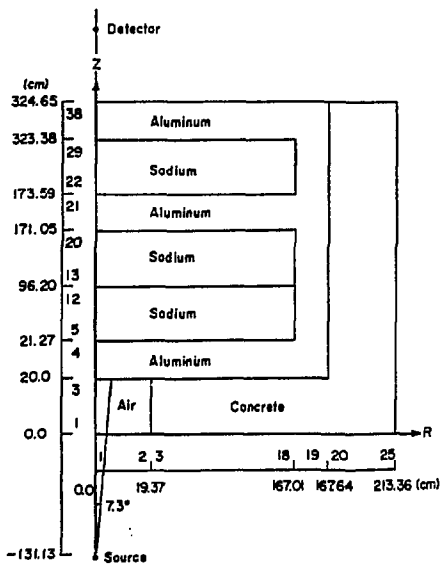

Fig. 1 Calculational model for DOT-3.5

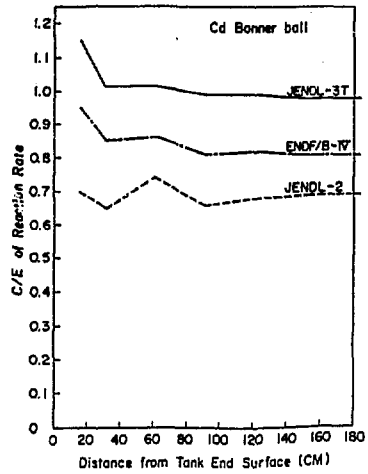

Fig. 2 C/E's of Cd-BB reaction rates

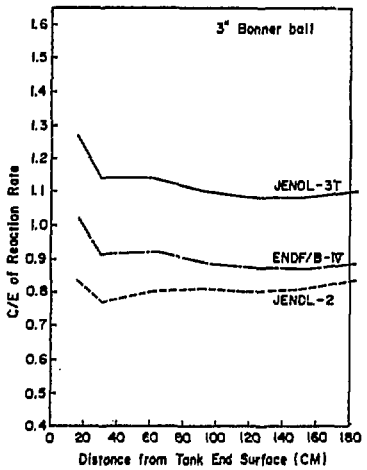

Fig. 3 C/E's of 3" BB reaction rates

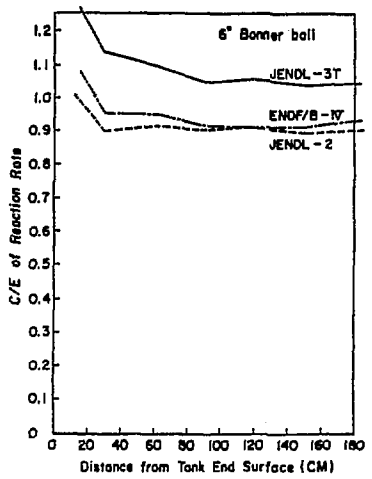

Fig. 4 C/E's of 6" BB reaction rates

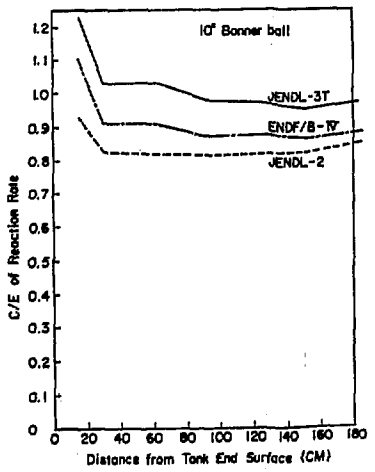

Fig. 5 C/E's of 10" BB reaction rates

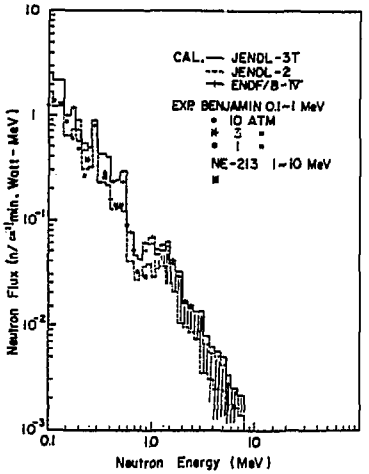

Fig. 6 Comparison of calculated spectra with measured spectrum

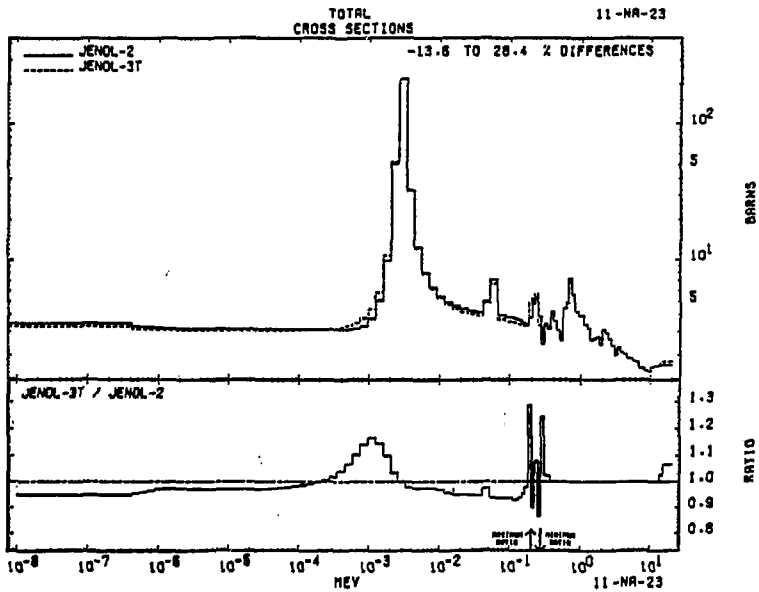

Fig. 7 Sodium neutron cross sections in JENDL-3T and -2

3.11 Evaluation of Secondary Gamma-Ray Production Cross Sections of Iron in the JENDL-3T through an Analysis on the 14-MeV Neutron Penetration Experiment of SUS-304 at the ORNL

Kiyoshi Sakurai
Japan Institute of Nuclear Safety

Kohtaro Ueki
Ship Research Institute

The 14-MeV neutron penetration experiment of SUS-304 carried out at the ORNL is a typical benchmark problem to evaluate not only a calculational method of fast neutrons but also neutron cross sections and secondary gamma-ray production cross sections, as well. The benchmark experiment was analyzed by the MORSE-CG code with the ENDF/B-IV and the JENDL-3T cross section libraries. The neutron and gamma-ray coupled cross sections were compiled by the RADHEAT-V4 code system.

1. Introduction

The 14-MeV neutron penetration experiment of SUS-304[1] carried out at the ORNL is a typical benchmark problem to evaluate not only a calculational method of fast neutrons but also neutron cross sections and secondary gamma-ray production cross sections, as well. The experimental configuration is shown in Fig.1. The benchmark experiment was analyzed by the Monte calro code MORSE-CG[2] with the ENDF/B-IV[3] and the JENDL-3T[4]* cross section libraries. The neutron and gamma-ray coupled cross sections were compiled by the RADHEAT-V4[5] code system. The Monte Carlo results of the neutron and the secondary gamma-ray energy spectra penetrated through the SUS-304 are shown, and the reliability of cross section libraries are discussed with the Monte Calro results in this study.

2. Calculational Techniques and Results

The energy group structures employed in the calculations were same as the Santro's analysis[1] by the DOT-3.5 code ; 53 groups for neutrons, 21 groups for gamma rays, and Legendre expansion coefficients were taken up to P_9. In the analysis with the JENDL-3T, the nuclides in the materials (air, iron, and concrete), except the SUS-304, were obtained from the ENDF/B-IV library. Also, there was no data on secondary gamma-ray production cross sections of manganese in the SUS-304, the cross sections were taken from the ENDF/B-IV library. The atomic number density of manganese in the SUS-304 ocupies only 2w/o. The calculations were performed by the MORSE-CG code with the splitting. In the case 1, only the iron cross sections in the SUS-304 was obtained from the JENDL-3T, and in the case 2, the iron, nickel, and chromium cross sections were taken from the JENDL-3T. The calculated energy spectra were processed by the resolution of the NE-213 detector. The Monte Calro results in the case 1 are shown in Fig.2 for the neutron spectrum and also in Fig.3 for the gamma-ray spectrum.

3. Discussions

The calculated secondary gamma-ray energyspectrum agreed well with the measured values and there were no distinct differences between the calculated results with the ENDF/B-IV and the ones with the JENDLE-3T. However, as indicated in Fig.4 the values of GAMGEN's (i.e., Σ_γ / Σ_T) in the MORSE-CG code indicated that the values of the JENDL-3T were larger than those of the ENDF/B-IV as much as a factor of 2~3, in the neutron energy region of 0.3~0.9MeV. Fortunately, the magnitude of the secondary gamma-ray production numbers for a neutron between 0.3 and 0.9 MeV is less than that of the other energy regions by a factor of 10. Accordingly, the secondary gamma-rays produced by neutrons between 0.3 and 0.9 MeV energy region would be a less contribution in the secondary gamma-ray energy spectrum. The iron cross sections in the ENDF/B-IV are not taken into account

the inelastic scattering cross sections of ^{57}Fe ; on the other hand, the cross sectionsin the JENDL-3T are deliberated on the inelastic cross sections of it. Accordingly, the iron cross sections in the JENDL-3T have better reliability than those of the ENDF/B-IV.

---

* JENDL-3T is a temporary file for testing the evaluated data which are for JENDL-3. The data in JENDL-3T will be partly revised in JENDL-3.

References

1) Santro, R.T., et al., Nucl. Sci. Eng., 78, 259(1981)

2) M.B.Emmett "The MORSE Monte Carlo Radiation Transport Code System," ORNL-4972 (1975).

3) "ENDF/B Summary Documentation," BNLNCS-17541(ENDF-201), 2nd ed. (ENDF/B-IV), D. Garber, Ed., available from the National Nuclear Date Center, Brookhaven National Laboratory, Upton, New York (Oct.1975).

4) JENDL Compilation Group (Nuclear Data Center, JAERI); JENDL-3T, private communication (1987).

5) N.Yamano, K.Koyama, K.Minami, "Development of Integrated Shielding Analysis Code System RADHEAT-V4," Proc. of Sixth Int. Conf., May 1983, Tokyo, Vol. 1, P.331, JAERI(1983).

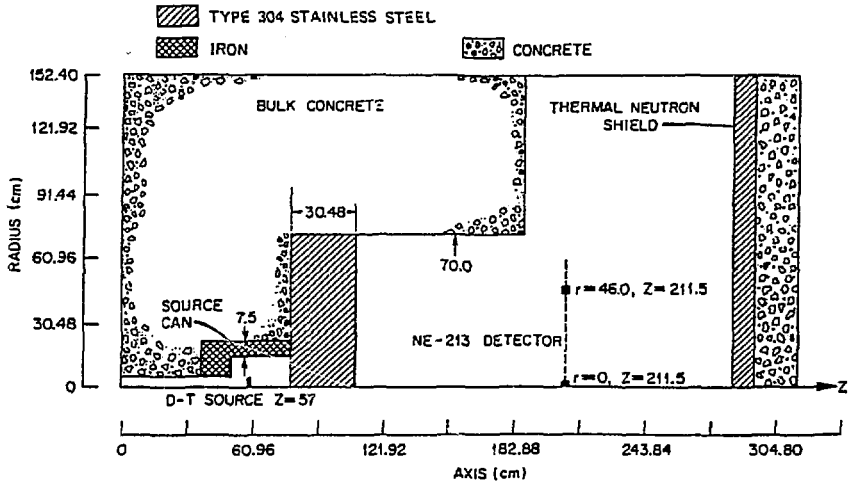

Fig. 1. Two-dimensional calculational model of the experimental configuration.

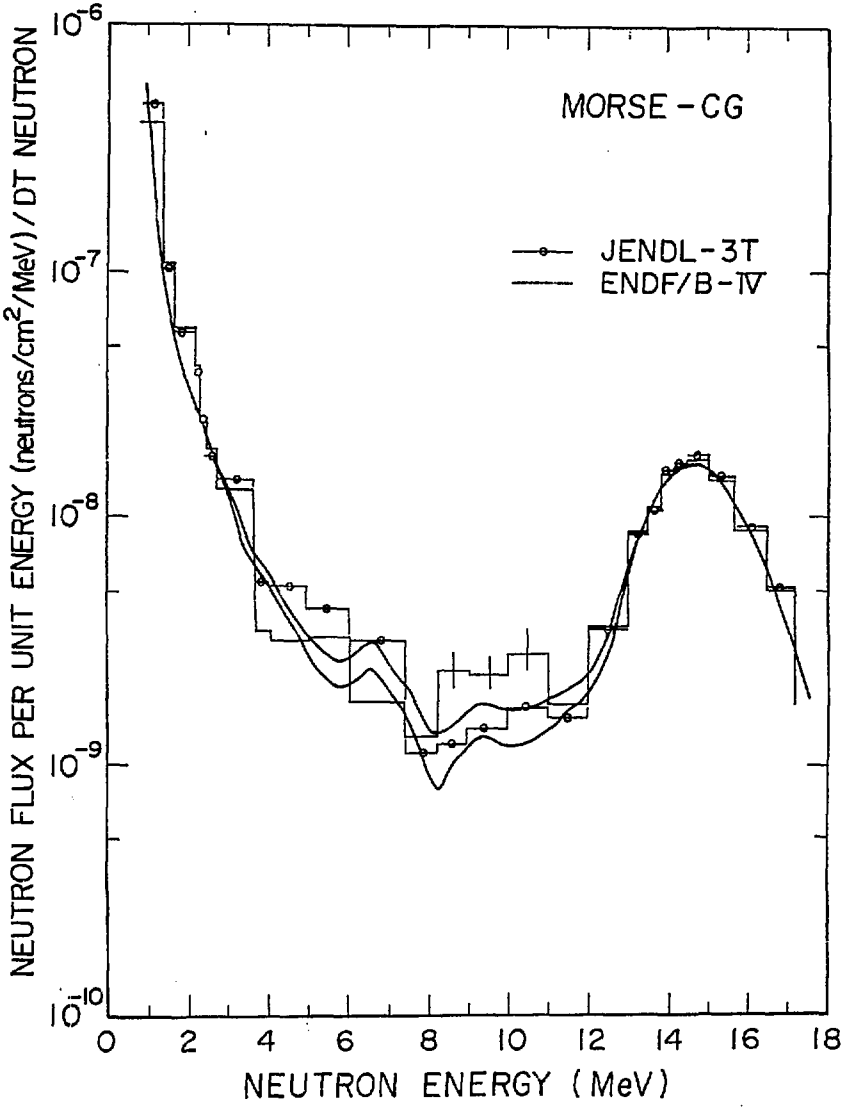

Fig. 2 Neutron flux per unit energy versus neutron energy for Type 304 stainless steel of 30.48 cm-thick.

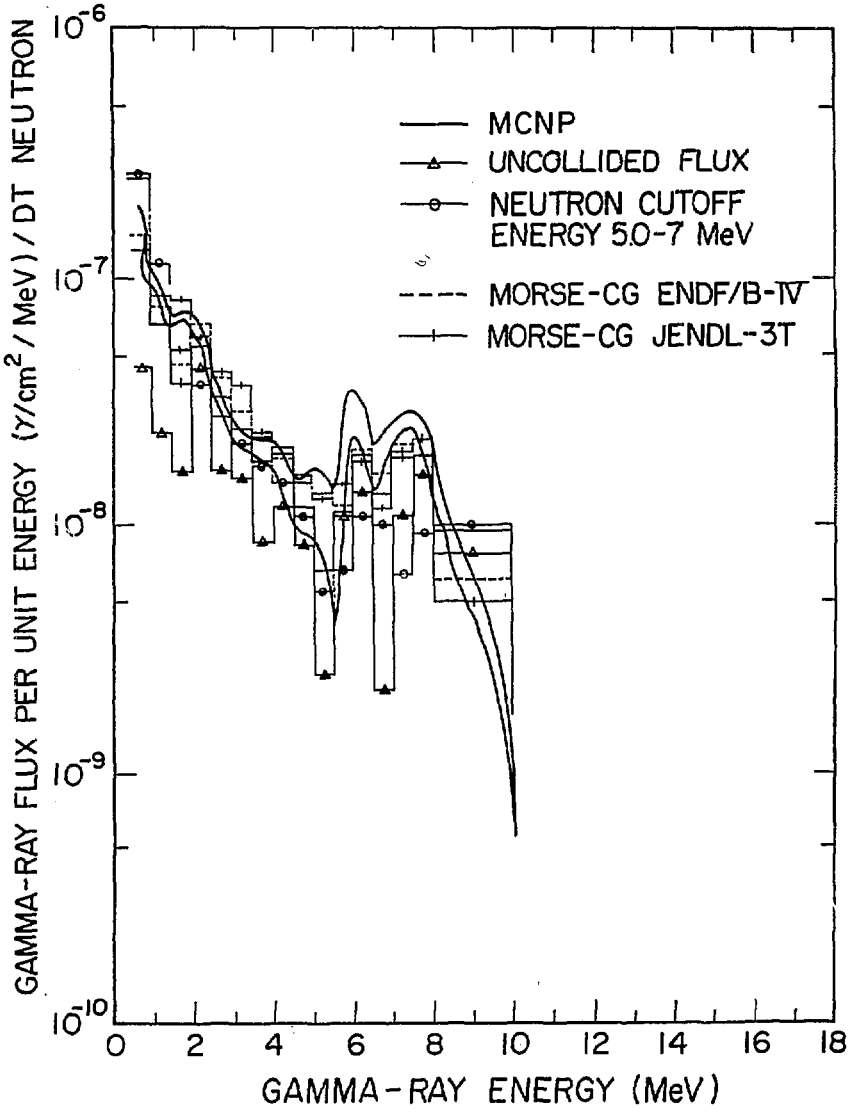

Fig. 3 Gamma-ray flux per unit energy versus gamma-ray energy for Type 304 stainless steel of 30.48 cm-thick.

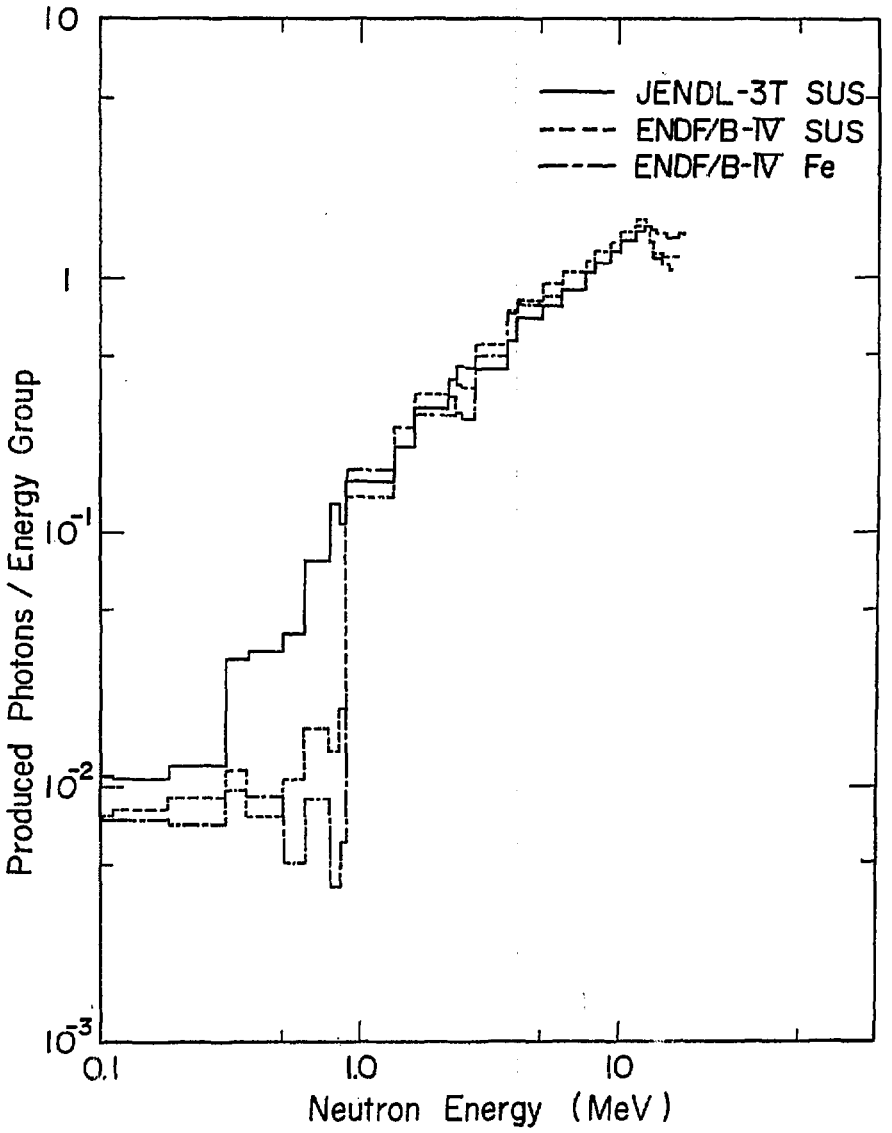

Fig.4 Values of GAMGEN's(i.e., Σ_γ / Σ_T) in the MORSE-CG code.

3.12 Neutron Integral Test of Graphite Cross Sections in MeV Energy Region for the JENDL-3T through an Analysis of the WINFRITH Shielding Experiment

Kohtaro Ueki
Ship Research Institute
Shinkawa, Mitaka-shi, Tokyo 181

Kiyoshi Sakurai
Japan Institute of Nuclear Safety
Mita, Minato-ku, Tokyo 181

The neutron integral tests of graphite cross sections in MeV neutron energy region for the ENDF/B-IV, JENDL-2, JENDL-3PR1 and -3T were performed through the Monte Carlo analysis of the graphite shielding experiment at the WINFRITH. The measured values were on the reaction rates of $^{115}In(n,n')^{115m}In$, $^{27}Al(n,\alpha)^{24}Na$, $^{32}S(n,p)^{32}P$, and $^{103}Rh(n,n')^{103m}Rh$ threshold detectors located in the graphite slabs, so that the experiment on the graphite was good at the integral test of neutron cross sections in MeV energy resion.

1. Introduction

To evaluate the reliability of graphite cross sections in the JENDL-3T[1)]*, the neutron integral tests of graphite cross sections in MeV neutron energy region were performed not only for the JENDL-3T but also for the ENDF/B-IV[2)], JENDL-2[3)], and JENDL-3PR1[4,5)] through the Monte Carlo analysis of the graphite shielding experiment at the WINFRITH[6)]. The experimental configuration is shown in Fig. 1. The measured values were on the reaction rates of $^{115}In(n,n')^{115m}In$, $^{27}Al(n,\alpha)^{24}Na$, $^{32}S(n,p)^{32}P$, and $^{103}Rh(n,n')^{103m}Rh$ threshold detectors located in the graphite slabs, so that the experiment on the graphite was suitable for the integral test of neutron cross sections in MeV energy resion.

2. Calculational techniques and Results

The cross sections prepared to calculate this experiment were compiled by using the RADHEAT-V4[7] code system ; neutron 100 groups and the Legendre expansion coefficients were taken up to P_9. The Monte Carlo code MORSE-CG[8] with the splitting technique was employed to the analysis and the reaction cross sections of the threshold detectors were compiled by the IRDF-82 library. The NESX(Next Event Surface Crossing) Estimator was used to reduce the FSD (fractional standard deviation) in all the calculations. The calculated results of those threshold detectors are shown in Table 1. There is no distinct difference in the value of C/E(Calculated/Experiment) by each cross section library employed in the calculations. The differences of the total cross sections between ENDF/B-IV and the other three libraries were only a few percents in the energy resion of 0.1-10 MeV. The Rh(n,n') reaction rates obtained from the Monte Carlo calculations were a little less than those of the experiment. However, the reason of the under estimation does not depend on the cross sections of graphite, but it may be due to calculational techniques or measured data on its own.

3. Discussions

Through the Monte Carlo analysis of the threshold detectors located as far as 50-cm-depth in the graphite slabs, there was no distinct difference in the value of C/E by each cross section library. Consequently, the reliability of the graphite cross sections in MeV energy resion of the JENDL-3T were demonstrated by the present investigations of the integral test.

---

* JENDL-3T is a temporary file for testing the evaluated date which are for JENDL-3. The date in JENDL-3T will be partly revised in JENDL-3.

References

1) JENDL Compilation Group (Nuclear Date Center, JAERI); JENDL-3T, private communication (1987).

2) "ENDF/B Summary Documentation," BNLNCS-17541(EBDF-201), 2nd ed. (ENDF/B-IV), D. Garber, Ed., available from the National Nuclear Date Center, Brookhaven National Laboratory, Upton, New York (Oct.1975).

3) Y.Kikuchi, et al., "Second Version of Japanese Evaluated Nuclear Date Library (JENDL-2)," J. Nucl. Sci. Tech., 22, 593 (1985).

4) T.Asami "Status of JENDL-3PR1 & -3PR2." JAERI-M 86-029, 15 (1986).

5) K. Shibata "Evaluation of Neutron Nuclear Date for ^{12}C" JAERI-M 83-221 (1983).

6) M.D. Carter, M.M. Chestnutt, and A.K. McCracken, "The ASPIS Iron Benchmark Experiment-Results and Calculational Model," Proc. of Specialists' Meeting on Nuclear Data and Benchmarks for Reactor Shielding, Oct. 1980, Paris, p. 297 (1980).

7) N.Yamano, K.Koyama, K.Minami, "Development of Integrated Shielding Analysis Code System RADHEAT-V4," Proc. of Sixth Int. Conf., May 1983, Tokyo, Vol. 1, P.331, JAERI(1983).

8) M.B.Emmett "The MORSE monte Carlo Radiation Transport Code System," ORNL-4972 (1975).

Table 1 Values of C/E (Calculated/Experiment) for each threshold detector.

DETECTOR & LOCATION(cm)		ENDF/B-4	JENDL-2	JENDL-3PR1	JENDL-3T
In(n,n')	0	1.04 ±0.04	1.00 ± 0.03	1.00 ± 0.04	1.00 ± 0.03
	10	1.00 ±0.05	0.90 ± 0.03	0.95 ± 0.04	0.94 ± 0.03
	30	0.87 ± 0.09	0.84 ± 0.04	0.96 ± 0.10	0.87 ± 0.04
	50	1.00 ± 0.20	0.82 ± 0.08	0.97 ± 0.23	0.90 ± 0.10
Al(n, α)	0	0.96 ± 0.10	0.92 ± 0.05	1.00 ± 0.11	0.95 ± 0.05
	10	1.07 ± 0.17	1.03 ± 0.07	1.08 ± 0.22	1.02 ± 0.10
	30	0.96 ± 0.12(*)	0.93 ± 0.12	1.17 ± 0.26	1.10 ± 0.11
S(n,p)	0	1.05 ± 0.05	1.01 ± 0.04	1.03 ± 0.07	1.00 ± 0.04
	10	1.05 ± 0.06	0.98 ± 0.04	1.07 ± 0.07	1.00 ± 0.05
	30	1.03 ± 0.14	0.90 ± 0.05	1.09 ± 0.17	0.98 ± 0.05
	50	1.09 ± 0.40	0.88 ± 0.09	1.06 ± 0.26	1.03 ± 0.10
Rh(n,n')	0	1.00 ± 0.06	0.96 ± 0.03	0.96 ± 0.03	0.96 ± 0.03
	10	0.92 ± 0.04	0.84 ± 0.03	0.88 ± 0.04	0.90 ± 0.04
	30	0.73 ± 0.06	0.71 ± 0.03	0.81 ± 0.07	0.80 ± 0.05
	50	0.78 ± 0.14	0.65 ± 0.05	0.75 ± 0.15	0.70 ± 0.10

(*) Calculated with the splitting.

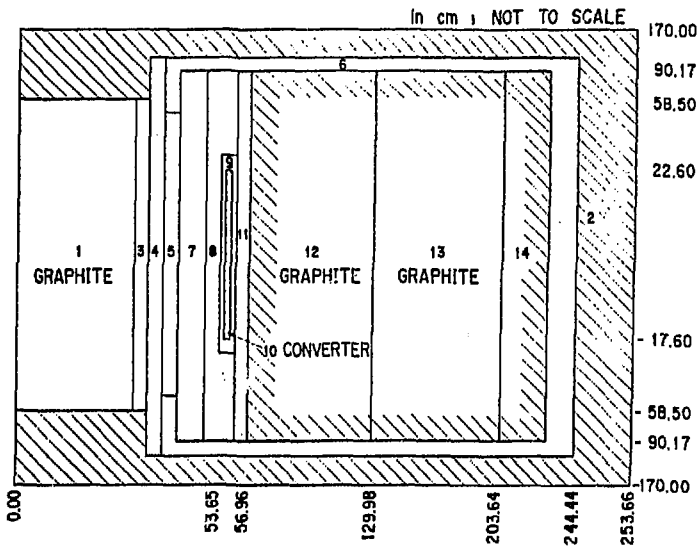

Fig. 1 Schematic arrangement of graphite shielding experiment at the WINFRITH[6] (1, 7, 12, 13, 14 ; Graphite, 2 ; Concrete, 3, 5, 9, 11 ; Aluminum, 4, 8 ; Void 6 ; Mild Steel, 10 ; U/Al Fuel).

3.13 $^{7}Li + \vec{p}$ Reactions at 12, 14 and 16 MeV

N. Koori, I. Kumabe, M. Hyakutake, K. Orito, K. Akagi, Y. Watanabe, K. Ogawa, N. Oda, J. Yano and A. Iida

Department of Nuclear Engineering, Kyushu University, Fukuoka, 812 Japan

and

K. Sagara, H. Nakamura, K. Maeda, T. Nakashima and M. Kamimura

Department of Physics, Kyushu University, Fukuoka, 812 Japan

Abstract: Double differential cross sections and analyzing powers for $^{7}Li(p,p')$, (p,d) and (p,t) reactions have been measured at incident energies of 12, 14 and 16 MeV. Experimental results are briefly summarized. Theoretical analyses are also given; two sets of the optical potential parameters were obtained from calculations based on the spherical optical model and based on the coupled channel method. Furthermore, adoptability of the coupled discretized-continuum channel method and final state interaction theory are discussed for continuum regions of proton and triton energy spectra, respectively.

1. Introduction

Nuclear data for $^{6,7}Li$ isotopes are important for the fusion reactor development. Especially, tritium production cross sections and double differential cross sections (DDX) for inelastic scatterings are related to the tritium breeding ratio in the reactor and neutron transport in the reactor blanket. Precise measurements were recently reported on $^{6,7}Li(n,t)$ and (n,n') reactions(1-4) to refine their nuclear data.

In evaluations of nuclear data for lithium isotopes, experimental data are treated by simple theories(5) because of difficulties in theoretical analyses including three-body breakup processes. It is highly necessary to establish nuclear theories for reactions involving lithium

isotopes. The coupled discretized-continuum channel (CDCC) calculation has successfully reproduced lithium breakup reactions(6). Furthermore, the Faddeev approach for three-body breakup reactions has been developed extensively for rather simple systems(7). For study of their adoptability to the reactions, precise double differential cross sections and analyzing powers have to be measured. Proton induced reactions have advantages in precision against neutron induced reactions.

As concerns the ^{7}Li(n,n') scattering data, the 1st excited state (0.478 MeV) peak could not be separated from the elastic peak by means of TOF spectrometers. The optical potential for ^{7}Li was searched by the use of only differential cross sections including the ground and 1st excited states. Furthermore, the spin dependent terms of V_{so}, r_{so} and a_{so} were fixed a priori in the search. Experiments with polarized beams are required to determine the spin dependent terms. Measurements of analyzing powers, however, have been performed only for ^{6}Li(n,n) elastic scattering(3); for reaction channels polarization data have not been reported.

On the other hand, there are no experimental data of polarized proton induced reactions on the lithium isotopes in an energy region of 10-18 MeV. Systematic study of scatterings and reactions on the lithium isotopes by the use of polarized proton beams will give valuable information for modelling of nuclear reactions involving the isotopes.

This report describes measurements of ^{7}Li(p,p'), (p,d) and (p,t) reactions induced by polarized protons of 12, 14 and 16 MeV, and results of theoretical analyses of the data.

2. Experimental Procedure

Polarized and unpolarized proton beams from the tandem accelerator at Kyushu University were used for measurements of ^{7}Li(p,p'), (p,d) and (p,t) reactions at incident energies E_l of 12.0, 14.0 and 16.0 MeV. Emitted particles were detected with a counter telescope, which consisted of 15.5 μm and 75 μm thick transmission-type Si detectors and a 2000 μm thick Si detector. The lowest energy for the measurement was 1.0 MeV for protons, 1.3 MeV for deuterons and 1.5 MeV for tritons. The over-all energy resolution for protons was about 95 keV in fwhm, which was mainly due to the kinematical spreading.

Self-supporting ^{7}Li metallic foils used have thicknesses of 0.867 mg/cm^2 thick (for measurements at 12 and 14 MeV), and 0.324 mg/cm^2 thick

(for measurements at 16 MeV).

The beam polarization was monitored at the down stream of the scattering chamber. The polarimeter consisted of a ^{4}He gas target and two ΔE+E Si detector systems fixed at ± 113° with respect to the beam direction, where the analyzing power of ^{4}He was known to be 1.00 - 0.98 for 12 - 16 MeV protons.

3. Experimental Results

3-1 ^{7}Li(p,p') scattering.

The differential cross sections and analyzing powers for 12, 14 and 16 MeV are shown in Figs. 1(a - c) for the ground(3/2-), 1st excited (0.478MeV, 1/2-), and 2nd excited (4.63MeV, 7/2-) states.

Examples of DDX spectra of the (p,p') scattering are shown for 14 MeV in Fig. 2(a). The continuum region of spectra are mainly due to three-body breakup process of ^{7}Li(p,p')tα. Differential cross sections for the continuum region corresponding to the three-body breakup process were estimated by fits of the phase space distributions. The estimated cross sections are shown in Fig. 2(b).

3-2. ^{7}Li(p,d) reaction.

The differential cross sections and analyzing powers for 12, 14 and 16 MeV are shown in Figs. 3(a - c) for the ground (1+), 1st excited (2.185 MeV, 3+), and 2nd excited (3.562 MeV, 0+) states. The continuum region of the DDX spectra of the (p,d) reaction is mainly due to the three-body breakup process of ^{7}Li(p,d)dα.

3-3. ^{7}Li(p,t) reaction.

Typical DDX spectra of the (p,t) reaction are shown for 14 MeV in Fig. 4. An enhancement observed in the highest energy region of the spectra is due to the p-α final state interaction, and a bump in the middle region is attributed to the t-α final state interaction through decays from excited states of ^{7}Li.

4. Theoretical Analyses and Discussion

4-1. DWBA analyses of (p,p') scattering and optical potential.

First, the optical potential parameters including spin dependent terms were searched with a code 'ELAST2' from the elastic scattering data of differential cross sections and analyzing powers. The spherical optical model was applied for ^{7}Li and the standard form of optical potential with the Woods-Saxson type form factor was employed in the ELAST2 code. The

obtained parameters are listed in Table 1(a), and good fits were obtained not only for differential cross sections but also for analyzing powers as indicated by solid lines in Fig. 1(a). Inelastic scatterings were calculated with a DWBA code 'DWUCK', in which the optical potential parameters obtained above were used and the momentum transfer was assumed to be l=2. Deformation parameters were determined for the 1st and 2nd excited states so as to reproduce well their differential cross sections. The results are indicated by solid lines in Figs. 1(b and c) for the excited states.

Second, the coupled channel calculation was performed with a code 'ECIS79', in which lower states up to the 3rd state were assumed to be coupled and to belong to K=1/2 band in the rotational model(8). Starting from the resultant parameters from the ELAST2 calculation, the ECIS79 code searched the optical potential and deformation parameters so as to give a good fit with the experimental differential cross sections for the ground, 1st excited, and 2nd excited states, and with the analyzing powers for the ground states. If the analyzing powers for the 1st and 2nd excited states were included for the search, the search procedure could not settle reasonably. The obtained parameters are listed in Table 1(b). The calculated results indicated by dashed lines in Figs. 1(a-c) reproduces very well the differential cross sections and analyzing powers, except for analyzing powers of the 1st and 2nd excited states.

4-2. DWBA calculation for (p,d) reactions.

The angular distributions and analyzing powers for the (p,d) reaction leading to the ground, 1st excited, and 2nd excited states of ^{6}Li were calculated in the framework of the zero-range DWBA using the DWUCK code. One neutron pickup process from the 1p3/2 orbit was assumed in the calculation. The optical potential used in the entrance channel was that obtained in the DWBA analyses of the (p,p) elastic scattering. The exit channel optical potential was derived from ^{6}Li(d,d) experimental data and its energy dependence was ignored. The calculated results are indicated by solid lines in Figs. 3(a - c). The results reproduce well the angular distributions in the forward angles, but in backward angles not so well. The analyzing powers are not reproduced.

4-3 DWBA calculation with discretized-continuum states.

The proton continuum spectrum is mainly due to the ^{7}Li(p,p')tα three-body breakup reaction. Instead of complete CDCC calculations, we tried to calculate the spectrum in the framework of the DWBA using the ^{7}Li

form factors extended to resonant and non-resonant continuum states. The form factors were obtained on the basis of a microscopic t-α cluster model by Sakuragi et al. (9) Transition probabilities were calculated from the ground state to 15 excited states, among which 11 states are discretized-continuum ones. The optical potential derived from the ELAST2 calculation was used in the entrance channel. The real and imaginary parts of the central force in the potential for the exit channel were assumed to have energy dependences given by Dave and Gould(10).

Proton energy spectra were constructed from the 15 calculated angular distributions; the resonant and non-resonant components were added. As the resonant components of the 2nd (7/2) and 3rd (5/2) excited states have widths Γ of 0.1 MeV and 1.0 MeV, respectively, they were spread in accordance to the Lorentzian distribution. The calculated spectra were fit with optimized normalization factors. The results are compared with the measured ones for 12, 14 and 16 MeV in Fig. 5. The non-resonant breakups are presented by dashed lines and the total breakups including resonant ones through the 7/2 and 5/2 excited states by solid lines in the figures. Good agreements are indicated in rather wide region except for the low energy region. The DWBA calculation with the form factors for discretized-continuum states explains qualitatively the measured continuum spectra. Measured angular variation of the spectra, however, was not reproduced well, because the results of DWBA calculations did not agree so well with the angular distributions of the 2nd 7/2 excited state. More comprehensive CDCC calculation is necessary.

4-4 Calculation by final state interaction theory.

Triton spectra were calculated by means of the final state interaction (FSI) theory(11), which included only the p-α and t-α FSI and direct-breakup processes as main contributions. The p-wave (3/2) phase shift of p-α scattering was taken from the R-matrix theory(11), and the f-wave (7/2) phase shift of t-α scattering from the experimental data of Spiger et al. (12). Decay through the 7/2 excited state of ^{7}Li was interpreted as the t-α FSI. These three contributions were added incoherently so as to give good fits with the measured spectra. Fig. 6 shows examples of comparisons for 12, 14 and 16 MeV. Analyzing powers of the spectra, as shown in the figures, indicate rather large asymmetries at the FSI regions; they can not be predicted in the framework of FSI theory. The differential cross sections obtained by integration of the calculated spectra for each contribution are shown in Fig. 7 above the threshold

energy of 1.5 MeV. The p-α FSI contribution shows distinctly an oscillating shape of angular distribution, which agrees with that of (n,t) reaction at 14 MeV. It is suggested in the present analysis with the FSI theory that these typical processes are rather independent of each other in the ^{7}Li(p,t)pα three-body breakup reaction.

4-5 Total triton production cross sections and comparison with the neutron induced reactions.

The total triton production cross section were estimated from integrations of angular distribution for continuum region and the 2nd excited (7/2) state, as well as from the (p,t) reaction spectra. With the aid of the theoretical calculation fit, as described above, spectra in an energy region below the measurement threshold were estimated. The obtained total cross sections are summarized in Table 2. Since the (p,p') data are larger than that obtained from the (p,t) reaction, it is necessary to estimate other processes such as the statistical process of (p,xp') reactions, which do not emit tritons.

Since similarity in shape are indicated between the (p,p') and (n,n') spectra and between the (p,t) and (n,t) spectra, the analyses performed in the present work may be applicable to the neutron induced reactions. The n-α FSI and p-α FSI agree in their angular distributions and in absolute differential cross sections. However, the other process could not be compared directly because the (n,t) reaction spectra were not measured in the low energy region if compared with the (p,t) reaction spectra. The total triton production cross sections in proton induced reaction are smaller than those of neutron induced reaction, which are compiled in JENDL-3(5).

5. Summary

Double differential cross sections and analyzing powers were measured for ^{7}Li(p,p'), (p,d) and (p,t) reactions at 12.0, 14.0 and 16.0 MeV. The experimental data of the elastic scattering were excellently reproduced by calculations based on the spherical optical model and the coupled channel method. The DWBA and CC calculations did not predict correctly the analyzing powers in the inelastic channels leading to the 1st and 2nd excited states of ^{7}Li. The three-body breakup process observed in (p,p') continuum spectra were qualitatively explained by DWBA calculations with discretized continuum states; this method is a simplified one for the complete CDCC calculation. Continuum spectra of the (p,t) reaction were

reproduced well on the basis of the FSI theory; the p-α and t-α FSI seems to be rather independent processes in the three-body breakup reaction. Distinct asymmetries in analyzing powers, furthermore, were observed in FSI regions of the (p,t) spectra.

We are continuing this type of study on ^{6}Li; measurements have been finished and the data analysis is in progress.

Acknowledgements

The authors are indebted to Dr. Y. Sakuragi (Osaka City University) for valuable discussion on theoretical analyses.

References

(1) S. Higuchi, K. Shibata, S. Shirato and H. Yamada, Nucl. Phys. A384, 51 (1982).

(2) S. Chiba, M. Baba, H. Nakashima, M. Ono, N. Yabuta, S. Yukinori and N. Hirakawa, J. Nucl. Sci. Technol. 22, 771 (1985).

(3) H.H. Hogue, P.L. von Behren, D.W. Glasgow, S.G. Giendinning, P.W. Lisowski, C.E. Nelson, F.O. Purser, W. Tornow, C.R. Gould and L.W. Seagondollar, Nucl. Sci. Eng. 68, 22 (1979).

(4) A. Takahashi, J. Yamamoto, K. Oshima, M. Ueda, M. Fukazawa, Y. Yanagi, J. Miyaguchi and K. Sumita, J. Nucl. Sci. Technol. 21, 577 (1984).

(5) K. Shibata, "Evaluation of Neutron Nuclear Data of ^{6}Li for JENDL-3", JAERI-M 198 (1984); "Evaluation of Neutron Nuclear Data of ^{7}Li for JENDL-3" JAERI-M 204 (1984).

(6) M. Kamimura, Y. Sakuragi, M. Yahiro and M. Tanifuji, J. Phys. Soc. Jpn. Suppl. 55, 205 (1986).

(7) See Proc. 11th Int. Conf. on Few-Body Systems in Particle and Nuclear Physics, Nucl. Phys. A463 (1987).

(8) C.M. Chesterfield and B.M. Spicer, Nucl. Phys. 41, 675 (1963).

(9) Y. Sakuragi, M. Yahiro and M. Kamimura, Prog. Theor. Phys. 70, 1047 (1983).

(10) J.H. Dave and C.R. Gould, Phys. Rev. C28, 2212 (1983).

(11) T. Rausch, H. Zell, D. Wallenwein and W. Von Witsch, Nucl. Phys. A222, 429 (1974).

(12) R.J. Spiger and T.A. Tombrello, Phys. Rev. 163, 964 (1967).

Table 1 Parameters of optical potential for the ^{7}Li+p system.

(a) ELAST2 (spherical optical model).

	V (MeV)	r_0 (fm)	a_0 (fm)	W (MeV)	r_i (fm)	a_i (fm)	V_{so} (MeV)	r_{so} (fm)	a_{so} (fm)	χ_σ^2/N	χ_A^2/N
12 MeV	47.56	1.337	0.643	10.05	1.416	0.342	7.530	1.240	0.580	2.61	16.37
14 MeV	49.55	1.331	0.605	9.737	1.220	0.484	6.358	1.205	0.457	0.40	9.16
15 MeV	49.30	1.299	0.600	8.840	1.209	0.553	7.718	1.240	0.406	0.86	3.11

(b) ECIS79 (coupled channel method).

	V (MeV)	r_0 (fm)	a_0 (fm)	W (MeV)	r_i (fm)	a_i (fm)	V_{so} (MeV)	r_{so} (fm)	a_{so} (fm)	β_2	χ_σ^2/N	χ_A^2/N
12 MeV	49.90	1.193	0.545	1.935	1.760	0.702	5.929	1.084	0.337	0.9852	23.83	5.68
14 MeV	52.45	1.127	0.583	2.529	1.571	0.732	6.565	1.141	0.432	0.9610	24.12	4.19
16 MeV	52.56	1.130	0.575	2.957	1.296	0.766	6.250	1.112	0.371	0.9850	26.77	5.29

The optical potential form:

$$U = -V \cdot f(r,r_0,a_0) + 4i\,a_i \cdot W \cdot \frac{d}{dr} f(r,r_i,a_i) + \left(\frac{\hbar}{m_\pi c}\right)^2 \cdot V_{so} \cdot \frac{\vec{s}\cdot\vec{\ell}}{r} \cdot \frac{d}{dr} f(r,r_{so},a_{so}),$$

where $f(r,r_x,a_x) = 1 + \exp\{(r - r_x \cdot A^{1/3})/a_x\}^{-1}$ (the Woods-Saxson type form factor).

Table 2 Total cross sections of the ^{7}Li(p,t) reaction.

Ep (MeV)	σ p(cont) (mb)	σ p(2nd) (mb)	σ p(sum) (mb)	σ t(cal) (mb)	σ t(exp) (mb)	σ (n,t) (mb)
12	152	84	236	212	147	322
14	160	75	235	193	144	286
16	152	66	218	---	146	237

σ p(cont): from the continuum region of ^{7}Li(p,p') spectra.
σ p(2nd) : from the ^{7}Li(p,p') scattering to the 2nd state.
σ p(sum) : sum of σ p(cont) and σ p(2nd).
σ t(cal) : from calculated triton spectra.
σ t(exp) : from measured triton spectra (Et ≧ 1.5 MeV).
σ (n,t) : the total cross section of ^{7}Li(n,t) reaction from JENDL-3.

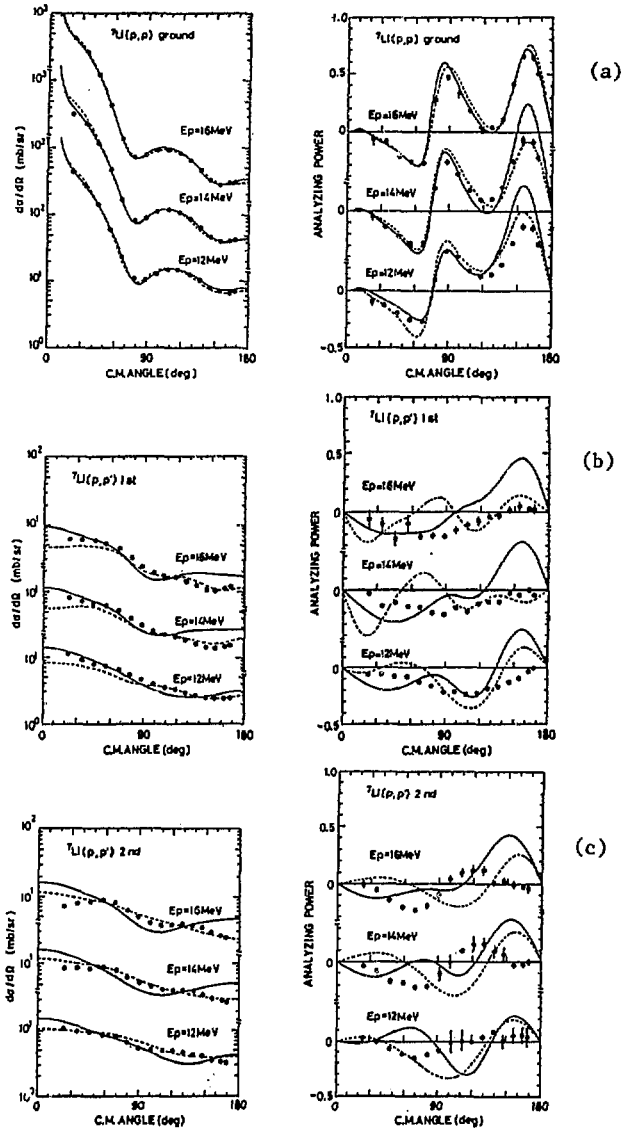

Fig. 1 Differential cross sections and analyzing powers of (p,p') scatterings for the ground state (a), for the 1st state (b) and for the 2nd state (c). Solid lines are for calculations with spherical optical model(for the ground state) and with DWBA (for the excited states), and dashed lines for CC calculations.

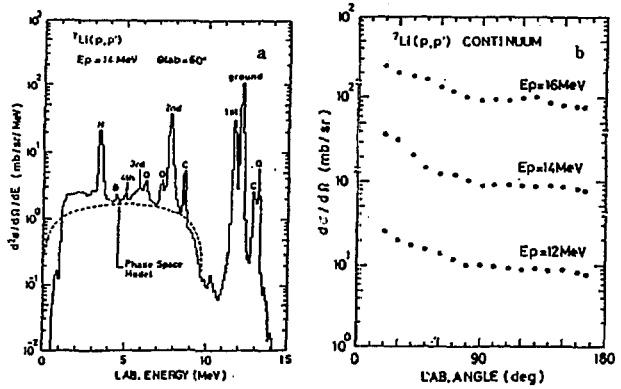

Fig. 2 Fitting of the (p,p') continuum spectrum with the phase space distribution (a) and differential cross sections of the continuum region (b).

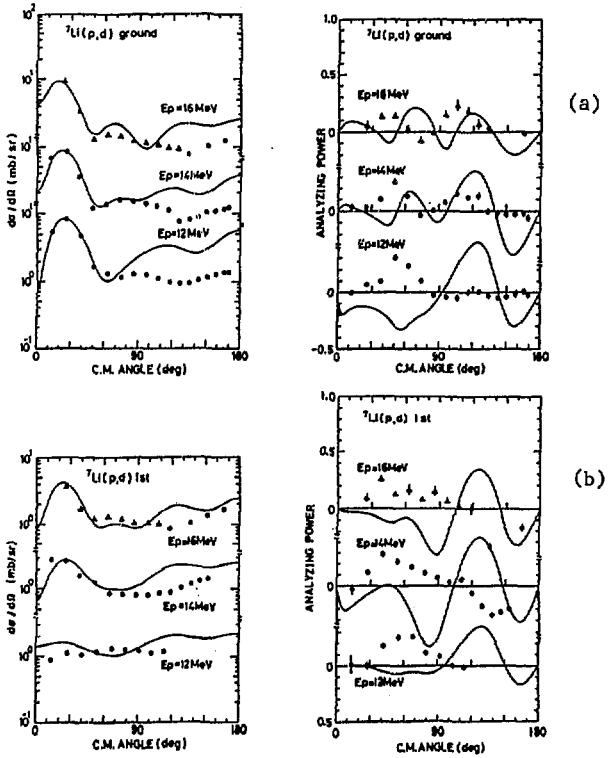

Fig. 3 Differential cross sections and analyzing powers of (p,d) reactions for the ground state (a), for the 1st state (b) and for the 2nd state (c). Solid lines are for DWBA calculations.

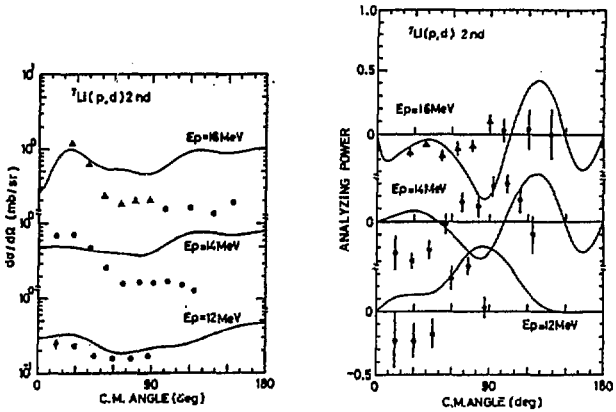

Fig. 3 (continued)

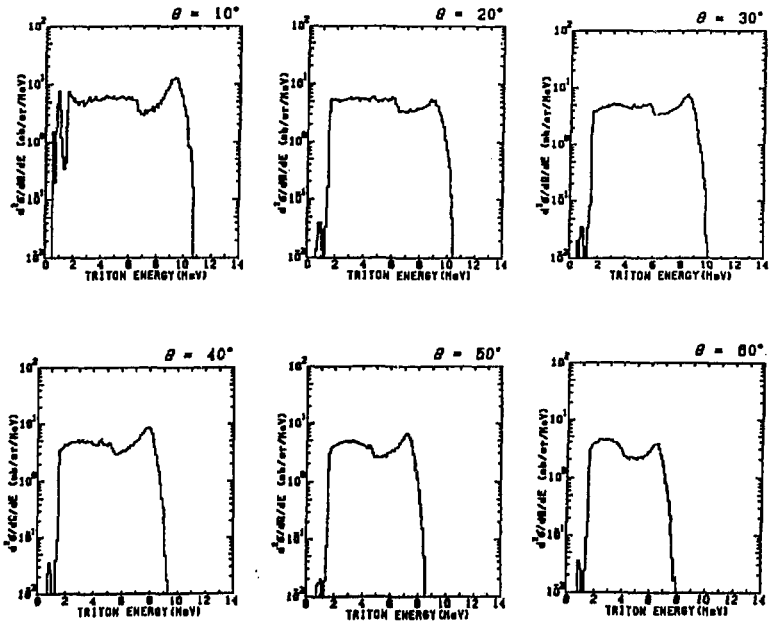

Fig. 4. Examples of DDX spectra of (p, t) reaction for 14 MeV.

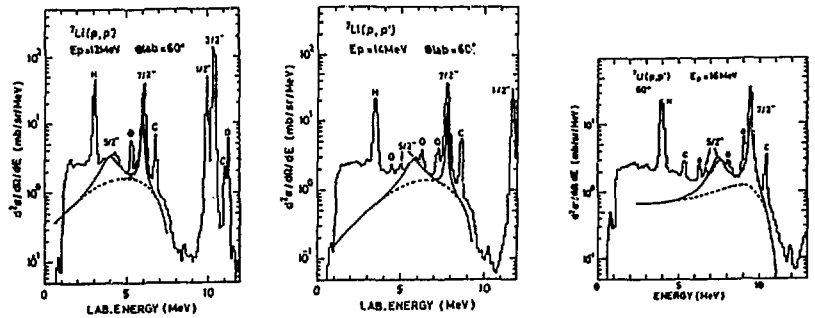

Fig. 5 Comparisons of theoretical calculations by DWBA with proton continuum spectra.

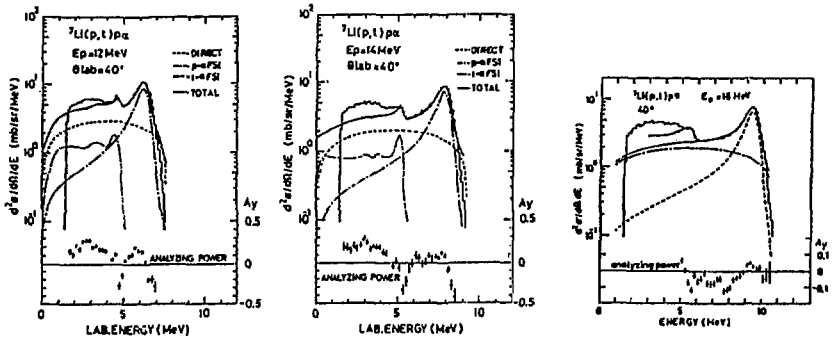

Fig. 6 Comparisons of theoretical calculations by FSI theory with triton spectra.

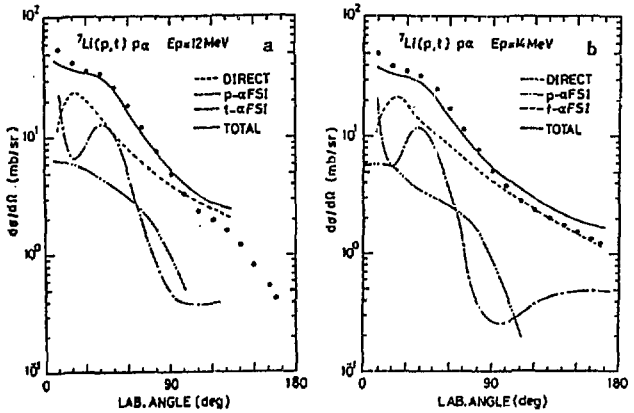

Fig. 7 Differential cross sections for (p, t) reactions at 12 MeV (a), and 14 MeV (b).

3.14 Shell and Odd-even Effects in Preequilibrium (p,p') and (n,n') Processes

Y. Watanabe, I. Kumabe, N. Koori, M. Hyakutake* and A. Takahashi**
Department of Nuclear Engineering, Kyushu University, Fukuoka

ABSTRACT

We have systematically measured energy spectra of protons emitted from 18 MeV (p,xp) reactions on ^{90}Zr, ^{93}Nb, ^{92,94,96,98,100}Mo, ^{106}Pd, and Ag, and of neutrons emitted from 14.1 MeV (n,xn) reactions on Ag, Cd, In, Sn, Sb, and Te in order to investigate the shell and odd-even effects in the preequilibrium (p,p') and (n,n') processes. It was found that there are no appreciable shell and odd-even effects in the preequilibrium (p,p') and (n,n') spectra corresponding to excitations above 4 MeV of the residual nuclei. The experimental results were reasonably interpreted using the state densities derived from realistic single particle levels introducing a shell gap. The effect of the direct process in continuum spectrum region was also examined in terms of collective excitations of the low energy octupole resonance(LEOR).

1. INTRODUCTION

Neutron nuclear data in the incident energies of 10-50 MeV are needed for fusion energy applications. Theoretical calculations based on nuclear models provide an important tool in evaluating nuclear data in the energy and mass regions, where available experimental data lack. In 10-50 MeV neutron induced reactions, preequilibrium process becomes a significant reaction mechanism for particle emitted with relatively high energies. Most of fusion reactor candidate materials are metals or their alloys which consist of atoms with shell closed nuclei and nuclei near the shell closures. Therefore, studies on the shell and odd-even effect in the preequilibrium process in neutron induced reactions are of great importance for enhancing our understanding of the reaction mechanism as well as for meeting nuclear data needs for fusion energy applications.

In general, experimental data of proton induced reactions are superior

* Sasebo Technical College, Sasebo
** Department of Nuclear Engineering, Osaka University, Osaka

to those of neutron induced reactions in terms of accuracy. First, we have measured double differential cross sections of 18 MeV (p,xp) reactions on ^{90}Zr, ^{93}Nb, ^{92,94,96,98,100}Mo, ^{106}Pd, and Ag [1] in order to investigate the shell and odd-even effects in the preequilibrium process of inelastic scattering. After analyses of the (p,p') scattering, we have performed another measurement for energy spectra of neutrons emitted from 14.1 MeV (n,xn) reactions on Ag, Cd, In, Sn, Sb, and Te to obtain a consistent understanding between (p,p') and (n,n') scatterings.[2]

2. 18 MeV (p,p') SCATTERING

The experiment was performed using an 18 MeV proton beam from the tandem Van de Graaff accelerator at Kyushu University. The experimental procedure and data processing have been described in detail elsewhere.[1]

Fig.1 shows the measured angle-integrated (p,xp) spectra for all target nuclei. The proton spectra for shell closed nuclei (^{90}Zr and ^{92}Mo) with neutron number 50 have noticeable structures in outgoing energies above 10 MeV. On the other hand, the spectra for nuclei away from the shell closure become flat and smooth with increasing neutron number, and have a similar shape and almost the same magnitude within several percent in the preequilibrium region above 10 MeV.

Part(a) and (b) in Fig.2 shows the cross sections(σ_a and σ_b) integrated over 10-13 MeV after subtraction of the equilibrium component estimated in two ways; (a) one is the calculated cross section using the Hauser-Feshbach model, (b) the other is the measured cross section at a backward angle θ =160° that was assumed to correspond to the equilibrium component with an isotropic angular distribution. Although the absolute values of the nonequilibrium cross sections σ_a and σ_b are different, each is nearly equal within the error among the measured isotopes. These experimental results, therefore, show that there are no appreciable shell and odd-even effects in the (p,p') spectra in the outgoing energy region corresponding to excitations above 4 MeV, where preequilibrium emissions are dominant.

These observations were reasonably interpreted on the basis of the state densities generated from two sets of single particle levels using the recursion method of Williams et al.[3]; one is based on the spherical Nilsson model[4][Fig.3(a)] and the other on the modified uniform spacing (MUS) model[1,5,6] [Fig.3(b)] in which a shell gap is introduced into the

uniform spacing (US) model[Fig.3(c)]. In the calculation, the pairing correlation was taken into account under the quasi-particle approximation.[7] As shown for ^{92,96,100}Mo in Fig.4, the influence of a shell gap on the calculated $(n)(n)^{-1}$ state densities for the neutron shell is reduced significantly in the excitation energies above 4 MeV. In the case of an odd- and even-A pair of ^{107}Ag and ^{106}Pd, the $(p)(p)^{-1}$ states created by excitations of an unpaired proton appear obviously below ~2 MeV for ^{107}Ag. However the $(p)(p)^{-1}$ state density of ^{107}Ag is almost equal to that of ^{106}Pd above 2 MeV, because excitations of broken proton pairs are dominant.

The emission from n=3 initial configuration in the composite nucleus has a large fraction in the preequilibrium emissions. According to the formulas of the exciton model[1], the energy spectrum of emitted particles from n=3 is proportinal to the 1p-1h $[(n)(n)^{-1}$ or $(p)(p)^{-1}]$ state density of the residual nucleus. Thus, it can be understood from the above results of the state densities that there are no appreciable shell and odd-even effects in the preequilibrium (p,p') process which leaves the residual nucleus in excitations above 4 MeV. As can been seen in Fig.4, the MUS and US models reproduced well the averaged behavior of state densities obtained from the spherical Nilsson model in the region above 4 MeV. This indicates that the Williams formula[8] commonly used in the preequilibrium models is a reasonable approximation above 4 MeV even for nuclei near the shell closure.

In Figs. 5 and 6, the measured angle-integrated proton spectra were compared with those calculated on the basis of the exciton model and the Hauser-Feshbach model in which the isospin selection rule is taken into account. The details of calculations have been described in Ref.[1]. Good agreement between the experimental and calculated spectra was obtained in the outgoing proton energy region of 3-14 MeV for all targets, regardless of rough assumptions on the isospin mixing.

3. 14.1 MeV (n,n') SCATTERING

The experiment was performed with an 85° TOF spectrometer using a 14.1 MeV pulsed neutron beam at OKTAVIAN in Osaka University. The details of this facility and the experimental procedures have been described elsewhere[2,9].

Double differetial neutron emission cross sections measured at 70° are

shown for Ag, Cd, In, Sn, Sb, and Te in Fig.7. In the energy region of 5-10 MeV of interest, where the preequilibrium emission is dominant, the measured spectra are similar in shape except for Te. The (n,xn) spectrum for Te has such structure that some small peaks overlap, and the magnitude is somewhat larger than those for the other spectra.

In Fig.7, the experimental spectra are compared with $1/4\pi$ of the angle-integrated spectra obtained on the basis of the evaporation model and the exciton model. In the calculations, the isotope with the mass number almost equal to the atomic weight was assumed as the target nucleus (i.e. ^{107}Ag, ^{112}Cd, ^{115}In, ^{116}Sn, ^{121}Sb, and ^{128}Te). The parameters used were the same as those in the (p,p') calculation, except for the K-value in the exciton model calculation. As shown in Fig.7, the calculated spectra are in good agreement with the experimental ones in the outgoing energy region of 1-10 MeV, although some underestimation is seen in 7-10 MeV for Te.

In Fig. 8, comparisons of the experimental cross sections integrated over 7-10 MeV are shown by the solid circles. The cross sections increase monotonically with increasing mass number from Ag to Sb. However the cross section for Te increases discontinuously. As an interpretation on the discontinuous incease, we can suggest the possibility of strong excitation of low energy octupole resonance(LEOR) by the direct reaction process.

In a systematic study on the LEOR[11], it has been indicated that the excitation of the LEOR is not appreciably observed if the first 3$^-$ transition occured strongly. From comparisons of the deformation parameters β_3[12,13] for the first 3$^-$ state listed in Table I, it was found that β_3 values for ^{128,130}Te[13] are considerably smaller than those for the others. We derived the deformation parameter β_{LEOR} for the LEOR under some assumptions. The derivation of β_{LEOR} is mentioned in details elsewhere[2]. Following the direct reaction theory, the cross section for excitations of LEOR was predicted from the expression $\beta_{LEOR}{}^2 \cdot \sigma_{DW}$, where σ_{DW} is the DWBA cross section. The predicted LEOR cross section for Te was 17-50% larger than those for the other nuclei. The cross sections after subtraction of the LEOR cross section from the experimental ones are shown by open circles in Fig.8. The obtained cross sections increase monotonically over the whole mass region including Te and showed no appreciable shell and odd-even effects. This component would be considered to be the preequilibrium component, because excitations of the coherent motion such as LEOR can not be treated in the framework of the preequilibrium model such as the exciton

model.[14]

As mentioned in Sec.2, preequilibrium energy spectra are closely related to the state density of the residual nucleus. In the case of the (n,n') scattering by nuclei in the Sn region, a consideration for the state densities of proton configuration can provide a reasonable explanation on A- or Z- dependence of the preequilibrium (n,n') cross sections shown by open circles in Fig.8. The components of direct process may also be included in the continuum region of (p,p') spectra. We calculated the σ_{LEOR} for the (p,p') scattering by nuclei in the Mo region, and obtained the preequilibrium cross sections from subtraction of the calculated σ_{LEOR}. The results also led to a consistent conclusion with that of the (n,n') scattering.

4. SUMMARY

We have systematically measured energy spectra of protons emitted from 18 MeV (p,xp) reactions on ^{90}Zr, ^{93}Nb, ^{92,94,96,98,100}Mo, ^{106}Pd, and Ag, and of neutrons emitted from 14.1 MeV (n,xn) reactions on Ag, Cd, In, Sn, Sb, Te, in order to investigate the shell and odd-even effects in the preequilibrium (p,p') and (n,n') processes.

The experimental results showed that there were no appreciable shell and odd-even effects in the preequilibrium component in continuum (p,p') and (n,n') spectra corresponding to residual excitations above 4 MeV. These facts could be qualitatively explained in terms of the calculated state densities from realistic single particle schemes introducing a shell gap under the quasi-particle approximation.

The (p,p') and (n,n') energy spectra were calculated on the basis of the exciton model for the preequilibrium process and the Hauser-Feshbach model or the evaportion model for the equilibrium process. The results showed good agreements with the experimental ones; some underestimation was seen in 7-10 MeV for Te(n,n') scattering. The underestimation was reasonably explained by taking into account the contribution from the collective excitation of the LEOR by direct processes.

Finally, it will be required to examine the application of the present results to nuclear data evaluation for fusion energy developement.

References

1) Y. Watanabe, I. Kumabe, M. Hyakutake, N. Koori, K. Ogawa, K. Orito, K. Akagi, and N. Oda, Phys. Rev. C 36, 1325(1987).

2) Y. Watanabe, I. Kumabe, M. Hyakutake, A. Takahashi, H. Sugimoto, E. Ichimura, and Y. Sasaki, to be published in Phys. Rev. C.

3) F.C. Williams.Jr., A. Mignerey, and M. Blann, Nucl. Phys. A207, 619 (1973)

4) S.G. Nilsson, Mat. Fys. Medd. Dan. Vid. Selsk., 29, No.16 (1955).

5) I. Kumabe and Y. Watanabe, Phys. Rev. C 36, 543 (1987).

6) I. Kumabe, Y. Mito, M. Hyakutake, N. Koori, H. Sakai, and Y. Watanabe, Phys. Rev. C 35, 467 (1987).

7) A. Bohr and B.R. Mottelson, Nuclear Structure (Benjamin, Reading, MA, 1975), Vol.II, p. 649.

8) F.C. Williams, Jr., Nucl. Phys. A166, 231 (1971).

9) A. Takahashi, H. Sugimoto, and E. Ichimura, Proc. Int. Conf. Fast Neutron Physics, Dubrovnik, May 26-31, 1986 (Ruder Boskovic Institute Pub. 1986).

10) E. Ichimura and A. Takahashi, OKTAVIAN Report A-87-02 (unpublished).

11) J.M. Moss, D.R. Brown, D.H. Youngblood, C.M. Rozsa, and J.D. Bronson, Phys. Rev. C 18, 741 (1978).

12) R.L. Robinson, J.L.C. Ford,Jr., P.H. Stelson, and G.R. Satcher, Phys. Rev. 146, 816 (1966).

13) W. Makofske, W. Savin, H. Ogata, and T.H. Kruse, Phys. Rev. 174, 1429 (1968).

14) P.E. Hodgson, G.M. Field, H. Gruppelaar, and P. Nagel, Proc. Int. Conf. on Nuclear data for Basic and Applied Science, Santa Fe, May 13-17, 1985 (Gordon and Breach Science Pub., 1986), Vol.2, p.1033.

Table 1 Comparisons of experimental values of the deformation parameters β_3 for the first 3^- state, estimated β_{LEOR}, and cross sections for the excitation of the LEOR by the direct process.

Nuclei	first 3^- a)			LEOR		σ_{DW} (mb/sr)	σ_{LEOR} (mb/sr)
	Energy(MeV)	β_3(exp.)	EWSR(%)	β_3	EWSR(%)		
^{107}Ag	2.07	0.15	8.7	0.124	21.3	147.1	2.3
^{112}Cd	1.97	0.164	10.9	0.114	19.1	166.7	2.2
^{115}In	1.95	0.160	10.6	0.113	19.4	177.8	2.3
^{118}Sn	2.32	0.168	14.7	0.098	15.3	187.8	1.8
^{121}Sb	2.39	0.159	14.0	0.099	16.0	196.4	1.9
^{128}Te	2.50	0.110	7.8	0.111	22.2	213.9	2.7
^{130}Te	2.77	0.10	7.3	0.112	22.7	218.9	2.7

a) The excitation energies and β_3 for odd nuclei(^{107}Ag, ^{115}In, and ^{121}Sb) were those for the neighboring even-even nuclei(^{106}Pd, ^{114}Cd and ^{120}Sn, respectively). Experimental data for excitation energies and β_3 were taken from Ref./2 for ^{106}Pd and Ref./3 for the other isotopes.

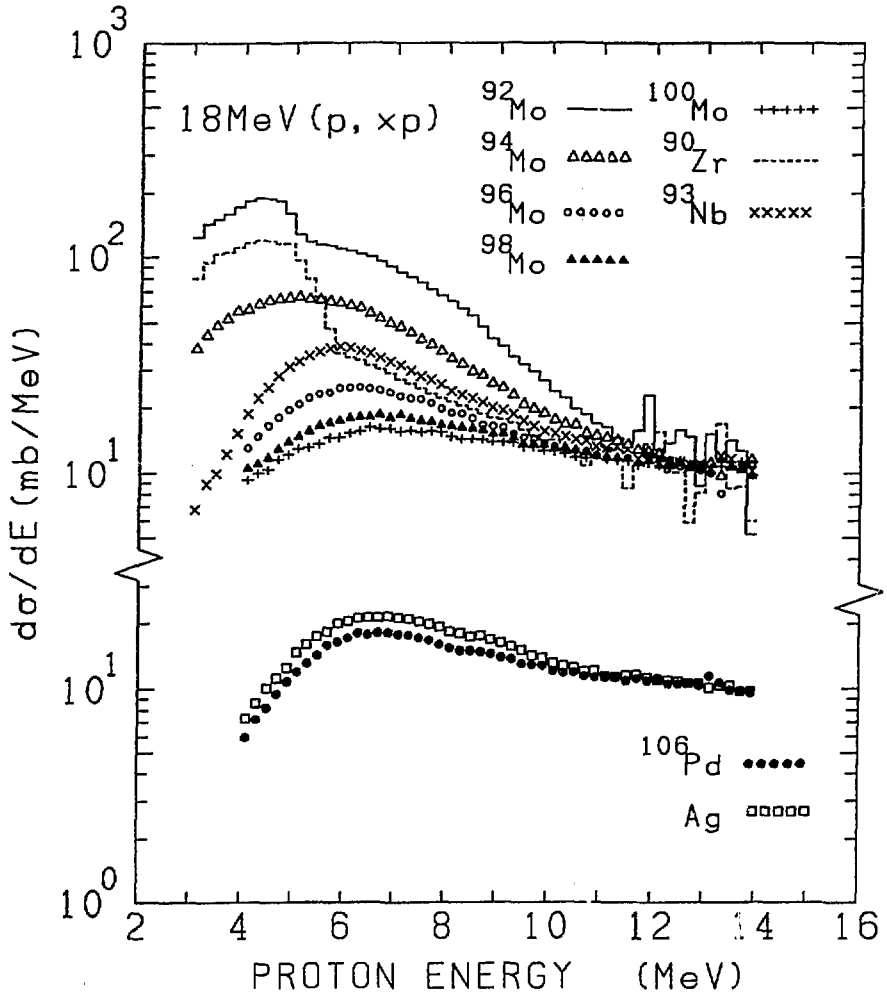

Fig. 1 Angle-integrated energy spectra of protons emitted from 18 MeV (p,xp) reactions

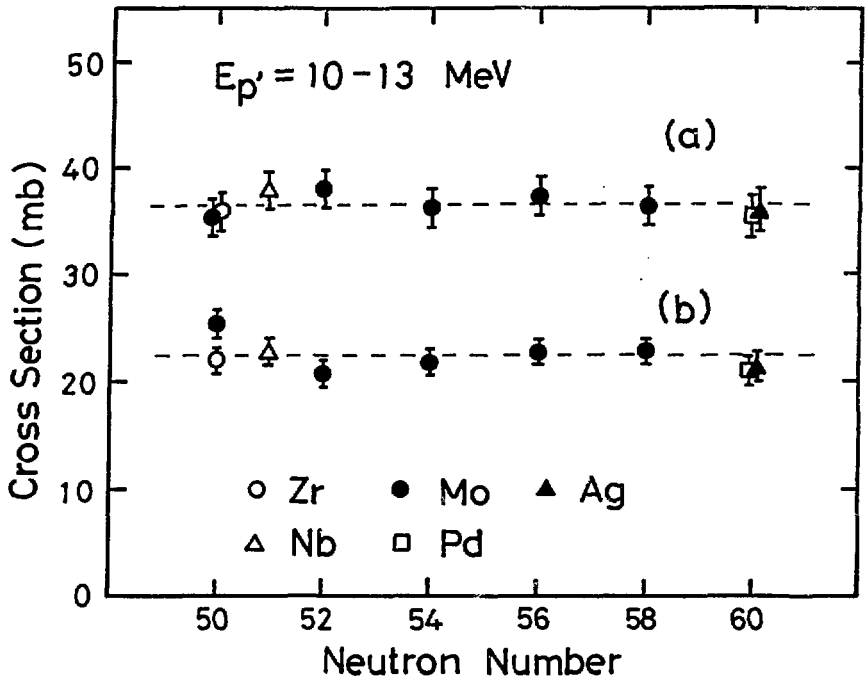

Fig. 2 Nonequilibrium cross sections integrated over 10-13 MeV after subtraction of equilibrium component. Dashed horizontal lines denote the averaged nonequilibrium cross section.

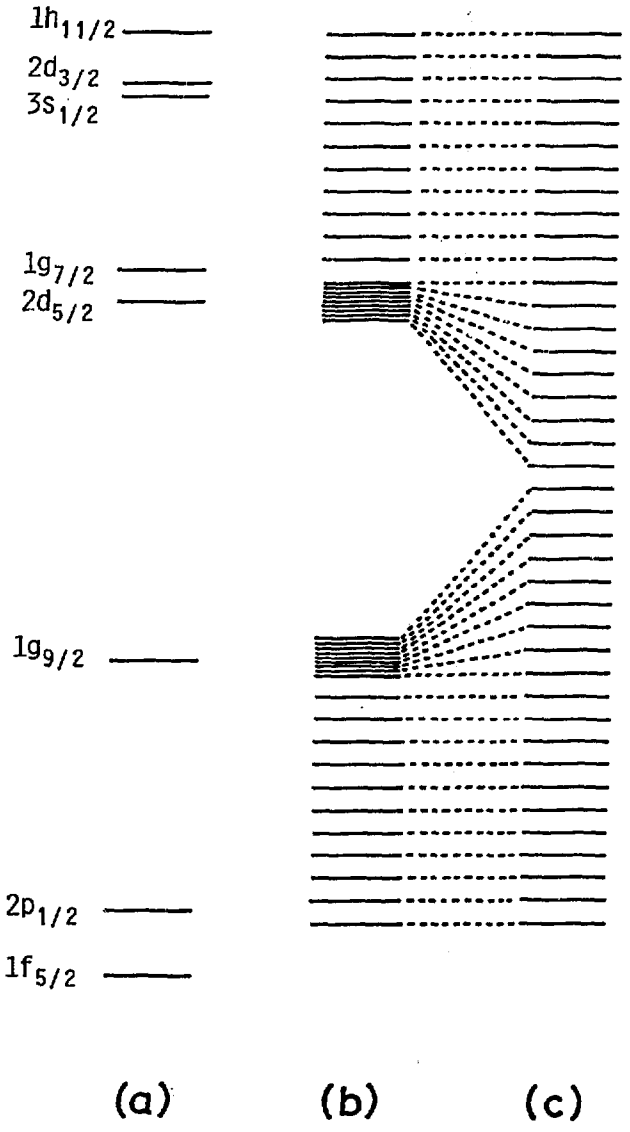

Fig. 3 Single particle level schemes for neutron shell; (a) Spherical Nilsson model (b) Modified uniform spacing model (c) Uniform spacing model.

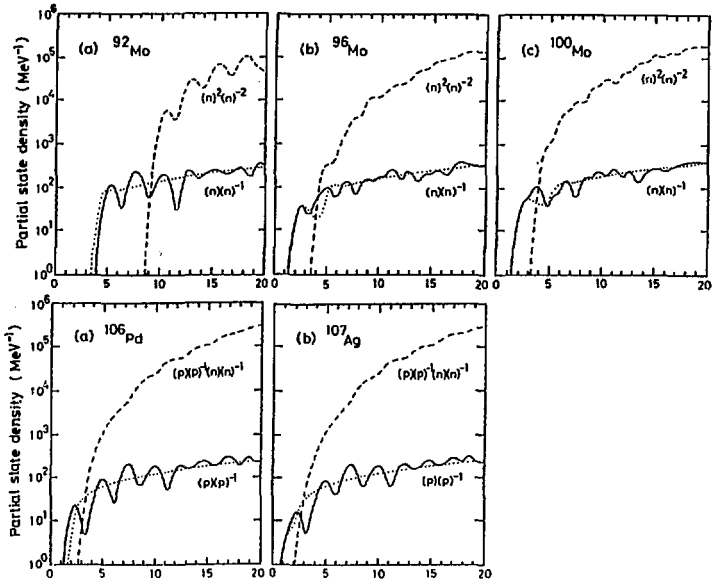

Fig. 4 Partial state densities for 1p-1h neutron configurations $[(n)(n)^{-1}]$ and 2p-2h neutron ones $[(n)^2(n)^{-2}]$ for ^{92,96,100}Mo, and for 1p-1h proton configurations $[(p)(p)^{-1}]$ and one proton particle-one proton hole and one neutron particle-one neutron hole configurations $[(p)(p)^{-1}(n)(n)^{-1}]$ for ^{106}Pd and ^{107}Ag. Solid and dashed curves represent state densities generated using the spherical Nilsson model. Dotted curves are the results of the modified uniform spacing model.

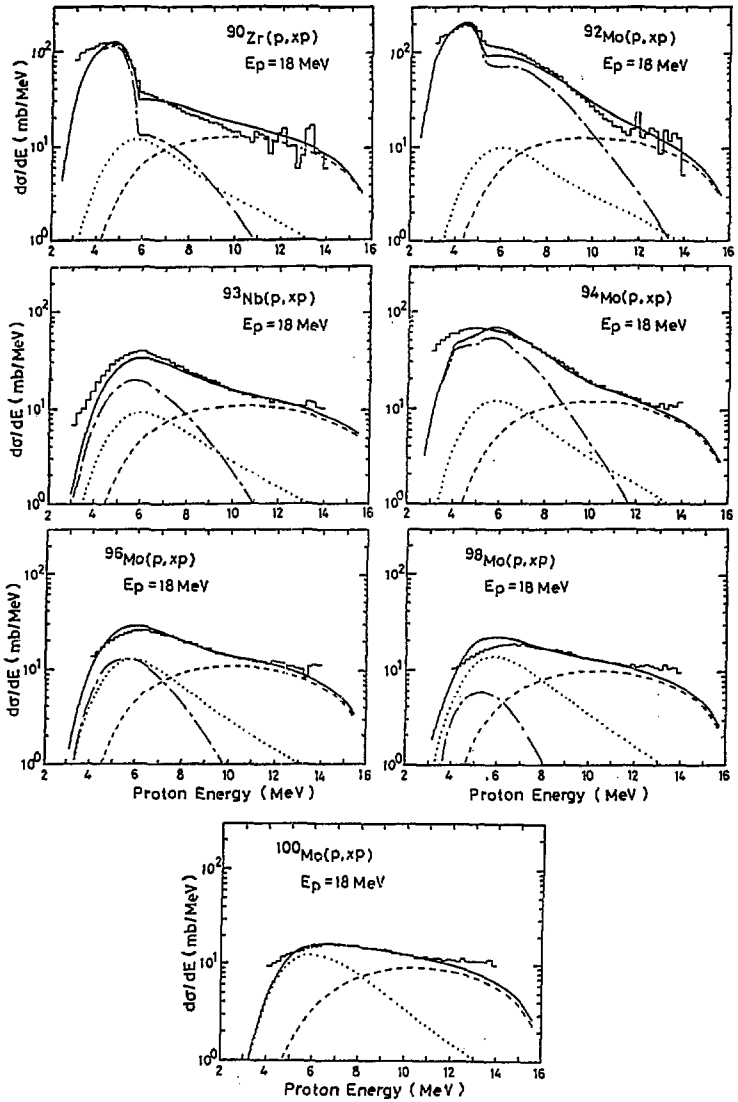

Fig. 5 Calculated and experimental (p,xp) spectra for ^{90}Zr, ^{93}Nb, ^{92,94,96,98,100}Mo. Histgrams represent the experimental angle-integrated spectra. Solid curves are the total calculated energy spectra. Dashed curves are $T_<$ component of the calculated preequilibrium energy spectra using the exciton model; Dotted curves are $T_>$ component of those. Dashed-dotted curves show the calculated equilibrium spectra using the Hauser-Feshbach model.

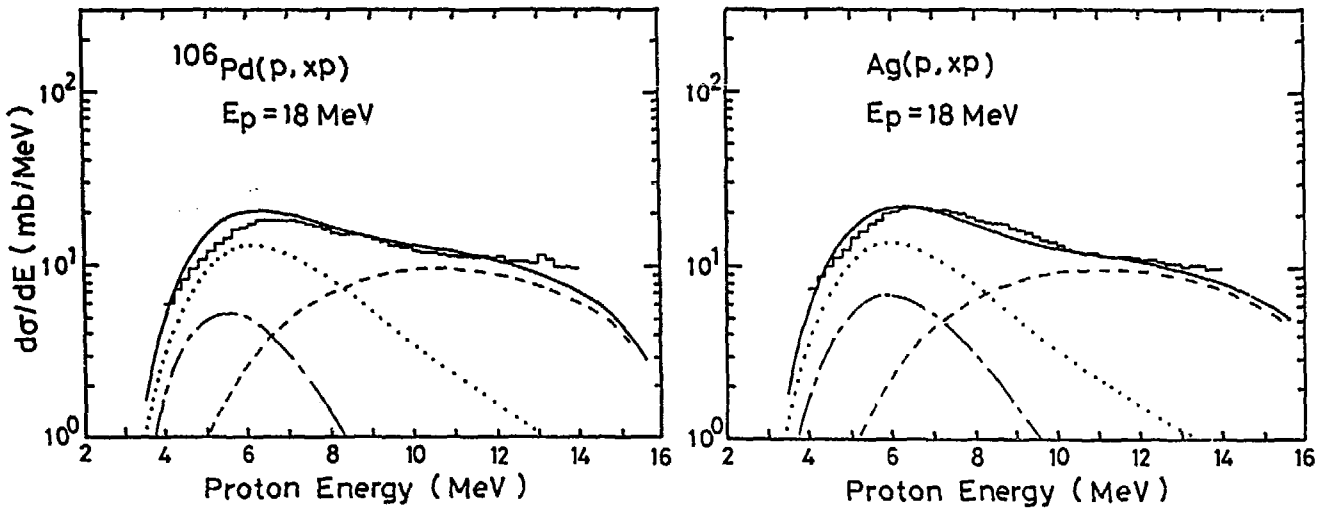

Fig. 6 Calculated and experimental (p,xp) spectra for ^{106}Pd and Ag. See also the caption of Fig.5.

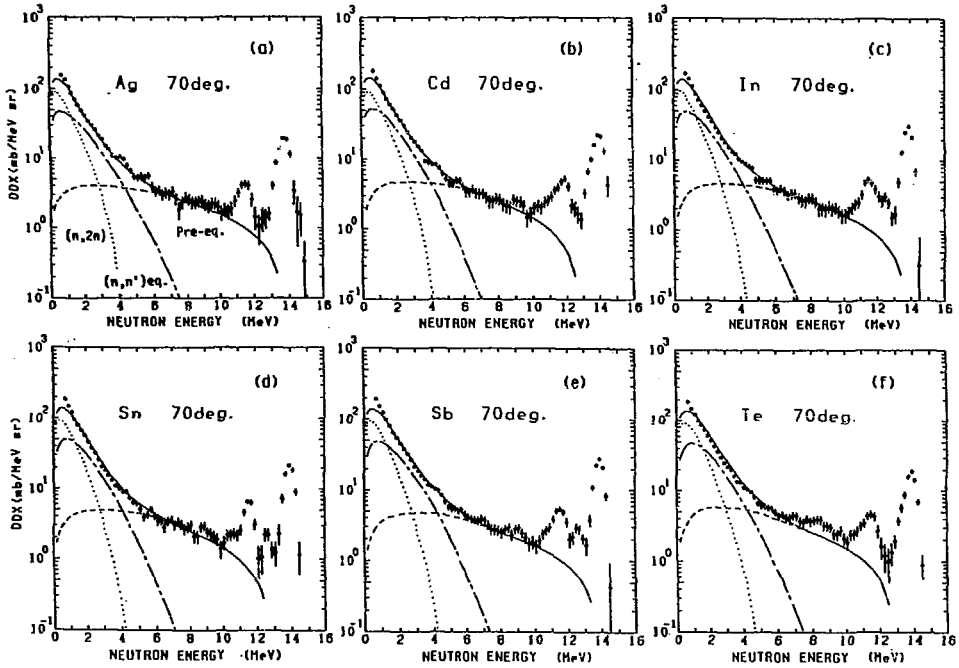

Fig. 7 Comparisons of the experimental and calculated double differential neutron emission cross sections for Ag, Cd, In, Sn, Sb, and Te. Dashed curves are the calculated preequilibrium spectra using the exciton model. Dashed-dotted curves and dotted curves show the calculated evaporation spectra for emissions of one neutron and two neutrons, respectively. Solid curves are the sum of them.

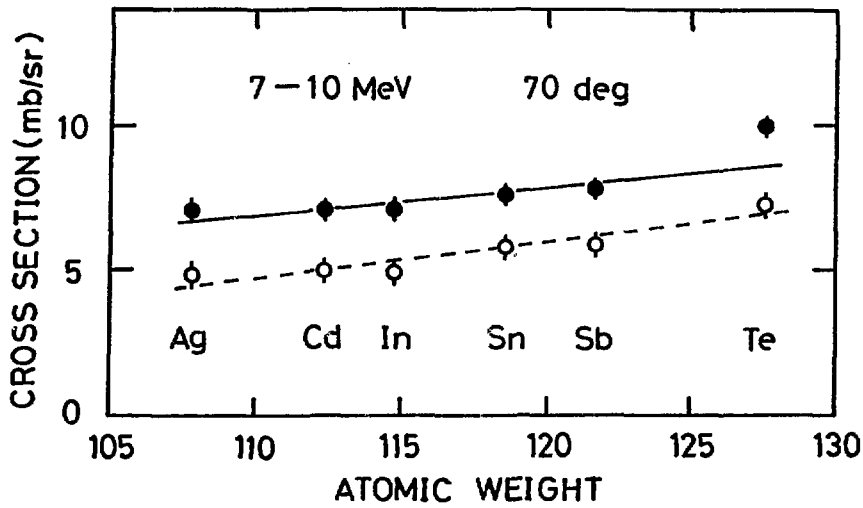

Fig.8 Dependence of integrated cross sections over 7-10 MeV on the atomic weight of scatterers. Solid circles represent the measured cross sections at 70°. Open circles are the results after subtraction of the predicted LEOR cross sections.

3.15 Critical Experiment and Analysis on Thorium Test Assembly in UTR-KINKI － A Note on Nuclear Data Library of Thorium －

Ryota MIKI, Tetsuo ITOH
Atomic Energy Research Institute, Kinki University
3-4-1, Higashi-Osaka, Osaka 577 Japan
and
Keichiro TSUCHIHASHI*

A b s t r a c t

Integral critical experiment on thorium test assemblies which are installed at the center of internal graphite reflector of UTR-KINKI, Kinki University Reactor, has been performed. The experiment includes (1) Measurement of the reactivity effect of the space between thorium metal plates in the test assemblies and (2) Measurement of detailed relative vertical neutron flux distribution in the test assemblies. Analytic calculations by JEARI Thermal Reactor Standard Code System for Reactor Design and Analysis (SRAC Code System[1]) on the reactivity effect of thorium test assembly and on the neutron flux distribution were also performed. The measured values agree fairly well with the calculated results when JENDL-3T data file was used. The cross section data of thorium in JENDL-2 library give somewhat lower C/E values on reactivity effect.

1. Introduction

The recent renewed interest in alternative fuel cycles has stimulated the investigation of the neutronic data of thorium which have not yet been well established. Since late 1970's, critical experiments with thorium have been made at several institutes around the world to check the evaluated neutronic data files of thorium.

In 1980, Atomic Energy Research Institute of Kinki University started a program to complement a series of experiments planned and performed at KUCA, Kyoto University Critical Assembly[2-4]. In this paper, we present some of the results of our integral critical experiments which have been made in UTR-KINKI, Kinki University Reactor, and of the analytic calculations with SRAC Code System.

UTR-KINKI is a light-water moderated and cooled, graphite reflected, heterogeneous, highly enriched uranium thermal reactor with 46 cm-separated 2-slab fuel arrangement. There are 12 fuel elements, each consists of 12 aluminum-clad, flat MTR-type fuel plates. The basic design of UTR-KINKI was developed from the "Argonaut" research reactor.

*Japan Atomic Energy Research Institute, Tokai-mura, Ibaraki-Ken, Japan

The maximum thermal neutron flux at the center of internal graphite reflector in the core is about 1.5×10^7 n/cm²-sec. The 46-cm wide internal graphite reflector region between the two fuel tanks has almost flat and isotropic neutron flux distribution and an enlarged vertical stringer at the center of internal reflector can be withdrawn to provide the space for insertion of thorium test assembly. Due to the small power and low residual radioactivity in the core of UTR-KINKI, "dry access" to the core is possible. This feature allows us to set up and unload the thorium test assembly into the core easily and safely. The reactor cross section (north to south) and the core plan of UTR-KINKI are shown in Figs. 1 and 2.

2. Experimental

Thorium test assembly

The thorium test assemblies used in this integral critical experiment consist of nine pillar elements, 55.3mm square and 73cm long, tightly packed in 3-row and 3-line configuration. Each test assembly was inserted into the vacant space which was provided by withdrawal of the enlarged central vertical stringer in the internal graphite reflector. At the top and bottom of each test assembly, graphite blocks 24.5cm in height were placed. Details of enlarged vertical stringer and thorium test assembly are shown in Fig. 3. In the central region of each test assembly, five 2"-square thorium metal plates, 1/8" in thickness, were loaded at regular intervals together with square graphite plates of different thickness. The remaining space was filled with square graphite plates. Each element was enclosed with 55.3mm square and 73cm long aluminum sheath, 1.5mm in thickness. The total amount of thorium loaded in each test assembly was about 4.1kg. The thorium test assemblies were named Th-1, Th-2, Th-3, Th-4 and Th-5 according to the intervals between the thorium metal plates, 1/2", 1",2", 3", and 4", respectively. The loading patterns of thorium metal plates in each element of thorium test assemblies are shown in Fig. 4.

Measurement of reactivity effect

The reactivity effect of thorium test assemblies was measured as the difference of excess reactivity between the reference core and individual core loaded with thorium test assembly. As the reference core, standard core configuration with no thorium metal plates was chosen. The positive period method was used in the measurement of excess reactivity. The effective delayed neutron fraction, 7.653×10^{-3}, and prompt neutron life time, 1.45×10^{-4} sec., were used for deriving reactivity from period.

Measurement of relative neutron flux distribution in test assemblies

Measurement of relative neutron flux distribution along the vertical center line of each test assembly was measured by bare gold foil activation method. Gold foils, 0.05mm in thickness, were placed at regular intervals between metal or graphite plates along the center line of the central element of each test assembly and irradiated for 1.5 hours at 1W. After irradiation, relative induced radioactivities were measured by automatic well-type scintillation counter.

Analytic calculations by SRAC Code System

Analytic calculations on reactivity effect of thorium test assemblies and distribution of bare gold foil reaction rate were performed by SRAC Code System. The system consists of neutron cross section libraries and auxiliary processing codes, neutron spectrum routines, a variety of transport routines, 1-D, 2-D and 3-D diffusion routines, dynamic parameters, etc. The fundamental group constant library has been produced from SRACTLIB-JENDL2 and SRACTLIB JENDL-3T[5] nuclear data files with energy group structure of 107 groups. In unit cell calculation for multi-group constants (fast 31 groups and thermal 22 groups), collision probability method was used . Multi-groups core calculation for few group constants (fast 5 groups and thermal 5 groups) was done by 1-D diffusion code in cylindrical geometry. In few-group (10 groups) full core calculation, 3-D CITATION code in X-Y-Z geometry was used. The reaction rate of bare gold foils was calculated by similar procedures described above, except that for few groups full core calculation, 2-D (R, Z) TWOTRAN Code using 16-group (fast 11 and thermal 5 groups) constants were employed. The details of calculation procedures including the two-dimensional (R,Z) geometric model for the core configuration have been reported elsewhere[6,7]

3. Results and discussion

Reactivity effect

The experimental and calculated results of the reactivity effects of thorium test assemblies are tabulated in Table 1. The reactivity effect is expressed as the difference of excess reactivity between the reference core and the individual core loaded with thorium test assembly. The reactivity effects of thorium test assemblies have its maximum negative value in Th-3 assembly. The measured values agree fairly well to the calculated results, but discrepancies are slightly larger when JENDL-2 nuclear data file was used. In Fig. 5, the reactivity effects of thorium test assemblies are shown.

Relative neutron flux distribution

The relative neutron flux distributions along the vertical center

line in each thorium test assembly measured by reaction rate of bare gold foils inserted at regular intervals in the central element are shown in Figs.6-8, together with the results calculated by SRAC Code System. The measured values agree well to the calculated results. In summary, the cross section data of thorium in JENDL-2 library give somewhat lower C/E values on reactivity effect as long as the integral critical experiment and analysis on thorium test assemblies in UTR-KINKI are concerned.

Acknowledgement

Part of this work was partially supported by the Special Research on Energy under the Grant-in-Aid of the Scientific Research of the Ministry of Education, Science and Culture.

References

1. K. Tuchihashi, et al.: "SRAC: JAERI Thermal Reactor Standard Code System for Reactor Design and Analysis", JAERI 1285 (1983) and "Revised SRAC Code System", JAERI 1302 (1986).
2. K. Kobayashi, et al.: Reactivity measurements in a thorium critical assembly, Nucl. Sci. Eng., 71 143 (1979)
3. K. Kanda, et al.: Reactor physics experiment using KUCA, J.Atom. Energy Soc. Japan, 21 557 (1979)
4 .K. Kanda, et al.: Critical experiment with thorium using KUCA, Thorium Fuel Reactors, Atom. Energy Soc. Japan (1985)
5. H. Takano: Private communication (1987)
6. T. Itoh, et al.: Critical experiment and analysis on thorium assembly in Kinki University Reactor, Ann. Rep. Kinki Univ. Atom. Energy Res. Inst., 22 15 (1985)
7. T. Itoh, et al.: Critical experiment on natural uranium assembly in Kinki University Reactor, Ann. Rep. Kinki Univ. Atom. Energy Res. Inst., 23 39 (1986)

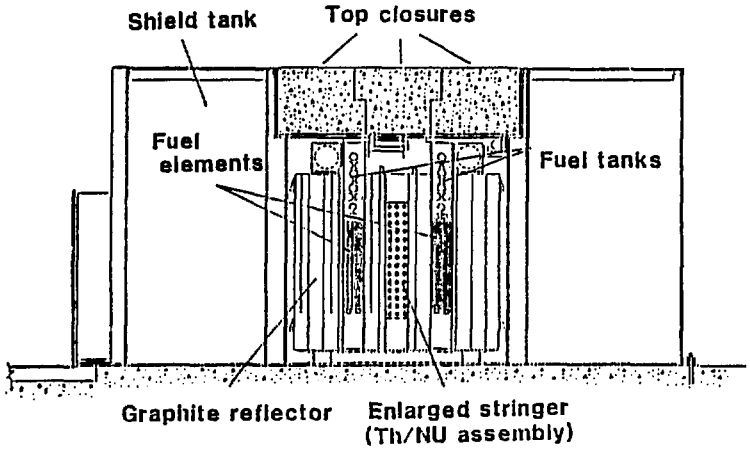

Fig. 1 Reactor cross section of UTR-KINKI

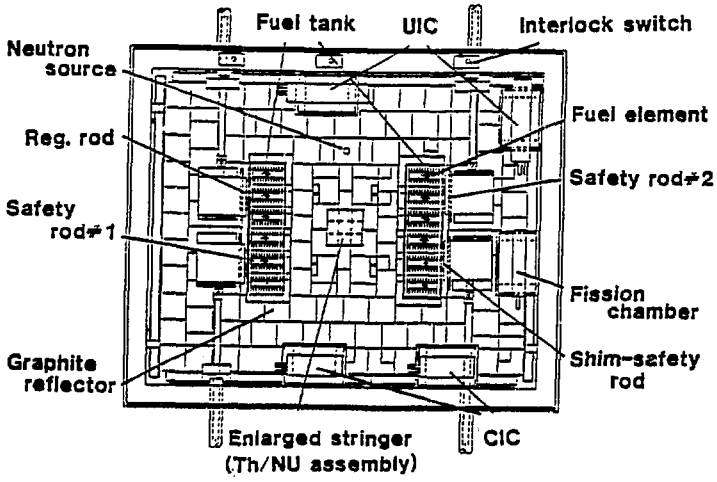

Fig. 2 Reactor core plan of UTR-KINKI

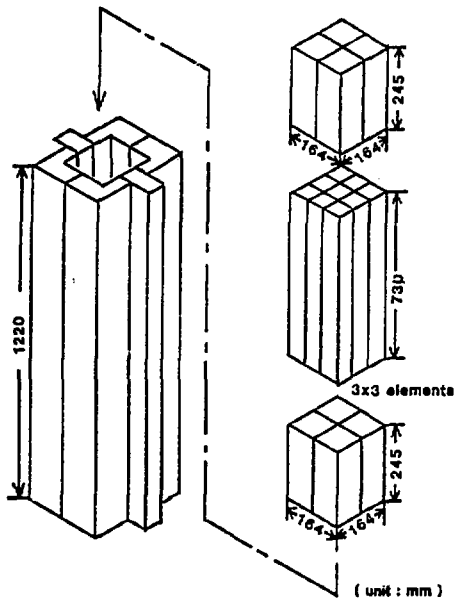

Fig. 3 Details of enlarged stringer and thorium test assembly

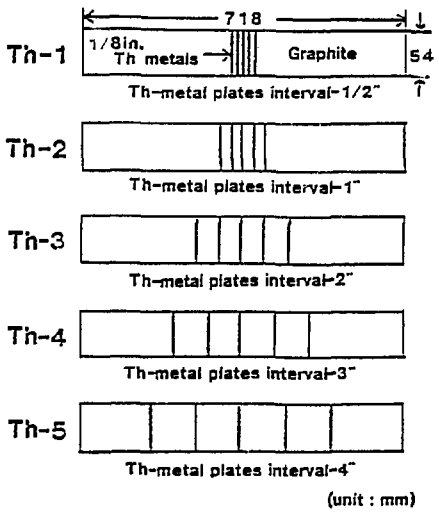

Fig. 4 Loading patterns of thorium element

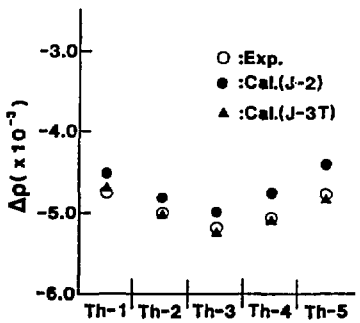

Fig. 5 Reactivity effects of thorium test assemblies

Table 1 Measured and calculated values of reactivity effects of various thorium assemblies

Th assembly	Th metal Plate interval	Reactivity differences ($-\Delta k \times 10^{-3}$)			C／E	
		Exp. value	Cal. value			
			J-2 (10-G)	J-3T(10-G)	J-2 (10-G)	J-3T (10-G)
Th-1	1/2"	4.76	4.51	4.69	0.946	0.985
Th-2	1"	5.01	4.81	5.03	0.961	1.005
Th-3	2"	5.19	4.95	5.25	0.954	1.012
Th-4	3"	5.06	4.77	5.11	0.943	1.010
Th-5	4"	4.75	4.42	4.84	0.930	1.019

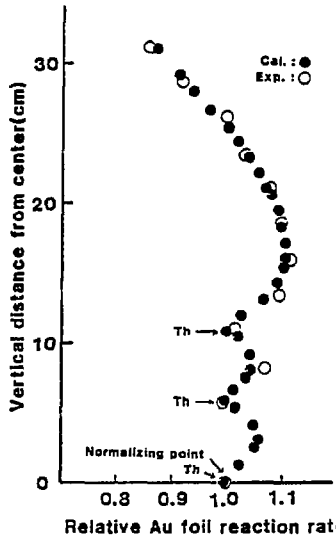

Fig. 6 Relative Au foil reaction rate distribution in Th-3 assembly (thorium metal plate interval—2")

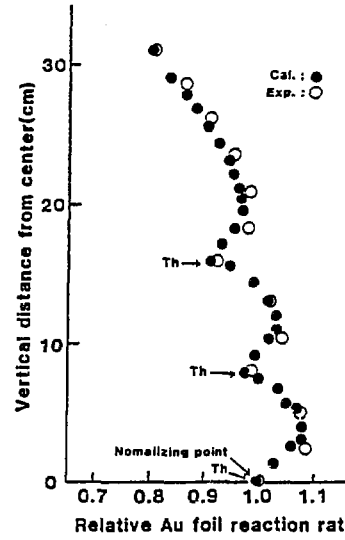

Fig. 7 Relative Au foil reaction rate distribution in Th-4 assembly (thorium metal plate interval—3")

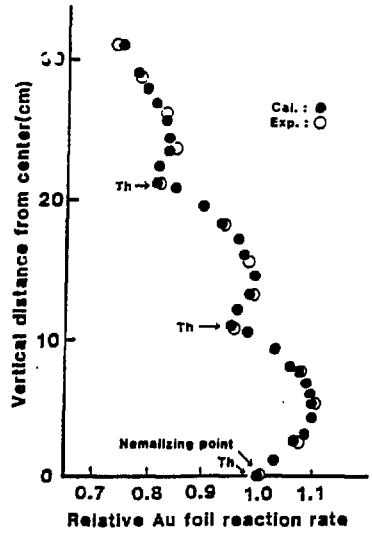

Fig. 8 Relative Au foil reaction rate distribution in Th-5 assembly (thorium metal plate interval—4")

3.16 Prototyping of an Expert System for Nuclear Data Evaluation

S. Iwasaki, N. Odano, M. Takahashi, M. Kitamura, K. Sugiyama

Department of Nuclear Engineering, Tohoku University
Aramaki-Aoba, Sendai 980, Japan

A prototype guidance system for the nuclear cross section calculation has been developed in a 16-bit personal computer. The system was consisted of two main parts: the first part is for selection of the code system, and the second one is for selection of the best input parameters for the selected codes. Priciples of guidance were taken from several literatures and recomendations.

I Introduction

An expert system in the field of the nuclear data evaluation is considered to be one of the solutions to the rapidly increasing requests on the nuclear data for various applied fields in Japan in spite of deficiency of the mon-power for the evaluation.

There are many kinds of nuclear codes for various cross section calculation, and only limited experienced researchers know which code is good for their purposes , how to use the selected codes correctly, and how to choose the input parameters to the codes.

If the collection of various kinds of knowledge about the nuclear codes and proper way of usage are systematized and implemented in a computer system (knowledge base system) so as to be accessed easily, it is very convenient for beginners, unskilled persons in the nuclear calculation, and even for the experts. The knowledge base system will be very flexible to revision and modification according to the progress of the theories, techniqeus and development of codes for the nuclear calculation.

In the present paper, an atempt of making a proto-type guidance system for nuclear cross section calculation by some nuclear codes is described. In the system we have assumed that the objective area of the nueleus is limited to the structural material near iron and the range of the incidnent neutron energy is fast neutron region above 1MeV. The guidance principles were taken from proceedings of several recent meetings[1-5] and papers[6-11], and was implemented in the system for the methods of code selection and detemination of the input parameters. Outline of the principles are described in sections 2 and 3.

II Outline of the guidance principles

II-1 Selection of code

Proper codes should be selected according to the several conditions: region of target nuclei in the periodic table, and

region of the incident neutron energy (resonance, unresolved, or fast neutron region).

If they hope to calculate the neutron cross sections in the energy range less than several MeV, they should use the statistical model (Hauser-Feshbach model) code with width fluctuation effect such as CASTHY[12]. Above this energy region, the number of open channels increases and the width fluctuation effect becomes small. Multistep Hauser-Feschbach (MSHF) model code, such as GNASH[13], is suitable for the calculations in the energy range. The GANSH code has a capability of tracing the all open channels upto the 8 CN's (parent nuclei) and 4 decay modes of the CN's. Therefore they can use this code up to the incident energies of about 50 MeV. Of cource, it is necessary to prepare all transmission coefficients of all outgoing particles for every CN by mean of other optical model codes prior to use. Another MSHF code, TNG[14] is also available and has different features[15] from GNASH.

Above 10 MeV, the contributions of the precompound (PC) reaction mechanism become important for (n,xn'ycp) reactions, where x=1,2 or 3 or y=0,1,2 and cp=charged particles. The nuclear theory of this mechanism are now under development and there has been no definite model. In all available MSHF codes, a sort of the PC model is built in. For this reason we had better use the PC model which is included in the existent code exept for minor modification, if necessary. If someone want to use a recently developed model, he has to implement the model into the code by himself, and this process is usually not recomended except for the experts.

In this energy region, the direct reaction (DR) mechanism may also dominate in the elastic and inelastic scatterings. If it is necessary to evaluate properly both scatterings in magnitude and angular distributions, usage of the DWBA or coupled channel(CC) model calculation are inevitable. Especially the CC model is recomended if apparently the ground state of the target nucleus couples strongly to the collectively excitated states.

In Fig.1, a diagram of typical code systems and relationship between them for the nuclear data calculation given by Yamamuro et al.[16] is shown.

II-2 Selection of various input parameters

In this section, outline of the priciples of input parameter determination mainly for the optical model potential, level density formula and gamma-strength functions.

II-2-1 Optical model potential parameters

The most important input parameters are those for the neutron optical model (OPM) potential. These parameters should be determined very carefully because almost the result of the calculation would be determined by them[11]. According to several recent model calculation studies[6-11], there are three methods to choose the parameters.

The first one is to adopt a global opticlal model parameter set. Modern global parameter sets are more superior than old

ones in general[5]. However the most global parameters were determined by fitting the data of the representative nuclei in the periodic table, and not the best parameters in the specific nuclei. Therefore the global parameters are suitalble to the purpose of rough calculation or the initial parameter set of the detailed and iterative calculations. The second way is to choose the parameter set which had been determined in a previous evaluation/calculation which reprocduced the cross sections well. Those parameters, however, are not always the best ones when the new experimental data come out after the evaluation. The third way is to determine the parameters independently on the previous works, but this process is tedious and not prefereable in general.

In any cases described above, the parameter values must be reevaluated by comparing the results with the recent reliable experimental data set. First, the parameter set should be checked by the Lagrange's criterion, so called "SPRT" method[11]. The optical model parameters should reproduce the important optical model quantities, such as S- and P- wave strength functions and scattering radius R' for the slow neutrons. The optical model calculation should reproduce the total (T) cross section behavior in the entire energy range, except for the resonance structure. In order to get best results, the iteration porocess is necessary. Volume integrals of both real and imaginary well depth show sometime good index of the parameter systematics[5].

The proton and alpha-particle optical potentials are also important because the recent nuclear development needs the accurate cross sections of the charged particle emission reactions in the high energy regions, and the cross section of the particle emission is very sensitive to the parameters. The charged particle optical potentials, however, have not been studied extensively as the neutrons. Usually, these charged particle parameters are selected among the global parameter sets. Among many paramere sets, the Huizenga and Igo's set[17] for alpha is considered not to be suitable, because that parameter set results in the abnormally large cross sections[18].

II-2-2 Level density parameters

Level density (LD) formula and its parameters are also important for determining not only the cross sections itself but also the energy distribution of the emmitted particles[4,11].

Usually as the LD model in the cross section calculations, the phenomenological Fermi-gas formula have commonly been used, because the formula has rather simple expression and have been studied comprehensively and improved. In spite of recent remarkable impovement of the microscopic model of the density, these trend will continue for comming five to ten years.

First, the Gilbert-Cameron formula[19] is recommeded, because this formula have been used in almost every calculation code available in Japan. The parameters of the formula are also studied for almost every nucleus. However, the back-shifted Fermi-gas formula[20] should be tested if the former one failed the fitting because It is very easy to replace by the latter.

For any formula and paramerers, the result should be checked

by comparing the results to the recent experimental data. Average resonance level spacing[21] is one of the important experimental data. Particle (neutrons and charged particles) emission spectra are very sensitive to the desity parameters. Particularly, the Grimes' data[22] should be refered. Reasonable parameter set must be searched by iteration process.

II-2-3 Gammma-ray transmission coefficient (GTC)

These parameters are influential not only to the gamma-ray production cross sections and spectra but also to the particle cross sections through the competition processes.

The profile of the GTC are usually so called giant-dipole resonance type whose parameters are taken from the systematics by Gardner et al[23]. Specific nuclei's parameters are determined by interpolation.

Absolute value of the GTC should be normalized to the ratio of the experimental data of the gamma width $\langle\ \rangle$ and average level spacing $\langle D \rangle$. However the experimental data sometime have large systematic errors. In the important nuclei, the coefficient should be renormalized so that the reliable capture cross sections at low energy region are reproduced.

II-2-4 Other parameters

Other important parameters in the cross section calculations are the following ones,

.Precompound (PC) model parameters
.Direct reaction (DR) calculation
and others which are unique to the code.

In the PC model parameters, the Kalbach's constant[24] or its related parameter is important. We had better consider that this parameter is an adjustable one[11], especially for alpha.

In the direct reaction calculation, the coupling scheme and the deformation parameters are important. These parameters are also selected in similar manners discussed above.

III Guidance System

III-1 Expert shell

The knowledge and recomended processes for the calculations should be implemented in the knowledge base. Considering the prototype one, we chose the small expert construction system, TELL[25] (expert shell) which ran in a 16-bit microcomputor with 2-Mbyte extended RAM.

TELL is based on the PROLOG language (PROLOG-KABA[26]) with its extension tool, WING[27]. TELL supports three kinds of knowledge expression, such as 'production rules' for backward and foreward inference, 'frame expression' and 'table inference'. The last one is a fuzzy like inference with a values table and unique to the TELL. Table header of the table will be fired when the sum of weight(-99 - 99) of fired items in the table excede the predetermined threshold value (0 - 999). Thus the table inference is effective for reduction of the redundant production rules.

TELL also supports Japanese input and output, multi-window system, mouse interface and graphics, and is accessible to the data base file made by dBASE-II[28].

III-2 Basic structure of the system

The system is consisted of two main parts. The first one corresponds to the code selection, and the second one to the parameter determination.

In the first part, the system asks two basic questions to the user on the nuclei to be calculated and the region of energy. The system checks the whether the answered regions are covered by the system: structural material elements near iron and the energy less than 50MeV.

The system asks additional questions to the user on kinds of reactions (assumled to be neutron, proton and alpha-particle emission) and a kind of calculation purpose, detailes or rough calculation (estimation), etc. Some time in the rough calculations the systematical model or simple model such as PEGASUS[29] are preferable rather than the MSHF model codes because of the simpleness of parameter input and fast calculation. The reasoning of the code selections are the table one. The typical example of the table inference and its values is presetnted in Fig 2.

In the socond part of the system, the part is devided into 5 independent rule blocks, such as the block for the OPM and parameters, for the LD formula and parameters, for the GTC's, for the PC part, and for the DR. The first OPM part is devided into subblocks, for the neutron, proton and alpha-particle, respectively.

Almost rules implemented in the second part are the production rules. Example of the questions, answers and guidance dialogue for the case of the neutron OPM parameter selection is shown in Fig. 3. For the present, no experimental data base is included in the system, the user should consult the other data bases or some references in order to answer the questions given from the system.

IV Summary

A prototype guidance system for the nuclear cross section calculation has been developed in the 16-bit personal computer. Test run of the system showed that it presented proper guide and was useful for the biginners. However, the system is far from the application use, because the system is limited in the small region of the nuclei, adopted rules are limited and the experimental data base has not been included. It is also necessary to develop new technique of the determination of the best parameter set from a lot of and various types of the experimental data, and criteria for fitting the cross sections.

In future, it is not impossible to develope a semi-automated nuclear data evaluation system which will be a large scale system in a main frame computor linked with other codes and data base systems, and be accessible from remote areas in the country by computor network.

References

1) Proc. of Consultants' Meeting on the use of Nuclear Theory in Neutron Nuclear Data Evaluation, vol.I & II, IAEA-190, Trieste, 8-11 Dec. 1975 (IAEA, Viena 1976).
2) Proceedings of Workshop on Evaluation Methods and Procedures, BNL, Upton NY BNL, 22-25 Oct., 1980 (Upton, 1980).
3) Proc. NEANDC/NEACRP Specialist's Meeting on Fast Neutron Capture Cross Sections, April 20-23, 1982 ANL, ANL-83-4 (Argonne 1983).
4) Proc. of a Advisory Group Meeting on Basic and Applied Problems of Nuclear Level Densities, Upton NY, 11-15 April, 1983, BNL-NCS-51694 , M.R.Bhat (Ed.), (IAEA and USDOE 1983).
5) Proc. on Specialist Meeting on Use of the Optical Model for the Calculation of Neutron Cross Sections below 20 MeV, Paris 13-15 Nov., 1985 (OECD 1986).
6) Arthur, E.D and Young, P.G.: LA-8626-MS(ENDF-304),UC-34c (LANL 1980).
7) Arthur, E.D.: Proceeding of Consultants' Meeting on Structural Materials (IAEA), Vienna, Austria, November 2-4, (1983), and LA-UR 83-3137 LANL (1983).
8) Prince, A.: Proc. International Conference on Nuclear Data for Science and Technology, Antwerp, Sep. 6-10, 1982, pp, ECSC,EEC,EAEC,Brussels and Luxembourg (1983).
9) Strohmaier, B and Uhl, M.: ibid., pp552-555.
10) Hetrick, D.M., Fu, C.Y. and Larson, D.C.: ORNL/TM-9086 ENDF-337 (ORNL 1984).
11) Yamamuro, N.: private communications (1986).
12) Igarashi, S.: J. Nucl. Sci. Technl., 12, 67 (1975).
13) Young, P.G. and Arthur, E.D.: LA-6947, LASL (1977).
14) Fu, C.Y.: ORNL/TM-7042 (1980).
15) Shibata, K.: JAERI-M 87-025, p.331 (1987).
16) Yamamuro, N. and Hida, K.: ibid., p.347 (1987).
17) Heizenga, J.R. and Igo, G.: Nucl. Phys., 29, 462 (1962).
18) Vonach, H.: Proc. IAEA Adv. Gr. Meet. on Nucl. Level Densities, BNL-NCS-51694, p.247 (1983).
19) Gilbert, A. and Cameron, A.G.W.: Canadian Journal of Physics, 43, pp1446-1496,(1965).
20) Dilg, W., et al., Nucl. Phys., A217, (1973).
21) Mughabghab, S.F., Divadeenam, M.and Holden, N.E.: "Neutron Cross Sections, vol1&2 Neutron Resonance Parameters and Thermal Cross Sections, Part A:Z=1-60 ", Academic Press (New York, 1981).
22) Grimes, S.M., et al.: Phys. Rev., C19, 2127 (1979).
23) Gardner, D.G., Gardner, M.A. and Dietrich, F.S.: Lawrence Livermore Lab.,(1980).
24) Kalbach, C.: A. Physik, A283, 401 (1977).
25) Hagino, T., et al.: "PROLOG-KABA reference manual" (in Japanese) ASTEC Co., (Tokyo,1986)
26)Inaba, T., et al.: "WING reference manual" (in Japanese), Iwasaki Giken Kogyo Co., (Tokyo, 1986).
27) "AIPLAN TELL users manual"(in Japanese), Iwasaki Giken Kogyo Co.,(Tokyo 1987).
28) dBASE-II, Ashton-Tate, Co., USA.
29) Iijima, S., et al.: JEARI-M 87-025, P337 (1987).

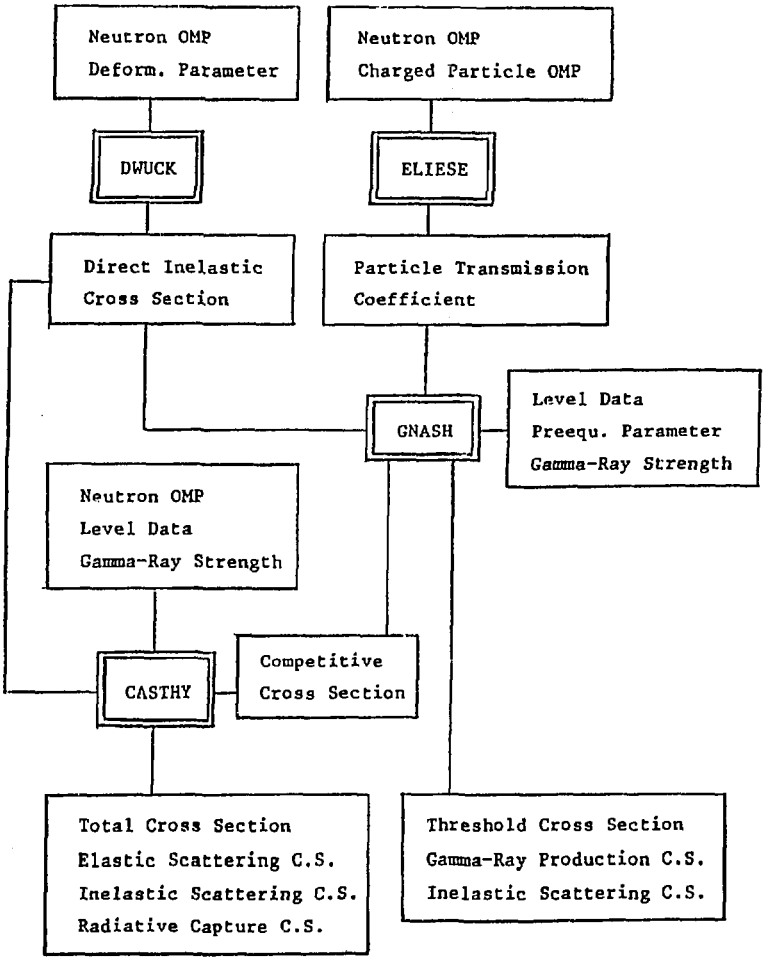

Adoption of Inelastic Scattering Cross Section

$E \leq Ej$ CASTHY + DWUCK

$E > Ej$ GNASH + DWUCK

Fig.1 Example of code system for the nuclear cross section calculations, given by Yamamuro et al[16].

I. Table Header : calculation code candidate GNASH*

Threshold value: 100

TABLE ITEMS	VALUE	WEIGHT	Ex.
[50MeV>incident energy>several MeV,	YES	100]	
[20MeV>incident energy>several MeV,	YES	60]	o
[incident energy<several MeV,	YES	-200]	
[include direct reaction calc.,	YES	30]	o
[Gilbert-Cameron level density,	YES	30]	o
[angular distribution for secondary neutrons,	YES	-200]	o
[simple calculation,	YES	-50]	
[widely used code,	YES	50]	o
[easy preparation for transmission coefficients,	YES	50]	o
[ENDF format output	YES	-50]	

Ex.: 60+30+30+(-200)+50+50=20<50 then GNASH is not recomended.

*this GNASH is first version (1975) and recent one is much improved.

II. Table Header : TNG

Threshold value: 100

ITEM	VALUE	WIGHT	Ex.
[50MeV>incident energy>several MeV,	YES	-100]	
[20MeV>incident energy>several MeV,	YES	60]	o
[incident energy <several MeV,	YES	50]	
[include direct reaction calc.,	YES	30]	o
[Gilbert-Cameron level density,	YES	30]	o
[angular distribution for secondary neutrons,	YES	100]	o
[simple calculation,	YES	-50]	
[widely used code,	YES	-50]	o
[easy preparation for transmission coefficients,	YES	30]	o
[ENDF/B format output	YES	30]	

Ex.: 60+30+30+100+(-50)+50=220 > 50 then TNG is recomended with the certainty factor of 220.

Fig. 2 Two examples of the 'table inference' for code selection.

```
[Start rule block for the neutron optical potential selection]
     > assumed answer for basic question : Fe-54 and 56
     >           for additional questions: detailed calculation
     >                                     etc.
Q1:is there any recent (after 1980) calculation/evaluation
   for the nuclei?
A1: YES [then go to ...] (not shown)
  : NO [then G1]
G1: It is recomended to adopt a global optical potential
 Q2: do you have definite GOPM candidate to be selected?
 A2: YES [then go to ...] (not shown)
   : NO
     [start rule block for GOP selection]
     [read the frame block of the NEUTRON GOPM]
     [select the best GOPM from its slot values]
 G2: use Walter and Gass GOP as a starting value
     [start rule block for best OPM determination]
  Q3:do you want to revise the OPM parameter once(1),
     or twice or more(2)?
  A3: 1 then go to ...(not shown)
    : 2 [start SPRT checking rule]
  G3: calculate s-wave (S0) and p-wave (P0) strength
      functions and potential scattering radius,
      and compare with the recent exp. data.
   Q4: good agreement?
   A4: YES [then go to ..] (not shown)
       NO
   G4: vary V,aR,rR and WI,aI,rI and get best fitting
    Q5: good agreement?
    A5: NO [then go to...] (not shown)
        YES
    G5: calculate total (T) cross section curve
        in the entire energy range,
        and compare with the best experimental data.
     Q6: good agreement?
     A6: NO [then go to ...] (not shown)
       : YES
     G6: calculate elastic( ang. dist.), inelastic1 and
         noelastic cross section in the entire energy range,
         compare with the best experiment.
      Q7: good agreement?
      A7: YES [then go to ...] (not shown)
          NO
      G7: include the deformation parameters in the OPM.

          ..... (continued)
```

Fig. 3 Example of a part of dialogue between user and the present expert system.
Q: questions asked from the system
A: answers by user
G: guidances given by the system
[inference processes of the system]

3.17 Expert System for Estimation of Uncertainty on Experimental Nuclear Data

Yuji Uenohara, Mitsuhaya Tsukamoto, Toshiya Mori, Mitsuru Kihara, and Yukinori Kanda

Department of Energy Conversion Engineering, Kyushu University
Kasuga, Fukuoka 816, Japan

Abstract

We tried to design an expert system for evaluation of the systematic errors. The knowledge base and inference engine of the expert system are written in the computer programing language LISP. The systematic errors of $^{238}U(n,f)$ cross section data in EXFOR file were evaluated for an example.

Introduction

Covariances of evaluated nuclear data are important in the field of nuclear engineering. Error information on experimental cross section data are important sources for the evaluation of covariances. Systematic errors of experimental cross section data play a significant role in the evaluation of covariances. It, however, is impossible to evaluate accurately systematic errors. The information on systematic errors are given in nuclear reaction database. They, however, are not always described in detail. Ones hardly obtain the information on systematic errors in the nuclear reaction database. The systematic errors, however, show patterns with respect to experimental conditions e.g. facilities, detectors, and so on. Evaluators can roughly deduce systematic errors. The deduction is performed by using their abundant knowledge and experiences. This work becomes hard and troublesome with the number of

experimental data. Many experts on the evaluation are required for the evaluation of systematic errors. A mechanical evaluation of systematic errors interests us. The knowledge cannot be almost represented by mathematical formulas and numerical data. The traditional computer programing technique are unsuitable to the development of it.

A knowledge engineering has recently been developed. This technique can be applied in many fields. An expert system is the most successful technique in the knowledge engineering. We have tried to design the expert system for evaluation of the systematic errors. The knowledge base and inference engine of the expert system are written in the computer programing language LISP. The systematic errors of an experiment of $^{238}U(n,f)$ cross section data in EXFOR[1] file were evaluated for an example.

Production System

A production system in a knowledge engineering is characterized by an inference engine and knowledge base[2]. The traditional computer program was composed of the program and data parts. The procedure of problem solving was only in the program part. In the case of production system, it is in the data part. It is represented by the form of knowledge. A set of knowledge is called knowledge base. It is composed of facts and rules. The program part is called inference engine. The inference engine deduces new facts by using knowledge base. The present system is designed by using the technique of the production system. The block diagram of this system is shown in Fig. 1. The implementation of the system by LISP is referred to the reference[3].

EXFOR file

An EXFOR(EXchange FORmat) is the format for experimental

nuclear reaction database. The numerical data of experimental cross section are almost stored and circulated to users in the EXFOR format. This database includes experimental conditions in detail. The EXFOR file is a set of entries, e.g. reports. An ENTRY is a set of some subentries, e.g. experiments. A SUBENTRY is a minimum unit identifying experiment. The example of EXFOR file is shown in Fig. 2. The bibliography and experimental conditions are stored in the BIB section. The keywords identify the experimental and bibliographic information in EXFOR file. Keywords are specified by codes and free documentations. The structure of component in BIB section is written by

KEYWORD, CODE, FREE_DOCUMENTATION.

We represent this structure as

(KEYWORD CODE FREE_DOCUMENTATION)

by the LISP. If code and free documentation are not given, they are replaced by a NIL, which means a null set. The changed database into LISP is shown in Fig. 3.

Knowledge Base

The knowledge bases of present system are categorized into three types as shown in Fig. 1.

The first is the knowledge for searching keywords in EXFOR file. These knowledge are written with the form of production rule. The inference engine is driven by using these knowledge. If the keyword, ERR-ANALYS, is not found in a given subentry, the inference engine searches every keywords concerned with the systematic errors by the backward reasoning. The second is a global knowledge with respect to cross section measurements. The code for keyword searched by using the rules are specified by using these knowledge. They are represented with the form of

frames. The third is a systematic error table.

Example

In this example, the present system estimates a partial error derived from estimation of neutron flux. The example experiment is the measurement of fission cross section ratio of ^{238}U and ^{235}U. In order to test the present system, the keywords of FACILITY and N-SOURCE are omitted in this subentry. The knowledge used in this example are shown in Fig. 4 and 5. The system tries to match between ERR-ANALYS and keywords in this subentry. Since the operator cannot find the neutron flux error, the inference engine searches to the keywords related neutron flux error. The first rule in Fig. 4 tells us that facility and neutron source are required for the deduction of neutron flux errors. The keywords, FACILITY and N-SOURCE, are not found in the subentry. In the next step, the inference engine searches the keywords for deduction of FACILITY and N-SOURCE. Other rules tell us that neutron energy ranges, the number of energy points, and institute are required for the deduction of facility and neutron source. These keywords are given in the subentry. The inference engine concludes that the estimation of neutron flux error enable. This process is backward reasoning. The facility and neutron source are specified by the global knowledge shown in Fig. 5. Obtaining the information on experimental conditions, the values of systematic errors are decided by the error tables. The outputs of the operation are shown in Fig. 6. In the present status, this system is handled by an operator at the real time. The operator is required for the analysis of free documentation.

Concluding remark

We have designed an expert system for evaluation of systematic uncertainty on experimental cross section data and

tried to construct the prototype of the system.

The EXFOR format can be converted to LISP, easily. Using LISP interpreter, the inference engine and knowledge base can be implemented to the main frame FACOM780, easily. The LISP is very powerful tool to program this system.

The knowledge base is the most important to make this system fit for practical use. The knowledge of neutron cross section measurement needs to be collected internationally for the purpose of improvement of quality. Many discussions by experts on experiments are necessary to polish up the knowledge. It is expected that the discussions contribute to the improvement of experimental technique.

References

[1] Lemmel, H.D. ed., NDS EXFOR Manual, International Atomic Energy Agency Nuclear Data Services, 1979.

[2] Rich, E., "Artificial Intelligence", McGrqw-Hill Book Company, 1983.

[3] Winston, P.H. and Horn, B.K.P., "LISP", Addision-Wesley Publishing Company, Inc., 1981.

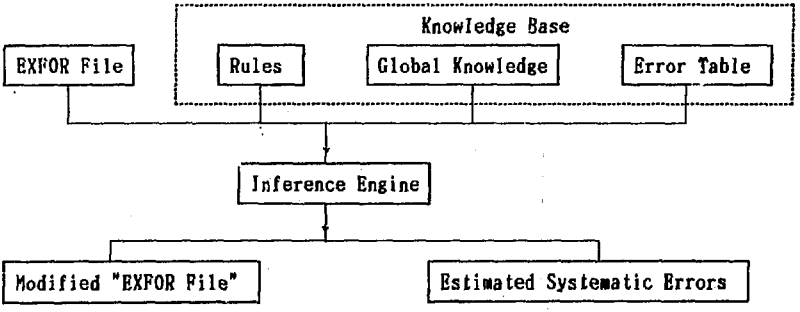

Fig. 1 Block diagram of the present system.

INSTITUTE (1USAANL)
REFERENCE (J,NSE,49,310,7211)
(R,INDC(USA)-38,72)
AUTHOR (J.W.MEADOWS)
TITLE THE RATIO OF THE URANIUM-238 TO URANIUM-235 FISSION CROSS SECTIONS FROM 1 TO 5 MEV
INC-SPECT ENERGY RESOLUTION GIVEN REFERS TO FULL ENERGY SPREAD.
METHOD (TOF) TIME-OF-FLIGHT USED TO REDUCE AND MEASURE TIME-INDEPENDENT BACKGROUND.
CORRECTION CORRECTED FOR SECOND LI7(P,N) GROUP, OTHER URANIUM ISOTOPES, INELASTIC SCATTERING IN SAMPLE BACKINGS, PULSE-HEIGHT EXTRAPOLATION, AND BACKGROUND. EFFECTS DUE TO ELASTIC SCATTERING IN SAMPLE SUPPORTS, SAMPLE GEOMETRY, AND MOMENTUM EFFECTS ELIMINATED BY THE NORMALIZATION OR BY MEASUREMENTS IN BOTH COUNTER ORIENTATIONS.
STATUS (APRVD) APPROVED BY AUTHOR
HISTORY (721030C)
(750905A) BIB CHANGES.
ISO-QUANT ((92-U-238,NF)/(92-U-235,NF))
SAMPLE MEASUREMENTS MADE WITH DEPOSITS OF KNOWN MASS RATIOS. DETERMINED BY TWO METHODS - 1.SPECIFIC ALPHA ACTIVITIES, 2.RELATIVE THERMAL FISSION RATES OF PURE U-235 SAMPLE AND OF U-238 SAMPLE CONTAINING SEVERAL PERCENT U-235.
ERR-ANALYS ERROR ANALYSIS FOR THE ABSOLUTE MEASUREMENT AT 2.51MEV

ERROR DUE TO	METHOD 1(PER-CENT)	METHOD 2(PER-CENT)
MASS RATIO	1.0	0.5
COUNTING STATISTICS	0.35	0.35
COMBINED ERROR	1.25	0.91

RATIO ERROR GIVEN INCLUDES MASS RATIO, COUNTING STATISTICS AND RELATIVE CONSISTENCY.

Fig. 2 Example of BIB section in EXFOR file. The strings in the first to 11th columns are keywords. The next strings enclosed by parenthesis are codes. The others are free documentations.

```
(
 (INSTITUTE (1USAANL) NIL)
 (REFERENCE  (J,NSE,49,310,7211
             R,INDC/(USA/)-38,72) NIL)
 (AUTHOR      (J.W.MEADOWS) NIL)
 (TITLE       NIL (THE RATIO OF THE URANIUM-238 TO URANIUM-235 FISSION
              CROSS SECTIONS FROM 1 TO 5 MEV))
 (METHOD      (TOF) (TIME-OF-FLIGHT USED TO REDUCE AND MEASURE
              TIME-INDEPENDENT BACKGROUND.))
 (CORRECTION NIL  (CORRECTED FOR SECOND LI7/(P,N/) GROUP, OTHER URANIUM
             ISOTOPES, INELASTIC SCATTERING IN SAMPLE BACKINGS,
             PULSE-HEIGHT EXTRAPOLATION, AND BACKGROUND. EFFECTS
             DUE TO ELASTIC SCATTERING IN SAMPLE SUPPORTS, SAMPLE
             GEOMETRY, AND MOMENTUM EFFECTS ELIMINATED BY THE
             NORMALIZATION OR BY MEASUREMENTS IN BOTH COUNTER
             ORIENTATIONS.))
 (STATUS      (APRVD) (APPROVED BY AUTHOR))
 (HISTORY     (75) (BIB CHANGES.))
 (ISO-QUANT   (92-U-238,NF // 92-U-235,NF) NIL)
 (SAMPLE      NIL (MEASUREMENTS MADE WITH DEPOSITS OF KNOWN MASS RATIOS.
              DETERMINED BY TWO METHODS - 1/.SPECIFIC ALPHA
              ACTIVITIES, 2*RELATIVE THERMAL FISSION RATES OF PURE
              U-235 SAMPLE AND OF U-238 SAMPLE CONTAINING SEVERAL
              PERCENT U-235.))
 (ERR-ANALYS  NIL (ERROR ANALYSIS FOR THE ABSOLUTE MEASUREMENT
      ERROR DUE TO     METHOD 1(PER-CENT)  METHOD 2(PER-CENT)
      -----------      ------------------  ------------------
      MASS RATIO             1/.0                0/.5
      COUNTING STATISTICS    0/.35               0/.35
      COMBINED ERROR         1/.25               0/.91

           RATIO ERROR GIVEN INCLUDES MASS RATIO, COUNTING
           STATISTICS AND RELATIVE CONSISTENCY.))
  (RANGE (1 5) NIL)
  (POINT (40) NIL)
)
```

Fig. 3 The example of EXFOR files changed into LISP. The new keywords, RANGE, and POINT denote neutron energy range and the number of data, respectively. They are added temporarily. These keywords are not defined in the original EXFOR format.

```
          .
          .
 (RULE IDENTIFY7
       (IF (FACILITY)
           (N-SOURCE))
       (THEN (FLUX-ERROR)))
 (RULE IDENTIFY8
       (IF (INSTITUTE)
           (HISTORY))
       (THEN (FACILITY)))
 (RULE IDENTIFY9
       (IF (RANGE))
       (THEN (FACILITY)
             (N-SOURCE)))
 (RULE IDENTIFY11
       (IF (POINT))
       (THEN (FACILITY)
             (N-SOURCE)))
          .
          .
```

Fig. 4 Production rules for inference of unknown keywords. The first rule means if keywords, INSTITUTE and HISTORY are given in SUBENTRY, the facility can be found.

```
(INSTITUTE
    (
          .
          .
     ((INSTITUTE (1USAANL) NIL)
         ( ((FACILITY (DYNOM) NIL) (HISTORY (72) NIL))
           ((FACILITY (VDG)   NIL)   (HISTORY (72) NIL))
           ((FACILITY (LINAC) NIL)  (HISTORY (75) NIL))
         )
     )
          .
          .
   )
)
```

Fig. 5 Example of global facts for institute. This knowledge shows the facilities which belong to Algonne National Laboratory.

```
>(MAIN)

 (ERROR ANALYSIS FOR THE ABSOLUTE MEASUREMENT AT 2.51MEV
           ERROR DUE TO    METHOD 1(PER-CENT)  METHOD 2(PER-CENT)
           ------------    ------------------  ------------------
           MASS RATIO            1/.0                0/.5
           COUNTING STATISTICS   0/.35               0/.35
           COMBINED ERROR        1/.25               0/.91

     RATIO ERROR GIVEN INCLUDES MASS RATIO, COUNTING
           STATISTICS AND RELATIVE CONSISTENCY.)


 ((FLUX-ERROR) IS-DESCRIPTED-IN-ERR-ANALYS?)

>NO
(IDENTIFY7 (FACILITY))
(IDENTIFY8 (N-SOURCE))
(IDENTIFY6 (MONITOR))
(IDENTIFY5 (FLUX-ERROR))
(HYPO (FLUX-ERROR) IS-TRUE)
HYPOTHESES-IS-END
```

Fig. 6-1 Operation of the present system. The under scored lines are operator's input. The LIST, (MAIN), is the function name of the inference engine. The system displayed the free documentation in ERR-ANALYS on the monitor and asked to operator whether flux error was descripted in ERR-ANALYS. As there was no information, the operator answered "NO". The inference engine, then, tested the hypothesis, "Flux Error can be deduced.". In the example, the hypothesis is true.

```
>FACT
(
      (((N-SOURCE (P-LI7) NIL) (N-SOURCE (D-D) NIL))
       ((FACILITY (VDG) NIL))
      (INSTITUTE (1USAANL) NIL)
      (REFERENCE  (J,NSE,49,310,7211
                R,INDC/(USA/)-38,72) NIL)
      (AUTHOR     (J.W.MEADOWS) NIL)
      (TITLE       NIL (THE RATIO OF THE URANIUM-238 TO URANIUM-235 FISSION
                   CROSS SECTIONS FROM 1 TO 5 MEV))
      (METHOD     (TOF) (TIME-OF-FLIGHT USED TO REDUCE AND MEASURE
                   TIME-INDEPENDENT BACKGROUND.))
      (PART-DET   (FF) (FISSION FRAGMENTS))
      (CORRECTION NIL (CORRECTED FOR SECOND LI7/(P,N/) GROUP, OTHER URANIUM
                   ISOTOPES.))
      (STATUS     (APRVD) (APPROVED BY AUTHOR))
      (HISTORY    (75) (BIB CHANGES.))
      (ISO-QUANT  (92-U-238,NF // 92-U-235,NF) NIL)
      (SAMPLE     NIL (MEASUREMENTS MADE WITH DEPOSITS OF KNOWN MASS RATIOS.
                   DETERMINED BY TWO METHODS - 1/.SPECIFIC ALPHA
                   ACTIVITIES, 2*RELATIVE THERMAL FISSION RATES OF PURE
                   U-235 SAMPLE AND OF U-238 SAMPLE CONTAINING SEVERAL
                   PERCENT U-235.))
      (ERR-ANALYS  NIL (ERROR ANALYSIS FOR THE ABSOLUTE MEASUREMENT
           ERROR DUE TO    METHOD 1(PER-CENT)  METHOD 2(PER-CENT)
           ------------    ------------------  ------------------
           MASS RATIO            1/.0                0/.5
           COUNTING STATISTICS   0/.35               0/.35
           COMBINED ERROR        1/.25               0/.91

                RATIO ERROR GIVEN INCLUDES MASS RATIO, COUNTING
                 STATISTICS AND RELATIVE CONSISTENCY.))
       (RANGE (1 5) NIL)
       (POINT (40) NIL)
)
)

>ERROR
((FLUX-ERROR IS 1 %))
```

Fig. 6-2 Operation of the present system. The under scored lines are operator's input. The modified EXFOR file is shown in this figure. At the top of the LIST, the deduced facts are added. The values of flux error is stored in the atom, ERROR.

3.18 Calculation of Double Differential Cross Sections for Structural Materials by PEGASUS Code

T. Sugi, T. Nakagawa, T. Nishigori and S. Iijima

*) Japan Atomic Energy Research Institute
**) Osaka University
***) NAIG Nuclear Research Laoratory

The neutron induced neutron and proton emission double differential cross sections were calculated with PEGASUS code for Cr, Fe and Ni and their isotopes. Results are in fair agreement with experimental data for neutron energy near 14 MeV, confirming that PEGASUS may be applied successfully to produce the double differential cross section data for JENDL.

1. Introduction

Neutron-induced double differential cross sections (DDX) of structural materials are required from fusion neutronics calculation and the evaluation of radiation damage of materials. In JENDL-3 general purpose file, the DDX for direct inelastic scattering to discrete levels are included but not for the particle emissions to the continuum levels of residual nuclei. It is anticipated that the extensive DDX data will be required in very near future for many applications, especially to calculate the primary knock-on atom spectra for radiation damage study and medical applications.

A recently developed code PEGASUS(1), based on the pre-equilibrium and the multi-step evaporation theory, is capable of calculating the angular distributions of neutrons and protons from the preequilibrium stage. The calculation is based on the theory of Mantzouranis et al.(2) with the effect of refraction of incident neutrons at the nuclear surface(3).

This scheme has been applied by many authors to calculate the neutron angular distributions, and seems to have been almost established. However, to the author's knowledge, the realistic applications to important structural materials including the statistical or the evaporation components and also proton emissions have not been made sufficiently.

The aim of the present study is to test PEGASUS through the comparison of calculation and experimental data of DDX for neutron and proton emissions induced by neutrons of energy of about 14 MeV. The goal is to apply PEGASUS to implement the JENDL DDX files.

2. Method of calculation

The preequilibrium angular distributions of neutrons and protons are calculated by the method of Mantzouranis et al.(2) together with the refraction of incident neutrons at the nuclear surface(3). Infinite refraction index is assumed. The angular distributions of alpha particles are not treated. The particle emissions from the second stage on are calculated by evaporation theory and are isotropic.

The angular distributions of emitted nucleons are then written in the form :

$$\sigma_{n,x\beta}(E_N,\varepsilon_\beta,\theta_\beta)=\sigma_{n,x\beta}(E_N,\varepsilon_\beta)\sum_{\ell}\frac{2\ell+1}{4\pi}f_\ell(E_N,\varepsilon_\beta)P_\ell(\cos\theta_\beta), \quad (1)$$

$$f_\ell(E_N,\varepsilon_\beta)=\frac{\sigma_{comp}(E_N)}{\sigma^{pre}_{n,x\beta}(E_N,\varepsilon_\beta)}\sum_{n=3}^{\bar{n}}W_\beta(n,\varepsilon_\beta)\tau(n)\mu_\ell^{\frac{n+1}{2}}, \quad (\ell\geq 1) \quad (2)$$

Here, σ_{comp} is the composite nucleus formation cross section, $W_\beta(n,\varepsilon_\beta)$ the particle emission rate from the state of exciton

number n, and $\tau(n)$ the exciton life time.

The eigenvalues are : $\mu_0=1$, $\mu_1=2/3$, $\mu_2=1/4$, $\mu_3=0$, etc. The maximum order of Legendre expansion Lmax = 2 is sufficient. Since the preequilibrium particle emission is dominant from the state of exciton number 3, the Legendre coefficient f_ℓ may be further simplified as :

$$f_\ell(E_N,\varepsilon_\beta) \approx \mu_\ell^2 \cdot \sigma^{Pre}_{n,x\beta}(E_N,\varepsilon_\beta) \Big/ \sigma_{n,x\beta}(E_N,\varepsilon_\beta) . \quad (3)$$

Figure 1 illsustrate the neutron angular distributions from Ni-58 induced by 15 MeV neutrons calculated by Eqs. (2) and (3), showing that a simplified formula, Eq.(3) is a good approximation. The corresponding particle spectra and the Legendre coefficients spectra are shown in Fig. 2.

3. The model parameters

The calculations were performed for Cr, Fe and Ni isotopes. The inverse cross sections are calculated from the optical potentials used for evaluation of JENDL-3 cross sections. These are fixed to the values for the dominant target nuclides, i.e., Cr-52, Fe-56 and Ni-58. Figure 3 shows the inverse cross sections for neutron, protons and alpnas.

Level density parameters are essentially the same as those adopted in JENDL-3 evaluation and of the Gilbert and Cameron type. In case of chromium, where the back-shifted Fermi gas model was used in JENDL-3 evaluation, the parameters of Gilbert-Cameron type had to be re-determined. These parameters were adjusted to some extent depending on

the target nuclides to fit the excitaition cross sections and the particle spectra. Original values and the adjusted values are listed in Table 1. Only the Fermi gas parameter a and the temperature value T of the constant temperature formula are given in the table. Remaining parameters are easily obtained by the condition of the smooth continuity. Pairing energy data were adopted from Gilbert and Cameron. Figure 4 shows the level density parameters as a function of mass number. The dotted lines indicate the systematics which was used in the present study when the level density parameters were difficult to determine from the slow neutron resonance data and/or the low-lying level scheme data. It is seen that the product aT is nearly constant with respect to the mass number of this range.

The Kalbach's constant K, representing the strength of two-body interaction matrix, was determined to fit the high energy part of the particle spectra. The adopted values are listed in Table 2.

Another important parameter is the eigenvalue μ_ℓ . As understood from Eq. (3), the angular distributions are sensitive to the values of μ_ℓ . In fact, Gruppelaar et al.(4) suggests the modified values of μ_ℓ to fit the angular distributions. In the present study the eigenvalues were kept fixed to the original values.

4. Comparison with experimental data

The particle emission spectra as well as DDX were calculated for incident neutron energy near 14 MeV and are compared with the experimental data. The angular

distributions are calculated in the center-of-mass frame. No conversion from the C.M. to the laboratory frame was made.

The integrated and the double differential neutron emission spectra from natural Cr, Fe and Ni were calculated for neutron energy 14.5Mev. Fig. 5(a) compares with the integrated spectrum data of Vonach et al.(5) at 14.8 MeV and of Hermsdorf et al.(6) at 14.1 MeV. In Fig. 5(b) the double differential spectrum data of Tohoku University(7) at 14.1 MeV were compared with the calculation at angles 30 and 150 degrees. Although there remains need for futher adjustment of the parameters, a reasonable overall agreement with experimental data is obtained.

Figures 6(a) and 6(b) compare in the same manner the calculation of the proton emission spectra from dominant isotopes with the data of Grimes et al.(8) at 14.8 MeV. The agreement between calculation and experiment is fairly well.

The angle-integrated alpha particle emission spectra are shown in Figs. 7 for dominant isotopes. Though not depicted, the experimental data of Grimes et al.(8) exhibit the strong anisotropy in the angular distributions. There seems to be no reliable method of calculating the angular distributions of cluster particles at present.

5. Discussions

As understood from the basic theoretical expressions and the comparison with experimental data, the high energy particle spectra in forward directions are predominantly of the preequilibrium nature, while in the backward directions the spectra are almost purely of the statistical nature.

This point is useful in determining the model parameters from the comparison with experimental DDX data.

The appicabilty of PEGASUS to the present problem may be considered as established. It will be also certain that a simplified expression, , Eq.(3), of the Legendre coefficients is valid. This enables the calculation of DDX very simple and make possible an effective storage of DDX cross sections without the use of an enormous storage in the form of double differential data file. It may be particularly useful to prepare the special purpose data file in plan for DPA cross sections, Kerma factor and the primary knock-on atom spectra.

Acknowldgement

Authors are thankful to M. Baba at Tohoku University for providing us with the double differential cross sections data for Cr, Fe and Ni prior to publication. They appreciate the discussions with A.Iwamoto at JAERI and K. Harada (JAERI, now at Nihon Energy Co.) concerning the method of calculation.

References

(1) Program PEGASUS : Iijima,S., Nakagawa,T., Nishigori, T., Sugi,T. : JAERI Report (to be pusblished)
(2) Mantzouranis,G.,Weidenmüller,H.A., Agassi,D. : Z. Phys. A276 145 (1976)
Mantzouranis,G.,Agassi,D.,Weidenmüller,H.A. : Phys. Lett. 578 220 (1975)
(3) Akkermans,J.M., Gruppelaar,H : Calculation of pre-equilibrium angular distributions with the exciton model code PREANG, ECN-60 (1979), Netherlands Energy Research Foundation
(4) Gruppelaar,H., Akkermans,J.M. : Comparison of experimental and calculated neutron emission spectra and angular distri-butions, ECN-84 (1980), Netherlands Energy Research Foundation
(5) Vonach,H. et al.: BNL-NCS-51245 p.343 (1980)
(6) Hermsdorf,d. et al.: Zfk-277(u), 1977
(7) Baba,M: priv. comm. (1987)
(8) Grimes,S.M. et al. : Phys. Rev. C19 2127 (1979)

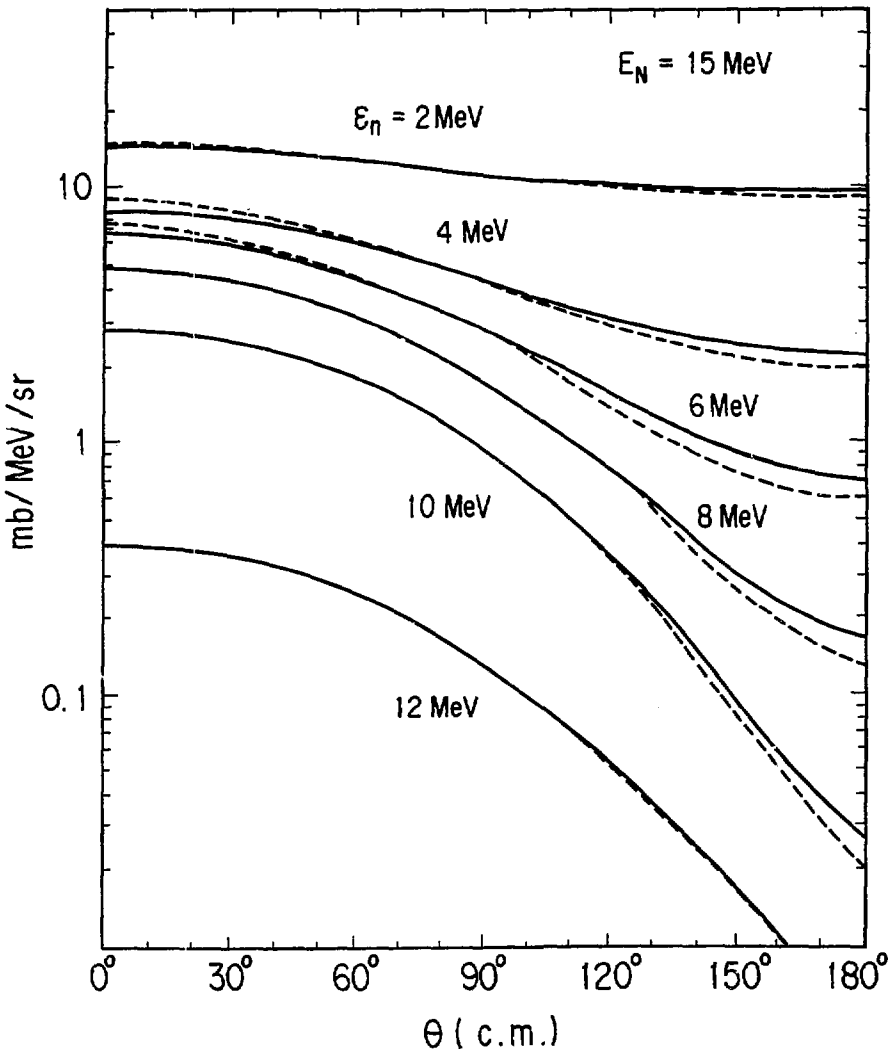

Fig. 1 Neutron angular distributions from ^{58}Ni induced by 15 MeV neutrons

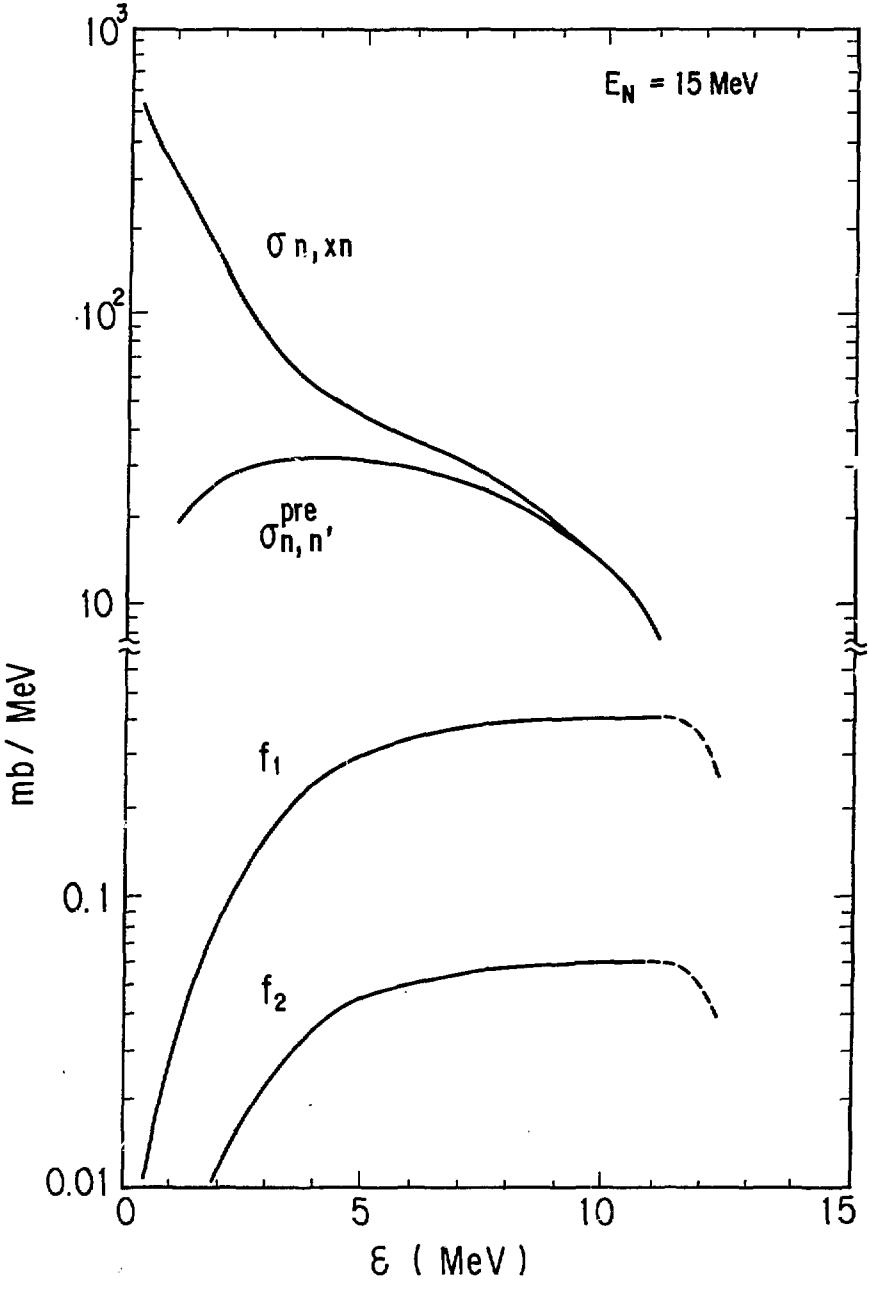

Fig. 2 Neutron spectra from ^{58}Ni induced by 15 MeV neutrons

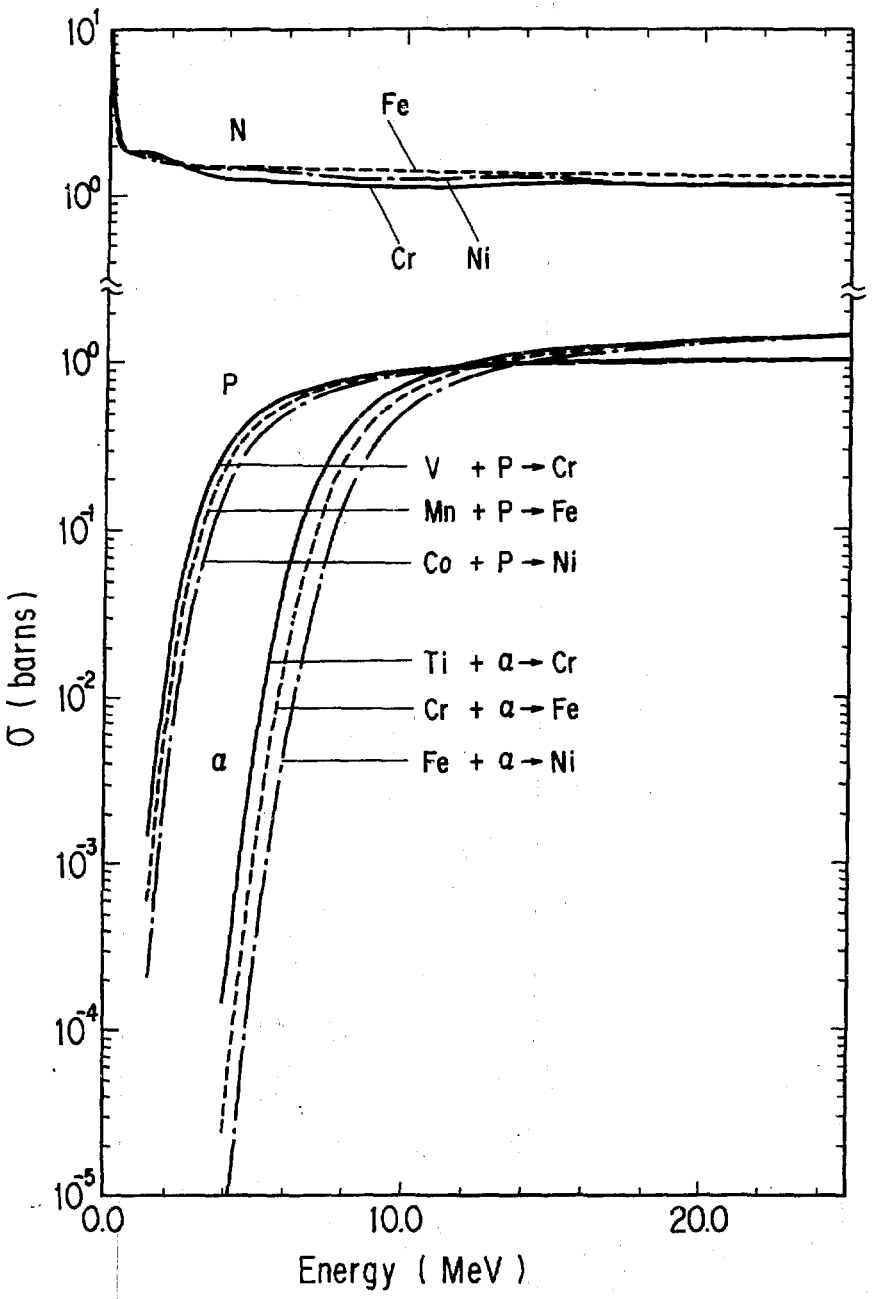

Fig. 3 Inverse cross sections

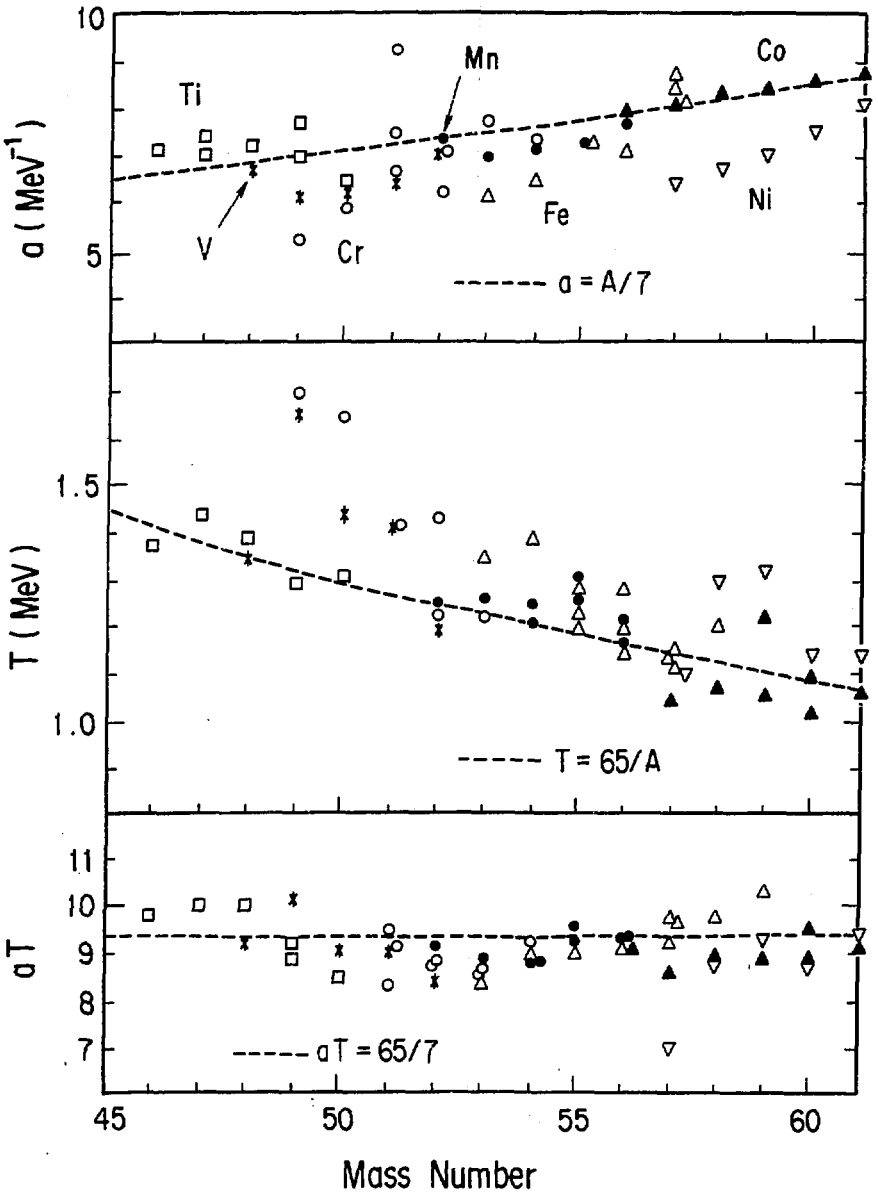

Fig. 4 Level density parameters

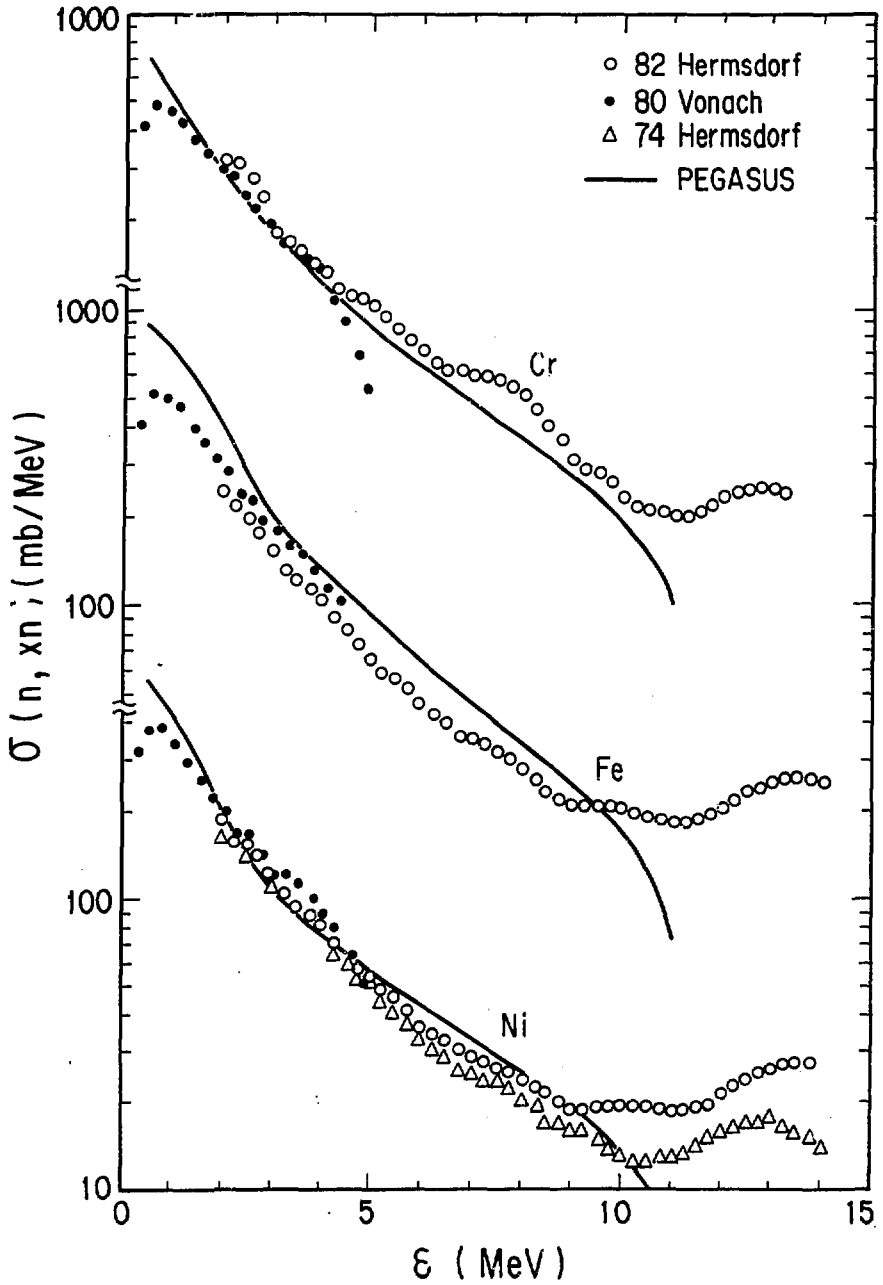

Fig. 5(a) Comparison of neutron spectra at incident neutron energy of 14.8 MeV

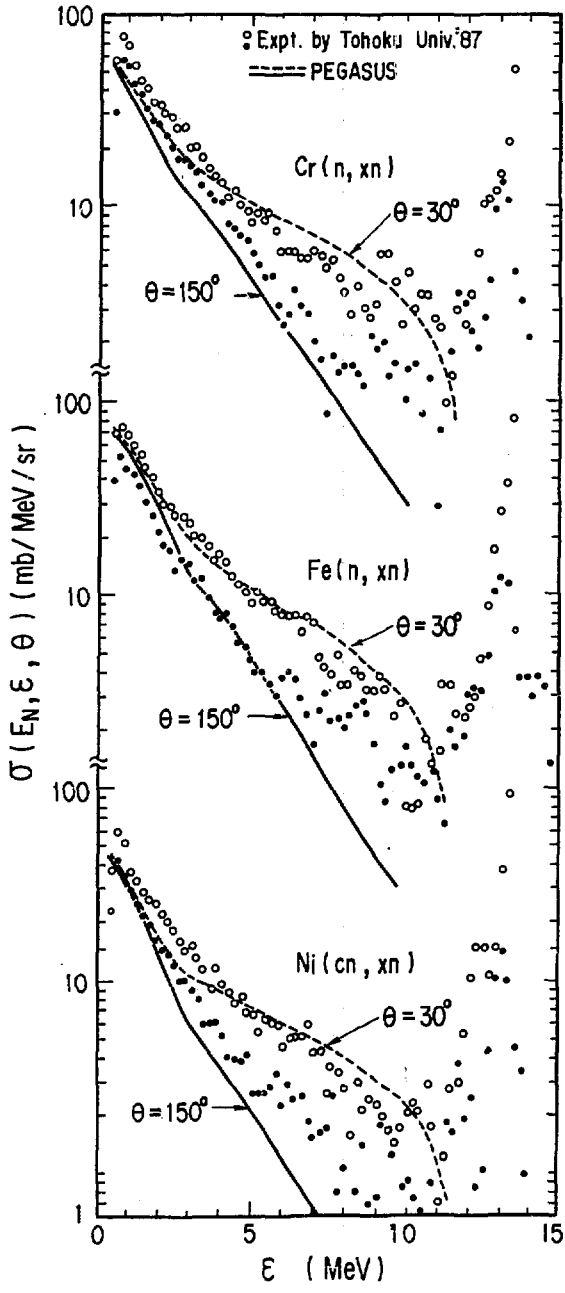

Fig. 5(b) Comparison of DDX at incident neutron energy of 14.1 MeV

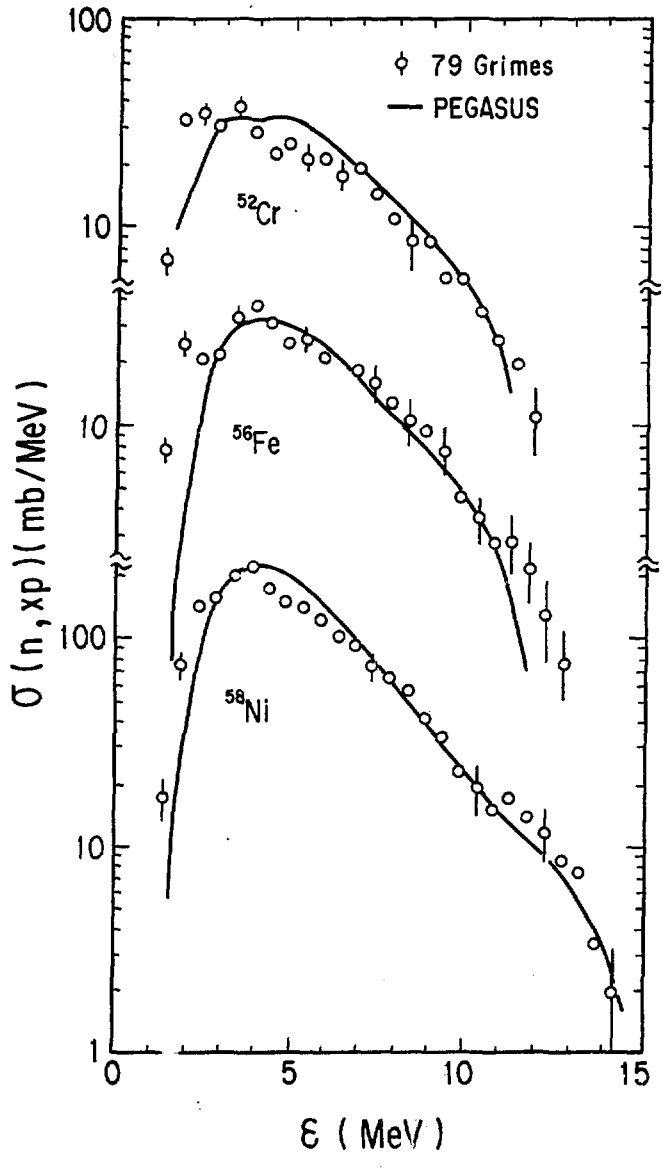

Fig. 6(a) Comparison of proton spectra at incident energy of 14.8 MeV

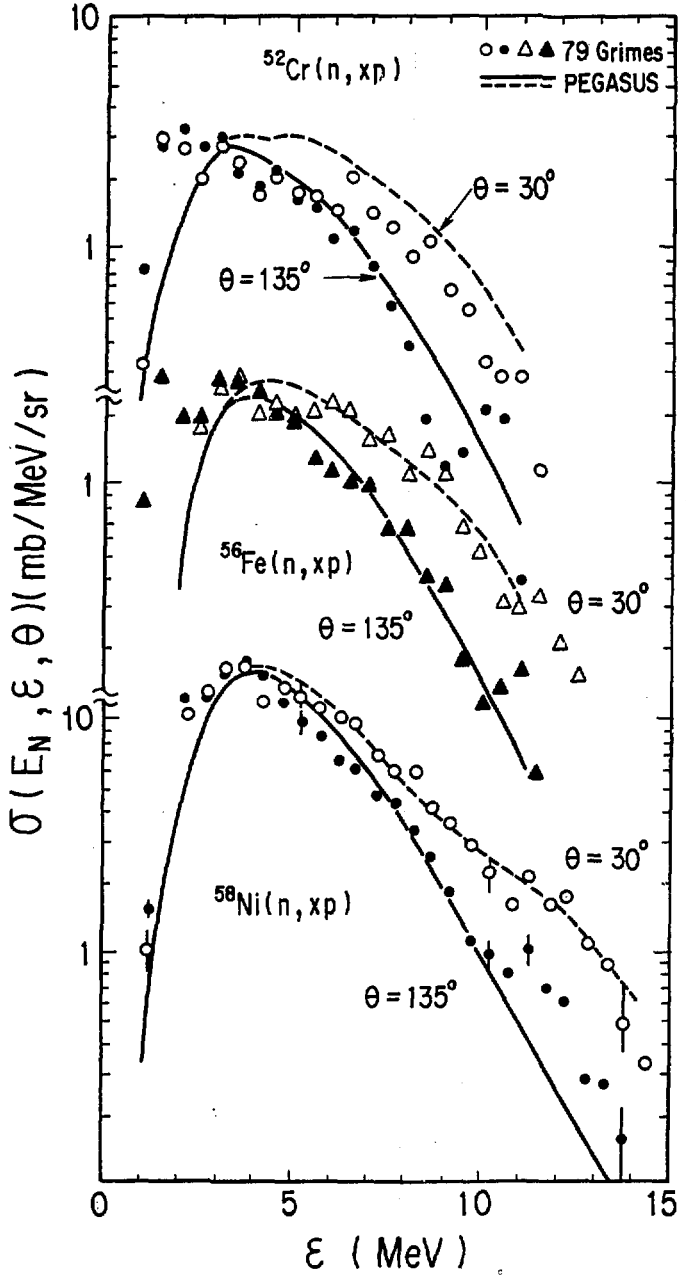

Fig. 6(b) Comparison of proton DDX at incident energy of 14.8 MeV

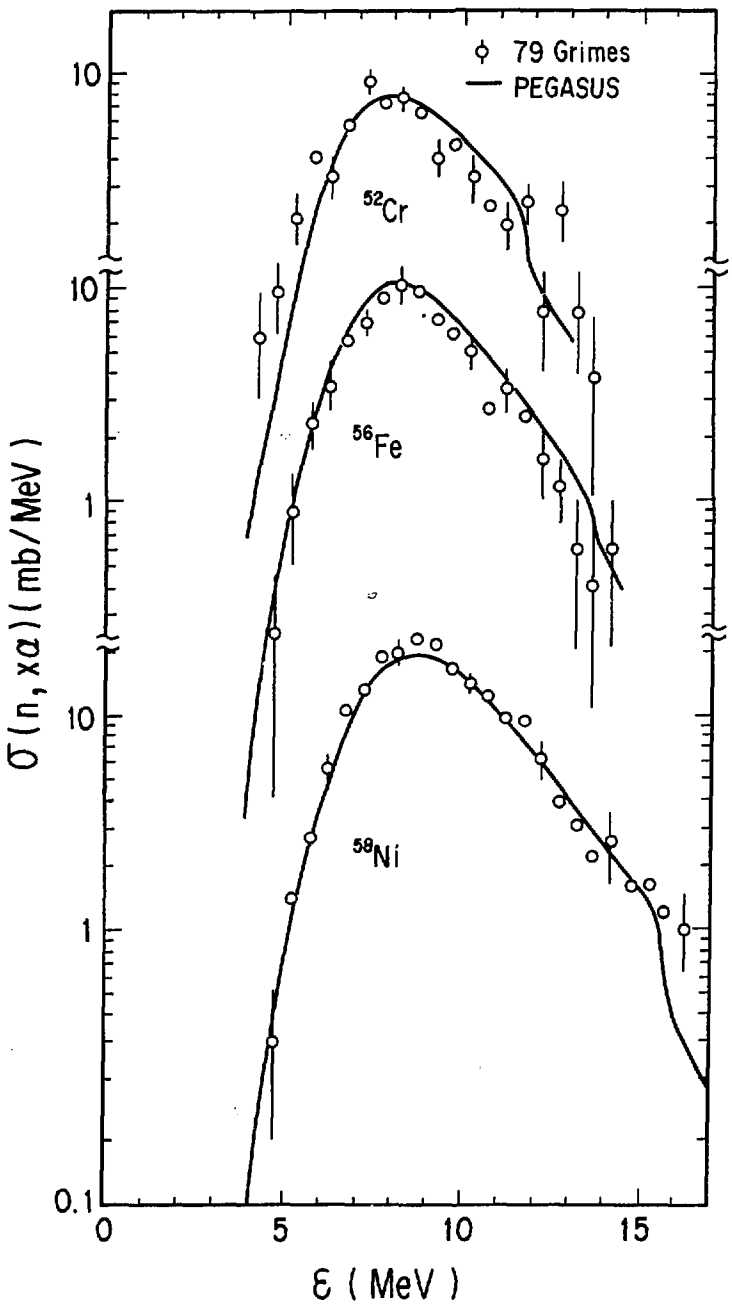

Fig. 7(a) Comparison of alpha particle spectra at incident neutron energy of 14.8 MeV

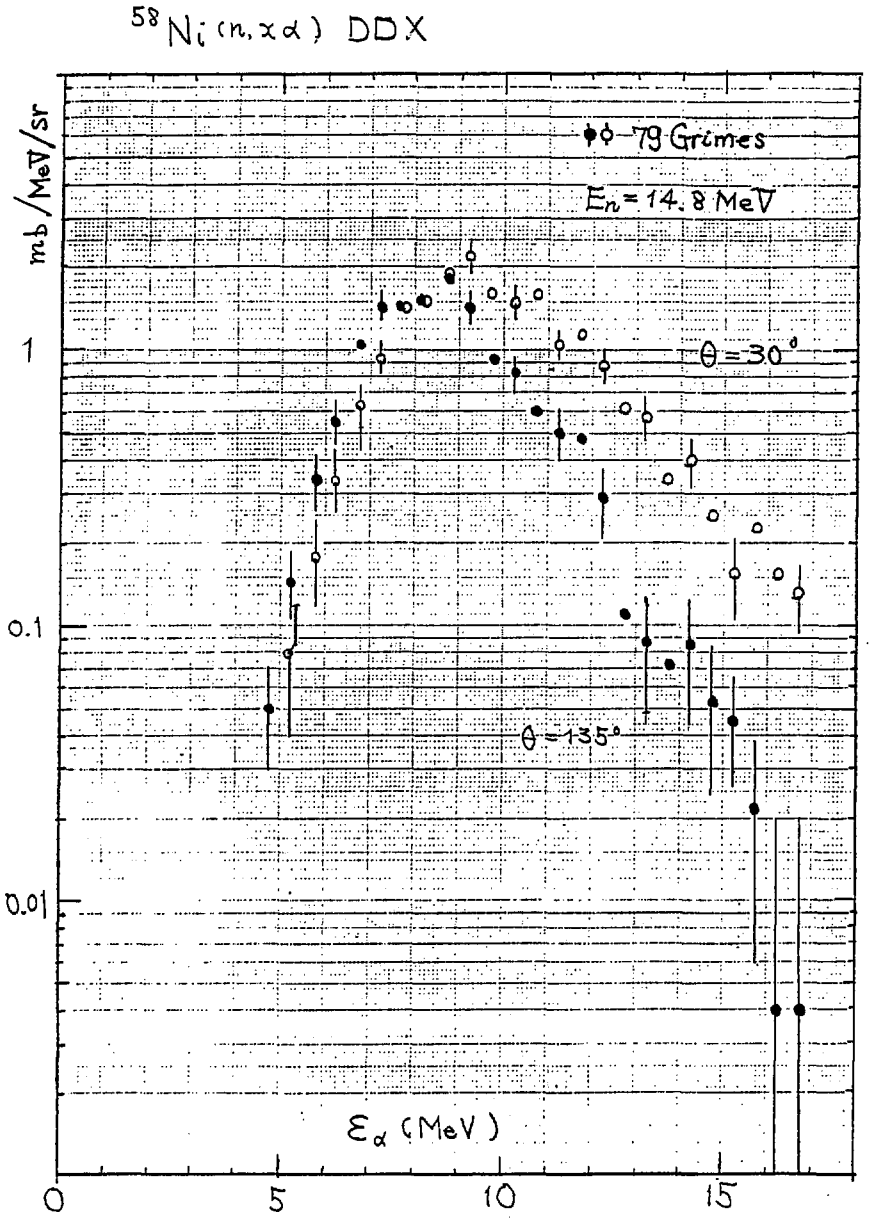

Fig. 7(b) Comparison of alpha DDX of ^{58}Ni at incident neutron energy of 14.8 MeV

4. Free Discussion on JENDL-3

Chairman : My name is Atsushi Zukeran of the Energy Research Lab. of Hitachi Ltd and I will serve as the chairman of this seminar. I would like to ask for your kind cooperation.

Extensive evaluations have been made by about 20 members for JENDL-3, and new and huge amounts of experimental data have been processed for it. The results of the integral test, however, are are unfavorable, and some analysts are saying that we do not need JENDL-3 and only JENDL-2 well do ! Ladies and gentlemen !, what do you think about this situation ? At first, I would like to have some comments from the users of JENDL-3 regarding their reactor design.

Chairman :

Dr. Seki of FBEC, could you give some comments on the results of the integral test, and do you use this new version for your core design ?

Dr. Seki :

I think it depends on the timing whether we use the JENDL-3 for our design or not. We completed the final design of the demonstration FBR "MONJU" based on the mock-up critical experiment MOZART made at the Winfrith Laboratory of UKAEA. We seriously investigated the discrepancies observed in the experimental and analyses from physical points of view, and finally determined the most reliable core performance parameters. If we use the present new version JENDL-3 for MONJU, we are obliged to trace back to the MOZART experiment analysis and re-evaluate the result from the design basis. This may be impossible and a time-consuming job when we consider the time schedule. However, as the next commercial FBR the JENDL-3 should be welcomed.

Chairman :

Dr. Kamei of NAIG, how about your comments as another user ?

Dr. Kamei :

I think, we can made a minor adjustment, a few percent, for multi-group cross section as far as the error of experimental data, although the adjustable range does depends on the type of integral data, for instance, for reaction rate distribution, 3 % seems to be acceptable. Such a minor adjustment is no problem since the error of experimental data is governed by statistics.

Chairman :

Please, Dr. Takeda of Osaka University.

Dr. Takeda :

As is well known, the uncertainties of nuclear characteristics of FBRs come from the cross section uncertainties, and thus, I think, an adjustment of multi-group cross section based on the integral data is one efficient procedure to reproduce the experimental results by using the cross section data based on JENDL-3 and the method employed for its core design.

Chairman :

Please, Dr. Iijma of NAIG.

Dr. Iijima :

Don't worry about whether JENDL-3 will be used for fission and fusion reactors or not ! There are many, and wide fields where JENDL-3 can be extensively used.

Chairman :

Are you talking about your forthcoming "multipurpose file' !? This is an advertisement yours, isn't it ?

Chairman :

Please, Dr. Asami of JAERI.

Dr. Asami :

As the manager of the JENDL-3 project, the saying "JENDL-2 is preferred over JENDL-3" causes significant problems! I would like to delete such a comment from the proceedings of this seminar.

Chairman :

In order to complete JENDL-3A, about 20 members have contributed to the nuclear data evaluation;i.e., data collection and extensive evaluation tasks, and we thought the new one would be superior to JENDL-2. However, our pride has been crushed by the integral test group. Well, I would like to have some comments from the evaluators.

Dr. Kawai of NAIG, do you have any counter opinions towards the integral test group view ?

Dr. Kawai :

I'm one of evaluators who have some doubt about the results of the integral test. For instance, as shown in the figure of Keff C/E vs. the fertile-to-fissile ratio, presented by Dr. Takano, an abnormal discrepancy occurs at ZPR-6-6A. I would like to ask a question," Do you believe that your test is well made for the evaluated micro-scopic data by such poor data?". I think your neutron flux is not carefully evaluated .

Dr. Takeda :

Surely, Keff C/E-value of ZPR-6-6A is usually extremely underestimated in comparison to others.

Chairman :

As pointed out by Dr. Kawai, it seems to inherently contain the method uncertainty in the analysis of integral data. For instance, as shown by Dr. Takano, both radial power distributions based on JENDL-2 and JENDL-3 nuclear data files have remarkable spatial dependence; that is, C/E-values imply that the neutron spectra cannot be reasonably reproduced by calculation. Such

method uncertainty may be enhanced in the spatial power distribution of thermal reactors.

What do you think, Dr. Takano of JAERI ?

Dr. Takano :

Certainly, our method still has some methodological problems. At present, re-confirmation is in progress using VIM code.

Chairman :

Please, Dr. Kanda of Kyusyu University !

Dr. Kanda :

I also have studied the difference between microscopic and macroscopic experiments. As shown in Fig. 1, in both experiments, where detectors 1 and 2 are quite the same and also the experimental techniques are essentially same, the only difference is in the neutron field denoted by the neutron fluxes. Therefore, both experiments have nearly same errors, belonging to the same source. These facts imply that if the integral experiment is correct, in the same sense the microscopic experiments can have the same reliability as the integral. Thus, I do not agree with the opinion that micro-scopic data given as an evaluated data file are doubtful, since the calculated integral quantity does not agree with the experimental data.

Chairman :

Please, Dr. Maekawa of JAERI !

Dr. Maekawa :

I'll agree with Dr. Kanda, that is, I would like to point out that both experiments can have errors in the same source, and in the calculation since the neutron spectra depends on the calculational model, its method uncertainty might reflect to the criticality or especially the reaction rate distribution.

Chairman :

Please, Dr. Kikuchi of JAERI !

Dr. Kikuchi :

As far as the figures showing the adjusted smooth cross section obtained by simultaneous evaluation in comparison with the experimental data, I think, there seems to be no allowable range for capture and fission cross section to be modified, but on the contrary the fission neutron yield (ν -value), fission spectrum(χ), inelastic scattering cross section (σ_{inel}) and so on, which are left unchanged, may affect the results of the analysis of integral data.

Chairman :

Well, Dr. Igarashi of the JAERI Nuclear Data Centre, when do you want to remove the letter "T" attached to JENDL-3 as JENDL-3T*) ?

*) "T" : stands for "Test", "Tentative" or "Temporary" as you prefer.

Dr. Igarashi :

I wish to get rid of it as soon as we can !

Chairman :

Thank you so much ! We wish to continue this fruitful discussion, but our time is up. So, I would like to conclude;

(1) ν -values, which had been easily accepted from experimental data, significantly affect the Keff C/E-values of Benchmark cores.

(2) Simultaneous evaluation of the smooth cross section above 50 KeV gave consistent results among several kinds of reaction cross sections, and thus it could be concluded that this method has been established as a powerful tool for data evaluation. If

possible, it's desirable to add the integral quantities to its variables.

(3) If further simultaneous evaluations taking ν , σ_{inel} and χ into account are possible, our method will be close to the goal, since for instance the fission spectrum χ rolled to harden the neutron spectra and over estimated the threshold reaction rate ratios.

(4) It seemed that there exist some inconsistencies due to methodological uncertainty which are enhanced in the spatial distributions of reaction rate. As a possible source of uncertainty, discussion focussed on the difference of neutron spectra in the microscopic and macroscopic measurements.

Thank you very much for your earnest cooperation in carrying out this session.

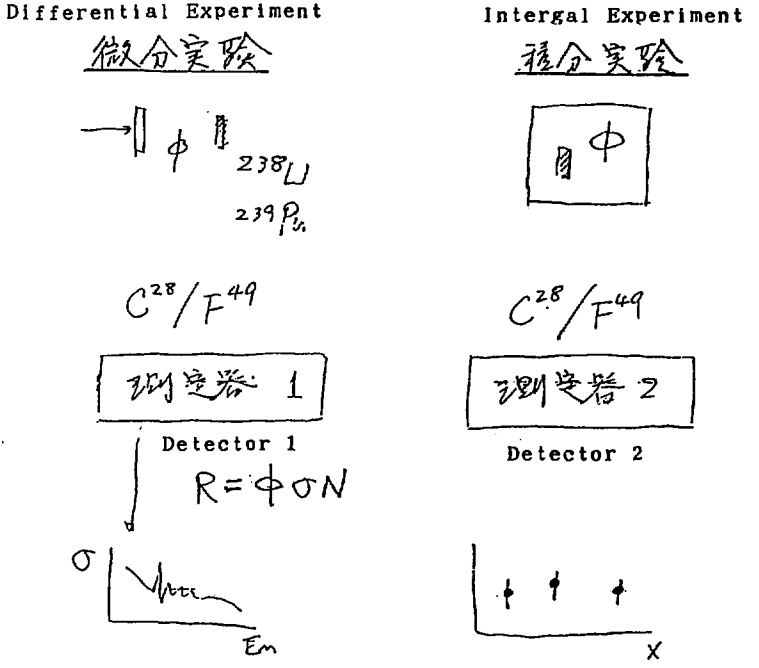

Fig. 1 Comparison of Integral Experimwnt with Differential One

Acknowledgements

The editors wish to acknowledge all the oral and poster presentaters for their interesting presentations at the Seminar and for providing the manuscripts for this report. The editors also acknowledge the session chairmen for their efforts in guiding the fruitful discussion at the seminar. The staff of the Nuclear Data Center of JAERI must be acknowledged for their great help in preparing announcements, program, letters, and arranging the meeting place and reception. Finally the editors acknowledge the members of the program committee for their good ideas regarding the seminar program.